frontiers | Research Topics

Cardiac regeneration

Edited by
Ajit Magadum, Rajika Roy and Claudio de Lucia

Published in
Frontiers in Cardiovascular Medicine

ISSN 1664-8714
ISBN 978-2-83252-137-3
DOI 10.3389/978-2-83252-137-3

About Frontiers

Frontiers is more than just an open access publisher of scholarly articles: it is a pioneering approach to the world of academia, radically improving the way scholarly research is managed. The grand vision of Frontiers is a world where all people have an equal opportunity to seek, share and generate knowledge. Frontiers provides immediate and permanent online open access to all its publications, but this alone is not enough to realize our grand goals.

Frontiers journal series

The Frontiers journal series is a multi-tier and interdisciplinary set of open-access, online journals, promising a paradigm shift from the current review, selection and dissemination processes in academic publishing. All Frontiers journals are driven by researchers for researchers; therefore, they constitute a service to the scholarly community. At the same time, the *Frontiers journal series* operates on a revolutionary invention, the tiered publishing system, initially addressing specific communities of scholars, and gradually climbing up to broader public understanding, thus serving the interests of the lay society, too.

Dedication to quality

Each Frontiers article is a landmark of the highest quality, thanks to genuinely collaborative interactions between authors and review editors, who include some of the world's best academicians. Research must be certified by peers before entering a stream of knowledge that may eventually reach the public - and shape society; therefore, Frontiers only applies the most rigorous and unbiased reviews. Frontiers revolutionizes research publishing by freely delivering the most outstanding research, evaluated with no bias from both the academic and social point of view. By applying the most advanced information technologies, Frontiers is catapulting scholarly publishing into a new generation.

What are Frontiers Research Topics?

Frontiers Research Topics are very popular trademarks of the *Frontiers journals series*: they are collections of at least ten articles, all centered on a particular subject. With their unique mix of varied contributions from Original Research to Review Articles, Frontiers Research Topics unify the most influential researchers, the latest key findings and historical advances in a hot research area.

Find out more on how to host your own Frontiers Research Topic or contribute to one as an author by contacting the Frontiers editorial office: frontiersin.org/about/contact

Cardiac Regeneration

Topic editors

Ajit Magadum — Temple University, United States

Rajika Roy — Temple University, United States

Claudio de Lucia — Local Health Authority Naples 1 Center, Italy

Citation

Magadum, A., Roy, R., de Lucia, C., eds. (2023). *Cardiac regeneration*. Lausanne: Frontiers Media SA. doi: 10.3389/978-2-83252-137-3

Table of contents

frontiers | Frontiers in Cardiovascular Medicine

TYPE Editorial
PUBLISHED 27 March 2023
DOI 10.3389/fcvm.2023.1178440

OPEN ACCESS

EDITED AND REVIEWED BY
Paolo Madeddu,
University of Bristol, United Kingdom

*CORRESPONDENCE
Ajit Magadum
ajit23882@gmail.com
tun83483@temple.edu

SPECIALTY SECTION
This article was submitted to Cardiovascular Biologics and Regenerative Medicine, a section of the journal Frontiers in Cardiovascular Medicine

RECEIVED 02 March 2023
ACCEPTED 06 March 2023
PUBLISHED 27 March 2023

CITATION
Roy R, de Lucia C, Joladarashi D and Magadum A (2023) Editorial: Cardiac regeneration.
Front. Cardiovasc. Med. 10:1178440.
doi: 10.3389/fcvm.2023.1178440

Editorial: Cardiac regeneration

Rajika Roy[1], Claudio de Lucia[2], Darukeshwara Joladarashi[1] and Ajit Magadum[1]*

[1]Center for Translational Medicine, Lewis Katz School of Medicine, Temple University, Philadelphia, PA, United States, [2]Geriatric Center Frullone, ASL (Azienda Sanitaria Locale - Local Health Authority) Napoli 1 Centro, Naples, Italy

KEYWORDS

cardiac regeneration, cardiomyocyte proliferation, gene therapy (GT), cell therapy, cardiac regeneration animal models, small molecule screening

Editorial on the Research Topic
Cardiac regeneration

Cardiovascular diseases (CVD) are the leading cause of morbidity and mortality worldwide, with 19.05 million deaths in 2020. Heart failure (HF) is primarily due to the inability of the adult mammalian heart to replace the lost cardiomyocytes (CMs) following injury. Current treatments are focused on prevention rather than therapies. Therefore, developing novel therapies and finding novel molecular and cellular mechanisms are of great importance. The research topic comprises a series of original articles and reviews, and summarizes and discusses intuitive concepts, strategies, and novel inventions to regenerate or repair the injured heart.

With the focus on CM proliferation, there is a need to monitor and distinguish between cycling and non-cycling CMs. Murganti et al. described a Florescent Ubiquitination-based Cell Cycle Indicator (FUCCI) that can differentiate between cycling and non-cycling CMs and combined that with time-lapse microscopy to distinguish between cytokinesis and karyokinesis. The authors used human induced pluripotent cell (TNNT2-FUCCI)-derived CMs and screened for 94 autophagy-regulating small molecules to find a novel CM proliferator inducer. Similarly, Magadum et al. also used the FUCCI approach and developed a stable CM7/1-hgem mouse embryonic stem cell line, further differentiated into CMs to screen for novel inducers of CM proliferation. By screening the Spectrum Collection small molecule library subset, 18 potential inducers of CM proliferation were identified. Among the top four candidates were two cardiac glycosides, peruvoside and convallatoxin, and osajin and efaroxan hydrochloride. Inhibition of PTEN and GSK-3β enhanced cell cycle re-entry and progression upon stimulation with cardiac glycosides and osajin.

Myc expression has been shown to induce CM proliferation in mouse hearts when co-expressed with Cyclin T1. Boikova et al. explored the collective ability of Myc and HRas (known to stabilize Cyclin T1) in inducing CM proliferation. The overexpression of HRas*G12V* and constitutive Myc mutually induced adult mammalian CM proliferation but also caused CM death. Since combinatorial Cyclin T1 and Myc expression does not induce CM death in mice hearts post-MI, it could be therapeutically used. Separately, Sun et al. found cyclin-dependent kinase 9 (CDK9) an attractive therapeutic target in cardiac regeneration. CDK9 is highly expressed in the neonatal period and is usually not detected in the adult heart. CDK9 stimulates cardiac regeneration *via* serine-threonine-protein kinase 3 (SGK3) and downstream glycogen synthase kinase-3 beta (GSK-3β)/β-catenin pathway. The overexpression of CDK9 significantly stimulated mature CMs to

re-enter the cell cycle and promoted cardiac repair after MI in adult mice, while CDK9 inhibition repressed CM proliferation in neonatal mice post-injury.

Duan et al. proposed metabolism (fatty acid oxidation, glycolysis, amino acid metabolism, and the tricarboxylic acid cycle), a key modulator of cardiac regeneration, to be considered as a therapeutic target. The detailed review article by Miao et al. highlighted the role of nicotinamide adenine dinucleotide phosphate oxidase (NOXs) in myocardial remodeling and its potential as a therapeutic target (Miao et al.). Amongst the different isoforms of NOX, NOX1, NOX2, NOX4, and NOX5 are found in cardiac tissue. Besides structural remodeling, NOX isoforms also play a role in modulating inflammatory responses and metabolism. In mouse models, NOX inhibitors have been shown to improve outcomes of pathological remodeling and can be further explored for clinical testing. Sierra-Pagan et al. described the role of different novel factors in cardiovascular lineage development and reprogramming that can be further exploited to better develop regenerative therapies for cardiovascular disease.

Wang et al., in a review, highlighted recent advances in cell and cell-free-based therapies for ischemic heart diseases. It is well known that the transplantation efficiency of human pluripotent stem cell (hPSC)-derived CMs (hPSC-CMs) is low because of poor cell survival in the ischemic heart. The authors listed numerous factors that regulate CM proliferation and cardiac regeneration from the last two decades.

Post-injury scar tissue lacks perfusion due to loss of vasculature. To promote re-vascularization, Spiroski et al. utilized a good manufacturing practice (GMP)-compatible human embryonic stem cell-derived endothelial cell product (hESC-ECP) that has been previously tested for its angiogenic potential. Fourteen days after cell transplantation, cardiac structure and function were better preserved. Graber et al. reported that the mechanical stimulus of shockwave therapy (SWT) could incite regenerative effects in ischemic tissue through growth factor release, modulation of the inflammatory response, and angiogenesis with functional improvement. SWT to the ischemic heart has limitations, such as the heart having a small acoustic window, restriction in accessing the treatment regions, and risk of potential lung injuries.

To study mechanistic details of *in vivo* processes, Maselli et al. established a protocol to obtain and culture 3D organotypic heart slices from porcine hearts containing intact epicardium. This approach allows cost-effective slice preparation compared to large animal testing, the ability to study an integrated group of cells instead of individual cells, and elucidating cell-ECM interactions.

In summary, the "Cardiac Regeneration" research topic addresses novel strategies and inventions, a broad explanation, and intuitive concepts on cardiac regeneration. Readers will undoubtedly appreciate the concise summaries of the contributions given in this issue that describe different ideas and strategies to induce cardiac regeneration. We hope that the ongoing efforts of investigators in cardiovascular regeneration and the published papers within this issue will one day lead to groundbreaking advances in the treatment of CVD in patients.

Author contributions

RR, CDL, AM have written and edited the manuscript. DJ has provided critical inputs for the writing and has edited the manuscript. All authors contributed to the article and approved the submitted version.

Conflict of interest

The authors declare that the research was conducted in the absence of any commercial or financial relationships that could be construed as a potential conflict of interest.

Publisher's Note

frontiers | Frontiers in Cardiovascular Medicine

ORIGINAL RESEARCH
published: 25 April 2022
doi: 10.3389/fcvm.2022.840147

FUCCI-Based Live Imaging Platform Reveals Cell Cycle Dynamics and Identifies Pro-proliferative Compounds in Human iPSC-Derived Cardiomyocytes

Francesca Murganti[1†], Wouter Derks[1†], Marion Baniol[2], Irina Simonova[1], Palina Trus[1], Katrin Neumann[1], Shahryar Khattak[1,3], Kaomei Guan[4] and Olaf Bergmann[1,2]*

[1] Center for Regenerative Therapies Dresden, TU Dresden, Dresden, Germany, [2] Karolinska Institute, Cell and Molecular Biology (CMB), Stockholm, Sweden, [3] Royal College of Surgeons Ireland (RCSI) in Bahrain, Adliya, Bahrain, [4] Institute of Pharmacology and Toxicology, TU Dresden, Dresden, Germany

OPEN ACCESS

Edited by:
Rajika Roy,
Temple University, United States

Reviewed by:
Michela Noseda,
Imperial College London,
United Kingdom
Joe Z. Zhang,
Shenzhen Bay Laboratory, China

***Correspondence:**
Olaf Bergmann
olaf_bergmann@tu-dresden.de

[†]These authors have contributed equally to this work

Specialty section:
This article was submitted to Cardiovascular Biologics and Regenerative Medicine, a section of the journal Frontiers in Cardiovascular Medicine

Received: 20 December 2021
Accepted: 16 March 2022
Published: 25 April 2022

Citation:
Murganti F, Derks W, Baniol M, Simonova I, Trus P, Neumann K, Khattak S, Guan K and Bergmann O (2022) FUCCI-Based Live Imaging Platform Reveals Cell Cycle Dynamics and Identifies Pro-proliferative Compounds in Human iPSC-Derived Cardiomyocytes. Front. Cardiovasc. Med. 9:840147. doi: 10.3389/fcvm.2022.840147

One of the major goals in cardiac regeneration research is to replace lost ventricular tissue with new cardiomyocytes. However, cardiomyocyte proliferation drops to low levels in neonatal hearts and is no longer efficient in compensating for the loss of functional myocardium in heart disease. We generated a human induced pluripotent stem cell (iPSC)-derived cardiomyocyte-specific cell cycle indicator system (TNNT2-FUCCI) to characterize regular and aberrant cardiomyocyte cycle dynamics. We visualized cell cycle progression in TNNT2-FUCCI and found G2 cycle arrest in endoreplicating cardiomyocytes. Moreover, we devised a live-cell compound screening platform to identify pro-proliferative drug candidates. We found that the alpha-adrenergic receptor agonist clonidine induced cardiomyocyte proliferation *in vitro* and increased cardiomyocyte cell cycle entry in neonatal mice. In conclusion, the TNNT2-FUCCI system is a versatile tool to characterize cardiomyocyte cell cycle dynamics and identify pro-proliferative candidates with regenerative potential in the mammalian heart.

Keywords: cardiomyocyte, cell cycle activity, cell cycle indicator, fluorescence ubiquitination cell cycle indicator, induced pluripotent stem cell, clonidine, polyploidy

INTRODUCTION

Heart regeneration in mammals is restricted to the neonatal period when cardiomyocytes can still proliferate (1–3). Cardiomyocyte proliferation gradually declines after birth and remains at a low level in adulthood (4, 5). Although multiple factors, including changes in metabolism (6), extracellular matrix (7), and endocrine signaling (8), contribute to this loss of proliferative activity, the exact underlying mechanism that drives cardiomyocyte cell cycle exit still needs further elucidation.

While cardiomyocyte proliferation declines, aberrant cell cycle activity becomes more dominant, leading to multinucleation and endoreplication during the first postnatal weeks (1). The increase in polyploidy is implicated in the loss of regenerative capacity in postnatal hearts (9). To date, it is not clear which cues determine the fate of cycling cells and how one can direct non-productive cell cycle activity to cytokinesis and proliferation. Moreover, this non-productive cell cycling

has made the identification of cardiomyocyte proliferation challenging and has previously led to misinterpretation of the cardiomyocyte renewal capacity (10).

The Fluorescence Ubiquitin Cell Cycle Indicator (FUCCI) system is a genetically encoded, protein-based two-color cell cycle indicator that allows for the identification of cycling and non-cycling cells and relies on the ubiquitination and degradation of the cell cycle regulators Cdt1 and Geminin (11, 12). The combination of FUCCI cell cycle indicators with time-lapse microscopy can unequivocally determine whether the outcome of the cardiomyocyte cell cycle is productive (cytokinesis) or non-productive (endoreplication) (13–16).

Human induced pluripotent stem cell-derived cardiomyocytes (hiPSC-derived CMs) can currently be robustly generated using established protocols (17), diminishing the need for cardiomyocytes isolated from rodents, which do not fully recapitulate human physiology.

Depending on their level of maturity, hiPSC-derived CMs still have the capacity to proliferate (18). Thus, hiPSC-derived CMs represent an ideal model system to study the kinetics and regulation of human cardiomyocyte proliferation.

Here, we generated a troponin T2-FUCCI (TNNT2-FUCCI) hiPSC line and showed aberrant cell cycle kinetics with G2 arrest in endoreplicating cardiomyocytes compared to those undergoing proliferation and multinucleation. Moreover, we investigated our TNNT2-FUCCI hiPSC-derived CMs with an autophagy compound library in a live-cell screening approach and identified the alpha-adrenergic agonist clonidine to promote cardiomyocyte proliferation in hiPSC-derived CMs and cell cycle entry in mouse neonatal cardiomyocytes (mNCMs).

METHODS

Generation of TNNT2-FUCCI hiPSC

The pCAG-Fucci2a plasmid (the RIKEN Center for Life Science Technologies, RDB13080) was obtained through RIKEN (19, 20). mCherry was kindly provided by Shaner et al. (21). The Fucci2a portion (mCherry-hCdt1-T2A-mVenus-hGem) was PCR amplified and cloned in frame downstream of the TNNT2 start codon into a custom synthesized (Thermo Fisher Scientific) plasmid backbone containing the ColE1 origin of replication, ampicillin resistance, 1,000 bp 5′ and 980 bp 3′ homology arms to the hTNNT2 (NM_000364.4) transcription start site, IRES-Puro and an FRT-flanked PGK-hygromycin selection cassette to generate the targeting vector using the NEBuilder High-Fidelity DNA Assembly Cloning Kit (NEB, E5520). Twenty-one bp downstream of the start codon, including the sgRNA target sites, was excluded from the targeting vector to protect it from CRISPR/Cas9-induced double-strand breaks. The resulting targeting vector was verified by Sanger sequencing, linearized by restriction with SspI and SfiI enzymes and phenol–chloroform-extracted. Two different sgRNAs (*spacer sequences below*), each targeting the region behind the start codon of hTNNT2 that was excluded from the targeting vector, were transcribed *in vitro* using an EnGen® sgRNA Synthesis Kit (NEB, E3322S). The generation and characterization of CRTD5 hiPSCs (hPSCreg, CRTDi005-B) was previously described (22). CRTD5 hiPSCs (800,000) were electroporated with 10 μg linearized targeting vector, 1 μg of each sgRNA and 60 pmol Cas9-NLS protein (EnGen® Spy Cas9 NLS, NEB, M0646 M) with the Lonza 4D X-unit, pulse CB-150 and Primary Cell 4D-Nucleofector Kit L (V4XP-3024, Lonza). Transfected cells were seeded at clonal density in dishes coated with hESC-qualified Matrigel (Corning Life Sciences, 354277) in mTeSR1 medium (StemCell Technologies, 85850) supplemented for 3 days with 10 μM Rock inhibitor Y-27632 (StemCell Technologies, 78003). Cells were selected with 50 μg/ml hygromycin B (Thermo Fisher Scientific, 10687010) starting on Day 3 after nucleofection for 7 days, and resistant colonies were manually selected, clonally expanded and screened for correctly targeted clones by colony PCRs amplifying the 5′ and 3′ junction of the targeted alleles from outside of the homology arms into the insert as well as the presence of an intact second allele. Heterozygously targeted clones were selected, and the complete insert was analyzed by Sanger sequencing. The selected complete clone CRTD5-TNNT2-FUCCI #19 was karyotyped by Giemsa banding and showed an intact chromosome set 46,XY[cp20], similar to the parental line (**Supplementary Figure 1A**).

hTNNT2-sgRNA#3: 5′- GACCATGTCTGACATAGAAG-A3′
hTNNT2-sgRNA#4: 5′- GGTGGTGGAAGAGTACGAGG-3′

hiPSC Culture and Maintenance

The hiPSC line (CRTD5) generated from human fibroblasts was used in this study as a control and was obtained from the Stem Cell Engineering facility of the Center for Molecular and Cellular Bioengineering (CMCB), TU Dresden. Research with CRTD5 hiPSC was approved by the *Ethikkommission an der Technischen Universität Dresden* (BO-EK-38012020). Cells were propagated using ReLeSR (StemCell Technologies, 05873) and maintained in mTESR1™ (StemCell Technologies, 85850) on Matrigel™-coated plates (Corning Life Sciences, 354234) under standard culturing conditions (37 °C, 5% CO_2). Cell cultures were routinely checked for mycoplasma using the LookOut® Mycoplasma PCR Detection Kit (Sigma Aldrich, D9307).

hiPSC Differentiation Into Cardiomyocytes

Differentiation of CRTD5 and FUCCI-CRTD5 lines was induced by adaptation of a previously described protocol (17, 23). Briefly, undifferentiated hiPSCs were passaged into 12-well plates using Versene (Thermo Fisher Scientific, 15040066). When hiPSC culture reached 90–95% confluency, differentiation was induced using CDM3 medium (17) supplemented with the GSK3β inhibitor CHIR99021 (4 μM, Sigma, SML1046) for 48 h followed by treatment with IWP2 (5 μM, Tocris, 3533) for an additional 48 h. After, cells were cultured in CDM3 medium. At Day 15 of differentiation, hiPSC-derived CMs were gently detached from the plate by incubating with 1 mg/ml collagenase B dissolved in CDM3 medium for 30 min at 37°C. hiPSC-derived CMs were further dissociated using 0.25% trypsin-EDTA for 5 min at 37°C. The reaction was stopped by adding a double volume of stop medium (80% CDM3, 20% FBS, ROCK inhibitor). Cells were plated at a density of 1,000,000 cells/well into Matrigel-coated 12-well plates. CDM3 was exchanged every second day until further analysis.

Imagestream-X Analysis

hiPSC-derived CMs were detached from the plate by incubating with 1 ml of TrypLE (Thermo Fisher Scientific, 12604013) for 5 min at 37°C. A double volume of PBS was added to stop the reaction, and the cells were passed through a 100 μm cell strainer. hiPSC-derived CMs were centrifuged at 200 g for 5 min, fixed with 1% PFA for 20 min and washed 3x with PBS. hiPSC-derived CMs were incubated with primary antibodies against mVenus (Biorbyt, orb334993, 1:800) and mCherry (Abcam, ab125096, 1:250) and anti-cardiac troponin T-APC (Miltenyi Biotec, 130-120-403, 1:50) in blocking buffer (PBS, 4% donkey serum, 0.1% Triton X-100 in PBS, 2 mM EDTA) for 2 h at RT. After washing, the cells were incubated with the secondary antibodies anti-goat Alexa Fluor® 488 (Jackson ImmunoResearch, 705-546-147, 1:500), anti-rabbit Alexa Fluor® 555 (Abcam, ab150062, 1:500) and Hoechst 33342 (Thermo Fisher Scientific, H21492) for 1 h at 4°C. Cells were then washed 3x with PBS and centrifuged at 200 g for 5 min. Finally, 5 million cells were resuspended in 500 μl of FACS buffer (PBS, 2% FBS, EDTA) and kept on ice until further analysis. Cells were analyzed on Amnis ImageStream-X MkII (Luminex, United States).

hiPSC Immunohistochemistry

Cells were fixed with 4% formaldehyde solution in PBS for 10 min and stained overnight at 4°C with primary antibodies against mVenus (1:800, Biorbyt, orb334993) and mCherry (1:250, Abcam, ab125096) and anti-cardiac troponin T (1:250, Thermo Fisher Scientific, MA5-12960) in blocking buffer (PBS, 4% donkey serum, 0.1% Triton X-100 in PBS, 2 mM EDTA). Cells were then washed 3x with PBS and incubated with the following secondary antibodies in PBS: anti-goat Alexa Fluor® 488 (1:500, Jackson ImmunoResearch, 705-546-147), anti-rabbit Alexa Fluor® 555 (1:500, Abcam, ab150062), anti-mouse Alexa Fluor® 647 (1:500, Jackson ImmunoResearch, 715-606-151) and Hoechst 33342 (Thermo Fisher Scientific, H3570).

Measurement of Cell Area and Sarcomere Spacing

CRTD5 and FUCCI-CRTD5 cardiomyocytes at Day 25 of differentiation were first costained with antibodies against TNNT2 (mouse, Thermo Fisher Scientific, MA5-12960) and α-actinin (rabbit, ThermoFisher Scientific, 701914). Imaging of single cardiomyocytes was performed using a Zeiss LSM 700. For cell area analysis, using ImageJ-Fiji software, a defined region of interest (ROI) was defined to outline the outer edges of the cell, and the cell area was measured for each cardiomyocyte. For sarcomere spacing measurements, an ROI with at least 10 sarcomeres was defined. The intensity or the ROI shows a series of peaks that correspond to the spatial frequency of the sarcomeric pattern, and the amplitude between the peaks was determined to assess the sarcomere spacing.

Primary mNCMs Culture

Whole litters of C57BL/6JRj mice (P0) were used for isolation of mNCMs. C57BL/6JRj mice were originally obtained from Janvier labs and bred internally in CRTD animal facilities. All procedures were approved by the local ethics committee, Landesdirektion Sachsen (TVT-1/2017). P0 mNCMs were isolated using the Neonatal Heart Dissociation kit (Miltenyi Biotec, 130-098-373) following the manufacturer's instructions. Cells were seeded in plating medium (20% M199 (Thermo Fisher Scientific, 12340030), 65% DMEM (Thermo Fisher Scientific, 31966021), 5% FBS (fetal bovine serum), and 10% HS (horse serum) at a seeding density of 35,000 cells/well in a 96-well plate coated with Matrigel (Corning Life Sciences, 354234). Cells recovered for 1 day in an incubator (37°C, 5% CO_2).

Live Imaging and Analysis of TNNT2-FUCCI hiPSCs

HiPSC-derived CMs at different time points post cardiomyocyte induction (0, 6, and 30 days) were imaged using a Keyence BZ-X800E microscope (Keyence, Japan). Images were acquired using brightfield, YFP and Cy3 filter sets. For time-lapse imaging, FUCCI hiPSC-derived CMs at Day 30 of differentiation were seeded in CDM3 medium at a density of 150,000 cells per well in a 24-well plate (Cellvis, P24-0-N) coated with Matrigel (Corning Life Sciences, 354234). Time-lapse imaging was performed as previously described (14). Briefly, FUCCI hiPSC-derived CMs were imaged every 20 min for 72 h, and the quantification of the mCherry and mVenus fluorescent intensities was performed using Keyence image measurement and analysis software (Keyence, Japan) and ImageJ-Fiji software. A region around the cell was first defined as the background region, and the cell nucleus was segmented using the brightfield signal. The mCherry and mVenus intensities were detected in both the background region and the nucleus. The background signal was subtracted from the nuclear intensity. Single-cell intensity data were aligned based on the peak mVenus intensity and plotted over a period of 40 h using GraphPad Prism.

Analysis of Ploidy and Binucleation in Cardiomyocytes

Culture hiPSC-derived CMs or mNCMs were fixed with 4% formaldehyde solution in PBS for 10 min and stained overnight at 4 °C with primary antibodies against cardiac troponin I (1:500, Abcam, ab56357) and Ki-67 (CellSignaling, 9449T) in blocking buffer (PBS, 4% donkey serum, 0.1% Triton X-100 in PBS, 2 mM EDTA). Cells were then washed 3x with PBS and stained with the secondary antibodies anti-goat Alexa Fluor® 488 (Jackson ImmunoResearch, 705-546-147, 1:500), anti-rabbit Alexa Fluor® 555 (1:500, Abcam, ab150062), and Vybrant DyeCycle Violet Stain (Invitrogen, V35003) in PBS. Images were acquired using a Keyence BZ X800 fluorescence microscope (Keyence, Japan) equipped with an imaging cytometer (BZ-H4XI). Image analysis was performed in the open source software CellProfiler 4.2.1 (24). Nuclei segmentation was performed using the identify primary objects module with an adaptive thresholding method to account for background variances. Cardiac troponin I and Ki-67 intensities were measured in segmented nuclei, and thresholds were determined according to their histograms. DNA staining intensities of non-cycling (Ki-67$^-$) cardiomyocyte nuclei (cardiac troponin I$^+$) were measured, and ploidy levels were plotted as histograms, from which ploidy thresholds

were determined (**Supplementary Figure 3**). The number of nuclei per cardiomyocyte was determined manually analyzing a minimum of 15 field of views for each biological replicate.

Cell Plating and Culturing and Screen Conditions

TNNT2-FUCCI hiPSC-CMs were differentiated as described above. hiPSC-CMs were used 30 days after starting the differentiation. hiPSC-CMs were plated on 96-well glass bottom plates (Cellvis, P96-1-N) coated with Matrigel (Corning Life Sciences, 354277) at a seeding density of 4000 cells per well. Cells were seeded in a volume of 50 μl RPMI20 medium (RPMI 1640 with 20% FBS). Outer wells were left unused and filled with PBS to exclude well plate edge effects. The medium was changed the next day for RPMI 1640 (Thermo Fisher Scientific, 32404014) + B27 (Thermo Fisher Scientific, 17504044) + 0.1% FBS (Thermo Fisher Scientific, 10500064). Subsequently, hiPSC-CMs were left for 3 days to reduce the baseline level of proliferation induced by the plating medium before starting the screen.

Four days after seeding the cells, the autophagy library (ENZO, BML-2837-0100) was added to wells by total medium exchange at an end concentration of 25 μM. Then, the medium was supplemented with nontoxic concentrations of Hoechst 33342 (10 ng/ml, Thermo Fisher Scientific, H3570) and EdU (5 μM, Thermo Fisher Scientific, C10340). The compound library and controls were divided over two template plates, from which the compounds in the medium were transferred into triplicate screening plates. All pipetting was performed with automated channel pipets to avoid interwell variation. Medium with compounds was not exchanged throughout the 72 h duration of the screen.

Image Acquisition

All images were acquired using a Keyence BZ-X800E compact fluorescence microscope equipped with live imaging cytometer (BZ-H4XI) and CO_2 control (BZ-H4XT) modules. Live images were acquired using the 10x objective and DAPI, YFP and Cy3 filter sets. Binning was set to 3x3, the gain to 6 dB and exposure times were 28 ms for DAPI, 666 ms for YFP and 167 ms for Cy3 channels. The resulting images were 640x480 pixels. Five non-overlapping sites were imaged per well. LIVE imaging was performed at Day 0 directly after adding the compound library and every 24 h until 72 h. After the last LIVE acquisition, hiPSC-CMs were fixed by incubation with 4% formaldehyde solution in PBS for 15 min. Subsequently, an EdU click-it reaction (Thermo Fisher Scientific, C10340) was performed according to the manufacturer's protocol to visualize EdU incorporation. Images of fixed cells were acquired using DAPI and Cy5 channels, binning was set to 3x3, gain to 6 dB and exposure times were 100 ms for DAPI and 10 ms for Cy3.

Automated Image Analysis

Automated image analysis was performed in the open source software CellProfiler 4.2.1 (24). Briefly, single channel images from DAPI, YFP, and Cy3 channels were imported into the program. In the first module, the YFP images were enhanced to reduce uneven backgrounds. Subsequently, the DAPI channel was used to identify all nuclei and assign them as primary objects. In the next modules, the intensity of mVenus and mCherry from the YFP and Cy3 channel images within the nuclei was measured, and a threshold was set to categorize the nuclei as positive (+) or negative (–) for these channels. In the following modules, we assigned all nuclei to a single category as follows: mVenus- and mCherry- nuclei: BLUE; $mCherry^+$ and $mVenus^-$ nuclei: RED; $mCherry^+$ and $mVenus^+$ nuclei: YELLOW; $mVenus^+$ and $mCherry^-$ nuclei: GREEN. In the last module, counts were exported into spreadsheets for further data analysis.

Data Analysis of the TNNT2-FUCCI Screen

Data analysis was performed using the open-source data analytics software KNIME (Konstanz Information Miner) version 4.3.1. The general approach for screen analysis was followed as described by Stöter et al. (25). Briefly, CellProfiler output files were imported, and the following steps were performed: quality control, filtering, grouping, normalization, and statistics. As a first step, data from individual sites were excluded from analysis if the number of nuclei was far below (>2 STDEV) mean levels (indicating problems with focus, e.g.,). In the second step, the results from imaging sites were grouped by wells, giving mean values per well from the five sites imaged. In the next steps, the data from wells were matched with locations on the plates and the compound information. The percentages per compound were normalized to the control (100%). Next, wells were grouped by treatment, and if parameters showed STDEVs larger than half the value of the parameter, they were excluded as quality controls. Data were exported into Excel, and the main parameter (% of $mVenus^+$ in all $FUCCI^+$) was plotted using GraphPad Prism software.

Clonidine Treatment of Neonatal Mice

Animals were housed in the Comparative Medicine Biomedicum (Karolinska Institutet, Stockholm) animal facility on a 12-h light/dark cycle and were provided food and water *ad libitum*. All breeding and organ collection protocols were performed in accordance with the Swedish and European Union guidelines and approved by the institutional ethics committee (Stockholms Norra Djurförsöksetiska Nämnd). C57BL/6N neonatal mice were injected subcutaneously with a volume of 0.1 ml of PBS with EdU (20 mg/kg, Invitrogen, E10187) and clonidine (60 ng/pup, Sigma, C7897). Clonidine was given for an estimated weight of 1.5 g/pup throughout the experiment; therefore, a fixed dose of 60 ng/pup was used. Neonatal mice were sacrificed at P7 by decapitation, and hearts were dissected and collected in PBS, cryoprotected in 30% sucrose and flash-frozen in isopentane.

Immunohistochemistry Staining of P7 Neonatal Mouse Hearts

Frozen hearts were sectioned into 10 μm thick sections at the cryostat. After washing with PBS sections were fixed by

incubating in 2% formaldehyde solution for 10 min. Primary antibodies against rabbit PCM-1 (1:100, Santa Cruz, sc-67204), mouse SMA-Cy3 (1:1000, SigmaAldrich, C6198), and biotinylated isolectin B4 (Vector labs, B-1205, 1:500) were diluted in blocking buffer (PBS, 4% donkey serum, 0.1% Triton X-100 in PBS, 2 mM EDTA) and sections were incubated overnight at RT. Sections were then washed 3x with PBS (15 min) and stained with matching secondary antibody anti-rabbit Alexa Fluor® 488 (1:500, Jackson ImmunoResearch, 711-546-152) and Streptavidin-Alexa Fluor 647® (1:1000, ThermoFisher, S21374) in PBS. Subsequently, Click-iT™ EdU Cell Proliferation Kit for Imaging, Alexa Fluor™ 647 or 488 dyes (ThermoFisher, C10340 and C10637) was used to detect EdU. Slides were then washed and mounted using ProLong Gold Antifade Mountant with DAPI (ThermoFisher, P36931). Images were acquired using a Keyence BZ X800 fluorescence microscope (Keyence, Japan) and Zeiss LSM 750 confocal microscopy from at least three regions of the left ventricle per heart.

Neonatal Cardiomyocyte Isolation and Immunocytochemistry

Frozen hearts were placed on ice, cut into small pieces, fixed in four percent paraformaldehyde for 1 h, and digested for 2 h at 37°C (3.6 mg/ml collagenase B, 4.8 mg/ml collagenase D, in PBS). Cells were incubated with primary antibody against α-Actinin (Thermofisher, A7811, 1:500) and Connexin-43 (SigmaAldrich, C6219, 1:1000) for 30 min to label cardiomyocyte cytoplasm and borders. After washing with PBS, cells were resuspended with matched secondary antibodies [AF488-coupled (Abcam, ab150110, 1:1000) and AF555-coupled (Jackson Immuno Research, 711-546-152, 1:500)] for 30 minutes. Cardiomyocytes were placed on a slide with a mounting medium (Invitrogen™ ProLong™ Gold Antifade Mountant with DAPI). Images were acquired using a Keyence BZ X800 fluorescence microscope (Keyence, Japan) equipped with an imaging cytometer (BZ-H4XI). Image analysis was performed in the open source software CellProfiler 4.2.1 (24). Nuclei segmentation was performed using the identify primary objects module with an adaptive thresholding method to account for background variances. α-Actinin intensities were measured in segmented nuclei, and thresholds were determined according to their histograms. DNA staining intensities of cardiomyocyte nuclei were measured, and ploidy levels were plotted as histograms, from which ploidy thresholds were determined (**Supplementary Figure 4**). The number of nuclei per cardiomyocyte was determined manually analyzing a minimum of 15 field of views for each biological replicate.

RESULTS

Generation and Validation of TNNT2-FUCCI in hiPSC-Derived CMs

We generated a TNNT2-FUCCI hiPSC line using a CRISPR–Cas9 approach (see Methods). TNNT2-FUCCI hiPSCs expressed the FUCCI construct under the control of the cardiomyocyte-specific TNNT2 promoter (**Figure 1A** and **Supplementary Figure 1A**). The generated TNNT2-FUCCI hiPSC line showed a normal karyotype, and pluripotency characterization showed high expression of bona fide pluripotency markers and could generate three germ layers (**Supplementary Figures 1B–D**). FUCCI fluorescence (mCherry/mVenus) became visible from Day 6 post differentiation into cardiomyocytes (**Figure 1A**). At Day 30, in most cells, FUCCI signal was detected (**Figure 1A**), and all FUCCI-expressing cells were TNNT2$^+$ (**Figure 1B**). To further confirm the cardiomyocyte-specific expression of TNNT2-FUCCI fluorescence, we used imaging flow cytometry. We analyzed 50,000 cells defined by their TNNT2 expression and found that 85.4% were mCherry-Cdt1$^+$ (G0/G1 phase), 5.1% were mVenus-geminin$^+$ (G2/M phase) and 1.6% of the cardioymocytes were both mCherry-Cdt1 and mVenus-geminin$^+$ (G1/S phase) (**Figure 1C**). Importantly, we found no FUCCI expression in the TNNT2$^-$ cell fraction. However, some signal in the TNNT2$^-$ fraction detected in the green and red fluorescence channels could be assigned to autofluorescence (**Supplementary Figure 2A**).

To demonstrate that the TNNT2-FUCCI signal reliably indicates the cell cycle status of cardiomyocytes, we costained FUCCI cardiomyocytes with cyclin-dependent kinase-1 (CDK1) and found a complete overlap of mVenus$^+$ and CDK1$^+$ nuclei, supporting that mVenus$^+$ cardiomyocytes indeed represent cells in the S/G2/M phase of the cell cycle (**Supplementary Figure 2B**).

TNNT2-FUCCI cardiomyocytes showed a similar sarcomere spacing pattern (1.97 μm ± 0.06 μm SEM) and cell size (2525.4 μm^2 ± 259.2 μm^2 SEM) as controls (**Supplementary Figures 2C,D**), suggesting that the integration of the TNNT2-FUCCI knock-in did not compromise the functionality of the TNNT2-FUCCI cardiomyocytes.

In summary, we showed that TNNT2-FUCCI expression is limited to cardiomyocytes and reliably detects cell cycle progression.

Live Cell Imaging of TNNT2-FUCCI Cardiomyocytes Shows Differences in Cell Cycle Progression With G2 Phase Arrest in Polyploidy

We tracked single TNNT2-FUCCI cardiomyocytes over 72 h (**Figure 2**) Among 570 cardiomyocytes analyzed, 90.4% ± 10.6% SEM did not show any cell cycle activity, 5.1 % ± 1.5% SEM underwent cytokinesis and cell division, 3.2% ± 1.5% SEM became binucleated, and 1.40% ± 0.8% SEM underwent polyploidization (**Figure 2A**). We could not detect any binucleated or polyploid cardiomyocyte undergoing cell division, supporting the notion that mainly diploid mononucleated cardiomyocytes show proliferative capacity (9). Next, we plotted the FUCCI oscillation pattern for cardiomyocytes undergoing cell division, multinucleation and polyploidization (**Figures 2B–D** and **Supplementary Movies 1–3**). In all three cycling populations, mVenus-geminin fluorescence started to increase concomitant with the reduction of the mCherry-Cdt1 signal, marking the end of the G1 phase and the beginning of

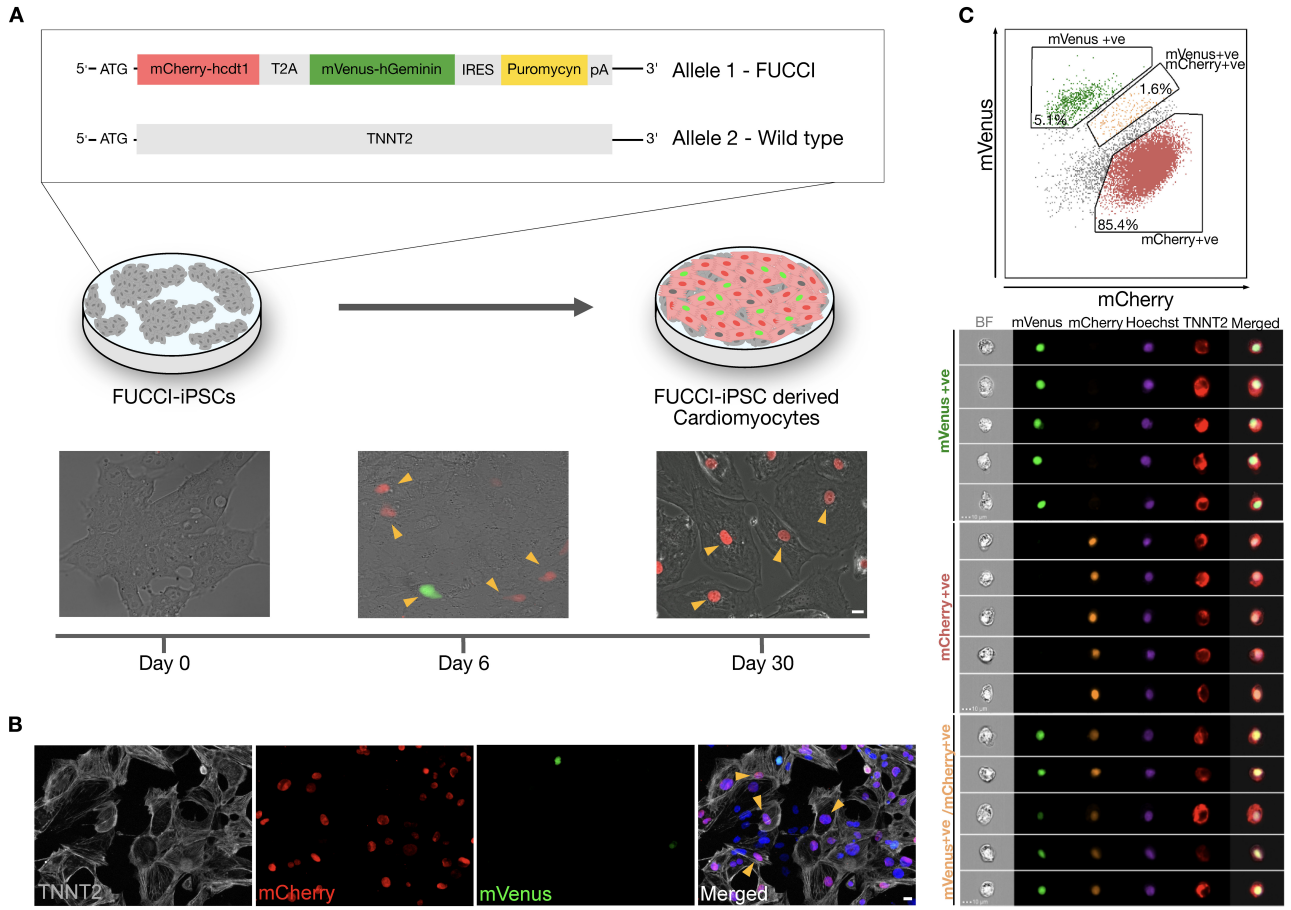

FIGURE 1 | Generation and validation of TNNT2-FUCCI in hiPSC-derived CMs. **(A)** Schematic representation showing TNNT2-FUCCI reporter cell line generation and differentiation towards cardiomyocytes. Upon differentiation into cardiomyocytes, the FUCCI signal became visible at Day 6. Arrowheads indicate FUCCI$^+$ nuclei. Scale bar, 20 μm. **(B)** Immunocytochemistry showing cardiomyocytes at Day 30 of differentiation. Arrowheads indicate cardiomyocytes (TNNT2$^+$) that were FUCCI$^+$, demonstrating the specificity of the FUCCI reporter. Scale bar, 20 μm. **(C)** Imaging flow cytometry shows TNNT2$^+$ cells expressing nuclear mVenus and/or mCherry, indicating cardiomyocyte specificity of the TNNT2-FUCCI system.

the S/G2 phase. In early mitosis, mVenus fluorescence dropped sharply concomitant with nuclear envelope breakdown in dividing and multinucleating TNNT2-FUCCI cardiomyocytes (**Figures 2B,C**). The average duration of the S/G2/M phase was 16.38 h ± 0.84 SEM h in dividing cells and 17.29 h ± 0.55 SEM h in multinucleating cells, with no significant difference between the two populations ($p > 0.05$, **Figure 2E**). In contrast, polyploid cells showed a different FUCCI oscillation pattern. An increase in the mCherry signal was detected before the loss of mVenus, which dropped slowly, suggesting G2 phase arrest without activation of the anaphase-promoting complex (26). Accordingly, no mitotic features, such as cell rounding or cytoplasmic localization of mVenus, were detected (**Figure 2D**). Moreover, mVenus expression was detected over a significantly longer period in polyploid cells compared to dividing ($p = 0.0009$) and multinucleating ($p = 0.0029$) cells, with an average duration of the S/G2 phase of 24.5 h ± 2.77 h SEM (**Figure 2E**). These data suggest that hiPSC-derived CMs that become polyploid do not enter mitosis and remain arrested in the G2 phase.

Live Image-Based TNNT2-FUCCI Screening Identifies Cell Cycle Activators

Next, we devised a live screening platform in which we probed TNNT2-FUCCI cardiomyocytes for cell cycle entry using a library of 94 autophagy-related compounds (**Figure 3A**, and Methods). TNNT2-FUCCI live cardiomyocytes were imaged, and mVenus and mCherry nuclear fluorescence was documented at 24 h, 48 h, and 72 h (**Figure 3A**). Proproliferative activity was determined as the percentage of mVenus$^+$ (S/G2/M phase) cardiomyocyte nuclei and normalized to the control group at all three time points (**Figure 3B** and **Supplementary Figures 3A,B**). The acquisition time point of 48 h with the smallest coefficient of variance (24 h, 48 h, 72 h; 13.1%, 12.1%; 28.0%, respectively) was chosen to select six pro-proliferative candidates. We

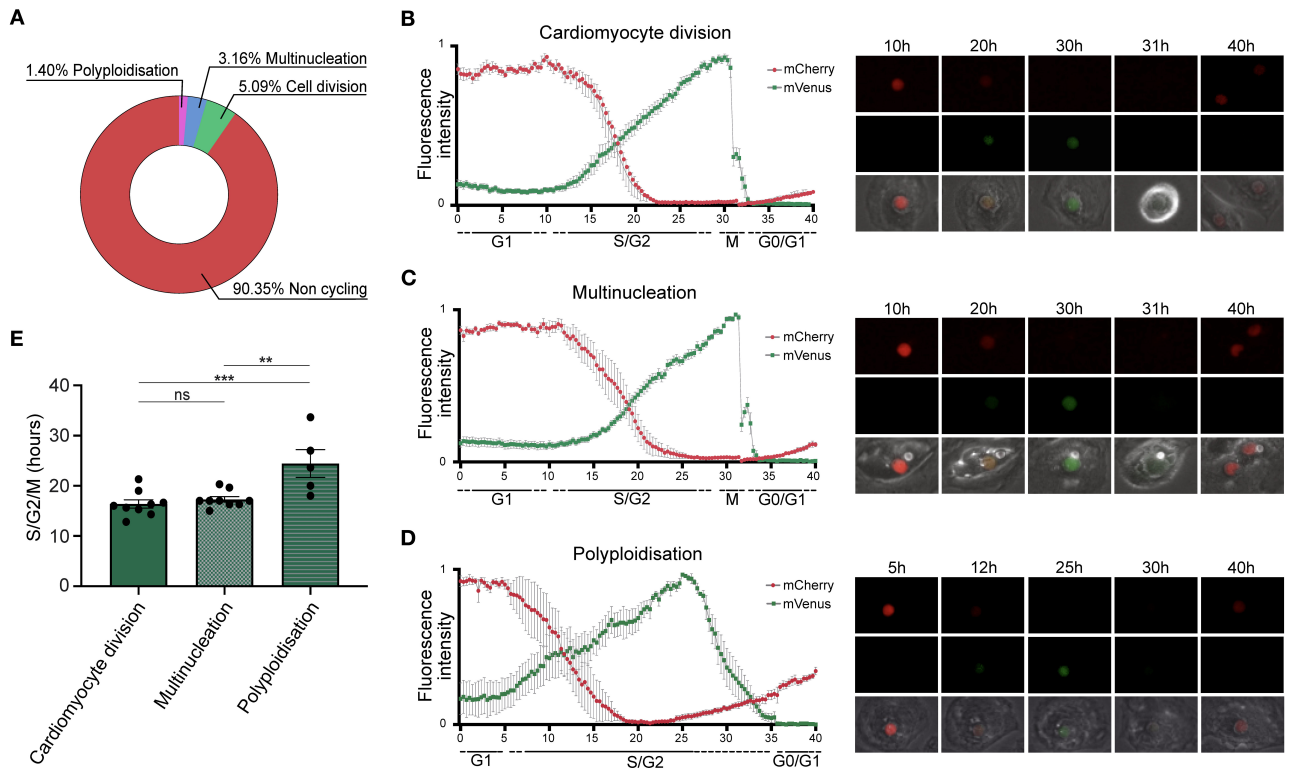

FIGURE 2 | Quantification of cell cycle duration using live cell imaging of hiPSC-derived CMs. **(A)** Pie chart showing the percentage of non-cycling and cycling cardiomyocytes ($n = 570$) collected from 20 movies. **(B–D)** left panels show oscillation patterns of FUCCI fluorescence measured by live imaging in cardiomyocytes undergoing **(B)** cell division ($n = 9$), **(C)** multinucleation ($n = 9$), and **(D)** polyploidization ($n = 5$). Data show mean intensity ± SEM. Right panels show images of selected intervals of the movies. **(E)** Quantification of the total duration of the combined S, G2, and M phases shows a significant increase in cell cycle duration in cardiomyocytes undergoing polyploidization ($n = 5$) compared to multinucleation ($n = 9$) and polyploidization ($n = 9$). Data show mean intensity ± SEM. *P*-value was determined by one-way ANOVA. $^{**}p < 0.01$, $^{***}p < 0.001$.

selected the six pro-proliferative candidate compounds based on their increase in the percentage of mVenus$^+$ nuclei and their biological significance (see Methods and **Supplementary Figures 3A,B**).

Validation of Pro-proliferative Candidate Compounds in mNCMs

The six selected compounds were tested at three different concentrations to establish potential concentration dependencies (2.5 nM, 250 nM, 25 μM) in mNCMs. Cell cycle activation was validated by EdU incorporation after 72 h which can detect DNA synthesis during S-phase (**Figure 3C**). We found two compounds that significantly increased cell cycle activity at all tested concentrations. Of these, the alpha-adrenergic and imidazoline receptor agonist clonidine showed the most pronounced concentration-dependent effect (2.78-fold increase compared to untreated, $p < 0.0001$) on cell cycle activity in mNCMs (**Figures 3C,D** and **Supplementary Figure 3C**). Hence, we continued to explore the pro-proliferative potential of clonidine (**Supplementary Figure 3D**).

Clonidine Triggers Proliferation in hiPSC-Derived CMs and Cell Cycle Activity in mNCMs

We assessed whether clonidine-induced cell cycle activity results in proliferation or polyploidy in hiPSC-derived CMs (**Figures 4A–E**). Cell cycle activity was first determined by Ki-67 expression. A cell cycle related gene, which expression is gradually increased during cell cycle progression, reaching a maximum at G2/S (27). Although there are reports that Ki-67 expression is linked to DNA damage response (27, 28), Ki-67 is widely used to demonstrate cell cycle activity (28). We could show a high fidelity of Ki-67 in detecting cell cycle progression (S/G2/M) in neonatal mice (14). We measured an increase in cell cycle activity after clonidine treatment through Ki-67 expression from 9.0% ± 1.23% SEM to 22.0% ± 4.51% SEM at 72 h after treatment in hiPSC-CMs ($p = 0.03$, **Figure 4A**). Clonidine did not cause any changes in polyploidy ($p > 0.05$, **Figure 4B**, and **Supplementary Figure 4A**) or in binucleation ($p > 0.05$, **Figure 4C**), suggesting that most clonidine-induced cell cycle activity results in proliferation. Consistent with these findings, we found an increase in aurora B kinase (AurKB)-positive midbodies, indicative of late phase cytokinesis, from

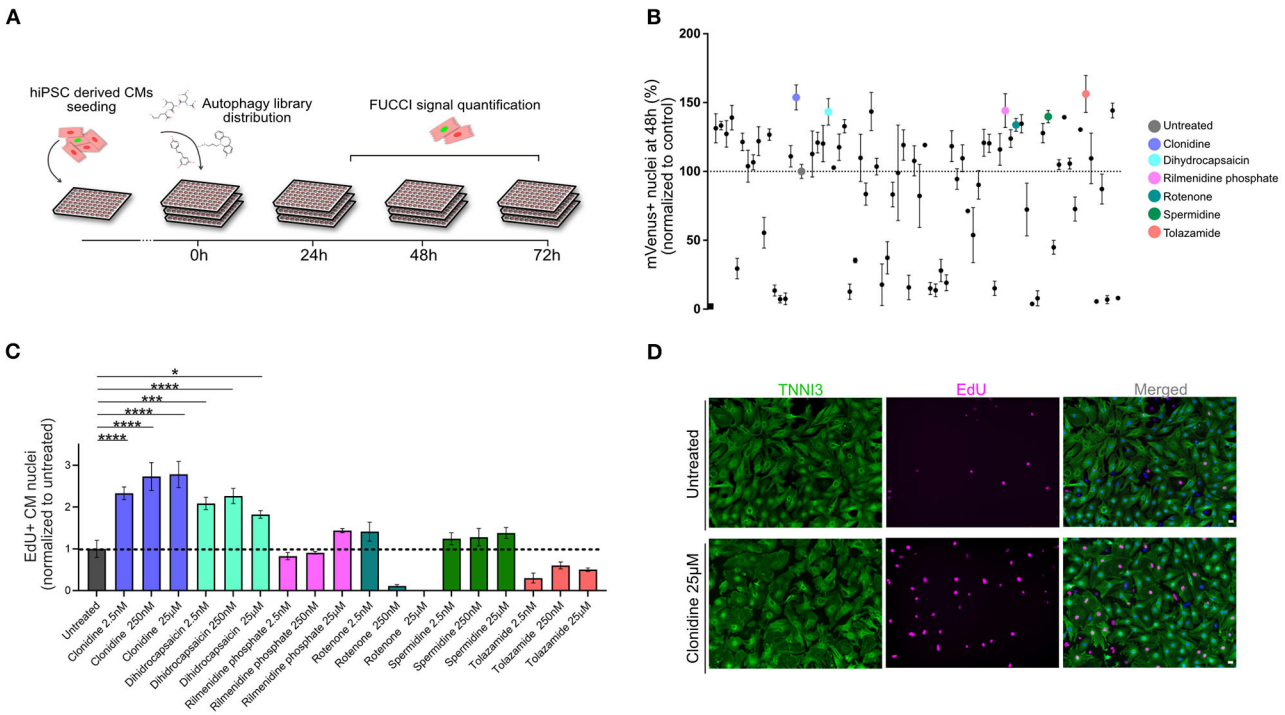

FIGURE 3 | Live-image-based TNNT2-FUCCI hiPSC-derived cardiomyocyte screen identifies compounds that induce cell cycle activity. **(A)** Schematic drawing of the screening experiment. hiPSC-derived CMs were seeded in 96-well plates and stimulated with 94 compounds of an autophagy-related compound library at a concentration of 25 μM. FUCCI signal was documented at 24 h, 48 h, and 72 h. **(B)** The effect of each compound is shown as the percentage of mVenus$^+$ nuclei relative to the control at the 48 h time point. Results are from one screen with three replicate wells on separate plates. Error bars represent STDEV between the triplicates. Six compounds that increased the percentage of mVenus$^+$ cardiomyocyte nuclei were subjected to further validation, these are indicated with colors. **(C)** Six compounds were further tested in mNCMs at three different concentrations (2.5 nM, 250 nM and 25 μM). Cell cycle activity was validated by EdU incorporation and subsequent detection at 72 h. The experiment was repeated three times, each with three replicates wells. Values are mean ± SEM. P-values were determined by one-way ANOVA. $^*p < 0.05$, $^{***}p < 0.001$, $^{****}p < 0.0001$. **(D)** Representative immunocytochemistry images of untreated and clonidine-treated mNCMs with EdU incorporation detected in magenta and cardiac troponin I in green. Scale bar, 20 μm.

0.83% ± 0.17% SEM in untreated hiPSC-derived CMs to 1.69% ± 0.24% SEM in clonidine-treated hiPSC-derived CMs ($p = 0.04$, **Figures 4D,E**).

Next, we investigated whether clonidine elicits similar effects in mNCMs that are more restricted in their capacity to proliferate. We found an increase in cell cycle activity, measured through Ki-67 expression, from 10.97% ± 1.68% SEM in untreated mNCMs to 23.23% ± 2.63% SEM in clonidine-treated mNCMs ($p = 0.002$, **Figure 4F**). The ratio of binucleated cardiomyocytes was not altered by clonidine treatment ($p > 0.05$, **Figure 4H**), but we found an increase in nuclear ploidy with an increase in the tetraploid fraction from 26.52% ± 0.54% SEM in untreated mNCMs to 38.93% ± 2.32% SEM in clonidine-treated mNCMs ($p = 0.0004$, **Figure 4G**, **Supplementary Figure 4B**), suggesting that a substantial proportion of clonidine-induced cell cycle activity can be attributed to nuclear polyploidy. Additionally, we performed AurKB staining on clonidine-treated and control mNCMs. Although we observed AurKB$^+$ cardiomyocyte nuclei in all cultures (**Supplementary Figure 4C**), we could not detect any positive midbodies in these cultures (more than 10,000 cardiomyocytes analyzed), suggesting that clonidine does not stimulate cytokinesis in cell cycle-active mNCMs. In agreement with this, cardiomyocyte cell count did not show any significant increase ($p > 0.05$, **Supplementary Figure 5D**) in the number of cardiomyocytes after clonidine treatment.

Clonidine Induces Cell Cycle Activity in the Neonatal Mouse Heart

To explore whether clonidine triggers cell cycle activity in the mouse heart, similar to what we found *in vitro*, we administered clonidine to neonatal mice. Clonidine was given along with EdU daily from P1 to P5 (60 ng/day), and the hearts were collected for analysis at P7 (**Figure 5A**). The number of EdU$^+$ cardiomyocyte nuclei (EdU$^+$/PCM-1$^+$) was significantly increased in the clonidine-treated group (36.15% ± 2.72% SEM) compared to control animals (25.54% ± 1.80% SEM) ($p = 0.02$, **Figures 5B,C**), demonstrating that clonidine triggers cardiomyocyte cell cycle activity as more cells have entered S-Phase in both *in vitro* and *in vivo* mouse neonatal hearts. In contrast to neonatal cardiomyocyte *in vitro*, nuclear ploidy levels remained constant (**Figures 5D,F** and **Supplementary Figure 5C**), whereas the fraction of mononucleated cardiomyocytes

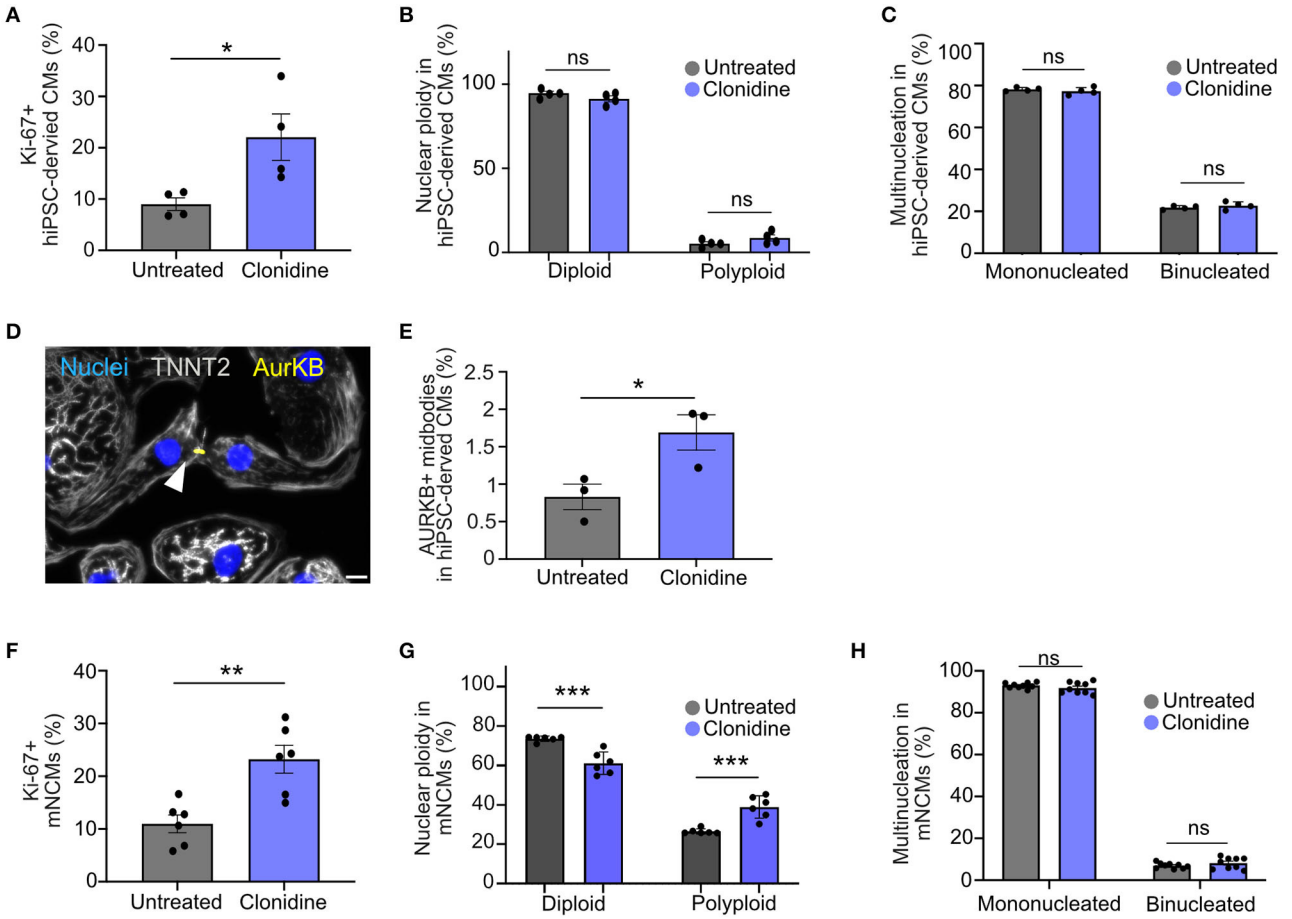

FIGURE 4 | Effect of clonidine on cell cycle activity and proliferation in human and mouse cardiomyocytes **(A)** Quantification of Ki-67$^+$ hiPSC-derived CMs after 72 h of clonidine treatment. *P*-values were determined by unpaired t-test. Datapoints represent four individual wells from one experiment. **(B,C)** Cell cycle activity induced by clonidine did not show any changes in **(B)** nuclear ploidy or **(C)** binucleation. Datapoints represent four individual wells with 11 fields of view analyzed per well. *P*-values were determined by two-way ANOVA. **(D,E)** AurKB$^+$ midbodies, indicative of late phase cytokinesis, increased significantly in clonidine-treated hiPSC-derived CMs. Datapoint represent three individual wells. Scale bar, 20 μm. *P*-values were determined by unpaired *t-test*. **(F)** Clonidine significantly increased the percentage of Ki-67$^+$ mNCMs. Datapoints represent six individual wells, P-values were determined by unpaired *t-test*. **(G)** Quantification showed an increase in nuclear ploidy in mNCMs treated with clonidine. Datapoints represent six individual wells. *P*-values were determined by two-way ANOVA. **(H)** Ratios of binucleated mNCMs were not altered by clonidine treatment. P-values were determined by two-way ANOVA. Values are mean ± SEM. *$P < 0.05$, **$p < 0.01$, ***$p < 0.001$. Datapoints represent nine wells with three fields of view analyzed for each well.

was reduced in clonidine treated animals from 14.8% ± 1.3 SEM%, compared to 22.3% ± 1.7% SEM in controls ($p = 0.01$, **Figure 5E**), demonstrating mitotic activity without cytokinesis.

As alpha adrenergic signaling is not restricted to cardiomyocytes (29), we explored the possibility that cell cycle activity is altered in other cell types of the heart. Whereas, we did not see any changes in fraction of EdU$^+$ endothelial cells (control: 29.4% ± 2.8% SEM vs. clonidine: 30.1% ± 1.7% SEM, $p = 0.85$), we found an increase in smooth muscle cell cycle activity from 44.2% (29.4–46.9%, interquartile range) in controls to 59.3% (51.9–61.7%, interquartile range) in clonidine treated animals ($p = 0.04$, **Supplementary Figures 5D–F**).

DISCUSSION

Heart failure is among the leading causes of death in the Western world, and currently available treatment is limited to salvaging existing cardiomyocytes or heart transplantation. Augmenting the proliferation of existing cardiomyocytes is often proposed as a promising future strategy for reverting disease progression (30). To achieve this goal, detailed knowledge of the human cardiomyocyte cell cycle and how it can be manipulated is crucial. Here, we generated TNNT2-FUCCI cardiomyocytes to reveal cell cycle kinetics in human cardiomyocytes undergoing proliferation, binucleation and polyploidization. To show the versatility of TNNT2-FUCCI, we devised a live cell

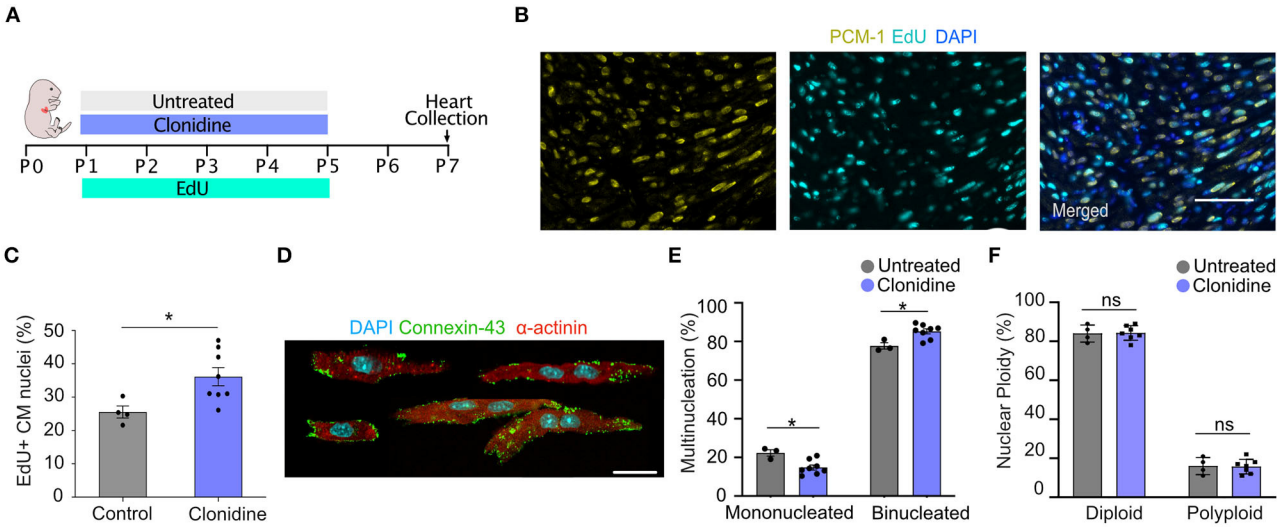

FIGURE 5 | Clonidine induces cell cycle activity in neonatal mice. **(A)** Neonatal mice were subjected to four days (P1-P5) of clonidine (60 ng/pup) and EdU treatment (20mg/kg). Pups were sacrificed and hearts were collected at P7. **(B,C)** Quantification of EdU$^+$ cardiomyocyte (PCM-1$^+$) nuclei in sectioned mouse hearts showed an increase in EdU incorporation in clonidine-treated neonatal mice. Three sites per heart section were imaged and a minimum of 100 cardiomyocytes nuclei were analyzed per sample. Each point represents a biological replicate, clonidine n = 8, untreated n = 4. Values are mean ± SEM. P-value was determined by unpaired *t-test*. *$P < 0.05$. Scale bar, 50 μm. **(D)** Shows compilation of individual representative images of digested P7 cardiomyocytes stained with α-actinin and connexin-43. Scale bar, 20 μm. **(E)** Quantification of mono and binucleated cardiomyocytes with clonidine treatment ($n = 8$) and untreated ($n = 3$). At least 100 cardiomyocytes per biological replicate were analyzed. Values are mean ± SEM. *P*-value was determined by unpaired *t-test*. *$P < 0.05$. **(F)** Quantification of nuclear ploidy on cardiomyocytes with clonidine treatment ($n = 8$) and untreated ($n = 4$) shows no significant difference. At least 422 cardiomyocyte nuclei were analyzed per mouse.

screening platform to assess the pro-proliferative effects of compounds from an autophagy library. Using this platform, we identified clonidine as a compound that induces cell cycle activity in cardiomyocytes, resulting in the proliferation of hiPSC-CMs.

Generation and Characterization of a hiPSC Line With the Cardiomyocyte-Specific TNNT2-FUCCI Reporter

The identification of cycling cardiomyocytes is critical for studying cardiomyocyte proliferation (10, 14, 31–34). Here, we generated the TNNT2-FUCCI hiPSC reporter line and differentiated it into cardiomyocytes. Consistent with previous data, we showed that inactivation of one TNNT2 locus by FUCCI knock-in did not cause structural impairments in cardiomyocytes (35). After 6 days in culture, we found the first cells expressing TNNT2-FUCCI along with the appearance of beating cardiomyocytes at Day 8 of differentiation (17). We found a complete overlap of cyclin-dependent kinase 1 (CDK1), which oscillates in the cell cycle and shows activity in S/G2/M phases (36), with mVenus-geminin$^+$ cardiomyocytes, verifying the fidelity of geminin expression and thereby with the TNNT2 -FUCCI system.

Single-Cell Live Imaging of Cycling Cardiomyocytes

Video time-lapse microscopy is considered the gold standard to unequivocally determine the outcome of the cardiomyocyte cell cycle as division, multinucleation or polyploidization (10, 14, 37). Here, we combined time-lapse microscopy with our TNNT2-FUCCI sensor to determine the length and distinct phases of the cardiomyocyte cell cycle. We found that the S/G2/M phase took approximately 18 h for both dividing and binucleating cells with similar TNNT2-FUCCI fluorescent oscillation patterns, documenting a slightly longer cell cycle length than in mouse embryonic E14.5 cardiomyocytes (10.4 h) (15) and in mNCMs at P0 (15.1 h) (14). In contrast, human cardiomyocytes undergoing polyploidy showed a longer S/G2/M phase duration of ∼25 h and prominent changes in the TNNT2-FUCCI fluorescence intensity pattern, exemplifying the difficulty in estimating annual cell cycle activity rates based on a fixed duration of cell cycle length (38, 39). Furthermore, our data suggest that polyploidy is not only a result of karyokinesis failure (40) because we did not observe nuclear envelope breakdown in cardiomyocytes but can also be a result of G2-phase arrested cycling cardiomyocytes.

Live TNNT-FUCCI Screening Platform

Here, we developed a fluorescence-based live imaging screening platform based on the TNNT2-FUCCI system. This screening

platform does not require immunofluorescence staining and eliminates the need for total cell counts and the incorporation of nucleotide analogs (e.g., BrdU and EdU). Live imaging of cycling cardiomyocytes allows for multiple imaging time points to establish the efficacy time course of pro-proliferative compounds. Due to the cardiomyocyte specificity of the TNNT2-FUCCI system, we eliminated false-positive detection of proliferative events originating from non-depleted cycling non-cardiomyocytes. Moreover, TNNT-FUCCI cardiomyocyte specificity allows sophisticated cocultures of cardiomyocytes with other cell types and could even be combined with recently developed cardiac organoids (41, 42). Our platform can be used with any type of library to identify pro-proliferative candidates. In this study, we subjected TNNT2-FUCCI hiPSC-derived CMs to a library of compounds regulating autophagy. Autophagy has been implicated in heart regeneration (43) and exerts numerous roles in myocardial stress responses (44). Autophagy reduces cellular stress caused by reactive oxygen species, which in turn plays a role in cardiomyocyte cell cycle exit (45).

Validation of Screen-Identified Compounds in mNCMs

We selected six compounds for further validation in mNCMs (**Supplementary Table 1**), which are considered more mature than iPSC-derived CMs (18), with a partial loss of their capacity to proliferate. We found that only two of the six compounds significantly enhanced cell cycle activity, potentially due to higher levels of maturation in mNCMs compared to hiPSC-derived CMs and cross-species variation in cardiomyocyte physiology. One of these two compounds was dihydrocapsaicin, an analog of the active component of chili pepper with documented effects on cardiomyocytes, including autophagy induction (46) and attenuation of mitochondrial function (47).

The most robust and dose-dependent effect on cardiomyocyte cell cycle entry was elicited by the alpha-adrenergic and imidazoline agonist clonidine. Although clonidine is an alpha2-adrenergic agonist, it also shows binding to alpha1-adrenergic receptors (48). Furthermore, clonidine activates the imidazoline receptor, leading to a decrease in the level of cAMP in cells, resulting in downstream autophagy activation (49). Alpha-adrenergic receptors are predominantly found on smooth muscle cells of blood vessels, mediating vasoconstriction (29), but can also be detected on cardiomyocytes (50). Accordingly, we found an increase in cell cycle activity of smooth muscle cells in clonidine treated neonatal hearts. Single cell RNA sequencing data, re-analyzed from our previous study (14), showed expression of alpha1B and beta1 adrenergic receptors in P0 and P7 mNCMs. Apart from adrenergic receptor expression, we also found nischarin (Nisch), the mouse homolog of human imidazoline receptor I1 candidate (51), robustly expressed in mNCMs (**Supplementary Figures 5A,B**). We hypothesized that clonidine mainly elicits its pro-proliferative effects via direct alpha1 adrenergic receptor (50), and imidazoline receptor interaction on cardiomyocytes (52). Alpha1 adrenergic receptors are members of the G protein-coupled receptor superfamily. They activate mitogenic responses and regulate growth and proliferation of many cell types through several downstream signaling cascades such as the c-Jun NH2-terminal kinase (JNK) and the mitogen activated protein kinase (MAPK) pathways (53). Thus, we chose to further investigate whether clonidine treatment in addition to cell cycle entry also results in successful mitosis and cytokinesis.

Based on detected AurKB$^+$ midbodies, clonidine promotes cytokinesis in hiPSC-derived CMs. While the increase in cell cycle activity did not alter the ratio between diploid and polyploid cells in hiPSC-derived CMs, in mNCMs, we did observe an increase in polyploid cardiomyocytes and no AurKB$^+$ midbody formation after clonidine treatment. The latter indicates that clonidine-induced cell cycle activity was not productive and that for successful completion of mitosis and cytokinesis in mNCMs, additional stimuli are required. Cardiomyocyte maturation is linked to a number of processes including changes in structure, metabolism and gene expression, and plays a major role in cardiomyocyte cell cycle exit (54). Whereas, immature hiPSC-derived CMs still have the capacity to divide given optimal condition (55), mNCMs gradually lose their proliferative capacity during the first postnatal days (1, 2, 45). Silencing of cell cycle and cytokinesis related genes such as AURKB and ECT2 along with an activation of mitochondrial biogenesis and a metabolic switch to oxidative phosphorylation has been attributed to a proliferation-to-hypertrophy transition in the developing and neonatal heart (45, 56). These changes could explain why clonidine acts differently on hiPSC-derived CMs and mNCMs in this study.

In conclusion, we generated TNNT2-FUCCI hiPSCs and demonstrated that TNNT2-FUCCI hiPSC-derived CMs enable analysis of cell cycle entry and progression, providing a powerful platform for screening and validation of pro-proliferative candidates in human cardiomyocytes.

DATA AVAILABILITY STATEMENT

The original contributions presented in the study are included in the article/**Supplementary Material**, further inquiries can be directed to the corresponding author/s.

ETHICS STATEMENT

The studies involving human participants were reviewed and approved by Ethikkommission an der Technischen Universität Dresden (BO-EK-38012020). Written informed consent for participation was not required for this study in accordance with the national legislation and the institutional requirements. The animal study was reviewed and approved by Stockholm Local Ethics Committee and Landesdirektion Sachsen.

AUTHOR CONTRIBUTIONS

FM, MB, WD, IS, and PT: methodology. FM, MB, WD, KN, SK, PT, and OB: investigation. FM, WD, and OB:

conceptualization, writing—original draft, and writing—review and editing. FM, WD, KG, and OB: supervision. OB: funding acquisition. All authors contributed to the article and approved the submitted version.

FUNDING

OB was supported by the Center for Regenerative Therapies Dresden, the Karolinska Institute, the Swedish Research Council, the Ragnar Söderberg Foundation, the Åke Wiberg Foundation, and the LeDucq Foundation.

ACKNOWLEDGMENTS

The CRTD5-TNNT2-FUCCI reporter hiPSC line was generated by the Stem Cell Engineering Facility, a core facility of the Center for Molecular and Cellular Bioengineering (CMCB) at Technische Universität Dresden. Giemsa staining and analysis of metaphase chromosomes were performed at the Molecular Cytogenetics lab at Jena University Hospital. We thank Marc Bickle from MPI-CBG in Dresden for advice on image acquisition strategies and for helping to set up the analysis in KNIME. We thank the Light Microscopy and Flow Cytometry core facilities of BIOTEC/CRTD for their help with imaging and flow cytometry analyses. A preprint of this article was published at bioRxiv: (57).

SUPPLEMENTARY MATERIAL

The Supplementary Material for this article can be found online at: https://www.frontiersin.org/articles/10.3389/fcvm.2022.840147/full#supplementary-material

Supplementary Movie 1 | Time-lapse recording of a TNNT2-FUCCI cardiomyocyte undergoing polyploidization.

Supplementary Movie 2 | Time-lapse recording of a TNNT2-FUCCI cardiomyocyte undergoing cytokinesis.

Supplementary Movie 3 | Time-lapse recording of a TNNT2-FUCCI cardiomyocyte undergoing binucleation.

Supplementary Figure 1 | Characterization of TNNT2-FUCCI hiPSC line. **(A)** Schematic representation of the FUCCI technology. The FUCCI system is based on two cell cycle regulator proteins, Geminin and Cdt1, which are fused to a green (mVenus) and red (mCherry) fluorescent protein respectively. During the cell cycle, Geminin and Cdt1 are ubiquitinated by specific ubiquitin E3 ligases and are then targeted to the proteosome for degradation. During the G0/G1 phase, Geminin is degraded and only Cdt1 is present and therefore the nuclei of the cells appear red. During the G1/S transition and S phase both proteins are present and the nuclei appear yellow. During the G2/M phase Cdt1 is degraded and only Geminin tagged with mVenus is present, resulting in green nuclei. At the end of the M phase and at the beginning of G0/G1 phase both proteins are absent and the nuclei appear colorless. **(B)** The CRTD5-TNNT2-FUCCI hiPSC line was karyotyped by Giemsa banding and showed an intact chromosome set similar to the parental line. **(C)** Immunocytochemistry staining shows the capacity to differentiate into the three germ layers; markers are shown in green. **(D)** Flow cytometry analysis showing high levels of expression of the pluripotency markers OCT4, SOX2, SSEA4 and TRA1-60. Blue markers indicate no antibody control, and red indicates the antibody-stained sample. The percentages shown refer to antibody-stained sample.

Supplementary Figure 2 | Characterization of TNNT2-FUCCI cardiomyocytes. **(A)** Imaging flow cytometry recordings of non-myocytes. All signals observed in the $TNNT2^-$ fraction in the green and red fluorescence channels could be assigned to autofluorescence. **(B)** Co-staining of FUCCI cardiomyocytes with cyclin-dependent kinase-1 (CDK1) shows an overlap of $mVenus^+$ and $CDK1^+$ nuclei. Scale bar, 20 μm. **(C)** TNNT2-FUCCI cardiomyocytes showed similar sarcomere spacing patterns, as determined using TNNT2 and α-actinin staining. Datapoints represent the analysis from a single cardiomyocyte ($n = 10$), from a two well experiment. Scale bar, 20 μm. **(D)** Cell size was not compromised in FUCCI cardiomyocytes. Scale bar, 20 μm. Datapoints represent the analysis from a single cardiomyocyte ($n = 30$), from a two well experiment.

Supplementary Figure 3 | Autophagy compound screen of TNNT2-FUCCI cardiomyocytes. **(A,B)** Plots showing additionally acquired timepoint of the screen. The effect of each compound is shown as the percentage of $mVenus^+$ nuclei relative to the DMSO control (=100%). Timepoints of 24 h and 72 h were used to generate these graphs. Error bars represent STDEV between triplicates. **(C)** Quantification and representative immunocytochemistry images of untreated and clonidine (25 μM and 100 μM)-treated mNCMs with EdU incorporation in purple and cardiac troponin I in green. $N = 6$ individual wells. Scale bar, 50 μm. Values are mean ± SEM. $^*P < 0.05$, $^{**}p < 0.01$. **(D)** Schematic representation of the experimental strategy for the validation of Clonidine as an inducer of cell cycle activity in hiPSC-derived CMs and in mNCMs *in vitro* and *in vivo*.

Supplementary Figure 4 | Ploidy of noncycling in mNCMs. **(A,B)** Histograms showing the DNA intensity distribution of non-cycling nuclei (cardiac troponin I^+/Ki-67^-) of **(A)** hiPSC-derived CMs and **(B)** mNCMs. Mean of 1203 ± -211 SEM cardiomyocyte nuclei were analyzed to generate these 4 histograms. **(C)** Nuclear AurKB staining (red) indicates G2/M activity of mNCMs (green, arrowheads). More than 10,000 cardiomyocytes were analyzed, but no $AurKB^+$ midbody assembly at the site of abscission was detected. Arrowheads indicate nuclear localization of AurKB in cardiomyocytes. Scale bar 20 μm. **(D)** No significant difference in cardiomyocyte cell count was found after clonidine treatment. Datapoints represent individual wells ($n = 9$).

Supplementary Figure 5 | Receptor expression and cell cycle activity in cardiomyocytes and non-cardiomyocytes *in vivo*. **(A,B)** Expression levels of adrenergic receptor and imidazolin-1 receptor genes measured by single cell RNA sequencing in ventricular cardiomyocytes from P0 **(A)** and P7 **(B)** neonatal mouse hearts (expression plotted as normalized log counts). Data taken from (14) **(C)** Histograms showing the DNA intensity distribution of P7 cardiomyocyte nuclei (troponin I^+) untreated or with clonidine treatment. Mean of 19028 ± -13009 SEM cardiomyocyte nuclei were analyzed to generate the histograms. **(D)** Immunohistochemistry images showing smooth muscle cells (α-SMA) and endothelial cells (Isolectin B4) and cells that have incorporated EdU. Scale bar, 20 μm. **(E)** Quantification of percentage of EdU^+ of α-SMA^+ cells, Values are Median ± quartile. $^*P = 0.04$, Mann-Whitney U test shows a significant increase in cycling smooth muscle cells. **(F)** Quantification of percentage of EdU^+ of isolectin $B4^+$ cells, values are Mean ± SEM.

Supplementary Table 1 | Characterization of candidate compounds.

Supplementary Graphical Abstract | FUCCI-based live imaging platform reveals cell cycle dynamics and identifies pro-proliferative compounds in human iPSC-derived CMs.

REFERENCES

1. Alkass K, Panula J, Westman M, Wu TD, Guerquin-Kern JL, Bergmann O. No evidence for cardiomyocyte number expansion in preadolescent mice. *Cell.* (2015) 163:1026–36. doi: 10.1016/j.cell.2015.10.035
2. Porrello ER, Mahmoud AI, Simpson E, Hill JA, Richardson JA, Olson EN, et al. Transient regenerative potential of the neonatal mouse heart. *Science.* (2011) 331:1078–80. doi: 10.1126/science.1200708
3. Ye L, D'Agostino G, Loo SJ, Wang CX, Su LP, Tan SH, et al. Early regenerative capacity in the porcine heart. *Circulation.* (2018) 138:2798–808. doi: 10.1161/CIRCULATIONAHA.117.031542
4. Bergmann O, Zdunek S, Felker A, Salehpour M, Alkass K, Bernard S, et al. Dynamics of cell generation and turnover in the human heart. *Cell.* (2015) 161:1566–75. doi: 10.1016/j.cell.2015.05.026
5. Senyo SE, Steinhauser ML, Pizzimenti CL, Yang VK, Cai L, Wang M, et al. Mammalian heart renewal by pre-existing cardiomyocytes. *Nature.* (2013) 493:433–6. doi: 10.1038/nature11682
6. Honkoop H, de Bakker DE, Aharonov A, Kruse F, Shakked A, Nguyen PD, et al. Single-cell analysis uncovers that metabolic reprogramming by ErbB2 signaling is essential for cardiomyocyte proliferation in the regenerating heart. *Elife.* (2019) 8:e50163. doi: 10.7554/eLife.50163.sa2
7. Bassat E, Mutlak YE, Genzelinakh A, Shadrin IY, Baruch Umansky K, Yifa O, et al. The extracellular matrix protein agrin promotes heart regeneration in mice. *Nature.* (2017) 547:179–84. doi: 10.1038/nature22978
8. Hirose K, Payumo AY, Cutie S, Hoang A, Zhang H, Guyot R, et al. Evidence for hormonal control of heart regenerative capacity during endothermy acquisition. *Science.* (2019) 364:184–8. doi: 10.1126/science.aar2038
9. Patterson M, Barske L, Van Handel B, Rau CD, Gan P, Sharma A, et al. Frequency of mononuclear diploid cardiomyocytes underlies natural variation in heart regeneration. *Nat Genet.* (2017) 49:1346–53. doi: 10.1038/ng.3929
10. Leone M, Magadum A, Engel FB. Cardiomyocyte proliferation in cardiac development and regeneration: a guide to methodologies and interpretations. *Am J Physiol Heart Circ Physiol.* (2015) 309:H1237–50. doi: 10.1152/ajpheart.00559.2015
11. Sakaue-Sawano A, Kurokawa H, Morimura T, Hanyu A, Hama H, Osawa H, et al. Visualizing spatiotemporal dynamics of multicellular cell-cycle progression. *Cell.* (2008) 132:487–98. doi: 10.1016/j.cell.2007.12.033
12. Zielke N, Edgar BA. FUCCI sensors: powerful new tools for analysis of cell proliferation. *Wiley Interdiscip Rev Dev Biol.* (2015) 4:469–87. doi: 10.1002/wdev.189
13. Alvarez, R. Jr., Wang BJ, Quijada PJ, Avitabile D, Ho T, et al. Cardiomyocyte cell cycle dynamics and proliferation revealed through cardiac-specific transgenesis of fluorescent ubiquitinated cell cycle indicator (FUCCI). *J Mol Cell Cardiol.* (2019) 127:154–64. doi: 10.1016/j.yjmcc.2018.12.007
14. Baniol M, Murganti F, Smialowska A, Panula J, Lázár E, Brockman V, et al. Identification and characterization of distinct cell cycle stages in cardiomyocytes using the FUCCI transgenic system. *Exp Cell Res.* (2021) doi: 10.1101/2021.08.11.455626
15. Hashimoto H, Yuasa S, Tabata H, Tohyama S, Hayashiji N, Hattori F, et al. Time-lapse imaging of cell cycle dynamics during development in living cardiomyocyte. *J Mol Cell Cardiol.* (2014) 72:241–9. doi: 10.1016/j.yjmcc.2014.03.020
16. Hashimoto H, Yuasa S, Tabata H, Tohyama S, Seki T, Egashira T, et al. Analysis of cardiomyocyte movement in the developing murine heart. *Biochem Biophys Res Commun.* (2015) 464:1000–7. doi: 10.1016/j.bbrc.2015.07.036
17. Burridge PW, Matsa E, Shukla P, Lin ZC, Churko JM, Ebert AD, et al. Chemically defined generation of human cardiomyocytes. *Nat Methods.* (2014) 11:855–60. doi: 10.1038/nmeth.2999
18. Karbassi E, Fenix A, Marchiano S, Muraoka N, Nakamura K, Yang X, et al. Cardiomyocyte maturation: advances in knowledge and implications for regenerative medicine. *Nat Rev Cardiol.* (2020) 17:341–59. doi: 10.1038/s41569-019-0331-x
19. Mort RL, Ford MJ, Sakaue-Sawano A, Lindstrom NO, Casadio A, Douglas AT, et al. Fucci2a: a bicistronic cell cycle reporter that allows Cre mediated tissue specific expression in mice. *Cell Cycle.* (2014) 13:2681–96. doi: 10.4161/15384101.2015.945381
20. Sakaue-Sawano A, Kobayashi T, Ohtawa K, Miyawaki A. Drug-induced cell cycle modulation leading to cell-cycle arrest, nuclear mis-segregation, or endoreplication. *BMC Cell Biol.* (2011) 12:2. doi: 10.1186/1471-2121-12-2
21. Shaner NC, Campbell RE, Steinbach PA, Giepmans BN, Palmer AE, Tsien RY. Improved monomeric red, orange and yellow fluorescent proteins derived from *Discosoma* sp. red fluorescent protein. *Nat Biotechnol.* (2004) 22:1567–72. doi: 10.1038/nbt1037
22. Kutsche LK, Gysi DM, Fallmann J, Lenk K, Petri R, Swiersy A, et al. Combined experimental and system-level analyses reveal the complex regulatory network of miR-124 during human neurogenesis. *Cell Syst.* (2018) 7:438–52 e438. doi: 10.1016/j.cels.2018.08.011
23. Lian X, Zhang J, Azarin SM, Zhu K, Hazeltine LB, Bao X, et al. Directed cardiomyocyte differentiation from human pluripotent stem cells by modulating Wnt/beta-catenin signaling under fully defined conditions. *Nat Protoc.* (2013) 8:162–75. doi: 10.1038/nprot.2012.150
24. Carpenter AE, Jones TR, Lamprecht MR, Clarke C, Kang IH, Friman O, et al. CellProfiler: image analysis software for identifying and quantifying cell phenotypes. *Genome Biol.* (2006) 7:R100. doi: 10.1186/gb-2006-7-10-r100
25. Stoter M, Janosch A, Barsacchi R, Bickle M. CellProfiler and KNIME: open-source tools for high-content screening. *Methods Mol Biol.* (2019) 1953:43–60. doi: 10.1007/978-1-4939-9145-7_4
26. Ballabeni A, Melixetian M, Zamponi R, Masiero L, Marinoni F, Helin K. Human geminin promotes pre-RC formation and DNA replication by stabilizing CDT1 in mitosis. *EMBO J.* (2004) 23:3122–32. doi: 10.1038/sj.emboj.7600314
27. Uxa S, Castillo-Binder P, Kohler R, Stangner K, Muller GA, Engeland K. Ki-67 gene expression. *Cell Death Differ.* (2021) 28:3357–70. doi: 10.1038/s41418-021-00823-x
28. Sun X, Kaufman PD. Ki-67: more than a proliferation marker. *Chromosoma.* (2018) 127:175–86. doi: 10.1007/s00412-018-0659-8
29. Jensen BC, O'Connell TD, Simpson PC. Alpha-1-adrenergic receptors in heart failure: the adaptive arm of the cardiac response to chronic catecholamine stimulation. *J Cardiovasc Pharmacol.* (2014) 63:291–301. doi: 10.1097/FJC.0000000000000032
30. Tzahor E, Poss KD. Cardiac regeneration strategies: staying young at heart. *Science.* (2017) 356:1035–9. doi: 10.1126/science.aam5894
31. Ang KL, Shenje LT, Reuter S, Soonpaa MH, Rubart M, Field LJ, et al. Limitations of conventional approaches to identify myocyte nuclei in histologic sections of the heart. *Am J Physiol Cell Physiol.* (2010) 298:C1603–9. doi: 10.1152/ajpcell.00435.2009
32. Derks W, Bergmann O. Polyploidy in cardiomyocytes: roadblock to heart regeneration? *Circ Res.* (2020) 126:552–65. doi: 10.1161/CIRCRESAHA.119.315408
33. Hesse M, Doengi M, Becker A, Kimura K, Voeltz N, Stein V, et al. Midbody positioning and distance between daughter nuclei enable unequivocal identification of cardiomyocyte cell division in mice. *Circ Res.* (2018) 123:1039–52. doi: 10.1161/CIRCRESAHA.118.312792
34. Raulf A, Horder H, Tarnawski L, Geisen C, Ottersbach A, Röll W, et al. Transgenic systems for unequivocal identification of cardiac myocyte nuclei and analysis of cardiomyocyte cell cycle status. *Basic Res Cardiol.* (2015) 110:489. doi: 10.1007/s00395-015-0489-2
35. Ahmad F, Banerjee SK, Lage ML, Huang XN, Smith SH, Saba S, et al. The role of cardiac troponin T quantity and function in cardiac development and dilated cardiomyopathy. *PLoS ONE.* (2008) 3:e2642. doi: 10.1371/journal.pone.0002642
36. Bashir T, Pagano M. Cdk1: the dominant sibling of Cdk2. *Nat Cell Biol.* (2005) 7:779–81. doi: 10.1038/ncb0805-779
37. Leone M, Engel FB. Advances in heart regeneration based on cardiomyocyte proliferation and regenerative potential of binucleated cardiomyocytes and polyploidization. *Clin Sci.* (2019) 133:1229–53. doi: 10.1042/CS20180560
38. Bergmann O, Jovinge S. Cardiac regeneration *in vivo*: mending the heart from within? *Stem Cell Res.* (2014) 13(Pt. B):523–31. doi: 10.1016/j.scr.2014.07.002
39. Bergmann O, Zdunek S, Alkass K, Druid H, Bernard S, Frisén J. Identification of cardiomyocyte nuclei and assessment of ploidy for the analysis of cell turnover. *Exp Cell Res.* (2011) 327:188–94. doi: 10.1016/j.yexcr.2010.08.017

40. Han L, Choudhury S, Mich-Basso JD, Ammanamanchi N, Ganapathy B, Suresh S, et al. Lamin B2 levels regulate polyploidization of cardiomyocyte nuclei and myocardial regeneration. *Dev Cell.* (2020) 53:42–59 e11. doi: 10.1016/j.devcel.2020.01.030
41. Hofbauer P, Jahnel SM, Papai N, Giesshammer M, Deyett A, Schmidt C, et al. Cardioids reveal self-organizing principles of human cardiogenesis. *Cell.* (2021) 184:3299–317 e3222. doi: 10.1016/j.cell.2021.04.034
42. Lewis-Israeli YR, Wasserman AH, Gabalski MA, Volmert BD, Ming Y, Ball KA, et al. Self-assembling human heart organoids for the modeling of cardiac development and congenital heart disease. *Nat Commun.* (2021) 12:5142. doi: 10.1038/s41467-021-25329-5
43. Xie F, Xu S, Lu Y, Wong KF, Sun L, Hasan KMM, et al. Metformin accelerates zebrafish heart regeneration by inducing autophagy. *NPJ Regen Med.* (2021) 6:62. doi: 10.1038/s41536-021-00172-w
44. Delbridge LMD, Mellor KM, Taylor DJ, Gottlieb RA. Myocardial stress and autophagy: mechanisms and potential therapies. *Nat Rev Cardiol.* (2017) 14:412–425. doi: 10.1038/nrcardio.2017.35
45. Puente BN, Kimura W, Muralidhar SA, Moon J, Amatruda JF, Phelps KL, et al. The oxygen-rich postnatal environment induces cardiomyocyte cell-cycle arrest through DNA damage response. *Cell.* (2014) 157:565–79. doi: 10.1016/j.cell.2014.03.032
46. Wei J, Lin J, Zhang J, Tang D, Xiang F, Cui L, et al. TRPV1 activation mitigates hypoxic injury in mouse cardiomyocytes by inducing autophagy through the AMPK signaling pathway. *Am J Physiol Cell Physiol.* (2020) 318:C1018–29. doi: 10.1152/ajpcell.00161.2019
47. Qiao Y, Hu T, Yang B, Li H, Chen T, Yin D, et al. Capsaicin alleviates the deteriorative mitochondrial function by upregulating 14-3-3eta in anoxic or anoxic/reoxygenated cardiomyocytes. *Oxid Med Cell Longev.* (2020) 2020:1750289. doi: 10.1155/2020/1750289
48. Gil DW, Cheevers CV, Kedzie KM, Manlapaz CA, Rao S, Tang E, et al. Alpha-1-adrenergic receptor agonist activity of clinical alpha-adrenergic receptor agonists interferes with alpha-2-mediated analgesia. *Anesthesiology.* (2009) 110:401–407. doi: 10.1097/ALN.0b013e3181943226
49. Williams A, Sarkar S, Cuddon P, Ttofi EK, Saiki S, Siddiqi FH, et al. Novel targets for Huntington's disease in an mTOR-independent autophagy pathway. *Nat Chem Biol.* (2008) 4:295–305. doi: 10.1038/nchembio.79
50. Woodcock EA, Du XJ, Reichelt ME, Graham RM. Cardiac alpha 1-adrenergic drive in pathological remodelling. *Cardiovasc Res.* (2008) 77:452–62. doi: 10.1093/cvr/cvm078
51. Zhang J, Abdel-Rahman AA. Nischarin as a functional imidazoline (I1) receptor. *FEBS Lett.* (2006) 580:3070–4. doi: 10.1016/j.febslet.2006.04.058
52. Maltsev AV, Kokoz YM, Evdokimovskii EV, Pimenov OY, Reyes S, Alekseev AE. Alpha-2 adrenoceptors and imidazoline receptors in cardiomyocytes mediate counterbalancing effect of agmatine on NO synthesis and intracellular calcium handling. *J Mol Cell Cardiol.* (2014) 68:66–74. doi: 10.1016/j.yjmcc.2013.12.030
53. Hawes BE, van Biesen T, Koch WJ, Luttrell LM, Lefkowitz RJ. Distinct pathways of Gi- and Gq-mediated mitogen-activated protein kinase activation. *J Biol Chem.* (1995) 270:17148–53. doi: 10.1074/jbc.270.29.17148
54. Guo Y, Pu WT. Cardiomyocyte maturation: new phase in development. *Circ Res.* (2020) 126:1086–106. doi: 10.1161/CIRCRESAHA.119.315862
55. Buikema JW, Lee S, Goodyer WR, Maas RG, Chirikian O, Li G, et al. Wnt activation and reduced cell-cell contact synergistically induce massive expansion of functional human iPSC-derived cardiomyocytes. *Cell Stem Cell.* (2020) 27:50–63 e55. doi: 10.1016/j.stem.2020.06.001
56. van den Berg CW, Okawa S, Chuva de Sousa Lopes SM, van Iperen L, Passier R, Braam SR, et al. Transcriptome of human foetal heart compared with cardiomyocytes from pluripotent stem cells. *Development.* (2015) 142:3231–8. doi: 10.1242/dev.123810
57. Murganti F, Derks W, Baniol M, Simonova I, Neumann K, Khattak S, et al. FUCCI-based live imaging platform reveals cell cycle dynamics and identifies pro-proliferative compounds in human iPSC-derived cardiomyocytes. *bioRxiv.* (2021). doi: 10.1101/2021.12.20.473521

Conflict of Interest: The authors declare that the research was conducted in the absence of any commercial or financial relationships that could be construed as a potential conflict of interest.

Publisher's Note: All claims expressed in this article are solely those of the authors and do not necessarily represent those of their affiliated organizations, or those of the publisher, the editors and the reviewers. Any product that may be evaluated in this article, or claim that may be made by its manufacturer, is not guaranteed or endorsed by the publisher.

frontiers | Frontiers in Cardiovascular Medicine

REVIEW
published: 12 May 2022
doi: 10.3389/fcvm.2022.875965

Cardiac Shockwave Therapy – A Novel Therapy for Ischemic Cardiomyopathy?

*Michael Graber[1,2], Felix Nägele[1], Jakob Hirsch[1], Leo Pölzl[1,3], Victor Schweiger[4], Sophia Lechner[1], Michael Grimm[1], John P. Cooke[2], Can Gollmann-Tepeköylü[1] and Johannes Holfeld[1]**

[1] Department of Cardiac Surgery, Medical University of Innsbruck, Innsbruck, Austria, [2] Department of Cardiovascular Sciences, Center for Cardiovascular Regeneration, Houston Methodist Research Institute, Houston, TX, United States, [3] Division of Clinical and Functional Anatomy, Medical University of Innsbruck, Innsbruck, Austria, [4] Department of Cardiology, University Hospital Zurich, Zurich, Switzerland

Over the past decades, shockwave therapy (SWT) has gained increasing interest as a therapeutic approach for regenerative medicine applications, such as healing of bone fractures and wounds. More recently, pre-clinical studies have elucidated potential mechanisms for the regenerative effects of SWT in myocardial ischemia. The mechanical stimulus of SWT may induce regenerative effects in ischemic tissue *via* growth factor release, modulation of inflammatory response, and angiogenesis. Activation of the innate immune system and stimulation of purinergic receptors by SWT appears to enhance vascularization and regeneration of injured tissue with functional improvement. Intriguingly, small single center studies suggest that SWT may improve angina, exercise tolerance, and hemodynamics in patients with ischemic heart disease. Thus, SWT may represent a promising technology to induce cardiac protection or repair in patients with ischemic heart disease.

Keywords: shockwaves, angiogenesis, regeneration, ischemic heart disease, translational research

OPEN ACCESS

Edited by:
Ajit Magadum,
Temple University, United States

Reviewed by:
Ahmed Mahmoud,
University of Wisconsin–Madison, United States
Eng Leng Saw,
Boston University, United States

***Correspondence:**
Johannes Holfeld
johannes.holfeld@i-med.ac.at

Specialty section:
This article was submitted to Cardiovascular Biologics and Regenerative Medicine, a section of the journal Frontiers in Cardiovascular Medicine

Received: *14 February 2022*
Accepted: *12 April 2022*
Published: *12 May 2022*

Citation:
Graber M, Nägele F, Hirsch J, Pölzl L, Schweiger V, Lechner S, Grimm M, Cooke JP, Gollmann-Tepeköylü C and Holfeld J (2022) Cardiac Shockwave Therapy – A Novel Therapy for Ischemic Cardiomyopathy? Front. Cardiovasc. Med. 9:875965. doi: 10.3389/fcvm.2022.875965

BACKGROUND

Ischemic heart disease (IHD) remains the most frequent cause of death in the Western World (1). IHD can result in necrotic death of cardiomyocytes and their subsequent replacement by non-functional scar tissue (2). Contractile function of the scarred and ischemic myocardium is impaired in ischemic cardiomyopathy (ICMP). One strategy to preserve myocardial tissue is myocardial protection. For example, myocardial protection may be achieved during cardiac surgery by applying cold cardioplegic solution to decrease myocardial oxygen consumption and thus, avoid myocardial damage during ischemia. Remodeling of the heart is an alteration in the dimensions of the ventricular wall and/or chambers. Correction of myocardial ischemia can lead to reduced left ventricle chamber volume. Myocardial regeneration is achieved when new myocardial cells (cardiomyocytes, endothelial and/or vascular smooth muscle cells) are generated from progenitor cells or proliferation of resident cardiac cells. The optimal management of ICMP would restore perfusion, increase proliferation and function of cardiac cells, to improve ventricular function and structure.

One way of improving heart function is the re-establishment of adequate blood supply to perfuse the chronically ischemic border zone recruiting hibernating myocardium (3). Surgical

or interventional revascularization is limited to large coronary vessels, and a microvascular deficit may remain.

Angiogenic and regenerative treatment options may address this deficit. Cardiac shockwave therapy (SWT) has had promising effects in small clinical trials, and pre-clinical studies indicate that this benefit may be due to angiogenic, vasculogenic, and tissue regenerative responses (4–7). Several studies over the past years have repeatedly confirmed the angiogenic and regenerative effects of SWT in cell culture and various animal models, including hind limb ischemia and acute or chronic myocardial ischemia (8–11). In parallel, clinical studies investigating cardiac SWT have observed symptomatic relief in patients with refractory angina (5, 12, 13) as well as improvement of left ventricular function in patients with ICMP (14–16) indicating its promise in clinical use.

This review summarizes our present knowledge on this promising technology and addresses gaps of knowledge that have yet to be answered in future trials.

SAFETY ASPECTS

Shockwaves are specific sound-pressure waves appearing as transient pressure oscillations with characteristic wave profiles. The specific features defining the different types of shockwaves and the four technologies currently available to produce them have been discussed in previous reviews (17, 18). Notably, only focused shockwaves are used in the context of heart failure therapy. Shockwaves were originally applied for the purpose of lithotripsy to disintegrate kidney and urethral stones (19). As an incidental finding, iliac bone thickening was observed upon SWT. This serendipitous observation led to studies to assess SWT for bone regeneration in patients with non-unions and bone defects (20). Subsequent studies revealed that SWT could enhance healing of soft tissue defects or non-healing wounds (21, 22).

The observed regenerative effects were mainly attributed to inducing micro-injuries to the tissue, followed by subsequent repair. However, studies published over the recent years clearly showed a beneficial effect of SWT even at lower energies. Thorough examinations of tissues after SWT were not able to detect any signs of cellular damage. Transmission electron microscopy analyses of hearts treated with SW showed no changes of the myocardial ultrastructure upon therapy (7). Treatment of ischemic hearts in large animal models resulted in no signs of arrhythmia or functional impairment (23). A recent paper provided evidence for a therapeutic range of SWT, showing no cellular damage of cardiac cells beneath energy levels of 0.27 mJ/mm^2 total flux density. Regenerative effects including endothelial cell proliferation and angiogenic gene expression are induced dose-dependently until 0.15 mJ/mm^2 energy flux density. *In vitro* studies to characterize the effects of SWT revealed that in addition to the intensity of shockwaves, the effects of SWT were influenced by the geometry of the cell culture flask due to physical phenomena including reflection and interference (24). Moreover, the number of impulses has an impact on cell viability (25). However, there is no evidence that SWT induces cellular damage when used within a therapeutic range.

PROLIFERATION

One crucial mechanism underlying the regenerative effect of SWT is the induction of cellular proliferation. With respect to the heart, this proliferative effect was described mainly for endothelial cells. Although SWT induces proliferation of fibroblast cell lines *in vitro* possibly *via* transforming growth factor beta (TGF-β) upregulation (25), there is no evidence of proliferation of cardiac fibroblasts upon SWT *in vivo* (24). As cardiomyocytes are post-mitotic cells with very limited capacity of proliferation, it seems very unlikely that SWT might cause proliferation in primary cardiac myocytes. Indeed, *in vitro* studies of a cardiomyocyte cell line showed no proliferative effects of SWT upon treatment, irrespective of treatment dose (24).

There is ample evidence that SWT induces proliferation of endothelial cells (26). This might be due to the release of vascular endothelial growth factor (VEGF) and activation of VEGF receptor 2 (VEGFR2) with subsequent activation of AKT/ERK pathways resulting in endothelial cell proliferation (growth factor release upon SWT is discussed below). Interestingly, the proliferative effects of SWT are abolished upon inhibition of VEGF or VEGFR2 (27). Moreover, proliferation of endothelial cells upon SWT was described *in vivo* after induction of hind limb ischemia (28).

PRO-SURVIVAL/ANTI-APOPTOTIC

Myocardial hypoxia causes loss of cardiac cells. Tissue necrosis within the ischemic core is accompanied by apoptosis of cells in adjacent cardiac tissue, especially in the border zone of infarcted areas (29). At the same time, the evolutionary conserved process of autophagy is initiated, recycling damaged cellular components (30). Autophagy allows cells to adapt to various environmental stresses *via* degradation of defective proteins or organelles by lysosomes. Post-mitotic cells rely on autophagic processes upon stress since cell replacement is not an option (31). In rat cardiomyocytes, SWT promotes autophagy after hypoxia, probably *via* regulation of mammalian target of rapamycin (mTOR) and subsequent activation of AMP-activated kinase (AMPK) and Beclin 1 (32).

The limitation of cell death upon infarction is a valuable therapeutic strategy to preserve cardiac function after ischemia (33). SWT inhibits apoptosis in a myocardial cell line upon *in vitro* hypoxia and increases cell viability, thereby having a protective rather than regenerative effect on cardiomyocytes. It increases the expression of the crucial anti-apoptotic protein Bcl-2 and decreases the expression of the pro-apoptotic protein Bax. This effect reduces the activation of Caspase 3, a crucial mediator of the intrinsic pathway of apoptosis. The anti-apoptotic effects might depend on phosphorylation of AKT (34) (**Figure 1**).

GROWTH FACTOR RELEASE

The release of growth factors is crucial for successful regeneration. Growth factors are tissue-specific proteins with

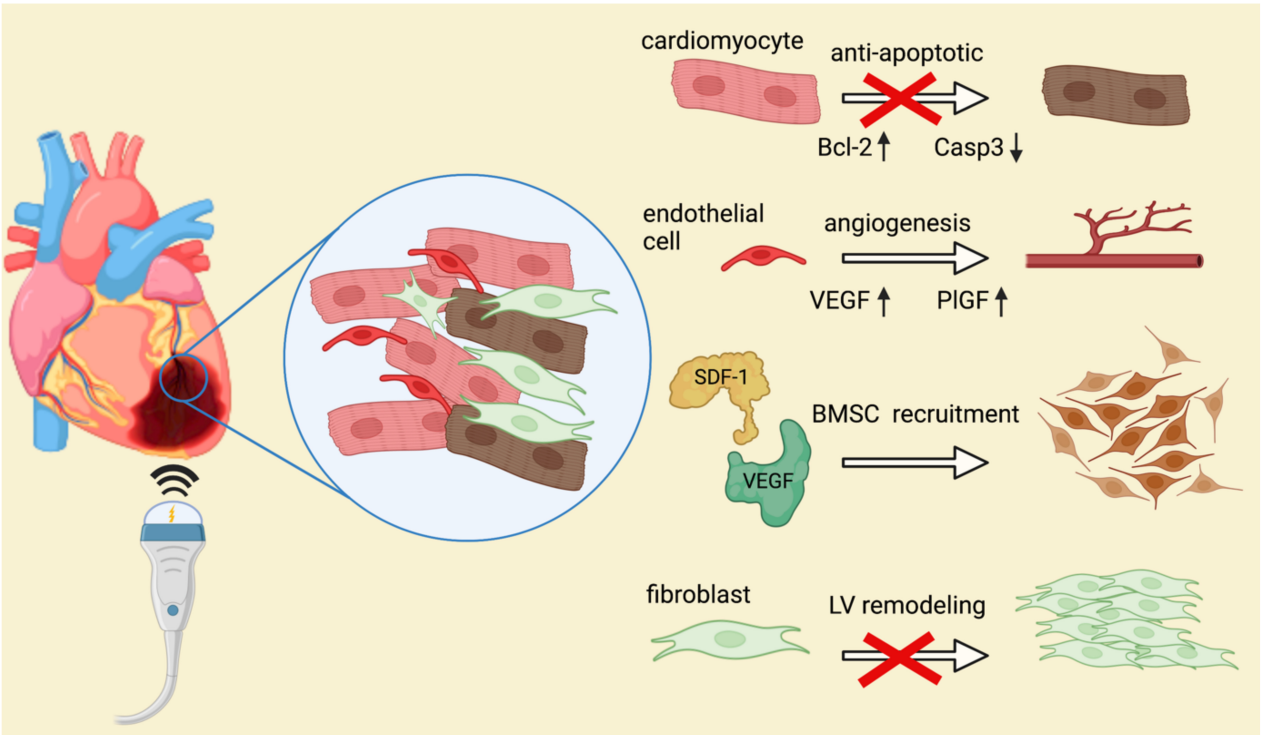

FIGURE 1 | Molecular mechanisms of shockwave therapy in ischemic heart disease. Several mechanisms of positive impacts mediated by SWT on the course of ischemic heart disease have been described. By regulation of anti-apoptotic proteins, cardiomyocyte survival is enhanced and hence, cardiac damage limited. Angiogenesis upon shockwave therapy is mediated *via* release of endothelial growth factors VEGF and PlGF. SDF-1 acts as a chemoattractant of angiogenic bone marrow derived stem cells. Migration of these progenitor cells is crucial for induction of vasculogenesis and revascularization of ischemic tissue. Moreover, shockwave therapy was shown to reduce the number of fibrocytes within chronic ischemic myocardium, thereby promoting reverse LV remodeling.

pivotal roles in both development and healing. The subtype of released growth factor upon SWT depends on the treated tissue and pathology. Regenerative effects of SWT in musculoskeletal disorders are mediated by released TGF-β, insulin-like growth factor 1 (IGF-1) and bone morphogenetic proteins (BMPs) (35, 36). These growth factors regulate proliferation of mesenchymal cells, thereby mediating bone, cartilage, and tendon repair. On the other hand, healing of chronic wounds depends on different factors, as these wounds are associated with persistent inflammatory dysregulation. SWT has beneficial effects on the healing of chronic wounds by modulating the inflammatory response. The release of platelet-derived growth factor (PDGF) modulates macrophage recruitment and function and thus contributes to wound healing (37). Macrophages play a prominent role in wound healing by creating granulation tissue, protecting from infection, and facilitating re-epithelization (38). Besides modulation of inflammation, induction of angiogenesis is the key for successful wound healing. Angiogenic growth factors such as VEGF and fibroblast growth factor (FGF) are major determinants of microvessel formation (27, 39). In ischemic tissue, including the heart, SWT induces the release of angiogenic growth factors including VEGF, placenta growth factor (PlGF) and FGF (26, 27, 40). These growth factors might be stored in the extracellular matrix and released upon mechanical stimulus (27).

ANGIOGENESIS

Angiogenesis is a vital part in regeneration of ischemic tissue. It improves perfusion preventing further ischemic damage and restores tissue function. Angiogenesis is defined as the formation of new capillaries from pre-existing vessels. This process is initiated by angiogenic growth factors driving the sprouting and proliferation of endothelial cells. The most prominent and angiogenic factor is VEGF. VEGF appears in four isoforms, VEGF-A, VEGF-B, VEGF-C, and VEGF-D (41). These peptides bind to and activate their receptors VEGFR1, VEGFR2, and VEGFR3. VEGFR3 is activated by VEGF-C and VEGF-D and generally limited to lymphatic endothelial cells. VEGFR2 binds the most abundant form VEGF-A and facilitates endothelial cell proliferation, migration and survival. Activation of VEGFR1 by VEGF-B and PlGF, another member of the VEGF-subfamily, leads to monocyte recruitment rather than induction of angiogenesis (41). Hence, decisive angiogenic mechanism are depending on VEGFR2 activation. SWT induces VEGF release and subsequent VEGFR2 activation in endothelial cells *in vitro*, resulting in endothelial cell proliferation (42). Moreover, SWT promotes the sprouting of new vessels from *ex vivo* cultured aortic rings (40). In this assay, the same molecular mechanisms are observed.

Similarly, SWT induces angiogenesis in a variety of animal models and tissues. Shockwaves enhance blood flow in epigastric skin flaps and hence, improves skin flap survival. In this case, the increase in microvascular density is associated with the generation of VEGF and nitric oxide (NO) (43, 44). NO is synthesized by endothelial nitric oxide synthase (eNOS), a direct downstream target of VEGFR2-signaling. NO is a potent vasodilator, which also regulates endothelial cell growth and cellular homeostasis (45). SWT similarly improves limb perfusion and function in a hind limb ischemia model in rodents, an effect which is associated with an increase in VEGF and VEGFR2 activation. The treatment increases the number of endothelial cells and capillaries in the ischemic limb musculature (28). Similar results are obtained in the ischemic heart. Shockwave therapy enhances capillary density in the border zones of experimental myocardial infarction, resulting in decreased infarct size and hence, improved cardiac function (27). In addition to angiogenesis, the increase in capillary density might also be due to vasculogenesis, the process by which circulating progenitor cells contribute to the microvasculature. Of interest, shockwave-treated hearts show a greater number of arterioles within the ischemic myocardium, indicative of arteriogenesis, which is the positive remodeling of existing collateral channels.

PROGENITOR CELLS

Circulating progenitor cells may play a role in revascularization. Such circulating cells may be capable of differentiation toward mature endothelial cells and participate directly in the formation of new vessels (46). On the other hand, other circulating progenitor cells may act in a paracrine fashion by releasing growth factors and creating an angiogenic milieu. Physiologically, endothelial progenitor cells (EPCs) and mesenchymal stem cells (MSCs) are involved in revascularization of ischemic tissue. EPCs are capable of both differentiation toward endothelial cells and release of growth factors (46). Only a small subset of EPCs is of true endothelial lineage in humans, most being of hematopoietic lineage. The great majority of these circulating angiogenic cells promote angiogenesis by secreting angiogenic cytokines and matrix metalloproteinases (47, 48). Some circulating cells that contribute to angiogenesis may be derived from mature endothelial cells from other sites that are mobilized into the systemic circulation by angiogenic cytokines released from the ischemic tissue (49). In addition, resident tissue MSCs may differentiate into pericytes stabilizing the endothelial network and supporting blood vessel growth *via* paracrine secretion (50).

Shockwave therapy may affect progenitor cells in several ways. First of all, SWT induces the release of stromal-derived factor 1 (SDF-1), a chemoattractant and ligand of CXC chemokine receptor 4 (CXCR-4) on EPCs (28, 51, 52). Hence, increased numbers of EPCs migrate to the ischemic tissue and contribute to the process of new vessel formation. Enhanced recruitment of multipotent cells and concomitant vasculogenesis is observed in shockwave-treated ischemic hind limbs as well as in chronic IHD (28, 53). Since SWT improves migration of intrinsic multipotent cells *via* upregulation of chemoattractants, it is also able to induce homing of systemically injected stem cells (52). In addition, SWT appears to enhance regenerative potential of injected cardiac stem cells significantly in human patients (54). Mechanistically, AKT-mediated upregulation of eNOS upon SWT induces beneficial effects on migration, proliferation, and angiogenic potential of injected cells (52). Moreover, SWT induces the release of adenosine tri-phosphate (ATP) from mesenchymal cells and, activation of purinergic receptors (55). Purinergic signaling enhances stem cell proliferation significantly. Notably, treated progenitor cells maintain multipotency *in vitro* and improve wound healing significantly by their enhanced differentiation potential (55, 56).

LEFT VENTRICULAR REMODELING

Acute myocardial infarction leads to a loss of cardiomyocytes and subsequent replacement of viable myocardium with non-contractile fibrotic scar tissue. Notably, extensive fibrosis emerging from the infarction border zone can be found as well in non-infarcted myocardium. This process of adverse left ventricular (LV) remodeling extends tissue damage, further impairs cardiac function, and ultimately worsens heart failure. LV remodeling is associated with poor prognosis and revascularization often fails to ameliorate this pathologic process. Several studies observed beneficial effects of mechanical stimulation with SWT after acute myocardial infarction. Thereby, cardiac function is preserved, possibly by limiting fibrotic remodeling of the heart (15). Effects are accompanied by angiogenesis as well as lower numbers of fibrocytes within the infarction border zone (9). Similarly, a reduced number of TGF-β positive cells is found upon SWT in a model of acute myocardial infarction in rats (57). A potential mechanism by which SWT reduces cardiac fibrosis in ischemic hearts might be through the regulation of the phosphoinositide-3-kinase (PI3K)/AKT pathway, as inhibition of PI3K abolished the observed improvement of left ventricular function and reduced cardiac fibrosis (58). Notably, similar effects are observed in myocardial ischemia/reperfusion injury (59). This model is of high clinical relevance, as SWT might be beneficial to alleviate cardiac ischemia/reperfusion injury.

INFLAMMATION

Upon myocardial infarction, subsequent inflammation determines the fate of the myocardium contributing to cell death, fibrosis, healing, and scar formation. Wound healing upon myocardial infarction occurs in a biphasic manner with an initial strong pro-inflammatory response followed by a prolonged resolution of inflammation, which governs tissue repair and scar formation (60). Accordingly, a balanced inflammatory response is crucial for adequate healing (61). An early proinflammatory

response is necessary to remove cellular debris after ischemia, whereas the later anti-inflammatory response promotes a milieu of angiogenesis and tissue repair (62).

SWT improves myocardial function *via* modulation of the inflammatory response. SWT of endothelial cells induces the release of endogenous RNA, causing activation of innate immune receptor Toll-Like receptor 3 (TLR3) (63). This inflammatory signaling *via* TLR3 activation promotes angiogenesis after SWT in ischemic hind limbs. *In vivo*, restoration of blood flow in ischemic tissue is abolished in $Tlr3^{-/-}$ animals (63). TLR3 typically activates an early pro-inflammatory and a late anti-inflammatory response (64). In this manner, shockwave-induced activation of TLR3 leads to an initial release of pro-inflammatory cytokines including cyclophilin A and interleukin 6 (IL-6). With some delay after treatment, anti-inflammatory interleukin 10 (IL-10) is upregulated (65). IL-10 is a major regulator of inflammation by restricting excessive pro-inflammatory cytokine production of migrating immune cells (66). Migrating immune cells, primarily macrophages, are mainly responsible for cytokine production within ischemic tissue (67). In the tissue, macrophages polarize toward a M1 or M2 subtype. M1 macrophages maintain the inflammatory cytokine production and enhance the further recruitment of immune cells (68). M2 macrophages on the other hand suppress the immune response and resolve acute inflammation (67). Polarization toward anti-inflammatory M2 macrophages is driven again by IL-10 and SWT thereby enhances this process (69). Similar observations of enhanced M2-presence are observed in ischemic mouse hind limbs treated with SWT (70).

In addition, SWT elevates NO levels *via* eNOS (51, 57) and neural NOS (71) induction and even non-enzymatic NO formation (72). Elevated NO levels increase local blood flow and thereby reduce ischemic necrosis and ensuing inflammatory processes (21). Thus, SWT reduced inflammation in a porcine model of myocardial ischemia (51). In the ischemic rat heart, it suppresses the infiltration of TGF-β positive cells and reduces the release of several pro-inflammatory cytokines while enhancing anti-inflammatory cytokines (57). Overall, these findings confirm that a modified inflammatory response mediated by TLR3 is involved in the positive effects elicited by SWT (**Figure 2**).

Besides the above-described mechanisms, recent research showed an emerging role of TLR3-mediated inflammation on cellular plasticity and concomitant cell fate transitions. This process, termed transflammation, may provide a mechanism by which mechanical activation of immune signaling facilitates angiogenesis in ischemic tissue.

TRANSFLAMMATION

As described earlier, activation of pattern recognition receptors (such as TLR3) by cellular damage or pathogens triggers cell-autonomous inflammatory signaling that leads to the release of inflammatory cytokines and chemokines that initiate tissue inflammation. We have discovered another limb of this pathway that mediates cellular plasticity.

Specifically, we have observed that inflammatory signaling causes a global alteration in the expression and activity of epigenetic modifiers. For example, activation of TLR3 by retroviral RNA increases the expression of histone acetyltransferases (HATs) and reduces the expression of histone deacetylases (HDAC). This change in the balance of epigenetic enzymes favors histone acetylation and thereby an open chromatin state, which can facilitate cell fate transitions (73). Furthermore, inflammation leads to nuclear translocation of inducible nitric oxide synthase (iNOS). There, it binds to, and S-nitrosylates epigenetic modifiers such as elements of the polycomb repressive complex (PRC1) and the NURD complex, causing these suppressive epigenetic enzymes to dissociate from the chromatin, enabling access to previously repressed transcriptional programs (74, 75). Finally, this inflammatory pathway activates a glycolytic switch, which supplies more citric acid to the nucleus, where it is converted to Acetyl-CoA to facilitate histone modifications (76).

This process of transflammation is required for changes in somatic cell fate, such as that which occurs when a fibroblast is reprogrammed to an induced pluripotent stem cell, or to an endothelial cell (73, 77, 78). Furthermore, transflammation appears to be activated in the setting of ischemia and may play a role in perfusion recovery. Specifically, we have observed a role for transflammation in the transdifferentiation of resident fibroblasts to endothelial cells in recovery of limb ischemia. Anti-inflammatory agents impair the transdifferentiation of fibroblasts to endothelial cells, impair perfusion recovery, and exacerbate tissue necrosis in a murine model of limb ischemia (79).

Since the underlying mechanism of this regenerative process is a modest activation of inflammatory signaling, as observed after shockwave therapy, further research should be done to clarify if mechanical conditioning could potentially have its effect on therapeutic cell fate transitions.

MECHANOTRANSDUCTION

The beneficial effects of SWT were initially thought to be due to mechanical, non-selective tissue damage followed by repair mechanisms. However, more recent work indicates that SWT induces a specific tissue response. How the physical stimulus of SWT is translated into a specific biological response is beginning to be elucidated. Cells are equipped with mechanosensors responsible for the translation of mechanical input to a biological response, a process termed "mechanotransduction" (80). Integrins play a major role within the process of mechanosensing. Integrins are cell surface receptors binding proteins of the extracellular matrix (80). They are linked intracellularly to actin filaments of the cytoskeleton, initiating their reorganization, and transducing molecular mechanism among others *via* AKT/ERK activation. Mechanical stimulation of cells with shockwaves induces this particular integrin-mediated AKT/ERK signaling (81). Besides activation of cellular mechanosensors, the cellular membrane itself is highly

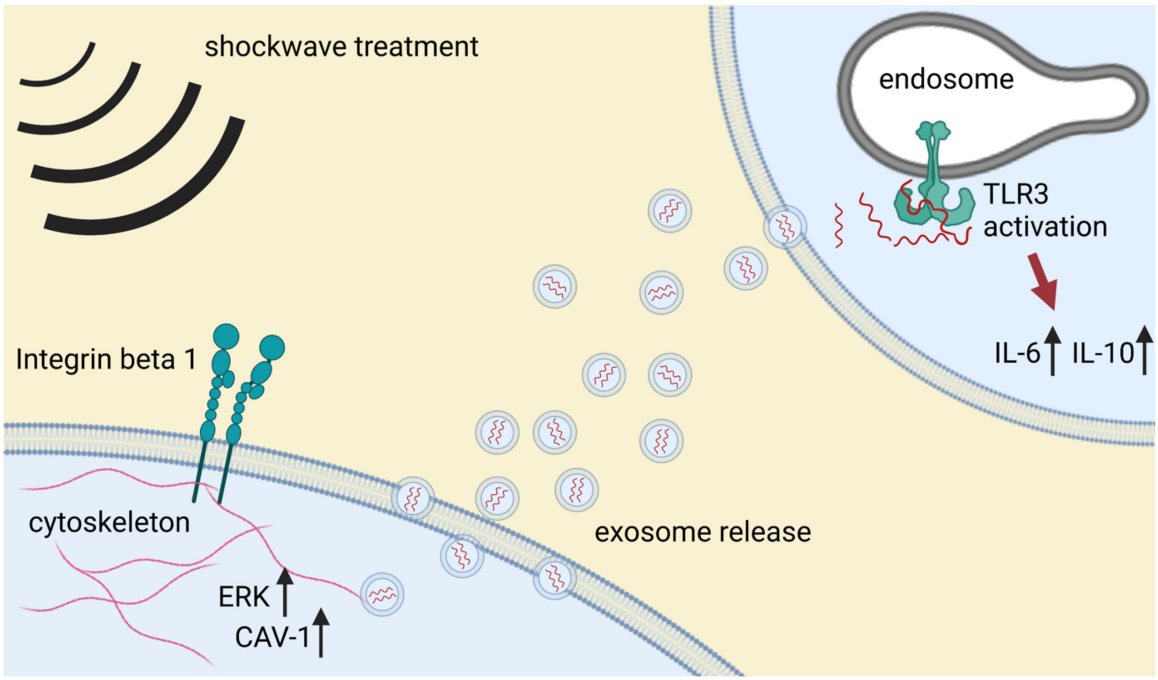

FIGURE 2 | Mechanotransduction and modulation of inflammatory response upon SWT. Mechanical stimulation with shockwaves induces cellular mechanosensing. Activation of beta 1 integrin on the cell surface induces intracellular upregulation of ERK, which in turn activates caveolin 1 (CAV-1). Caveolin is a potent regulator of microvesicle release and hence, intercellular communication. Microvesicles, particularly exosomes, are loaded with specific cargo and released to the extracellular space. Uptake of shockwave-derived exosomes activates the innate immune receptor TLR3. TLR3 signaling results in an inflammatory response that may induce epigenetic alterations required for the regenerative effects of SWT.

responsible to mechanical stimulation. Under the influence of SWT, the membrane can release vesicles from its surface. These reactive mechanisms rely on expression of caveolin 1 (CAV-1), which is upregulated upon SWT (81). CAV-1 governs the release of microvesicles, an important component of intercellular communication (82).

These observations are consistent with findings that SWT induces paracrine effects, as transfer of supernatant from SWT-treated cells recapitulates the direct effect of SWT. Treated supernatants contained increased amounts of released growth factors, protein/RNA complexes as well as exosomes (26, 83, 84). These specific extracellular vesicles are derived from cytosolic multivesicular bodies upon treatment and show distinct angiogenic potential *in vitro* as well as *in vivo*. Shockwave-derived exosomes improve vascularization and cardiac function in ischemic hearts. Of interest, inhibition of exosome release abolished the angiogenic effects of SWT. Intriguingly, shockwave-derived exosomes differ from control exosomes by their cargo. The angiogenic microRNA miR19a-3p mediates angiogenesis and reduction of myocardial fibrosis upon SWT (83). Use of miR19a-3p obtained the same results as shockwave-derived exosomes, whereas antagonizing this specific miRNA abolished the angiogenic potential of SWT exosomes. Further studies are needed to elucidate the exact mechanisms of extracellular vesicle release upon SWT and their potential interplay with innate immunity (**Figure 2**).

DISCUSSION AND PERSPECTIVE

Ischemic heart disease and ischemic heart failure are ever increasing in the western world. Together they are a leading cause of death and disability, representing a major socio-economic burden for healthcare systems (1). Current treatment strategies fail to regenerate damaged heart muscle. Cell-based regenerative options have been disappointing (85). However, small single-center studies suggest that SWT may be useful in patients with ICMP (5). However, most clinical studies of cardiac SWT used symptomatic relief as a primary endpoint rather than objective improvement in heart function. Moreover, all available clinical data was generated by extracorporeal application of SWT. Extracorporeal application of SWT to the ischemic heart has several limitations: (a) a small acoustic window, (b) accessible treatment regions being restricted to the anterior myocardium, and (c) the risk of potential lung injuries (86, 87). Hence, a direct epicardial approach during surgical procedures may be more favorable to obtain optimal treatment efficacy since beneficial effects are directly associated with the intensity of mechanical stimulation (24). A new clinical trial of direct epicardial SWT in patients with ICMP undergoing coronary artery bypass grafting aims to determine if direct application of SWT to the myocardium can increase cardiac function (88).

To conclude, effects of shockwaves have been studied extensively in ischemic tissue, including the ischemic heart. Thereby, it is application has been tested in models of both acute

and chronic myocardial ischemia (23, 27, 58). In both settings SWT showed positive effects on cardiac function, although clinical settings are mainly focused on chronic IHD. SWT induces various molecular mechanisms leading to the release of angiogenic growth factors, enhanced survival of hypoxic cells and regenerative epigenetic mechanisms *via* induction of inflammatory signaling. Underlying these observed effects is the process of mechanotransduction, the translation of a mechanic stimulus to a biological signal. The cell membrane is highly responsive to shockwaves and sheds extracellular vesicles upon treatment. These vesicles have angiogenic activity and are capable of improving vascularization in ischemic tissue (83). The effect of SWT to induce angiogenesis may not fully explain the observed improvement of LV remodeling. Although angiogenesis is the most prominent factor in regenerating chronic ischemic tissue, mechanical conditioning also seems to have a protective role *via* anti-apoptotic effects. Both effects are accompanied by reduction of cardiac fibrosis, either by preventing its initial formation or by degradation of fibrotic material when tissue perfusion is restored. Further research should show whether mechanical stimulation *via* shockwaves may induce cardiac-specific mechanisms in comparison to other soft tissue applications. Furthermore, it remains to be clarified which cell types within the ischemic heart are primarily responding to the mechanical stimulation with shockwaves since different cell types showed varying effects upon treatment *in vitro* (24). In addition, further in-depth analysis of the SWT-induced release of exosomes and their cargo is required to provide more comprehensive insight how this may interplay with or activate other crucial mechanisms such as the inflammatory response. Although the molecular mechanisms are incompletely characterized, evidence is accumulating that SWT has beneficial effects in patients suffering from myocardial ischemia. Notably, existing data is restricted to small observational monocentric studies with limitations regarding variations in extent of myocardial injury, treatment protocols and endpoint analyses. Therefore, multi-center adequately powered randomized double-blind studies are warranted to assess the safety and efficacy of SWT in IHD.

AUTHOR CONTRIBUTIONS

MGa: conceptualization, writing original draft, and writing review and editing. FN, JHi, LP, VS, MGi, and JC: review and editing. CG-T and JHo: conceptualization, supervision, and writing review and editing. All authors contributed to the article and approved the submitted version.

FUNDING

This work was supported in part by NIH grants to JC (R0-1 HL148338 and HL133254).

ACKNOWLEDGMENTS

Figures were created with BioRender.com.

REFERENCES

1. Moran AE, Forouzanfar MH, Roth GA, Mensah GA, Ezzati M, Flaxman A, et al. The global burden of ischemic heart disease in 1990 and 2010: the global burden of disease 2010 study. *Circulation.* (2014) 129:1493–501.
2. Richardson WJ, Clarke SA, Quinn TA, Holmes JW. Physiological Implications of myocardial scar structure. *Compr Physiol.* (2015) 5:1877–909.
3. Wijns W, Vatner SF, Camici PG. Hibernating myocardium. *N Engl J Med.* (1998) 339:173–81.
4. Holfeld J, Lobenwein D, Tepeköylü C, Grimm M. Shockwave therapy of the heart. *Int J Surg.* (2015) 24:218–22. doi: 10.1016/j.ijsu.2015.09.070
5. Burneikaitė G, Shkolnik E, Čelutkienė J, Zuozienė G, Butkuvienė I, Petrauskienė B, et al. Cardiac shock-wave therapy in the treatment of coronary artery disease: systematic review and meta-analysis. *Cardiovasc Ultrasound.* (2017) 15:11. doi: 10.1186/s12947-017-0102-y
6. Di Meglio F, Nurzynska D, Castaldo C, Miraglia R, Romano V, De Angelis A, et al. Cardiac shock wave therapy: assessment of safety and new insights into mechanisms of tissue regeneration. *J Cell Mol Med.* (2012) 16:936–42. doi: 10.1111/j.1582-4934.2011.01393.x
7. Liu B, Zhang Y, Jia N, Lan M, Du L, Zhao D, et al. Study of the safety of extracorporeal cardiac shock wave therapy: observation of the ultrastructures in myocardial cells by transmission electron microscopy. *J Cardiovasc Pharmacol Ther.* (2018) 23:79–88. doi: 10.1177/1074248417725877
8. Nishida T, Shimokawa H, Oi K, Tatewaki H, Uwatoku T, Abe K, et al. Extracorporeal cardiac shock wave therapy markedly ameliorates ischemia-induced myocardial dysfunction in pigs in vivo. *Circulation.* (2004) 110:3055–61. doi: 10.1161/01.CIR.0000148849.51177.97
9. Uwatoku T, Ito K, Abe K, Oi K, Hizume T, Sunagawa K, et al. Extracorporeal cardiac shock wave therapy improves left ventricular remodeling after acute myocardial infarction in pigs. *Coron Artery Dis.* (2007) 18:397–404. doi: 10.1097/MCA.0b013e328089f19b
10. Fu M, Sun CK, Lin YC, Wang CJ, Wu CJ, Ko SF, et al. Extracorporeal shock wave therapy reverses ischemia-related left ventricular dysfunction and remodeling: molecular-cellular and functional assessment. *PLoS One.* (2011) 6:e24342. doi: 10.1371/journal.pone.0024342
11. Lei PP, Tao SM, Shuai Q, Bao YX, Wang SW, Qu YQ, et al. Extracorporeal cardiac shock wave therapy ameliorates myocardial fibrosis by decreasing the amount of fibrocytes after acute myocardial infarction in pigs. *Coron Artery Dis.* (2013) 24:509–15. doi: 10.1097/MCA.0b013e3283640ec7
12. Ruiz-Garcia J, Lerman A. Cardiac shock-wave therapy in the treatment of refractive angina pectoris. *Interv Cardiol.* (2011) 3:191–201. doi: 10.2217/ica.11.5
13. Wang J, Zhou C, Liu L, Pan X, Guo T. Clinical effect of cardiac shock wave therapy on patients with ischaemic heart disease: a systematic review and meta-analysis. *Eur J Clin Invest.* (2015) 45:1270–85. doi: 10.1111/eci.12546
14. Vasyuk YA, Hadzegova AB, Shkolnik EL, Kopeleva MV, Krikunova OV, Iouchtchouk EN, et al. Initial clinical experience with extracorporeal shock wave therapy in treatment of ischemic heart failure. *Congest Hear Fail.* (2010) 16:226–30. doi: 10.1111/j.1751-7133.2010.00182.x
15. Kagaya Y, Ito K, Takahashi J, Matsumoto Y, Shiroto T, Tsuburaya R, et al. Low-energy cardiac shockwave therapy to suppress left ventricular remodeling in patients with acute myocardial infarction: a first-in-human study. *Coron Artery Dis.* (2017) 29:294–300. doi: 10.1097/MCA.0000000000000577
16. Myojo M, Ando J, Uehara M, Daimon M, Watanabe M, Komuro I. Feasibility of extracorporeal shock wave myocardial revascularization therapy for post-acute myocardial infarction patients and refractory angina pectoris patients. *Int Heart J.* (2017) 58:185–90. doi: 10.1536/ihj.16-289
17. Rassweiler JJ, Knoll T, Köhrmann K-U, McAteer JA, Lingeman JE, Cleveland RO, et al. Shock wave technology and application: an update. *Eur Urol.* (2011) 59:784–96. doi: 10.1016/j.eururo.2011.02.033
18. van der Worp H, van den Akker-Scheek I, van Schie H, Zwerver J. ESWT for tendinopathy: technology and clinical implications. *Knee Surg*

Sports Traumatol Arthrosc. (2013) 21:1451–8. doi: 10.1007/s00167-012-2009-3
19. Chaussy C, Brendel W, Schmiedt E. Extracorporeally induced destruction of kidney stones by shock waves. *Lancet.* (1980) 2:1265–8. doi: 10.1016/s0140-6736(80)92335-1
20. Elster EA, Stojadinovic A, Forsberg J, Shawen S, Andersen RC, Schaden W. Extracorporeal shock wave therapy for nonunion of the tibia. *J Orthop Trauma.* (2010) 24:133–41. doi: 10.1097/BOT.0b013e3181b26470
21. Mittermayr R, Antonic V, Hartinger J, Kaufmann H, Redl H, Téot L, et al. Extracorporeal shock wave therapy (ESWT) for wound healing: technology, mechanisms, and clinical efficacy. *Wound Repair Regen.* (2012) 20:456–65. doi: 10.1111/j.1524-475X.2012.00796.x
22. Ottomann C, Stojadinovic A, Lavin PT, Gannon FH, Heggeness MH, Thiele R, et al. Prospective randomized phase II Trial of accelerated reepithelialization of superficial second-degree burn wounds using extracorporeal shock wave therapy. *Ann Surg.* (2012) 255:23–9. doi: 10.1097/SLA.0b013e318227b3c0
23. Holfeld J, Zimpfer D, Albrecht-Schgoer K, Stojadinovic A, Paulus P, Dumfarth J, et al. Epicardial shock-wave therapy improves ventricular function in a porcine model of ischaemic heart disease. *J Tissue Eng Regen Med.* (2014) 10:1057–64. doi: 10.1002/term.1890
24. Pölzl L, Nägele F, Hirsch J, Graber M, Lobenwein D, Kirchmair E, et al. Defining a therapeutic range for regeneration of ischemic myocardium via shock waves. *Sci Rep.* (2021) 11:409. doi: 10.1038/s41598-020-79776-z
25. Berta L, Fazzari A, Ficco AM, Enrica PM, Catalano MG, Frairia R. Extracorporeal shock waves enhance normal fibroblast pro- liferation in vitro and activate mRNA expression for TGF- β 1 and for collagen types I and III. *Acta Orthop.* (2009) 80:612–7. doi: 10.3109/17453670903316793
26. Peng YZ, Zheng K, Yang P, Wang Y, Li RJ, Li L, et al. Shock wave treatment enhances endothelial proliferation via autocrine vascular endothelial growth factor. *Genet Mol Res.* (2015) 14:19203–10. doi: 10.4238/2015.December.29.30
27. Gollmann-Tepeköylü C, Lobenwein D, Theurl M, Primessnig U, Lener D, Kirchmair E, et al. Shock wave therapy improves cardiac function in a model of chronic ischemic heart failure: evidence for a mechanism involving vegf signaling and the extracellular matrix. *J Am Heart Assoc.* (2018) 7:e010025. doi: 10.1161/JAHA.118.010025
28. Tepekoylu C, Wang FS, Kozaryn R, Albrecht-Schgoer K, Theurl M, Schaden W, et al. Shock wave treatment induces angiogenesis and mobilizes endogenous CD31/CD34-positive endothelial cells in a hindlimb ischemia model: implications for angiogenesis and vasculogenesis. *J Thorac Cardiovasc Surg.* (2013) 146:971–8. doi: 10.1016/j.jtcvs.2013.01.017
29. Saraste A, Pulkki K, Kallajoki M, Henriksen K, Parvinen M, Voipio-Pulkki LM. Apoptosis in human acute myocardial infarction. *Circulation.* (1997) 95:320–3.
30. Abdellatif M, Sedej S, Carmona-Gutierrez D, Madeo F, Kroemer G. Autophagy in cardiovascular aging. *Circ Res.* (2018) 123:803–24.
31. Schiattarella GG, Hill JA. Therapeutic targeting of autophagy in cardiovascular disease. *J Mol Cell Cardiol.* (2016) 95:86–93. doi: 10.1016/j.yjmcc.2015.11.019
32. Du L, Shen T, Liu B, Zhang Y, Zhao C, Jia N, et al. Shock wave therapy promotes cardiomyocyte autophagy and survival during hypoxia. *Cell Physiol Biochem.* (2017) 42:673–84. doi: 10.1159/000477885
33. Yaoita H, Ogawa K, Maehara K, Maruyama Y. Apoptosis in relevant clinical situations: contribution of apoptosis in myocardial infarction. *Cardiovasc Res.* (2000) 45:630–41. doi: 10.1016/s0008-6363(99)00349-1
34. Yu W, Shen T, Liu B, Wang S, Li J, Dai D, et al. Cardiac shock wave therapy attenuates H9c2 myoblast apoptosis by activating the AKT signal pathway. *Cell Physiol Biochem.* (2014) 33:1293–303. doi: 10.1159/000358697
35. Hsu SL, Chou WY, Hsu CC, Ko JY, Jhan SW, Wang CJ, et al. Shockwave therapy modulates the expression of bmp2 for prevention of bone and cartilage loss in the lower limbs of postmenopausal osteoporosis rat model. *Biomedicines.* (2020) 8:E614. doi: 10.3390/biomedicines8120614
36. Chen Y, Wang C, Yang KD, Kuo Y, Huang H, Huang Y, et al. Extracorporeal shock waves promote healing of collagenase-induced Achilles tendinitis and increase TGF- p 1 and IGF-I expression. *J Orthop Res.* (2004) 22:854–61. doi: 10.1016/j.orthres.2003.10.013
37. Holsapple JS, Cooper B, Berry SH, Staniszewska A, Dickson BM, Taylor JA, et al. Low intensity shockwave treatment modulates macrophage functions beneficial to healing chronic wounds. *Int J Mol Sci.* (2021) 22:7844. doi: 10.3390/ijms22157844
38. Krzyszczyk P, Schloss R, Palmer A, Berthiaume F. The role of macrophages in acute and chronic wound healing and interventions to promote pro-wound healing phenotypes. *Front Physiol.* (2018) 9:419. doi: 10.3389/fphys.2018.00419
39. Yun Y, Won JE, Jeon E, Lee S, Kang W, Jo H, et al. Fibroblast growth factors: biology, function, and application for tissue regeneration. *J Tissue Eng.* (2010) 2010:218142. doi: 10.4061/2010/218142
40. Holfeld J, Tepeköylü C, Blunder S, Lobenwein D, Kirchmair E, Dietl M, et al. Low energy shock wave therapy induces angiogenesis in acute hind-limb ischemia via VEGF receptor 2 phosphorylation. *PLoS One.* (2014) 9:e103982. doi: 10.1371/journal.pone.0103982
41. Holmes DIR, Zachary I. The vascular endothelial growth factor (VEGF) family: angiogenic factors in health and disease. *Genome Biol.* (2005) 6:209. doi: 10.1186/gb-2005-6-2-209
42. Rohringer S, Holnthoner W, Hackl M, Weihs AM, Ru D, Skalicky S, et al. Molecular and cellular effects of in vitro shockwave treatment on lymphatic endothelial cells. *PLoS One.* (2014) 9:e114806. doi: 10.1371/journal.pone.0114806
43. Mittermayr R, Hartinger J, Antonic V, Meinl A, Pfeifer S, Stojadinovic A, et al. Extracorporeal shock wave therapy (ESWT) minimizes ischemic tissue necrosis irrespective of application time and promotes tissue revascularization by stimulating angiogenesis. *Ann Surg.* (2011) 253:1024–32. doi: 10.1097/SLA.0b013e3182121d6e
44. Yan X, Zeng B, Chai Y, Luo C, Li X. Improvement of blood flow, expression of nitric oxide, and vascular endothelial growth factor by low-energy shockwave therapy in random-pattern skin flap model. *Ann Plast Surg.* (2008) 61:646–53. doi: 10.1097/SAP.0b013e318172ba1f
45. Cooke JP, Connor JH, Jain A. Acute and chronic cardiovascular manifestations of COVID-19: role for endotheliopathy. *Methodist Debakey Cardiovasc J.* (2021) 17:53–62. doi: 10.14797/mdcvj.1044
46. Hou L, Kim JJ, Woo YJ, Huang NF. Stem cell-based therapies to promote angiogenesis in ischemic cardiovascular disease. *Am J Physiol Heart Circ Physiol.* (2016) 310:H455–65. doi: 10.1152/ajpheart.00726.2015
47. Yoon CH, Hur J, Park KW, Kim JH, Lee CS, Oh IY, et al. Synergistic neovascularization by mixed transplantation of early endothelial progenitor cells and late outgrowth endothelial cells: the role of angiogenic cytokines and matrix metalloproteinases. *Circulation.* (2005) 112:1618–27. doi: 10.1161/circulationaha.104.503433
48. Grunewald M, Avraham I, Dor Y, Bachar-Lustig E, Itin A, Jung S, et al. VEGF-induced adult neovascularization: recruitment, retention, and role of accessory cells. *Cell.* (2006) 124:175–89. doi: 10.1016/j.cell.2005.10.036
49. Aicher A, Rentsch M, Sasaki K, Ellwart JW, Fändrich F, Siebert R, et al. Nonbone marrow-derived circulating progenitor cells contribute to postnatal neovascularization following tissue ischemia. *Circ Res.* (2007) 100:581–9. doi: 10.1161/01.RES.0000259562.63718.35
50. King A, Balaji S, Keswani SG, Crombleholme TM. The role of stem cells in wound angiogenesis. *Adv Wound Care.* (2014) 3:614–25. doi: 10.1089/wound.2013.0497
51. Sheu JJ, Lee FY, Yuen CM, Chen YL, Huang TH, Chua S, et al. Combined therapy with shock wave and autologous bone marrow-derived mesenchymal stem cells alleviates left ventricular dysfunction and remodeling through inhibiting inflammatory stimuli, oxidative stress & enhancing angiogenesis in a swine myocardial. *Int J Cardiol.* (2015) 193:69–83. doi: 10.1016/j.ijcard.2015.03.044
52. Aicher A, Heeschen C, Sasaki Ki, Urbich C, Zeiher AM, Dimmeler S. Low-energy shock wave for enhancing recruitment of endothelial progenitor cells: a new modality to increase efficacy of cell therapy in chronic hind limb ischemia. *Circulation.* (2006) 114:2823–30. doi: 10.1161/CIRCULATIONAHA.106.628623
53. Can G, Daniela L, Markus T, Uwe P, Daniela L, Elke K, et al. Shock wave therapy improves cardiac function in a model of chronic ischemic heart failure: evidence for a mechanism involving VEGF signaling and the extracellular matrix. *J Am Heart Assoc.* (2018) 7:e010025. doi: 10.1161/JAHA.118.010025
54. Assmus B, Walter DH, Seeger FH, Leistner DM, Lutz A, Dimmeler S. Effect of shock wave – facilitated intracoronary cell therapy on LVEF in patients with chronic heart failure: the CELLWAVE randomized clinical trial. *JAMA.* (2013) 309:1622–31. doi: 10.1001/jama.2013.3527

55. Weihs AM, Fuchs C, Teuschl AH, Hartinger J, Slezak P, Mittermayr R, et al. Shock wave treatment enhances cell proliferation and improves wound healing by ATP release-coupled extracellular signal-regulated kinase (ERK) activation. *J Biol Chem.* (2014) 289:27090–104. doi: 10.1074/jbc.M114.580936
56. Priglinger E, Schuh CMAP, Steffenhagen C, Wurzer C, Maier J, Nuernberger S, et al. Improvement of adipose tissue–derived cells by low-energy extracorporeal shock wave therapy. *Cytotherapy.* (2017) 19:1079–95. doi: 10.1016/j.jcyt.2017.05.010
57. Abe Y, Ito K, Hao K, Shindo T, Ogata T, Kagaya Y, et al. Extracorporeal low-energy shock-wave therapy exerts anti-inflammatory effects in a rat model of acute myocardial infarction. *Circ J.* (2014) 78:2915–25. doi: 10.1253/circj.cj-14-0230
58. Wang L, Tian X, Cao Y, Ma X, Shang L, Li H, et al. Cardiac shock wave therapy improves ventricular function by relieving fibrosis through PI3K/Akt signaling pathway: evidence from a rat model of post-infarction heart failure. *Front Cardiovasc Med.* (2021) 8:563. doi: 10.3389/fcvm.2021.693875
59. Ito Y, Ito K, Shiroto T, Tsuburaya R, Yi GJ, Takeda M, et al. Cardiac shock wave therapy ameliorates left ventricular remodeling after myocardial ischemia-reperfusion injury in pigs in vivo. *Coron Artery Dis.* (2010) 21:304–11. doi: 10.1097/mca.0b013e32833aec62
60. Prabhu SD. Healing and repair after myocardial infarction: the forgotten but resurgent basophil. *J Clin Invest.* (2021) 131:e150555. doi: 10.1172/JCI150555
61. Nahrendorf M, Swirski FK, Aikawa E, Stangenberg L, Wurdinger T, Figueiredo JL, et al. The healing myocardium sequentially mobilizes two monocyte subsets with divergent and complementary functions. *J Exp Med.* (2007) 204:3037–47. doi: 10.1084/jem.20070885
62. Nahrendorf M, Pittet MJ, Swirski FK. Monocytes: protagonists of infarct inflammation and repair after myocardial infarction. *Circulation.* (2010) 121:2437–45. doi: 10.1161/CIRCULATIONAHA.109.916346
63. Holfeld J, Tepeköylü C, Reissig C, Lobenwein D, Scheller B, Kirchmair E, et al. Toll-like receptor 3 signalling mediates angiogenic response upon shock wave treatment of ischaemic muscle. *Cardiovasc Res.* (2016) 109:331–43. doi: 10.1093/cvr/cvv272
64. Ramnath D, Powell EE, Scholz GM, Sweet MJ. The toll-like receptor 3 pathway in homeostasis, responses to injury and wound repair. *Semin Cell Dev Biol.* (2017) 61:22–30. doi: 10.1016/j.semcdb.2016.08.014
65. Holfeld J, Tepekoylu C, Kozaryn R, Urbschat A, Zacharowski K, Grimm M, et al. Shockwave therapy differentially stimulates endothelial cells: implications on the control of inflammation via toll-like receptor 3. *Inflammation.* (2014) 37:65–70. doi: 10.1007/s10753-013-9712-1
66. Couper KN, Blount DG, Riley EM. IL-10: the master regulator of immunity to infection. *J Immunol.* (2008) 180:5771–7. doi: 10.4049/jimmunol.180.9.5771
67. Mantovani A, Sica A, Sozzani S, Allavena P, Vecchi A, Locati M. The chemokine system in diverse forms of macrophage activation and polarization. *Trends Immunol.* (2004) 25:677–86. doi: 10.1016/j.it.2004.09.015
68. Szabo SJ, Sullivan BM, Peng SL, Glimcher LH. Molecular mechanisms regulating Th1 immune responses. *Annu Rev Immunol.* (2003) 21:713–58. doi: 10.1146/annurev.immunol.21.120601.140942
69. Sukubo NG, Tibalt E, Respizzi S, Locati M, d'Agostino MC. Effect of shock waves on macrophages: a possible role in tissue regeneration and remodeling. *Int J Surg.* (2015) 24:124–30. doi: 10.1016/j.ijsu.2015.07.719
70. Tepeköylü C, Lobenwein D, Urbschat A, Graber M, Pechriggl EJ, Fritsch H, et al. Shock wave treatment after hindlimb ischaemia results in increased perfusion and M2 macrophage presence. *J Tissue Eng Regen Med.* (2018) 12:e486–94. doi: 10.1002/term.2317
71. Ciampa AR, de Prati AC, Amelio E, Cavalieri E, Persichini T, Colasanti M, et al. Nitric oxide mediates anti-inflammatory action of extracorporeal shock waves. *FEBS Lett.* (2005) 579:6839–45. doi: 10.1016/j.febslet.2005.11.023
72. Gotte G, Amelio E, Russo S, Marlinghaus E, Musci G, Suzuki H. Short-time non-enzymatic nitric oxide synthesis from L-arginine and hydrogen peroxide induced by shock waves treatment. *FEBS Lett.* (2002) 520:153–5. doi: 10.1016/s0014-5793(02)02807-7
73. Lee J, Sayed N, Hunter A, Au KF, Wong WH, Mocarski ES, et al. Activation of innate immunity is required for efficient nuclear reprogramming. *Cell.* (2012) 151:547–58. doi: 10.1016/j.cell.2012.09.034
74. Meng S, Zhou G, Gu Q, Chanda PK, Ospino F, Cooke JP. Transdifferentiation requires iNOS activation. *Circ Res.* (2016) 119:e129–38. doi: 10.1161/CIRCRESAHA.116.308263
75. Chanda PK, Meng S, Lee J, Leung HE, Chen K, Cooke JP. Nuclear S-nitrosylation defines an optimal zone for inducing pluripotency. *Circulation.* (2019) 140:1081–99. doi: 10.1161/CIRCULATIONAHA.119.042371
76. Lai L, Reineke E, Hamilton DJ, Cooke JP. Glycolytic switch is required for transdifferentiation to endothelial lineage. *Circulation.* (2019) 139:119–33. doi: 10.1161/CIRCULATIONAHA.118.035741
77. Sayed N, Wong WT, Ospino F, Meng S, Cooke JP. Transdifferentiation of human fibroblasts to endothelial cells: role of innate immunity. *Circulation.* (2015) 131:300–9.
78. Zhou G, Meng S, Li Y, Ghebre YT, Cooke JP. Optimal ROS signaling is critical for nuclear reprogramming. *Cell Rep.* (2016) 15:919–25. doi: 10.1016/j.celrep.2016.03.084
79. Meng S, Lv J, Chanda PK, Owusu I, Chen K, Cooke JP. Reservoir of fibroblasts promotes recovery from limb ischemia. *Circulation.* (2020) 142:1647–62. doi: 10.1161/CIRCULATIONAHA.120.046872
80. Martino F, Perestrelo AR, Vinarský V, Pagliari S, Forte G. Cellular mechanotransduction: from tension to function. *Front Physiol.* (2018) 9:824. doi: 10.3389/fphys.2018.00824
81. Hatanaka K, Ito K, Shindo T, Kagaya Y, Ogata T, Eguchi K, et al. Molecular mechanisms of the angiogenic effects of low-energy shock wave therapy: roles of mechanotransduction. *Am J Physiol Cell Physiol.* (2016) 311:C378–85. doi: 10.1152/ajpcell.00152.2016
82. Ni K, Wang C, Carnino JM, Jin Y. The evolving role of caveolin-1: a critical regulator of extracellular vesicles. *Med Sci.* (2020) 8:46.
83. Gollmann-Tepekoylu C, Polzl L, Graber M, Hirsch J, Nagele F, Lobenwein D, et al. miR-19a-3p containing exosomes improve function of ischemic myocardium upon shock wave therapy. *Cardiovasc Res.* (2019) 116:1226–36. doi: 10.1093/cvr/cvz209
84. Tepeköylü C, Primessnig U, Pölzl L, Graber M, Lobenwein D, Nägele F, et al. Shockwaves prevent from heart failure after acute myocardial ischaemia via RNA/protein complexes. *J Cell Mol Med.* (2017) 21:791–801. doi: 10.1111/jcmm.13021
85. Banerjee MN, Bolli R, Hare JM. Clinical studies of cell therapy in cardiovascular medicine. *Circ Res.* (2018) 123:266–87. doi: 10.1161/CIRCRESAHA.118.311217
86. Cassar A, Prasad M, Rodriguez-Porcel M, Reeder GS, Karia D, DeMaria AN, et al. Safety and efficacy of extracorporeal shock wave myocardial revascularization therapy for refractory angina pectoris. *Mayo Clin Proc.* (2014) 89:346–54. doi: 10.1016/j.mayocp.2013.11.017
87. Malhotra V, Rosen RJ, Slepian RL. Life-threatening hypoxemia after lithotripsy in an adult due to shock-wave-induced pulmonary contusion. *Anesthesiology.* (1991) 75:529–31. doi: 10.1097/00000542-199109000-00023
88. Pölzl L, Nägele F, Graber M, Hirsch J, Lobenwein D, Mitrovic M, et al. Safety and efficacy of direct cardiac shockwave therapy in patients with ischemic cardiomyopathy undergoing coronary artery bypass grafting (the CAST-HF trial): study protocol for a randomized controlled trial. *Trials.* (2020) 21:447. doi: 10.1186/s13063-020-04369-0

Conflict of Interest: JHo, MGi, and JC were shareholders of Heart Regeneration Technologies GmbH, an Innsbruck Medical University spin-off aiming to develop cardiac shockwave therapy (www.heart-regeneration.com).

The remaining authors declare that the research was conducted in the absence of any commercial or financial relationships that could be construed as a potential conflict of interest.

Publisher's Note: All claims expressed in this article are solely those of the authors and do not necessarily represent those of their affiliated organizations, or those of the publisher, the editors and the reviewers. Any product that may be evaluated in this article, or claim that may be made by its manufacturer, is not guaranteed or endorsed by the publisher.

frontiers | Frontiers in Cardiovascular Medicine

REVIEW
published: 08 July 2022
doi: 10.3389/fcvm.2022.933060

Metabolic Regulation of Cardiac Regeneration

Xuewen Duan[1], Xingguang Liu[2] and Zhenzhen Zhan[1]**

[1] Key Laboratory of Arrhythmias of the Ministry of Education of China, Institute of Heart Failure, Shanghai East Hospital, Tongji University School of Medicine, Shanghai, China, [2] Department of Pathogen Biology, Naval Medical University, Shanghai, China

The mortality due to heart diseases remains highest in the world every year, with ischemic cardiomyopathy being the prime cause. The irreversible loss of cardiomyocytes following myocardial injury leads to compromised contractility of the remaining myocardium, adverse cardiac remodeling, and ultimately heart failure. The hearts of adult mammals can hardly regenerate after cardiac injury since adult cardiomyocytes exit the cell cycle. Nonetheless, the hearts of early neonatal mammals possess a stronger capacity for regeneration. To improve the prognosis of patients with heart failure and to find the effective therapeutic strategies for it, it is essential to promote endogenous regeneration of adult mammalian cardiomyocytes. Mitochondrial metabolism maintains normal physiological functions of the heart and compensates for heart failure. In recent decades, the focus is on the changes in myocardial energy metabolism, including glucose, fatty acid, and amino acid metabolism, in cardiac physiological and pathological states. In addition to being a source of energy, metabolites are becoming key regulators of gene expression and epigenetic patterns, which may affect heart regeneration. However, the myocardial energy metabolism during heart regeneration is majorly unknown. This review focuses on the role of energy metabolism in cardiac regeneration, intending to shed light on the strategies for manipulating heart regeneration and promoting heart repair after cardiac injury.

Keywords: heart regeneration, cardiomyocyte proliferation, fatty acid metabolism, glucose metabolism, amino acid metabolism, metabolism regulation

OPEN ACCESS

Edited by:
Claudio de Lucia,
Scientific Clinical Institute Maugeri (ICS Maugeri), Italy

Reviewed by:
Felix B. Engel,
University Hospital Erlangen, Germany
Ahmed Mahmoud,
University of Wisconsin-Madison, United States
Mauro Giacca,
King's College London, United Kingdom

***Correspondence:**
Zhenzhen Zhan
zhanzz@tongji.edu.cn
Xingguang Liu
liuxg@immunol.org

Specialty section:
This article was submitted to Cardiovascular Biologics and Regenerative Medicine, a section of the journal Frontiers in Cardiovascular Medicine

Received: *30 April 2022*
Accepted: *13 June 2022*
Published: *08 July 2022*

Citation:
Duan X, Liu X and Zhan Z (2022) Metabolic Regulation of Cardiac Regeneration. Front. Cardiovasc. Med. 9:933060. doi: 10.3389/fcvm.2022.933060

INTRODUCTION

Heart failure is a burgeoning public health problem (1). It is a common and complex disease and has a poor prognosis in most patients. Ischemia is one of the main factors that contribute to heart failure. Following myocardial infarction (MI), the function and morphology of the cardiac cells begin to change. In the early phase of ischemia, cardiomyocytes lack oxygen and nutrients, resulting in a large-scale loss. Myofibroblasts in the heart became activated and produce collagen and other extracellular matrix components to compensate for the maintenance of the basic heart structure. In the later phase of ischemia, a large number of myofibroblasts accumulate, which thickens the ventricular wall and changes the mechanics of the heart, thereby impairing the cardiac pump function (2). As the proliferative capacity of adult cardiomyocytes is very low, they fail to repair the damaged area. This results in maladaptive cardiac remodeling and fibrosis, which ultimately progresses to an irreversible late-stage heart failure (3). With the exception of heart transplantation, current treatments, such as ventricular assist devices, fail to replenish the massive loss of cardiomyocytes

after injury. Xenotransplantation and cardiac tissue engineering are achieving the encouraging progress for replacing damaged heart tissues (4). However, cardiac regeneration through altering cardiomyocyte fate plasticity is emerging as a promising approach to compensate for the loss of functional cardiomyocytes and repair cardiac functions.

A previous study revealed that in several non-mammalian lower vertebrates, endogenous cardiac regeneration occurs after cardiac damage (5). However, there has been a long-standing assumption that the mammalian heart is a terminally differentiated organ and that the adult mammalian heart cells are incapable of cell division and proliferation. Intriguingly, a study by Engel et al. (6) for the first time showed that adult mammalian ventricular cardiomyocytes could be induced not only to enter the cell cycle but also to undergo cytokinesis resulting in cell division. However, previous research showed that neonatal mice possessed remarkable endogenous cardiomyocyte proliferation and cardiac regeneration capacity before postnatal day 7 (P7) (7). Further evidence revealed that the heart of P3 mice/rat could not regenerate anymore, which might be due to cell cycle withdrawal and changes in energy metabolism occurring around P3 in mice and rats (8). Thus, establishing a neonatal mouse cardiac regeneration model provides a way to elucidate the mechanisms of cardiac regeneration. After birth, there is a shift in the source of nutrition from placenta-dependent to postnatal nutrition. This in turn triggers a dramatic change in the availability of energy substrates and leads to a shift in the metabolism of cardiomyocytes. Moreover, from embryonic to adult life, the oxygen status alters, thereby shifting the energy metabolism of cardiomyocytes. Interestingly, the shift in myocardial energy metabolism coincides with the time point of cardiomyocyte cycle withdrawal and loss of myocardial regenerative capacity in postnatal mice (9). This raises a question whether changes in metabolism are the cause of cell cycle exit or a consequence thereof. To sum up, these researches insinuate that myocardial metabolism plays a key role in the regenerative capacity of the heart.

In this review, we summarize the changes in major energy metabolic pathways, including fatty acid oxidation, glycolysis, amino acid metabolism, and tricarboxylic acid cycle (TCA), occurring during heart regeneration. We also discuss the key metabolic targets that point the way to research on cardiac regeneration.

ENERGY METABOLISM IS INVOLVED IN HEART REGENERATION

Oxygen Content Is Closely Related to the Regenerative Capacity in Lower Vertebrates

Lower vertebrates, such as zebrafish (*Danio rerio*) and axolotl, have the incredible potential for heart regeneration. The Mexican cavefish have been reported to regenerate their hearts after an injury (10). Zebrafish have the ability to regenerate cardiac muscles throughout their lifetime (11). After removing 20% of the ventricular volume, the heart can be completely regenerated within 2 months, with myocardial contractility returning to normal levels (11). The reasons for the high regenerative capacity of lower vertebrates might be divided into three aspects. First, the circulatory system of zebrafish is relatively hypoxic. This is because the zebrafish heart consists of a single atrium and a single ventricle, causing mixing of arterial and venous blood, which leads to low oxygen content in circulating blood (12, 13). Second, previous research found that centrosomes were intact in cardiomyocytes of zebrafish and salamander, while in mammalian cardiomyocytes they were disintegrated, impairing proper cell division (14). Finally, zebrafish cardiomyocytes are small and mononuclear throughout their life cycle and maintain proliferative potential (13, 15, 16). In addition, the oxygen content in the natural aquatic habitat of zebrafish is 1/30 of that in atmospheric air (17, 18). A previous study found that hypoxia promoted myocardial regeneration by altering the metabolic state. In contrast, exposing zebrafish to hyperoxic water at 45 kPa (vs. normoxic water at 21 kPa) inhibited myocardial regeneration (19). In addition, the change in environmental oxygen level from embryonic to adult stage triggers a switch in energy metabolism of the postnatal heart, which generates mitochondrial reactive oxygen species (ROS). The DNA damage response (DDR) is triggered, and the cell cycle of postnatal cardiomyocytes is thus stalled (17). Moreover, a research found that ROS altered the activity of metabolically critical enzymes and hence played a role in cardiac regeneration of zebrafish. Since elevated H_2O_2 levels are detrimental, investigators identify protein tyrosine phosphatase 1b (Ptp1b) as a downstream target of ROS and propose that inhibition of Ptp1b promotes myocardial regeneration (20). In addition, MSI-1436, a small molecule inhibitor, selectively represses Ptp1b and hence promotes regeneration (21). Dual-specificity phosphatase 6 (Dusp6), a member of the PTP family, is sensitive to the redox effects of ROS. Moreover, the change in Dusp6 expression correlates with the regenerative window of the heart, which suggests Dusp6 might have a key role in the early cardiac regeneration process (22). Furthermore, by single-cell transcriptome analysis of regenerated zebrafish myocardium, researchers found that cardiomyocytes in the proliferative border zone underwent a shift in energy metabolism after heart cryoinjury (23). This suggests that proliferation and regeneration of cardiomyocytes after cardiac injury in zebrafish involve energy metabolism.

Energy Metabolism in Cardiac Regeneration of Mammals

Morphology of murine neonatal heart is similar to that of zebrafish heart (24). Hence, researchers turned their attention to find out whether mammalian heart could regenerate after damage. The size of human cardiomyocyte increases approximately 8.6-fold during the first 20 years of life (25). Although adult cardiomyocytes can temporarily self-renew, their self-renewal rate is extremely low (26). In addition, the regeneration ability of adult cardiomyocytes is very limited and is not enough to repair the damaged myocardial tissue. Hence,

adult mammalian myocardial tissue cannot regenerate after heart damage. However, recent data suggest that cardiomyocyte renewal occurs in adulthood in mammals including humans (27, 28). Interestingly, in 2011, researchers discovered that neonatal mice had an amazing myocardial regenerative potential (7). This study showed that 1-day-old newborn mice heart had the ability to regenerate resected myocardium after apical resection. Nonetheless, this regenerative ability is lost after 7 days of birth (7).

Further, on investigating the reasons for reduced regenerative capacity of adult mice, researchers found that differences in the type of energy metabolism were influential factors that determined the ability of the myocardium to regenerate. There are two main ways by which cardiac energy in mice is altered. On the one hand, a change in oxygen status from embryonic to postnatal causes a shift in cardiac metabolism. Due to exposure to relatively hypoxic environment, embryonic blood shunt circulation in the mammalian heart results in significant mixing of arteriovenous blood (29). However, after birth, the shift in circulation and the rapid increase in arterial oxygen change the oxygenation status of cardiomyocytes within minutes (17). Therefore, mammalian cardiomyocytes are capable of generating energy through metabolic conversion to adapt to high energy demands after birth (30). The main source of adenosine triphosphate (ATP) is cardiac metabolism, and ATP maintains cardiac homeostasis and function (31, 32). Mitochondria perform energy conversion, and more than 95% of the ATP is produced through energy substrates for the heart (33). After birth of mice, energy metabolism of neonatal cardiomyocytes changes, and the number of cardiomyocyte mitochondria dramatically increases in the adult heart (34). One research found that mitochondrial DNA copy number was lower in the neonatal murine heart compared with the adult murine heart (17). At present, many studies focus on understanding the regulation of mitochondrial metabolism in postnatal cardiomyocyte cycle arrest and influencing future regeneration strategies.

On the other hand, nutrient supply is altered after birth of mice (35), and the shift in metabolic pattern causes cardiomyocyte maturation and cell cycle exit (36). Previous studies on porcine and rabbit hearts indicated that postnatal cardiomyocytes underwent a shift in energy source compared with embryonic cardiomyocytes due to different nutrients (37, 38). Therefore, the increased oxygen content at sharp atmosphere stress and changes in metabolic matrix postnatally together alter the type of energy metabolism in cardiomyocytes and reduce their proliferation capacity (**Figure 1**). In all, the regenerative capacity of the myocardium is related to the metabolism of cardiomyocytes.

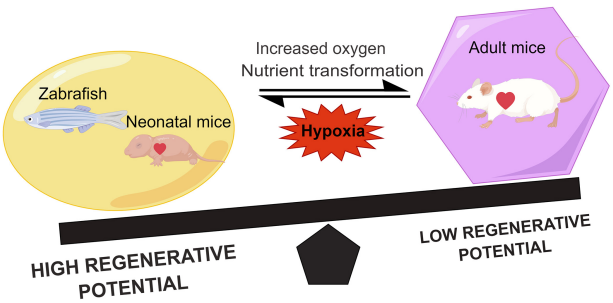

FIGURE 1 | Comparison of the regenerative capacity of representative lower vertebrates, neonatal, and adult mammals. Hypoxia can promote heart regeneration and increase the regenerative capacity. During the growth of neonatal mice, the shift in metabolic state of the heart due to the increased oxygen and nutrients leads to a decrease in the myocardial regenerative capacity.

HYPOXIA REGULATES METABOLIC REPROGRAMING TO PROMOTE CARDIAC REGENERATION

Hypoxia refers to reduced and insufficient oxygen supply, and it influences myocardial energy metabolism and cardiac contractile function (39, 40). Chronic hypoxia decreases the activity of fatty acid oxidase (40), which in turn reduces fatty acid uptake and oxidation in mitochondria (41). In addition, it increases glycolysis and glycolytic enzyme activity (42). Moreover, chronic hypoxia decreases mitochondrial utilization of fatty acid and pyruvate substrates and reduces the enzymatic activities of electron transport chain (ETC) complexes I, II, and IV in the mitochondria of cardiomyocytes, thereby lowering the production of ROS (43). Hence, the regenerated cardiomyocytes show characteristics of proliferative cardiomyocytes in the embryonic stage, which exhibits hypoxic environment.

Professor Sadek's team found that moderate hypoxia promoted myocardial regeneration after myocardial infarction (44). They reported that gradually reducing inhaled oxygen by 1% and maintaining oxygen concentration level at 7% for 2 weeks, reduced ROS production and DDR, however, restarted mitosis in cardiomyocytes. Hypoxia-inducible factor (HIF)-1 family adjusts the cells to hypoxic environment. HIF-1 is a class of specialized heterodimers composed of unstable alpha subunits (HIF-α). HIF-1α protein is steady under hypoxic conditions and activates transcription of multiple genes involved in glycolysis, fatty acid metabolism, mitochondrial metabolism, and cell cycle regulation (45). Stem cells or progenitor cells of some organs are relatively hypoxic and maintain their normal physiological functions by stabilizing the HIF-1α subunit (46). In 2012, researchers found that hypoxia promoted cardiomyocyte dedifferentiation and myocardial regeneration in adult zebrafish, and HIF-1α played the important role in this (19). However, another study found that the complete activation of HIF-1α signal led to the dilated cardiomyopathy and heart failure (47, 48). These findings suggest that the moderate activation of HIF-1α hypoxia signal may be a potential strategy for heart regeneration. In addition, the authors found that HIF-1α deficiency impaired glycolysis and inhibited proliferation of hypoxic fetal cardiomyocytes, which in turn led to transient reprograming of amino acid metabolism and activation of HIF2 (19, 49, 50). This shows that the embryonic heart is metabolically flexible.

In conclusion, chronic severe hypoxia enhances the expression of glycolytic and cell cycle genes, whereas it inhibits the

expression of fatty acid oxidation genes and cell cycle inhibitory genes (51), and thus, it metabolically reprograms embryonic heart. These genetic and metabolic changes promote myocardial regeneration, which is referred to as the hypoxia-induced cardiomyocyte proliferation and the infarcted zone revascularization.

DIFFERENT TYPES OF ENERGY METABOLISM AFFECT THE MYOCARDIAL REGENERATIVE CAPACITY

The heart is the most energy-intensive organ of the body (52). In the physiological state, the heart of adult mouse produces ATP in two ways to maintain its contractile function. Mitochondrial oxidative metabolism produces approximately 95% of the cardiac energy, while glycolysis produces only 5% of it. About 40–60% of the energy in mitochondrial oxidative metabolism is generated through free fatty acids and glucose metabolism, while the remainder of this is produced by the oxidation of ketones, lactate, and amino acids (53, 54). Compared with glucose oxidation, fatty acid oxidation requires more oxygen. Hence, the aerobic oxidation efficiency of glucose is higher than that of fatty acids (53). During the perinatal period, glycolysis and lactate oxidation are the main sources of cardiac ATP (55–57), while fatty acid oxidation produces only a small fraction of ATP (55). In the early postnatal period (from P1 to P7), glycolysis produces almost half of the ATP for the neonatal murine heart (55). While 7 days post-birth, glycolysis gradually decreases, providing only a small amount (10%) of ATP for cardiomyocyte metabolism. However, there is a significant increase in fatty acid oxidation to maintain cardiomyocyte energy metabolism (38, 55). In the neonatal period, the source of cardiac energy is β-oxidation of fatty acids, which produces ATP at levels close to those found in the heart of adult animals (58). The researchers measured metabolite levels, such as fatty acids, in the cardiac arteries of fetal, newborn (1–4 days), and juvenile (7 weeks) lambs (57, 59). They found that fatty acid flux was zero in the embryonic heart. Interestingly, there was an increase in fatty acids in the myocardium of newborn lambs, but there was no net flux of fatty acid (57). And the flux of fatty acids was increased in the juvenile lambs (57). Glucose and lactate were sources of energy metabolism for embryonic and neonatal (3–15 days) lamb hearts (60). In addition, a research found that fatty acids promoted proliferation of P4 cardiomyocytes but inhibited proliferation of P5 cardiomyocytes (61). In all, different developmental stages and oxygen levels result in altered energy sources for the mouse heart. This leads to varying metabolic states of cardiomyocytes that affect their proliferative capacity (**Figure 2**).

Fatty Acid Metabolism and Cardiac Regeneration

Studies indicate that fatty acid oxidation is the main source of cardiac energy for the adult heart (62). After entering cardiomyocytes, fatty acids generate ATP mainly through oxidation *via* the TCA in the mitochondria. Among all energy substrates, fatty acids produce the highest ATP content and have the highest oxygen demand. Therefore, fatty acids are myocardial energy substrates with the lowest metabolic efficiency (ATP production/oxygen consumption) (33).

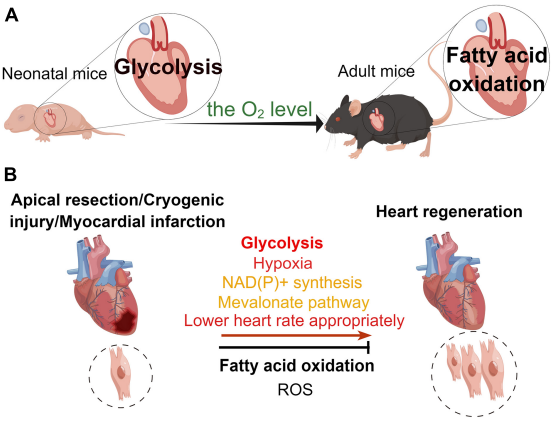

FIGURE 2 | Different metabolic patterns in physiological and pathological states affect the myocardial regenerative capacity. **(A)** Under physiological conditions, the main mode of metabolism in the murine neonatal heart is glycolysis, whereas that in the hearts of adult mice is fatty acid oxidation. **(B)** In the pathological state, glycolysis, hypoxia, NAD(P)+ synthesis, mevalonate pathway, and appropriate reduction in heart rate promote heart regeneration, while fatty acid oxidation and reactive oxygen species (ROS) inhibit myocardial regeneration in the neonatal mouse heart regeneration models (apical resection, cryoinjury, or myocardial infarction).

A research found that feeding fatty acid-deficient milk to postnatal mice prolonged the proliferation window of their hearts (63). Carnitine palmitoyltransferase 1 (CPT1) transfers fatty acids from the cytoplasm to the mitochondria and is the key enzyme regulating fatty acid oxidation. CPT1 activity in the neonatal murine heart is very low, while it increases significantly in the heart of a 7-day-old mouse, which coincides with the time when mammalian cardiomyocytes lose their ability to proliferate (64). One research found that etomoxir (ETO) could inhibit the activity of CPT1, thereby reducing fatty acid oxidation and promoting proliferation of neonatal mouse cardiomyocytes and heart regeneration in neonatal mice (61). Previous study showed that the low expression of carnitine palmitoyltransferase 2 (CPT2), which is an essential enzyme for fatty acid oxidation (65), could promote cardiomyocyte proliferation in P14 mice (66). Acyl-CoA synthetase long-chain family member 1 (ACSL1) mediates the uptake of cellular lipids and is a key enzyme regulating lipid metabolism. On examining the expression of glycolipid-related enzymes in heart tissue of mice at different ages, it was found that ASCL1 expression increases with the age of mice (67). Inhibition of ACSL1 expression with a corresponding decrease in cardiomyocyte lipid uptake in cardiomyocytes of adult mice post-MI and primary neonatal mouse cardiomyocytes upregulated the expression of cell cycle-activating genes, but downregulated the expression of cell cycle-inhibiting genes (67).

However, the view that fatty acid oxidation inhibits myocardial regeneration is still debatable. A research

found that peroxisome proliferator-activated receptor alpha (PPARα)-mediated β-oxidation of fatty acid promoted primary neonatal mouse cardiomyocyte hypertrophy and maturation and enhanced the presence of binucleated cardiomyocytes at postnatal day 5. Moreover, it caused the withdrawal of cardiomyocytes from cell cycle (61). Nevertheless, it is interesting to note that PPARα-mediated β-oxidation of fatty acid promoted G0/G1 cell cycle entry rate and proliferation of cardiomyocytes in mice at postnatal day 4 (61). What makes fatty acid oxidation has opposite regulatory effects on myocardial regeneration? In this context, the authors speculate that the reduced proliferation rate of cardiomyocytes at postnatal day 5 is due to the presence of binucleated cardiomyocytes and cardiomyocytes leaving the cell cycle (61). These results suggest that the effect of fatty acids on myocardial regeneration is inconclusive and needs to be studied in the future.

Glucose Metabolism and Cardiac Regeneration

Glycolysis is the primary mode of energy metabolism in the neonatal murine heart. A previous study reported that glycolysis promoted myocardial regeneration in adult zebrafish (68). Glucose is an important fuel and produces ATP through cytoplasmic glycolysis and mitochondrial oxidation in the heart. In the heart, glucose transporter 1 (GLUT1) and GLUT4 transport glucose into cardiomyocytes. Under physiological conditions, GLUT1, whose the expression increases by HIF-1α (69), is the main glucose transporter in embryonic and neonatal hearts (70, 71). A research found that overexpression of GLUT1 promoted glycolysis in the neonatal murine heart (72, 73) and increased nucleotide synthesis, thereby promoting myocardial regeneration by enhancing glucose metabolism after cryogenic injury in neonatal mice at P21 and P40 (9).

The key glycolytic enzymes play important roles in myocardial regeneration. Phosphofructokinase 2 (PFK2) regulates the level of fructose-2,6-bisphosphate (Fru-2,6-P2) by phosphorylating fructose-6-phosphate (F6P) during glycolysis. A research revealed that PFK2 could increase the contractility of hypoxic cardiomyocytes in mice, suggesting that it affects the metabolism of cardiomyocytes while maintaining their function (74). Pyruvate dehydrogenase kinase (PDK) inhibits the activity of pyruvate dehydrogenase (PDH). Previous studies found a significantly high expression of PDK in the infarct area of the adult heart (71) and zebrafish (68) after cryogenic injury of the heart. Moreover, PDK4 deletion promoted cardiac regeneration in adult mice after MI and proliferation of primary adult mouse cardiomyocytes by increasing glycolysis (63). In contrast, a report implied that PDK3 overexpression promoted cardiomyocyte proliferation by enhancing glycolysis during the early stages of cardiac regeneration in zebrafish, while there was no scar repair in the later stages (68). What is the reason for the difference between early and late stages? Since PDK3 overexpression can promote cardiomyocyte proliferation, can it also promote maturation of new cardiomyocytes to replace injured cardiomyocytes, and thus promote scar repair? Of note, PDK3 and PDK4 are both isozymes of PDK, so why do they exhibit opposite effects on cardiomyocyte proliferation? Their distributions are different, but the mechanisms involved require further study. Notably, studies have shown that M2-pyruvate kinase (PKM2) can promote the phosphopeptide pathway and inhibit oxidative stress (75, 76). A research found that knockout of PKM2 in mice post-MI promoted catenin beta 1 (Ctnnb1) translocation to the nucleus and trans-activation of key genes that mediate cell cycle progression (77). In zebrafish, the *Pkma2* gene encodes M2-pyruvate kinase. It has been found that pkma2 knockdown in zebrafish decreases glycolysis and thereby inhibits cardiomyocyte proliferation (68). Magadan's team found that overexpression of PKM2 promoted cardiomyocyte proliferation and regeneration after MI in adult mice, by increasing the expression of glucose-6-phosphate dehydrogenase (G6PD) (78). Therefore, PDK and PKM2 serve as promising treatment strategies for promoting cardiac repair and regeneration.

Interestingly, some key regulatory genes can regulate cardiac regeneration by promoting glycolysis. Myeloid ecotropic viral integration site 1 (MEIS1) is an important transcription factor that regulates the cardiomyocyte cycle. A research found that myocardium-specific knockout of MEIS1 in neonatal mice could extend the proliferation window of cardiomyocytes and that these cardiomyocytes could re-enter the cell cycle (79). Conversely, another finding indicated that inhibiting MEIS1 expression in primary fetal and neonatal sheep cardiomyocytes resulted in the increased mitochondrial activity and decreased glycolytic genes, leading to the enhanced cardiomyocyte maturation (80). The discrepancy in MEIS1 function between mice and sheep may be related to the differences in cardiomyocytes themselves from these two species. Further studies are needed to understand the mechanism of MEIS1 regulation on the metabolic state as well as the cell cycle of cardiomyocytes.

It is worth noting that cardiomyocyte proliferation-related pathways can also affect glycolysis. Furthermore, Yes-associated protein (YAP), a component of the Hippo pathway, is involved in glycolytic metabolism during heart development (81). A previous study found that the defect in Hippo pathway could activate Yap signaling to promote cardiomyocyte proliferation in adult mice (82–84). Studies on adult cardiomyocytes showed that direct and indirect target genes of activated Yap were associated with glycolysis and mitochondrial metabolism (84–86). In addition, the interaction between neuregulin 1 (NRG1) and its receptors, ErbB2 or ErbB4, facilitated glycolysis and inhibited mitochondrial oxidative phosphorylation (87), which was vital for cardiomyocyte proliferation in zebrafish (88) and newborn mice (89). Researchers showed that ErbB2 affected cardiac regeneration *via* downstream activation of YAP (81). Moreover, Wnt/β-catenin and ERK/MYC signaling pathways promoted glycolysis and cell proliferation by upregulating cyclin–CDK complex in neonatal mouse cardiomyocytes and immature human pluripotent stem cell-derived cardiomyocyte (hPSC-CM) (90, 91). Overexpression of c-Myc could promote glycolysis and cardiomyocyte proliferation in mice during both gestation and adult life (92). In contrast, Wnt/β-catenin signaling in adult mice was cardioprotective but

did not induce cardiomyocyte proliferation (91). Thus, the role of Wnt/β-catenin signaling in mice at different stages depends on the metabolic state of cardiomyocytes (91). Taken together, these pathways and genes can regulate cardiomyocyte proliferation by influencing glycolysis. However, which gene or component of the glycolytic pathway is affected is not yet elucidated. Moreover, whether these pathways only affect glycolysis or also affect lipid and other metabolic pathways remains to be determined.

In all, these studies indicate that glycolysis plays an essential role in modulating cardiomyocyte proliferation and cardiac regeneration after injury. As a result, targeting glucose metabolism is an interesting strategy to promote adult heart regeneration.

Amino Acid Metabolism Followed by Heart Regeneration

Cardiomyocytes require protein synthesis during growth, after birth, and during maturation. The increased protein synthesis results in the increased amino acid metabolism. Amino acid oxidation is also a source of cardiac ATP, with branched-chain amino acids (BCAAs) playing a major role. BCAA includes three amino acids, namely, leucine, isoleucine, and valine. Although BCAA oxidation produces only 2% of the total ATP generated by the heart (93), BCAAs play an important role in regulating cardiac signaling pathways, including insulin and mTOR signaling pathways (94).

Metabolomic analysis of mouse heart tissues at different developmental stages revealed that BCAAs showed differential levels in the heart at different developmental stages (95). Valine, leucine, and isoleucine concentrations gradually increased postnatally reaching a peak at day 9 and then decreased until they reached to the postnatal day 1 (P1) level on P23 (95). Most of the differentially expressed genes (DEGs) directly correlated with BCAA concentrations and were upregulated at the mRNA level between P9 and P23 (95). Therefore, we speculate whether inhibiting enzymes of the BCAA breakdown pathway could promote cardiomyocyte proliferation.

Glutamine is an amino acid transporter. Elevated glutamine expression in zebrafish and neonatal mouse cardiomyocytes activated the amino acid-driven mTOR signaling pathway, which promoted mitochondrial maturation and regulated cardiomyocyte proliferation (96). In addition, high concentrations of leucine and glutamate were found to activate the mTOR pathway and promote regeneration (96). Since leucine concentration rises in the postnatal week, does the concentration of BCAA also affect the ability of cardiomyocytes to proliferate? Researchers found that cardiomyocyte injury initiated Wnt/β-catenin signaling during zebrafish cardiomyocyte regeneration, which in turn initiated mTOR activation and metabolic remodeling (97). As previously described, Wnt/β-catenin signaling pathway promoted glycolysis and activated mTOR signaling pathway together with BCAAs (91, 98). This suggests that metabolic pathways are not independent but interact with each other. Thus, alterations in amino acid metabolism in cardiomyocytes affect their proliferation. However, studies in this research area are limited and need to be investigated in the future.

Tricarboxylic Acid Cycle Metabolites and Cardiac Regeneration

Tricarboxylic acid cycle occurs in the mitochondrial matrix. It is the metabolic center of the carbohydrate–lipid–amino acid linkage and the last metabolic pathway of the three nutrients. The transformation of energy metabolism and an increase in mitochondrial DNA after birth of mice lead to a significant increase in ROS produced by mitochondria (17). This increased ROS production damages proteins, lipids, and DNA and leads to cell cycle arrest (99–102). Therefore, clarifying the role of mitochondrial metabolites in regulating metabolic switch is essential for identifying metabolic targets that will promote adult heart regeneration.

To begin with, the primary approach to promote cardiomyocyte proliferation by inhibiting mitochondrial metabolism is to suppress ROS production by mitochondrial oxidation. Studies have reported that overexpression of mitochondrial catalase (mCAT) and the ROS scavenger *N*-acetylcysteine (NAC) system reduces DDR and promotes cardiomyocyte proliferation (17). Martin's team found that the activation of the antioxidant response after cardiac injury could reduce ROS and thereby promote cardiac repair (84). In cardiomyocytes, nuclear factor-erythroid-2-related factor 2 (Nrf2) directly regulates the expression and subcellular location of paired-like homeodomain 2 (Pitx2). Genome analysis indicated that Pitx2 activates genes in response to oxidative response by recruiting YAP (103). The knockdown of Pitx2 in the neonatal mouse heart leads to the failure of regeneration after cardiac injury. This suggests that antioxidant stress response pathways are critical for cardiomyocyte proliferation and cardiac regeneration (84). These include genes encoding ETC components and ROS eliminator that protect cells from ROS damage and promote cardiomyocyte regeneration (84, 103). Pei et al. (104) confirmed that hydrogen sulfide (H2S) could scavenge ROS, and hence, cardiomyocytes could re-enter the proliferation cycle. Researchers used propargylglycine (PAG) to inhibit H2S synthesis and found that it promoted the deposition of ROS in the murine neonatal heart and inhibited proliferation of cardiomyocytes (104). In contrast, sodium hydrosulfide hydrate (NaHS), an H2S donor, could reduce ROS accumulation and promote cardiomyocyte proliferation and regeneration by alleviating H2S-mediated cardiomyocyte injury (104). These findings reveal that antioxidant pathways play an important role in the regeneration of the heart. In addition, cardiac sarcomere contraction after birth promoted mitochondrial metabolism and activated p53 to produce ROS and DNA damage responses (105). It is known that p53 causes cardiomyocytes to exit the cell cycle by repressing *Cyclin B1* gene (106). We speculate that cardiac sarcomere contraction affects the proliferative capacity of cardiomyocytes by regulating their metabolism. However, this speculation remains to be validated. Overall, sarcomere disassembly in cardiomyocytes can preclude ROS production and promote proliferation of cardiomyocytes (105).

Succinate dehydrogenase (SDH) converts succinate to fumarate in the TCA cycle. During ischemia, succinate concentration increases and inhibits SDH activity. A previous study revealed that injecting succinic acid in neonatal mice

inhibited the proliferation of cardiomyocytes. In contrast, malonate, an SDH inhibitor, prolonged the regeneration window of the heart after birth and promoted the proliferation of cardiomyocytes and heart regeneration in adult mice after MI (107). Similarly, malonate injection in neonatal mice promoted myocardial regeneration after an injury (108). In addition, malonic acid induced the formation of a new coronary vascular system within the infarcted tissue (108), given that glycolysis promoted angiogenesis through apical cell formation (109). In short, malonate promotes proliferation of cardiomyocytes and vascularization would be a candidate therapeutic target. In terms of clinical translation, delivery of SDH inhibitors directly to the heart may be more effective because SDH deficiency can lead to tumorigenesis (108). Nonetheless, the role of other critical enzymes of the TCA cycle is not yet clear. In short, these studies suggest that in addition to glycolipid metabolism, changes in the activity of critical enzymes of the TCA cycle also have different impacts on cardiomyocyte proliferation.

SEVERAL BIOSYNTHETIC PATHWAYS AFFECT THE MYOCARDIAL REGENERATIVE CAPACITY

Interestingly, researchers found that in addition to classical metabolic pathways, several biosynthetic pathways could affect cardiomyocyte proliferation. A study revealed that simvastatin inhibited cardiomyocyte proliferation by inhibiting the mevalonate pathway of isoprene synthesis in cardiomyocytes of human-induced pluripotent stem cell (hiPSC)-cardiac organoids (110). Previous studies found that the expression of genes that regulated ancillary biosynthetic pathway enzymes increased in cardiomyocytes in response to cell cycle stimulation by four cell cycle factors, namely, cyclin B1, cyclin D1, CDK1, and CDK4. These enzymes were related to the hexosamine biosynthesis pathway (HBP), serine biosynthesis pathway, protein *O*-GlcNAcylation, and those involved in NAD(P)+ (111). Researchers found that overexpression of *O*-GlcNAcase (OGA) was associated with HBP and prevented cardiomyocyte cycle entry and progression, while knockdown of nicotinamide phosphoribosyltransferase (NAMPT) inhibited cycle entry of human iPSC cardiomyocytes (hiPSC-CM) (111). In addition, investigators found that overexpression of phosphoenolpyruvate carboxykinase 2 (PCK2), a gluconeogenic pathway enzyme that catalyzed the transformation of oxaloacetate to phosphoenolpyruvate, promoted proliferation of hiPSC-CM (111). In general, the crossover point metabolites in these synthetic pathways are provided by the glycolytic pathway, which again highlights the importance of the glycolytic pathway in the process of myocardial regeneration.

Previous research found that cardiomyocyte-specific overexpression of PPARδ induced cell cycle progression in cardiomyocytes after MI in mice and improved cardiac function (112). In addition, carbacyclin, a PPARδ activator, induced proliferation of neonatal and adult rat mononuclear cardiomyocytes *via* (PPARδ)/PDK1/Akt/GSK3β/β-catenin pathway (112). Glycogen synthase kinase-3β (GSK-3β) is a serine/threonine kinase originally identified as a key enzyme in glycogen synthesis. The authors do not indicate whether myocardial metabolism is altered during PPARδ-mediated myocardial regeneration. In addition, we cannot speculate whether PPARδ ultimately promotes myocardial regeneration by enhancing glycogen synthesis during this process. In contrast, previous studies have shown that PPARβ/δ overexpression in the heart increases glucose utilization by enhancing the expression of glucose transporter protein type 4 (Glut4) (113, 114). Can this be considered that PPARδ promotes cardiomyocytes to enter the cell cycle by enhancing glycolysis? This should be further delved into future studies.

In addition to its ability to regulate glycolysis, PKM2 has been reported to redirect glucose carbon flow to oxidative pentose phosphate pathway (PPP), thereby reducing oxidative stress and causing increased expression of cell cycle genes in postnatal cardiomyocytes (78). It has been shown that overexpression of the glucose transporter protein Glut1 leads to an increase in glucose metabolites and thus nucleotide supply in heart regeneration of neonatal mice (9). Recently, researchers have found that metabolic pathways can combine with biosynthetic pathways to affect the cardiomyocyte proliferation. Moderate heart rate reduction (HRR) can induce cardiomyocyte proliferation by altering the metabolic pattern of cardiomyocytes (115). On the one hand, glucose metabolism enzymes exert non-enzymatic activity to promote cell cycle progression. On the other hand, the PPP is activated to supply the biosynthetic metabolic demand required for promoting cardiomyocyte proliferation (115). In addition, researchers found that lowering the heart rate upregulated the expression of cyclin D1. Moreover, they also observed an increase in the nuclear transport of PKM2, which promoted cyclin D1 and thus restarted cardiomyocyte proliferation (115). This suggests that the three biological properties of cardiomyocytes, namely continuous rhythmic beating, unique energy metabolic pattern, and limited proliferative capacity, are intrinsically linked. In addition, PPP may be a prospective regenerative strategy for cardiac injury. Overall, reducing the heart rate of cardiomyocytes can affect their energy metabolic patterns and thus promote cardiac regeneration. However, some questions have not been explored yet. For example, what specific molecules and signaling pathways of PPP are affected by HRR regulation? Are there any other biosynthetic pathways that are also affected? Furthermore, this suggests that future studies combine metabolism and synthesis, rather than a single aspect, to explain the phenomenon of cardiac regeneration.

DIFFERENCES IN ENERGY METABOLISM BETWEEN THE FETAL HEART AND THE FAILING HEART

Heart failure is the end stage of many heart diseases, including the ischemic cardiomyopathy and non-ischemic cardiomyopathy. In this regard, MI is a common ischemic cardiomyopathy, while cardiac hypertrophy due to pressure-loaded cardiomyopathy is a

TABLE 1 | Summary of recent studies demonstrating the role of metabolism in heart regeneration.

Metabolic pathway	Species	Cells	Intervention targets	Results	References
Fatty acid oxidation	Postnatal mice	—	Fatty acid availability	Fatty acid-deficient milk prolonged the proliferation window of their hearts	(63)
	Infant mice	Primary neonatal mouse cardiomyocytes and primary 3-week-old mouse cardiomyocytes	Carnitine palmitoyltransferase 1 (CPT1)	Inhibition of the activity of CPT1 reduced fatty acid oxidation and increased cardiomyocyte proliferation	(61)
	P14 mice	—	Carnitine palmitoyltransferase 2 (CPT2)	Partial depletion of CPT2 enhanced cardiomyocyte proliferation	(66)
	Adult mice post-MI	Primary neonatal mouse cardiomyocytes	Acyl-CoA synthetase long-chain family member 1 (ACSL1)	ACSL1 knockdown inhibited fatty acid oxidation and enhanced the cardiomyocyte proliferation	(67)
	Infant mice	Primary neonatal mouse cardiomyocytes and primary 3-week-old mouse cardiomyocytes	Peroxisome proliferator-activated receptor (PPAR) α	PPARα-mediated fatty acid β-oxidation promoted proliferation of cardiomyocytes in P4 mice, while it enhanced the presence of binucleated cardiomyocytes in P5 mice	(61)
Glycolysis	Mouse embryo	Fatal mouse cardiomyocytes	Hypoxia-inducible factor α (HIF-α)	HIF-1α deficiency impaired glycolysis in mouse heart and inhibited cardiomyocyte proliferation	(19, 49, 50)
	Heart cryoinjury of P21 and P40 mice	—	Glucose transporter 1 (GLUT1)	The increase in glucose metabolism mediated by Glut1 overexpression promoted cardiac regeneration in neonatal mouse heart	(9)
	Adult mice after myocardial ischemia-reperfusion	Isolated adult mouse cardiomyocytes	Phosphofructokinase (PFK) 2	PFK2 overexpression increased the contractility of hypoxic cardiomyocytes	(74)
	Adult mice post-MI	Primary adult mouse cardiomyocytes	Pyruvate dehydrogenase kinase (PDK) 4	PDK4 deletion decreases DNA damage and promotes cardiac regeneration	(63)
	Zebrafish and adult mice post-MI	Neonatal rat CMs and adult mouse CMs	M2-pyruvate kinase (PKM2)	Pkma2 knockdown in zebrafish decreased glycolysis and inhibited cardiomyocyte proliferation; overexpression of PKM2 promoted cardiomyocyte proliferation and regeneration after MI in adult mice	(68, 78)
	Neonatal sheep	Primary fetal and neonatal sheep cardiomyocytes	Myeloid ecotropic viral integration site 1 (MEIS1)	Inhibiting MEIS1 expression promoted sheep cardiomyocyte maturation by decreasing glycolytic genes expression	(80)
	Adult murine heart	Adult mouse cardiomyocytes	Yes-associated protein (YAP)	Activation of YAP enhanced glycolysis and promoted cardiomyocyte proliferation	(84–86)
	Neonatal mice and zebrafish	Neonatal, juvenile and adult CMs	Neuregulin 1 (Nrg1)- Erbb2	Activation of Nrg1-Erbb2 enhanced glycolysis and promoted cardiomyocyte proliferation	(88, 89)
	Neonatal mice	Immature human pluripotent stem cell-derived cardiomyocyte (hPSC-CM)	β-catenin	Activation of β-catenin enhanced glycolysis and promoted cardiomyocyte proliferation	(91)
	Fatal and adult mice	Islet1^{+} cardiac progenitors and primary adult mouse cardiomyocytes	c-Myc	Activation of c-Myc enhanced glycolysis and promoted cardiomyocyte proliferation	(92)
TCA cycle metabolism	Neonatal mice	Primary neonatal mouse cardiomyocytes	Paired-like homeodomain 2 (Pitx2)	Pitx2 knockdown inhibited myocardial regeneration of neonatal mice through producing ROS	(84)
	Adult mice after MI and neonatal mice	Adult mouse cardiomyocytes	Succinate dehydrogenase (SDH)	Malonate (SDH inhibitor) promoted adult mouse cardiomyocyte proliferation by reducing succinate accumulation	(107)
Anabolic pathways	Neonatal mice and adult mice	Human PSC-cardiac organoids and hPSC-derived cardiomyocytes (hPSC-CM)	Simvastatin	Simvastatin suppressed cardiomyocyte proliferation by inhibiting the mevalonate pathway of isoprene synthesis	(110)
	—	Human iPSC cardiomyocytes (hiPSC-CM)	*O*-GlcNAcase (OGA)	Overexpression of *O*-GlcNAcase (OGA) was associated with HBP and prevented cardiomyocyte cell cycle entry	(111)
	—	Human iPSC cardiomyocytes (hiPSC-CM)	Nicotinamide phosphoribosyltransferase (NAMPT)	Knockdown of (NAMPT) inhibited cardiomyocyte cycle entry	(111)
	—	Human iPSC cardiomyocytes (hiPSC-CM)	Phosphoenolpyruvate carboxykinase 2 (PCK2)	Overexpression of PCK2 promoted proliferation of hiPSC-CM	(111)

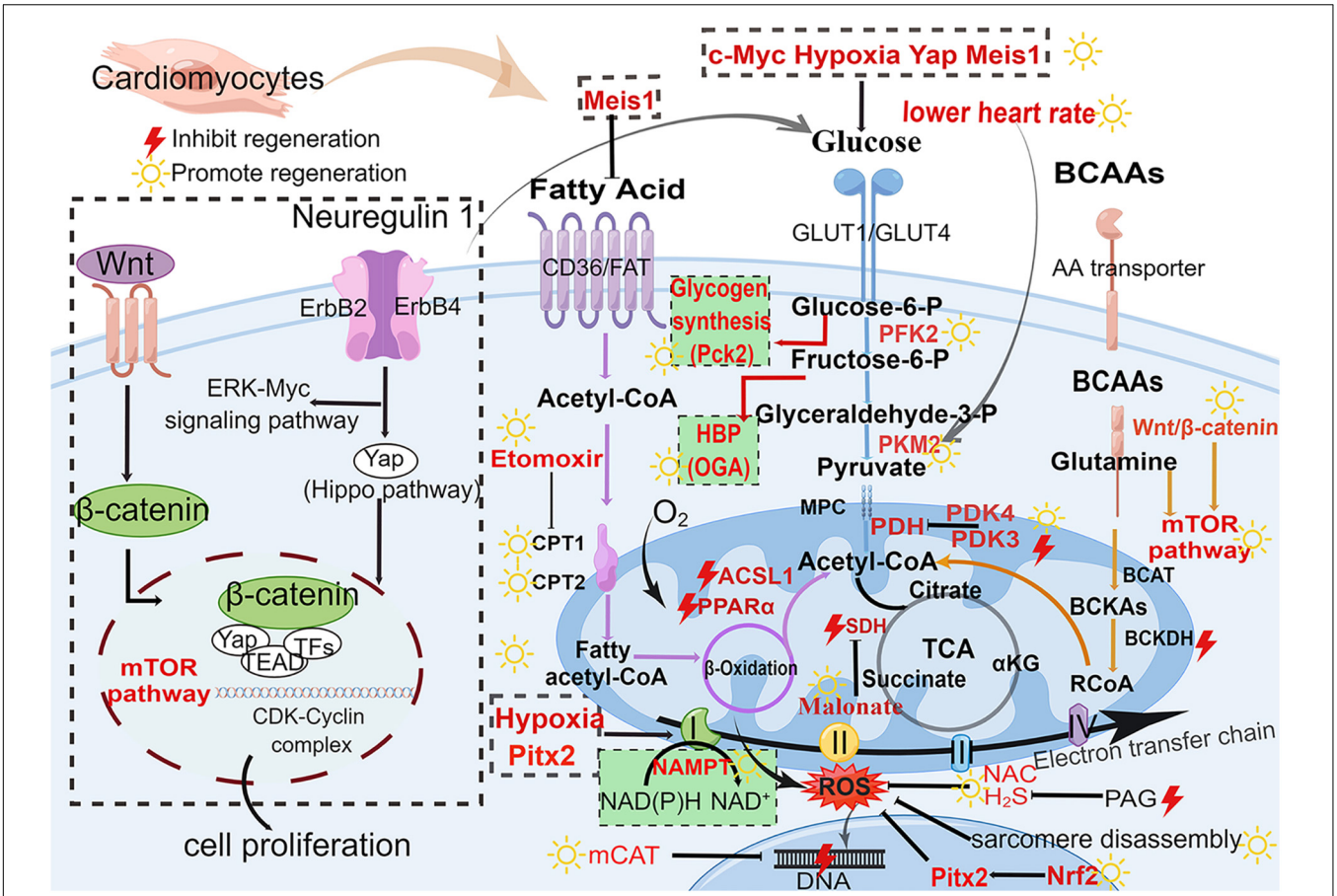

FIGURE 3 | Major metabolic pathways and signaling pathways in heart regeneration after cardiac injury. Glucose metabolism (blue), fatty acid metabolism (purple), BCAA metabolism (orange), and biosynthetic pathways (green background). The boxed section shows the factors affecting the metabolic pathways. Wnt/β-catenin pathway and Nrg1-ErbB pathway affect the metabolism of heart regeneration. Acetyl-CoA is the final effector of these three metabolism pathways (fatty acid oxidation, glycolysis, and amino acid metabolism) and regulates the initiation of the TCA cycle. GLUT, glucose transporter type; Glucose-6-P, glucose-6-phosphate; Fructose-6-P, fructose-6-phosphate; Glyceraldehyde-3-P, glyceraldehyde-3-phosphate; PFK, phosphofructokinase; PKM2, M2-pyruvate kinase; PDK, pyruvate dehydrogenase kinase; PDH, pyruvate dehydrogenase; CD36, cluster of differentiation; FAT, fatty acid transport carrier; CPT, carnitine palmitoyltransferase; BCAAs, branched-chain amino acids; BCAT, branched-chain amino acid transferase; BCKA, branched-chain alpha-keto acids; BCKDH, branched-chain alpha-keto acid dehydrogenase; mTOR, mammalian target of rapamycin; TCA, tricarboxylic acid cycle; SDH, succinate dehydrogenase; αKG, α-ketoglutarate; ROS, reactive oxygen species; H_2S, hydrogen sulfide; NAC, *N*-acetylcysteine; NAMPT, nicotinamide phosphoribosyltransferase; PAG, propargylglycine; mCAT, mitochondrial catalase; Pitx2, paired-liked homeodomain transcription factor 2; Nrf2, nuclear factor-erythroid-2-related factor 2; CDK, cyclin-dependent kinases; HBP, hexosamine biosynthesis pathway; Pck2, phosphoenolpyruvate carboxykinase 2; OGA, *O*-GlcNAcase. The yellow sun represents the promotion of heart regeneration, while the red lightning represents the inhibition of heart regeneration.

common non-ischemic cardiomyopathy. These processes include a wide range of remodeling in metabolism, cardiac structure, and cardiac electrophysiology (116). There is growing evidence that metabolic remodeling precedes most pathological processes and may play an important role in myocardial hypertrophy and heart failure (33, 117–119). In the failing heart, mitochondrial ROS production increases and also mitochondrial autophagy decreases. This results in the impaired mitochondrial function and reduced mitochondrial oxidative metabolism (120, 121). Hence, to increase the ATP supply, there is a compensatory increase in glycolysis (122). In addition, the energy metabolism shifts to a "fetal"-like pattern of energy substrate metabolism after cardiac hypertrophy (123, 124). That is, glycolysis increases and fatty acid oxidation decreases in pressure-overload cardiac hypertrophy (122, 125).

Although major changes in glycolysis and fatty acid oxidation in both failing and hypertrophic hearts resemble the major metabolic pattern of the embryonic heart, the cardiomyocyte proliferation capacity varies. For this reason, the specific metabolic patterns in the embryonic and failing hearts are intrinsically different. The primary difference is the substrate of energy metabolism and the way of metabolism.

In the ischemic heart, anaerobic glycolysis is the main source of cardiac ATP and leads to the production of lactate (126). In the absence of blood perfusion, glucose is not available to cardiomyocytes, and hence, previously stored glycogen is used to produce ATP (127). Since glycolysis produces less ATP than oxidative phosphorylation, ATP is consumed more than it is produced. The intracellular lactic acid accumulates, leading to cellular acidosis, and inhibits enzymes of the glycolytic

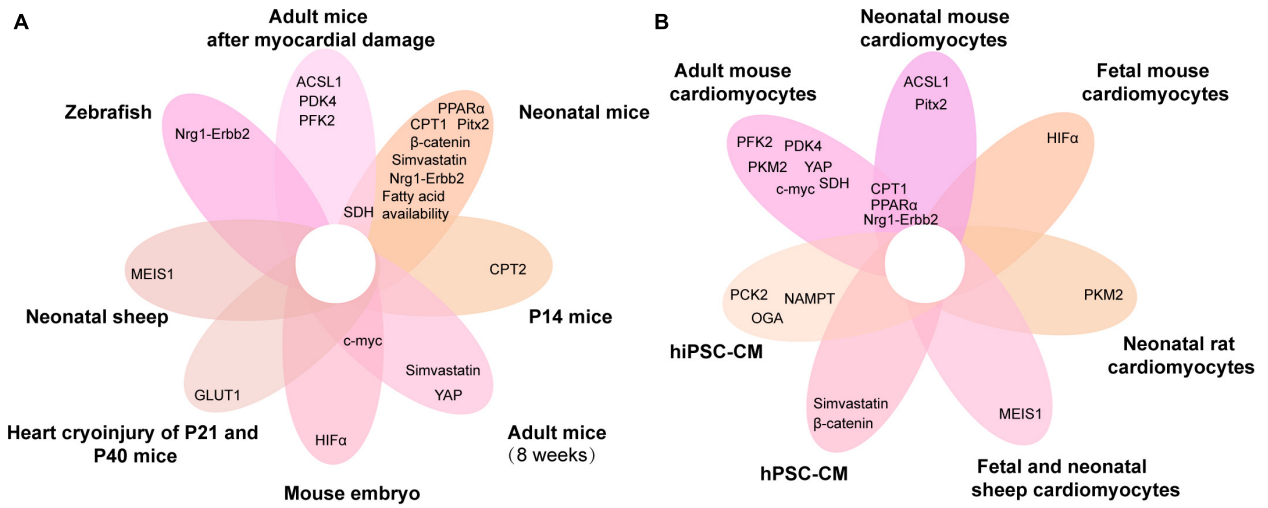

FIGURE 4 | Venn diagram of metabolic genes associated with cardiomyocyte proliferation overlapping in different animals and cardiomyocytes. **(A,B)** The metabolic genes associated with cardiomyocyte proliferation in different animals **(A)** and cardiomyocytes **(B)**. ACSL1, acyl-CoA synthetase long-chain family member 1; PFK, phosphofructokinase 2; PPARα, peroxisome proliferator-activated receptor; HIF-α, hypoxia-inducible factor α; PDK4, pyruvate dehydrogenase kinase 4; MEIS1, myeloid ecotropic viral integration site 1; PCK2, phosphoenolpyruvate carboxykinase 2; CPT, carnitine palmitoyltransferase; NAMPT, nicotinamide phosphoribosyltransferase; YAP, yes-associated protein; Nrg1, neuregulin 1; SDH, succinate dehydrogenase; GLUT1, glucose transporter 1; Pitx2, paired-like homeodomain 2; hiPSC-CM, human-induced pluripotent stem cell cardiomyocytes; hPSC-CM, human pluripotent stem cell-derived cardiomyocytes; P14, postnatal day 14; P21, postnatal day 21; P40, postnatal day 40.

pathway (116). Hence, the efficiency of glycolysis decreases during prolonged ischemia (127). Glycolysis ceases despite the availability of glycogen stores in cardiomyocytes (127). In addition, the lack of blood perfusion leads to the accumulation of intracellular protons that inhibits glycolysis in a feedback manner (128, 129). However, during the embryonic period, the heart obtains energy mainly through glucose. Due to low oxygen concentration during the embryonic period, the embryonic heart produces energy mainly through anaerobic glycolysis, which promotes heart regeneration (68). This suggests that the substrates of energy metabolism are different in the ischemic and regenerative heart.

On the one hand, researchers found that aerobic glycolysis was the main source of cardiac ATP in pressure-overload-induced heart failure (130–132), whereas, anaerobic glycolysis was the main source of cardiac ATP during myocardial regeneration in neonatal mice (133). On the other hand, glucose oxidation was lower in hypertrophied hearts than that in non-hypertrophied hearts (134, 135). When the heart rates were appropriately reduced, P1 cardiomyocytes were more dependent on glucose oxidation (115). This suggests that glucose oxidation promotes myocardial proliferation. Thus, regenerative and hypertrophic hearts are metabolized in different ways. Besides, researchers tested 13 key genes for energy metabolic substrates, including "adult" isoform genes and "fetal" isoform genes. They found that the expression of "adult" isoform of metabolic genes was reduced in the failing adult heart (124). This suggests that the reversion of the metabolic pattern in the failing heart is similar to the metabolic pattern of the embryonic heart (124). However, some studies had different conclusions. It was found that fatty acid oxidation (FAO) was either unchanged or increased, whereas glycolysis was either unchanged or decreased in the hypertrophied heart (132). Another research showed that myocardial FAO was unchanged, glycolysis was slightly reduced, and glucose and lactate oxidation was decreased in angiotensin II-induced myocardial hypertrophy (136). These discrepancies suggest that the metabolism of failing and regenerating hearts is different. Hence, the failing cardiac metabolism evolving from infarction and myocardial hypertrophy is different from the cardiac metabolism of neonatal mice.

CONCLUDING REMARKS AND PERSPECTIVES

Heart failure is by far the leading cause of mortality and disability throughout the world. Neonatal mice have an ability of myocardial regeneration and thus serve as a model for the treatment of heart failure. In this review, we summarize the current status of research on the metabolic regulation of myocardial regeneration, including recent findings and controversies (**Table 1** and **Figure 3**). Glycolipid–amino acid metabolism and biosynthesis are critical for the regulation of heart regeneration. Based on this, changing metabolism of related components, making cardiomyocytes to re-enter the cell cycle, promoting proliferation of cardiomyocytes, and enhancing cardiac regeneration serve as effectives therapies for heart diseases that eventually evolve into heart failure (**Figure 4** and **Table 1**). However, further studies are required to find solutions for the following problems: For example, several metabolic pathways are closely related to each other, so which

molecule or mechanism controls the direction of metabolic changes? What are the mechanisms by which the metabolic alterations eventually affect the cardiomyocytes proliferation and heart regeneration? Many metabolisms end up affecting the intranuclear epigenetic mechanisms. So, whether the combination of metabolism and epigenesis influences the process of heart regeneration? In addition to the four major metabolisms discussed in this review, are other metabolic pathways involved in the regulation of cardiac regeneration? For example, is the current and popularly studied novel metabolism of metal ions (iron and copper metabolism) related to other heart diseases?

The primary step of heart regeneration is to promote the cardiomyocytes to enter the cell cycle for division and proliferation. The interphase of the cell cycle is metabolically active and is the period during which the cells synthesize various enzymes, RNA, DNA, and proteins. During the S-phase, the cell cycle can be promoted by metabolic enzymes and proliferation pathways that target nucleic acid and protein synthesis, thereby promoting entry of cardiomyocytes into the cell cycle. However, specific biosynthetic pathways and metabolic enzymes need to be further explored, in order to increase the proliferative capacity of cardiomyocytes.

Certain questions are still unanswered. For example, are there other cardiac component cells (such as immune cells, endothelial cells, and fibroblasts) that interact with cardiomyocytes to influence their metabolism and thus alter their proliferative potential? Macrophages are required for myocardial regeneration in neonatal mice (137). However, it is unclear whether macrophages reprogram cardiomyocyte metabolism through intercellular interaction or paracrine effects. The angiogenesis of vascular endothelium supports regenerating cardiomyocytes after MI (138). The vascular endothelium supplies paracrine factors to cardiomyocytes so that they participate in regeneration. However, whether it affects the metabolism of cardiomyocytes is unclear. Besides, the investigators suggest that *in situ* modulation of cardiac cells in infarct foci can promote cardiomyocyte proliferation to repair scars and thus avoids the need of transplantation (139). Cardiac fibroblasts constitute a large proportion of the cardiac cells, and previous studies suggest that the cocktail therapy could potentially reprogram the fibroblasts in infarct foci directly into cardiomyocytes by modulating the transcription factors (139). Nonetheless, it is unclear whether cardiomyocyte metabolism is altered in this case? In addition, is it possible to enhance the proliferation of cardiomyocytes directly with small molecule drug-targeted metabolites?

Currently, hypoxia-induced glycolysis is the most studied among the metabolic pathways and has the greatest impact on myocardial regeneration. In future, translational studies can be conducted in depth from glycolysis to provide new targets for future clinical translation. It is important to further explore the relationship between myocardial regeneration mechanisms and changes in myocardial energy metabolism. However, we should note that almost none of the published studies have proven that their manipulations improve cardiac function by directly increasing the number of cardiomyocytes. The improved heart function is mainly correlated with the enhanced cell cycle activity and the improved functioning of the remaining cardiomyocytes, which might be due to a metabolic shift. Thus, it is essential to uncover the signaling pathways and key regulatory factors that affect energy metabolism accompanied by myocardial regeneration to develop effective therapeutic approaches. In all, we are optimistic that it will be possible to achieve great progress in human heart regeneration.

AUTHOR CONTRIBUTIONS

ZZ and XL conceived and designed the study and revised the manuscript. XD analyzed the data and wrote the manuscript. All authors listed and approved the manuscript for publication.

FUNDING

This work was supported by the National Key R&D Program of China (2019YFA0801502), the National Natural Science Foundation of China (82070415, 82071790, and 81771695), the Shuguang Program sponsored by Shanghai Education Development Foundation and Shanghai Municipal Education Commission (19SG17 and 18SG33), and the Shanghai Science & Technology Development Foundation (AX-2105).

ACKNOWLEDGMENTS

We thank Figdraw (www.figdraw.com) for the help in drawing the figures.

REFERENCES

1. Eriksson H. Heart failure: a growing public health problem. *J Intern Med.* (1995) 237:135–41. doi: 10.1111/j.1365-2796.1995.tb01153.x
2. Laflamme MA, Zbinden S, Epstein SE, Murry CE. Cell-based therapy for myocardial ischemia and infarction: pathophysiological mechanisms. *Annu Rev Pathol.* (2007) 2:307–39. doi: 10.1146/annurev.pathol.2.010506.092038
3. Laflamme MA, Murry CE. Heart regeneration. *Nature.* (2011) 473:326–35. doi: 10.1038/nature10147
4. Reardon S. First pig-to-human heart transplant: what can scientists learn? *Nature.* (2022) 601:305–6. doi: 10.1038/d41586-022-00111-9
5. Becker RO, Chapin S, Sherry R. Regeneration of the ventricular myocardium in amphibians. *Nature.* (1974) 248:145–7. doi: 10.1038/248145a0
6. Engel FB, Schebesta M, Duong MT, Lu G, Ren S, Madwed JB, et al. P38 map kinase inhibition enables proliferation of adult mammalian cardiomyocytes. *Genes Dev.* (2005) 19:1175–87. doi: 10.1101/gad.1306705
7. Porrello ER, Mahmoud AI, Simpson E, Hill JA, Richardson JA, Olson EN, et al. Transient regenerative potential of the neonatal mouse heart. *Science.* (2011) 331:1078–80. doi: 10.1126/science.1200708
8. Notari M, Ventura-Rubio A, Bedford-Guaus SJ, Jorba I, Mulero L, Navajas D, et al. The local microenvironment limits the regenerative potential of the mouse neonatal heart. *Sci Adv.* (2018) 4:eaao5553. doi: 10.1126/sciadv.aao5553
9. Fajardo VM, Feng I, Chen BY, Perez-Ramirez CA, Shi B, Clark P, et al. Glut1 overexpression enhances glucose metabolism and promotes neonatal heart regeneration. *Sci Rep.* (2021) 11:8669. doi: 10.1038/s41598-021-88159-x

10. Stockdale WT, Lemieux ME, Killen AC, Zhao J, Hu Z, Riepsaame J, et al. Heart regeneration in the Mexican cavefish. *Cell Rep.* (2018) 25:1997–2007.e7. doi: 10.1016/j.celrep.2018.10.072
11. Poss KD, Wilson LG, Keating MT. Heart regeneration in zebrafish. *Science.* (2002) 298:2188–90. doi: 10.1126/science.1077857
12. Staudt D, Stainier D. Uncovering the molecular and cellular mechanisms of heart development using the zebrafish. *Annu Rev Genet.* (2012) 46:397–418. doi: 10.1146/annurev-genet-110711-155646
13. Leone M, Magadum A, Engel FB. Cardiomyocyte proliferation in cardiac development and regeneration: a guide to methodologies and interpretations. *Am J Physiol Heart Circ Physiol.* (2015) 309:H1237–50. doi: 10.1152/ajpheart.00559.2015
14. Zebrowski DC, Vergarajauregui S, Wu CC, Piatkowski T, Becker R, Leone M, et al. Developmental alterations in centrosome integrity contribute to the post-mitotic state of mammalian cardiomyocytes. *Elife.* (2015) 4:e05563. doi: 10.7554/eLife.05563
15. Poss KD. Getting to the heart of regeneration in zebrafish. *Semin Cell Dev Biol.* (2007) 18:36–45. doi: 10.1016/j.semcdb.2006.11.009
16. Wills AA, Holdway JE, Major RJ, Poss KD. Regulated addition of new myocardial and epicardial cells fosters homeostatic cardiac growth and maintenance in adult zebrafish. *Development.* (2008) 135:183–92. doi: 10.1242/dev.010363
17. Puente BN, Kimura W, Muralidhar SA, Moon J, Amatruda JF, Phelps KL, et al. The oxygen-rich postnatal environment induces cardiomyocyte cell-cycle arrest through DNA damage response. *Cell.* (2014) 157:565–79. doi: 10.1016/j.cell.2014.03.032
18. Rees BB, Sudradjat FA, Love JW. Acclimation to hypoxia increases survival time of zebrafish, danio rerio, during lethal hypoxia. *J Exp Zool.* (2001) 289:266–72. doi: 10.1002/1097-010x(20010401/30)289:43.0.co;2-5
19. Jopling C, Suñé G, Faucherre A, Fabregat C, Izpisua Belmonte JC. Hypoxia induces myocardial regeneration in zebrafish. *Circulation.* (2012) 126:3017–27. doi: 10.1161/circulationaha.112.107888
20. Helston O, Amaya E. Reactive oxygen species during heart regeneration in zebrafish: lessons for future clinical therapies. *Wound Repair Regen.* (2021) 29:211–24. doi: 10.1111/wrr.12892
21. Smith AM, Maguire-Nguyen KK, Rando TA, Zasloff MA, Strange KB, Yin VP. The protein tyrosine phosphatase 1b inhibitor Msi-1436 stimulates regeneration of heart and multiple other tissues. *NPJ Regen Med.* (2017) 2:4. doi: 10.1038/s41536-017-0008-1
22. Missinato MA, Saydmohammed M, Zuppo DA, Rao KS, Opie GW, Kühn B, et al. Dusp6 attenuates Ras/Mapk signaling to limit zebrafish heart regeneration. *Development.* (2018) 145:dev157206. doi: 10.1242/dev.157206
23. Honkoop H, de Bakker DE, Aharonov A, Kruse F, Shakked A, Nguyen PD, et al. Single-cell analysis uncovers that metabolic reprogramming by Erbb2 signaling is essential for cardiomyocyte proliferation in the regenerating heart. *Elife.* (2019) 8:e50163. doi: 10.7554/eLife.50163
24. Rubin N, Harrison MR, Krainock M, Kim R, Lien CL. Recent advancements in understanding endogenous heart regeneration-insights from adult zebrafish and neonatal mice. *Semin Cell Dev Biol.* (2016) 58:34–40. doi: 10.1016/j.semcdb.2016.04.011
25. Li F, Wang X, Capasso JM, Gerdes AM. Rapid transition of cardiac myocytes from hyperplasia to hypertrophy during postnatal development. *J Mol Cell Cardiol.* (1996) 28:1737–46. doi: 10.1006/jmcc.1996.0163
26. Ali SR, Hippenmeyer S, Saadat LV, Luo L, Weissman IL, Ardehali R. Existing cardiomyocytes generate cardiomyocytes at a low rate after birth in mice. *Proc Natl Acad Sci U S A.* (2014) 111:8850–5. doi: 10.1073/pnas.1408233111
27. Bergmann O, Bhardwaj RD, Bernard S, Zdunek S, Barnabé-Heider F, Walsh S, et al. Evidence for cardiomyocyte renewal in humans. *Science.* (2009) 324:98–102. doi: 10.1126/science.1164680
28. Bergmann O, Zdunek S, Felker A, Salehpour M, Alkass K, Bernard S, et al. Dynamics of cell generation and turnover in the human heart. *Cell.* (2015) 161:1566–75. doi: 10.1016/j.cell.2015.05.026
29. Dawes GS, Mott JC, Widdicombe JG. The foetal circulation in the lamb. *J Physiol.* (1954) 126:563–87. doi: 10.1113/jphysiol.1954.sp005227
30. Vivien CJ, Hudson JE, Porrello ER. Evolution, comparative biology and ontogeny of vertebrate heart regeneration. *NPJ Regen Med.* (2016) 1:16012. doi: 10.1038/npjregenmed.2016.12
31. Neely JR, Morgan HE. Relationship between carbohydrate and lipid metabolism and the energy balance of heart muscle. *Annu Rev Physiol.* (1974) 36:413–59. doi: 10.1146/annurev.ph.36.030174.002213
32. Kolwicz SC Jr., Purohit S, Tian R. Cardiac metabolism and its interactions with contraction, growth, and survival of cardiomyocytes. *Circ Res.* (2013) 113:603–16. doi: 10.1161/circresaha.113.302095
33. Doenst T, Nguyen TD, Abel ED. Cardiac metabolism in heart failure: implications beyond ATP production. *Circ Res.* (2013) 113:709–24. doi: 10.1161/circresaha.113.300376
34. Ritterhoff J, Tian R. Metabolism in cardiomyopathy: every substrate matters. *Cardiovasc Res.* (2017) 113:411–21. doi: 10.1093/cvr/cvx017
35. Maroli G, Braun T. The long and winding road of cardiomyocyte maturation. *Cardiovasc Res.* (2021) 117:712–26. doi: 10.1093/cvr/cvaa159
36. Mills RJ, Titmarsh DM, Koenig X, Parker BL, Ryall JG, Quaife-Ryan GA, et al. Functional screening in human cardiac organoids reveals a metabolic mechanism for cardiomyocyte cell cycle arrest. *Proc Natl Acad Sci U S A.* (2017) 114:E8372–81. doi: 10.1073/pnas.1707316114
37. Ascuitto RJ, Ross-Ascuitto NT, Chen V, Downing SE. Ventricular function and fatty acid metabolism in neonatal piglet heart. *Am J Physiol.* (1989) 256:H9–15. doi: 10.1152/ajpheart.1989.256.1.H9
38. Lopaschuk GD, Spafford MA. Energy substrate utilization by isolated working hearts from newborn rabbits. *Am J Physiol.* (1990) 258:H1274–80. doi: 10.1152/ajpheart.1990.258.5.H1274
39. Essop MF. Cardiac metabolic adaptations in response to chronic hypoxia. *J Physiol.* (2007) 584:715–26. doi: 10.1113/jphysiol.2007.143511
40. Cole MA, Abd Jamil AH, Heather LC, Murray AJ, Sutton ER, Slingo M, et al. On the pivotal role of PPARα in adaptation of the heart to hypoxia and why fat in the diet increases hypoxic injury. *Faseb J.* (2016) 30:2684–97. doi: 10.1096/fj.201500094R
41. Daneshrad Z, Garcia-Riera MP, Verdys M, Rossi A. Differential responses to chronic hypoxia and dietary restriction of aerobic capacity and enzyme levels in the rat myocardium. *Mol Cell Biochem.* (2000) 210:159–66. doi: 10.1023/a:1007137909171
42. Dang YM, Huang YS, Zhou JL, Zhang JP, Yan H, Zhang M. [An experimental study on the influence of hypoxia induction Factor-1alpha on the glycolysis of the rat myocardial cell under hypoxic condition]. *Zhonghua Shao Shang Za Zhi.* (2005) 21:339–42.
43. Heather LC, Cole MA, Tan JJ, Ambrose LJ, Pope S, Abd-Jamil AH, et al. Metabolic adaptation to chronic hypoxia in cardiac mitochondria. *Basic Res Cardiol.* (2012) 107:268. doi: 10.1007/s00395-012-0268-2
44. Nakada Y, Canseco DC, Thet S, Abdisalaam S, Asaithamby A, Santos CX, et al. Hypoxia induces heart regeneration in adult mice. *Nature.* (2017) 541:222–7. doi: 10.1038/nature20173
45. Kaelin WG Jr. The Von Hippel-Lindau protein, HIF hydroxylation, and oxygen sensing. *Biochem Biophys Res Commun.* (2005) 338:627–38. doi: 10.1016/j.bbrc.2005.08.165
46. Wu D, Liu L, Fu S, Zhang J. Osteostatin improves the osteogenic differentiation of mesenchymal stem cells and enhances angiogenesis through Hif-1α under hypoxia conditions in vitro. *Biochem Biophys Res Commun.* (2022) 606:100–7. doi: 10.1016/j.bbrc.2022.02.085
47. Moslehi J, Minamishima YA, Shi J, Neuberg D, Charytan DM, Padera RF, et al. Loss of hypoxia-inducible factor Prolyl hydroxylase activity in cardiomyocytes phenocopies ischemic cardiomyopathy. *Circulation.* (2010) 122:1004–16. doi: 10.1161/circulationaha.109.922427
48. Lei L, Mason S, Liu D, Huang Y, Marks C, Hickey R, et al. Hypoxia-inducible factor-dependent degeneration, failure, and malignant transformation of the heart in the absence of the Von Hippel-Lindau protein. *Mol Cell Biol.* (2008) 28:3790–803. doi: 10.1128/mcb.01580-07
49. Menendez-Montes I, Escobar B, Gomez MJ, Albendea-Gomez T, Palacios B, Bonzon-Kulichenko E, et al. Activation of amino acid metabolic program in cardiac HIF1-alpha-deficient mice. *iScience.* (2021) 24:102124. doi: 10.1016/j.isci.2021.102124
50. Guimarães-Camboa N, Stowe J, Aneas I, Sakabe N, Cattaneo P, Henderson L, et al. HIF1α represses cell stress pathways to allow proliferation of hypoxic fetal cardiomyocytes. *Dev Cell.* (2015) 33:507–21. doi: 10.1016/j.devcel.2015.04.021

51. Cardoso AC, Pereira AHM, Sadek HA. Mechanisms of neonatal heart regeneration. *Curr Cardiol Rep.* (2020) 22:33. doi: 10.1007/s11886-020-01282-5
52. Wang Z, Ying Z, Bosy-Westphal A, Zhang J, Schautz B, Later W, et al. Specific metabolic rates of major organs and tissues across adulthood: evaluation by mechanistic model of resting energy expenditure. *Am J Clin Nutr.* (2010) 92:1369–77. doi: 10.3945/ajcn.2010.29885
53. Karwi QG, Uddin GM, Ho KL, Lopaschuk GD. Loss of metabolic flexibility in the failing heart. *Front Cardiovasc Med.* (2018) 5:68. doi: 10.3389/fcvm.2018.00068
54. Neubauer S. The failing heart–an engine out of fuel. *N Engl J Med.* (2007) 356:1140–51. doi: 10.1056/NEJMra063052
55. Lopaschuk GD, Spafford MA, Marsh DR. Glycolysis is predominant source of myocardial ATP production immediately after birth. *Am J Physiol.* (1991) 261:H1698–705. doi: 10.1152/ajpheart.1991.261.6.H1698
56. Werner JC, Sicard RE. Lactate metabolism of isolated, perfused fetal, and newborn pig hearts. *Pediatr Res.* (1987) 22:552–6. doi: 10.1203/00006450-198711000-00016
57. Bartelds B, Gratama JW, Knoester H, Takens J, Smid GB, Aarnoudse JG, et al. Perinatal changes in myocardial supply and flux of fatty acids, carbohydrates, and ketone bodies in lambs. *Am J Physiol.* (1998) 274:H1962–9. doi: 10.1152/ajpheart.1998.274.6.H1962
58. Itoi T, Lopaschuk GD. The contribution of glycolysis, glucose oxidation, lactate oxidation, and fatty acid oxidation to ATP production in isolated biventricular working hearts from 2-week-old rabbits. *Pediatr Res.* (1993) 34:735–41. doi: 10.1203/00006450-199312000-00008
59. Onay-Besikci A. Regulation of cardiac energy metabolism in newborn. *Mol Cell Biochem.* (2006) 287:1–11. doi: 10.1007/s11010-006-9123-9
60. Bartelds B, Knoester H, Beaufort-Krol GC, Smid GB, Takens J, Zijlstra WG, et al. Myocardial lactate metabolism in fetal and newborn lambs. *Circulation.* (1999) 99:1892–7. doi: 10.1161/01.cir.99.14.1892
61. Cao T, Liccardo D, LaCanna R, Zhang X, Lu R, Finck BN, et al. Fatty acid oxidation promotes cardiomyocyte proliferation rate but does not change cardiomyocyte number in infant mice. *Front Cell Dev Biol.* (2019) 7:42. doi: 10.3389/fcell.2019.00042
62. Isu G, Robles Diaz D, Grussenmeyer T, Gaudiello E, Eckstein F, Brink M, et al. Fatty acid-based monolayer culture to promote in vitro neonatal rat cardiomyocyte maturation. *Biochim Biophys Acta Mol Cell Res.* (2020) 1867:118561. doi: 10.1016/j.bbamcr.2019.118561
63. Cardoso AC, Lam NT, Savla JJ, Nakada Y, Pereira AHM, Elnwasany A, et al. Mitochondrial substrate utilization regulates cardiomyocyte cell cycle progression. *Nat Metab.* (2020) 2:167–78.
64. Brown NF, Weis BC, Husti JE, Foster DW, McGarry JD. Mitochondrial carnitine palmitoyltransferase I isoform switching in the developing rat heart. *J Biol Chem.* (1995) 270:8952–7. doi: 10.1074/jbc.270.15.8952
65. Ceccarelli SM, Chomienne O, Gubler M, Arduini A. Carnitine Palmitoyltransferase (CPT) modulators: a medicinal chemistry perspective on 35 years of research. *J Med Chem.* (2011) 54:3109–52. doi: 10.1021/jm100809g
66. Hirose K, Payumo AY, Cutie S, Hoang A, Zhang H, Guyot R, et al. Evidence for hormonal control of heart regenerative capacity during endothermy acquisition. *Science.* (2019) 364:184–8. doi: 10.1126/science.aar2038
67. Li Y, Yang M, Tan J, Shen C, Deng S, Fu X, et al. Targeting ACSL1 promotes cardiomyocyte proliferation and cardiac regeneration. *Life Sci.* (2022) 294:120371. doi: 10.1016/j.lfs.2022.120371
68. Fukuda R, Marín-Juez R, El-Sammak H, Beisaw A, Ramadass R, Kuenne C, et al. Stimulation of glycolysis promotes cardiomyocyte proliferation after injury in adult zebrafish. *EMBO Rep.* (2020) 21:e49752. doi: 10.15252/embr.201949752
69. Huang Y, Lei L, Liu D, Jovin I, Russell R, Johnson RS, et al. Normal glucose uptake in the brain and heart requires an endothelial cell-specific HIF-1α-dependent function. *Proc Natl Acad Sci U S A.* (2012) 109:17478–83. doi: 10.1073/pnas.1209281109
70. Shao D, Tian R. Glucose transporters in cardiac metabolism and hypertrophy. *Compr Physiol.* (2015) 6:331–51. doi: 10.1002/cphy.c150016
71. Sugden MC, Langdown ML, Harris RA, Holness MJ. Expression and regulation of pyruvate dehydrogenase kinase isoforms in the developing rat heart and in adulthood: role of thyroid hormone status and lipid supply. *Biochem J.* (2000) 352(Pt 3):731–8.
72. Pereira RO, Wende AR, Olsen C, Soto J, Rawlings T, Zhu Y, et al. Inducible overexpression of Glut1 prevents mitochondrial dysfunction and attenuates structural remodeling in pressure overload but does not prevent left ventricular dysfunction. *J Am Heart Assoc.* (2013) 2:e000301. doi: 10.1161/jaha.113.000301
73. Liao R, Jain M, Cui L, D'Agostino J, Aiello F, Luptak I, et al. Cardiac-specific overexpression of Glut1 prevents the development of heart failure attributable to pressure overload in mice. *Circulation.* (2002) 106:2125–31. doi: 10.1161/01.cir.0000034049.61181.f3
74. Wang Q, Donthi RV, Wang J, Lange AJ, Watson LJ, Jones SP, et al. Cardiac phosphatase-deficient 6-phosphofructo-2-kinase/fructose-2,6-bisphosphatase increases glycolysis, hypertrophy, and myocyte resistance to hypoxia. *Am J Physiol Heart Circ Physiol.* (2008) 294:H2889–97. doi: 10.1152/ajpheart.91501.2007
75. Mazurek S. Pyruvate kinase Type M2: a key regulator of the metabolic budget system in tumor cells. *Int J Biochem Cell Biol.* (2011) 43:969–80. doi: 10.1016/j.biocel.2010.02.005
76. Luo W, Semenza GL. Pyruvate kinase M2 regulates glucose metabolism by functioning as a coactivator for hypoxia-inducible factor 1 in cancer cells. *Oncotarget.* (2011) 2:551–6. doi: 10.18632/oncotarget.299
77. Hauck L, Dadson K, Chauhan S, Grothe D, Billia F. Inhibiting the Pkm2/B-catenin axis drives in vivo replication of adult cardiomyocytes following experimental MI. *Cell Death Differ.* (2021) 28:1398–417. doi: 10.1038/s41418-020-00669-9
78. Magadum A, Singh N, Kurian AA, Munir I, Mehmood T, Brown K, et al. Pkm2 regulates cardiomyocyte cell cycle and promotes cardiac regeneration. *Circulation.* (2020) 141:1249–65. doi: 10.1161/circulationaha.119.043067
79. Muralidhar SA, Sadek HA. Meis1 regulates postnatal cardiomyocyte cell cycle arrest. In: Nakanishi T, Markwald RR, Baldwin HS, Keller BB, Srivastava D, Yamagishi H editors. *Etiology and Morphogenesis of Congenital Heart Disease: From Gene Function and Cellular Interaction to Morphology*. Tokyo: Springer Copyright 2016, The Author(s) (2016). p. 93–101.
80. Lindgren IM, Drake RR, Chattergoon NN, Thornburg KL. Down-regulation of Meis1 promotes the maturation of oxidative phosphorylation in perinatal cardiomyocytes. *Faseb J.* (2019) 33:7417–26. doi: 10.1096/fj.201801330RR
81. Aharonov A, Shakked A, Umansky KB, Savidor A, Genzelinakh A, Kain D, et al. Erbb2 drives yap activation and EMT-like processes during cardiac regeneration. *Nat Cell Biol.* (2020) 22:1346–56. doi: 10.1038/s41556-020-00588-4
82. Leach JP, Heallen T, Zhang M, Rahmani M, Morikawa Y, Hill MC, et al. Hippo pathway deficiency reverses systolic heart failure after infarction. *Nature.* (2017) 550:260–4. doi: 10.1038/nature24045
83. Xin M, Kim Y, Sutherland LB, Murakami M, Qi X, McAnally J, et al. Hippo pathway effector yap promotes cardiac regeneration. *Proc Natl Acad Sci U S A.* (2013) 110:13839–44. doi: 10.1073/pnas.1313192110
84. Tao G, Kahr PC, Morikawa Y, Zhang M, Rahmani M, Heallen TR, et al. Pitx2 promotes heart repair by activating the antioxidant response after cardiac injury. *Nature.* (2016) 534:119–23. doi: 10.1038/nature17959
85. Monroe TO, Hill MC, Morikawa Y, Leach JP, Heallen T, Cao S, et al. Yap partially reprograms chromatin accessibility to directly induce adult cardiogenesis in vivo. *Dev Cell.* (2019) 48:765–79.e7. doi: 10.1016/j.devcel.2019.01.017
86. Li L, Tao G, Hill MC, Zhang M, Morikawa Y, Martin JF. Pitx2 maintains mitochondrial function during regeneration to prevent myocardial fat deposition. *Development.* (2018) 145:dev168609. doi: 10.1242/dev.168609
87. Ding Y, Liu Z, Desai S, Zhao Y, Liu H, Pannell LK, et al. Receptor tyrosine kinase Erbb2 translocates into mitochondria and regulates cellular metabolism. *Nat Commun.* (2012) 3:1271. doi: 10.1038/ncomms2236
88. Gemberling M, Karra R, Dickson AL, Poss KD. Nrg1 is an injury-induced cardiomyocyte mitogen for the endogenous heart regeneration program in zebrafish. *Elife.* (2015) 4:e05871. doi: 10.7554/eLife.05871
89. D'Uva G, Aharonov A, Lauriola M, Kain D, Yahalom-Ronen Y, Carvalho S, et al. ERBB2 triggers mammalian heart regeneration by promoting cardiomyocyte dedifferentiation and proliferation. *Nat Cell Biol.* (2015) 17:627–38. doi: 10.1038/ncb3149

90. Ahuja P, Zhao P, Angelis E, Ruan H, Korge P, Olson A, et al. Myc controls transcriptional regulation of cardiac metabolism and mitochondrial biogenesis in response to pathological stress in mice. *J Clin Invest.* (2010) 120:1494–505. doi: 10.1172/jci38331
91. Quaife-Ryan GA, Mills RJ, Lavers G, Voges HK, Vivien CJ, Elliott DA, et al. B-Catenin drives distinct transcriptional networks in proliferative and nonproliferative cardiomyocytes. *Development.* (2020) 147:dev193417. doi: 10.1242/dev.193417
92. Villa Del Campo C, Clavería C, Sierra R, Torres M. Cell competition promotes phenotypically silent cardiomyocyte replacement in the mammalian heart. *Cell Rep.* (2014) 8:1741–51. doi: 10.1016/j.celrep.2014.08.005
93. Murashige D, Jang C, Neinast M, Edwards JJ, Cowan A, Hyman MC, et al. Comprehensive quantification of fuel use by the failing and nonfailing human heart. *Science.* (2020) 370:364–8. doi: 10.1126/science.abc8861
94. Lopaschuk GD, Karwi QG, Tian R, Wende AR, Abel ED. Cardiac energy metabolism in heart failure. *Circ Res.* (2021) 128:1487–513. doi: 10.1161/circresaha.121.318241
95. Talman V, Teppo J, Pöhö P, Movahedi P, Vaikkinen A, Karhu ST, et al. Molecular atlas of postnatal mouse heart development. *J Am Heart Assoc.* (2018) 7:e010378. doi: 10.1161/jaha.118.010378
96. Saxton RA, Sabatini DM. mTOR signaling in growth, metabolism, and disease. *Cell.* (2017) 168:960–76. doi: 10.1016/j.cell.2017.02.004
97. Miklas JW, Levy S, Hofsteen P, Mex DI, Clark E, Muster J, et al. Amino acid primed mTOR activity is essential for heart regeneration. *iScience.* (2022) 25:103574. doi: 10.1016/j.isci.2021.103574
98. Zhang P, Shan T, Liang X, Deng C, Kuang S. Mammalian target of rapamycin is essential for cardiomyocyte survival and heart development in mice. *Biochem Biophys Res Commun.* (2014) 452:53–9. doi: 10.1016/j.bbrc.2014.08.046
99. Moos PJ, Edes K, Fitzpatrick FA. Inactivation of wild-type P53 tumor suppressor by electrophilic prostaglandins. *Proc Natl Acad Sci U S A.* (2000) 97:9215–20. doi: 10.1073/pnas.160241897
100. Marnett LJ, Riggins JN, West JD. Endogenous generation of reactive oxidants and electrophiles and their reactions with DNA and protein. *J Clin Invest.* (2003) 111:583–93. doi: 10.1172/jci18022
101. Hoeijmakers JH. DNA damage, aging, and cancer. *N Engl J Med.* (2009) 361:1475–85. doi: 10.1056/NEJMra0804615
102. Elhelaly WM, Lam NT, Hamza M, Xia S, Sadek HA. Redox regulation of heart regeneration: an evolutionary tradeoff. *Front Cell Dev Biol.* (2016) 4:137. doi: 10.3389/fcell.2016.00137
103. Liu S, Martin JF. The regulation and function of the hippo pathway in heart regeneration. *Wiley Interdiscip Rev Dev Biol.* (2019) 8:e335. doi: 10.1002/wdev.335
104. Pei J, Wang F, Pei S, Bai R, Cong X, Nie Y, et al. Hydrogen sulfide promotes cardiomyocyte proliferation and heart regeneration *via* ros scavenging. *Oxid Med Cell Longev.* (2020) 2020:1412696. doi: 10.1155/2020/1412696
105. Pettinato AM, Yoo D, VanOudenhove J, Chen YS, Cohn R, Ladha FA, et al. Sarcomere function activates a P53-Dependent DNA damage response that promotes polyploidization and limits in vivo cell engraftment. *Cell Rep.* (2021) 35:109088. doi: 10.1016/j.celrep.2021.109088
106. Taylor WR, Stark GR. Regulation of the G2/M transition by P53. *Oncogene.* (2001) 20:1803–15. doi: 10.1038/sj.onc.1204252
107. Bae J, Salamon RJ, Brandt EB, Paltzer WG, Zhang Z, Britt EC, et al. Malonate promotes adult cardiomyocyte proliferation and heart regeneration. *Circulation.* (2021) 143:1973–86. doi: 10.1161/circulationaha.120.049952
108. McNamara JW, Porrello ER. From fragrances to heart regeneration: malonate repairs broken hearts. *Circulation.* (2021) 143:1987–90. doi: 10.1161/circulationaha.121.054313
109. Yetkin-Arik B, Vogels IMC, Nowak-Sliwinska P, Weiss A, Houtkooper RH, Van Noorden CJF, et al. The role of glycolysis and mitochondrial respiration in the formation and functioning of endothelial tip cells during angiogenesis. *Sci Rep.* (2019) 9:12608. doi: 10.1038/s41598-019-48676-2
110. Mills RJ, Parker BL, Quaife-Ryan GA, Voges HK, Needham EJ, Bornot A, et al. Drug screening in human PSC-cardiac organoids identifies pro-proliferative compounds acting *via* the mevalonate pathway. *Cell Stem Cell.* (2019) 24:895–907.e6. doi: 10.1016/j.stem.2019.03.009
111. Abouleisa RRE, McNally L, Salama ABM, Hammad SK, Ou Q, Wells C, et al. Cell cycle induction in human cardiomyocytes is dependent on biosynthetic pathway activation. *Redox Biol.* (2021) 46:102094. doi: 10.1016/j.redox.2021.102094
112. Magadum A, Ding Y, He L, Kim T, Vasudevarao MD, Long Q, et al. Live cell screening platform identifies PPARδ as a regulator of cardiomyocyte proliferation and cardiac repair. *Cell Res.* (2017) 27:1002–19. doi: 10.1038/cr.2017.84
113. Burkart EM, Sambandam N, Han X, Gross RW, Courtois M, Gierasch CM, et al. Nuclear receptors PPARbeta/delta and PPARalpha direct distinct metabolic regulatory programs in the mouse heart. *J Clin Invest.* (2007) 117:3930–9. doi: 10.1172/jci32578
114. Magadum A, Engel FB. PPARβ/Δ: linking metabolism to regeneration. *Int J Mol Sci.* (2018) 19:2013. doi: 10.3390/ijms19072013
115. Tan J, Yang M, Wang H, Shen C, Wu M, Xu H, et al. Moderate heart rate reduction promotes cardiac regeneration through stimulation of the metabolic pattern switch. *Cell Rep.* (2022) 38:110468. doi: 10.1016/j.celrep.2022.110468
116. Tran DH, Wang ZV. Glucose metabolism in cardiac hypertrophy and heart failure. *J Am Heart Assoc.* (2019) 8:e012673. doi: 10.1161/jaha.119.012673
117. Ashrafian H, Frenneaux MP, Opie LH. Metabolic mechanisms in heart failure. *Circulation.* (2007) 116:434–48. doi: 10.1161/circulationaha.107.702795
118. Kundu BK, Zhong M, Sen S, Davogustto G, Keller SR, Taegtmeyer H. Remodeling of glucose metabolism precedes pressure overload-induced left ventricular hypertrophy: review of a hypothesis. *Cardiology.* (2015) 130:211–20. doi: 10.1159/000369782
119. Gibb AA, Hill BG. Metabolic coordination of physiological and pathological cardiac remodeling. *Circ Res.* (2018) 123:107–28. doi: 10.1161/circresaha.118.312017
120. Zhou B, Tian R. Mitochondrial dysfunction in pathophysiology of heart failure. *J Clin Invest.* (2018) 128:3716–26. doi: 10.1172/jci120849
121. Knowlton AA, Chen L, Malik ZA. Heart failure and mitochondrial dysfunction: the role of mitochondrial fission/fusion abnormalities and new therapeutic strategies. *J Cardiovasc Pharmacol.* (2014) 63:196–206. doi: 10.1097/01.fjc.0000432861.55968.a6
122. Allard MF, Schönekess BO, Henning SL, English DR, Lopaschuk GD. Contribution of oxidative metabolism and glycolysis to ATP production in hypertrophied hearts. *Am J Physiol.* (1994) 267:H742–50. doi: 10.1152/ajpheart.1994.267.2.H742
123. Lorell BH, Grossman W. Cardiac hypertrophy: the consequences for diastole. *J Am Coll Cardiol.* (1987) 9:1189–93. doi: 10.1016/s0735-1097(87)80326-1
124. Razeghi P, Young ME, Alcorn JL, Moravec CS, Frazier OH, Taegtmeyer H. Metabolic gene expression in fetal and failing human heart. *Circulation.* (2001) 104:2923–31. doi: 10.1161/hc4901.100526
125. Wambolt RB, Henning SL, English DR, Dyachkova Y, Lopaschuk GD, Allard MF. Glucose utilization and glycogen turnover are accelerated in hypertrophied rat hearts during severe low-flow ischemia. *J Mol Cell Cardiol.* (1999) 31:493–502. doi: 10.1006/jmcc.1998.0804
126. Kübler W, Spieckermann PG. Regulation of glycolysis in the ischemic and the anoxic myocardium. *J Mol Cell Cardiol.* (1970) 1:351–77. doi: 10.1016/0022-2828(70)90034-9
127. Frangogiannis NG. Pathophysiology of myocardial infarction. *Compr Physiol.* (2015) 5:1841–75. doi: 10.1002/cphy.c150006
128. Opie LH. Myocardial ischemia–metabolic pathways and implications of increased glycolysis. *Cardiovasc Drugs Ther.* (1990) 4(Suppl. 4):777–90. doi: 10.1007/bf00051275
129. Jaswal JS, Keung W, Wang W, Ussher JR, Lopaschuk GD. Targeting fatty acid and carbohydrate oxidation–a novel therapeutic intervention in the ischemic and failing heart. *Biochim Biophys Acta.* (2011) 1813:1333–50. doi: 10.1016/j.bbamcr.2011.01.015
130. Ritterhoff J, Young S, Villet O, Shao D, Neto FC, Bettcher LF, et al. Metabolic remodeling promotes cardiac hypertrophy by directing glucose to aspartate biosynthesis. *Circ Res.* (2020) 126:182–96. doi: 10.1161/circresaha.119.315483
131. Kolwicz SC Jr., Olson DP, Marney LC, Garcia-Menendez L, Synovec RE, Tian R. Cardiac-specific deletion of Acetyl Coa Carboxylase 2 prevents metabolic remodeling during pressure-overload hypertrophy. *Circ Res.* (2012) 111:728–38. doi: 10.1161/circresaha.112.268128

132. Zhang L, Jaswal JS, Ussher JR, Sankaralingam S, Wagg C, Zaugg M, et al. Cardiac insulin-resistance and decreased mitochondrial energy production precede the development of systolic heart failure after pressure-overload hypertrophy. *Circ Heart Fail.* (2013) 6:1039–48. doi: 10.1161/circheartfailure.112.000228
133. Graham N, Huang GN. Endocrine influence on cardiac metabolism in development and regeneration. *Endocrinology.* (2021) 162:bqab081. doi: 10.1210/endocr/bqab081
134. Allard MF, Henning SL, Wambolt RB, Granleese SR, English DR, Lopaschuk GD. Glycogen metabolism in the aerobic hypertrophied rat heart. *Circulation.* (1997) 96:676–82. doi: 10.1161/01.cir.96.2.676
135. Wambolt RB, Lopaschuk GD, Brownsey RW, Allard MF. Dichloroacetate improves postischemic function of hypertrophied rat hearts. *J Am Coll Cardiol.* (2000) 36:1378–85. doi: 10.1016/s0735-1097(00)00856-1
136. Mori J, Basu R, McLean BA, Das SK, Zhang L, Patel VB, et al. Agonist-induced hypertrophy and diastolic dysfunction are associated with selective reduction in glucose oxidation: a metabolic contribution to heart failure with normal ejection fraction. *Circ Heart Fail.* (2012) 5:493–503. doi: 10.1161/circheartfailure.112.966705
137. Aurora AB, Porrello ER, Tan W, Mahmoud AI, Hill JA, Bassel-Duby R, et al. Macrophages are required for neonatal heart regeneration. *J Clin Invest.* (2014) 124:1382–92. doi: 10.1172/jci72181
138. Li M, Wu Y, Ye L. The role of amino acids in endothelial biology and function. *Cells.* (2022) 11:1372. doi: 10.3390/cells11081372
139. Ieda M, Fu JD, Delgado-Olguin P, Vedantham V, Hayashi Y, Bruneau BG, et al. Direct reprogramming of fibroblasts into functional cardiomyocytes by defined factors. *Cell.* (2010) 142:375–86. doi: 10.1016/j.cell.2010.07.002

Conflict of Interest: The authors declare that the research was conducted in the absence of any commercial or financial relationships that could be construed as a potential conflict of interest.

frontiers | Frontiers in Cardiovascular Medicine

METHODS
published: 18 July 2022
doi: 10.3389/fcvm.2022.920013

Porcine Organotypic Epicardial Slice Protocol: A Tool for the Study of Epicardium in Cardiovascular Research

Davide Maselli[1], *Rolando S. Matos*[1], *Robert D. Johnson*[1], *Davide Martella*[2,3], *Valeria Caprettini*[2,3], *Ciro Chiappini*[2,3], *Patrizia Camelliti*[1] *and Paola Campagnolo*[1]*

[1] Cardiovascular Section, Department of Biochemical Sciences, University of Surrey, Guildford, United Kingdom, [2] London Centre for Nanotechnology, King's College London, London, United Kingdom, [3] Centre for Craniofacial and Regenerative Biology, King's College London, London, United Kingdom

The epicardium has recently gained interest in the cardiovascular field due to its capacity to support heart regeneration after ischemic injury. Models to study the epicardium of large animals *in vitro* are limited and mainly based on epicardial cell isolation/differentiation from stem cells, followed by 2D cells culture. In this method paper, we describe the procedure to obtain and culture 3D organotypic heart slices presenting an intact epicardium, as a novel model to study the epicardial physiology and activation. Epicardial slices are obtained from porcine hearts using a high-precision vibratome and retain a healthy epicardial layer embedded in its native extracellular environment and connected with other cardiac cells (cardiomyocytes, fibroblasts, vascular cells etc.). Epicardial slices can be cultured for 72 h, providing an ideal model for studying the epicardium physiology or perform pharmacological interventions/gene therapy approaches. We also report on methods to assesses the viability and composition of the epicardial slices, and evaluate their architecture in 3D through tissue decoloration. Finally, we present a potential application for a nanomaterial-based gene transfer method for tracking of epicardial cells within the slice. Crucially, given the similarity in morphology and physiology of porcine heart with its human counterpart, our system provides a platform for translational research while providing a clinically relevant and ethical alternative to the use of small animals in this type of research.

Keywords: epicardium, *ex vivo* model, organotypic culture model, regenerative medicine, myocardial infarction

OPEN ACCESS

Edited by:
Rajika Roy,
Temple University, United States

Reviewed by:
Ching-Ling Lien,
Children's Hospital of Los Angeles, United States
Jun Jie Tan,
Universiti Sains Malaysia (USM), Malaysia

***Correspondence:**
Paola Campagnolo
p.campagnolo@surrey.ac.uk

Specialty section:
This article was submitted to Cardiovascular Biologics and Regenerative Medicine, a section of the journal Frontiers in Cardiovascular Medicine

Received: *14 April 2022*
Accepted: *30 May 2022*
Published: *18 July 2022*

Citation:
Maselli D, Matos RS, Johnson RD, Martella D, Caprettini V, Chiappini C, Camelliti P and Campagnolo P (2022) Porcine Organotypic Epicardial Slice Protocol: A Tool for the Study of Epicardium in Cardiovascular Research. Front. Cardiovasc. Med. 9:920013. doi: 10.3389/fcvm.2022.920013

INTRODUCTION

After myocardial injury, adult epicardial cells transiently re-express embryonic genes and actively participate to cardiac repair both through direct differentiation into cardiac cells and by producing reparative paracrine factors (1, 2). Recent discoveries of the role of the epicardium in heart repair have generated interest in developing strategies to exploit its regenerative potential for patient therapy (3–5). Due to the biological complexity of the cardiovascular system, the choice of the animal model is critical owing to significant inter-species differences (6, 7). Currently, studies on the epicardium are based either on 2D *in vitro* culture systems or on fate-tracking animal models, such as zebrafish and mice. *In vitro* experiments conducted with stem cell-derived epicardial cell lines, immortalized cell lines or primary isolated epicardial cells, provided a comprehensive knowledge

of the secretome and transcriptional profiling of the epicardium (4, 8–12). *In vivo*, zebrafish represent an interesting model due to its remarkable heart regeneration capacity, which is dependent on epicardial signals and epicardial cell trans-differentiation (13–16). Zebrafish studies have provided valuable mechanistic insights into the regenerative process of the heart and specifically the epicardial contribution (16). Mouse models are extensively utilized for their amenability to genetic modification, which allows the study of single gene function *in vivo* and fate mapping studies. These animal models were crucial in the identification of the pivotal role of the transcription factors WT1, Tbx18 and TCF21 in guiding the epicardium development and driving its repair potential (2, 17–19). However, for research aimed at clinical translation, it is essential that results from small vertebrates' studies are confirmed in a large animal models that more closely resemble the human heart physiology (6, 19).

Cardiac slices are well-established *ex vivo* models consisting of thin tissue slices obtained from the cardiac muscle (20, 21), and have been used in the past two decades for electrophysiological and pharmacological drug testing (21, 22). In our recent paper we described for the first time the preparation and characterization of heart slices derived from the epicardial portion of the heart, and their use for the investigation of this intriguing reservoir of regenerative cells (23). Our epicardial slices encompass the epicardial/myocardial interface while also preserving the cellular and extracellular structure of the cardiac tissue. Here we aim at producing an extensive and detailed protocol to support interested user in the production of epicardial slices, and their culture.

In part, this is due to technical difficulties as the epicardium is normally sacrificed to attach the specimen to the vibratome holder in order to ensure the alignment of the myocardial fibers within the tissue during cutting (24, 25). In this protocol, we modified previously developed tissue embedding (26, 27) and cutting (28, 29) procedure by flattening the tissue against a compliant surface during the embedding and then cutting the tissue starting from the epicardial side. This protocol exclusively enables to preserve the epicardial layer and obtain both healthy epicardial slices and functional cardiac slices. Epicardial slices contain both the epicardium and the myocardium and are amenable to culture for up to 72 h, maintaining vitality and morphology of the epicardial cells. They provide a suitable platform for multiplexing assays for drug/gene therapy discovery focused on the epicardium, and to study its interaction with the myocardial tissue, in a tunable culture system.

Importantly, epicardial slices have the potential to replace and reduce the use of small animals for research on the epicardium. Our slices were successfully derived from both experimental and abattoir porcine tissues, and with an adult heart yielding to 15–25 slices, each providing one experimental sample. This enables the multiplexing of assays, improving consistency and helping reducing the number of small animals used in cardiovascular research.

In summary, in this method paper we described in detail a robust and efficient protocol for obtaining and culturing epicardial slices, that can be used to study the physiological and reparative roles of the epicardium in an easy and cost-effective manner. Our system is based on large animal tissue, which closely resembles the human heart and has the potential to substitute or reduce the use of small animals in this type of research.

MATERIALS AND EQUIPMENT

Tissue Samples

Four to Six weeks old piglet hearts were obtained from The Pirbright Institute, UK. Animal procedures were carried out under the Home Office Animals (Scientific Procedures) Act (1986) and approved by the Animal Welfare and Ethical Review Board (AWERB) of The Pirbright Institute. The animals were housed in accordance with the Code of Practice for the Housing and Care of Animals Bred. All procedures were conducted by Personal License holders who were trained and competent and under the Project License PPL70/8852. Sixteen to twenty weeks old pig heart were obtained from Newman's Abattoir (Farnborough, UK).

Preparation of Solutions

Preparation of cardioplegia solution: This solution is required for the perfusion of the piglets' hearts and the transportation of cardiac tissue. To prepare 1 liter of solution, add the following: 6.43 g of sodium chloride (final concentration: 110 mM), 1.19 g of potassium chloride (final concentration: 16 mM), 3.25 g of magnesium chloride (final concentration: 16 mM) and 0.13 g of calcium chloride (final concentration: 1.2 mM), in 800 ml of double-distilled water (ddH_2O). Once all the reagents are dissolved, measure and adjust the pH to 7.4 with 10 mM sodium bicarbonate solution and then add ddH_2O to reach final volume (1 L). Cool down the solution to 4°C (see info in **Table 1**).

Preparation of Normal Tyrode's (NT) solution: Cardiac tissue is cut in ice cold NT solution with the addition of 2,3-Butanedione monoxime (BDM), an excitation–contraction uncoupler that block cardiomyocytes' beating preventing their damage during slicing. After cutting, the epicardial slices recover for at least 30 min at room temperature in the same solution. To make 1 liter of NT solution, add the following to 800 ml of ddH_2O: 1.00 g of BDM (final concentration: 10 mM), 4.09 g of sodium chloride (final concentration: 140 mM), 0.45 g of potassium chloride (final concentration: 6 mM), 1.8 g of glucose (final concentration: 10 mM), 2.38 g of HEPES (final concentration: 10 mM), 0.20 g of magnesium chloride (final concentration: 1 mM) and 0.20 g of calcium chloride (final concentration: 1.8 mM). Once all the reagents are dissolved, adjust the pH of the solution to 7.4 by adding drops of 2 M sodium hydroxide solution (Sigma-Aldrich) and then add ddH_2O to reach final volume (1 L). **Tip**: to improve slice viability, measure and fine tune the pH at the working temperature of the NT solutions (4°C for slicing NT solution and room temperature for recovery NT solution) and check the osmolarity of the NT solution to be in between 290 and 320 mOsm/L (see info in **Table 1**).

Equipment and Reagents

Equipment and reagents to obtain epicardial slices are listed separately for each phase of the protocol.

TABLE 1 | Components of solution.

Cardioplegia			Normal Tyrode's solution			Normal Tyrode's solution for recording		
Composition	**Manufacturer**	**Concentration (mM)**	**Composition**	**Manufacturer**	**Concentration (mM)**	**Composition**	**Manufacturer**	**Concentration (mM)**
NaCl	VWR Chemicals	110	NaCl	VWR Chemicals	140	NaCl	VWR Chemicals	140
CaCl2	Sigma-Aldrich	1.2	CaCl2	Sigma-Aldrich	1.8	CaCl2	Sigma-Aldrich	1.8
KCl	Sigma-Aldrich	16	KCl	Sigma-Aldrich	6	KCl	Sigma-Aldrich	4.5
MgCl2	VWR Chemicals	16	MgCl2	VWR Chemicals	1	MgCl2	VWR Chemicals	1
			Glucose	Sigma-Aldrich	10	Glucose	Sigma-Aldrich	10
			HEPES	VWR Chemicals	10	HEPES	VWR Chemicals	10
			BDM	Sigma-Aldrich	10			
*add NaHCO3 (10mM) to pH 7.4			*add NaOH (10M) to pH 7.4			*add NaOH (10M) to pH 7.4		

**The component needs to be added to adjust the pH of the solution.*

Excision of the Heart

- Anatomical forceps, Curved, 10 cm (Graefe)
- Disposable sterile scalpel (Torge Surgical Scalpels -size 21)
- Hermetic plastic box
- Scissors, straight, 16.5cm (Lexer)

Heart Perfusion

- 3-way valve (Tro-venoflow 3, Torge)
- Anatomical forceps, curved, 10 cm (Graefe)
- Nylon cable ties 100 × 2.5 mm
- Polycarbonate connector female luer hose barb adapter 1/4" (Masterflex Fitting)
- Polystyrene box with lid
- Scissors, straight, 16.5 cm (Lexer)
- Syringe 100 ml sterile (BD Plastipak Catheter-Tip)

Reagents:

- Cardioplegia solution 1L at 4°C

Slicing

- 2× Petri dishes 92 × 16 mm (Sarstedt)
- 3–4× Sterile plastic Pasteur pipettes (Agar scientific)
- 3D printed plastic ring (details in **Supplementary File 1**)
- 6- well Millicell cell culture inserts, pore size 0.4μm (Merck)
- 6-well plates ×3 (Customized with holes in the base of each well, Sarstedt)
- Anatomical forceps, curved, 10 cm (Graefe)
- Disposable sterile scalpel (Torge surgical scalpels -size 21)
- Double edge razor blades (Wilkinson Sword)
- High precision vibratome (Leica, VT1200S)
- Plastic box 30 × 40 × 7cm
- Polystyrene Box 60 × 40 × 40cm
- Self-sealing sterilization pouch (Qualitix)
- Single edge steel blades (Fast Mover Tools)
- Thermometer (RS PRO Digital Thermometer)
- Water bath set at 37°C

Reagents:

- Agarose (Invitrogen UltraPure Agarose)
- Cyanoacrylate glue (Solv-X)
- Low melting agarose (ThermoScientific, TopVision Low Melting Point Agarose)
- NT solution: 0.5 L at 4°C and 1 L at room temperature

Culture

- 12- well plates (Sarstedt)
- 3D-printed petri dish insert (**Supplementary File 2**)
- 8 mm-high Polydimethylsiloxane (PDMS) pillars array
- Anatomical forceps, curved, 10cm (Graefe)
- BioFlo120® control station (Eppendorf)
- CO_2 incubator (Galaxy® 48R – Eppendorf)
- Entomologist pins (A1 - 0.14 × 10 mm, Watkins & Doncaster)
- Petri dish 92 × 16mm (Sarstedt)
- Self-sealing sterilization pouch (Qualitix)
- Syringe Filter Unit, 0.22 μm, polyethersulfone, 33 mm (Medical Millex-GP, Merck)

Reagents:

- Polydimethylsiloxane (PDMS) (SYLGARD 184)
- 2,3-Butanedione monoxime (BDM) (Sigma-Aldrich)
- Ethanol 70% (AnalaR NORMAPUR)
- NT solution: 50 ml at room temperature
- Medium 199 (Sigma-Aldrich)
- Insulin, transferrin, and sodium selenite (ITS) Liquid Media Supplement (100×) (Sigma-Aldrich)
- Penicillin-Streptomycin (Sigma-Aldrich)

METHODS

This protocol uses hearts from animals euthanized for research purposes or human consumption obtained from the Pirbright Institute (Pirbright, UK) or the Newman's Abattoir (Farnborough, Hampshire, UK). Before transportation, adult hearts are dissected and piglets' hearts are perfused. Tissue samples are then transferred to the laboratory (within 20–30 min) submerged in cardioplegia solution to arrest the heart in non-contracted state, preventing tissue damage. Once in the lab, 8 × 8 mm cubes are obtained from the cardiac tissue and embedded in low meting agarose and sliced. Our embedding procedure allows to maintain flat and alive the epicardium during slicing. Tissue slices are then transferred to

the recovery bath for at least 30 min before further handling. In the following paragraphs we describe in detail the steps to produce epicardial/myocardial slices for *ex vivo* culture.

Excision of the Heart

Piglets weighing between 6 and 12 kg are euthanized with an intravenous administration of 10 ml of pentobarbital (Dolethal 200 mg/ml solution for injection, Vetoquinol UK Ltd). After exsanguination, the thorax is opened with a sterile scalpel by practicing two symmetrical cuts from the sternum toward the diaphragm membrane along the costal margins, severing the costal cartilages. Mediastinum is exposed by pulling down the severed portion toward the bladder with sterile forceps, and a transversal incision of the sternum allows the access to the heart. After transection of the great vessels, the heart is removed maintaining the pericardial membrane intact and immediately submerged in a hermetic plastic box filled with iced cold cardioplegia solution (∼300 ml) to wash the excess blood. Next, piglets' hearts are perfused as described in 3.2.

Adult pig hearts are obtained from farm pigs euthanized at the abattoir and immediately washed with iced cold cardioplegia. Upon excision, ventricles are immediately surgically separated from the rest of the tissue by cutting along the left anterior descending artery and the posterior descending artery and transported in a hermetic plastic box containing 500–600 ml of ice cold cardioplegia solution.

In both cases, the transportation is performed in an insulated polystyrene box filled with cooler packs.

Heart Perfusion

- Critical step: to ensure maximum/maximal survival of tissues, heart perfusion must be performed within few minutes from the excision.
- Screw a polycarbonate connector to one end of a 3-way valve, insert the luer in the aorta, and block it in position with a nylon cable tie (**Figure 1**).
- Fill a 100 ml sterile syringe with cold cardioplegia and connect at the 3-way valve, carefully pushing the cardioplegia though the valve. Tip: to avoid the formation of bubbles, turn the valve to direct the flow through the open end and flush the bubbles out before commencing the heart perfusion.
- Slowly inject the cardioplegia into the heart (c.a. 10–20 ml/min). Tip: successful perfusion can be assessed by monitoring the displacement of the blood by the colorless cardioplegia within the coronary arteries.
- After perfusion, the pericardial membrane is opened and the epicardium exposed.
- The ventricles are then removed and washed from any residual blood with cardioplegia and are ready for transportation (**Figure 2**). Important tip: for best results limit transportation time to a maximum of 1 h.

Tissue Embedding and Slicing

Tip: Upon arrival in the laboratory, the solution temperature must be measured to ensure the preservation of the cold environment between 3 and 6°C.

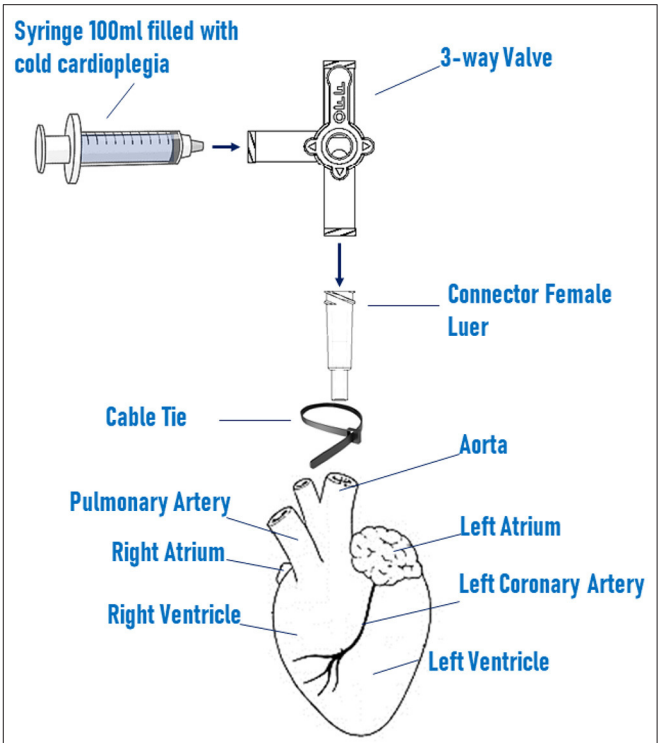

FIGURE 1 | Schematic setting of heart perfusion system. Heart is perfused with cold cardioplegia *via* a 100 ml sterile syringe connected to a the 3-way valve. The valve is screw to a female luer connector, which is inserted in the ascending aorta and fixed in position by a nylon cable tie.

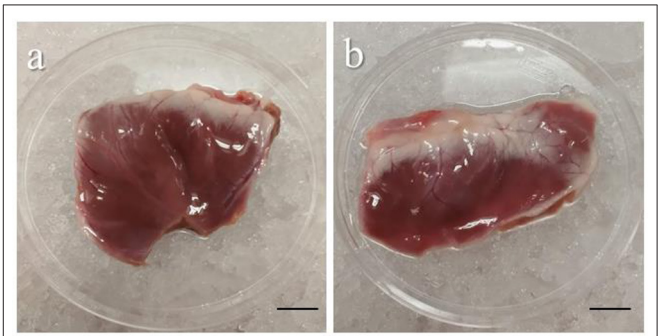

FIGURE 2 | Representative images of piglet's ventricles after excision. Images showing the left **(a)** and the right **(b)** ventricles carefully removed from a piglet heart after heart perfusion. Freshly dissected tissue can be stored for up to 1 h in cold cardioplegia without affecting the epicardial viability. Scale bar, 1 cm. Source: Maselli et al. (23).

NOTE: the equipment must be set up as described below before sample arrival:

Vibratome Setup

Clean the vibratome with 70% ethanol and distilled water and mount the blade (Wilkinson sword). It is essential to check the optimum positioning of the blade using Leica's VibroCheck, which minimizes the vertical vibration during cutting avoiding damage to the tissue. Set the cutting amplitude at 1.5 mm and

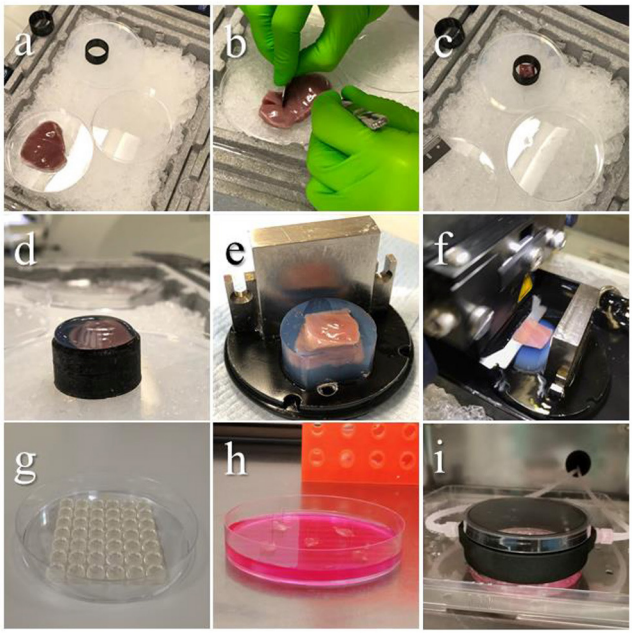

FIGURE 3 | Embedding procedure and slicing. Images showing the steps of tissue preparation for cutting epicardial slices. **(a)** The ventricles are isolated avoiding any direct handling of the epicardium and placed on ice throughout the procedure. **(b)** Tissue blocks are dissected by making an incision through the ventricular wall with a single edge steel blade and **(c)** placed on cold agarose inside a 3D printed plastic ring, the epicardium facing down. **(d)** The plastic ring is filled with low melting agarose. **(e)** Once solidified, the block is removed from the ring, squared and mounted on the holder using cyanoacrylate glue. **(f)** Epicardial slices are cut using a vibratome, with the blade speed at 0.03 mm/s. **(g–i)** Epicardial slices are pinned to pillared Petri dishes, and either cultured in static conditions changing medium every 24 h, or connected to BioFlo120® benchtop bioprocessor through a custom 3D-printed insert, enabling flow culture and control of the culture conditions. Source: Maselli et al. (23).

adjust z-axis deflection of the blade, following the manufacturer instructions, at values comprised between −0.2 and 0.2 μm. Once the blade alignment is optimal, the vibratome bath can be mounted. The outer part of the bath is filled with ice, the inner part is filled to the top with cold NT solution (4°C). The solution is bubbled with 99.5% oxygen for at least 30 min before starting to cut.

Preparation of Tissue Dissecting and Embedding Equipment

For the tissue dissection and embedding area the following material is needed: a polystyrene box full of ice, a petri dish and the agarose cushion already prepared, organized as in **Figure 3a**. Tip: to avoid delays, set up the dissection area in the vicinity of a water bath and a fridge.

- To prepare tissue embedding solution, dissolve 5% low melting agarose in NT solution (w/v). Heat the mixture and stir it until the agarose has completely melted. Leave the solution to cool down in a water bath set at 37°C.
- Tissue embedding is performed on a cushion of 2% (w/v) cold agarose prepared in NT solution. To prepare the agarose cushion, dissolve 2% (w/v) agarose in NT solution, and after heating, pour the melted agarose solution into a petri dish lid and let solidified at room temperature.
- Additional required equipment are single edge steel blades, anatomical forceps, 3D printed plastic ring (**Supplementary File 1**), plastic Pasteur pipettes and cyanoacrylate glue.

Preparation of Recovery Bath

The recovery bath for the epicardial slices should be prepared in advance by placing 6-well dishes with central holes in a large plastic box filled with recovery solution at room temperature and bubbled with 99.5% oxygen. In each well of the 6-well plate, place a cell culture insert.

Once the low melting agarose solution is equilibrated at 37°C, the dissecting area is prepared and the agarose cushion is set, it is possible to start cutting the epicardial slices.

- Place the ventricle on a petri dish on ice (epicardium up), dissect out an 8 × 8 mm tissue block by making incisions through the full thickness of the ventricular wall with a single edge steel blade (**Figure 3b**).
- Lightly blot the surfaces of the tissue block, avoiding touching the epicardium, to remove the excess of solution.
- Gently place the tissue block on the agarose cushion with the epicardium facing the cushion and make the whole surface adhere to the agarose to flatten the cutting surface. **Critical step**: if the epicardial surface does not adhere completely to the agarose surface the viability of the myocardial side of the slice will be compromised.
- Place the 3D printed plastic ring to surround the tissue (**Figure 3c**) and use a Pasteur pipette to transfer the low melting agarose solution into the plastic ring (5–8 ml). Continue adding until all the tissue is covered and the solution is over the edge of the ring (**Figure 3d**).
- Once solidified, remove the block from the cushion and cut off the excess of the agarose along the ring top.
- Carefully remove the block from the ring and square one side of the agarose cylinder to obtain a flat surface and orientate the tissue on the specimen holder facilitating the alignment of the blade (**Figure 3e**).
- Apply a drop of cyanoacrylate glue on the specimen holder and place on it the endocardial side of the embedded tissue block, waiting until the block is firmly glued on the holder, then mount on the vibratome.
- Position the vibratome' blade on top of the block and set this position as starting point, then set the cutting thickness to 400–500μm and start slicing (**Figure 3f**). Critical step: this step is critical to obtain thin and homogenous tissue slices, and to minimize the difference between the setup value and the final thickness. The critical point is to set the starting point as close as possible to the block surface. Tip: the blade has to make contact with the block surface to improve precision of the positioning. If possible, ensure this is done on the agarose surrounding the tissue. Avoid sliding the blade over the epicardial layer.

- While slicing, advance the blade at 0.03 mm/s. Once the blade has completely cut through the tissue, reaching the agarose on the posterior part of the block, stop the blade and return it to the starting position. Carefully collect the slices with the forceps by holding it from the corner, removing the excess agarose, and transfer in one of the cell culture inserts in the recovery bath. Let the slices recover at least 30 min to up to 4–5 h in the recovery bath. Slices might start to curl, but this will not affect viability, their culture or the outcome of the experiments.
- Multiple epicardial slices can be obtained from different blocks. After the removal of the epicardial slice, myocardial slices can be cut from the same block.

Culture of Epicardial/Myocardial Slices

Once recovered, slices can be cultured epicardium-up in Petri dishes modified by creating a PDMS pillar arrays at the bottom. Culture system is a modification of the previously published air/liquid interface method (24). The pillars are used to pin the slices, positioning an entomologist pin at each of the four corners of slice. This helps maintaining flatness and maximizes the contact between the tissue and the culture medium. Here is described an efficient and inexpensive method to produce the pillar array.

PDMS Pillar Array Fabrication

The PDMS is prepared by mixing the liquid silicone base with the curing agent (10:1, w/w) and carefully mixing avoiding formations of bubbles. To create the pillar array, pour 25 ml of the elastomer mixture in a shallow container (such as the lid of a multi-well dish) and press a 1,000 ml tip rack on top, ensuring that the solution fills the holes. Any master mold with spaced holes 5–8 millimeters deep would be appropriate. Polymer is cross-linked at 65°C for 3 h. Once solidified, the array can be cut to fit in the Petri dish as in **Figure 3g** and autoclaved in a sterilization pouch. The same array can be washed, autoclaved and re-used multiple times.

Culture System Setting

Epicardial slices can be cultured efficiently in the pillared Petri dish, changing medium every 24 hours (**Figure 3h**). However, here we describe a tunable culture method which enables a fine and real-time control/adjustment of the culture parameters, such as: pH, dissolved O_2 and CO_2, and medium exchange rate. We implemented this culture method using the BioFlo120® benchtop bioprocessor which monitors and regulates these parameters in a reservoir and pumps the medium from the reservoir to the culture dish via a custom 3D-printed insert, as shown in **Figure 3i**. The insert, made of thermo-resistant plastic (PA12 Nylon), was printed according to the design in the **Supplementary File 2**. Before culture, the reservoir is filled with 300 ml of medium (Medium 199 + 1X ITS Liquid Media Supplement + 1% Penicillin/Streptomycin Penicillin-Streptomycin + 10 mM of BDM) and parameters are set at pH 7.4, 21% oxygen level and medium flow of 4 ml/min, following to the manufacturer's instructions. The 3D insert must be autoclaved with input and output valves closed with caps before every use.

The following steps must be carried out in a sterile laminar flow hood:

- Transfer the slices from the recovery bath to the hood using a clean multi-well plate. Then, under the hood, move the slices in a new sterile multi-well plate and wash the slices by gently adding 0.22 μm filtered NT solution supplemented with 2% Penicillin-Streptomycin.
- Using sterile forceps, put the slice on top of the pillar array, and stick each corner on a pillar using entomologist pins, previously sterilized with 70% ethanol. Add 25 ml of medium into the dish.
- Place the 3D printed insert in between the plate and the lid and move the plate to the incubator, before removing the caps and connecting the input and output tubes.
- Activate the medium flow and incubate at 37°C in 5% CO_2 for up to 72 h.

Immunohistochemical Analysis

The slice viability, morphology and cellular composition can be assessed by histological analysis. Following is a protocol to obtain cross sections of the slices and perform immunohistochemical analysis.

- Fix the slices in 4% PFA (Paraformaldehyde, Santa Cruz Biotechnology) overnight at 4°C.
- Wash with phosphate buffer saline (PBS) and incubate overnight in 30% sucrose (Sigma-Aldrich) solution in PBS (w/v).
- To embed slices, lay them flat in a mold, cover in OCT Compound (Agar scientific) and snap freeze in isopentane cooled in liquid nitrogen.
- Cut 5 μm thick longitudinal cryosections (Hyrax C25 Cryostat, Zeiss), perpendicular to the epicardial surface, and collect them on SuperFrost slides (Menzel-Glaser, Germany). Slides can be stored at −20°C for up to 3 months.
- Hematoxylin/eosin staining can be performed for histological investigations. Results in **Figure 5** were obtained using Hematoxylin and Eosin Stain Kit (Vector Laboratories, H-3502) following the manufacturer's instructions.
- Antibody staining conditions must be optimized by the operator; however, below are some suggestions to improve the results of desired immunohistochemical assays:
    - Antigen retrieval is performed using citrate buffer (0.1 M Citric Acid, pH 6.0) for 5 min, 3 times in microwave at 759 W.
    - For nuclear antigens, permeabilize at room temperature for 30 min with 0.1% Triton-X 100 (v/v) in PBS (Sigma-Aldrich).
    - Block unspecific antigen binding using 20% (v/v) Goat serum (Sigma-Aldrich) in PBS for 1 h.
    - Incubate with primary antibody at 4°C overnight. Results in **Figure 5** were obtained using the following antibodies and concentrations: WT1 1:50 (ab89901), CD31 1:100

(ab28364) both from Abcam; Mesothelin 1:100 (NB110-85538) from Novus Biologicals; α-Actinin (Sarcomeric) 1:800 (A7732), α-smooth muscle actin (α-SMA) 1:400 (A5228) both from Sigma-Aldrich; Connexin 43 1:300 (71-0700), Vimentin 1:100 (MA5-11883) both from Thermo Fisher Scientific, followed by the appropriate Goat anti-Mouse and/or Goat anti-Rabbit Alexa Fluor (Thermo Fisher Scientific) secondary antibody diluted 1:200 for 1 h at 37°C.

- Stain the nuclei with DAPI 1 ug/ml (4′,6-Diamidine-2′-phenylindole dihydrochloride, Sigma-Aldrich) for 10 min at room temperature.
- To help to reduce tissue autofluorescence, incubate 30 min with 0.1% (w/v) Sudan Black (Sudan Black B, Santa Cruz Biotechnology) solution in 70% ethanol (w/v).

Whole mount histological analysis can be performed after tissue fixation (4% PFA, overnight at 4°C) and decoloration with CUBIC (Clear, Unobstructed Brain/body Imaging cocktails and Computational analysis) solution made with 25% (w/v) of urea (Sigma-Aldrich), 25% (w/v) of N,N,N,N-tetrakis(2-hydroxypropyl)ethylenediamine (Alfa Aesar) and 15% (w/v) Triton X-100 (Sigma-Aldrich) in water (30, 31). Briefly, whole slice decolouration is carried out for 6 days at room temperature on a slow shaker, changing solution every 2 days. Slices are then blocked with 20% (v/v) Goat serum (Sigma-Aldrich) in PBS for 24 h. Primary antibody incubation is performed at room temperature for 48 h (as in **Figure 6**, WT1 1:50 from Abcam and Mesothelin 1:100, from Novus Biologicals), followed by washing for 6 h in PBS. Finally, incubate with the appropriate Goat anti-Mouse and/or Goat anti-Rabbit Alexa Fluor secondary antibody at room temperature for 48 h and wash in PBS for 24 h.

Nanoneedle-Mediated Tracking of Epicardial Cells

Nanoneedles are an innovative nanoscale transfection tool (32–34) capable of transferring a variety of payloads, including nucleic acids and fluorescent quantum-dots, into the cytoplasm of cells without affecting their viability. Porous silicon nanoneedles are arranged vertically in an array with 2 μm spacing on an 8 × 8 mm chip; each needle is tailored to be 5 μm long with tips <50 nm and 50–70% porosity. The high porosity and the sharp tip geometry combine a high loading capacity with an efficient intracellular delivery (32, 35). Using this platform, we can deliver plasmids expressing reporter genes or cell impermeable dyes to the cells residing on the surface of the slice, within the epicardium.

Here we describe a protocol to deliver pcDNA3.1-GFP plasmid to the epicardial cells situated on the superficial layer of our slices using nanoneedles. Tagging the cells will enable fate mapping studies in large animals' adult tissues *ex vivo*. Similar approaches can be devised to transfer other genes of interest exclusively to the epicardium, to test their function.

- Nanoneedles are fabricated as previously reported (35) and treated with oxygen plasma for 10 min (0.4 mbar, 200 Watt), followed by coating 1 h with poly-L-lysine solution 0.1% (w/v, Sigma-Aldrich) in H_2O at room temperature. Nanoneedles are then washed for 30 s with 2N HCl (Sigma-Aldrich) followed by two washes for 30 s with distilled water.
- Plasmid loading is performed by incubating the chip surface for 15 min at room temperature with 20 μl of 1 μg/ml plasmid solution in H_2O, followed by a quick wash with sterile PBS.
- Nanoneedle chips are then applied on epicardial surface of the tissue slices for 30 min and then carefully removed.
- GFP expression is visualized with Nikon Eclipse Ts2 inverted microscope after 48 h of culture (as described above).

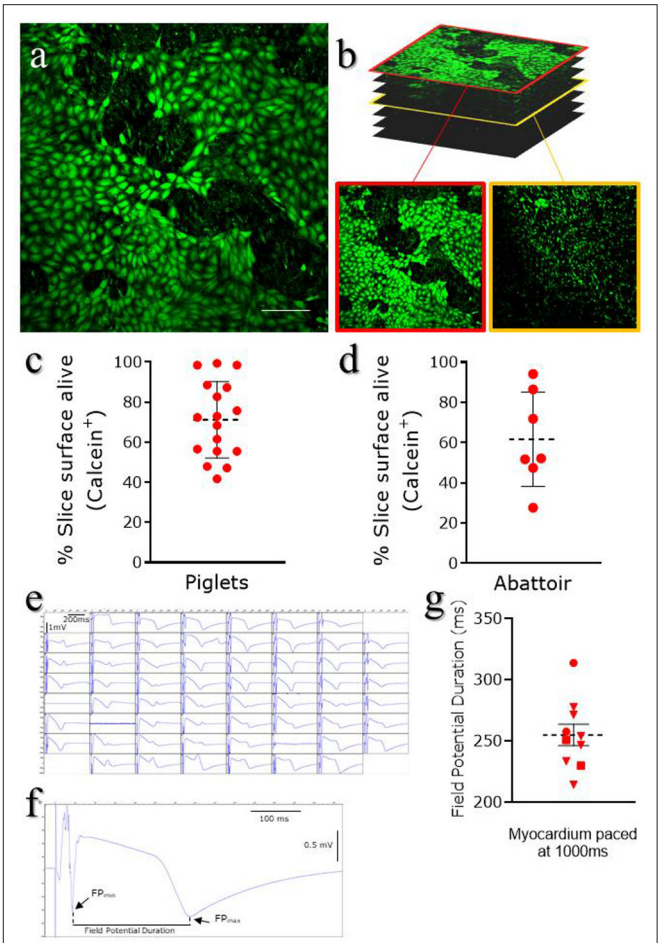

FIGURE 4 | Epicardial slices viability. Viability was assessed using Calcein AM live staining. Live cells are stained green. **(a)** Representative image of live staining of an epicardial slice imaged using confocal microscopy. Scale bar, 100 μm. **(b)** Representative images of Z-stack confocal acquisition of live/dead staining of epicardial slice, showing epicardial cells monolayer on the surface of the slice (red outline) and underlying fibroblasts/myocardium (yellow outline). **(c)** Quantification of alive area of the surface of piglet slices (*Mean and SEM*: 71.21 ± 4.61%; N of slices = 17/ N of Pigs = 10) and **(d)** abattoir-derived slices (*Mean and SEM*: 61.65 ± 8.88%; N of slices = 7/ N of Pigs = 4). **(e)** Representative field potential traces recorded from cardiomyocytes within the epicardial slices and **(f,g)** field potential duration, measured as the time between the depolarisation peak (FP_{MIN}) and the repolarization peak (FP_{MAX}) (*Mean and SEM* was 254.87 ± 8.86 ms; N of slices = 10/ N of Pigs = 3).

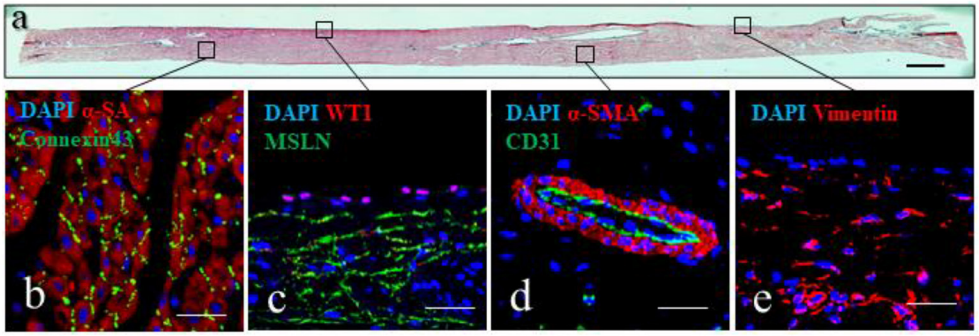

FIGURE 5 | Epicardial slices structure analysis. **(a)** Tissue architecture evaluation of epicardial slices performed using hematoxylin and eosin coloration. Scale bar, 500 μm. **(b–e)** Immunohistochemical staining and confocal microscopy of epicardial slices. **(b)** Cardiomyocytes are stained with α-sarcomeric actin and the intercalated disk is stained with connexin-43 antibody. **(c)** Epicardial cells highlighted with WT1 and mesenchymal derived cells stained with MSLN. **(d)** Microvasculature is stained with α- smooth muscle actin and the endothelial marker CD31. **(e)** Mesenchymal cells are stained with vimentin. Nuclei are labeled with DAPI. Scale bars, 50 μm.

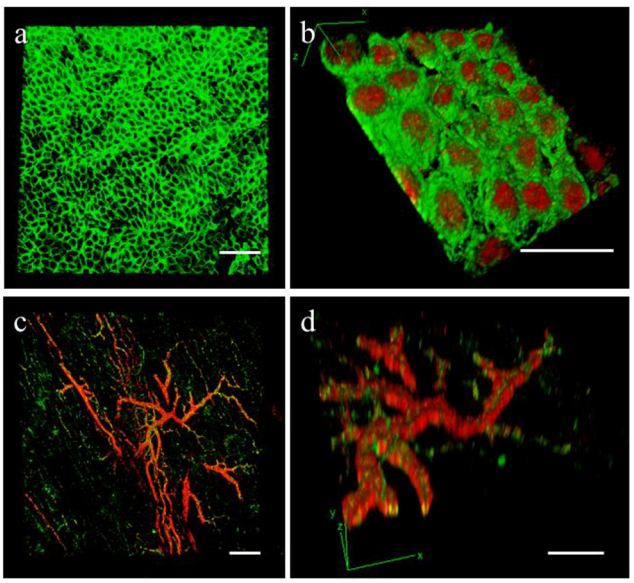

FIGURE 6 | Epicardial slices decolouration. Immunohistochemical staining and confocal analysis 3D reconstruction of decolorized epicardial slices obtained from piglet hearts, showing **(a)** low magnification image of the epicardial layer stained with MSLN (green) and **(b)** high magnification image showing the epicardial monolayer stained with MSLN (green) and WT1 (red) from the bottom. Low magnification **(c)** and detail view **(d)** of the vasculature present into the epicardial slice a stained with smooth muscle marker α-SMA (red) and the endothelial marker CD31 (green). Scale bars, 50 μm.

(ANTICIPATED) RESULTS

Viability of Slices

We used different assays to test the viability of the epicardial/myocardial slices. Epicardial cells metabolic activity/viability can be evaluated by Calcein acetoxymethyl (Calcein AM) (Thermo-Fisher) live staining, while for the myocardium utilized multi-electrode array (MEA) (MEA1060, Multi Channel Systems, Reutlingen, Germany) which allow non-invasive multifocal recording of extracellular field potential.

Live Staining

Calcein AM (Thermo Fisher Scientific, C1430) is a cell-permeant compound, converted in green fluorescent calcein by intracellular esterases. Microscopic imaging of the tissue stained with Calcein AM provides both functional and morphological information: the fluorescent conversion indicates the metabolic activity of cells and highlight the typical cobblestone morphology of the squamous epithelium (**Figure 4a**). Sporadic interruptions of the epicardial monolayer exposes the underlaying connective tissue and fibroblasts (**Figure 4b**). Morphological evaluation of the slices is fundamental to assess the outcome of the slice cutting protocol, with successful preparations presenting brightly fluorescent epicardium and extensive epicardial coverage. Briefly, slices are stained in NT solution supplemented with 10 μM Calcein AM cell-permeant dye at room temperature for 45 min under continuous shaking. Slices are then washed twice for 5 min with NT solution to remove all the Calcein AM residues and kept on ice until imaging by confocal microscopy. Z-stack confocal images are captured from random fields of the slice surface, using a 10× objective on a Nikon Eclipse Ti A1-A confocal laser scanning microscope and max projection images are quantified to estimate the percentage of live surface. We found that on average 71.21 ± 4.61% of the surface of epicardial slices from piglets (**Figure 4c**) and 61.65 ± 8.88% of the abattoir-derived slices were viable (**Figure 4d**).

Multi-Electrode Array Measurements

MEA system can be utilized to electrically stimulate the myocardial fibers present on the underside of the slices, evaluating the electrophysiology of the tissue (29). Data were acquired using a dish which contains 60-microelectrode arranged in an 8 × 8 matrix and an inter-electrode distance of 700 μm, providing a recording area of 4.9 × 4.9 mm^2. Slices are positioned in the center of the MEA dish, over the recording area, and submerged in oxygenated NT solution for recording at 37°C (see info in **Table 1**). Myocardial fibers within the epicardial slices exhibit viable field potential traces in the large majority of microelectrodes within the first 5 h following cutting, when elicited by 1 Hz stimulation (**Figure 4e**). This result

demonstrates full functionality and the maintenance of electrical connections between cardiomyocytes within the cardiac slices. The measurement of the field potential duration (**Figure 4f**), which is defined as the time between the depolarisation peak (FP_{MIN}) and the repolarisation peak (FP_{MAX}), estimates the action potential duration at 90% of repolarisation (APD90) (36). Our analysis, performed with Clampfit software (Axon Instruments, USA), indicate an average baseline of field potential duration of 254.87 ± 8.86 ms, which is in line with the value of field potential duration measured in cardiac slices of comparable size mammals (29) (**Figure 4g**).

Morphological Analysis

The tissue architecture of the slices can be investigated using different techniques. Here we show the results from the hematoxylin and eosin coloration and immunohistochemistry, following tissue sectioning, and the whole mount staining on decolorated epicardial/myocardial slices.

Tissue Sections

Histochemical analysis of the epicardial/myocardial slices performed with hematoxylin and eosin (**Figure 5a**) shows the orientation of myocardial fibers running parallel to the epicardial layer. Large coronary vessels and low levels of adipose tissue and connective tissue are also visible. High magnification images show the results obtainable from immunofluorescence staining of the slices (**Figures 5b–e**). Sarcomeric actin (α-SA) and connexin43 staining indicate the preservation of the myocardial tissue architecture, with sarcomeric structures and intact gap junctions (**Figure 5b**). Retention of intact epicardial monolayer is assessed by the expression of the epicardial progenitor transcription factor WT1 and the membrane marker mesothelin (MSLN) (**Figure 5c**). Preserved vascular tree is evidenced by the staining of capillaries, venules and arterioles with endothelial cell marker CD31, in some cases enveloped by α-SMA+ perivascular cells (**Figure 5d**). Connective tissue is identified by the expression of vimentin, which is typically highly expressed by mesenchymal/fibroblast cells (**Figure 5e**).

Slices Decoloration

We used the optical clearing method to visualize the expression of WT1 and MSLN in the full thickness of the epicardial monolayer (**Figures 6a,b**). We also obtained a comprehensive 3D map of the macro- and micro-vasculature within the slices by CD31 and α-SMA labeling (**Figures 6c,d**).

Culture

To keep the epicardial/myocardial slices alive, we developed a culture system which builds on the air-liquid interface protocol previously reported for the culture of myocardial slices (37). Our method allows tissue-medium contact at both epicardial and myocardial side, which is proven to be positive for the performance of the slices in culture (38). Notably, *en face* staining showed high epicardial cells viability and the retention of the typical cobblestone morphology in both piglets and adult swine hearts after 72 h of culture (**Figures 7a,b**).

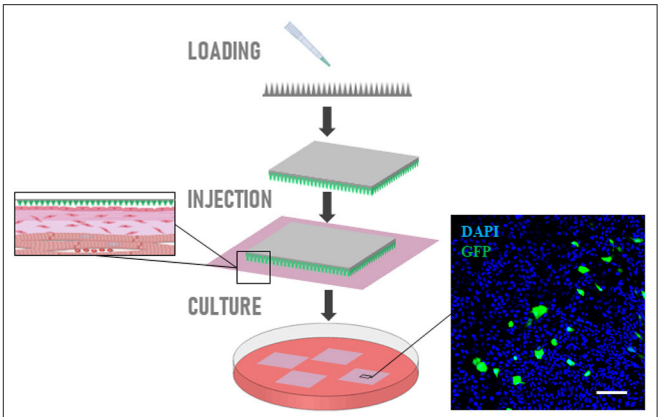

FIGURE 8 | Nanoinjection of plasmid. Schematic representation of nanoneedles-mediated delivery of GFP-carrying plasmid on epicardial cells. Confocal imaging indicated expression of GFP 48 h after nanoinjection in the epicardium of cultured slices. Scale bars, 50 μm.

Nanoinjection of Plasmid

GFP-carrying plasmid can be efficiently loaded on nanoneedles and delivered to the epicardial cells on the slice surface. Confocal imaging indicated expression of GFP 48 h after nanoinjection in the epicardium of cultured slices (**Figure 8**).

TROUBLESHOOTING GUIDE

In this section, we address the most common issues related to the preparation of epicardial/myocardial slices and suggest some possible solutions.

Tissue Block Shows Decoloration at the Edges After Embedding

- Low melting agarose solution is too warm:
  - Check the temperature of the solution and ensure the water bath is set at 37°C.

Blade Is Unable Cut the Tissue

- Blade is damaged or not mounted correctly:
  - Remove and replace the blade (check the z-axis deflection with VibroCheck).
- Tissue block is dis-homogeneous due to adipose or connective tissue:
  - Epicardial/myocardial slice integrity and viability are compromised, remove the tissue block and proceed with another embedding. This issue is more frequent in proximity of big vessels, try to avoid these areas when preparing the tissue block.

Epicardium Slice Is Not Flat

- Embedding agarose block is not flat or not well glued on to the specimen holder:
  - Myocardial side viability is compromised, this affects the viability of the whole slice in long-term culture. Remove the tissue block and proceed with another embedding. Be

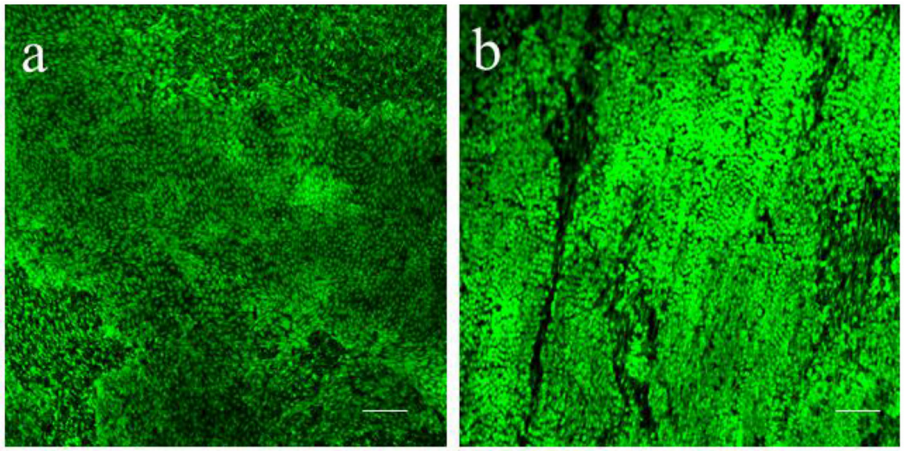

FIGURE 7 | Epicardial slices viability in culture. Calcein AM live staining performed on **(a)** piglet and **(b)** adult swine-derived slices, after 72 h of culture. Both tissues display large portion of living epicardial cells and the retention of the typical cobblestone morphology. Scale bars, 100 μm.

careful during the embedding and when removing the block from the plastic ring not to damage the agarose or press in correspondence of the tissue as this might cause the epicardium to bulge.

Epicardial Slice Appear to Be Thick

- Wrong position of the blade:
  - This can affect the viability of the slice. Remove the tissue block and proceed with another embedding. Set the vibratome's z-axis cutting blade starting position at the top edge of tissue block, ensure the blade is in contact with tissue/agarose when you set it.

Epicardial Slices Curl-Up Quickly in Recovery Solution

- Solutions were made incorrectly:
  - Slice viability can be compromised. Prepare the solution using ultrapure sterile water, adjust the pH at the exact working temperature of the solution, check the osmolarity to be in between 290 and 320 mOsm/L.

Poor Survival in Culture

- Lack of air-liquid interface:
  - The culture medium must skim the edges of the slice while leaving the epicardium partially exposed to the atmosphere, ensuring liquid interchange by capillarity. The correct amount of medium and the pump's speed need to be calibrated by the users.

ADVANTAGES AND LIMITATIONS

The increasing interest in the epicardium's regenerative capacity stimulated the development of numerous protocols to obtain cell systems for *in vitro* studies. Epicardial cells can be isolated by enzymatic digestion, by exploiting their ability to migrate from epicardial explant or by differentiation from stem cell sources (39–41). In terms of isolation strategy, epicardial outgrowth implies a degree of cell activation, while marker expression-based isolation and differentiation is complicated by the heterogeneity of the epicardial population, and the ectopic expression of markers (e.g., WT1) (23, 42, 43). The resulting cell population might therefore be contaminated by unwanted cell types and/or present different characteristics as compared to the *in vivo* counterpart. Furthermore, these primary cell lines have a tendency to undergo spontaneous epithelial-to-mesenchymal transition in culture, limiting their suitability for this type of studies (40). While primary cell studies have undoubtedly yielded important findings, epicardial slices represent a powerful tool in the investigation of the epicardium. Indeed, epicardial cells within the slices are embedded in their natural microenvironment, reducing spontaneous differentiation while at the same time enabling studies of the interaction between different cell populations within the cardiac tissue (23). In addition, epicardial/myocardial slices present significant advantages in respect to the currently available models: (i) Organotypic slices can be easily obtained and cultured *in vitro* while preserving the complexity of the tissue *in vivo,* maintaining tissue/cell morphology and the connections within cells and with the extracellular matrix. This integrated system allows to measure the effect of a treatment on multiple cell targets at once, providing information on epicardial, myocardial and non-contractile cells of the heart as well as the extracellular matrix. (ii) Slice preparation is cost effective as compared to large animal experiments. Moreover, from a single heart is possible to obtain up to 15–20 slices, increasing the number of samples/replicates and reducing the intra-assay variability. (iii) Our *ex vivo* model is accessible to the majority of the laboratories, as epicardial slices can be obtained from abattoir-derived hearts. (iv) Additionally, the wider application of epicardial/myocardial

slices will encourage the reduction of the number of animals used in research, replacing in part the use of rodents, large animals and zebrafish. At the same time, given the close similarities between porcine and human heart, results obtained on the slices will be clinically relevant.

While presenting some obvious advantages, slices also have some limitations: (i) The procedure is time-consuming and requires training and some preparatory experiments to ensure the success of the procedure. However, this limitation has to be weighed against the equally complex and time-consuming and ethically challenging training for *in vivo* work. (ii) Short-term viability in culture, as compared to classic *in vitro* models. Slices can be cultured up to 72 h, that could represent a limitation when mimicking chronic disease onset. Extended culture might be possible, although we expect some loss of viability in the myocardial compartment, and further studies are required to increase the lifespan of the slices. (iii) Lack of the inflammatory cells in the culture environment. Due the increasing interest for the role of the immune system in cardiovascular diseases, the integration of inflammatory cells in slices culture is one of the main targets for the development of this model. Immune cells and inflammatory stimuli can be added to the culture media as in a normal *in vitro* experiment, helping to identify specific mediators. (iv) Difficulties to distinguish the epicardial contribution due to the complexity of the tissue. The role of the epicardium can be assessed both by tracking the cells using methods such as the nanoinjection described here, or by comparison with myocardial slices obtained from the same block.

DATA AVAILABILITY STATEMENT

The raw data supporting the conclusions of this article will be made available by the authors, without undue reservation.

ETHICS STATEMENT

This study was reviewed and approved by the Animal Welfare and Ethical Review Board (AWERB) of The Pirbright Institute.

AUTHOR CONTRIBUTIONS

DMas conceived and planned the experiments and analyzed the data. RM, RJ, DMar, and VC provided key experimental expertise. DMas and PCamp wrote the manuscript and prepared the figures with support of CC and PCame. PCamp, PCame, and CC conceived the original idea and supervised the project. All authors contributed to the article and approved the submitted version.

FUNDING

This work PCamp and DMas were supported by the National Centre for the Replacement, Refinement & Reduction of Animals in Research (grant numbers: NC/R001006/1 and NC/T001216/1). RM is supported by the Doctoral College studentship award (University of Surrey) and CC, DMar, and VC by the European Research Council (grant reference: StG EnBioN 759577). PCame and RJ acknowledge support from the British Heart Foundation (grant number: FS/17/33/32931), the Royal Society (RSG/R1/180198) and the HEIF Strategic Fund.

ACKNOWLEDGMENTS

We thank Drs. L. Dixton, A. Reis, and M. Henstock from the Pirbright Institute (Pirbright, UK) and the personnel at Newman's Abattoir (Farnborough, UK) for their support in procuring the animal tissues. Prof. John McVey and the Department of Biochemical Sciences at the University of Surrey, especially the technical team, for their continuing support.

SUPPLEMENTARY MATERIAL

The Supplementary Material for this article can be found online at: https://www.frontiersin.org/articles/10.3389/fcvm.2022.920013/full#supplementary-material

REFERENCES

1. Zhou B, Honor LB, He H, Qing M, Oh JH, Butterfield C, et al. Adult mouse epicardium modulates myocardial injury by secreting paracrine factors. *J Clin Invest.* (2011) 121:1894–094. doi: 10.1172/JCI45529
2. van Wijk B, Gunst QD, Moorman AFM, van den Hoff MJB. Cardiac regeneration from activated epicardium. *PLoS ONE.* (2012) 7:e44692. doi: 10.1371/journal.pone.0044692
3. Smart N, Bollini S, Dubé KN, Vieira JM, Zhou B, Davidson S, et al. *De novo* cardiomyocytes from within the activated adult heart after injury. *Nature.* (2011) 474:640–4. doi: 10.1038/nature10188
4. Bollini S, Vieira JMN, Howard S, Dubè KN, Balmer GM, Smart N, et al. Re-activated adult epicardial progenitor cells are a heterogeneous population molecularly distinct from their embryonic counterparts. *Stem Cells Dev.* (2014) 23:1719–30. doi: 10.1089/scd.2014.0019
5. Bock-Marquette I, Shrivastava S, Pipes GCT, Thatcher JE, Blystone A, Shelton JM, et al. Thymosin β4 mediated PKC activation is essential to initiate the embryonic coronary developmental program and epicardial progenitor cell activation in adult mice *in vivo*. *J Mol Cell Cardiol.* (2009) 46:728–38. doi: 10.1016/j.yjmcc.2009.01.017
6. Tsang HG, Rashdan NA, Whitelaw CBA, Corcoran BM, Summers KM, MacRae VE. Large animal models of cardiovascular disease. *Cell Biochem Funct.* (2016) 34:113–32. doi: 10.1002/cbf.3173
7. Camacho P, Fan H, Liu Z, He JQ. Small mammalian animal models of heart disease. *Am J Cardiovasc Dis.* (2016) 6:70–80.
8. Austin AF, Compton LA, Love JD, Brown CB, Barnett J V. Primary and immortalized mouse epicardial cells undergo differentiation in response to TGFβ. *Dev Dyn.* (2008) 237:366–76. doi: 10.1002/dvdy.21421
9. Delaughter DM, Clark CR, Christodoulou DC, Seidman CE, Scott Baldwin H, Seidman JG, et al. Transcriptional profiling of cultured, embryonic epicardial cells identifies novel genes and signaling pathways regulated by TGFβR3 *in vitro*. *PLoS ONE.* (2016) 11:e0159710. doi: 10.1371/journal.pone.0159710
10. Gambardella L, McManus SA, Moignard V, Sebukhan D, Delaune A, Andrews S, et al. BNC1 regulates cell heterogeneity in human pluripotent stem cell-derived epicardium. *Development.* (2019) 146:dev174441. doi: 10.1242/dev.174441

11. Velecela V, Torres-Cano A, García-Melero A, Ramiro-Pareta M, Müller-Sánchez C, Segarra-Mondejar M, et al. Epicardial cell shape and maturation are regulated by Wt1 via transcriptional control of Bmp4. *Development.* (2019) 146:dev178723. doi: 10.1242/dev.178723
12. Vieira JM, Howard S, Villa del Campo C, Bollini S, Dubé KN, Masters M, et al. BRG1-SWI/SNF-dependent regulation of the Wt1 transcriptional landscape mediates epicardial activity during heart development and disease. *Nat Commun.* (2017) 8:16034. doi: 10.1038/ncomms16034
13. Poss KD, Wilson LG, Keating MT. Heart regeneration in zebrafish. *Science.* (2002) 298:2188–90. doi: 10.1126/science.1077857
14. Schnabel K, Wu CC, Kurth T, Weidinger G. Regeneration of cryoinjury induced necrotic heart lesions in zebrafish is associated with epicardial activation and cardiomyocyte proliferation. *PLoS ONE.* (2011) 6:e18503. doi: 10.1371/journal.pone.0018503
15. Wang J, Panáková D, Kikuchi K, Holdway JE, Gemberling M, Burris JS, et al. The regenerative capacity of zebrafish reverses cardiac failure caused by genetic cardiomyocyte depletion. *Development.* (2011) 138:3421–30. doi: 10.1242/dev.068601
16. Choi WY, Poss KD. Cardiac regeneration. In: *Current Topics in Developmental Biology*. San Diego, CA: Academic Press Inc. (2012). p. 319–44. doi: 10.1016/B978-0-12-387786-4.00010-5
17. Uygur A, Lee RT. Mechanisms of cardiac regeneration. *Dev Cell.* (2016) 36:362–74. doi: 10.1016/j.devcel.2016.01.018
18. Martínez-Estrada OM, Lettice LA, Essafi A, Guadix JA, Slight J, Velecela V, et al. Wt1 is required for cardiovascular progenitor cell formation through transcriptional control of Snail and E-cadherin. *Nat Genet.* (2010) 42:89–93. doi: 10.1038/ng.494
19. Chong JJH, Murry CE. Cardiac regeneration using pluripotent stem cells-Progression to large animal models. *Stem Cell Res.* (2014) 13:654–65. doi: 10.1016/j.scr.2014.06.005
20. de Boer TP, Camelliti P, Ravens U, Kohl P. Myocardial tissue slices: organotypic pseudo-2D models for cardiac research & development. *Fut Cardiol.* (2009) 5:425–30. doi: 10.2217/fca.09.32
21. Pillekamp F, Halbach M, Reppel M, Rubenchyk O, Pfannkuche K, Xi JY, et al. Neonatal murine heart slices. A robust model to study ventricular isometric contractions. *Cell Physiol Biochem.* (2007) 20:837–46. doi: 10.1159/000110443
22. Bursac N, Papadaki M, White JA, Eisenberg SR, Vunjak-Novakovic G, Freed LE. Cultivation in rotating bioreactors promotes maintenance of cardiac myocyte electrophysiology and molecular properties. *Tissue Eng.* (2004) 9:1243–53. doi: 10.1089/10763270360728152
23. Maselli D, Matos RS, Johnson RD, Chiappini C, Camelliti P, Campagnolo P. Epicardial slices: an innovative 3D organotypic model to study epicardial cell physiology and activation. *npj Regen Med.* (2022) 7:1–16. doi: 10.1038/s41536-021-00202-7
24. Kang C, Qiao Y, Li G, Baechle K, Camelliti P, Rentschler S, et al. Human organotypic cultured cardiac slices: new platform for high throughput preclinical human trials. *Sci Rep.* (2016) 6:1–13. doi: 10.1038/srep28798
25. Watson SA, Scigliano M, Bardi I, Ascione R, Terracciano CM, Perbellini F. Preparation of viable adult ventricular myocardial slices from large and small mammals. *Nat Protoc.* (2017) 12:2623–39. doi: 10.1038/nprot.2017.139
26. He S, Wen Q, OShea C, Muu-Min R, Kou K, Grassam-Rowe A, et al. A protocol for transverse cardiac slicing and optical mapping in murine heart. *Front Physiol.* (2019) 10:755. doi: 10.3389/fphys.2019.00755
27. Wen Q, Gandhi K, Capel RA, Hao G, O'Shea C, Neagu G, et al. Transverse cardiac slicing and optical imaging for analysis of transmural gradients in membrane potential and Ca2+ transients in murine heart. *J Physiol.* (2018) 596:3951–65. doi: 10.1113/JP276239
28. Bussek A, Wettwer E, Christ T, Lohmann H, Camelliti P, Ravens U. Tissue slices from adult mammalian hearts as a model for pharmacological drug testing. *Cell Physiol Biochem.* (2009) 24:527–36. doi: 10.1159/000257528
29. Camelliti P, Al-Saud SA, Smolenski RT, Al-Ayoubi S, Bussek A, Wettwer E, et al. Adult human heart slices are a multicellular system suitable for electrophysiological and pharmacological studies. *J Mol Cell Cardiol.* (2011) 51:390–8. doi: 10.1016/j.yjmcc.2011.06.018
30. Kolesová H, Capek M, Radochová B, Janáček J, Sedmera D. Comparison of different tissue clearing methods and 3D imaging techniques for visualization of GFP-expressing mouse embryos and embryonic hearts. *Histochem Cell Biol.* (2016) 146:141–52. doi: 10.1007/s00418-016-1441-8
31. Tainaka K, Kubota SI, Suyama TQ, Susaki EA, Perrin D, Ukai-Tadenuma M, et al. Whole-body imaging with single-cell resolution by tissue decolorization. *Cell.* (2014) 159:911–24. doi: 10.1016/j.cell.2014.10.034
32. Chiappini C, Campagnolo P, Almeida CS, Abbassi-Ghadi N, Chow LW, Hanna GB, et al. Mapping local cytosolic enzymatic activity in human esophageal mucosa with porous silicon nanoneedles. *Adv Mater.* (2015) 27:5147–52. doi: 10.1002/adma.201501304
33. Chiappini C, Chen Y, Aslanoglou S, Mariano A, Mollo V, Mu H, et al. Tutorial: using nanoneedles for intracellular delivery. *Nat Protoc.* (2021) 16:4539–63. doi: 10.1038/s41596-021-00600-7
34. Chiappini C, Martinez JO, De Rosa E, Almeida CS, Tasciotti E, Stevens MM. Biodegradable nanoneedles for localized delivery of nanoparticles *in vivo*: exploring the biointerface. *ACS Nano.* (2015) 9:5500–9. doi: 10.1021/acsnano.5b01490
35. Chiappini C, De Rosa E, Martinez JO, Liu X, Steele J, Stevens MM, et al. Biodegradable silicon nanoneedles delivering nucleic acids intracellularly induce localized *in vivo* neovascularization. *Nat Mater.* (2015) 14:532–9. doi: 10.1038/nmat4249
36. Halbach MD, Egert U, Hescheler J, Banach K. Estimation of action potential changes from field potential recordings in multicellular mouse cardiac myocyte cultures. *Cell Physiol Biochem.* (2003) 13:271–84. doi: 10.1159/000074542
37. Brandenburger M, Wenzel J, Bogdan R, Richardt D, Nguemo F, Reppel M, et al. Organotypic slice culture from human adult ventricular myocardium. *Cardiovasc Res.* (2012) 93:50–9. doi: 10.1093/cvr/cvr259
38. Watson SA, Duff J, Bardi I, Zabielska M, Atanur SS, Jabbour RJ, et al. Biomimetic electromechanical stimulation to maintain adult myocardial slices *in vitro*. *Nat Commun.* (2019) 10:1–15. doi: 10.1038/s41467-019-10175-3
39. Ramesh S, Singh A, Cibi DM, Hausenloy DJ, Singh MK. *In vitro* culture of epicardial cells from mouse embryonic heart. *J Vis Exp.* (2016) 2016:53993. doi: 10.3791/53993
40. Dronkers E, Moerkamp AT, van Herwaarden T, Goumans MJ, Smits AM. The isolation and culture of primary epicardial cells derived from human adult and fetal heart specimens. *J Vis Exp.* (2018) 2018:57370. doi: 10.3791/57370
41. Guadix JA, Orlova VV, Giacomelli E, Bellin M, Ribeiro MC, Mummery CL, et al. Human pluripotent stem cell differentiation into functional epicardial progenitor cells. *Stem Cell Rep.* (2017) 9:1754–64. doi: 10.1016/j.stemcr.2017.10.023
42. Rudat C, Kispert A. Wt1 and epicardial fate mapping. *Circ Res.* (2012) 111:165–9. doi: 10.1161/CIRCRESAHA.112.273946
43. Christoffels VM, Grieskamp T, Norden J, Mommersteeg MTM, Rudat C, Kispert A. Tbx18 and the fate of epicardial progenitors. *Nature.* (2009) 458:E8–9. doi: 10.1038/nature07916

Conflict of Interest: The authors declare that the research was conducted in the absence of any commercial or financial relationships that could be construed as a potential conflict of interest.

frontiers | Frontiers in Cardiovascular Medicine

TYPE Original Research
PUBLISHED 23 August 2022
DOI 10.3389/fcvm.2022.970745

OPEN ACCESS

EDITED BY
Claudio de Lucia,
Scientific Clinical Institute Maugeri (ICS Maugeri), Italy

REVIEWED BY
Nibaldo C. Inestrosa,
Pontificia Universidad Católica de Chile, Chile
Enrique Gallego-Colon,
Barzilai Medical Center, Israel

*CORRESPONDENCE
Liansheng Wang
drlswang@njmu.edu.cn

†These authors have contributed equally to this work

SPECIALTY SECTION
This article was submitted to Cardiovascular Biologics and Regenerative Medicine, a section of the journal Frontiers in Cardiovascular Medicine

RECEIVED 16 June 2022
ACCEPTED 08 August 2022
PUBLISHED 23 August 2022

CITATION
Sun J, Yang T, Wei T, Zhou L, Shan T, Chen J, Gu L, Chen B, Liu L, Jiang Q, Du C, Ma Y, Wang H, Chen F, Guo X, Ji Y and Wang L (2022) CDK9 binds and activates SGK3 to promote cardiac repair after injury via the GSK-3β/β-catenin pathway. *Front. Cardiovasc. Med.* 9:970745. doi: 10.3389/fcvm.2022.970745

CDK9 binds and activates SGK3 to promote cardiac repair after injury via the GSK-3β/β-catenin pathway

Jiateng Sun[1†], Tongtong Yang[1†], Tianwen Wei[1†], Liuhua Zhou[1], Tiankai Shan[1], Jiawen Chen[1], Lingfeng Gu[1], Bingrui Chen[1], Liu Liu[1], Qiqi Jiang[1], Chong Du[1], Yao Ma[1], Hao Wang[1], Feng Chen[2], Xuejiang Guo[3], Yong Ji[4,5] and Liansheng Wang[1*]

[1]Department of Cardiology, The First Affiliated Hospital of Nanjing Medical University, Nanjing, China, [2]Department of Biostatistics, School of Public Health, China International Cooperation Center for Environment and Human Health, Nanjing Medical University, Nanjing, China, [3]State Key Laboratory of Reproductive Medicine, Department of Histology and Embryology, Nanjing Medical University, Nanjing, China, [4]Key Laboratory of Cardiovascular and Cerebrovascular Medicine, Collaborative Innovation Center for Cardiovascular Disease Translation, Nanjing Medical University, Nanjing, China, [5]Key Laboratory of Targeted Intervention of Cardiovascular Disease, Collaborative Innovation Center for Cardiovascular Disease Translation, Nanjing Medical University, Nanjing, China

The mammalian heart possesses entire regeneration capacity after birth, which is lost in adulthood. The role of the kinase network in myocardial regeneration remains largely elusive. SGK3 (threonine-protein kinase 3) is a functional kinase we identified previously with the capacity to promote cardiomyocyte proliferation and cardiac repair after myocardial infarction. However, the upstream signals regulating SGK3 are still unknown. Based on the quantitative phosphoproteomics data and pulldown assay, we identified cyclin-dependent kinase 9 (CDK9) as a novel therapeutic target in regeneration therapy. The direct combination between CDK9 and SGK3 was further confirmed by co-immunoprecipitation (Co-IP). CDK9 is highly expressed in the newborn period and rarely detected in the adult myocardium. *In vitro*, the proliferation ratio of primary cardiomyocytes was significantly elevated by CDK9 overexpression while inhibited by CDK9 knockdown. *In vivo*, inhibition of CDK9 shortened the time window of cardiac regeneration after apical resection (AR) in neonatal mice, while overexpression of CDK9 significantly promoted mature cardiomyocytes (CMs) to re-enter the cell cycle and cardiac repair after myocardial infarction (MI) in adult

mice. Mechanistically, CDK9 promoted cardiac repair by directly activating SGK3 and downstream GSK-3β/β-catenin pathway. Consequently, our study indicated that CDK9 might be a novel target for MI therapy by stimulating myocardial regeneration.

KEYWORDS

myocardial regeneration, myocardial infarction, CDK9, cardiac repair, GSK-3β/β-catenin pathway

Introduction

Myocardial infarction (MI) and subsequent heart failure are the leading causes of morbidity and mortality in patients with cardiovascular disease (CVD) worldwide (1). Therefore, myocardial regenerative therapy for MI has become a research hotspot in recent years, and the discovery of the neonatal myocardial regeneration period provides a new theoretical basis for studying endogenous myocardial regeneration (2). Neonatal mice can achieve complete functional and structural repair by endogenous myocardial regeneration within 7 days after MI or apical resection (AR), but this ability is rapidly lost (3). Therefore, the relevant studies based on the regulation of the myocardial regeneration period can indicate the return of mature cardiomyocytes (CMs) to the cell cycle after injury to achieve myocardial regeneration and repair.

The cyclin-dependent kinases (CDKs) family has a remarkable role in promoting proliferation. CDKs control critical cell cycle checkpoints and transcriptional events in response to extracellular and intracellular signals leading to mammalian cell proliferation. The intervention of CDKs has been a hot topic in cancer therapy, among which inhibitors that block the activity of CDK4 and CDK6 enzymes (CDK4/6) have been approved by the FDA to treat metastatic hormone receptor-positive breast cancer (4). Positive cell cycle regulators such as cyclin D1, CDK4/6, Rb, and E2F transcription factors are highly expressed in fetal CMs but significantly down-regulated in neonatal and adult CMs, consistent with postnatal CMs cycle arrest (5). DiStefano et al. found that neonatal and adult CMs could re-enter the cell cycle by knocking out endogenous CDKs inhibitors (6). The results suggest that neonatal and adult CMs can achieve proliferative capacity by regulating CDKs key nodes. Recently, the combined expression of CDK1, CDK4, cyclin B1, and cyclin D1 can induce nuclear replication and division in mice, rats, and human cardiac muscle and achieve cardiac proliferation through stable cytoplasmic separation (7).

The role of protein kinases in CVD has also gradually gained attention (8, 9). Cyclin-dependent kinase 9 (CDK9) is the most representative member of the CDKs family and plays an essential role in the development and progression of cardiac hypertrophy (10). Sano et al. found that the expression of CDK9 was upregulated, and its activity increased during myocardial hypertrophy, while chronic activation of CDK9 led to heart failure in the myocardium of adult mice (11). Besides, CDK9 could be a potential biomarker of atherosclerosis, which significantly increases in the serum of patients with CVD, and plays a vital role in inflammatory diseases (12). In addition, CDK9 inhibitor LDC000067 and siRNA-mediated CDK9 knockdown could reverse low-density lipoprotein-induced inflammation and phenotypic conversion from contractile to synthetic phenotypes of human vascular smooth muscle cells (HVSMCs) by inhibiting the NF-kB signaling pathway in HVSMCs (13). As a core component of positive transcription elongation factor b, CDK9 has been involved in differentiating mice embryonic stem cells into CMs by interacting with GATA4 (14).

Our previous study found that serine/threonine-protein kinase 3 (SGK3) remains highly expressed during the neonatal stage (myocardium with regenerative capacity), consistent with the mammalian myocardial regenerative period. Additionally, overexpression of SGK3 kinase induces proliferation of CMs by mediating the GSK-3β/β-catenin signaling pathway, protecting against myocardial I/R injury (9). In exploring the mechanism of SGK3 in myocardial protection, we surprisedly found that CDK9 and SGK3 directly bind, and CDK9 could act as the upstream regulator of SGK3 expression, which may play a more significant role in promoting CMs proliferation. Therefore, CDK9 warrants further investigation of the relevant effects as a therapeutic target on CMs proliferation in mammals.

Abbreviations: SGK3, threonine-protein kinase 3; CDK9, cyclin-dependent kinase 9; Co-IP, co-immunoprecipitation; P1, postnatal day 1; AR, apical resection; MI, myocardial infarction; CVD, cardiovascular disease; CMs, cardiomyocytes; CDKs, cyclin-dependent kinases; CDK4/6, CDK4 and CDK6 enzymes; HVSMCs, human vascular smooth muscle cells; IACUC, Institutional Animal Care and Use Committee; ICR, Institute of Cancer Research; SPF, specific pathogen-free; LVEF, left ventricular ejection fraction; LVFS, left ventricular fraction shortening; EdU, 5-ethynyl-2′-deoxyuridine; DAPI, 4′, 6-diamidino-2-phenylindole; CTD, C-terminal domain; RNAP II, RNA polymerase II; IGF, insulin-like growth factor; PPAR δ, peroxisome proliferator-activated receptor δ.

Materials and methods

Mice

Neonatal 1-day-old and 8-week-old mice were used in our study. Institute of Cancer Research (ICR) mice were purchased from the Animal Core Facility of Nanjing Medical University and raised in the specific pathogen-free (SPF) environment with 12 h dark and 12 h light cycle. The mice were all healthy and had free access to water and food. As shown below, mice received AR at 1 day of age and MI at 8 weeks of age (All experiments involving animals are carried out following the Guidelines for the Use and Care of Laboratory Animals. All animal protocols have been approved by the Animal Care and Use Committee of Nanjing Medical University).

Apical resection and apical intra-myocardial microinjection

AR surgery was performed on neonatal mice 1 day after birth. P1 mice were anesthetized on an ice bed for 3–4 min. The skin was cut from the left fourth intercostal space by microsurgery. The heart was squeezed out of the chest by pressing the abdomen of the mice. Surgical scissors were then used to remove 10–15% of the apex tissue from the left ventricle. After surgery, the heart was gently returned to the chest, and the thoracic wall and skin incision were closed immediately using 6-0 sutures. Finally, mice were placed on the thermostat to recover their body temperature quickly and put back into the cage after returning to normal activities. The sham-operated mice were subjected to the same procedure mentioned above without AR. All mice were sent to their mothers after surgery. After the apex of the heart is partially resected, Ad5: cTnT-CDK9i (The target sequence of shRNA for mice CDK9 was 5′-GGTCACCAAGTACGAGAAACT-3′) or Ad5: cTnT-CONi (the total amount of virus injected was $1*10^9$ PFU) was injected around the apex of the P1 heart by a microsyringe with a 36G needle as we previously described (15). Briefly, the virus dilution was pre-dyed by Trypan blue and injected to the ventricular myocardium of AR border zone. Blue staining of the marginal myocardium indicates a successful intra-myocardial injection.

Myocardial infarction and apical intra-myocardial microinjection

Male mice aged 8 weeks (P56) were anesthetized by intraperitoneal injection of 1.2% Avertin (Sigma-Aldrich, St. Louis, MO, United States) and artificially ventilated by a small animal ventilator. Ophthalmic scissors were used to cut the skin along with the left fourth costal space. The intercostal muscles were bluntly separated by ophthalmic forceps and then entered the chest to expose the left atrial appendage. The LAD was ligated with a 6-0 suture needle from the lowest margin of the left atrial appendage. Then the intercostal muscle and skin incision were sutured layer by layer with 3-0 sutures. After the operation, the mice were placed on the thermostat to wake up. The sham-operated mice were subjected to the same procedure mentioned above without MI. After LAD was ligated, adenovirus AAV9: cTnT-CDK9 or AAV9: cTnT-CON was injected around the apex of P56 using a microsyringe with a 36G needle as previously described (15) (the total virus dose was $1.5*10^9$ v.g.). Briefly, the virus dilution was pre-dyed by Trypan blue and injected into the ventricular myocardium of the infarct border zone, defined as the myocardial tissue 1 ∼ 2 mm away from the infarction edge. Blue staining of the marginal myocardium indicates a successful intra-myocardial injection.

Echocardiography

Cardiac function was determined by echocardiography Vevo 2100 (VisualSonics, Ontario, CA, United States) following AR/MI injury at the designed timepoint (1/22 day-post-AR, n = 7; 4/28 day-post-MI, n = 8). After aligning the transverse B-mode with the papillary muscles, cardiac function was measured on M-mode images. The left ventricular contractile function parameters (LVEF/LVFS) were automatically calculated using the accompanying software.

Histological staining and assessment of infarct size

For histological analysis, we collected and embedded the MI (28 days post-MI) hearts in paraffin. Three sections of each heart (5 μm for each slide, two adjacent slides interval of 200 μm) were collected, starting from the apex to the base. The heart slices were then used for Masson staining to visualize the scar area. For scar size measurement, we measured the entire left ventricle area and the scar area for each slice with Image J, and the mean scar size of 3 slices was used as the scar size (%) for each heart.

Neonatal primary cardiomyocytes isolation, culture and transfection

Neonatal ICR mice hearts were harvested at 1 day old (50–80 hearts each time). Neonatal hearts were chopped up, then transferred to a sterile flask for digestion with 20 ml of

the digestive solution containing 0.06 g/100 ml trypsin (Sigma, United States) and 0.04 g/100 ml collagenase-II (Worthington, OH, United States) for 6–7 min each time. Cycle digestion until the myocardial tissue is completely digested into a cellular state. The cell suspension was resuspended using DMEM containing 10% FBS and incubated in an incubator for 45 min to remove cardiac fibroblasts. The remaining suspension was centrifuged with Percoll liquid (3,000 rpm, 30 min, slowly rising and falling), and the CMs of the middle layer were collected and cultured in an incubator with 5% CO_2 at 37°C. After 24 h of culture, non-adherent cells were washed, and the remaining cells were cultured for another 24 h, then transfected with adenovirus for different experiments. To investigate the role of CDK9 in CMs and its effect on SGK3, we used the corresponding vector to transfect CMs for 48 h.

Recombinant adenovirus

Recombinant adenovirus of CDK9, SGK3 (Ad5: cTNT-CDK9, SGK3) and adenovirus of control (Ad5: cTNT-CON) were designed by CMs specific cTNT promoter obtained from GeneChem Company (Shanghai, China). Adenoviruses carrying scrambled shRNA for mice CDK9, SGK3 (Ad5: cTNT-CDK9i, SGK3i) and adenovirus of control (Ad5: cTNT-CONi) were also purchased from GeneChem Company (Shanghai, China). The adeno-associated virus type 9 (AAV9) is driven by CMs specific cTNT promoter cTNT: 3Flag-CDK9 (AAV9: cTNT-CDK9) and control adeno-associated virus type 9 (AAV9: cTNT-CON) were also purchased from GeneChem Company (Shanghai, China). In neonatal primary CMs, the MOI (multiplicity of infection) of the effective transfection dose for viral transfection was 50 (9, 15).

RNA extraction and quantitative real-time polymerase chain reaction

Total RNA was extracted using TRIzol reagent (Thermo Fisher Scientific) according to the manufacturer's instructions. The quantity and quality of RNA were determined by Nanodrop 2000 spectrophotometer (Thermo Fisher Scientific). Then the PrimeScript RT Master Mix kit (Takara Bio, Kusatsu, Japan) was used to synthesize complementary DNA. Gene amplification was performed in Roche LightCycler 96 using specific primers and SYBR Green (Vazyme Biotech, Nanjing, China; Q131-02). The relative expression of the target genes was normalized to the expression level of 18S. The sequences of qRT-PCR primers are as follows: 18S-F: TAACGAACGAGACTCTGGCAT, 18S-R: CGGACATCTAAGGGCATCACAG; CDK9-F: TGAAGGCTGCGAATGTG, CDK9-R: GTTGGTGTATCGGT TGGG.

Flow cytometry

At the required stage *in vitro*, primary neonatal mouse cardiomyocytes were washed and cultured with PBS, then 0.25% EDTA-free trypsin was added and cultured in a 37°C incubator for 5 min to digest the cells. The digestion was terminated with the complete medium containing 10% FBS; the cells were centrifuged (1,200 rpm, 5 min), washed with PBS and centrifuged again (1,200 rpm, 5 min). Afterward, the cell masses were resuspended in 70% ethanol and 20 μM filter dripping and fixing overnight at 4°C. The cells were centrifuged (1,200 rpm, 5 min), washed with PBS, and then centrifuged again (1,200 rpm, 5 min). The cells were resuspended in PI/RNase staining buffer (BD Biosciences, Franklin Lakes, NJ, United States) and incubated in a 37°C water bath for 40 min for flow cytometry detection. The data is generated by BD FACSVerse (Franklin Lakes, NJ, United States).

Immunofluorescence staining

Hearts were fixed with 4% paraformaldehyde overnight and then embedded in paraffin. The paraffin-embedded hearts were cut into 5 μm slices and boiled in antigen retrieval buffer for 10 min. Then, the slices were immersed in PBS containing 0.2% Triton X-100 for 15 min and blocked with 5% bovine serum albumin for 2 h. Click-iT EdU imaging Kits (Thermo Fisher), anti-Ki67 antibody (1:200, Abcam; Ab16667) and anti-phosphorylation-histone 3 (pH3) antibody (1:200, CST; 9701) were used to culture with slices to identify cell cycle activity. Anti-troponin T (cTNT, 1:200, Abcam; Ab8295) was used to label CMs and Hoechst to label nuclei. Wheat germ agglutinin (WGA) staining (Thermo Fisher; w32466) was performed to stain the cell membrane. *In vitro*, neonatal mice CMs grown on 24-well plates were fixed with 4% paraformaldehyde for 30 min. After being blocked with 10% goat serum for 1 h, 5-ethynyl-2′-deoxyuridine (EdU), Ki67, and pH3 staining were performed. cTnT or a-Actinin were used to label CMs, and 4′, 6-Diamidino-2-phenylindole (DAPI) to label nuclei. Quantitative data were obtained by confocal microscopy (Zeiss, Oberkochen, Germany) and Carl Zeiss Microscopy (Jena, Germany). To detect CM proliferation, we calculated the number of EdU^+, $Ki67^+$, and $pH3^+$ cardiomyocytes in the whole infarct border zone and their proportions in all border CMs.

Western blot

For Western blot analysis, heart tissues or cells were lysed with lysis buffer (including 0.5% PMSF, 0.1% protease inhibitor, and 1% phosphatase inhibitor) (GeneChem, Shanghai, China). Cytoplasmic extracts and nuclear extracts were prepared using a

nuclear and cytoplasmic extraction reagent kit (Thermo Fisher, United States). After determining the protein concentration by BCA Protein Assay, equal amounts of proteins were separated in SDS-PAGE gels and electro-transferred onto PVDF membranes (Millipore). And the membranes were incubated overnight at 4°C with primary antibodies (here, add specific primary antibody information) after blocking with bovine serum albumin (BSA). After washing three times for 30 min with TBST, membranes were cultured with the secondary antibodies diluted in blocking buffer for 2 h at room temperature. Quantification of band intensity was performed using Image J software (National Institutes of Health, Bethesda, MD, United States).

Pull-down assay and mass spectrometry

The CMs treated with Ad5: cTNT-SGK3 were collected and lysed using RIPA lysis buffer (Beyotime, China). After detecting the concentration, the protein solution was divided into two groups and incubated overnight with IgG or SGK3 antibody at 4°C. The protein-antibody complex was captured using agarose beads (Millipore Corp., United States) for 4 h of rotation. SDS-PAGE was then used to separate the target proteins, and silver staining was used to identify the different bands between the two groups. The eluted protein solutions were analyzed through mass spectrometry analysis (Wuhan Genecreate Biological Engineering Co., Ltd.) using LC-MS/MS (ekspertTMnanoLC; AB Sciex TripleTOF 5600-plus) instrument.

Co-immunoprecipitation

For the Co-IP assay, the Ad5: cTNT-SGK3 transfected CMs, neonatal and adult myocardial tissue were collected and lysed using RIPA lysis buffer (Beyotime, China). The proteins were incubated with SGK3 or CDK9 antibody overnight at 4°C. The protein-antibody complex was captured using PureProteome^{TM} Protein A Magnetic Beads (Millipore Corp., United States) for 4 h of rotation. Then wash twice with RIPA lysis buffer and centrifugate to obtain the residue. Finally, the complex with loading buffer was boiled for 10 min and analyzed by Western blot.

Statistical analysis

All data were statistically analyzed using SPSS 22.0 (IBM, Armonk, NY, United States) and expressed as mean ± SEM. The unpaired Student *t*-test was used to assess the statistical difference between the two groups. Comparisons between multiple groups were performed using either one-way ANOVA (using the Tukey multiple comparison test) or two-way ANOVA (using the *post hoc* Sidak test) to determine statistical differences. The results with P-values < 0.05 were considered statistically significant.

Results

CDK9 interacts with SGK3 and enhances SGK3 activity

Our previous study found and verified the critical role of SGK3 in promoting endogenous cardiomyocyte proliferation via the GSK-3β/β-catenin pathway. To unravel the upstream signals of SGK3, we first selected 26 proteins detected to directly bind to SGK3 by pulldown and mass spectrometry analysis of SGK3 (**Supplementary Figure 1** and **Supplementary Tables 1, 2**). Combined with previous studies, we screened out CDK9 as a potential SGK3-interacted kinase (**Figure 1A**). To verify the relationship between SGK3 and CDK9, we used IgG and SGK3 as baits to perform co-IP experiments in H9C2 cell lines and neonatal mice CMs, respectively. We detected significant CDK9 expression in the SGK3 group (**Figures 1B,C**). Given the high expression of CDK9 in neonatal hearts, we performed supplementary co-IP in P1 mice myocardium and obtained the same results (**Figure 1D**). Furthermore, the co-immunofluorescence images also indicated that CDK9 and SGK3 co-localized in the cytoplasm in the P1 myocardium (**Figure 1E**). Next, to clarify the exact relationship between SGK3 and CDK9, we overexpressed SGK3 or CDK9 in neonatal mice CMs, respectively. The results showed that overexpression of CDK9 could increase the phosphorylation activity of SGK3, while the intervention of SGK3 had no significant effect on the expression level and activity of CDK9 (**Figures 1F,G**).

Expression pattern of CDK9 correlates with myocardial regeneration

To verify whether CDK9 plays a vital role in myocardial regeneration in mice, we first examined the expression levels of CDK9 in myocardial tissues during the embryonic and postnatal period. The results showed that CDK9 was highly expressed during embryonic and 3 days after birth. While the expression level rapidly decreased after 7 days of life and was almost undetectable in the adult stage. This expression pattern matched the myocardial regeneration period (2, 3) (**Figures 2A,B**). In addition, we constructed AR in neonatal mice at P1 and found that CDK9 expression was significantly higher by western blot at P7 (**Figures 2C,D**). Next, to further reveal the expression characteristics of CDK9 from the dimension of time and space, we found by nucleocytoplasmic separation and western blot that CDK9 was markedly distributed in both the nucleus and cytoplasm, and the expression level was significantly higher at

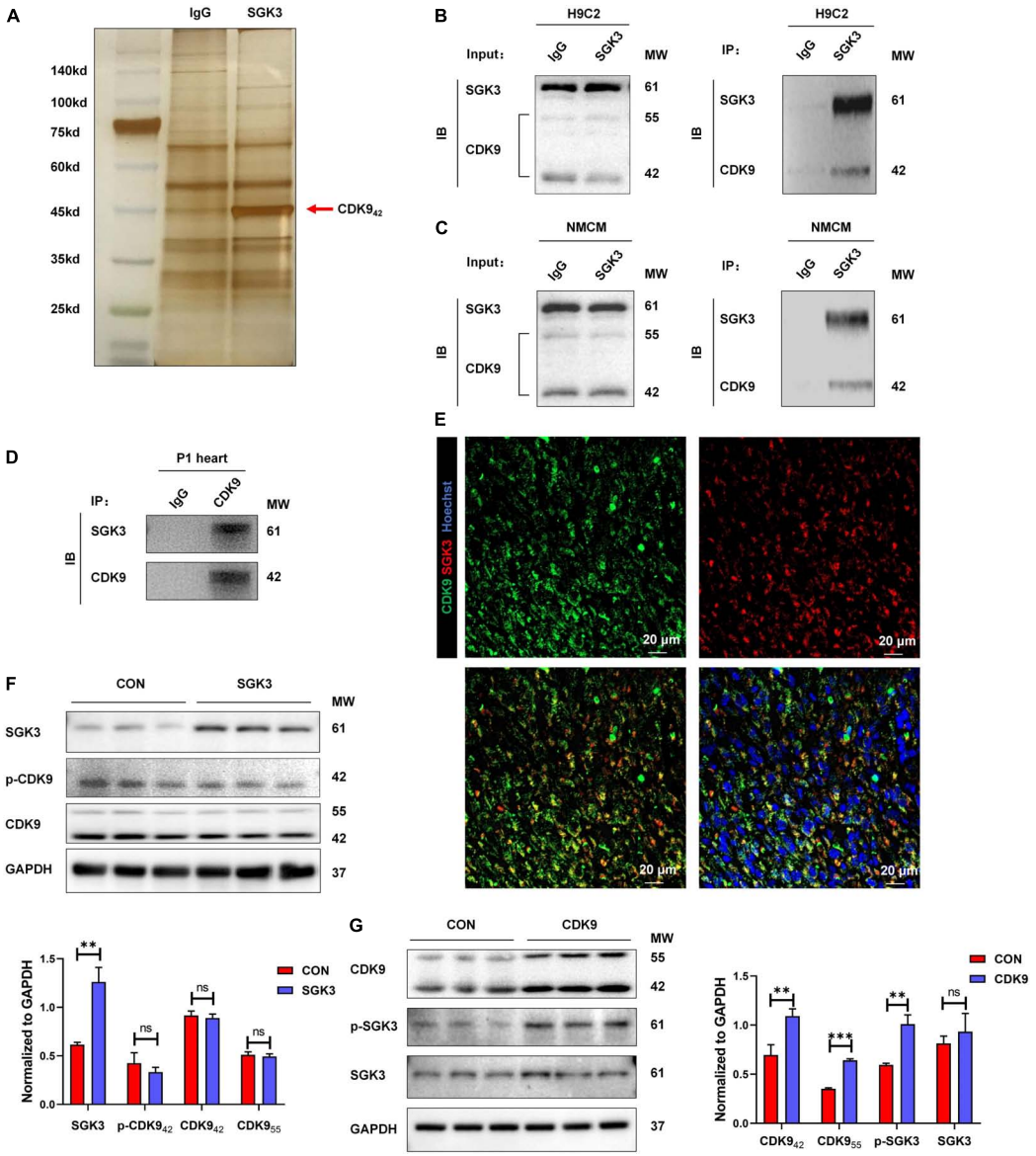

FIGURE 1
CDK9 interacts with SGK3 and enhances SGK3 activity. **(A–D)** Silver staining of a gel showing SGK3 and the control IgG pulldown proteins (CDK9, 42 kDa, red arrow) **(A)**. Co-immunoprecipitation reveals that CDK9$_{42}$ interacts with SGK3 in the H9C2 cell line **(B)**, neonatal CMs **(C),** and P1 heart **(D)**. **(E)** Co-localization of SGK3 and CDK9 in neonatal myocardium was detected by immunofluorescence. **(F)** SGK3, phosphorylated (p-) CDK9 and CDK9 proteins were detected by Western blot in CMs transfected with Ad5: cTnT-SGK3 (MOI = 50). **(G)** CDK9, SGK3 Thr320 and SGK3 proteins were detected by Western blot in CMs transfected with Ad5: cTnT-CDK9 (MOI = 50). CMs indicate cardiomyocytes, MW indicates molecular weight, MOI indicates a multiplicity of infection; statistical significance was calculated with the unpaired Student *t*-test; data are presented as mean ± SEM, $^{**}P \leq 0.01$, $^{***}P \leq 0.001$.

P1 day than P56 day. While the SGK3, as we previously revealed, was mainly distributed in the cytoplasm (Figure 2E).

CDK9 regulates cardiomyocytes proliferation *in vitro*

Based on the importance of CMs proliferation in myocardial regeneration, we next isolated and purified primary CMs *in vitro* and verified the effect of CDK9 on CMs proliferation. We first demonstrated the transfection efficiency of Ad5: cTNT-CDK9i, Ad5: cTNT-CON and Ad5: cTNT-CDK9 in CMs via western blot and qRT-PCR (Figures 3A,B). Then we used immunofluorescence to detect cell proliferation indicators, such as EdU (DNA synthesis), Ki67 (cell cycle activity) and pH3 (mitosis). The results showed that overexpression of CDK9 could improve the proliferative capacity of CMs (Figures 3C–E), while knockdown of CDK9 impaired the

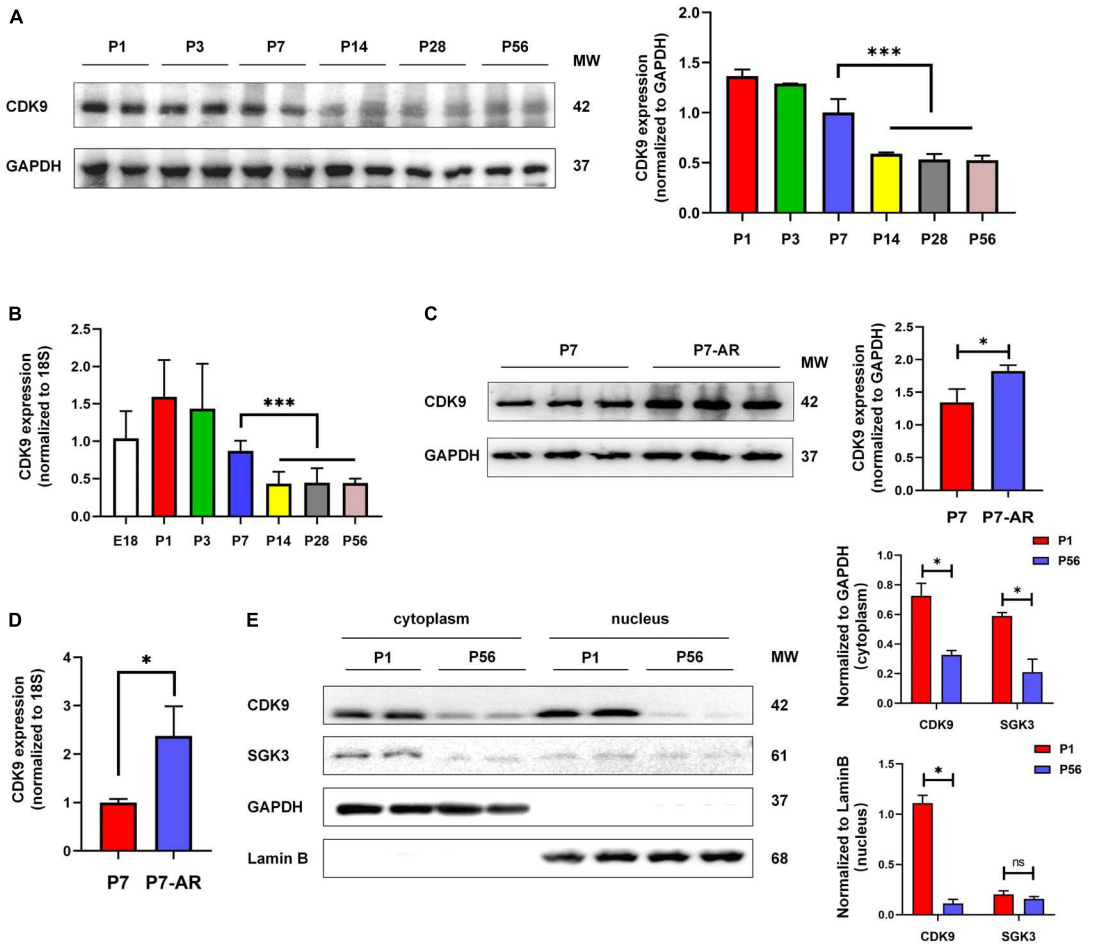

FIGURE 2
Expression pattern and subcellular localization of CDK9. **(A)** CDK9 proteins of ventricular myocardium detected by western blot in P1–P56 mice. **(B)** mRNA expression levels of CDK9 in embryo and P1–P56 mice. **(C)** CDK9 proteins of ventricular myocardium detected by western blot in P7 and P7-AR mice. **(D)** mRNA expression levels of CDK9 in P7 and P7-AR mice. **(E)** SGK3 and CDK9 proteins of ventricular myocardium in P1 and P56 mice submitted to nucleocytoplasmic fractionation. MW indicates molecular weight, AR indicates apical resection; statistical significance was calculated with the unpaired Student *t*-test; data are presented as mean ± SEM, $^{*}P \leq 0.05$, $^{***}P \leq 0.001$; each dot indicates a biological replicate.

proliferation ability of CMs (Figures 3F–H). In addition, flow cytometry analysis results also indicated that the proportion of G1-phase CMs decreased and S-phase and G2-phase CMs significantly increased after CDK9 overexpression, which was contrary in the CDK9 knockdown group (Figure 3I).

CDK9 knockdown impairs myocardial regenerative repair after apical resection in neonatal mice

To validate the effect of CDK9 on myocardial regenerative repair in neonatal mice, we performed AR surgery on P1 mice. Normal neonatal mice can recover entirely after AR surgery because of their active CMs proliferation capacity (2). We took intra-myocardial injections of Ad5: cTNT-CDK9 RNAi or Ad5: cTNT-CONi after AR surgery in neonatal mice. Premixed EdU solution was intraperitoneally injected 4 days after AR (5 μg/mouse diluted in PBS). Western blot analysis at 6 days after surgery showed that the CDK9 expression level in the AR + CDK9i group was significantly lower than in the AR + CONi group (Figure 4A). Besides, cell proliferation staining (EdU, Ki67, and pH3) of apical region tissues from the two groups revealed that the proliferation efficiency of CMs in the AR + CDK9i group was significantly lower than that in the AR + CONi group (Figures 4B–D). Masson staining at 22 days after surgery showed that the degree of myocardial fibrosis in the AR + CONi group was significantly lower than that in the AR + CDK9i group (Figure 4E). To verify the effect of CDK9 knockdown on postoperative cardiac function in neonatal mice, we performed echocardiography in the two groups of mice at 1 and 22 days after AR surgery. The results showed that

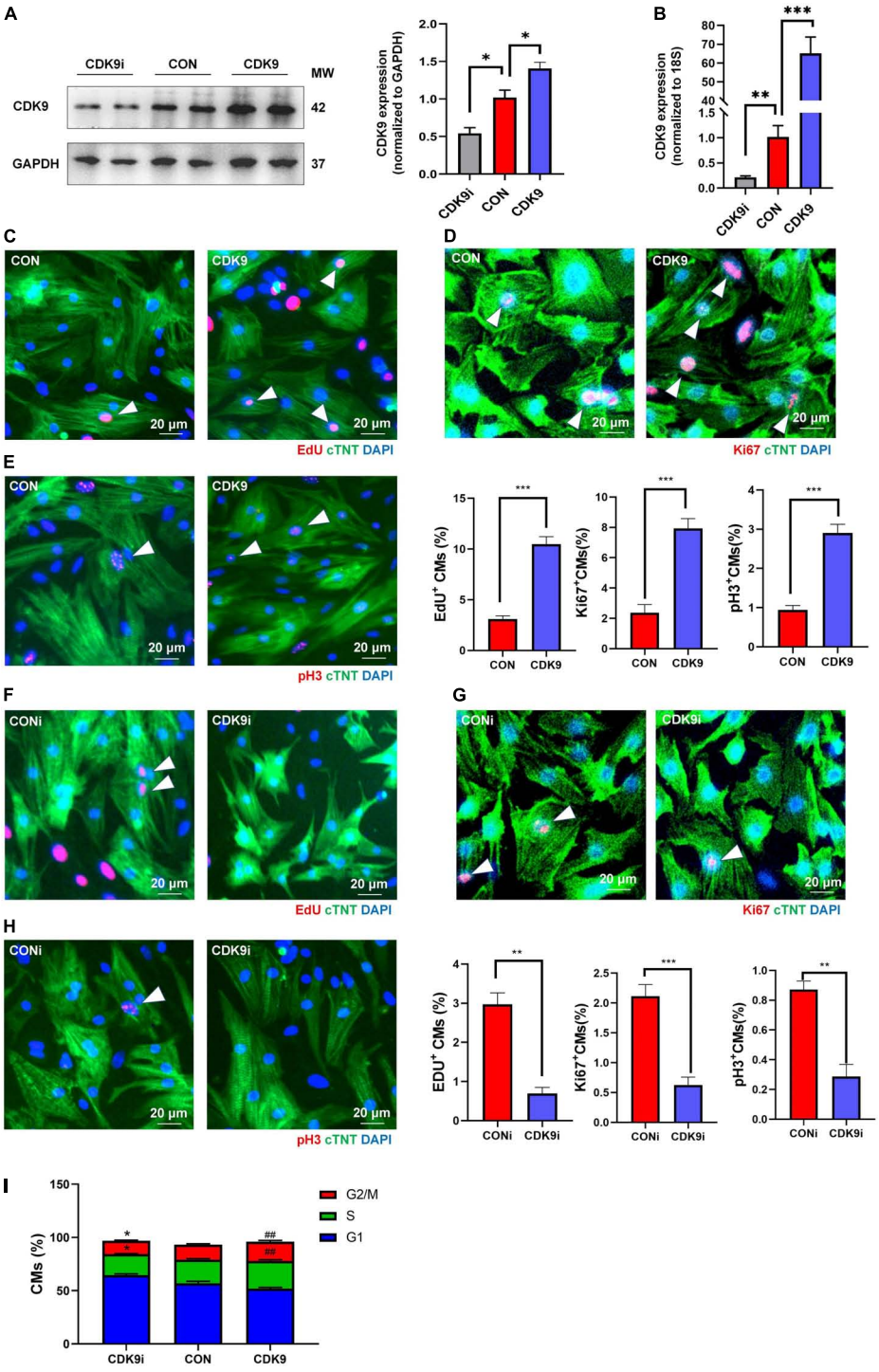

FIGURE 3
CDK9 promotes cardiomyocyte (CM) proliferation *in vitro*. **(A)** Knockdown and overexpression of CDK9 proteins confirmed by western blot in neonatal CMs treated with Ad5: cTnT-CON, Ad5: cTnT-CDK9 or Ad5: cTnT-CDK9 RNAi. **(B)** Knockdown and overexpression of CDK9 mRNA confirmed by qRT-PCR. **(C–E)** CM proliferation quantified in neonatal CMs transfected with Ad5: cTnT-CON or Ad5: cTnT-CDK9 by immunofluorescence for DNA synthesis **(C)**, cell-cycle activity **(D)**, and mitosis **(E)** (n = 6). **(F–H)** CM proliferation was quantified in neonatal CMs treated with Ad5: cTnT-CDK9 RNAi by immunofluorescence for DNA synthesis **(F)**, cell-cycle activity **(G)**, and mitosis **(H)** (n = 6). **(I)** CM cell cycle activity was detected by flow cytometry analysis after transfected with Ad5: cTnT-CON RNAi, Ad5: cTnT-CDK9, or Ad5: cTnT-CDK9 RNAi (CDK9i) (n = 3). White arrows in representative pictures point to the proliferating CMs; scale bars, 20 μm; CMs indicate cardiomyocytes, MW indicates molecular weight; statistical significance was calculated with the unpaired Student t-test; data are presented as mean ± SEM, $^{*}P \leq 0.05$, $^{**}P \leq 0.01$, $^{\#\#}P \leq 0.01$, $^{***}P \leq 0.001$; each dot indicates a biological replicate.

10.3389/fcvm.2022.970745

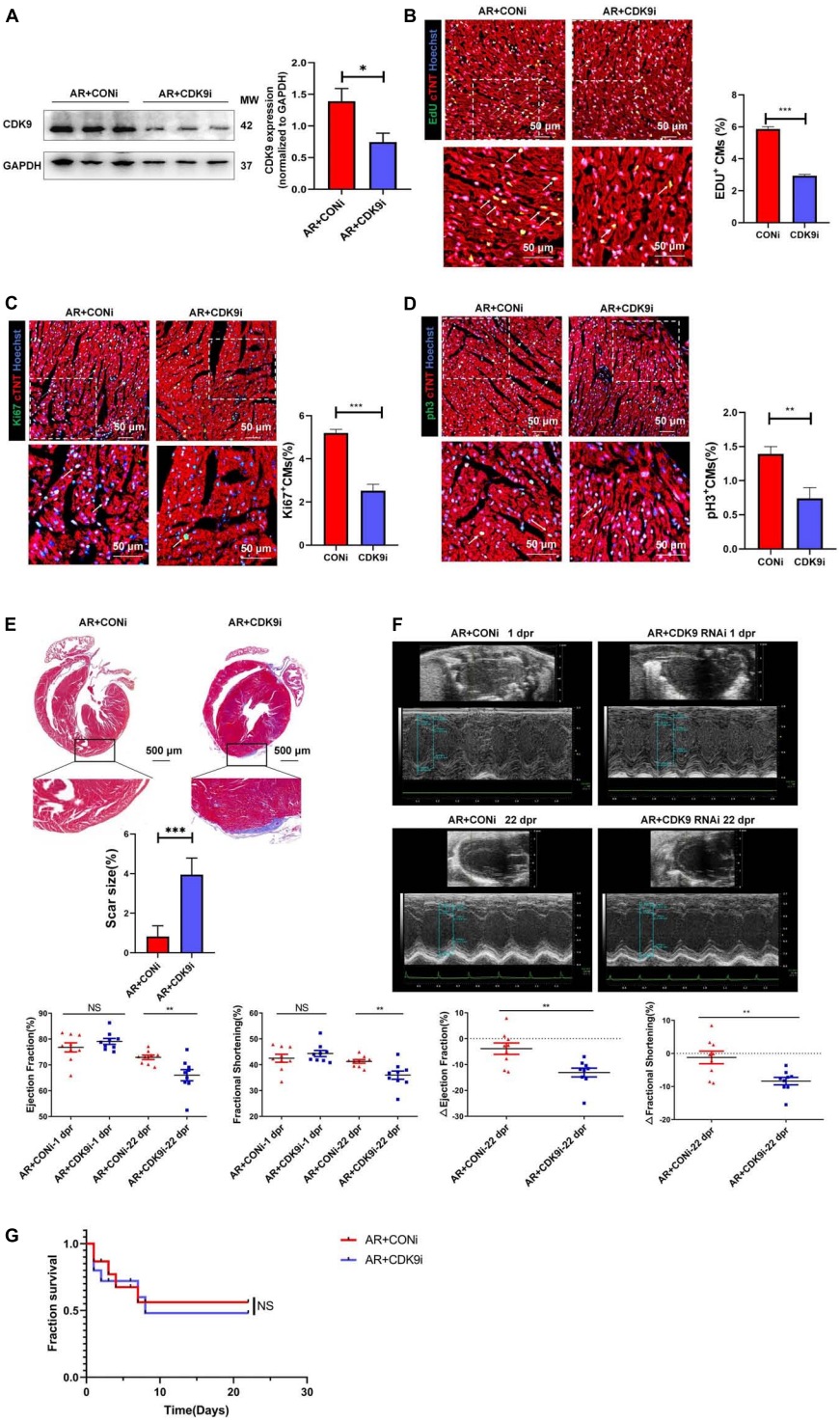

FIGURE 4

CDK9 knockdown impairs myocardial regeneration after AR in neonatal mice. **(A)** CDK9 protein of ventricular myocardium in neonatal mice injected Ad5: cTnT-CON RNAi or Ad5: cTnT-CDK9 RNAi (CDK9i) after AR surgery detected by western blot at 6 days after surgery. **(B–D)** CM proliferation in neonatal myocardial tissue after intra-myocardial injection with CDK9i or CONi quantified by immunofluorescence for DNA synthesis **(B)**, cell-cycle activity **(C)**, mitosis **(D)** (n = 3). **(E)** Comparison of scar size by Masson staining between the CONi and CDK9i groups at 22 days after AR surgery (n = 6). **(F)** LVEF and LVFS in P1 AR mice at 1 and 22 days after CDK9i or CONi injection was detected by echocardiography (n = 8). **(G)** Overall survival rate in neonatal mice from AR + CONi and AR + CDK9i groups (n = 15). Scale bars, 500 μm; CM indicates cardiomyocyte, MW indicates molecular weight; statistical significance was calculated with the unpaired Student t-test; data are presented as mean ± SEM, $^{*}P \leq 0.05$, $^{**}P \leq 0.01$, $^{***}P \leq 0.001$; each dot indicates a biological replicate.

myocardial systolic function was impaired in both groups of mice at 1 day after surgery (LVEF: AR + CONi: 76.78 ± 1.772%, AR + CDK9i: 79.10 ± 1.143%, p = 0.724; LVFS: AR + CONi: 42.50 ± 1.549%, AR + CDK9i: 44.34 ± 1.186%, p = 0.755). In contrast, the recovery of cardiac function in the CDK9i group was significantly worse than in the CONi group at 22 days after surgery (LVEF: AR + CONi: 72.93 ± 0.851%, AR + CDK9i: 66.02 ± 2.160%, p = 0.0056; LVFS: AR + CONi: 41.28 ± 0.706%, AR + CDK9i: 35.97 ± 1.592%, p = 0.0034) (**Figure 4F**). The overall survival rate was similar between the AR + CONi and AR + CDK9i groups (**Figure 4G**).

CDK9 overexpression promotes myocardial regenerative repair after myocardial infarction in adult mice

To explore the effect of CDK9 on injury repair and CMs proliferative capacity after MI in adult mice, we orthotopically injected AAV9: cTNT-CDK9 or AAV9: cTnT-CON at the same time after ligation of LAD in adult mice. We harvested samples 14 days after injection to verify successful CDK9 overexpression via western blot (**Figure 5A**). The heart size, heart weight/body weight ratio, and CM size were similar between the MI + AAV9: cTnT-CON and MI + AAV9: cTnT-CDK9 groups (**Figures 5B,C**). Then we confirmed the proliferation efficiency of CMs in the infarct border zone by immunofluorescence staining, which showed that the proliferative activity of CMs in the infarct border zone was significantly higher in the CDK9 overexpression group relative to the MI + AAV9: cTnT-CON group (**Figures 5D,E**). Meanwhile, Masson staining at 28 days after operation showed that the area of fibrosis in the infarct area was significantly ameliorative in the CDK9 overexpression group than in the CON group (**Figure 5F**). In addition, the results of echocardiography at 28 days after surgery showed that cardiac function (LVEF and LVFS) and structure (LV Mass and LV Vol d/s) was significantly improved in the CDK9 overexpression group (LVEF: 57.04 ± 8.80%; LVFS: 29.83 ± 5.75%) than in the CON group (LVEF: 43.94 ± 6.46%, p = 0.008; LVFS: 21.95 ± 3.75%, p = 0.010) (**Figure 5G**). The overall survival rate was similar between the MI + AAV9: cTnT-CON and MI + AAV9: cTnT-CDK9 groups (**Figure 5H**).

CDK9 activates SGK3 and promotes cardiomyocytes proliferation via the GSK-3β/β-catenin pathway *in vitro*

Based on our previous results, we have verified the binding of SGK3 and CDK9 and the effect of CDK9 on myocardial

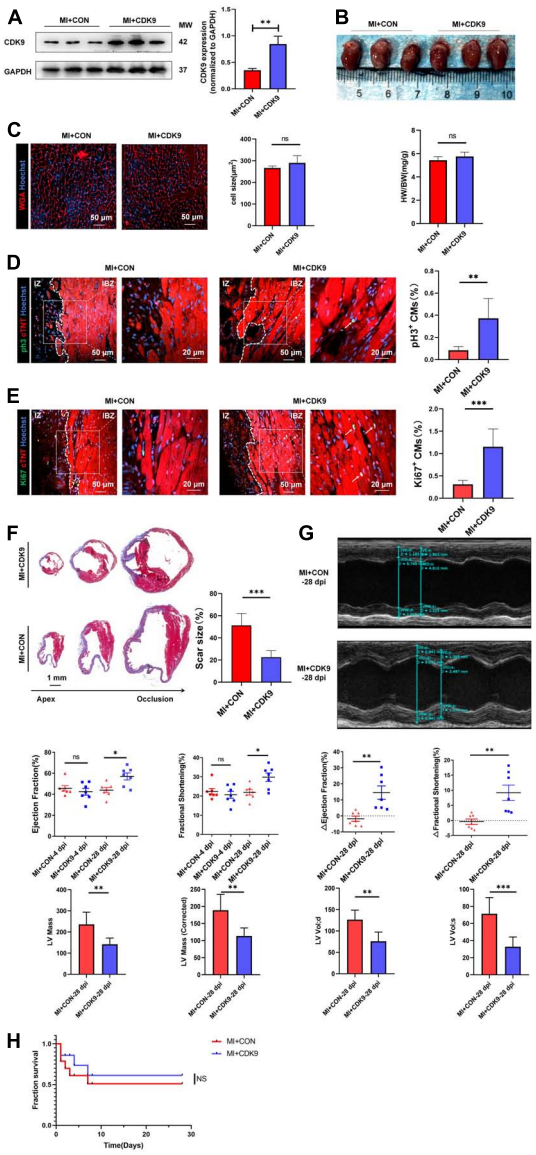

FIGURE 5
CDK9 overexpression promotes myocardial regeneration after MI in adult mice. **(A)** CDK9 protein of ventricular myocardium in adult mice injected with AAV9: cTnT-CDK9 or AAV9: cTnT-CON after MI detected by western blot (MI + CDK9 or MI + CON). **(B)** Left: cardiac morphology in adult mice subjected to MI + CDK9 or MI + CON at 14 dpi. Right: heart weight/Body weight (HW/BW) ratio in adult mice subjected to MI + CDK9 or MI + CON at 14 dpi (n = 6). **(C)** CM size in adult mice subjected to MI + CDK9 or MI + CON at 14 dpi was detected by wheat germ agglutinin (WGA) immunofluorescence (n = 6). **(D,E)** CM proliferation in adult myocardial tissue subjected to MI + CDK9 or MI + CON quantified by immunofluorescence for mitosis **(D)** and cell-cycle activity **(E)** (n = 6); white arrows point to the proliferating CMs. **(F)** Comparison of scar size by Masson staining between the CON and CDK9 groups at 28 days after MI (n = 6). **(G)** LVEF, LVFS, LV Mass and LV Vol d/s in adult MI mice at 4 and 28 days after CDK9 injection was detected by echocardiography (n = 7). **(H)** Overall survival rate in adult mice from MI + CON and MI + CDK9 groups (n = 14). Scale bars, 20/50 μm; CM indicates cardiomyocyte, MW indicates

(Continued)

FIGURE 5 (Continued)
molecular weight, IZ indicates infarct zone, IBZ indicates infarcted border zone (<2 mm outside IZ); statistical significance was calculated with the unpaired Student *t*-test; data are presented as mean ± SEM, $^{*}P \leq 0.05$, $^{**}P \leq 0.01$, $^{***}P \leq 0.001$; each dot indicates a biological replicate.

repair. Also, previous studies have shown that GSK-3β, β-catenin and cyclin D1 are downstream key targets of SGK3 (9). To further verify the effect of CDK9-SGK3 and its downstream signaling on proliferation in neonatal CMs, we examined relevant downstream including SGK3 after overexpression of CDK9 and found that overexpression of CDK9 significantly increased the phosphorylation levels of SGK3, significantly activated the phosphorylation site of GSK-3β at Ser9, and upregulated β-catenin and cyclin D1 expression (**Figure 6A**). Next, to verify whether CDK9 promotes CMs proliferation by regulating SGK3, we first examined the effect on CMs by intervening with CDK9 and SGK3 expression via western blot (**Figure 6B**). The immunofluorescence experiment showed that overexpression of CDK9 could promote CMs proliferation *in vitro*, and inhibition of SGK3 could weaken CMs proliferation ability. In contrast, simultaneous inhibition of SGK3 could partially attenuate the effect of CDK9 on CMs proliferation efficiency (EdU, Ki67, and pH3) (**Figures 6C–E**).

CDK9 regulates myocardial repair through SGK3/GSK-3β/β-catenin axis *in vivo*

After validating SGK3 as a critical target mediating CDK9 facilitated CMs proliferation *in vitro*, we needed to verify whether SGK3 mediated the function of CDK9 in promoting myocardial regenerative repair *in vivo*. We, therefore, constructed the mice AR model and orthotopically injected Ad5: cTNT-CDK9i simultaneously overexpressing SGK3. We first examined the effect on the myocardium by intervening with both CDK9 and SGK3 expression via western blot (**Figure 7A**). And the immunofluorescence results showed that the regenerative capacity of neonatal myocardium after AR was significantly impaired by CDK9 knockdown whereas partially alleviated by simultaneous SGK3 overexpression (**Figures 7B–D**).

Research pattern diagram

Our experimental results indicate that CDK9 drives CMs cycle activity in mice myocardium and promotes CMs proliferation and myocardial repair by directly binding to and activating SGK3 and its downstream signaling (**Figure 8**).

Discussion

The neonatal mammalian heart maintains regenerative capacity for a transient window, which declines rapidly after birth (16). The loss of the proliferative capacity of CMs involves alterations in gene expression and the activity of core regulatory components. SGK3 is a functional kinase we previously discovered and can promote CMs proliferation and cardiac repair after MI, while the underlying mechanism remains unknown (9). To uncover the upstream signals that regulate SGK3 and identify more potent key factors regulating myocardial regeneration, we performed a pulldown assay and mass spectrometry analysis of SGK3. We found CDK9 may have a pivotal role in CMs proliferation via interacting with SGK3. Therefore, CDK9 is expected to be a potential therapeutic target that can promote myocardial regeneration and repair by regulating SGK3.

It was reported that long-term overexposure to CDK9 may result in pathological cardiac hypertrophy; thus, CDK9 inhibitors have been investigated as new targets for treating hypertrophic cardiomyopathy (10). It is known that moderate hypertrophy of the myocardium after birth is regarded as a signature of myocardial maturation. Besides, recent studies have suggested that the proliferation and maturation of CMs are two sides of the same coin for myocardial regeneration, and the regulatory mechanisms of CMs proliferation and maturation have certain analogies: HIF1α can not only stimulate postnatal CMs to re-enter the cell cycle, but also promote CMs hypertrophy (17). Likewise, Igf1r is also thought to play an essential role in cardiac development and regenerative repair (18). Myocardial proliferation and physiological hypertrophy, as the crossroads of myocardial development and maturation, turn left or right, or even simultaneously, which is indeed an exciting truth to be further revealed (19). CDK9, which can regulate myocardial maturation, can also be used to explore the function of myocardial proliferation.

Gianfranco Matrone et al. showed that CDK9 plays a critical role in early cardiac development and CMs proliferation in zebrafish, and inhibition of CDK9 dephosphorylates its target site on the C-terminal domain of RNA polymerase II, thereby preventing regenerative repair after myocardial injury (20). Inhibition of CDK9 impairs the accumulation of neutrophils after injury and inhibits the recruitment of macrophages, thus hindering the repair of zebrafish heart damage. In contrast, transient inhibition of CDK9 can show positive effects (2-h window period) (21). In this study, we found that the expression pattern of CDK9 was consistent with the gradual loss of myocardial regenerative capacity *in vivo*, so we speculated that CDK9 might be a key regulator of myocardial regeneration. Our results indicated that the inhibition of CDK9 blocked CMs proliferation and myocardial repair after injury in neonatal mice. Exogenous overexpression of CDK9

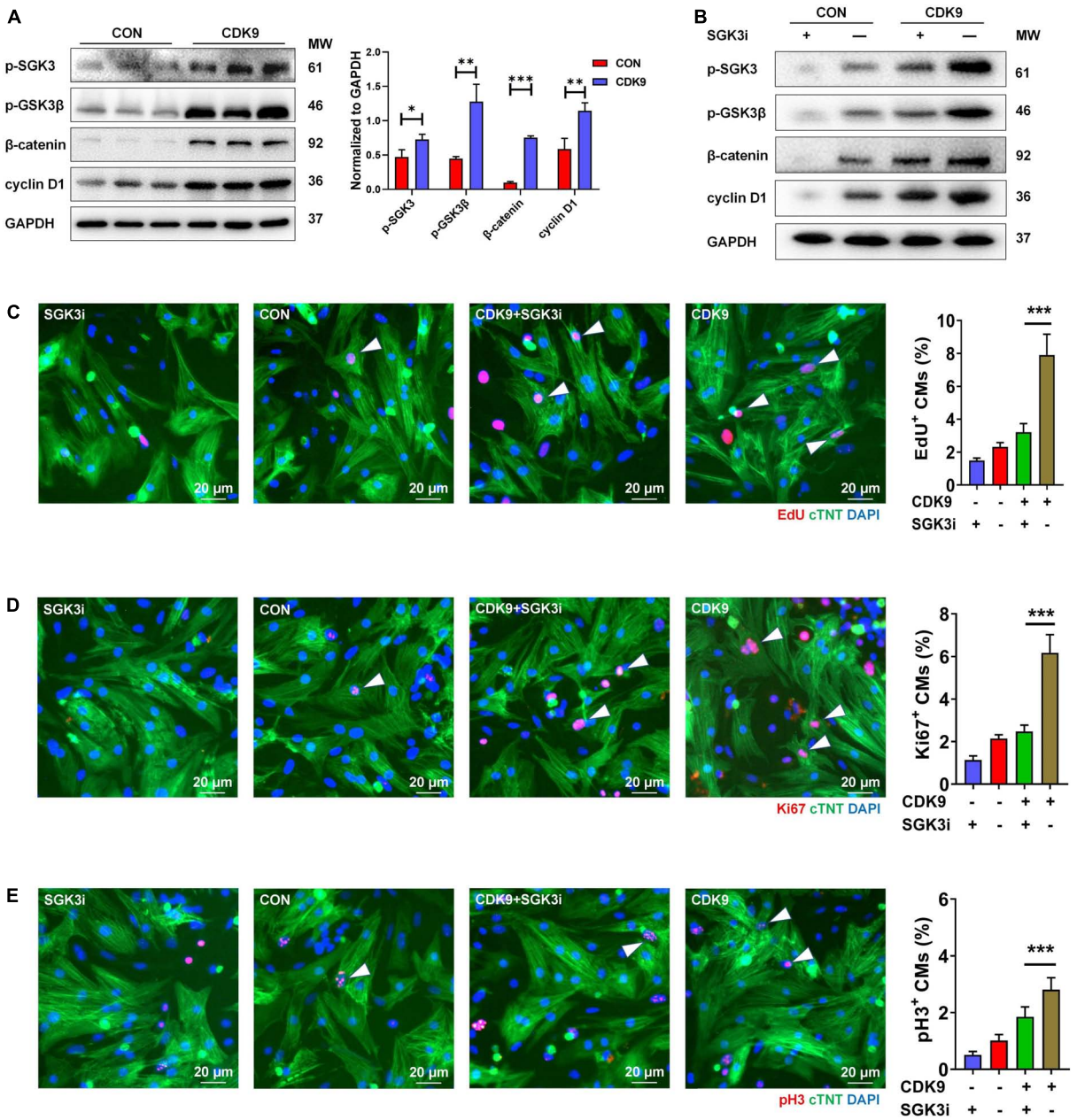

FIGURE 6
CDK9 regulates myocardial regeneration and repair through SGK3/GSK-3β/β-catenin axis *in vitro*. **(A)** p-SGK3, p-GSK3β, β-catenin and cyclin D1 proteins of ventricular myocardium in adult mice injected with Ad5: cTnT-CDK9 (CDK9) after MI detected by western blot. **(B)** p-SGK3, p-GSK3β, β-catenin and cyclin D1 proteins of neonatal CMs were detected by western blot after being transfected with CDK9 and/or Ad5:SGK3 RNAi (SGK3i). **(C–E)** CM proliferation is quantified by immunofluorescence for DNA synthesis **(C)**, cell-cycle activity **(D)**, and mitosis **(E)** in CMs transfected with CDK9 and/or SGK3i (n = 6). Scale bars, 20 μm; CMs indicate cardiomyocytes, MW indicates molecular weight; statistical significance was calculated with the unpaired Student t-test; data are presented as mean ± SEM, $^*P \leq 0.05$, $^{**}P \leq 0.01$, $^{***}P \leq 0.001$; each dot indicates a biological replicate.

significantly promoted CMs proliferation and regenerative repair in adult mice after MI.

CDK9 exists in two isoforms, the identified initially and more abundant one of 42kDa and the less abundant one of 55 kDa, the latter having an additional 117 aa at its N-terminus (22). These two isoforms are transcribed from the same *CDK9* gene but are composed of two different promoters. They are located more than 500 bp apart on the *CDK9* gene, of which the 42 kDa promoter is significantly more potent than the 55 kDa one (23). The expression of these two isoforms is differentially

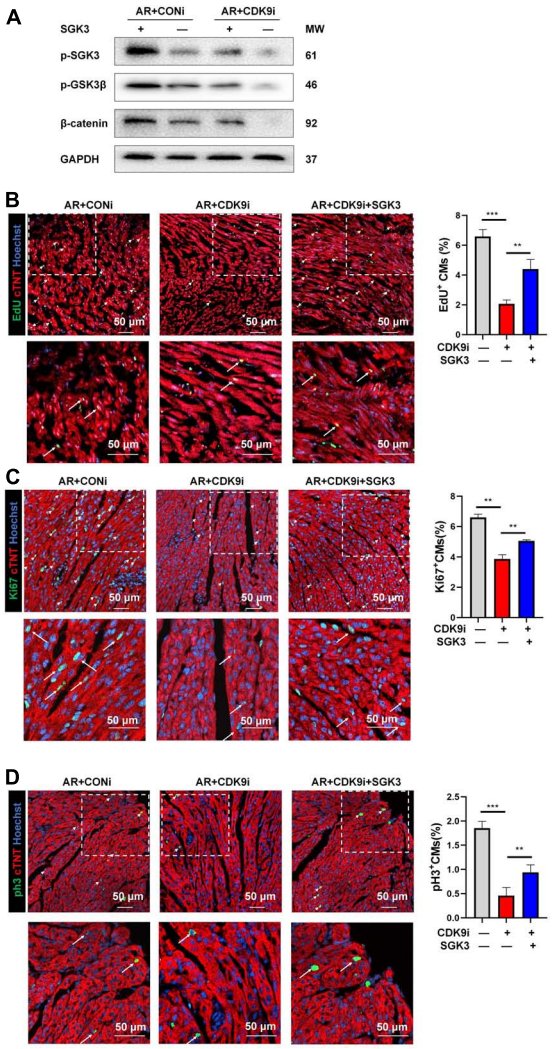

FIGURE 7
CDK9 regulates myocardial regeneration and repair through SGK3/GSK-3β/β-catenin axis *in vivo*. **(A)** p-SGK3, p-GSK3β and β-catenin proteins in neonatal myocardial tissue after intra-myocardial injection with Ad5: cTnT-CDK9 RNAi (CDK9i) and/or Ad5: cTnT-SGK3 (SGK3) after AR detected by western blot. **(B–D)** CM proliferation in neonatal AR myocardial tissue after intraperitoneal injection with CDK9i and/or SGK3 quantified by immunofluorescence for DNA synthesis **(B)**, cell-cycle activity **(C)**, mitosis **(D)** (n = 3). Scale bars, 50 μm; CMs indicates cardiomyocytes, AR indicates apical resection, MW indicates molecular weight; statistical significance was calculated with one-way ANOVA; data are presented as mean ± SEM, $^{**}P \leq 0.01$, $^{***}P \leq 0.001$; each dot indicates a biological replicate.

regulated in a signal-dependent and cell-type-specific manner. This study examined the expression of the two isoforms of CDK9 in primary CMs and myocardium under various physiological and pathological conditions. We found that the 42 kDa isoform plays a significant role in CMs proliferation. The classical part of CDK9 performs biological functions in the nucleus; CDK9 and cyclin T form a P-TEFb complex, which facilitates the transition from abortive to productive elongation by phosphorylating the CTD (C-terminal domain) of the large subunit of RNA polymerase II (RNAP II) POLR2A, SUPT5H and RDBP (22). CDK9 also regulates cytokine-induced transcriptional networks by promoting promoter recognition of target transcription factors (e.g., TNF-induced RELA/p65 activation and IL-6-induced STAT3 signaling), and plays a vital role in the genetics of cell growth, differentiation, and viral pathogenesis to promote RNA synthesis (4). However, little is known about the function of CDK9 in the cytoplasm, and the different subcellular localization of CDK9 is bound to mediate different modes of procedure. In the study of Zhao et al., function-guided proximity mapping unveils non-enzymatic PTMs in their non-canonical locales. CDK9 is hydroxynonenylated only in the cytoplasm and performs cross-compartment signaling (24).

This study demonstrates that CDK9 and SGK3 bind directly in the cytoplasm, and SGK3 is structurally highly homologous to AKT and can also regulate GSK-3β/β-catenin signaling (25). Activation of GSK-3β/β-catenin signaling is generally considered to be a common downstream pathway driving CMs proliferation and inhibiting CMs apoptosis (26, 27). In addition, our previous studies found that SGK3 can promote the recovery of cardiac function by inhibiting apoptosis. Therefore, the myocardial protective effect of CDK9 could be partly due to the inhibition of apoptosis by SGK3 (9). Previous studies have shown that Hippo/Yap, insulin-like growth factor (IGF), peroxisome proliferator-activated receptor δ (PPAR δ), neuregulin, and ERBB2 pathways are all involved in mediating the enhancement of downstream β-catenin signaling to stimulate CMs proliferation (28–31). GSK-3β/β-catenin pathway, as a part and essential loop of the Wnt signaling pathway, any intervention of arbitrary targets on this pathway could have a cascade amplifying effect on the target genes of the Wnt signaling pathway (32). Therefore, the further exploration of the relevant upstream signal initiators, such as Wnt ligands and Frizzled receptors, could bring more insights into the function of CDK9 in crosstalk between cardiomyocytes and other types of cells.

Moreover, we found that CDK9, as the upstream of SGK3, plays a critical role in promoting myocardial proliferation and cardiac repair after MI by activating the SGK3/GSK-3β/β-catenin pathway and even stimulates more pronounced CMs proliferation than SGK3. Notably, although our current findings suggest a positive effect of CDK9 on myocardial regenerative repair, appropriate treatment should be short-term and myocardial-specific, given the oncogenic property of CDK9. Myocardial regeneration is a holistic and dynamically regulated process, CMs proliferation is key to regenerating the lost myocardium following injury, which seems to be able to shape the cardiac microenvironment through the autonomous drive to achieve complete repair after injury (33, 34). Therefore, cardiomyocyte proliferation may play a guiding

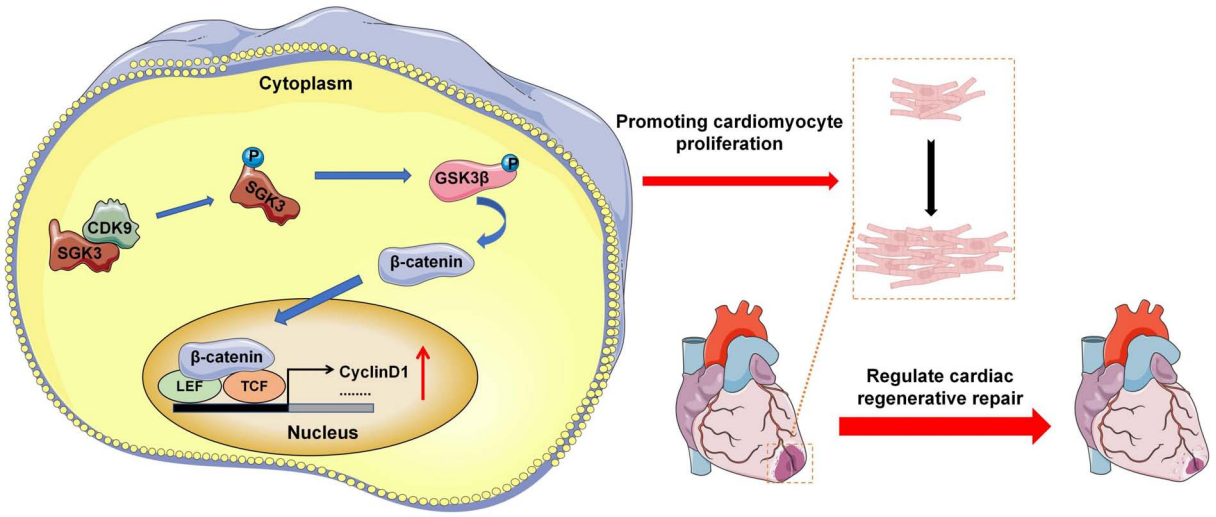

FIGURE 8
Research pattern diagram. Model depicting CDK9 binds to SGK3 and activates SGK3 and its downstream GSK-3β/β-catenin/cyclin D1 pathways to regulate the CM cycle activity, promoting CM proliferation and myocardial regeneration (CMs indicate cardiomyocytes).

or triggering role in the process of myocardial regenerative repair, which needs further work to verify. Additionally, CDK9 inhibitors are widely used in clinical tumor treatment. The undesirable cardiotoxicity caused by CDK9 treatment requires extra vigilance, as the death of patients receiving targeted therapy is not limited to tumor occurrence and metastasis but fatal cardiovascular complications such as severe heart failure and malignant arrhythmia (35). Therefore, strategies targeting CDK9 would be cardio-oncology new research directions.

Conclusion

Our study indicated that the expression pattern of CDK9 conforms to the changing trend of the mammalian myocardial regeneration period, and can interact with SGK3 to mediate cardiac repair and recovery after injury in the neonatal and adult heart through the GSK-3β/β-catenin pathway. The present work extends our knowledge of the kinase regulation in myocardial regeneration and indicates that targeting CDK9 and downstream signals might provide novel therapeutic implications in ischemic heart disease.

Data availability statement

The datasets presented in this study can be found in online repositories. The names of the repository/repositories and accession number(s) can be found below: iProX (https://www.iprox.cn/), Project ID: IPX0004689000.

Ethics statement

This animal study was reviewed and approved by Institutional Animal Care and Use Committee (IACUC) of Nanjing Medical University.

Author contributions

JS, TY, and TW performed the experiments and analyzed the data. JS, TY, LZ, and LG wrote the manuscript. TS and JC provided experimental advice and some experimental supplies. LW designed the experiments and provided financial support. All authors contributed to the editing of the review and approved the final version of the manuscript for submission.

Funding

This work was supported by grants from the National Natural Science Foundation of China (No. 82070367), the Postgraduate Research & Practice Innovation Program of Jiangsu Province (No. SJCX21_0615), and the Priority Academic Program Development of Jiangsu Higher Education Institutions (PAPD, No. KYZZ15_0263).

Acknowledgments

We are grateful for the technical assistance and support from Jiangsu Province Collaborative Innovation Center for

Cardiovascular Disease Translational Medicine. We thank all experimental model animals involved in the study for their sacrifice. **Figure 8** was modified from Servier Medical Art (http://smart.servier.com/).

Conflict of interest

The authors declare that the research was conducted in the absence of any commercial or financial relationships that could be construed as a potential conflict of interest.

Publisher's note

All claims expressed in this article are solely those of the authors and do not necessarily represent those of their affiliated organizations, or those of the publisher, the editors and the reviewers. Any product that may be evaluated in this article, or claim that may be made by its manufacturer, is not guaranteed or endorsed by the publisher.

Supplementary material

The Supplementary Material for this article can be found online at: https://www.frontiersin.org/articles/10.3389/fcvm.2022.970745/full#supplementary-material

SUPPLEMENTARY FIGURE 1
A Venn diagram describing proteins/peptides identified by pulldown-MS analysis from IgG and SGK3 group.

SUPPLEMENTARY TABLE 1
Details of proteins/peptides detected in IgG, SGK3, or both.

SUPPLEMENTARY TABLE 2
Descriptions of 26 SGK3-binded proteins and their biological functions.

References

1. Walli-Attaei M, Joseph P, Rosengren A, Chow CK, Rangarajan S, Lear SA, et al. Variations between women and men in risk factors, treatments, cardiovascular disease incidence, and death in 27 high-income, middle-income, and low-income countries (PURE): a prospective cohort study. *Lancet.* (2020) 396:97–109. doi: 10.1016/S0140-6736(20)30543-2

2. He L, Nguyen NB, Ardehali R, Zhou B. Heart regeneration by endogenous stem cells and cardiomyocyte proliferation: controversy, fallacy, and progress. *Circulation.* (2020) 142:275–91. doi: 10.1161/CIRCULATIONAHA.119.045566

3. Du C, Fan Y, Li YF, Wei TW, Wang LS. Research progress on myocardial regeneration: what is new? *Chin Med J.* (2020) 133:716–23. doi: 10.1097/CM9.0000000000000693

4. Mandal R, Becker S, Strebhardt K. Targeting CDK9 for anti-cancer therapeutics. *Cancers.* (2021) 13:2181. doi: 10.3390/cancers13092181

5. Zhao MT, Ye S, Su J, Garg V. Cardiomyocyte proliferation and maturation: two sides of the same coin for heart regeneration. *Front Cell Dev Biol.* (2020) 8:594226. doi: 10.3389/fcell.2020.594226

6. Di Stefano V, Giacca M, Capogrossi MC, Crescenzi M, Martelli F. Knockdown of cyclin-dependent kinase inhibitors induces cardiomyocyte re-entry in the cell cycle. *J Biol Chem.* (2011) 286:8644–54. doi: 10.1074/jbc.M110.184549

7. Mohamed TMA, Ang YS, Radzinsky E, Zhou P, Huang Y, Elfenbein A, et al. Regulation of cell cycle to stimulate adult cardiomyocyte proliferation and cardiac regeneration. *Cell.* (2018) 173:104–16.e12. doi: 10.1016/j.cell.2018.02.014

8. de Lucia C, Grisanti LA, Borghetti G, Piedepalumbo M, Ibetti J, Lucchese AM, et al. G protein-coupled receptor kinase 5 (GRK5) contributes to impaired cardiac function and immune cell recruitment in post-ischemic heart failure. *Cardiovasc Res.* (2022) 118:169–83. doi: 10.1093/cvr/cvab044

9. Li YF, Wei TW, Fan Y, Shan TK, Sun JT, Chen BR, et al. Serine/Threonine-protein kinase 3 facilitates myocardial repair after cardiac injury possibly through the glycogen synthase kinase-3β/β-catenin pathway. *J Am Heart Assoc.* (2021) 10:e022802. doi: 10.1161/JAHA.121.022802

10. Krystof V, Chamrád I, Jorda R, Kohoutek J. Pharmacological targeting of CDK9 in cardiac hypertrophy. *Med Res Rev.* (2010) 30:646–66. doi: 10.1002/med.20172

11. Sano M, Abdellatif M, Oh H, Xie M, Bagella L, Giordano A, et al. Activation and function of cyclin T-Cdk9 (positive transcription elongation factor-b) in cardiac muscle-cell hypertrophy. *Nat Med.* (2002) 8:1310–7. doi: 10.1038/nm778

12. Han Y, Zhan Y, Hou G, Li L. Cyclin-dependent kinase 9 may as a novel target in downregulating the atherosclerosis inflammation (Review). *Biomed Rep.* (2014) 2:775–9. doi: 10.3892/br.2014.322

13. Huang S, Luo W, Wu G, Wu G, Shen Q, Zhuang Z, et al. Inhibition of CDK9 attenuates atherosclerosis by inhibiting inflammation and phenotypic switching of vascular smooth muscle cells. *Aging.* (2021) 13:14892–909. doi: 10.18632/aging.202998

14. Sunagawa Y, Morimoto T, Takaya T, Kaichi S, Wada H, Kawamura T, et al. Cyclin-dependent kinase-9 is a component of the p300/GATA4 complex required for phenylephrine-induced hypertrophy in cardiomyocytes. *J Biol Chem.* (2010) 285:9556–68. doi: 10.1074/jbc.M109.070458

15. Fan Y, Cheng Y, Li Y, Chen B, Wang Z, Wei T, et al. Phosphoproteomic analysis of neonatal regenerative myocardium revealed important roles of checkpoint kinase 1 via activating mammalian target of rapamycin C1/ribosomal protein S6 kinase b-1 pathway. *Circulation.* (2020) 141:1554–69. doi: 10.1161/CIRCULATIONAHA.119.040747

16. Porrello ER, Mahmoud AI, Simpson E, Hill JA, Richardson JA, Olson EN, et al. Transient regenerative potential of the neonatal mouse heart. *Science.* (2011) 331:1078–80. doi: 10.1126/science.1200708

17. Guimarães-Camboa N, Stowe J, Aneas I, Sakabe N, Cattaneo P, Henderson L, et al. HIF1α represses cell stress pathways to allow proliferation of hypoxic fetal cardiomyocytes. *Dev Cell.* (2015) 33:507–21. doi: 10.1016/j.devcel.2015.04.021

18. Gallego-Colon E, Villalba M, Tonkin J, Cruz F, Bernal JA, Jimenez-Borregureo LJ, et al. Intravenous delivery of adeno-associated virus 9-encoded IGF-1Ea propeptide improves post-infarct cardiac remodelling. *NPJ Regener Med.* (2016) 1:16001. doi: 10.1038/npjregenmed.2016.1

19. Li H, Trager LE, Liu X, Hastings MH, Xiao C, Guerra J, et al. lncExACT1 and DCHS2 regulate physiological and pathological cardiac growth. *Circulation.* (2022) 145:1218–33. doi: 10.1161/CIRCULATIONAHA.121.056850

20. Matrone G, Wilson KS, Maqsood S, Mullins JJ, Tucker CS, Denvir MA. CDK9 and its repressor LARP7 modulate cardiomyocyte proliferation and response to injury in the zebrafish heart. *J Cell Sci.* (2015) 128:4560–71. doi: 10.1242/jcs.175018

21. Kaveh A, Bruton FA, Oremek MEM, Tucker CS, Taylor JM, Mullins JJ, et al. Selective CDK9 inhibition resolves neutrophilic inflammation and enhances cardiac regeneration in larval zebrafish. *Development.* (2022) 149:dev199636. doi: 10.1242/dev.199636

22. Morales F, Giordano A. Overview of CDK9 as a target in cancer research. *Cell Cycle.* (2016) 15:519–27. doi: 10.1080/15384101.2016.1138186

23. Shore SM, Byers SA, Maury W, Price DH. Identification of a novel isoform of Cdk9. *Gene.* (2003) 307:175–82. doi: 10.1016/s0378-1119(03)00466-9

24. Zhao Y, Miranda Herrera PA, Chang D, Hamelin R, Long MJC, Aye Y. Function-guided proximity mapping unveils electrophilic-metabolite sensing by

proteins not present in their canonical locales. *Proc Natl Acad Sci U.S.A.* (2022) 119:e2120687119. doi: 10.1073/pnas.2120687119

25. Liu M, Chen L, Chan TH, Wang J, Li Y, Zeng TT, et al. Serum and glucocorticoid kinase 3 at 8q13.1 promotes cell proliferation and survival in hepatocellular carcinoma. *Hepatology.* (2012) 55:1754–65. doi: 10.1002/hep.25584

26. Hernández-Reséndiz S, Palma-Flores C, De Los Santos S, Román-Anguiano NG, Flores M, de la Peña A. Reduction of no-reflow and reperfusion injury with the synthetic 17β-aminoestrogen compound prolame is associated with PI3K/Akt/eNOS signaling cascade. *Basic Res Cardiol.* (2015) 110:1. doi: 10.1007/s00395-015-0464-y

27. Kerkela R, Kockeritz L, Macaulay K, Zhou J, Doble BW, Beahm C, et al. Deletion of GSK-3beta in mice leads to hypertrophic cardiomyopathy secondary to cardiomyoblast hyperproliferation. *J Clin Invest.* (2008) 118:3609–18. doi: 10.1172/JCI36245

28. Tarazona OA, Pourquié O. Exploring the influence of cell metabolism on cell fate through protein post-translational modifications. *Dev Cell.* (2020) 54:282–92. doi: 10.1016/j.devcel.2020.06.035

29. Yu FX, Zhao B, Guan KL. Hippo pathway in organ size control, tissue homeostasis, and cancer. *Cell.* (2015) 163:811–28. doi: 10.1016/j.cell.2015.10.044

30. Magadum A, Ding Y, He L, Kim T, Dalvoy Vasudevarao M, Long Q, et al. Live cell screening platform identifies PPARδ as a regulator of cardiomyocyte proliferation and cardiac repair. *Cell Res.* (2017) 27:1002–19. doi: 10.1038/cr.2017.84

31. Xin M, Kim Y, Sutherland LB, Qi X, McAnally J, Schwartz RJ, et al. Regulation of insulin-like growth factor signaling by yap governs cardiomyocyte proliferation and embryonic heart size. *Sci Signal.* (2011) 4:ra70. doi: 10.1126/scisignal.2002278

32. Nusse R, Clevers H. Wnt/β-catenin signaling, disease, and emerging therapeutic modalities. *Cell.* (2017) 169:985–99. doi: 10.1016/j.cell.2017.05.016

33. Gladka MM, Kohela A, Molenaar B, Versteeg D, Kooijman L, Monshouwer-Kloots J, et al. Cardiomyocytes stimulate angiogenesis after ischemic injury in a ZEB2-dependent manner. *Nat Commun.* (2021) 12:84. doi: 10.1038/s41467-020-20361-3

34. Bae J, Salamon RJ, Brandt EB, Paltzer WG, Zhang Z, Britt EC, et al. Malonate promotes adult cardiomyocyte proliferation and heart regeneration. *Circulation.* (2021) 143:1973–86. doi: 10.1161/CIRCULATIONAHA.120.049952

35. Yeh ET, Bickford CL. Cardiovascular complications of cancer therapy: incidence, pathogenesis, diagnosis, and management. *J Am Coll Cardiol.* (2009) 53:2231–47. doi: 10.1016/j.jacc.2009.02.050

frontiers | Frontiers in Cardiovascular Medicine

TYPE Mini Review
PUBLISHED 23 August 2022
DOI 10.3389/fcvm.2022.972591

OPEN ACCESS

EDITED BY
Ajit Magadum,
Temple University, United States

REVIEWED BY
Robert Kelly,
UMR7288 Institut de Biologie du Développement de Marseille (IBDM), France

*CORRESPONDENCE
Daniel J. Garry
garry@umn.edu

SPECIALTY SECTION
This article was submitted to Cardiovascular Biologics and Regenerative Medicine, a section of the journal Frontiers in Cardiovascular Medicine

RECEIVED 18 June 2022
ACCEPTED 03 August 2022
PUBLISHED 23 August 2022

CITATION
Sierra-Pagan JE and Garry DJ (2022) The regulatory role of pioneer factors during cardiovascular lineage specification – A mini review. *Front. Cardiovasc. Med.* 9:972591. doi: 10.3389/fcvm.2022.972591

The regulatory role of pioneer factors during cardiovascular lineage specification – A mini review

Javier E. Sierra-Pagan[1] and Daniel J. Garry[1,2,3]*

[1]Cardiovascular Division, Department of Medicine, University of Minnesota, Minneapolis, MN, United States, [2]Stem Cell Institute, University of Minnesota, Minneapolis, MN, United States, [3]Paul and Sheila Wellstone Muscular Dystrophy Center, University of Minnesota, Minneapolis, MN, United States

Cardiovascular disease (CVD) remains the number one cause of death worldwide. Ischemic heart disease contributes to heart failure and has considerable morbidity and mortality. Therefore, alternative therapeutic strategies are urgently needed. One class of epigenetic regulators known as pioneer factors has emerged as an important tool for the development of regenerative therapies for the treatment of CVD. Pioneer factors bind closed chromatin and remodel it to drive lineage specification. Here, we review pioneer factors within the cardiovascular lineage, particularly during development and reprogramming and highlight the implications this field of research has for the future development of cardiac specific regenerative therapies.

KEYWORDS

pioneer factors, ETV2/ER71, ETS factors, cardiac regeneration, chromatin remodeling, reprogramming, epigenetics

Introduction

Cardiovascular disease is the number one cause of death in the U.S and worldwide. Vascular and cardiac disease results in considerable morbidity and mortality (1, 2). The only curative disease for end-stage cardiovascular disease is orthotopic heart transplantation (3). While it is estimated that more than 100,000 Americans could benefit from cardiac transplantation, only 3,000 to 3,500 recipients receive such therapy due to limited donor organ availability (4). Therefore, new therapies are warranted.

Reprogramming of lineages has received intense interest and several outstanding reviews are available and provide a comprehensive overview of the field (5, 6). This field had its genesis, in part, based on the discovery of master regulators—those factors that promote lineage specific gene expression when overexpressed in somatic cells such as fibroblasts (6). These assays were referred to as conversion assays and the first master regulator to be described was Myod and its family members (7). Subsequently, more than 200 master regulators have been described and their functional roles have been explored using gene disruption technologies (8).

While the role(s) of master regulators focused primarily on their ability as transcription factors to govern lineage specific gene expression, pioneer factors function to bind nucleosomal DNA and relax the chromatin landscape upstream of lineage specific genes (6, 8, 9). In this fashion, pioneer factors reside at the very top of the hierarchical molecular cascade. Moreover, there are only a limited number of rigorously defined pioneer factors (9). Here, we highlight the criteria necessary for inclusion as a pioneer factor, we provide an overview of the field itself and highlight the role and mechanisms of pioneer factors that govern the cardiovascular field.

Coordinated role of networks and lineage specification during cardiovascular development

Cardiovascular development is a well-coordinated and complex process that requires the specification, proliferation, migration and differentiation of progenitor cells that become coupled to form a functional syncytium within the heart (10–14). Progenitor cells arising from the mesodermal germ layer form the early cardiac crescent and fuse to form the linear heart tube. Progenitor cell populations and their derivatives contribute to the first and second heart fields. These respective progenitor cell populations contribute to distinct structures within the mature heart, and are combinatorily regulated by distinct and overlapping transcriptional networks (15). Stage specific transcription factors and signaling pathways have been defined and function as key regulators of cardiovascular development. As previously outlined, master regulatory genes govern the transcriptional cascades and direct cellular lineages during differentiation and cellular reprogramming. However, within this group of master regulators, a small subset of transcription factors known as pioneer factors, have the unique capacity to bind and remodel silent and compacted regions of chromatin (nucleosomal DNA) to drive the expression of lineage specific genes that allow for development and reprogramming to occur (Figure 1). Due to their unique capacity to bind nucleosomal DNA and drive lineage development, pioneer factors have been shown to be critical factors for regenerative sciences and cancer biology.

Role of master regulators during development

Essential transcription factors, known as master regulators, regulate cell fate and lineage commitment development. These master transcription factors regulate lineage commitment events, and can convert/reprogram cells (fibroblasts) to specific lineages (8, 16). In addition to the MYOD family, other prototypic master regulators include Pdx1, an important regulator of pancreas development (17). Global knockout of *Pdx1* in the mouse results in the absence of the pancreas and similar to MYOD, ectopic overexpression of PDX1 converts somatic cells to pancreatic acinar cells (18, 19). Other master regulators have been identified for each lineage including (but not limited to): MESP1, MYF5, NEUROD, ASCL1/MASH1, GATA2, GATA4, PAX3, PAX7, FOXO, FOXA, SCL/TAL1, HIF1 and others (7, 17, 20–24). These lineage specific transcription factors or master regulators are essential for the different combinations of reprogramming factors used to develop organ specific cellular therapies (6). Among these master regulators, a subset of transcription factors known as pioneer factors, initiate lineage specific regulatory events to open up or relax compacted (heterochromatic) DNA to govern developmental and reprogramming processes (6, 25, 26) (Figure 1).

Role of pioneer factors during lineage specification

Pioneer factors are a specialized group of lineage-specific transcription factors that bind heterochromatic regions of DNA to promote chromatin relaxation and recruit non-pioneer transcription factors for lineage development or reprogramming to occur (Figure 1) (9, 25, 26). This important functional role is due to their unique capacity to scan heterochromatin, recognize partial (non-canonical) DNA motifs that are exposed on the surface on nucleosomes and bind to them. The complexes that are formed (chromatin remodeling and non-pioneer factors) following the binding of a pioneer factor are context dependent (i.e., cell type specific) and serve to dictate the diverse mechanisms whereby pioneer factors can regulate lineage specification and development. Pioneer factors were discovered with the dissection and definition of the mechanisms whereby liver specific regulatory complexes were bound to heterochromatin early during development (27, 28). These studies identified FOXA1 as the first prototypical pioneer factor that regulates hepatic lineage specification during early embryonic development (Table 1) (25, 29). A distinct feature regarding FOXA1 is that its DNA binding domain (*forkhead*/winged helix domain) shares a similar structure to that of linker histones, which enables this pioneer transcription factor to displace linker histones from nucleosomes to remodel chromatin and promote liver development (30, 31). The discovery of FOXA1 as a pioneer factor has led to the identification and characterization of other pioneer factors (Table 1). Perhaps, the most recognized examples of pioneer factors are OCT4, SOX2 and KLF4 (OSK), which promote the reprogramming of terminally differentiated fibroblasts to induced pluripotent stem cells (iPSCs) (32, 33). While c-MYC is also necessary for the reprogramming process of fibroblasts to iPSCs, unlike OSK, which can bind partial DNA motifs in

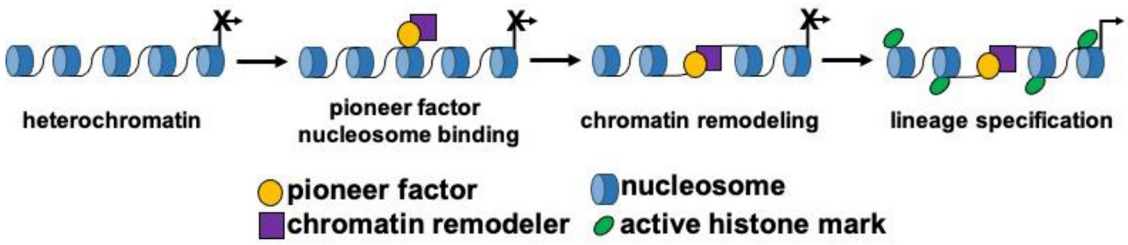

FIGURE 1
Pioneer factors drive lineage specification. Schematic model depicting the function of pioneer transcription factors during cellular lineage specification. Pioneer factors initially bind to nucleosomal DNA and then remodel chromatin by themselves or by recruiting a chromatin remodeling factor. These steps lead to the activation of gene expression and changes to the epigenetic landscape surrounding the DNA binding sites of the pioneer factor.

TABLE 1 Pioneer factors with established properties.

Pioneer	*Lineage (cell)*	*Nucleosome binding*	*Chromatin remodeling*	*Transcription factor cooperation*	*Ref.*
ASCL1	Neuron	Yes	Yes	BRN2	(126–129)
C/EBPα	Macrophage	Yes	Yes	PU.1	(119)
EBF1	B cell	Yes	Yes	PAX5	(117, 118)
ETV2	Endothelial cell	Yes	Yes	ELK3	(37)
FOXA1, FOXA2	Liver/Pancreas/Hormone dependent	Yes	Yes	GATA4,C/EBPβ,HNF4α /GATA6/Nuclear receptors	(29, 31, 130–137)
FOXH1	Mesendoderm	Yes	Yes	-	(138)
GRHL1, GRHL2, GRHL3	Epithelial cell	Yes	Yes	-	(139, 140)
GAF	Zygote	Yes	Yes	-	(141)
ISL1	Cardiac progenitor cell	Yes	Yes	GATA4	(44)
KLF4	iPS cells	Yes	Yes	MYC	(32, 33, 142)
MYOD1	Myoblast	Yes	Yes	-	(7)
PAX7	Melanotrope	Yes	Yes	TPIT	(34, 39, 143)
PU.1	Macrophage/ T cell	Yes	Yes	-	(115, 116, 120–122)
OCT4	iPS cells	Yes	Yes	MYC	(32, 33, 142)
OPA	Zygote	Yes	Yes	-	(144, 145)
SOX2	iPS cells	Yes	Yes	MYC	(32, 33, 142)
TCF1	T cell	Yes	Yes	-	(146)
ZELDA	Zygote	Yes	Yes	-	(147)

iPS, induced pluripotent stem cell.
Ref., reference.

nucleosomal DNA located in enhancers, c-MYC binds accessible regions in promoters and not nucleosomal DNA (25, 32, 33).

The molecular mechanisms whereby pioneer factors promote lineage specification and development remain ill-defined. One area of interest in the field is the effect of chromatin modifications (histones or DNA) on pioneer factor binding. A mechanism that has been observed is the binding of pioneer factors to nucleosomal DNA sites without any apparent effect. These regions are termed "pioneer factor resistant sites" and are being examined to define the co-regulatory mechanisms that are present in the chromatin environment to control cell fate by promoting or preventing chromatin remodeling and lineage specification by a pioneer factor following binding (34). For example, the pioneer factor PAX7 is able to bind facultative heterochromatin (H3K9me2) but not constitutive heterochromatin (H3M9me3) in order to regulate pituitary

progenitor cell development (33–35). This action highlights the need to characterize the role of different histone and DNA modifying enzymes that regulate pioneer factor function by directly interacting with them or by indirectly modifying the chromatin landscape during lineage specification (33).

A majority of the pioneer factor studies have focused on the characterization of the activation of lineage transcriptional programs and the initial functions of pioneer factors. However, the mechanisms driving lineage repression and the later stages of lineage specification are not well understood and warrant further investigation. ASCL1 is one of the few pioneer factors whose repressive role has been explored and found to recruit cooperating factors such as the myelin transcription factor 1-like protein (MYT1L), which represses the myogenic lineage program during the reprogramming of fibroblasts to neuronal cells (36). Studies on these cooperating or settler factors have demonstrated recruitment of both non-pioneer transcription factors as well as chromatin remodeling enzymes (p300 and BRG1) to allow for lineage specification to occur by activating gene expression, modifying chromatin or stabilizing the binding of pioneer factors to their DNA binding sites (9, 37, 38). Gaining a deeper understanding on how pioneer factor function is regulated by these settler factors may enhance reprogramming strategies to more efficiently drive lineage development in vivo to treat cardiovascular disease (6).

Role of chromatin modifying factors for the function of pioneer factors

While pioneer factors are required for the initial binding to nucleosomal DNA, cooperation with other (non-pioneer factors) is necessary in order to drive lineage development and reprogramming (9, 25, 39). Two important events are required following the binding of a pioneer factor and these include: (1) chromatin relaxation and (2) recruitment/interaction with other transcription factors (Figure 1). These two events enable the effects of pioneer factors and lineage development to occur by amplifying the signal and providing context dependent mechanisms in different regions of the genome (9, 25). Chromatin relaxation is a crucial step during lineage development where pioneer factors have been shown to promote remodeling by themselves (FOXA1) or with the assistance of the SWI/SNF complex (9, 25). The SWI/SNF complex of proteins is one of the most studied chromatin remodeling complexes. This complex increases DNA accessibility to regulate the development or reprogramming of pluripotent, neuronal, cardiac and endothelial cells (37, 40). SMARCA4 (BRG1), the ATPase subunit of the SWI/SNF complex, is an important regulator of early embryonic development as *Brg1* null embryos are lethal prior to implantation (41). Using in vitro differentiation and mouse studies, BRG1 has also been shown to be an important regulator of cardiovascular development and disease (42, 43). BRG1 also has been shown to be an important chromatin remodeler as it interacts with at least four different pioneer factors (OCT4, GATA3, ISL1 and ETV2) in a context dependent fashion to regulate chromatin remodeling and two of these pioneer factors are important regulators of cardiovascular development (Table 1) (37, 38, 44, 45).

Pioneer factors in the cardiovascular lineage

The cardiovascular lineage is composed of multiple lineages including: the muscle, vascular/endothelial and hematopoietic lineages (46–51). While many master regulators have been described and have important roles in the coordination of the development of the cardiovascular lineage, few pioneer factors have been identified within this lineage (8, 9). In part, this is due to the complexity associated with the different cellular lineages and structures within the cardiovascular system (13, 52). These pioneer factors are ISL1, GATA4 and ETV2, and in this section we will discuss the data supporting their pioneer role and function in the regulation of the cardiovascular lineage.

ISL1 is an important regulator for the development of the second heart field (SHF), and was recently identified as a pioneer factor (Table 1). *Isl1* KO mice lack the right ventricle, outflow tract and portions of the atria because of its role as an important regulator of SHF cardiac progenitor cells (CPCs) (53–56). In recent studies by Gao et al., they described that ISL1, like other pioneer factors, regulated the development of SHF CPCs by binding nucleosomal DNA and relaxing chromatin by forming a complex with BRG1-BAF60C (44). They also identified GATA4 as a cooperating factor in selected sites bound to ISL1, suggesting a potential interaction for ISL1 in the regulation of cardiovascular development. Together, ISL1 and GATA4 were shown to bind regulatory DNA regions of important cardiac genes such as *Hand2*, *Myocd*, *Ttn*, *Ryr2* and others. The exact mechanism whereby GATA4 promotes the pioneer function of ISL1 in these regulatory regions remains to be elucidated. These studies used both in vivo and in vitro assays to demonstrate that ISL1 binds nucleosomal DNA to regulate SHF development.

GATA4 is another important master regulator of cardiovascular development. Loss of *Gata4* has been shown to lead to early cardiac defects and results in bifed (non-fused) heart fields and embryonic lethality (57–62). Additionally, GATA4 has the capacity (along with other master regulators) to reprogram fibroblasts to induced cardiomyocytes (iCMs) *in vitro* and *in vivo* (63–67). While GATA4 is a key regulator of cardiovascular development, its role as a pioneer factor has only been described in hepatic progenitors and reprogramming of fibroblasts to hepatic-like cells (29, 68). A recent study combined scRNAseq, ATACseq, ChIPseq and machine learning to define the molecular mechanisms governing iCM reprogramming

using GATA4, MEF2C and TBX5 (GMT) and concluded that MEF2C and TBX5, but not GATA4 bind heterochromatin and promote chromatin remodeling during reprogramming (69). While these studies do not support the notion that GATA4 is a pioneer factor for the cardiac muscle lineage, further developmental studies are necessary to understand the heterochromatin binding and chromatin remodeling capabilities of GATA4 during cardiovascular development. The recent ISL1 studies suggest that GATA4 may bind to heterochromatin in the cardiovascular lineage independently but more mechanistic studies are needed (44).

More recently, ETV2 was identified as a pioneer factor for the cardiovascular lineage that regulates and reprograms endothelium (Table 1) (37). ETV2 is an essential transcription factor for the development of endothelial and hematopoietic lineages (51, 70–108). Its expression is observed in mesodermal progenitors and hemangioblasts that give rise to endocardial/endothelial and hematopoietic lineages, while repressing other lineages such as the cardiac and skeletal muscle lineages (49, 74, 79). Key regulatory genes and pathways for the cardiovascular lineage such as MESP1, NKX2-5, Wnt/Notch/BMP signaling (among others) have been shown to regulate ETV2 expression within the cardiovascular lineage (50, 74, 109, 110). Loss of *Etv2* results in lethality by E8.5 in developing mouse embryos due to the lack of all vascular and blood lineages. Moreover, congenital heart defects in aborted developing human fetuses have been reported to harbor *Etv2* mutations (50, 51, 111). Additionally, ETV2 overexpression (alone) reprograms terminally differentiated cells (fibroblasts) to endothelial cells both *in vitro* and *in vivo* (112). Our recent findings characterized the molecular mechanism whereby ETV2 regulates the endothelial lineage as a pioneer factor (37). ETV2 can scan the genome, bind nucleosomal DNA and remodel chromatin independent of its cellular context, whether it is related to fibroblast reprogramming or mouse embryonic stem cell (mESC) differentiation into endothelial progenitor cells (Figure 1). We characterized this functional role for ETV2 using scRNAseq, ATACseq, NOMEseq, ChIPseq and *in vitro* nucleosomal binding assays to unequivocally demonstrate that ETV2 binds nucleosomal DNA during endothelial lineage reprogramming/development. We identified canonical downstream targets for ETV2 such as *Emcn*, *Lmo2*, *Rhoj* and others that were bound by ETV2 during endothelial lineage development and reprogramming. Similar to ISL1, ETV2 recruits and directly interacts with BRG1. BRG1 is an essential co-factor for ETV2 to function as a pioneer factor as *Brg1* knockdown and conditional knockout significantly affected the ability of ETV2 to remodel chromatin and drive endothelial lineage formation in both reprogrammed fibroblasts and differentiating mESCs, respectively (37). This ETV2-BRG1 interaction was verified using mass spectrometry, Co-IP assays and GST-pulldown assays. Additionally, we demonstrated that this interaction was important for enacting epigenetic changes during endothelial lineage development such as the deposition of histone 3 lysine 27 acetylation (H3K27Ac) in regions surrounding ETV2-BRG1 bound sites. Lastly, by screening co-factors we identified ELK3 as a transcription factor that was recruited to ETV2-BRG1 bound sites following chromatin remodeling and ELK3 has an important role in endothelial cell development (Figure 1 and Table 1). Understanding how other factors might regulate chromatin remodeling and the pioneer activity of ETV2, such as FOXC2 which is known to regulate Fox-Ets enhancer motifs during endothelial lineage development in combination of ETV2, will be important for further dissecting this molecular mechanism (113). Forkhead transcription factors are important in the field of pioneer factors and chromatin remodeling because of their unique protein structure that resembles linker histones and allows (some of the *forkhead* family members) to remodel chromatin (31). Furthermore, the expression of ETV2 is transient during development, understanding how other downstream co-factors (i.e., ELK3, FLI1, SCL/TAL1, etc.) direct the developmental machinery following the downregulation of ETV2 will be important for the development of therapeutic strategies using ETV2 to develop mature vasculature that can be used for ischemic diseases such as the transplantation of human vasculature (71, 114).

ETV2 possesses an Ets DNA binding domain (DBD) characterized by a winged helix-turn-helix structure which needs to be studied in terms of how it interacts with nucleosomal DNA to allow for chromatin binding and remodeling to occur (75). Previous studies on *forkhead* factors have demonstrated that the winged helix DBD of the pioneer factor FOXA resembles that of the structure of linker histones, while Ets factors have been shown to use their short α-helix structure to bind the major groove of DNA to target nucleosomes (25). We hypothesize that the winged helix of ETV2 will most likely behave like that of previously described Ets factors, but it remains to be explored.

Unlike ISL1 and GATA4, the pioneer function of ETV2 in the cardiovascular lineage is independent of its cellular context, whether it is cellular differentiation or reprogramming, it functions in a similar fashion in both model systems. Future studies will need to focus on further characterization of the molecular mechanisms driving endothelial cell development/reprogramming by ETV2 to enhance therapeutic approaches to develop mature vasculature for ischemic diseases. While ETV2 is an essential regulator of hematopoietic development, we did not define ETV2 as a pioneer factor for hematopoietic lineages and therefore we hypothesize that other co-factors and pioneer factors might facilitate this developmental process. For example, EBF1, PU.1 and C/EBPα regulate hematopoietic development and act as pioneer factors for the B cells, DN3 t cells and macrophages (115–122) (Table 1). Whether these factors are regulated by ETV2 early on or they act independently of ETV2 to regulate the development of hematopoietic lineages remains to be

elucidated. Identifying this pioneer role for ETV2 has big implications for the development of regenerative therapies that aim to generate vasculature for ischemic diseases, particularly in the cardiovascular system (71, 112). Additionally, although not the focus of this review, the development of therapies that target pioneer factors in cancer will be very important. As ETV2 has been shown to have a role in cancer (82, 88, 98, 123), understanding whether its ability to remodel silent/compacted chromatin as a pioneer factor has important implications during angiogenesis, as therapeutic initiatives could target and inhibit ETV2 thereby impacting tumorigenesis (82, 98, 123). Additionally, it would be interesting to determine whether or not BRG1 or another chromatin remodeler also forms a complex with ETV2 in the context of cancer.

Conclusion(s)

More studies are emerging that claim to have characterized a novel pioneer transcription factor and this number will be expected to increase (8). This is in part due to the advances in molecular biology that facilitate the cellular characterization at the single cell level during embryogenesis. Further, these technologies will allow us to identify DNA binding sites for transcription factors (TF) and more importantly allow us to define the chromatin dynamics surrounding the DNA binding sites of such TFs. Importantly, the development of the Assay for Transposase-Accessible Chromatin followed by sequencing (ATAC-seq) allows for the definition of the chromatin landscape of differentiating or reprogramming cells using very few cells (50,000 cells or less) and support the claim that a TF is a pioneer factor (124, 125). While ATAC-seq characterization of cell populations can be insightful, we caution the reader that a more in-depth analysis is needed when assigning the role of pioneer factor. To designate a pioneer factor, three criteria need to be fulfilled: (1) pioneer factors need to bind nucleosomal DNA *in vivo* (sequencing) and *in vitro* (nucleosomal binding assay), (2) pioneer factors need to promote chromatin remodeling around DNA binding sites by themselves or by interacting with chromatin remodelers and (3) pioneer factors need to enact global epigenetic changes (i.e., demethylation) and recruit other co-factors that further promote the development or reprogramming of a cellular lineage (Figure 1; Table 1).

Further studies will be needed within the cardiovascular field to identify pioneer factors that regulate distinct cellular lineages and structures (i.e., first vs. second heart field) that comprise the four chambered organ. For example, while ETV2 sits at the top of the endothelial lineage developmental hierarchy, ISL1 and GATA4 are two of many regulators of the cardiac muscle lineage with very specific functions. We predict that multiple pioneer factors will be required to regulate cardiac muscle development and reprogramming. Other cellular lineages that were not discussed include: smooth muscle and cardiac fibroblasts as no pioneer factors have been identified for these lineages. Pioneer factors can be powerful tools for the development of regenerative therapies whose goal is to generate mature and functional cell lineages. Understanding the molecular mechanisms that drive lineage development by these and other pioneer factors within the cardiovascular lineage will be instrumental because coupling these pioneer factors along with chromatin remodelers and downstream targets genes can amplify the molecular effect needed to better develop regenerative therapies for cardiovascular disease.

Author contributions

JS-P and DG: conceived the review and wrote the manuscript. All authors contributed to the article and approved the submitted version.

Funding

We are grateful for the support of the Department of Defense (Grant # 3002-11765-00089113).

Conflict of interest

The authors declare that the research was conducted in the absence of any commercial or financial relationships that could be construed as a potential conflict of interest.

Publisher's note

References

1. Amini M, Zayeri F, Salehi M. Trend analysis of cardiovascular disease mortality, incidence, and mortality-to-incidence ratio: results from global burden of disease study 2017. *BMC Public Health.* (2021) 21:401. doi: 10.1186/s12889-021-10429-0

2. Roth GA, Mensah GA, Johnson CO, Addolorato G, Ammirati E, Baddour LM, et al. Global Burden of cardiovascular diseases and risk factors, 1990-2019: update from the GBD 2019 study. *J Am Coll Cardiol.* (2020) 76: 2982–3021.

3. Alraies MC, Eckman P. Adult heart transplant: indications and outcomes. *J Thorac Dis.* (2014) 6:1120–8. doi: 10.3978/j.issn.2072-1439.2014.06.44

4. Garry DJ, Masino AM, Naseem RH, Martin CM. Ponce de Leon's Fountain: stem cells and the regenerating heart. *Am J Med Sci.* (2005) 329:190–201. doi: 10.1097/00000441-200504000-00005

5. Aydin B, Mazzoni EO. Cell reprogramming: the many roads to success. *Annu Rev Cell Dev Biol.* (2019) 35:433–52. doi: 10.1146/annurev-cellbio-100818-125127

6. Wang H, Yang Y, Liu J, Qian L. Direct cell reprogramming: approaches, mechanisms and progress. *Nat Rev Mol Cell Biol.* (2021) 22:410–24. doi: 10.1038/s41580-021-00335-z

7. Tapscott SJ, Davis RL, Thayer MJ, Cheng PF, Weintraub H, Lassar AB. MyoD1: a nuclear phosphoprotein requiring a Myc homology region to convert fibroblasts to myoblasts. *Science.* (1988) 242:405–11. doi: 10.1126/science.3175662

8. Chan SS, Kyba M. What is a master regulator? *J Stem Cell Res Ther.* (2013) 3:114. doi: 10.4172/2157-7633.1000e114

9. Balsalobre A, Drouin J. Pioneer factors as master regulators of the epigenome and cell fate. *Nat Rev Mol Cell Biol.* (2022). doi: 10.1038/s41580-022-00464-z

10. Fishman MC, Olson EN. Parsing the heart: genetic modules for organ assembly. *Cell.* (1997) 91:153–6. doi: 10.1016/S0092-8674[00]80397-9

11. Olson EN, Srivastava D. Molecular pathways controlling heart development. *Science.* (1996) 272:671–6. doi: 10.1126/science.272.5262.671

12. Parmacek MS, Epstein JA. Pursuing cardiac progenitors: regeneration redux. *Cell.* (2005) 120:295–8. doi: 10.1016/j.cell.2005.01.025

13. Srivastava D. Making or breaking the heart: from lineage determination to morphogenesis. *Cell.* (2006) 126:1037–48. doi: 10.1016/j.cell.2006.09.003

14. Bruneau BG. The developmental genetics of congenital heart disease. *Nature.* (2008) 451:943–8. doi: 10.1038/nature06801

15. Evans SM, Yelon D, Conlon FL, Kirby ML. Myocardial lineage development. *Circ Res.* (2010) 107:1428–44. doi: 10.1161/CIRCRESAHA.110.227405

16. Davis TL, Rebay I. Master regulators in development: views from the Drosophila retinal determination and mammalian pluripotency gene networks. *Dev Biol.* (2017) 421:93–107. doi: 10.1016/j.ydbio.2016.12.005

17. Vinogradova TV, Sverdlov ED. PDX1: a unique pancreatic master regulator constantly changes its functions during embryonic development and progression of pancreatic cancer. *Biochemistry.* (2017) 82:887–93. doi: 10.1134/S000629791708003X

18. Ferber S, Halkin A, Cohen H, Ber I, Einav Y, Goldberg I, et al. Pancreatic and duodenal homeobox gene 1 induces expression of insulin genes in liver and ameliorates streptozotocin-induced hyperglycemia. *Nat Med.* (2000) 6:568–72. doi: 10.1038/75050

19. Heller RS, Stoffers DA, Bock T, Svenstrup K, Jensen J, Horn T, et al. Improved glucose tolerance and acinar dysmorphogenesis by targeted expression of transcription factor PDX-1 to the exocrine pancreas. *Diabetes.* (2001) 50:1553–61. doi: 10.2337/diabetes.50.7.1553

20. Davis RL, Weintraub H, Lassar AB. Expression of a single transfected cDNA converts fibroblasts to myoblasts. *Cell.* (1987) 51:987–1000. doi: 10.1016/0092-8674(87)90585-X

21. Boyer LA, Lee TI, Cole MF, Johnstone SE, Levine SS, Zucker JP, et al. Core transcriptional regulatory circuitry in human embryonic stem cells. *Cell.* (2005) 122:947–56. doi: 10.1016/j.cell.2005.08.020

22. Porcher C, Swat W, Rockwell K, Fujiwara Y, Alt FW, Orkin SH. The T cell leukemia oncoprotein SCL/tal-1 is essential for development of all hematopoietic lineages. *Cell.* (1996) 86:47–57. doi: 10.1016/S0092-8674(00)80076-8

23. Semenza GL. Hypoxia-inducible factor 1: master regulator of O2 homeostasis. *Curr Opin Genet Dev.* (1998) 8:588–94. doi: 10.1016/S0959-437X(98)80016-6

24. Bondue A, Lapouge G, Paulissen C, Semeraro C, Iacovino M, Kyba M, et al. Mesp1 acts as a master regulator of multipotent cardiovascular progenitor specification. *Cell Stem Cell.* (2008) 3:69–84. doi: 10.1016/j.stem.2008.06.009

25. Zaret KS. Pioneer transcription factors initiating gene network changes. *Annu Rev Genet.* (2020) 54:367–85. doi: 10.1146/annurev-genet-030220-015007

26. Zaret KS, Carroll JS. Pioneer transcription factors: establishing competence for gene expression. *Genes Dev.* (2011) 25:2227–41. doi: 10.1101/gad.176826.111

27. Gualdi R, Bossard P, Zheng M, Hamada Y, Coleman JR, Zaret KS. Hepatic specification of the gut endoderm *in vitro*: cell signaling and transcriptional control. *Genes Dev.* (1996) 10:1670–82. doi: 10.1101/gad.10.13.1670

28. McPherson CE, Shim EY, Friedman DS, Zaret KS. An active tissue-specific enhancer and bound transcription factors existing in a precisely positioned nucleosomal array. *Cell.* (1993) 75:387–98. doi: 10.1016/0092-8674(93)80079-T

29. Cirillo LA, Lin FR, Cuesta I, Friedman D, Jarnik M, Zaret KS. Opening of compacted chromatin by early developmental transcription factors HNF3 (FoxA) and GATA-4. *Mol Cell.* (2002) 9:279–89. doi: 10.1016/S1097-2765(02)00459-8

30. Iwafuchi-Doi M, Zaret KS. Cell fate control by pioneer transcription factors. *Development.* (2016) 143:1833–7. doi: 10.1242/dev.133900

31. Iwafuchi-Doi M, Donahue G, Kakumanu A, Watts JA, Mahony S, Pugh BF, et al. The pioneer transcription factor FoxA maintains an accessible nucleosome configuration at enhancers for tissue-specific gene activation. *Mol Cell.* (2016) 62:79–91. doi: 10.1016/j.molcel.2016.03.001

32. Soufi A, Garcia MF, Jaroszewicz A, Osman N, Pellegrini M, Zaret KS. Pioneer transcription factors target partial DNA motifs on nucleosomes to initiate reprogramming. *Cell.* (2015) 161:555–68. doi: 10.1016/j.cell.2015.03.017

33. Soufi A, Donahue G, Zaret KS. Facilitators and impediments of the pluripotency reprogramming factors' initial engagement with the genome. *Cell.* (2012) 151:994–1004. doi: 10.1016/j.cell.2012.09.045

34. Mayran A, Khetchoumian K, Hariri F, Pastinen T, Gauthier Y, Balsalobre A, et al. Pioneer factor Pax7 deploys a stable enhancer repertoire for specification of cell fate. *Nat Genet.* (2018) 50:259–69. doi: 10.1038/s41588-017-0035-2

35. Nicetto D, Donahue G, Jain T, Peng T, Sidoli S, Sheng L, et al. H3K9me3-heterochromatin loss at protein-coding genes enables developmental lineage specification. *Science.* (2019) 363:294–7. doi: 10.1126/science.aau0583

36. Lee QY, Mall M, Chanda S, Zhou B, Sharma KS, Schaukowitch K, et al. Pro-neuronal activity of Myod1 due to promiscuous binding to neuronal genes. *Nat Cell Biol.* (2020) 22:401–11. doi: 10.1038/s41556-020-0490-3

37. Gong W, Das S, Sierra-Pagan JE, Skie E, Dsouza N, Larson TA, et al. ETV2 functions as a pioneer factor to regulate and reprogram the endothelial lineage. *Nat Cell Biol.* (2022) 24:672–84. doi: 10.1038/s41556-022-00901-3

38. King HW, Klose RJ. The pioneer factor OCT4 requires the chromatin remodeller BRG1 to support gene regulatory element function in mouse embryonic stem cells. *Elife.* (2017) 6:e22631. doi: 10.7554/eLife.22631

39. Mayran A, Sochodolsky K, Khetchoumian K, Harris J, Gauthier Y, Bemmo A, et al. Pioneer and nonpioneer factor cooperation drives lineage specific chromatin opening. *Nat Commun.* (2019) 10:3807. doi: 10.1038/s41467-019-11791-9

40. Cenik BK, Shilatifard A, COMPASS. and SWI/SNF complexes in development and disease. *Nat Rev Genet.* (2021) 22:38–58. doi: 10.1038/s41576-020-0278-0

41. Bultman S, Gebuhr T, Yee D, La Mantia C, Nicholson J, Gilliam A, et al. A Brg1 null mutation in the mouse reveals functional differences among mammalian SWI/SNF complexes. *Mol Cell.* (2000) 6:1287–95. doi: 10.1016/S1097-2765(00)00127-1

42. Alexander JM, Hota SK, He D, Thomas S, Ho L, Pennacchio LA, et al. Brg1 modulates enhancer activation in mesoderm lineage commitment. *Development.* (2015) 142:1418–30. doi: 10.1242/dev.109496

43. Hang CT, Yang J, Han P, Cheng HL, Shang C, Ashley E, et al. Chromatin regulation by Brg1 underlies heart muscle development and disease. *Nature.* (2010) 466:62–7. doi: 10.1038/nature09130

44. Gao R, Liang X, Cheedipudi S, Cordero J, Jiang X, Zhang Q, et al. Pioneering function of Isl1 in the epigenetic control of cardiomyocyte cell fate. *Cell Res.* (2019) 29:486–501. doi: 10.1038/s41422-019-0168-1

45. Takaku M, Grimm SA, Shimbo T, Perera L, Menafra R, Stunnenberg HG, et al. GATA3-dependent cellular reprogramming requires activation-domain dependent recruitment of a chromatin remodeler. *Genome Biol.* (2016) 17:36. doi: 10.1186/s13059-016-0897-0

46. Ferretti E, Hadjantonakis AK. Mesoderm specification and diversification: from single cells to emergent tissues. *Curr Opin Cell Biol.* (2019) 61:110–6. doi: 10.1016/j.ceb.2019.07.012

47. Chang CP, Bruneau BG. Epigenetics and cardiovascular development. *Annu Rev Physiol.* (2012) 74:41–68. doi: 10.1146/annurev-physiol-020911-153242

48. Tam PP, Behringer RR. Mouse gastrulation: the formation of a mammalian body plan. *Mech Dev.* (1997) 68:3–25. doi: 10.1016/S0925-4773(97)00123-8

49. Rasmussen TL, Kweon J, Diekmann MA, Belema-Bedada F, Song Q, Bowlin K, et al. ER71 directs mesodermal fate decisions during embryogenesis. *Development.* (2011) 138:4801–12. doi: 10.1242/dev.070912

50. Ferdous A, Caprioli A, Iacovino M, Martin CM, Morris J, Richardson JA, et al. Nkx2-5 transactivates the Ets-related protein 71 gene and specifies an

endothelial/endocardial fate in the developing embryo. *Proc Natl Acad Sci.* (2009) 106:814–9. doi: 10.1073/pnas.0807583106

51. Lee D, Park C, Lee H, Lugus JJ, Kim SH, Arentson E, et al. ER71 acts downstream of BMP, Notch, and Wnt signaling in blood and vessel progenitor specification. *Cell Stem Cell.* (2008) 2:497–507. doi: 10.1016/j.stem.2008.03.008

52. Srivastava D, Olson EN. A genetic blueprint for cardiac development. *Nature.* (2000) 407:221–6. doi: 10.1038/35025190

53. Kwon C, Qian L, Cheng P, Nigam V, Arnold J, Srivastava D, et al. regulatory pathway involving Notch1/beta-catenin/Isl1 determines cardiac progenitor cell fate. *Nat Cell Biol.* (2009) 11:951–7. doi: 10.1038/ncb1906

54. Moretti A, Caron L, Nakano A, Lam JT, Bernshausen A, Chen Y, et al. Multipotent embryonic isl1+ progenitor cells lead to cardiac, smooth muscle, and endothelial cell diversification. *Cell.* (2006) 127:1151–65. doi: 10.1016/j.cell.2006.10.029

55. Laugwitz KL, Moretti A, Lam J, Gruber P, Chen Y, Woodard S, et al. Postnatal isl1+ cardioblasts enter fully differentiated cardiomyocyte lineages. *Nature.* (2005) 433:647–53. doi: 10.1038/nature03215

56. Cai CL, Liang X, Shi Y, Chu PH, Pfaff SL, Chen J, et al. Isl1 identifies a cardiac progenitor population that proliferates prior to differentiation and contributes a majority of cells to the heart. *Dev Cell.* (2003) 5:877–89. doi: 10.1016/S1534-5807(03)00363-0

57. Oka T, Maillet M, Watt AJ, Schwartz RJ, Aronow BJ, Duncan SA, et al. Cardiac-specific deletion of Gata4 reveals its requirement for hypertrophy, compensation, and myocyte viability. *Circ Res.* (2006) 98:837–45. doi: 10.1161/01.RES.0000215985.18538.c4

58. Bisping E, Ikeda S, Kong SW, Tarnavski O, Bodyak N, McMullen JR, et al. Gata4 is required for maintenance of postnatal cardiac function and protection from pressure overload-induced heart failure. *Proc Natl Acad Sci.* (2006) 103:14471–6. doi: 10.1073/pnas.0602543103

59. Zeisberg EM, Ma Q, Juraszek AL, Moses K, Schwartz RJ, Izumo S, et al. Morphogenesis of the right ventricle requires myocardial expression of Gata4. *J Clin Invest.* (2005) 115:1522–31. doi: 10.1172/JCI23769

60. Watt AJ, Battle MA Li J, Duncan SA. GATA4 is essential for formation of the proepicardium and regulates cardiogenesis. *Proc Natl Acad Sci.* (2004) 101:12573–8. doi: 10.1073/pnas.0400752101

61. Molkentin JD, Lin Q, Duncan SA, Olson EN. Requirement of the transcription factor GATA4 for heart tube formation and ventral morphogenesis. *Genes Dev.* (1997) 11:1061–72. doi: 10.1101/gad.11.8.1061

62. Kuo CT, Morrisey EE, Anandappa R, Sigrist K, Lu MM, Parmacek MS, et al. GATA4 transcription factor is required for ventral morphogenesis and heart tube formation. *Genes Dev.* (1997) 11:1048–60. doi: 10.1101/gad.11.8.1048

63. Fu JD, Srivastava D. Direct reprogramming of fibroblasts into cardiomyocytes for cardiac regenerative medicine. *Circ J.* (2015) 79:245–54. doi: 10.1253/circj.CJ-14-1372

64. Nam YJ, Song K, Olson EN. Heart repair by cardiac reprogramming. *Nat Med.* (2013) 19:413–5. doi: 10.1038/nm.3147

65. Fu JD, Stone NR, Liu L, Spencer CI, Qian L, Hayashi Y, et al. Direct reprogramming of human fibroblasts toward a cardiomyocyte-like state. *Stem Cell Rep.* (2013) 1:235–47. doi: 10.1016/j.stemcr.2013.07.005

66. Song K, Nam YJ, Luo X, Qi X, Tan W, Huang GN, et al. Heart repair by reprogramming non-myocytes with cardiac transcription factors. *Nature.* (2012) 485:599–604. doi: 10.1038/nature11139

67. Ieda M, Fu JD, Delgado-Olguin P, Vedantham V, Hayashi Y, Bruneau BG, et al. Direct reprogramming of fibroblasts into functional cardiomyocytes by defined factors. *Cell.* (2010) 142:375–86. doi: 10.1016/j.cell.2010.07.002

68. Huang P, He Z, Ji S, Sun H, Xiang D, Liu C, et al. Induction of functional hepatocyte-like cells from mouse fibroblasts by defined factors. *Nature.* (2011) 475:386–9. doi: 10.1038/nature10116

69. Stone NR, Gifford CA, Thomas R, Pratt KJB, Samse-Knapp K, Mohamed TMA, et al. Context-specific transcription factor functions regulate epigenomic and transcriptional dynamics during cardiac reprogramming. *Cell Stem Cell.* (2019) 25:87–102 e9. doi: 10.1016/j.stem.2019.06.012

70. Singh BN, Sierra-Pagan JE, Gong W, Das S, Theisen JWM, Skie E, et al. ETV2 (Ets variant transcription factor 2)-Rhoj cascade regulates endothelial progenitor cell migration during embryogenesis. *Arterioscler Thromb Vasc Biol.* (2020) 40:2875–90. doi: 10.1161/ATVBAHA.120.314488

71. Das S, Koyano-Nakagawa N, Gafni O, Maeng G, Singh BN, Rasmussen T, et al. Generation of human endothelium in pig embryos deficient in ETV2. *Nat Biotechnol.* (2020) 38:297–302. doi: 10.1038/s41587-019-0373-y

72. Singh BN, Gong W, Das S, Theisen JWM, Sierra-Pagan JE, Yannopoulos D, et al. Etv2 transcriptionally regulates Yes1 and promotes cell proliferation during embryogenesis. *Sci Rep.* (2019) 9:9736. doi: 10.1038/s41598-019-45841-5

73. Singh BN, Tahara N, Kawakami Y, Das S, Koyano-Nakagawa N, Gong W, et al. Etv2-miR-130a-Jarid2 cascade regulates vascular patterning during embryogenesis. *PLoS ONE.* (2017) 12:e0189010. doi: 10.1371/journal.pone.0189010

74. Koyano-Nakagawa N, Garry DJ. Etv2 as an essential regulator of mesodermal lineage development. *Cardiovasc Res.* (2017) 113:1294–306. doi: 10.1093/cvr/cvx133

75. Garry DJ. Etv2 is a master regulator of hematoendothelial lineages. *Trans Am Clin Climatol Assoc.* (2016) 127:212–23.

76. Singh BN, Kawakami Y, Akiyama R, Rasmussen TL, Garry MG, Gong W, et al. The Etv2-miR-130a network regulates mesodermal specification. *Cell Rep.* (2015) 13:915–23. doi: 10.1016/j.celrep.2015.09.060

77. Koyano-Nakagawa N, Shi X, Rasmussen TL, Das S, Walter CA, Garry DJ. Feedback mechanisms regulate Ets variant 2 (Etv2) gene expression and hematoendothelial lineages. *J Biol Chem.* (2015) 290:28107–19. doi: 10.1074/jbc.M115.662197

78. Rasmussen TL, Martin CM, Walter CA, Shi X, Perlingeiro R, Koyano-Nakagawa N, et al. Etv2 rescues Flk1 mutant embryoid bodies. *Genesis.* (2013) 51:471–80. doi: 10.1002/dvg.22396

79. Koyano-Nakagawa N, Kweon J, Iacovino M, Shi X, Rasmussen TL, Borges L, et al. Etv2 is expressed in the yolk sac hematopoietic and endothelial progenitors and regulates Lmo2 gene expression. *Stem Cells.* (2012) 30:1611–23. doi: 10.1002/stem.1131

80. Choi K, ETS. transcription factor ETV2/ER71/Etsrp in haematopoietic regeneration. *Curr Opin Hematol.* (2018) 25:253–8. doi: 10.1097/MOH.0000000000000430

81. Kim JY, Lee DH, Kim JK, Choi HS, Dwivedi B, Rupji M, et al. ETV2/ER71 regulates the generation of FLK1(+) cells from mouse embryonic stem cells through miR-126-MAPK signaling. *Stem Cell Res Ther.* (2019) 10:328. doi: 10.1186/s13287-019-1466-8

82. Lee TJ, Kang HK, Berry JC, Joo HG, Park C, Miller MJ, et al. ER71/ETV2 promotes hair regeneration from chemotherapeutic drug-induced hair loss by enhancing angiogenesis. *Biomol Ther.* (2021) 29:545–50. doi: 10.4062/biomolther.2021.022

83. Liu F, Li D, Yu YY, Kang I, Cha MJ, Kim JY, et al. Induction of hematopoietic and endothelial cell program orchestrated by ETS transcription factor ER71/ETV2. *EMBO Rep.* (2015) 16:654–69. doi: 10.15252/embr.201439939

84. Park C, Lee TJ, Bhang SH, Liu F, Nakamura R, Oladipupo SS, et al. Injury-Mediated Vascular Regeneration Requires Endothelial ER71/ETV2. *Arterioscler Thromb Vasc Biol.* (2016) 36:86–96. doi: 10.1161/ATVBAHA.115.306430

85. Xu CX, Lee TJ, Sakurai N, Krchma K, Liu F, Li D, et al. ETV2/ER71 regulates hematopoietic regeneration by promoting hematopoietic stem cell proliferation. *J Exp Med.* (2017) 214:1643–53. doi: 10.1084/jem.20160923

86. Zhao H, Choi K. A CRISPR screen identifies genes controlling Etv2 threshold expression in murine hemangiogenic fate commitment. *Nat Commun.* (2017) 8:541. doi: 10.1038/s41467-017-00667-5

87. Zhao H, Xu C, Lee TJ, Liu F, Choi K, ETS. transcription factor ETV2/ER71/Etsrp in hematopoietic and vascular development, injury, and regeneration. *Dev Dyn.* (2017) 246:318–27. doi: 10.1002/dvdy.24483

88. Baltrunaite K, Craig MP, Palencia Desai S, Chaturvedi P, Pandey RN, Hegde RS, et al. ETS transcription factors Etv2 and Fli1b are required for tumor angiogenesis. *Angiogenesis.* (2017) 20:307–23. doi: 10.1007/s10456-017-9539-8

89. Casie Chetty S, Sumanas S. Ets1 functions partially redundantly with Etv2 to promote embryonic vasculogenesis and angiogenesis in zebrafish. *Dev Biol.* (2020) 465:11–22. doi: 10.1016/j.ydbio.2020.06.007

90. Craig MP, Grajevskaja V, Liao HK, Balciuniene J, Ekker SC, Park JS, et al. Etv2 and fli1b function together as key regulators of vasculogenesis and angiogenesis. *Arterioscler Thromb Vasc Biol.* (2015) 35:865–76. doi: 10.1161/ATVBAHA.114.304768

91. Palencia-Desai S, Kohli V, Kang J, Chi NC, Black BL, Sumanas S. Vascular endothelial and endocardial progenitors differentiate as cardiomyocytes in the absence of Etsrp/Etv2 function. *Development.* (2011) 138:4721–32. doi: 10.1242/dev.064998

92. Sumanas S, Choi K, ETS. Transcription Factor ETV2/ER71/Etsrp in hematopoietic and vascular development. *Curr Top Dev Biol.* (2016) 118:77–111. doi: 10.1016/bs.ctdb.2016.01.005

93. Sumanas S, Gomez G, Zhao Y, Park C, Choi K, Lin S. Interplay among Etsrp/ER71, Scl, and Alk8 signaling controls endothelial and myeloid

cell formation. *Blood.* (2008) 111:4500–10. doi: 10.1182/blood-2007-09-110569

94. Wong KS, Proulx K, Rost MS, Sumanas S. Identification of vasculature-specific genes by microarray analysis of Etsrp/Etv2 overexpressing zebrafish embryos. *Dev Dyn.* (2009) 238:1836–50. doi: 10.1002/dvdy.21990

95. Chen PC, Hsueh YW, Lee YH, Tsai HW, Tsai KJ, Chiang PM, et al. primes angioblast formation by inducing ETV2 and LMO2 via FGFR1/BRAF/MEK/ERK. *Cell Mol Life Sci.* (2021) 78:2199–212. doi: 10.1007/s00018-020-03630-8

96. Chestnut B, Casie Chetty S, Koenig AL, Sumanas S. Single-cell transcriptomic analysis identifies the conversion of zebrafish Etv2-deficient vascular progenitors into skeletal muscle. *Nat Commun.* (2020) 11:2796. doi: 10.1038/s41467-020-16515-y

97. DiTacchio L, Bowles J, Shin S, Lim DS, Koopman P, Janknecht R. Transcription factors ER71/ETV2 and SOX9 participate in a positive feedback loop in fetal and adult mouse testis. *J Biol Chem.* (2012) 287:23657–66. doi: 10.1074/jbc.M111.320101

98. Kabir AU, Lee TJ, Pan H, Berry JC, Krchma K, Wu J, et al. Requisite endothelial reactivation and effective siRNA nanoparticle targeting of Etv2/Er71 in tumor angiogenesis. *JCI Insight.* (2018) 3:e97349. doi: 10.1172/jci.insight.97349

99. Kataoka H, Hayashi M, Kobayashi K, Ding G, Tanaka Y, Nishikawa S. Region-specific Etv2 ablation revealed the critical origin of hemogenic capacity from Hox6-positive caudal-lateral primitive mesoderm. *Exp Hematol.* (2013) 41:567–81 e9. doi: 10.1016/j.exphem.2013.02.009

100. Kataoka H, Hayashi M, Nakagawa R, Tanaka Y, Izumi N, Nishikawa S, et al. Etv2/ER71 induces vascular mesoderm from Flk1+PDGFRalpha+ primitive mesoderm. *Blood.* (2011) 118:6975–86. doi: 10.1182/blood-2011-05-352658

101. Kobayashi K, Ding G, Nishikawa S, Kataoka H. Role of Etv2-positive cells in the remodeling morphogenesis during vascular development. *Genes Cells.* (2013) 18:704–21. doi: 10.1111/gtc.12070

102. Lammerts van Bueren K, Black BL. Regulation of endothelial and hematopoietic development by the ETS transcription factor Etv2. *Curr Opin Hematol.* (2012) 19:199–205. doi: 10.1097/MOH.0b013e3283523e07

103. Moore JC, Sheppard-Tindell S, Shestopalov IA, Yamazoe S, Chen JK, Lawson ND. Post-transcriptional mechanisms contribute to Etv2 repression during vascular development. *Dev Biol.* (2013) 384:128–40. doi: 10.1016/j.ydbio.2013.08.028

104. Salanga MC, Meadows SM, Myers CT, Krieg PA, ETS. family protein ETV2 is required for initiation of the endothelial lineage but not the hematopoietic lineage in the Xenopus embryo. *Dev Dyn.* (2010) 239:1178–87. doi: 10.1002/dvdy.22277

105. Veldman MB, Lin S. Etsrp/Etv2 is directly regulated by Foxc1a/b in the zebrafish angioblast. *Circ Res.* (2012) 110:220–9. doi: 10.1161/CIRCRESAHA.111.251298

106. Veldman MB, Zhao C, Gomez GA, Lindgren AG, Huang H, Yang H, et al. Transdifferentiation of fast skeletal muscle into functional endothelium in vivo by transcription factor Etv2. *PLoS Biol.* (2013) 11:e1001590. doi: 10.1371/journal.pbio.1001590

107. Wareing S, Eliades A, Lacaud G, Kouskoff V. ETV2 expression marks blood and endothelium precursors, including hemogenic endothelium, at the onset of blood development. *Dev Dyn.* (2012) 241:1454–64. doi: 10.1002/dvdy.23825

108. Yamamizu K, Matsunaga T, Katayama S, Kataoka H, Takayama N, Eto K, et al. PKA/CREB signaling triggers initiation of endothelial and hematopoietic cell differentiation via Etv2 induction. *Stem Cells.* (2012) 30:687–96. doi: 10.1002/stem.1041

109. Chan SS, Shi X, Toyama A, Arpke RW, Dandapat A, Iacovino M, et al. Mesp1 patterns mesoderm into cardiac, hematopoietic, or skeletal myogenic progenitors in a context-dependent manner. *Cell Stem Cell.* (2013) 12:587–601. doi: 10.1016/j.stem.2013.03.004

110. Shi X, Zirbes KM, Rasmussen TL, Ferdous A, Garry MG, Koyano-Nakagawa N, et al. The transcription factor Mesp1 interacts with cAMP-responsive element binding protein 1 (Creb1) and coactivates Ets variant 2 (Etv2) gene expression. *J Biol Chem.* (2015) 290:9614–25. doi: 10.1074/jbc.M114.614628

111. Basel-Salmon L, Ruhrman-Shahar N, Barel O, Hagari O, Marek-Yagel D, Azulai N, et al. Biallelic variants in ETV2 in a family with congenital heart defects, vertebral abnormalities and preaxial polydactyly. *Eur J Med Genet.* (2021) 64:104124. doi: 10.1016/j.ejmg.2020.104124

112. Lee S, Park C, Han JW, Kim JY, Cho K, Kim EJ, et al. Direct reprogramming of human dermal fibroblasts into endothelial cells using ER71/ETV2. *Circ Res.* (2017) 120:848–61. doi: 10.1161/CIRCRESAHA.116.309833

113. De Val S, Chi NC, Meadows SM, Minovitsky S, Anderson JP, Harris IS, et al. Combinatorial regulation of endothelial gene expression by ets and forkhead transcription factors. *Cell.* (2008) 135:1053–64. doi: 10.1016/j.cell.2008.10.049

114. Garry DJ, Sierra-Pagan JE. *Mechanisms that Govern Endothelial Lineage Development and Vasculogenesis. Advanced Technologies in Cardiovascular Bioengineering.* Cham: Springer (2022). p. 31–48. doi: 10.1007/978-3-030-86140-7_3

115. Minderjahn J, Schmidt A, Fuchs A, Schill R, Raithel J, Babina M, et al. Mechanisms governing the pioneering and redistribution capabilities of the non-classical pioneer PU. *1 Nat Commun.* (2020) 11:402. doi: 10.1038/s41467-019-13960-2

116. Ungerback J, Hosokawa H, Wang X, Strid T, Williams BA, Sigvardsson M, et al. Pioneering, chromatin remodeling, and epigenetic constraint in early T-cell gene regulation by SPI1 (PU. 1). *Genome Res.* (2018) 28:1508–19. doi: 10.1101/gr.231423.117

117. Li R, Cauchy P, Ramamoorthy S, Boller S, Chavez L, Grosschedl R. Dynamic EBF1 occupancy directs sequential epigenetic and transcriptional events in B-cell programming. *Genes Dev.* (2018) 32:96–111. doi: 10.1101/gad.309583.117

118. Boller S, Ramamoorthy S, Akbas D, Nechanitzky R, Burger L, Murr R, et al. Pioneering activity of the C-terminal domain of EBF1 shapes the chromatin landscape for B cell programming. *Immunity.* (2016) 44:527–41. doi: 10.1016/j.immuni.2016.02.021

119. van Oevelen C, Collombet S, Vicent G, Hoogenkamp M, Lepoivre C, Badeaux A, et al. C/EBPalpha activates pre-existing and De Novo macrophage enhancers during induced pre-B cell transdifferentiation and myelopoiesis. *Stem Cell Reports.* (2015) 5:232–47. doi: 10.1016/j.stemcr.2015.06.007

120. Barozzi I, Simonatto M, Bonifacio S, Yang L, Rohs R, Ghisletti S, et al. Coregulation of transcription factor binding and nucleosome occupancy through DNA features of mammalian enhancers. *Mol Cell.* (2014) 54:844–57. doi: 10.1016/j.molcel.2014.04.006

121. Heinz S, Benner C, Spann N, Bertolino E, Lin YC, Laslo P, et al. Simple combinations of lineage-determining transcription factors prime cis-regulatory elements required for macrophage and B cell identities. *Mol Cell.* (2010) 38:576–89. doi: 10.1016/j.molcel.2010.05.004

122. Feng R, Desbordes SC, Xie H, Tillo ES, Pixley F, Stanley ER, et al. PU. 1 and C/EBPalpha/beta convert fibroblasts into macrophage-like cells. *Proc Natl Acad Sci U S A.* (2008) 105:6057–62. doi: 10.1073/pnas.0711961105

123. Zhao C, Gomez GA, Zhao Y, Yang Y, Cao D, Lu J, et al. ETV2 mediates endothelial transdifferentiation of glioblastoma. *Signal Transduct Target Ther.* (2018) 3:1–11. doi: 10.1038/s41392-018-0007-8

124. Buenrostro JD, Wu B, Litzenburger UM, Ruff D, Gonzales ML, Snyder MP, et al. Single-cell chromatin accessibility reveals principles of regulatory variation. *Nature.* (2015) 523:486–90. doi: 10.1038/nature14590

125. Buenrostro JD, Wu B, Chang HY, Greenleaf WJ. ATAC-seq: a method for assaying chromatin accessibility genome-wide. *Curr Protoc Mol Biol.* (2015) 109:21. doi: 10.1002/0471142727.mb2129s109

126. Luo C, Lee QY, Wapinski O, Castanon R, Nery JR, Mall M, et al. Global DNA methylation remodeling during direct reprogramming of fibroblasts to neurons. *Elife.* (2019) 8:e40197. doi: 10.7554/eLife.40197

127. Raposo A, Vasconcelos FF, Drechsel D, Marie C, Johnston C, Dolle D, et al. Ascl1 coordinately regulates gene expression and the chromatin landscape during neurogenesis. *Cell Rep.* (2015) 10:1544–56. doi: 10.1016/j.celrep.2015.02.025

128. Wapinski OL, Lee QY, Chen AC Li R, Corces MR, Ang CE, et al. Rapid chromatin switch in the direct reprogramming of fibroblasts to neurons. *Cell Rep.* (2017) 20:3236–47. doi: 10.1016/j.celrep.2017.09.011

129. Wapinski OL, Vierbuchen T, Qu K, Lee QY, Chanda S, Fuentes DR, et al. Hierarchical mechanisms for direct reprogramming of fibroblasts to neurons. *Cell.* (2013) 155:621–35. doi: 10.1016/j.cell.2013.09.028

130. Carroll JS, Liu XS, Brodsky AS Li W, Meyer CA, Szary AJ, et al. Chromosome-wide mapping of estrogen receptor binding reveals long-range regulation requiring the forkhead protein FoxA1. *Cell.* (2005) 122:33–43. doi: 10.1016/j.cell.2005.05.008

131. Cernilogar FM, Hasenoder S, Wang Z, Scheibner K, Burtscher I, Sterr M, et al. Pre-marked chromatin and transcription factor co-binding shape the pioneering activity of Foxa2. *Nucleic Acids Res.* (2019) 47:9069–86. doi: 10.1093/nar/gkz627

132. Laganiere J, Deblois G, Lefebvre C, Bataille AR, Robert F, Giguere V. From the cover: location analysis of estrogen receptor alpha target promoters reveals that FOXA1 defines a domain of the estrogen response. *Proc Natl Acad Sci U S A.* (2005) 102:11651–6. doi: 10.1073/pnas.0505575102

133. Lee K, Cho H, Rickert RW, Li QV, Pulecio J, Leslie CS, et al. FOXA2 is required for enhancer priming during pancreatic differentiation. *Cell Rep.* (2019) 28:382–93 e7. doi: 10.1016/j.celrep.2019.06.034

134. Lupien M, Eeckhoute J, Meyer CA, Wang Q, Zhang Y, Li W, et al. FoxA1 translates epigenetic signatures into enhancer-driven lineage-specific transcription. *Cell.* (2008) 132:958–70. doi: 10.1016/j.cell.2008.01.018

135. Sekiya S, Suzuki A. Direct conversion of mouse fibroblasts to hepatocyte-like cells by defined factors. *Nature.* (2011) 475:390–3. doi: 10.1038/nature10263

136. Serandour AA, Avner S, Percevault F, Demay F, Bizot M, Lucchetti-Miganeh C, et al. Epigenetic switch involved in activation of pioneer factor FOXA1-dependent enhancers. *Genome Res.* (2011) 21:555–65. doi: 10.1101/gr.111534.110

137. Wang Q, Li W, Zhang Y, Yuan X, Xu K, Yu J, et al. Androgen receptor regulates a distinct transcription program in androgen-independent prostate cancer. *Cell.* (2009) 138:245–56. doi: 10.1016/j.cell.2009.04.056

138. Charney RM, Forouzmand E, Cho JS, Cheung J, Paraiso KD, Yasuoka Y, et al. Foxh1 occupies cis-regulatory modules prior to dynamic transcription factor interactions controlling the mesendoderm gene program. *Dev Cell.* (2017) 40:595–607 e4. doi: 10.1016/j.devcel.2017.02.017

139. Jacobs J, Atkins M, Davie K, Imrichova H, Romanelli L, Christiaens V, et al. The transcription factor grainy head primes epithelial enhancers for spatiotemporal activation by displacing nucleosomes. *Nat Genet.* (2018) 50:1011–20. doi: 10.1038/s41588-018-0140-x

140. Nevil M, Gibson TJ, Bartolutti C, Iyengar A, Harrison MM. Establishment of chromatin accessibility by the conserved transcription factor Grainy head is developmentally regulated. *Development.* (2020) 147:dev185009. doi: 10.1242/dev.185009

141. Gaskill MM, Gibson TJ, Larson ED, Harrison MM. GAF is essential for zygotic genome activation and chromatin accessibility in the early Drosophila embryo. *Elife.* (2021) 10:e66668. doi: 10.7554/eLife.66668.sa2

142. Chronis C, Fiziev P, Papp B, Butz S, Bonora G, Sabri S, et al. Cooperative binding of transcription factors orchestrates reprogramming. *Cell.* (2017) 168:442–59 e20. doi: 10.1016/j.cell.2016.12.016

143. Budry L, Balsalobre A, Gauthier Y, Khetchoumian K. L'Honore A, Vallette S, et al. The selector gene Pax7 dictates alternate pituitary cell fates through its pioneer action on chromatin remodeling. *Genes Dev.* (2012) 26:2299–310. doi: 10.1101/gad.200436.112

144. Koromila T, Gao F, Iwasaki Y, He P, Pachter L, Gergen JP, et al. Odd-paired is a pioneer-like factor that coordinates with Zelda to control gene expression in embryos. *Elife.* (2020) 9:e59610. doi: 10.7554/eLife.59610.sa2

145. Soluri IV, Zumerling LM, Payan Parra OA, Clark EG, Blythe SA. Zygotic pioneer factor activity of odd-paired/Zic is necessary for late function of the Drosophila segmentation network. *Elife.* (2020) 9:e53916. doi: 10.7554/eLife.53916.sa2

146. Johnson JL, Georgakilas G, Petrovic J, Kurachi M, Cai S, Harly C, et al. Lineage-determining transcription factor TCF-1 initiates the epigenetic identity of T cells. *Immunity.* (2018) 48:243–57 e10. doi: 10.1016/j.immuni.2018.01.012

147. McDaniel SL, Gibson TJ, Schulz KN, Fernandez Garcia M, Nevil M, Jain SU, et al. Continued activity of the pioneer factor zelda is required to drive zygotic genome activation. *Mol Cell.* (2019) 74:185–95 e4. doi: 10.1016/j.molcel.2019.01.014

frontiers | Frontiers in Cardiovascular Medicine

TYPE Original Research
PUBLISHED 26 September 2022
DOI 10.3389/fcvm.2022.901396

OPEN ACCESS

EDITED BY
Rajesh Katare,
University of Otago, New Zealand

REVIEWED BY
Yuji Nakada,
University of Alabama at Birmingham, United States
Marie-José Goumans,
Leiden University Medical Center, Netherlands
Katherine Yutzey,
Cincinnati Children's Hospital Medical Center, United States
Wataru Kimura,
RIKEN Center for Biosystems Dynamics Research (BDR), Japan

*CORRESPONDENCE
Ajit Magadum
tun83483@temple.edu
Felix B. Engel
felix.engel@uk-erlangen.de

SPECIALTY SECTION
This article was submitted to Cardiovascular Biologics and Regenerative Medicine, a section of the journal Frontiers in Cardiovascular Medicine

RECEIVED 21 March 2022
ACCEPTED 10 August 2022
PUBLISHED 26 September 2022

CITATION
Magadum A, Renikunta HV, Singh N, Estaras C, Kishore R and Engel FB (2022) Live cell screening identifies glycosides as enhancers of cardiomyocyte cell cycle activity. *Front. Cardiovasc. Med.* 9:901396. doi: 10.3389/fcvm.2022.901396

Live cell screening identifies glycosides as enhancers of cardiomyocyte cell cycle activity

Ajit Magadum[1,2,3]*, Harsha V. Renikunta[1,4], Neha Singh[5], Conchi Estaras[3], Raj Kishore[3,6] and Felix B. Engel[1,7,8]*

[1]Department of Cardiac Development and Remodelling, Max-Planck-Institute for Heart and Lung Research, Bad Nauheim, Germany, [2]Cardiovascular Research Center, Icahn School of Medicine at Mount Sinai, New York, NY, United States, [3]Lewis Katz School of Medicine, Center for Translational Medicine, Temple University, Philadelphia, PA, United States, [4]Department of Cardiology, Charité Berlin - University Medicine, Berlin, Germany, [5]Department of Sports Biosciences, Central University of Rajasthan, Ajmer, India, [6]Department of Cardiovascular Sciences, Lewis Katz School of Medicine at Temple University, Philadelphia, PA, United States, [7]Experimental Renal and Cardiovascular Research, Department of Nephropathology, Institute of Pathology, Friedrich-Alexander-Universität Erlangen-Nürnberg (FAU), Erlangen, Germany, [8]Muscle Research Center Erlangen (MURCE), Erlangen, Germany

Promoting cardiomyocyte proliferation is a promising strategy to regenerate the heart. Yet, so far, it is poorly understood how cardiomyocyte proliferation is regulated, and no factor identified to promote mammalian cardiomyocyte proliferation has been translated into medical practice. Therefore, finding a novel factor will be vital. Here, we established a live cell screening based on mouse embryonic stem cell-derived cardiomyocytes expressing a non-functional human geminin deletion mutant fused to Azami Green (CM7/1-hgem-derived cardiomyocytes). We screened for a subset of compounds of the small molecule library Spectrum Collection and identified 19 potential inducers of stem cell-derived cardiomyocyte proliferation. Furthermore, the pro-proliferative potential of identified candidate compounds was validated in neonatal and adult rat cardiomyocytes as well as human induced pluripotent stem cell-derived cardiomyocytes. 18 of these compounds promoted mitosis and cytokinesis in neonatal rat cardiomyocytes. Among the top four candidates were two cardiac glycosides, peruvoside and convallatoxin, the flavonoid osajin, and the selective α-adrenoceptor antagonist and imidazoline I1 receptor ligand efaroxan hydrochloride. Inhibition of PTEN and GSK-3β enhanced cell cycle re-entry and progression upon stimulation with cardiac glycosides and osajin, while inhibition of IP3 receptors inhibited the cell cycle-promoting effect of cardiac glycosides. Collectively, we established a screening system and identified potential compounds to promote cardiomyocyte proliferation. Our data suggest that modulation of calcium handling and metabolism promotes cardiomyocyte proliferation, and cardiac glycosides might, besides increasing myocardial contraction force, contribute to cardiac repair by inducing cardiomyocyte proliferation.

KEYWORDS

cardiac glycosides, cardiomyocyte proliferation, calcium handling, live cell screening platform AG, Azami Green, stem cell, small molecules, cell cycle

Introduction

Heart failure remains a major socio-economic challenge. Despite significant achievements in medical practice resulting in reduced acute mortality of myocardial infarction (MI), the prevalence of heart failure is increasing (1). Thus, there is a great need to develop strategies that allow to increase the muscle mass of the heart to enhance heart function. In recent years, induction of cardiomyocyte proliferation has been proposed as an important approach for cardiac regeneration (2). An alternative is cardiac tissue engineering. Also in this context, induction of proliferation of stem cell-derived cardiomyocytes is of interest, for example, to enable the generation of compact cardiac tissues during biofabrication (3–5).

Human cardiac regeneration is limited due to low postnatal cardiomyocyte replicative rates as well as progressive polyploidization (2, 6). The mechanism underlying the establishment of the cell cycle arrest in mammalian cardiomyocytes remains poorly understood. Recently, several mechanisms have been suggested including sarcomere formation (7–9), cyclin G1 expression (10), heterochromatin formation (11), loss of centrosome integrity (12), as well as metabolic switch (13, 14). In addition, while initially very few factors were identified to induce significant cardiomyocyte proliferation, in the last decade, a large number of stimuli have been reported to induce cardiomyocyte proliferation and heart regeneration (2, 15–17). Yet, none of these factors has so far been translated into medical practice.

Here, we have applied a chemical approach to modulate proliferation of stem cell-derived cardiomyocytes, which has several advantages over conventional genetic methods such as enabling temporal control, rapid inhibition or activation, regulation of functionally overlapping targets, and applicability of the identified chemicals across similar species. Notably, many chemicals can be applied directly as therapeutic drugs. In addition, we have established a Fucci-based (18) live cell screening, which eliminates the need for techniques such as immunofluorescence staining, incorporation of nucleotide analogs, or cell count assays. In addition, a live cell screening can capture events that may develop at different times post-treatment, which may be potentially overlooked by end-point assays. Screening of over 700 compounds and validation in primary cardiomyocytes identified as the four most potent promotors of cardiomyocyte cell cycle progression two cardiac glycosides, peruvoside and convallatoxin, the flavonoid osajin, and the selective α-adrenoceptor antagonist and imidazoline I1 receptor ligand efaroxan hydrochloride. To date, no study reports that any of these four compounds have an effect on cardiomyocyte cell cycle progression or heart regeneration.

Cardiac glycosides are a group of compounds, which are secondary metabolites produced by certain plants, insects, and vertebrates. They are mainly known as inhibitors of the sodium-potassium pump in eukaryotic cells and are used as drugs to treat heart disease (e.g., cardiac arrhythmia, congestive heart failure, and atrial fibrillation) by increasing myocardial contraction force and, at the same time, lowering the frequency of this contraction (19–21). Interestingly, data are accumulating which indicate that cardiac glycosides have additional targets such as the nuclear receptor superfamily of transcription factors (19). However, their toxicity prevents their widespread use, and thus a better understanding of the function of cardiac glycosides is necessary (20).

Abbreviations: AG, Azami Green; ANOVA, analysis of variance; ara C, cytosine-D-arabinofuranoside; BIO, 6-bromoindirubin-3′-oxime; BrdU, 5-Bromo-2-deoxyuridine; cdc2, cyclin dependent kinase 1; cDNA, complementary deoxyribonucleic acid; DAPI, 4′, 6′-diamidino-2-phenylindole; DMEM, Dulbecco's Modified Eagle Medium; DMSO, Dimethylsulfoxid; DNA, deoxyribonucleic acid; EB, embryoid bodies; ES, embryonic stem; FASN, fatty acid synthase; FBS, fetal bovine serum; flk1, fetal liver kinase 1; FGF1, fibroblast growth factor 1; gapdh, glyceraldehyde-3-phosphate dehydrogenase; GSK-3, glycogen synthase kinase-3; H3P, histone H3 phosphorylation on serine10; hiPSC, human induced pluripotent stem cells; IP3, inositol trisphosphate; LIF, leukemia inhibitory factor; mAG-hGem(1/110), non-functional human geminin deletion mutant fused to a monomeric version of AG; MI, myocardial infarction; myh7, myosin heavy chain 7; nkx2-5, NK2 homeobox 5; oct, octamer binding transcription factor; P3, 3-day-old; p38i, mitogen-activated protein kinase inhibitor SB203580; PBS, phosphate-buffered saline; PI3K, phosphoinositide 3-kinase; PPAR, peroxisome proliferator-activated receptor; PTEN, phosphatase and tensin homolog; RNA, ribonucleic acid; RT-PCR, reverse transcription followed by polymerase chain reaction; SEM, standard error of the mean.

Methods

Isolation of primary cardiomyocytes

The investigation conforms with the guidelines from Directive 2010/63/EU of the European Parliament on the protection of animals used for scientific purposes. Extraction of organs and preparation of primary cell cultures were approved by the local Animal Ethics Committee in accordance with governmental and international guidelines on animal experimentation (protocol TS-9/2016 Nephropatho). Ventricular cardiomyocytes from 3-day-old (P3) and 12-week-old (adult) Sprague Dawley rats were isolated and cultured as described (22). Rats were first injected s.c. with 0.04 mg/kg buprenorphine and were anesthetized after 30 min by isoflurane inhalation (2 ml vaporized in a 5 l beaker). After loss of standing, eyelid and pedal reflexes, animals were sacrificed by exsanguination due to heart excision upon thoracotomy. Hearts from P3 rats were dissected upon decapitation with operating scissors (ROBOZ [RS-6845], no anesthesia), base

with atria removed, and the remaining ventricle minced. Cells were initially cultured for 48–72 h in the presence of 20 μM cytosine-D-arabinofuranoside (ara C) and 5% horse serum before stimulation to prevent non-myocyte proliferation. Cardiomyocytes were subsequently treated in the presence of fetal bovine serum (FBS) (neonatal: 0.2% FBS; adult: 0.5% FBS: adult) as indicated. Postnatal cardiomyocytes were stimulated once; adult cardiomyocytes every day.

Reagents

The chemical reagents and recombinant proteins were obtained from different companies: "Spectrum Collection" (MicroSource Discovery Systems, Inc., 10 mM stock solutions in dimethylsulfoxid (DMSO), purity > 90%), 6-bromoindirubin-3'-oxime (BIO), osajin, peruvotoxin, efaroxan hydrochloride, xestospongin C (Tocris bioscience), SB203580 (Calbiochem), fibroblast growth factor 1 (FGF1, R&D Systems), convallatoxin (Sigma), valeryl salicylate, bpV(HOpic) (Santa Cruz Biotechnology). Inhibitors were added 1 h before cardiomyocyte stimulation.

Generation of CM7/1-hgem mouse stem cell line

The mouse embryonic stem (ES) cell line CM7/1 (23) was cultured in stem cell medium [DMEM containing 2 mM L-glutamine (GIBCO), penicillin (100 U/mL), streptomycin (100 μg/mL) (Sigma), beta-mercaptoethanol (Merck), 3 mM Na-pyruvate (Thermo Fisher), and 15% FBS (PAA Laboratories)] for 2 days in the presence of leukemia inhibitory factor (LIF, Sigma). The cells were transfected with linear mAG-hGem (1/110) plasmid (18) using lipofectamine 2000 (Thermo Fisher). After 48 h, cells were selected for utilizing 200 μM Zeocin antibiotic (Thermo Fisher) for 2 weeks. Single growing colonies were selected and expanded, resulting in several cell lines. One of the cell lines showing Azami Green (AG) expression was differentiated into beating embryoid bodies (Ebs) and then dissociated into cardiomyocytes. This mouse stem cell line was called CM7/1-hgem and was used in this study.

Differentiation of CM7/1-hgem mouse stem cell line

CM7/1-hgem ES cells were cultured in stem cell medium for 2 days in the presence of LIF (Sigma). The cells were trypsinized with 0.005% trypsin (GIBCO) and counted by hemocytometer. For differentiation, 330,000 cells/ 10 ml differentiation medium (Dulbecco's Modified Eagle Medium (DMEM) containing 2 mM L-glutamine, penicillin (100 U/mL), streptomycin (100 μg/mL), and 3 mM Na-pyruvate, 10% FBS) were used for the hanging drop method. After 2 days, formed Ebs were transferred to suspension culture (10 cm cell culture plate) containing differentiation medium. The plates were stirred at 50 rpm. On day 9, when Ebs started to beat, differentiation medium was replaced with differentiation medium containing 400 μM G418 (Thermo Fisher) to eliminate non-myocytes. After 4–5 days, Ebs were dissociated with 1 mM collagenase B (Sigma) in phosphate-buffered saline (PBS) and centrifuged at 400 RCF for 5 min. Subsequently, single cells were seeded on fibronectin-coated cell culture plates (15,000 cells/well) in cardiomyocyte medium (DMEM containing 2 mM L-glutamine, penicillin (100 U/mL), streptomycin (100 μg/mL), and 3 mM Na-pyruvate, 0.2% FBS) and 400 μM G418 (100 μl/well) and cultured for 5 to 6 days. Then, cells were washed and treated with small molecules utilizing a cardiomyocyte medium.

Screening

CM7/1-hgem-derived cells were treated once with the indicated compounds at a concentration of 1 μM. More than 700 molecules were screened from the bioactive collection of the "Spectrum Collection" from MicroSource Discovery Systems, Inc. (Gaylordsville, CT) (Supplementary Table 1). We used cardiomyocyte medium with DMSO as negative control and 10% FBS and FGF1 + p38 mitogen-activated protein kinase inhibitor SB203580 (FGF1/p38i) as positive controls. AG expression was analyzed every 12 h (for quantitative analysis, around 100 cells were evaluated) for the following 4 days by visual inspection using a Leica fluorescence microscope. The maximal number of mAG-hGem(1/110)-positive cells were used to normalize the data against the DMSO-treated control as a fold-change. Hit compounds were defined as those giving an effect higher than 2-fold. Individual samples of hit compounds were picked from the original library and confirmed with the same method as in the primary screen for three times.

Reverse transcription followed by polymerase chain reaction (RT-PCR) analysis

Total ribonucleic acid (RNA) was isolated from Ebs derived from CM7/1-hgem mouse stem cells at different time points using the Rneasy Kit (Qiagen). The cDNA (complementary deoxyribonucleic acid) was prepared from isolated RNA using *MMLV* or superscript II reverse transcriptase and the oligo(dT) primer (Qiagen). PCR was performed according to standard protocols (Applied Biosystems). Primers: *octamer binding transcription factor* (*oct*)*3/4*: forward (F) 5′-TGAGAACCTTCA

GGAGATATGCAA – 3′,reverse©,5′-CTCAATGCTAGTTCG CTTTCTCTTC – 3′,nanog:F5′-AGTATCCCAGCATCCATTG C – 3′,R,5′-TTTCACCTGGTGGAGTCACA – 3′,brachyury:F 5′-CTCCAACCTATGCGGACAAT – 3′,R,5′-CCCCTTCATA CATCGGAGAA – 3′,isl1:F5′-GCGACATAGATCAGCCTGC T – 3′,R,5′-GTGTATCTGGGAGCTGCGAG – 3′,fetalliverkin ase1(flk1):F5′-GGGTTTGGTTTTGGAAGGTT-3′,R,5′-AGGA GCAAGCTGCATCATTT-3′,gata4:F5′-CTGTCATCTCACTA TGGGCA – 3′,R,5′-CCAAGTCCGAGCAGGAATTT – 3′,NK 2homeobox5(nkx2-5):F5′-AAGCAACAGCGGTACCTGTC-3′, R,5′-GCTGTCGCTTGCACTTGTAG – 3′,myosinheavychain7 (myh7):F5′-TTGGCACGGACTGCGTCATC – 3′,R,5′-GAGC CTCCAGAGTTTGCTGAAGGA – 3′,glyceraldehyde-3-phosp hatedehydrogenase(gapdh):F5′-CAGAAGACTGTGGATGGC CC-3′,R5′-AGTGTAGC- CCAGGATGCCCT-3′.

Immunofluorescence staining

Staining was performed as described (24). Primary antibodies: anti-tropomyosin (1:200, Sigma), anti-actinin (1:100, Abcam), anti-aurora B (1:200) (both BD Transduction Laboratories), rabbit polyclonal anti-troponin I, anti-cyclin A, anti-cyclin dependent kinase 1 (cdc2), anti-geminin (all 1:50, Santa Cruz Biotechnology), anti-phospho-histone H3 (Ser10) (1:200, Millipore), anti-pRb807/811 (1:100, Cell Signaling), anti-mAG (1:300, MBL), rat monoclonal anti-5-Bromo-2-deoxyuridine (BrdU) (1:100, Abcam). Immune complexes were detected with ALEXA 488- or ALEXA 594-conjugated secondary antibodies (1:200; Molecular Probes). DNA was visualized with DAPI'(4" 6'-diamidino-2-phenylindole, 0.5 μg/ml). For BrdU, cells were cultured in 30 μM BrdU (Sigma) (neonatal: last 24–48 h, adult: last 5 days).

Culture and cardiac differentiation of human induced pluripotent stem cells (HiPSC)

The line hiPSC 19-9-11 (WISC Bank) was utilized to generate cardiomyocytes based on a previously published protocol (25). In brief, hiPSCs were maintained in mTeSR1 media (STEMCELL Technologies). When hiPSCs reached the proper confluency (∼80%), they were passaged using trypsin-EDTA (Life Technologies) and plated at a density of 200,000 cells per well of a Matrigel (BD Biosciences)-coated 24-well plates containing mTeSR with 10 μM Rock Inhibitor (Y27632). After 24 h, media was changed with 0.5 mL mTeSR media without Rock inhibitor. At the following day, culture media was replaced with 50 nM XV (GSK3 inhibitor) in mTeSR media for hiPSC differentiation (Day 0). After 24 h, media was substituted with RPMI/B-27 minus insulin (Day 1). On Day 3, 50% of media was exchanged with RPMI/B-27 minus insulin and IWP-2 [Wnt signaling inhibitor, 7.5 μM (final concentration)]. On day 5, media was replenished with RPMI/B27 minus insulin. On day 7, media was changed with RPMI/B27. Then, media was renewed every 3 days (we kept the cells for 36 days). Next, cells were trypsinized with 0.25% (wt/vol) trypsin-EDTA and incubated the mixture in a 37°C, 5% CO_2 incubator for 5 min. The cells were centrifuged at 200 x g for 5 min and the cell pellet was distributed in RPMI20 + 5 μM Y27632 on a laminin-coated coverslip (25 μg/mL). After 2 days, the cells were kept in RPMI/B-27 medium and maintained for the desired time (for 2 days). HiPSC-derived cardiomyocytes were then stimulated with small molecules to analyze their effect on cell cycle progression.

MTS assay

Cell cytotoxicity was measured by an MTS assay (Abcam) according to the manufacture's instruction. Cardiomyocytes were treated with DMSO or individual small molecules for 72 h and absorbance was measured after MTS reagent addition at 4–0 - 500 nm using an Epoch microplate spectrophotometer (Biotek, USA).

Cell count

In order to determine whether compounds increase the number of cells, 100,000 neonatal rat cardiomyocytes were seeded per well of 24-well plates. Cells were then cultured for 48 h in the presence of 20 μM ara C and 5% horse serum and subsequently treated with the indicated compounds in the presence of 0.2% FBS as indicated. The number of cells was determined 5 days post-treatment after trypsinization utilizing a TC20 cell counter (Bio-Rad, USA) according to the manufacturer's instructions.

Statistical analysis

For immunofluorescence analyses, around 50 cardiomyocytes in five random fields of two different subpopulations were counted per experiment equaling a total cell number of around 500 cardiomyocytes. Data of at least three independent experiments are expressed as mean ± standard error of the mean (SEM). Results were analyzed by Graph Pad Prism (version 4.00, Graph Pad Software Inc.). Statistical significance was determined using a two-tailed Student's t-test or analysis of variance (ANOVA) were appropriate. The values of $p < 0.05$ were considered statistically significant.

Results

Live cell screening based on mouse stem cell-derived cardiomyocytes

In order to perform a screen for novel inducers of cardiomyocyte cell cycle activity, we have generated a mouse stem cell line that expresses a non-functional human geminin deletion mutant fused to a monomeric version of AG [mAG-hGem(1/110)] under the control of the ubiquitous CMV promoter (Figure 1A). Note, mAG-hGem(1/110) is only stable in S-/G2-/ and M-phase cells. In order to develop this cell line, we transfected the mouse ES cell line CM7/1 (26) with the plasmid mAG-hGem(1/110) (18), which allows selection for positive integration with Zeocin. The cell line CM7/1 expresses the neomycin-phospho-transferase gene under the control of the cardiomyocyte-specific *α-myosin heavy chain* promoter. This allows to obtain stem cell-derived cardiomyocyte cultures with a purity of > 99% after G418-treatment (26). This approach resulted in the establishment of the cell line CM7/1-hgem expressing AG (Figure 1B), which can be induced to differentiate into well beating EBs (Figures 1C,D). To ensure that cardiomyocytes derived from CM7/1-hgem express mAG-hGem(1/110), 12–14 days-old beating EBs were dissociated and seeded cells were stained for AG and a cardiomyocyte-specific marker (Figure 1E). This analysis revealed that 22.3 ± 6.8% of cardiomyocytes expressed mAG-hGem(1/110). That mAG-hGem(1/110) expression does not interfere with cardiogenesis of CM7/1-hgem was validated by normal temporal mRNA expression patterns of stem cell (*oct3/4*, *nanog*), mesodermal (*brachyury*), early progenitor (*gata4*), and cardiomyocyte (*myh7*) markers (Figure 1F). The actual screen for novel inducers of cardiomyocyte cell cycle activity was performed with cardiomyocytes obtained by treating CM7/1-hgem EBs at day 9 of differentiation with G418, dissociation of these EBs at day 12 to 14, plating the single cells on fibronectin-coated plates, and culturing them for another 6 days in the presence of G418. Immunofluorescence analysis revealed that the percentage of non-myocytes in the single cell culture decreased from 68.6 ± 5.8% at day 1 to <3.5 ± 0.4% at day 6 (mean ± SEM, ***: $p < 0.001$, Figures 1G,H).

To assess the base level of CM7/1-hgem-derived cardiomyocyte cell cycle activity, BrdU incorporation (24 h) assays were performed and the number of mAG-hGem(1/110)-, H3P (histone H3 phosphorylation on serine 10)-positive as well as Aurora B-positive cardiomyocytes was determined at day 1 (non-selected) and day 6 (selected) post-dissociation. The number of cardiomyocytes incorporating BrdU decreased from 38.8 ± 3.5% at day 1 to 4.8 ± 0.92% at day 6 (mean ± SEM, $p < 0.01$, Figures 2A,B). Assuming that completion of one cell cycle lasts less than 24 hours, all cycling cardiomyocytes should be BrdU-positive. The percentage of cardiomyocytes expressing mAG-hGem(1/110) decreased from 22.3 ± 3% to 3 ± 0.6% (mean ± SEM, $p < 0.01$, Figures 2B,C). The overall number of mAG-hGem(1/110)-positive cells is as expected lower than BrdU-positive cells, as mAG-hGem(1/110) is only stable in S-/G2-/ and M-phase cells. The number of H3P-positive cardiomyocytes decreased from 5.9 ± 0.45% to 0.45 ± 0.1% (Figure 2D). Note, histone H3 is only phosphorylated in late G2-phase cells and M-phase cells until late anaphase. Finally, the number of Aurora B-positive cardiomyocytes at the midbody decreased from 1.89 ± 0.1% to 0.25 ± 0.03% (Figures 2E,F). Note, Aurora B is only a marker for cytokinesis when localized to the midbody or cleavage furrow. The overall decrease of cycling cardiomyocytes from day 1 to day 6 is in agreement with the general observation that the proliferation rate of ES cell-derived cardiomyocytes decreases over time in culture (27).

In order to test whether cell cycle activity in CM7/1-hgem-derived cardiomyocytes can be promoted, cells were stimulated for 3 days with 10% FBS, which is known to promote cell cycle activity in fetal, neonatal, and adult mammalian cardiomyocytes (24, 28). FBS treatment induced in 37 ± 3.8% of cardiomyocytes BrdU incorporation (Figures 2G,H), in 21 ± 4.4% mAG-hGem(1/110) expression (Figures 2H,I), and in 6 ± 0.8% histone H3 phosphorylation (Figures 2J,K) compared to 4.8 ± 0.9% (BrdU), 3 ± 0.6% (AG), and 0.49 ± 0.09% (H3P) upon DMSO treatment, respectively (mean ± SEM, $p < 0.01$, Figures 2H,K).

Screening for small molecules inducing CM7/1-hgem-derived cardiomyocyte cell cycle activity

In order to identify novel inducers of cardiomyocyte cell cycle activity, a subset of compounds of the small molecule library "Spectrum Collection" from MicroSource Discovery Systems, Inc. (Gaylordsville, CT) was utilized. This library presents 2,560 compounds and includes drugs from three sources: (1) US drug collection of 1,040 drugs that have reached clinical trial stages in the USA whereby each compound has been assigned USAN or USP status. (2) An International Drug Collection of 240 drugs that are marketed in Europe and/or Asia. (3) The rest is a unique collection of pure natural products and their derivatives. Natural Products include simple and complex oxygen heterocycles, alkaloids, sesquiterpenes, diterpenes, pentacyclic triterpenes, sterols, and many other diverse representatives. For each compound, data can be obtained regarding its structure, CAS #, formula, molecular weight, biological profile, as well as generic and market name. In addition, literature references are available describing the use and toxicology of the individual compounds. CM7/1-hgem-derived EB's were dissociated on day 14, seeded at 15,000 cells per well in a 96-well plate (flat glass-bottomed), and cultured for 6 days in the presence of G418. Subsequently, cells were treated with a subset of compounds of the small molecule

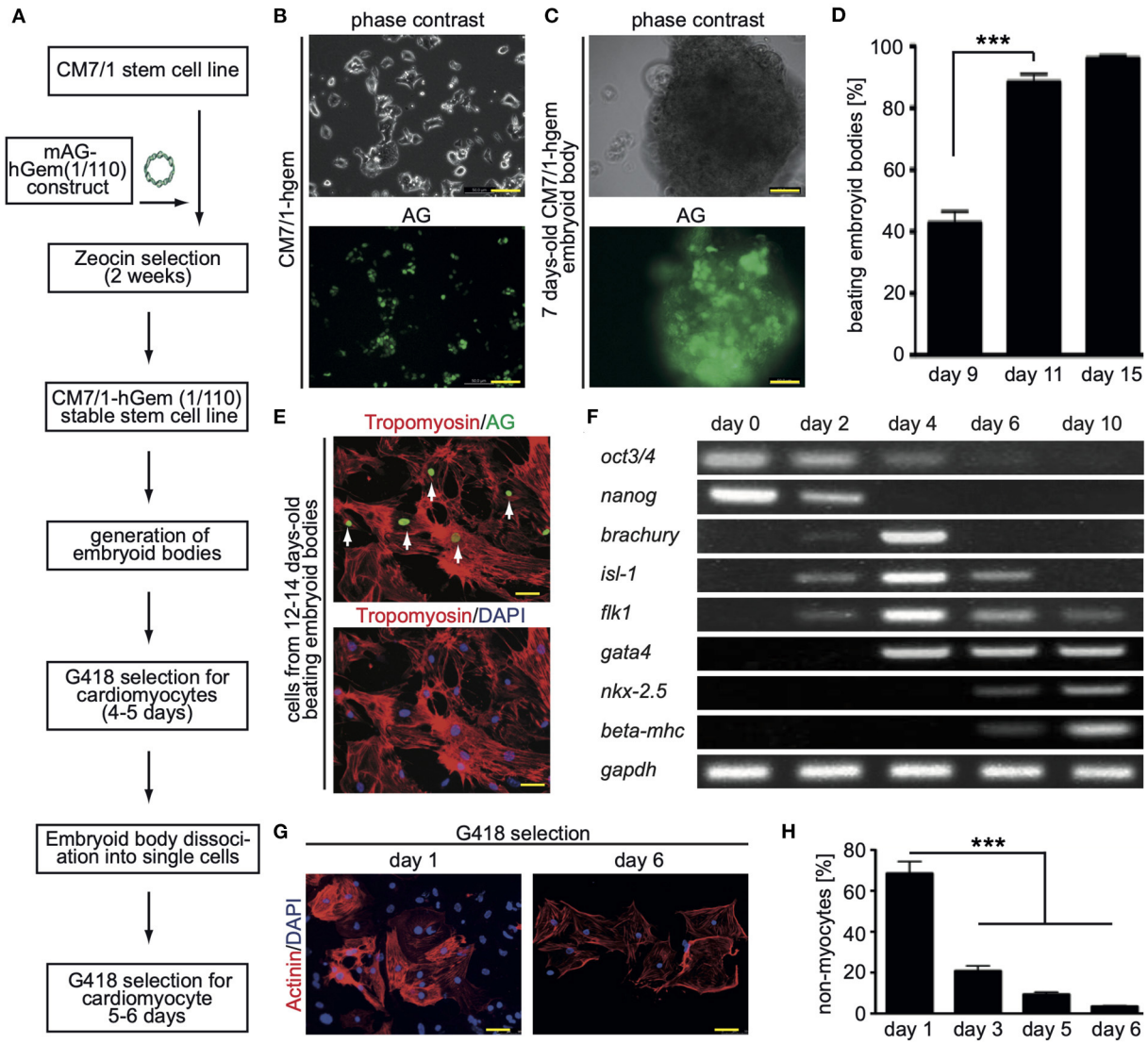

FIGURE 1
Generation of the CM7/1-hgem stem cell line and their differentiation. **(A)** Work flow of the generation of the CM7/1-hgem stem cell line. **(B)** Representative live pictures of nuclear expression of monomeric Azami Green (AG) in CM7/1 embryonic stem cells. **(C)** Representative live pictures of a 7-day-old differentiating embryonic body (EB) derived from CM7/1-hgem cells expressing AG. **(D)** Quantitative analysis of beating EBs at different time points ($n = 3$, mean ± SEM, ***: $p < 0.001$). **(E)** AG expression in CM7/1-hgem-derived cardiomyocytes. 12- to 14-day-old beating EBs were dissociated and stained for AG expression (green) and counterstained against cardiomyocyte-specific tropomyosin (red). DAPI was used to visualize nuclei (blue). **(F)** mRNA expression patterns of stem cell (oct3/4, nanog), mesodermal (brachyury), early progenitor (gata4), and cardiomyocyte (myh7) markers during differentiation of CM7/1-hgem stem cells into cardiomyocytes. **(G)** Enrichment for cardiomyocytes by treating 9-day-old EB with 400 μM G418 for 4 to 5 days. The EBs were then dissociated to single cell cultures and kept under 400 μM G418 for another 6 days. Representative examples of CM7/1-hgem cell-derived cardiomyocytes stained for sarcomeric alpha-actinin (red). Nuclei were visualized using DAPI (blue). **(H)** Quantitative analysis of **(G)** ($n = 3$, mean ± SEM, ***: $p < 0.001$). Scale bar = 50 μm in **(B,C,E,G)**.

library "Spectrum Collection" at a concentration of 1 μM. DMSO served as a negative control, 10% FBS and FGF1/p38i as positive controls. mAG-hGem(1/110)-positive cells per field were recorded for 4 days at intervals of 12 h (Figure 3A). As this was a pilot study, recording (image acquisition) and image analysis were performed manually, and the screen was performed only once. Note, to minimize the manual labor, only around 100 cells in the center of each well were evaluated utilizing a 20x objective. Data are represented as a fold-change increase of the observed maximal number of mAG-hGem(1/110)-positive cells per field in comparison to the maximal number in DMSO-treated cultures (Figure 3B). Note, in cases when compound treatment resulted in no mAG-hGem(1/110)-positive cell at markedly more time points

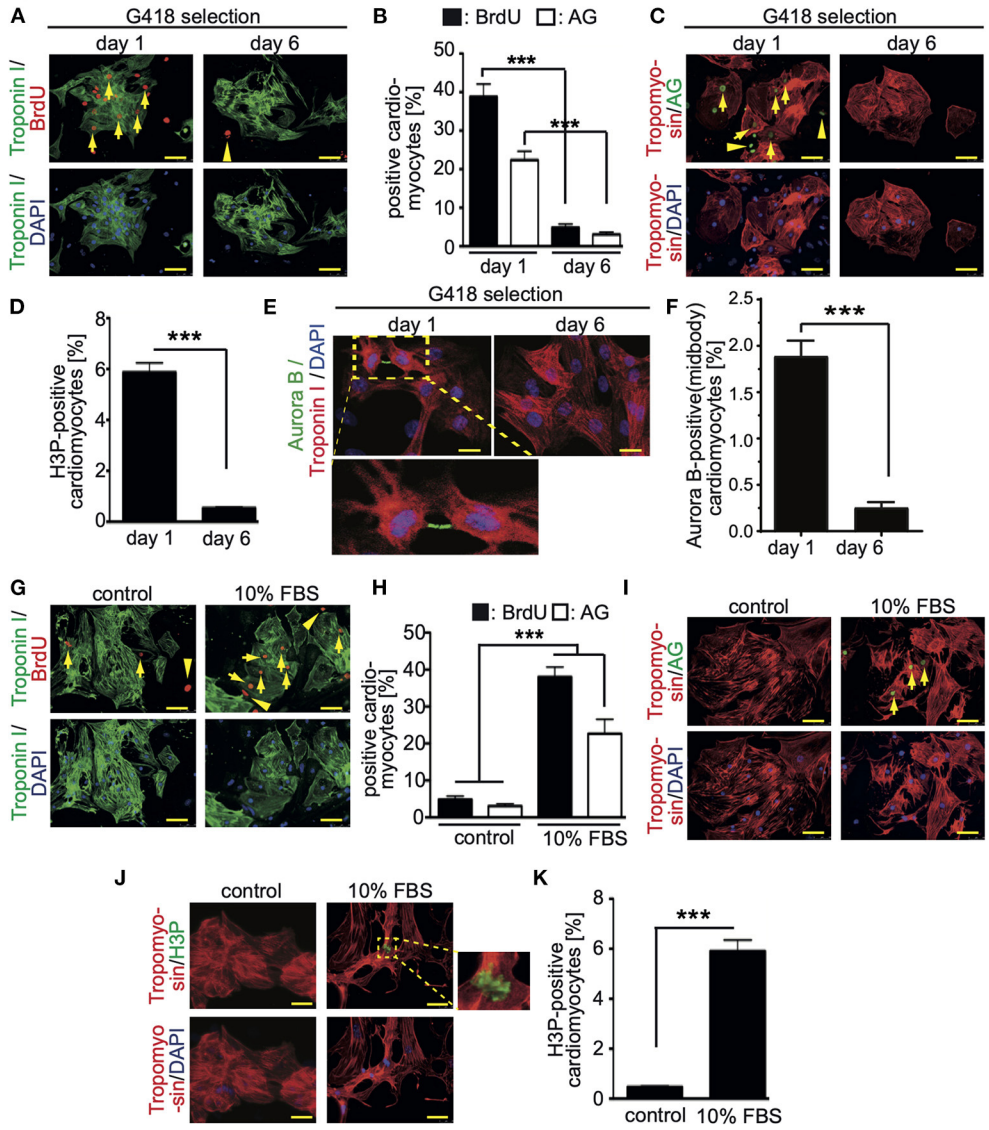

FIGURE 2
Cell cycle activity in CM7/1-hgem derived cardiomyocytes. **(A,C)** The number of BrdU- and Azami Green (AG)-positive CM7/1-hgem-derived cardiomyocytes decreased during differentiation. Representative examples of CM7/1-hgem-derived cardiomyocytes stained for troponin I (green) or tropomyosin (red) (cardiomyocyte-specific), BrdU (red) **(A)** or AG (green) **(C)**, and DAPI (nuclei, blue). Scale bar: 50 μm. $n = 6$. **(B)** Quantitative analysis of **(A,C)** ($n = 6$, mean ± SEM, ***:$p < 0.001$). **(D)** Quantitative analysis of H3P-positive CM7/1-hgem-derived cardiomyocytes ($n = 6$, mean ± SEM, ***:$p < 0.001$). **(E)** Representative examples of CM7/1-hgem-derived cardiomyocytes stained for troponin I (red) (cardiomyocyte-specific), Aurora B (green), and DAPI (nuclei, blue). Scale bar: 20 μm. **(F)** Quantitative analysis of Aurora B-positive CM7/1-hgem-derived cardiomyocytes at the midbody ($n = 6$, mean ± SEM, ***:$p < 0.001$). **(G–I)** Stimulation of cell cycle progression in CM7/1-hgem-derived cardiomyocytes by 10% FBS. Representative examples of CM7/1-hgem-derived cardiomyocytes stained for troponin I (green) **(G)** or tropomyosin (red) **(I)** (cardiomyocyte-specific), BrdU (red) **(G)** or AG (green) **(I)**, and DAPI (nuclei, blue). Scale bar: 50 μm. $n = 3$. **(F)** Quantitative analysis of **(G,I)** ($n = 6$, mean ± SEM, ***:$p < 0.001$). **(J)** Representative examples of CM7/1-hgem-derived cardiomyocytes stained for tropomyosin (red) (cardiomyocyte-specific), H3P (green), and DAPI (nuclei, blue). Scale bar: 50 μm. $n = 6$. **(K)** Quantitative analysis of **(J)** ($n = 6$, mean ± SEM, ***: $p < 0.001$).

(≥ 4) than in the DMSO control (1 of 8), the fold-change was defined as 0.5-fold. The number of observed mAG-hGem(1/110)-positive cells at the different 12 h time points for each treatment are provided in Supplementary Table 1. Our analysis revealed that 10% FBS as well as FGF1/p38i efficiently induced mAG-hGem(1/110) expression in CM7/1-hgem-derived cells enriched for cardiomyocytes (~10 fold and ~ 5-fold, respectively, Figures 3B,C). While most of the 722 tested compounds had no positive effect on mAG-hGem(1/110) expression, 19 compounds induced mAG-hGem(1/110)

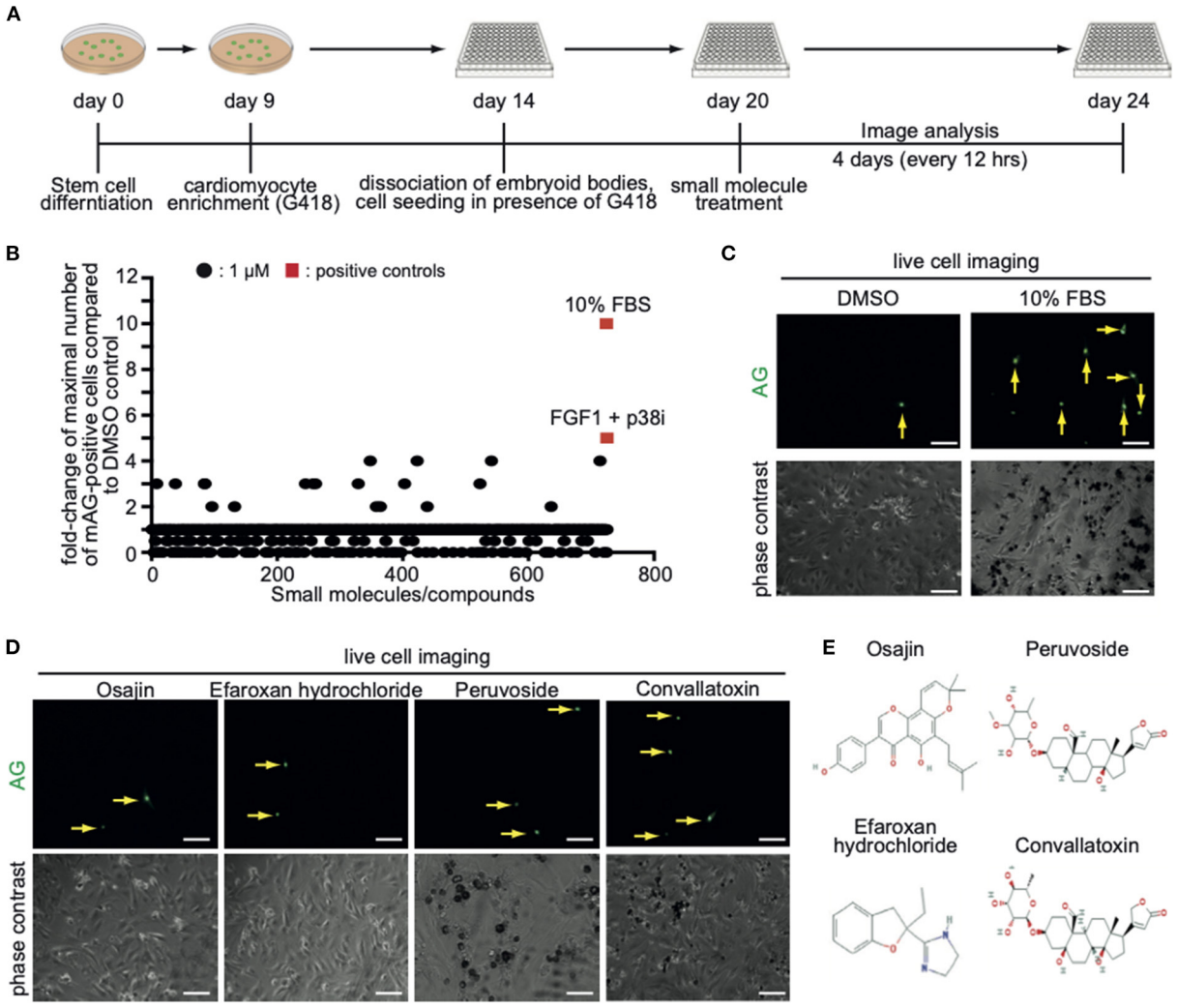

FIGURE 3
Screening of a small molecule library identifies novel compounds promoting CM7/1-hgem-derived cardiomyocyte cell cycle progression. **(A)** Workflow of the applied screening strategy. **(B)** Quantitative analysis of Azami Green (AG) expression in the screen of a Microsource spectrum small molecule screening library. **(C)** Representative live pictures of AG expression in control or 10% FBS-treated CM7/1-hgem-derived cardiomyocytes. Scale bar: 100 μm. **(D)** Representative live pictures of AG expression in osajin-, efaroxan hydrochloride-, peruvoside-, and convallatoxin-treated CM7/1-hgem-derived cardiomyocytes. Scale bar: 100 μm. **(E)** Molecular design of small molecule hits.

expression in at least twice as many cells as upon DMSO treatment (Figure 3B, Supplementary Table 1). The most effective compounds were osajin, efaroxan hydrochloride, peruvoside, and convallatoxin (all 4-fold) (Figures 3D,E).

Cell cycle-promoting effect of identified compounds on neonatal and adult primary rat cardiomyocytes

Stem cell-derived cardiomyocytes are considered immature exhibiting a behavior similar to late fetal cardiomyocytes (29). In order to assess whether the here identified 19 compounds could promote cell cycle progression also in more mature cardiomyocytes, neonatal rat cardiomyocytes were stimulated and analyzed 3 days later for BrdU incorporation (BrdU pulse-labeled for the final 24 h). For this purpose, cardiomyocytes were isolated from postnatal day 3 (P3) rats and stimulated once with the individual small molecules at concentrations of 50 nM, 250 nM, 1 μM, and 5 μM (Supplementary Figure 1).

Subsequently, cardiomyocytes were treated with the optimal concentrations of the individual compounds, cultured for 3 days and pulse-labeled with BrdU for the final 48 hours to assess also cardiomyocytes that already entered S phase after 24 h to 48 h post-treatment. In Supplementary Figure 1 (data from

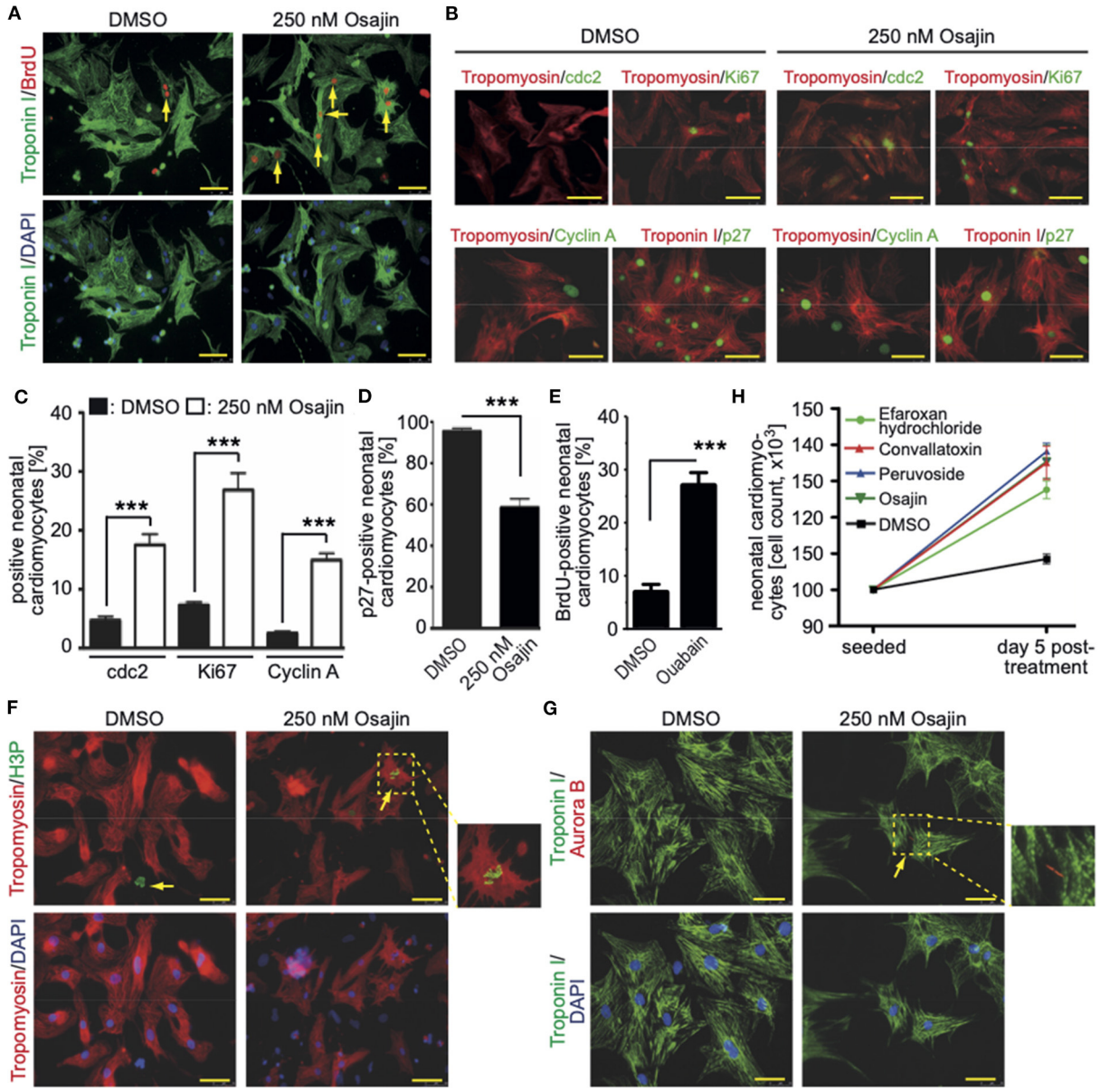

FIGURE 4
Promoting neonatal cardiomyocyte cell cycle progression by small molecules (Positive hits). **(A)** Osajin induced BrdU incorporation of P3 neonatal cardiomyocytes ($n = 6$). Representative example of neonatal cardiomyocytes stained for BrdU (red) and troponin I (green, cardiomyocyte-specific). Examples are indicated by arrows. DNA was visualized using DAPI (blue). **(B)** Osajin treatment induced increased expression of cell cycle promoting factors and decreased expression of cell cycle inhibitors (immunofluorescence analyses at 48 h after stimulation). Representative example of neonatal cardiomyocytes stained for cdc2, Ki67, cyclin A, or p27 (green) and tropomyosin (red, cardiomyocyte-specific). DNA was visualized using DAPI (blue). **(C,D)** Quantitative analysis of **(B)** ($n = 6$, mean ± SEM, ***: $p < 0.001$). **(E)** Quantitative analysis of the number of BrdU-positive cardiomyocytes after ouabain treatment ($n = 6$, mean ± SEM, ***: $p < 0.001$). **(F,G)** Representative examples of osajin-stimulated neonatal cardiomyocytes stained for tropomyosin (red) or troponin I (green, both cardiomyocyte-specific) undergoing mitosis (H3P, green) and cytokinesis (Aurora B, red). Examples are indicated by arrows. Arrowhead: H3P-positive non-myocyte. DNA was visualized using DAPI (blue). **(H)** Quantitative analysis of the increase in cell number five days after treatment with the indicated compounds ($n = 5$, mean ± SD). Scale bars: 50 μm.

six independent experiments per parameter) the data for the optimal concentration of each of the 19 compounds is provided whereby treatment with 250 nM osajin was most efficient in inducing BrdU incorporation in P3 rat cardiomyocytes (30.3 ± 2.4% *vs.* DMSO: 10.5 ± 0.9%, $p < 0.01$, Figure 4A). A deeper analysis showed that osajin treatment induced the expression of cell cycle perpetuating factors like cdc2, cyclin A, and Ki67 (Figures 4B,C) and the downregulation of the

TABLE 1 Cell cycle parameters in neonatal rat cardiomyocytes treated with selected small molecules.

Small molecule	conc.	48 h BrdU [%]	H3P [%]	aurora B [%]
Osajin	0.25 μM	30.3 ± 2.4	1.86 ± 0.3	1.73 ± 0.3
Efaroxan Hydrochloride	1 μM	29.6 ± 2.1	1.76 ± 0.3	1.65 ± 0.3
Peruvoside	1 μM	30.0 ± 2.6	1.32 ± 0.2	1.36 ± 0.2
Convallatoxin	1 μM	29.3 ± 3.0	1.35 ± 0.3	1.28 ± 0.2
Valeryl salycilate	0.25 μM	27.0 ± 2.5	1.35 ± 0.1	1.21 ± 0.1
Idebenone	1 μM	22.0 ± 2.6	0.97 ± 0.1	0.92 ± 0.2
Lobaric acid	5 μM	22.0 ± 1.5	0.92 ± 0.2	0.85 ± 0.2
PIDOTIMOD	1 μM	21.3 ± 2.0	0.85 ± 0.1	0.75 ± 0.1
Ferulic acid	1 μM	22.6 ± 2.0	0.80 ± 0.2	0.75 ± 0.2
Quircitrin	1 μM	22.6 ± 0.8	0.75 ± 0.2	0.75 ± 0.1
Glutathione	1 μM	24.6 ± 2.3	0.60 ± 0.2	0.65 ± 0.2
Acedoben	1 μM	20.0 ± 3.2	0.65 ± 0.1	0.61 ± 0.1
Isaxonine	1 μM	21.6 ± 2.4	0.60 ± 0.2	0.50 ± 0.1
Protoporphyrin	1 μM	16.6 ± 3.8	0.55 ± 0.1	0.50 ± 0.1
N-methylanthranilic acid	1 μM	17.3 ± 1.8	0.60 ± 0.1	0.50 ± 0.1
Gitoxin	1 μM	19.0 ± 2.1	0.60 ± 0.1	0.50 ± 0.1
Tiratricol	1 μM	25.3 ± 3.7	0.55 ± 0.1	0.47 ± 0.1
Bilirubin	1 μM	18.6 ± 1.9	0.56 ± 0.2	0.45 ± 0.1
Merogedunin	1 μM	19.0 ± 1.2	0.35 ± 0.1	0.30 ± 0.1
DMSO		10.5 ± 0.9	0.37 ± 0.1	0.35 ± 0.1

cell cycle inhibitor p27 (Figures 4B,D). Notably, also the cardiac glycosides convallotoxin and peruvoside, efficiently induced BrdU incorporation (Supplementary Figure 1). Thus, we also tested the effect of the cardiac glycoside ouabain on P3 cardiomyocyte proliferation. Similar to the other cardiac glycosides, ouabain induced efficiently BrdU incorporation (28.8 ± 2.9% vs. DMSO: 9.1 ± 0.7%, $p < 0.01$, Figure 4E). Analyses of H3P revealed that all tested cardiac glycosides and all other compounds stimulating BrdU incorporation, except merogedunin, also induced cell cycle progression into G2/M-phase (Table 1). For example, treatment with 250 nM osajin induced the number of H3P-positive cardiomyocytes ~5-fold compared to DMSO (1.86 ± 0.3% *vs.* DMSO: 0.37 ± 0.1%, $p < 0.01$) after 3 days of stimulation (Figure 4F). The analysis of aurora B expression suggests that most compounds, including osajin (1.73 ± 0.3%), efaroxan hydrochloride (1.65 ± 0.3%) as well as the cardiac glycosides peruvoside (1.36 ± 0.2%) and convallotoxin (1.28 ± 0.2% *vs.* DMSO: 0.35 ± 0.1%, $p < 0.01$), also induce cytokinesis (Table 1). Notably, cardiomyocytes exhibited in most cases a two-sided cleavage furrow, as shown for osajin (Figure 4G). Finally, cell count experiments revealed that the treatment of all compounds resulted 5 days post-treatment in a significantly increased cell number (Figure 4H). Notably, none of these compounds exhibited cytotoxic effects on cardiomyocytes based on MTS assays (Supplementary Figure 2). Taken together, our data suggest that our screening system allows the identification of molecules with the potential to promote neonatal cardiomyocyte proliferation such as cardiac glycosides.

To determine if cardiac glycosides can also promote cell cycle progression in adult rat cardiomyocytes, ventricular cardiomyocytes from 12-week-old rats were stimulated and analyzed for BrdU incorporation, histone H3 phosphorylation, and aurora B expression. Osajin as well as the cardiac glycosides peruvoside and convallotoxin efficiently induced cell cycle re-entry in adult rat cardiomyocytes (all > 0.6% BrdU-, > 0.07% H3P-, and > 0.06% aurora B-positive cardiomyocytes compared to < 0.002% for all parameters upon DMSO treatment, Figures 5A–C). Notably, cell cycle activity was observed in mono- as well as binucleated adult rat cardiomyocytes (Figures 5D–F). Collectively, these data show that cardiac glycosides can promote adult cardiomyocyte cell cycle progression.

Identified compounds promote cell cycle progression of HiPSC-derived cardiomyocytes

Aiming at evaluating the translation potential of the identified compounds, the effect of the positive hits, including cardiac glycosides, on cell cycle progression in hiPSC-derived cardiomyocytes was assessed. HiPSC-derived cardiomyocytes were treated with DMSO or peruvoside (100 nM), convallotoxin

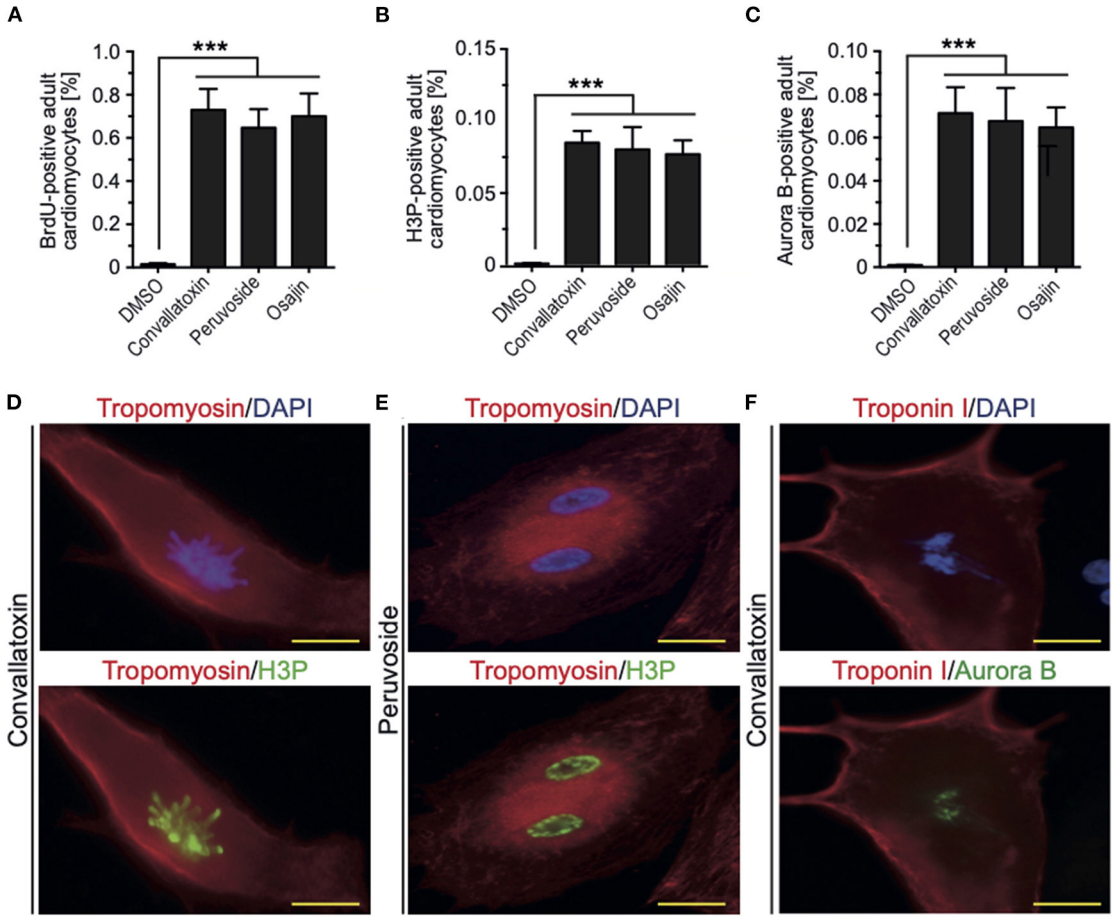

FIGURE 5
Osajin and cardiac glycosides promote adult cardiomyocyte cell cycle progression. **(A–C)** Quantitative analysis of cell cycle progression [BrdU incorporation, **(A)**], mitosis [H3P, **(B)**], and cytokinesis [Aurora B, **(C)**] ($n = 6$, mean ± SEM, ***: $p < 0.001$). **(D–F)** Representative examples of adult rat cardiomyocytes (tropomyosin- or troponin I-positive) utilized for the quantitative analysis in **(B,C)**. **(D)** Mononucleated adult rat cardiomyocyte stained for H3P in pro-metaphase. **(E)** Binucleated adult rat cardiomyocyte stained for H3P in G2 to prophase. **(F)** Binucleated adult rat cardiomyocyte stained for aurora B in G2 to prophase.

(100 nM), osajin (250 nM), and efaroxan hydrochloride (1 μM) and analyzed for changes in the expression of Ki67 or phosphorylation of histone H3 (H3P) 48 h post-treatment (Figures 6A–D). Pervuvoside significantly increased the number of both Ki67- and H3P-positive cardiomyocytes compared to DMSO (Ki67: 34.90 ± 2% *vs.* DMSO: 17.57 ± 0.97%, $p < 0.01$; H3P: 6.3 ± 0.23% *vs.* DMSO: 3.06 ± 0.36%, $p < 0.01$). Similarly, all other tested compounds exhibited a positive effect on cell cycle progression in hiPSC-derived cardiomyocytes (convallotoxin: Ki67: 32.07 ± 1.57%, H3P: 6.1 ± 0.28%; osajin: Ki67: 40.00 ± 2.0%, H3P: 7.04 ± 0.22%; efaroxan hydrochloride: Ki67: 34.25 ± 1.7%, H3P: 6.88 ± 0.58%; all $p < 0.01$, Figures 6A–D). Finally, we analyzed Aurora B-positive cardiomyocytes at midbody indicative for cell division. We found that pervuvoside significantly increased cardiomyocytes in cytokinesis compared to DMSO (Aurora B at midbody: 2.08 ± 0.08% *vs.* DMSO: 0.85 ± 0.04%, $p < 0.01$) (Figures 6E,F). Similarly, all other tested compounds exhibited a positive effect on cardiomyocyte cytokinesis (convallotoxin: 1.85 ±0.04%; osajin: 2.28 ± 0.12%; efaroxan hydrochloride: 2.21 ± 0.13%; all $p < 0.01$, Figure 6E). Taken together, these data suggest that cardiac glycosides, as well as osajin and efaroxan hydrochloride, also positively affect cell cycle progression in hiPSC-derived cardiomyocytes.

Inhibition of PTEN and GSK-3β enhance cell cycle progression induced by cardiac glycosides and osajin

Previously, others and we have shown that the phosphoinositide 3-kinase (PI3K)-Akt pathway is implicated in the regulation of cardiomyocyte proliferation (14, 24, 30)

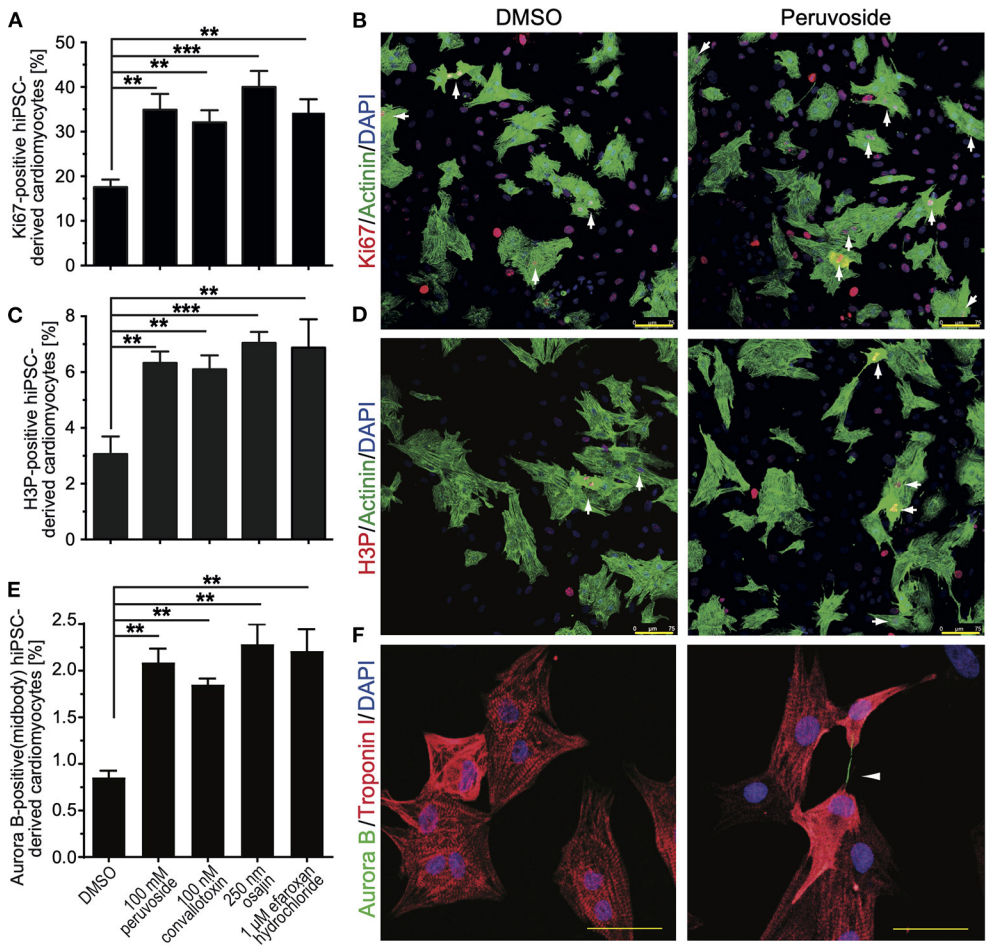

FIGURE 6
Small molecules (positive hits) promote cell cycle progression in hiPSC-derived cardiomyocytes. HiPSC-derived cardiomyocytes were stimulated with the indicated compounds for 2 days and subsequently analyzed in regards to cell cycle activity. **(A)** Quantitative analysis of the percentage of Ki67-positive cardiomyocytes ($n = 6$, mean ± SEM, **: $p < 0.01$, ***: $p < 0.001$). **(B)** Representative examples were utilized for the analysis in **(A)**. Ki67: red; Actinin: green (cardiomyocyte-specific). DNA (DAPI): blue. Examples of Ki67-positive cardiomyocytes are indicated by arrows. **(C)** Quantitative analysis of the percentage of H3P-positive cardiomyocytes ($n = 6$, mean ± SEM, **: $p < 0.01$, ***: $p < 0.001$). **(D)** Representative examples were utilized for the analysis in **(C)**. H3P: red; Actinin: green (cardiomyocyte-specific). DNA (DAPI): blue. Examples of H3P-positive cardiomyocytes are indicated by arrows. Scale bars: 75 µm. **(E)** Quantitative analysis of the percentage of Aurora B-positive cardiomyocytes at the midbody ($n = 6$, mean ± SEM, **: $p < 0.01$, ***: $p < 0.001$). **(F)** Representative examples were utilized for the analysis in **(E)**. Aurora B: Green; Troponin I: green (cardiomyocyte-specific). DNA (DAPI): blue. Example of an Aurora B-positive cardiomyocyte at the midbody is indicated by an arrowhead. Scale bars: 50 µm.

and phosphatase and tensin homolog (PTEN), an inhibitor of the PI3K pathway, inhibits periostin-induced cardiomyocyte cell cycle activity (30). Recently, it was shown that loss of PTEN promotes cardiomyocyte proliferation and cardiac repair after MI, suggesting the pathway has a substantial role in cardiomyocyte proliferation (31). Thus, we have tested whether bpv(HOpic), a potent inhibitor of PTEN, enhances the effect of osajin and the cardiac glycosides on BrdU incorporation in neonatal and adult cardiomyocytes. As expected, bpv(HOpic) increased the number of BrdU-positive cardiomyocytes in the control, but was less efficient than osajin and the cardiac glucosides (Figures 7A,B). Notably, bpv(HOpic) significantly enhanced the effect of osajin and the cardiac glucosides on inducing BrdU incorporation in primary neonatal (Figure 7A) as well as adult (Figure 7B) rat cardiomyocytes. In addition, we have previously demonstrated that the small molecule BIO, a specific inhibitor of glycogen synthase kinase-3 (GSK-3), promotes cell cycle progression into mitosis in neonatal and adult mammalian cardiomyocytes (14, 32). Thus, we have tested whether BIO enhances the effect of osajin and the cardiac glycosides in regards to aurora B expression in neonatal and adult cardiomyocytes (Figures 7C,E). While BIO had a moderate effect on aurora B expression in neonatal cardiomyocytes (Figure 7C) and aurora B-positive neonatal

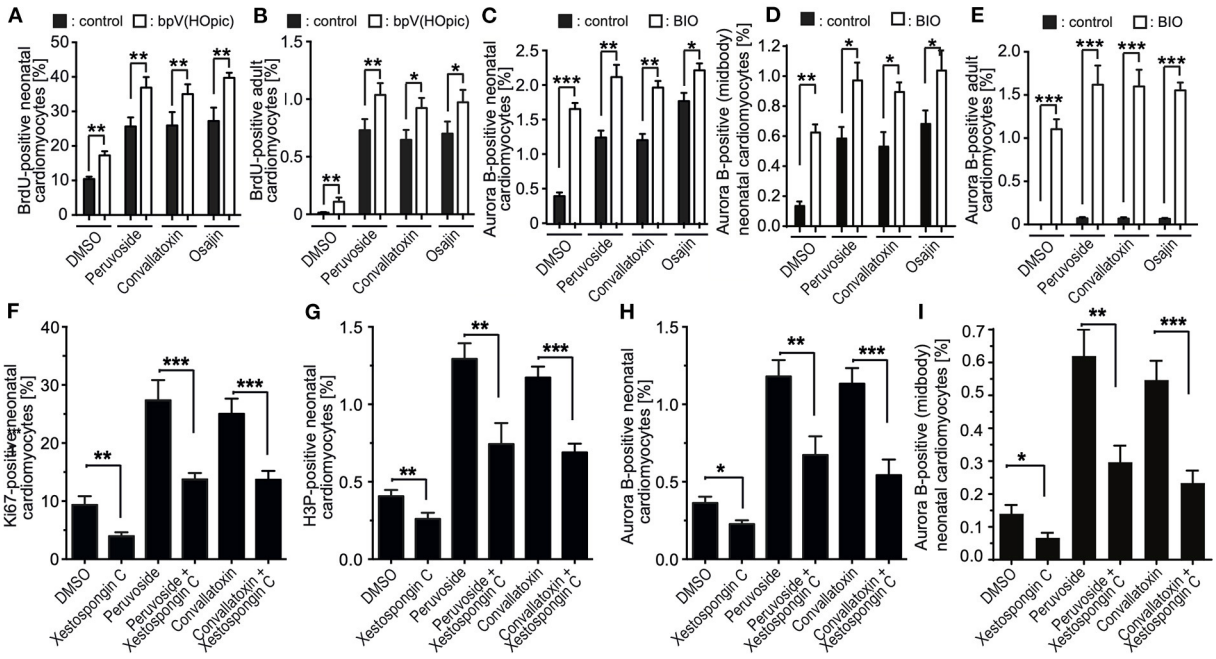

FIGURE 7
Mechanistic analysis of compound-enhanced cell cycle progression. **(A–E)** Inhibition of PTEN, as well as GSK-3β enhances cell cycle progression induced by cardiac glycosides and osajin. Quantitative analysis of BrdU- **(A,B)** and Aurora B- **(C,E)**, Aurora B at the midbody in neonatal cardiomyocytes **(D)**, positive neonatal **(A,C)** and adult **(B,E)** cardiomyocytes upon stimulation with cardiac glycosides and osajin in the presence and absence of PTEN inhibitor bpV (HOpic) **(A,B)** or GSK3-β inhibitor BIO **(C–E)**. $n = 6$, mean ± SEM, *: $p < 0.1$, **: $p < 0.01$, ***: $p < 0.001$. **(F–I)** Inhibition of IP3 receptor impedes peruvoside- and convallotoxin-induced cardiomyocyte cell cycle progression. Neonatal rat cardiomyocytes were stimulated with glycosides in the absence or presence of IP3 receptor inhibitor xestospongin C (1 μM) and the number of Ki67-, H3P-, and aurora B-positive cardiomyocytes were evaluated. Quantitative analysis of the percentage of Ki67- [cell cycle progression, **(F)**], H3P- [mitosis, **(G)**], and aurora B- [cytokinesis, **(H,I)**] positive cardiomyocytes ($n = 6$, mean ± SEM, *: $p < 0.05$), **: $p < 0.01$, ***: $p < 0.001$.

cardiomyocytes at the midbody (Figure 7D), it markedly enhanced aurora B expression in adult cardiomyocytes stimulated with osajin or the cardiac glycosides (Figure 7E). Yet, no adult cardiomyocytes positive for Aurora B at the midbody or cleavage furrow was observed. Yet, considering the rare observation of aurora B-positive adult cardiomyocytes and the short existence of the midbody, it is also rather unlikely to find an adult cardiomyocyte in this stage.

IP3 receptor inhibition reduces the cell cycle-promoting effect of cardiac glycosides

Cardiac glycosides increase the output force of the heart and decrease its rate of contractions by acting on the cellular sodium-potassium ATPase pump, Na^+K^+ATPase (20). As Na^+K^+ATPase is known to specifically regulate calcium transients *via* the inositol trisphosphate (IP3) receptors (33–35), we have tested the effect of the selective IP3 receptor antagonist xestospongin C (36) on cardiac glycoside-enhanced cardiomyocyte cell cycle progression. For this purpose, P3 rat cardiomyocytes were stimulated with glycosides in the absence or presence of 1 μM xestospongin C and the number of Ki67-, H3P-, aurora B-positive cardiomyocytes as well as cardiomyocytes positive for aurora B at the midbody were evaluated. This analysis revealed that the presence of xestospongin C significantly reduced the positive effect of peruvoside and convallotoxin on neonatal cardiomyocyte cell cycle progression (Figures 7F–I). These data suggest that Ca2+ levels regulated by glycosides might be important for the cell cycle promoting effect of cardiac glycosides.

Discussion

Here we developed a fluorescence-based live imaging screening assay based on mouse stem cells and the Fucci system to identify new inducers of cardiomyocyte proliferation. This system eliminates the need for immunofluorescence staining, incorporation of nucleotide analogs or cell count assays and allows to capture events that may develop at different times post-treatment, which may be potentially overlooked by end-point assays. As the system utilizes a ubiquitous promoter, this system can also be utilized to identify new inducers of

proliferation of other cell types, such as neurons. Validation of positive hits utilizing several independent assays in primary neonatal and adult mammalian cardiomyocytes identified among others cardiac glycosides as a novel potential inducer of mammalian postnatal cardiomyocytes. In addition, the effect of cardiac glycosides on cardiomyocyte cell cycle progression was enhanced by inhibition of PTEN as well as GSK-3β and inhibited by IP3 receptor antagonist xestospongin C, which is known to inhibit IP3-mediated Ca^{2+} release from endo- and sarcoplasmic reticulum (36).

The here developed assay proved to be valid to identify novel compounds to enhance cardiomyocyte cell cycle progression. While our study is a pilot study being limited in a number of compounds, a number of analyzed cells per time point, and repetitions, pipette robots and automated image analysis solutions will allow in the future unbiased, in-depth analyses of high-content compound libraries.

To date, no direct data are available regarding the effect of cardiac glycoside on cardiomyocyte proliferation. In general, cardiac glycosides inhibit the sodium-potassium pump resulting in an increased calcium concentration inside the cell. It is well known that Na^+K^+ATPase specifically regulates calcium transients *via* the IP3 receptors (33–35) and our data show that inhibition of the IP3 receptors with xestospongin C inhibits the cell cycle-promoting effect of glycosides. Notably, calcium plays, in general, a crucial role in cell proliferation and aberrant Ca^{2+}-signaling and loss of intracellular Ca^{2+} homeostasis contributes to tumor initiation and proliferation (37, 38). While cardiac glycosides became recently popular to inhibit tumor growth (39), there is evidence that cardiac glycosides can promote cell proliferation at lower, subsaturating concentrations. It has been reported that low concentrations of cardiac glycosides stimulate cell proliferation in astrocytes (40), vascular smooth muscle cells (41), renal tubule cells (42–44), Sertoli cells (45), human endothelial cells (46), and human umbilical vein smooth muscle cells (47). In addition, it has been indicated that voltage-gated L-type Ca^{2+} channels blockers enhance hiPSC-derived cardiomyocyte proliferation (48). Further, it has been reported that modulation of calcium channel activity controls proliferation vs. differentiation of cardiac progenitor cells (49). Finally, it has been suggested that cardiac glycosides can interfere with nuclear receptor signaling (19). For example, it has been shown that the cardiac glycosides digoxin and lanatoside C induce both the expression of peroxisome proliferator-activated receptor (PPAR) δ (50–52), which previously has been shown to promote cardiomyocyte proliferation (14). Taken together, our data indicate that cardiac glycosides can enhance cell cycle progression in cardiomyocytes.

Besides cardiac glycosides, we have identified the flavonoid osajin as a potent inducer of postnatal cardiomyocyte cell cycle progression. Previously, it has been shown that osajin exhibits a potential cardioprotective role in ischemia-reperfusion-induced injury in rat hearts. This cardioprotective role has been attributed to the suppression of oxidative stress resulting in improved ventricular function (53, 54). Yet, it has also been shown that osajin can inhibit fatty acid synthase (FASN) expression, a key enzyme for lipogenesis (55). This might enhance glycolysis, which has been associated with several processes during tissue repair and regeneration (56) as well as cardiomyocyte proliferation (13, 57). Concurrently, it has been shown that myocardial injury due to ischemia/reperfusion injury was significantly reduced by cardiac-specific PPARδ overexpression concomitant with increased myocardial glucose utilization (58).

Finally, we identified the selective α-adrenoceptor antagonist and imidazoline I_1 receptor ligand efaroxan hydrochloride as a promotor of cardiomyocyte cell cycle progression. α-adrenoceptor and imidazoline I_1 receptor are both expressed in cardiomyocytes and are involved in NO synthesis and intracellular calcium handling (59). Besides, efaroxan hydrochloride improved *in vivo* oral glucose tolerance (60). Yet, there is little evidence that efaroxan hydrochloride promotes proliferation. It has been reported that α2-adrenergic blockade by efaroxan hydrochloride increased primary breast tumor size and distant metastasis under non-stress conditions (61).

The efficiency of the investigated compounds to enhance cardiomyocyte cell cycle progression significantly decreased with the age of the cardiomyocytes. This phenomenon has been observed for a large number of measures to induce cardiomyocyte proliferation such as treatment with FGF1/p38 inhibitor, BIO or microRNAs as well as Meis1 deletion (24, 32, 62, 63). Thus, it will be important to elucidate the mechanisms promoting cardiomyocyte cell cycle progression utilized by the different stimuli, to determine the difference in the response of neonatal and adult cardiomyocytes to these stimuli, and to test if combinations of the different inhibitors might be able to induce robust proliferation in adult cardiomyocytes. Here, we have shown that the combinatorial approach of osajin or cardiac glycosides with PTEN or GSK3β inhibition enhances the effect on cardiomyocyte cell cycle progression. Similarly, it has been shown that the combinations of p38 MAP kinase inhibition/ PI3kinase/AKT signaling (24), GSK3β inhibition/AKT phosphorylation (4), and PPARδ signaling/GSK3β inhibition are more efficient in promoting cardiomyocyte cell cycle progression than the individual measures (14).

In the future, it will be important to determine whether the here identified drugs induce cell cycle re-entry of adult cardiomyocytes upon injury *in vivo* and to show that this contributes to improved function. Our data suggest that the positive effect of cardiac glycosides on heart function might not only increase myocardial contraction force by inhibiting the sodium-potassium pump but might also contribute to cardiac repair by inducing cardiomyocyte proliferation. Considering the toxicity of cardiac glycosides, the application of subsaturating

concentrations might open new avenues for the use of cardiac glycosides, which might benefit from the combination with other pro-proliferative drugs.

Conclusion

Considering that cardiovascular diseases represent a significant socio-economic burden affecting the pediatric as well as adult population and that currently no therapy is available to cure congenital heart disease or heart failure, the development of a cardiomyocyte proliferation screening system and the identification of novel inducers of cardiomyocyte proliferation, are potentially of great therapeutic value (64–66). Here, we identified, utilizing a novel screening system, potential compounds to promote cardiomyocyte proliferation including cardiac glycosides. Our data suggest that modulation of calcium handling and metabolism promotes cardiomyocyte proliferation and cardiac glycosides might, besides increasing myocardial contraction force, contribute to cardiac repair by inducing cardiomyocyte proliferation. The cardiomyocyte proliferation by cardiac glycosides at low concentrations enhanced by PTEN and GSK-3β inhibitors might contribute to cardiac repair by inducing cardiomyocyte proliferation. This study provides a translational perspective to investigate chemical compounds derived from the high throughput screening for their potential to improve cardiac tissue engineering approaches as well as to repair or regenerate the injured heart in pre-clinical models.

Data availability statement

The original contributions presented in the study are included in the article/Supplementary material, further inquiries can be directed to the corresponding authors.

Ethics statement

The animal study was reviewed and approved by the local Animal Ethics Committee Erlangen, Germany in accordance with governmental and international guidelines on animal experimentation (protocol TS-9/2016 Nephropatho).

Author contributions

AM designed and carried out most of the experiments, analyzed most of the data, and wrote the manuscript. HR performed *in vitro* cell culture and immunostaining. NS performed immunostainings. CE provided the human iPSC-derived differentiated cardiomyocytes. RK analyzed data and revised the manuscript. FE designed experiments, analyzed data, and wrote the manuscript. All authors contributed to the article and approved the submitted version.

Funding

This work was supported by the Emerging Fields Initiative of the Friedrich-Alexander-Universität Erlangen-Nürnberg (FAU) [EFI, CYDER: Cell Cycle in Disease and Regeneration to FE], the Alexander von Humboldt Foundation [Sofja Kovalevskaja Award to FE], and as well as the German Research Foundation (DFG) [INST 410/91-1 FUGG and IRTG 1566, PROMISE to FE].

Acknowledgments

We thank Atsushi Miyawaki for providing Fucci plasmid constructs and Robert Zweigerdt for the CM7/1 mouse stem cell line.

Conflict of interest

The authors declare that the research was conducted in the absence of any commercial or financial relationships that could be construed as a potential conflict of interest.

Publisher's note

Supplementary material

The Supplementary Material for this article can be found online at: https://www.frontiersin.org/articles/10.3389/fcvm.2022.901396/full#supplementary-material

SUPPLEMENTARY FIGURE 1
Dosage-dependent induction of DNA synthesis in neonatal cardiomyocytes. Quantitative analysis of BrdU-positive neonatal cardiomyocytes upon stimulation with the top 19 candidates at indicated concentrations. $n = 6$, mean ± SEM. Cardiomyocytes were isolated from postnatal day 3 rats, stimulated once with the individual small molecules, after 48 h BrdU was added, and after 24 h BrdU pulse-labeling the percentage of BrdU-positive cardiomyocytes was determined.

SUPPLEMENTARY FIGURE 2
Cardiac glycosides do not induce cell death in neonatal rat cardiomyocytes. Quantitative analysis of cardiomyocytes death by MTS assay ($n = 6$, mean ± SEM, **: $p < 0.01$, *: $p < 0.05$).

References

1. Virani SS, Alonso A, Benjamin EJ, Bittencourt MS, Callaway CW, Carson AP, et al. Heart Disease and Stroke Statistics-2020 Update: a report from the American Heart association. *Circulation.* (2020) 141:e139–596. doi: 10.1161/CIR.0000000000000757

2. Leone M, Engel FB. Advances in heart regeneration based on cardiomyocyte proliferation and regenerative potential of binucleated cardiomyocytes and polyploidization. *Clin Sci (Lond).* (2019) 133:1229–53. doi: 10.1042/CS20180560

3. Madonna R, Van Laake LW, Botker HE, Davidson SM, De Caterina R, Engel FB, et al. ESC Working Group on Cellular Biology of the Heart: position paper for Cardiovascular Research: tissue engineering strategies combined with cell therapies for cardiac repair in ischaemic heart disease and heart failure. *Cardiovasc Res.* (2019) 115:488–500. doi: 10.1093/cvr/cvz010

4. Buikema JW, Lee S, Goodyer WR, Maas RG, Chirikian O, Li G, et al. Wnt activation and reduced cell-cell contact synergistically induce massive expansion of functional human iPSC-derived cardiomyocytes. *Cell Stem Cell.* (2020) 27:50–63 e5. doi: 10.1016/j.stem.2020.06.001

5. Hesselbarth R, Esser TU, Roshanbinfar K, Schrufer S, Schubert DW, Engel FB. CHIR99021 promotes hiPSC-derived cardiomyocyte proliferation in engineered 3D microtissues. *Adv Healthc Mater.* (2021) 10:e2100926. doi: 10.1002/adhm.202100926

6. Bergmann O, Zdunek S, Felker A, Salehpour M, Alkass K, Bernard S, et al. Dynamics of cell generation and turnover in the human heart. *Cell.* (2015) 161:1566–75. doi: 10.1016/j.cell.2015.05.026

7. Becker JR, Deo RC, Werdich AA, Panakova D, Coy S, MacRae CA. Human cardiomyopathy mutations induce myocyte hyperplasia and activate hypertrophic pathways during cardiogenesis in zebrafish. *Dis Model Mech.* (2011) 4:400–10. doi: 10.1242/dmm.006148

8. Ben-Yair R, Butty VL, Busby M, Qiu Y, Levine SS, Goren A, et al. H3K27me3-mediated silencing of structural genes is required for zebrafish heart regeneration. *Development.* (2019) 146:dev178632. doi: 10.1242/dev.178632

9. Jiang J, Burgon PG, Wakimoto H, Onoue K, Gorham JM, O'Meara CC, et al. Cardiac myosin binding protein C regulates postnatal myocyte cytokinesis. *Proc Natl Acad Sci U S A.* (2015) 112:9046–51. doi: 10.1073/pnas.1511004112

10. Liu Z, Yue S, Chen X, Kubin T, Braun T. Regulation of cardiomyocyte polyploidy and multinucleation by CyclinG1. *Circ Res.* (2010) 106:1498–506. doi: 10.1161/CIRCRESAHA.109.211888

11. Sdek P, Zhao P, Wang Y, Huang CJ, Ko CY, Butler PC, et al. Rb and p130 control cell cycle gene silencing to maintain the postmitotic phenotype in cardiac myocytes. *J Cell Biol.* (2011) 194:407–23. doi: 10.1083/jcb.201012049

12. Zebrowski DC, Vergarajauregui S, Wu CC, Piatkowski T, Becker R, Leone M, et al. Developmental alterations in centrosome integrity contribute to the post-mitotic state of mammalian cardiomyocytes. *Elife.* (2015) 4. doi: 10.7554/eLife.05563

13. Cardoso AC, Lam NT, Savla JJ, Nakada Y, Pereira AHM, Elnwasany A, et al. Mitochondrial substrate utilization regulates cardiomyocyte cell cycle progression. *Nat Metab.* (2020) 2:167–78. doi: 10.1038/s42255-020-0169-x

14. Magadum A, Ding Y, He L, Kim T, Vasudevarao MD, Long Q, et al. Live cell screening platform identifies PPARdelta as a regulator of cardiomyocyte proliferation and cardiac repair. *Cell Res.* (2017) 27:1002–19. doi: 10.1038/cr.2017.84

15. Zebrowski DC, Becker R, Engel FB. Towards regenerating the mammalian heart: challenges in evaluating experimentally induced adult mammalian cardiomyocyte proliferation. *Am J Physiol Heart Circ Physiol.* (2016) 310:H1045–54. doi: 10.1152/ajpheart.00697.2015

16. Jung JH, Ikeda G, Tada Y, von Bornstadt D, Santoso MR, Wahlquist C, et al. miR-106a-363 cluster in extracellular vesicles promotes endogenous myocardial repair via Notch3 pathway in ischemic heart injury. *Basic Res Cardiol.* (2021) 116:19. doi: 10.1007/s00395-021-00858-8

17. Abbas N, Perbellini F, Thum T. Non-coding RNAs: emerging players in cardiomyocyte proliferation and cardiac regeneration. *Basic Res Cardiol.* (2020) 115:52. doi: 10.1007/s00395-020-0816-0

18. Sakaue-Sawano A, Kurokawa H, Morimura T, Hanyu A, Hama H, Osawa H, et al. Visualizing spatiotemporal dynamics of multicellular cell-cycle progression. *Cell.* (2008) 132:487–98. doi: 10.1016/j.cell.2007.12.033

19. Karas K, Salkowska A, Dastych J, Bachorz RA, Ratajewski M. Cardiac glycosides with target at direct and indirect interactions with nuclear receptors. *Biomed Pharmacother.* (2020) 127:110106. doi: 10.1016/j.biopha.2020.110106

20. Patel S. Plant-derived cardiac glycosides: Role in heart ailments and cancer management. *Biomed Pharmacother.* (2016) 84:1036–41. doi: 10.1016/j.biopha.2016.10.030

21. Muller-Ehmsen J, Nickel J, Zobel C, Hirsch I, Bolck B, Brixius K, et al. Longer term effects of ouabain on the contractility of rat isolated cardiomyocytes and on the expression of Ca and Na regulating proteins. *Basic Res Cardiol.* (2003) 98:90–6. doi: 10.1007/s00395-003-0396-9

22. Leone M, Engel FB. Isolation, culture, and live-cell imaging of primary rat cardiomyocytes. *Methods Mol Biol.* (2021) 2158:109–24. doi: 10.1007/978-1-0716-0668-1_9

23. Schroeder M, Niebruegge S, Werner A, Willbold E, Burg M, Ruediger M, et al. Differentiation and lineage selection of mouse embryonic stem cells in a stirred bench scale bioreactor with automated process control. *Biotechnol Bioeng.* (2005) 92:920–33. doi: 10.1002/bit.20668

24. Engel FB, Schebesta M, Duong MT, Lu G, Ren S, Madwed JB, et al. p38 MAP kinase inhibition enables proliferation of adult mammalian cardiomyocytes. *Genes Dev.* (2005) 19:1175–87. doi: 10.1101/gad.1306705

25. Lian X, Zhang J, Azarin SM, Zhu K, Hazeltine LB, Bao X, et al. Directed cardiomyocyte differentiation from human pluripotent stem cells by modulating Wnt/beta-catenin signaling under fully defined conditions. *Nat Protoc.* (2013) 8:162–75. doi: 10.1038/nprot.2012.150

26. Zweigerdt R, Burg M, Willbold E, Abts H, Ruediger M. Generation of confluent cardiomyocyte monolayers derived from embryonic stem cells in suspension: a cell source for new therapies and screening strategies. *Cytotherapy.* (2003) 5:399–413. doi: 10.1080/14653240310003062

27. Klug MG, Soonpaa MH, Field LJ, DNA. synthesis and multinucleation in embryonic stem cell-derived cardiomyocytes. *Am J Physiol.* (1995) 269:H1913–21. doi: 10.1152/ajpheart.1995.269.6.H1913

28. Engel FB, Schebesta M, Keating MT. Anillin localization defect in cardiomyocyte binucleation. *J Mol Cell Cardiol.* (2006) 41:601–12. doi: 10.1016/j.yjmcc.2006.06.012

29. Maxwell JT, Xu C. Stem-cell-derived cardiomyocytes grow up: start young and train harder. *Cell Stem Cell.* (2018) 22:790–1. doi: 10.1016/j.stem.2018.05.011

30. Kuhn B. del Monte F, Hajjar RJ, Chang YS, Lebeche D, Arab S, et al. Periostin induces proliferation of differentiated cardiomyocytes and promotes cardiac repair. *Nat Med.* (2007) 13:962–9. doi: 10.1038/nm1619

31. Liang T, Gao F, Jiang J, Lu YW, Zhang F, Wang Y, et al. Loss of phosphatase and tensin homolog promotes cardiomyocyte proliferation and cardiac repair after myocardial infarction. *Circulation.* (2020) 142:2196–9. doi: 10.1161/CIRCULATIONAHA.120.046372

32. Tseng AS, Engel FB, Keating MT. The GSK-3 inhibitor BIO promotes proliferation in mammalian cardiomyocytes. *Chem Biol.* (2006) 13:957–63. doi: 10.1016/j.chembiol.2006.08.004

33. Zhang L, Zhang Z, Guo H, Wang Y. Na+/K+-ATPase-mediated signal transduction and Na+/K+-ATPase regulation. *Fundam Clin Pharmacol.* (2008) 22:615–21. doi: 10.1111/j.1472-8206.2008.00620.x

34. Grisanti LA. Cardiomyocyte Na(+)/K(+)-ATPase-alpha2 overexpression confers protection in ischemic heart failure. *Am J Physiol Heart Circ Physiol.* (2021) 321:H736–H7. doi: 10.1152/ajpheart.00505.2021

35. Cellini A, Hofler D, Arias-Loza PA, Bandleon S, Langsenlehner T, Kohlhaas M, et al. The alpha2-isoform of the Na(+)/K(+)-ATPase protects against pathological remodeling and beta-adrenergic desensitization after myocardial infarction. *Am J Physiol Heart Circ Physiol.* (2021) 321:H650–H62. doi: 10.1152/ajpheart.00808.2020

36. Gafni J, Munsch JA, Lam TH, Catlin MC, Costa LG, Molinski TF, et al. Xestospongins: potent membrane permeable blockers of the inositol 1,4,5-trisphosphate receptor. *Neuron.* (1997) 19:723–33. doi: 10.1016/S0896-6273(00)80384-0

37. Varghese E, Samuel SM, Sadiq Z, Kubatka P, Liskova A, Benacka J, et al. Anti-cancer agents in proliferation and cell death: the calcium connection. *Int J Mol Sci.* (2019) 20. doi: 10.3390/ijms20123017

38. Pinto MC, Kihara AH, Goulart VA, Tonelli FM, Gomes KN, Ulrich H, et al. Calcium signaling and cell proliferation. *Cell Signal.* (2015) 27:2139–49. doi: 10.1016/j.cellsig.2015.08.006

39. Regulska K, Regulski M, Karolak B, Murias M, Stanisz B. Can cardiovascular drugs support cancer treatment? The rationale for drug repurposing. *Drug Discov Today.* (2019) 24:1059–65. doi: 10.1016/j.drudis.2019.03.010

40. Murata Y, Matsuda T, Tamada K, Hosoi R, Asano S, Takuma K, et al. Ouabain-induced cell proliferation in cultured rat astrocytes. *Jpn J Pharmacol.* (1996) 72:347–53. doi: 10.1254/jjp.72.347

41. Allen JC, Abramowitz J, Koksoy A. Low concentrations of ouabain activate vascular smooth muscle cell proliferation. *Ann N Y Acad Sci.* (2003) 986:504–8. doi: 10.1111/j.1749-6632.2003.tb07235.x

42. Khundmiri SJ, Metzler MA, Ameen M, Amin V, Rane MJ, Delamere NA. Ouabain induces cell proliferation through calcium-dependent phosphorylation of Akt (protein kinase B) in opossum kidney proximal tubule cells. *Am J Physiol Cell Physiol.* (2006) 291:C1247–57. doi: 10.1152/ajpcell.00593.2005

43. Nguyen AN, Jansson K, Sanchez G, Sharma M, Reif GA, Wallace DP, et al. Ouabain activates the Na-K-ATPase signalosome to induce autosomal dominant polycystic kidney disease cell proliferation. *Am J Physiol Renal Physiol.* (2011) 301:F897–906. doi: 10.1152/ajprenal.00095.2011

44. Li J, Zelenin S, Aperia A, Aizman O. Low doses of ouabain protect from serum deprivation-triggered apoptosis and stimulate kidney cell proliferation via activation of NF-kappaB. *J Am Soc Nephrol.* (2006) 17:1848–57. doi: 10.1681/ASN.2005080894

45. Lucas TF, Amaral LS, Porto CS, Quintas LE. Na+/K+-ATPase alpha1 isoform mediates ouabain-induced expression of cyclin D1 and proliferation of rat sertoli cells. *Reproduction.* (2012) 144:737–45. doi: 10.1530/REP-12-0232

46. Tverskoi AM, Sidorenko SV, Klimanova EA, Akimova OA, Smolyaninova LV, Lopina OD, et al. Effects of ouabain on proliferation of human endothelial cells correlate with Na+,K+-ATPase activity and intracellular ratio of Na+ and K. *Biochemistry (Mosc).* (2016) 81:876–83. doi: 10.1134/S0006297916080083

47. Abramowitz J, Dai C, Hirschi KK, Dmitrieva RI, Doris PA, Liu L, et al. Ouabain- and marinobufagenin-induced proliferation of human umbilical vein smooth muscle cells and a rat vascular smooth muscle cell line, A7r5. *Circulation.* (2003) 108:3048–53. doi: 10.1161/01.CIR.0000101919.00548.86

48. Woo LA, Tkachenko S, Ding M, Plowright AT, Engkvist O, Andersson H, et al. High-content phenotypic assay for proliferation of human iPSC-derived cardiomyocytes identifies L-type calcium channels as targets. *J Mol Cell Cardiol.* (2019) 127:204–14. doi: 10.1016/j.yjmcc.2018.12.015

49. Hotchkiss A, Feridooni T, Zhang F, Pasumarthi KB. The effects of calcium channel blockade on proliferation and differentiation of cardiac progenitor cells. *Cell Calcium.* (2014) 55:238–51. doi: 10.1016/j.ceca.2014.02.018

50. Fan SC Yu BC, Chen ZC, Chen LJ, Chung HH, Cheng JT. The decreased expression of peroxisome proliferator-activated receptors delta (PPARdelta) is reversed by digoxin in the heart of diabetic rats. *Horm Metab Res.* (2010) 42:637–42. doi: 10.1055/s-0030-1253373

51. Chen ZC Yu BC, Chen LJ, Cheng KC, Lin HJ, Cheng JT. Characterization of the mechanisms of the increase in PPARdelta expression induced by digoxin in the heart using the H9c2 cell line. *Br J Pharmacol.* (2011) 163:390–8. doi: 10.1111/j.1476-5381.2011.01212.x

52. Shi H, Mao X, Zhong Y, Liu Y, Zhao X, Yu K, et al. Lanatoside C Promotes Foam Cell Formation and Atherosclerosis. *Sci Rep.* (2016) 6:20154. doi: 10.1038/srep20154

53. Necas J, Bartosikova L, Florian T, Klusakova J, Suchy V, Naggar EM, et al. [Protective effects of the flavonoids osajin and pomiferin on heart ischemia-reperfusion]. *Ceska Slov Farm.* (2006) 55:168–74.

54. Florian T, Necas J, Bartosikova L, Klusakova J, Suchy V, Naggara EB, et al. Effects of prenylated isoflavones osajin and pomiferin in premedication on heart ischemia-reperfusion. *Biomed Pap Med Fac Univ Palacky Olomouc Czech Repub.* (2006) 150:93–100. doi: 10.5507/bp.2006.013

55. Huang SY, Huang GJ, Hsieh PF, Wu HC, Huang WC. Osajin displays potential antiprostate cancer efficacy via impairment of fatty acid synthase and androgen receptor expression. *Prostate.* (2019) 79:1543–52. doi: 10.1002/pros.23876

56. Magadum A, Engel FB. PPARbeta/delta: linking metabolism to regeneration. *Int J Mol Sci.* (2018) 19:2013. doi: 10.3390/ijms19072013

57. Fukuda R, Marin-Juez R, El-Sammak H, Beisaw A, Ramadass R, Kuenne C, et al. Stimulation of glycolysis promotes cardiomyocyte proliferation after injury in adult zebrafish. *EMBO Rep.* 2020:e49752. doi: 10.15252/embr.201949752

58. Burkart EM, Sambandam N, Han X, Gross RW, Courtois M, Gierasch CM, et al. Nuclear receptors PPARbeta/delta and PPARalpha direct distinct metabolic regulatory programs in the mouse heart. *J Clin Invest.* (2007) 117:3930–9. doi: 10.1172/JCI32578

59. Maltsev AV, Kokoz YM, Evdokimovskii EV, Pimenov OY, Reyes S, Alekseev AE. Alpha-2 adrenoceptors and imidazoline receptors in cardiomyocytes mediate counterbalancing effect of agmatine on NO synthesis and intracellular calcium handling. *J Mol Cell Cardiol.* (2014) 68:66–74. doi: 10.1016/j.yjmcc.2013.12.030

60. Lehner Z, Stadlbauer K, Adorjan I, Rustenbeck I, Belz M, Fenzl A, et al. Mechanisms of antihyperglycaemic action of efaroxan in mice: time for reappraisal of alpha2A-adrenergic antagonism in the treatment of type 2 diabetes? *Diabetologia.* (2012) 55:3071–82. doi: 10.1007/s00125-012-2679-x

61. Lamkin DM, Sung HY, Yang GS, David JM, Ma JC, Cole SW, et al. alpha2-Adrenergic blockade mimics the enhancing effect of chronic stress on breast cancer progression. *Psychoneuroendocrinology.* (2015) 51:262–70. doi: 10.1016/j.psyneuen.2014.10.004

62. Mahmoud AI, Kocabas F, Muralidhar SA, Kimura W, Koura AS, Thet S, et al. Meis1 regulates postnatal cardiomyocyte cell cycle arrest. *Nature.* (2013) 497:249–53. doi: 10.1038/nature12054

63. Eulalio A, Mano M, Dal Ferro M, Zentilin L, Sinagra G, Zacchigna S, et al. Functional screening identifies miRNAs inducing cardiac regeneration. *Nature.* (2012) 492:376–81. doi: 10.1038/nature11739

64. Neininger AC, Long JH, Baillargeon SM, Burnette DT, A. simple and flexible high-throughput method for the study of cardiomyocyte proliferation. *Sci Rep.* (2019) 9:15917. doi: 10.1038/s41598-019-52467-0

65. Mills RJ, Parker BL, Quaife-Ryan GA, Voges HK, Needham EJ, Bornot A, et al. Drug screening in human PSC-cardiac organoids identifies pro-proliferative compounds acting via the mevalonate pathway. *Cell Stem Cell.* (2019) 24:895–907 e6. doi: 10.1016/j.stem.2019.03.009

66. Murganti F, Derks W, Baniol M, Simonova I, Trus P, Neumann K, et al. FUCCI-based live imaging platform reveals cell cycle dynamics and identifies pro-proliferative compounds in human iPSC-derived cardiomyocytes. *Front Cardiovasc Med.* (2022) 9:840147. doi: 10.3389/fcvm.2022.840147

frontiers | Frontiers in Cardiovascular Medicine

TYPE Original Research
PUBLISHED 10 October 2022
DOI 10.3389/fcvm.2022.953211

OPEN ACCESS

EDITED BY
Rajika Roy,
Temple University, United States

REVIEWED BY
Marie-José Goumans,
Leiden University Medical Center (LUMC), Netherlands
Fujian Wu,
Jinan University, China

*CORRESPONDENCE
Andrew H. Baker
Andy.Baker@ed.ac.uk

SPECIALTY SECTION
This article was submitted to Cardiovascular Biologics and Regenerative Medicine, a section of the journal Frontiers in Cardiovascular Medicine

RECEIVED 25 May 2022
ACCEPTED 16 September 2022
PUBLISHED 10 October 2022

CITATION
Spiroski AM, McCracken IR, Thomson A, Magalhaes-Pinto M, Lalwani MK, Newton KJ, Miller E, Bénézech C, Hadoke P, Brittan M, Mountford JC, Beqqali A, Gray GA and Baker AH (2022) Human embryonic stem cell-derived endothelial cell product injection attenuates cardiac remodeling in myocardial infarction. *Front. Cardiovasc. Med.* 9:953211. doi: 10.3389/fcvm.2022.953211

Human embryonic stem cell-derived endothelial cell product injection attenuates cardiac remodeling in myocardial infarction

Ana-Mishel Spiroski[1,2], Ian R. McCracken[1], Adrian Thomson[3], Marlene Magalhaes-Pinto[1,2], Mukesh K. Lalwani[1], Kathryn J. Newton[1], Eileen Miller[1], Cecile Bénézech[4], Patrick Hadoke[1], Mairi Brittan[1,2], Joanne C. Mountford[5], Abdelaziz Beqqali[1], Gillian A. Gray[1] and Andrew H. Baker[1,2]*

[1]Centre for Cardiovascular Science, Queen's Medical Research Institute, University of Edinburgh, Edinburgh, United Kingdom, [2]BHF Centre for Vascular Regeneration, University of Edinburgh, Edinburgh, United Kingdom, [3]Edinburgh Preclinical Imaging, University of Edinburgh, Edinburgh, United Kingdom, [4]Centre for Inflammation Research, University of Edinburgh, Edinburgh, United Kingdom, [5]Scottish National Blood Transfusion Service, Edinburgh, United Kingdom

Background: Mechanisms contributing to tissue remodeling of the infarcted heart following cell-based therapy remain elusive. While cell-based interventions have the potential to influence the cardiac healing process, there is little direct evidence of preservation of functional myocardium.

Aim: The aim of the study was to investigate tissue remodeling in the infarcted heart following human embryonic stem cell-derived endothelial cell product (hESC-ECP) therapy.

Materials and methods: Following coronary artery ligation (CAL) to induce cardiac ischemia, we investigated infarct size at 1 day post-injection in media-injected controls (CALM, n = 11), hESC-ECP-injected mice (CALC, n = 10), and dead hESC-ECP-injected mice (CALD, n = 6); echocardiography-based functional outcomes 14 days post-injection in experimental (CALM, n = 13; CALC, n = 17) and SHAM surgical mice (n = 4); and mature infarct size (CALM and CALC, both n = 6). We investigated ligand–receptor interactions (LRIs) in hESC-ECP cell populations, incorporating a publicly available C57BL/6J mouse cardiomyocyte-free scRNAseq dataset with naive, 1 day, and 3 days post-CAL hearts.

Results: Human embryonic stem cell-derived endothelial cell product injection reduces the infarct area (CALM: 54.5 ± 5.0%, CALC: 21.3 ± 4.9%), and end-diastolic (CALM: 87.8 ± 8.9 uL, CALC: 63.3 ± 2.7 uL) and end-systolic ventricular volume (CALM: 56.4 ± 9.3 uL, CALC: 33.7 ± 2.6 uL). LRI analyses indicate an alternative immunomodulatory effect mediated *via* viable hESC-ECP-resident signaling.

Conclusion: Delivery of the live hESC-ECP following CAL modulates the wound healing response during acute pathological remodeling, reducing infarct area, and preserving functional myocardium in this relatively acute model. Potential intrinsic myocardial cellular/hESC-ECP interactions indicate that discreet immunomodulation could provide novel therapeutic avenues to improve cardiac outcomes following myocardial infarction.

KEYWORDS

myocardial infarction, hESC-ECP, cell therapy, scRNAseq, ligand–receptor interaction, immunomodulation

Introduction

Heart disease is responsible for the greatest proportion of death and disability attributed to a non-communicable disease worldwide (1, 2). In addition to the staggering economic and social cost of caring for patients with ischemic heart disease in the acute setting, greater survival rates translate to increased long-term investments in recovery and rehabilitation (1, 3). The window of opportunity to halt the progression of ischemic injury is narrow, and cell-based therapies have shown potential in the treatment of ischemic heart disease, albeit largely in the pre-clinical setting (4–6). Indeed, in the pre-clinical setting, cell derivation protocols that produce a heterogeneous range of endothelial cell (EC) lineages do show some angiogenic efficacy and long-term cell retention (7). However, progenitor cell-derived products that have been reported to promote angiogenesis in small mammal models have resulted in disappointing outcomes in clinical translation to date (8). The lack of characterization of cell products and their potential effects in *in vivo* paradigms of human disease stifles effective translation in this setting. Therefore, we have focused on producing a well-characterized human embryonic stem cell-derived product, trialed in multiple pre-clinical disease paradigms with physiologically relevant, clinically translatable outcomes.

Over the last decade, we have developed a robust good manufacturing practice (GMP)-compatible human embryonic stem cell-derived endothelial cell product (hESC-ECP) that promotes angiogenesis in ischemic tissue (9–11). This robust ECP is differentiated using a well-described method and can be derived from both human embryonic and induced pluripotent stem cell (iPSC) sources. Our work with the single-source hESC-ECP is not confounded by donor variation and can be genetically manipulated, and polarization is reliable with high cell viability (10). Our recent work has focused on single-cell RNA sequencing (scRNAseq) to characterize temporal changes in transcriptional dynamics throughout derivation of pluripotent, mesodermal, mesenchymal, and endothelial lineages (11). This robust protocol produces ∼60% ECs and 40% mesenchymal cells (MESs) expressing TGFB1, FLT1, and HIF1A across both EC and MES populations, in the absence of SOX2 and POU5F1 co-expression (11). These relatively immature ECs do not specify to an arterial, lymphatic, or venous lineage and are transcriptionally distinct from fetal, infant, and adult ECs from diverse vascular beds (11). These data suggest that the resultant "unspecified" EC population, which expresses angiogenic transcription factors *in vitro*, is primed for neo-angiogenesis if introduced to an appropriate cellular milieu. Indeed, we have shown that hESC-ECP injection improves capillary endowment and perfusion as measured by using a tissue Doppler in a mouse paradigm of peripheral vascular disease, even in the presence of co-morbidities (10). In that work, we demonstrated the therapeutic potential of this cell product for acute and chronic limb ischemia, with 1×10^6 cells injected intramuscularly at the time of surgery in immune-competent, -deficient, and type 2 diabetic mouse backgrounds, and injected 3 days post-surgical limb ischemia. Interestingly, superparamagnetic iron oxide nanoparticle (SPIO) magnetic resonance imaging (MRI) showed that the hESC-ECP does not persist in the hindlimb after the first week post-injection, despite gradually improving tissue perfusion compared with media-injected

Abbreviations: ARRIVE, Animal Research: Reporting of *In Vivo* Experiments; AWERB, Animal Welfare and Ethical Review Board; CAL, coronary artery ligation; CCL23, C-C motif chemokine ligand 23; CCL4L2, C-C motif chemokine ligand 4 like 2; EC, endothelial cell; EdU, 5-ethynyl-2′-deoxyuridine; EDV, end-diastolic volume; EF, ejection fraction; EKV, ECG-gated kilohertz visualization; ESV, end-systolic volume; FLT1, Fms-related receptor tyrosine kinase 1, vascular endothelial growth factor receptor 1; GLS, global longitudinal strain; GMP, good manufacturing practice; hESC-ECP, human embryonic stem cell-derived endothelial cell product; HIF1A, hypoxia inducible factor 1 subunit alpha; IGF2R, insulin-like growth factor 2 receptor; iPSC, induced pluripotent stem cell; KLRC1, killer cell lectin-like receptor C1; KLRK1, killer cell lectin-like receptor K1; LRI, ligand–receptor interaction; LV, left ventricle; Ly6C, lymphocyte antigen 6C; MES, mesenchymal cells; MI, myocardial infarction; MT, Masson's trichrome; NK, natural killer cells; PBS, phosphate-buffered saline; PFA, paraformaldehyde; PSC, pluripotent stem cell; POU5F1, POU class 5 homeobox 1; PWD, pulse-wave Doppler; scRNAseq, single-cell RNA sequencing; SOX2, SRY-box transcription factor 2; SPIO, superparamagnetic iron oxide nanoparticle; SSEA-4, stage-specific embryonic antigen 4; MRI, magnetic resonance imaging; PSR, picrosirius red; TGFB1, transforming growth factor beta 1; TRA-181, podocalyxin; TTC, triphenyltetrazolium chloride; VEGF, vascular endothelial growth factor.

control mice throughout the duration of the study. PET-based 18F-FLT cell tracking suggested ∼24% of transplanted cells is retained at 4 h post-transplantation, confirmed by immunohistochemistry. By qPCR, human DNA from the hESC-ECP persists in the mouse hindlimb 1 and 7 days post-transplantation at a reduced amount, 2.5- and 4.5-fold less, respectively, but induces angiogenesis without hESC-ECP retention. Our work shows that without cellular integration of the hESC-ECP, we are able to modify the cellular milieu, shifting the tissue response toward a pro-angiogenic outcome. Progressive recovery of blood flow in the absence of long-term hESC-ECP biodistribution suggests that the angiogenic efficacy of the cell product lies in its acute effects in ischemic tissue following transplantation. This suggests that angiogenesis occurs in response to integrated cellular cues driven by the tissue microenvironment. Promoting endogenous vascular regeneration and repair in peripheral tissues alters the cellular response and subsequent functional outcomes in peripheral vascular disease (12). Therefore, we hypothesize that the hESC-ECP activates intrinsic remodeling pathways, preserving myocardial tissue and vascular endowment.

Materials and methods

Ethical approval

All regulated animal experiments were performed in accordance with the Animals (Scientific Procedures) Act (UK) 1986 under the auspices of the home office project and personal licenses held in the University of Edinburgh facilities, following ethical review by the University of Edinburgh Animal Welfare and Ethical Review Board (AWERB) (project 70/8933, approved 29/04/2016), approved by the Bioresearch and Veterinary Services, University of Edinburgh, and conducted in accordance with Animal Research: Reporting of *In Vivo* Experiments (ARRIVE) guidelines (13). Human ESC line H9 (WiCell, Madison, WI, USA) was used in accordance with the U.K. Stem Cell Bank Steering Committee guidelines (Project Approvals SCSC11-51 and SCSC17-26) under the guidance of Dr. Jo Mountford, Scottish National Blood Transfusion Service. All cell culture and surgical techniques are routine within the Baker Lab.

Generation of experimental groups

To align with our established studies in HLI and chronic CAL and avoid compromising the innate response to cell injection, cardiac inflammation, and cardiotoxicity, such as with cyclophosphamide-induced immunosuppression, we used 8- to 10-week-old female Crl:CD1-Foxn1^{nu} mice (Charles River, Edinburgh, UK). The mice were group-housed, maintained in a 12-/12-h light/dark cycle and provided free access to food and water. After 1 week of facility acclimatization, the mice were anesthetized with 50 mg/kg ketamine (Velatar, Boehringer Ingelheim, Berkshire, UK)/5 mg/kg xylazine (Rompun, 2%, Bayer, Berkshire, UK) anesthesia by intraperitoneal injection, intubated, ventilated mechanically (MiniVent 845, Harvard Apparatus Ltd., Edenbridge, UK) with positive end-expiratory pressure and 100% oxygen, and provided homeothermic support (Physitemp, Clifton, NJ, USA). Anesthetic depth was monitored with corneal and withdrawal reflexes. A left thoracotomy was performed, the pericardium opened, and a 7-0 Prolene suture (Henry Schein, Gillingham, UK) placed around the proximal left anterior descending coronary artery to induce myocardial infarction by CAL. Immediately following CAL, intracardiac injection of either hESC-ECP or un-supplemented media into the left ventricle was administered within 1 mm of the ischemic peri-infarct border. The hESC-ECP was resuspended in fresh un-supplemented EBM-2 (Lonza, Basel, Switzerland), to provide 1 × 10^6 cells in 15 uL (CALC, n = 17). Either hESC-ECP (CALC) or un-supplemented EBM-2 media (CALM, n = 13) was injected at three sites (5 uL each) into the peri-infarct border. Warmed sterile 0.9% saline (0.2 mL) was injected into the thorax, and air removed from the chest cavity, and the thorax closed. Following skin closure with 6-0 Prolene suture (Henry Schein, Gillingham, UK), subcutaneous buprenorphine (0.05 mg/kg) was provided, anesthesia reversed with 1.0 mg/kg atipamezole (Antisedan, Henry Schein, Gillingham, UK), and an additional 0.2 mL 0.9% saline injected subcutaneously. From induction to recovery, each surgical procedure was completed in <15 min. Intubation was maintained until the mouse regained breathed spontaneously, and the blink and withdrawal reflexes were evident. Homeothermic support was provided, and following recovery, mice were group-housed in sterile individually ventilated cages with their established cage-mates, with free access to DietGel (ClearH2O, Portland, ME, USA), water, and food. The surgical sham mice (n = 5) underwent all procedures, except CAL and intracardiac injection. The mice were weighed and severity monitored as per facility guidance. Analgesia (0.05 mg/kg buprenorphine) and 0.5 mL warmed sterile 0.9% saline were injected subcutaneously 24 h following surgery. Intracardiac cell injection confounds using plasma cardiac troponin-I as a biomarker of infarct size. Therefore, to reduce post-surgical stress, we did not collect conscious blood samples 24 h post-surgery for troponin T analysis.

14-day coronary artery ligation

To investigate the cardiac cellular response and tissue remodeling induced by hESC-ECP injection in the ischemic mouse heart, both Crl:CD1-Foxn1nu mice were allocated to either the 14- or 1-day arm of the study. The mice allocated to the 14-day study (**Figure 1**) received 50 mg/kg intraperitoneal injections of Edu in 0.9% sterile saline at day 0 (0 d), 2, 4, 6, 9, and 12 d. These mice also underwent ultrasound

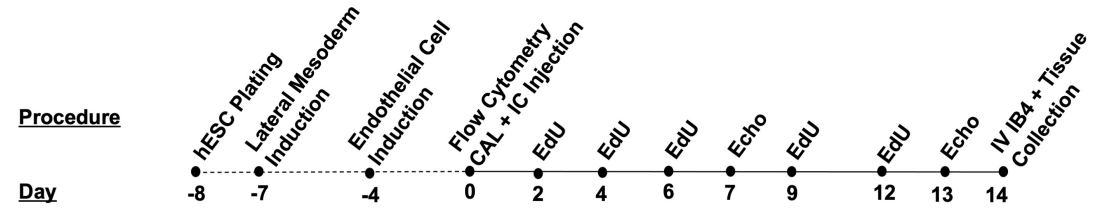

FIGURE 1
Timeline and design of human embryonic stem cell-derived endothelial cell product (hESC-ECP) differentiation and the 14-day study.

echocardiography at d7 and d14 and received an intravenous injection of 400 ng isolectin B4 (Sigma-Aldrich, UK) in 100 uL sterile saline 15 min prior to euthanasia with 150 mg/kg intraperitoneal pentobarbital sodium (Euthatal). A subset of mice (CALM and CALC, both $n = 6$) were perfused with PBS, perfusion-fixed with 4% paraformaldehyde in PBS, and hearts were excised, weighed, and cryoprotected overnight in 30% sucrose/PBS solution at 4°C (all from Thermo Fisher Scientific, Waltham, MA, USA). The hearts were embedded in Tissue-Tek O.C.T. Compound (Sakura, Netherlands) and stored at −80°C until sectioning. Then, 10 μm sections were collected and stored at −80°C until immunohistochemistry. Tissues from the remaining mice were micro-dissected and snap-frozen in liquid nitrogen for work outside the scope of this study.

1-day coronary artery ligation

The mice allocated to the 1-day arm of the study underwent a terminal procedure on 1 d post-surgery and injection. The mice (CALM, $n = 11$; CALC, $n = 10$) were anesthetized with intraperitoneal injection (50 mg/kg ketamine and 5 mg/kg, xylazine, as previously described). When the depth of anesthesia was sufficient, the aorta was catheterized, and the mouse perfused with PBS. Following PBS perfusion, Evans blue dye was perfused, and hearts were collected and processed, as previously described (14). In brief, the hearts were stained with 2% triphenyltetrazolium chloride (TTC) to assess the cardiac risk area and infarct area. The stained hearts were cut into 1-mm sections transverse to the apex/base axis to the level above the suture and incubated in 2% TTC for 30 min at 37°C. The hearts were blotted dry and post-fixed in 4% formalin. The sections were scanned, and risk and the infarct area were quantified manually in Fiji. The CALD mouse that survived 1 d post-surgery underwent this procedure as well.

Human embryonic stem cell-derived endothelial cell product differentiation

H9 (P43-47) hESCs were differentiated to an hESC-ECP, as previously described (10, 11). In brief, hESCs maintained in hESC StemPro SFM media (Thermo Fisher Scientific, Waltham, MA, USA) on a vitronectin matrix (Life Technologies, Paisley, UK) were dissociated at day 0 and seeded onto a fibronectin matrix (Sigma, St. Louis, MO, USA) in mTeSR1 media (STEMCELL Technologies, BC, Vancouver, Canada) supplemented with 10 μM ROCK inhibitor (Y27632) (Tocris, Bristol, UK). The lateral mesoderm was induced at day 1 with 25 ng/ml BMP4 (R&D Systems, Minneapolis, MN USA) and 7 μM GSK3 inhibitor CHIR99021 (Sigma, St. Louis, MO, USA) in N2B27/neurobasal/DMEM:F12 media (Life Technologies, Paisley, UK). At day 4, endothelial fate was induced with 200 ng/ml VEGF (R&D Systems, Minneapolis, MN, USA) and 2 μM Forskolin (Sigma, St. Louis, MO, USA) in StemPro34 media (Life Technologies, Paisley, UK), with a fresh media change at day 5. At day 6, cells were plated into a matrix-free T75 flask and maintained with daily media changes through day 8 with EGM-2 media (Lonza, Basel, Switzerland) supplemented with VEGF (50 ng/ml) and 1% human AB serum (Sigma, St. Louis, MO, USA). At day 8, the cells were visualized with the EVOS XL Core Cell Imaging System (Thermo Fisher Scientific, Waltham, MA, USA), detached with 1X TrypLE Express Enzyme (Thermo Fisher Scientific, Waltham, MA, USA), and kept on ice for flow cytometry assessment and *in vivo* use.

A group of mice ($n = 6$) were randomly allocated to receive freeze-thaw-killed (6) hESC-ECP injection (CALD). Only one mouse survived the procedure. This aspect of the study was discontinued to ensure alignment to ethical guidelines.

Cell staining and flow cytometry

At day 8, the cells were mixed 1:1 with trypan blue to identify dead cells, visualized, quantified (Bio-Rad, Hertfordshire, UK), and characterized for pluripotency and endothelial cell phenotype, as previously described (11). In brief, the cells were stained for pluripotency (SSEA-3 +/TRA-160 +) with PE rat anti-human SSEA-3, PE Rat IgM, κ isotype control, Alexa Fluor® 647 Mouse anti-Human TRA-1-60, Alexa Fluor® 647 Mouse IgM, and endothelial markers (CD31 +/CD144 +) with PE mouse anti-human CD144, PE mouse IgG1 κ isotype control (BD Biosciences), and APC anti-human CD31 and APC mouse IgG1 κ isotype control

(both eBioscience). Flow was conducted with an Attune NxT system (Thermo Fisher Scientific, Waltham, MA, USA) and data analyzed using FlowJo software (FlowJo LLC, Ashland, OR, USA). Preparations with an acceptable EC population (>60% EC, remaining cells mesenchymal) were used for this study.

Echocardiography

At day 8, the cells were mixed 1:1 with trypan blue to identify dead cells, visualized, quantified (Bio-Rad, HertfordshiCardiac function was assessed by ultrasound echocardiography with Doppler flow under isoflurane anesthesia (4% induction, ∼1.75% maintenance) on the Vevo 3100 Preclinical Imaging System and analyzed in Vevo Lab V3.2.6 image analysis software (FUJIFILM VisualSonics, Inc., Toronto, Canada). Post-CAL cardiac function (d7) was assessed to determine early post-injection cardiac function and late function at d14. Left ventricle (LV) function was assessed with brightness mode (B-mode), pulse wave Doppler (PWD), and motion mode (M-mode) in parasternal long axes, short axes and apical 4 chamber view (as appropriate), EKV (ECG-gated kilohertz visualization), and global longitudinal strain (GLS) in the long axis. All echocardiography analyses were blinded.

Immunohistochemistry

Slides were placed in ice-cold acetone for 10 min, followed by Masson's trichrome (MT) staining, as per the manufacturer's instructions (Thermo Fisher Scientific, UK) to investigate the infarct area. Collagen was stained using picrosirius red (PSR) for 1 h. Images were acquired in brightfield for MT and PSR on an Axioscan 2.1 slide scanner (Zeiss, Cambridge, UK), tiled at 40x, and the infarct and collagen areas (%) quantified manually in Fiji.

Immunofluorescence

Tissue staining was performed in blocking solution [0.5% Triton-X-100, 10% normal goat serum (NGS, Thermo Fisher Scientific)], and 1% bovine serum albumin. For antibodies raised in mouse, Mouse-on-Mouse blocking reagent (Vectorlab, MKB-2213-1) was used, as per the manufacturer's protocol. A range of conjugated and unconjugated antibodies were used (**Table 1**). In brief, the sections were stained overnight at 4°C or for 2 h at room temperature, then washed, and incubated with corresponding secondary antibodies for 2 h at room temperature. The sections were mounted in Fluoromount-GTM with DAPI (Invitrogen). Fluorescence microscopy images were obtained using a slide scanner Axioscan 2.1 (Zeiss, Cambridge, UK). Vessel density was quantified as the percentage of Isolectin IB4$^+$ cells measured at the infarct border using a vessel density Fiji macro. For Edu quantification, after Click-iT Edu Imaging Kit with Alexa Fluor 647, Edu$^+$/Troponin T$^+$ cells were manually counted at the infarct border.

Ligand–receptor interaction analysis

To investigate the potential hESC-EC and -MES ligand–receptor interactions (LRIs) from our previously published hESC-ECP dataset (GEO; GSE131736), we mined a publicly available (ArrayExpress: E-MTAB-7895) 10x Chromium C57BL/6J mouse cardiomyocyte-free scRNAseq dataset from naive, 1-, and 3-day CAL mouse hearts (15) with CellPhoneDB (16), similar to network analysis conducted by Wang and colleagues in ligated neonatal hearts (17).

CellPhoneDB (16) was used to identify potential ligand–receptor interactions (LRIs) between the hESC-ECP (GEO; GSE131736) and resident cardiac populations in a publicly available C57BL/6J mouse cardiomyocyte-free scRNA-seq dataset from naive, 1-, and 3-day CAL mouse hearts (15).

Data for the mouse cardiac MI were downloaded from ArrayExpress (E-MTAB-7895) and subsequently processed using the 10X Cell Ranger pipeline (v3.1.0) with the 10X pre-built Cell Ranger mm10-3.0.0 reference. Custom quality control was performed using the Scater package (18) using data from the standard filtered matrices. Cells with a total UMI count exceeding 4 median absolute deviations (MADs) from the median value or with fewer than 200 genes identified were removed from downstream analysis. In addition, the cells with a high proportion of counts from mitochondrial genes (>4 MADs) were also excluded. Prior to merging datasets, data normalization was performed using the MultiBatchNormalisation (19) to minimize batch effects between datasets. The top 2,000 most variable genes were subsequently identified using the standard FindVariableFeatures method (20). Normalized data were then scaled using the standard ScaleData method (20) and principal component analysis conducted using the previously identified variable genes. Harmony correction

TABLE 1 Immunofluorescence antibodies and dilutions.

Primary antibodies (dilution)	Manufacturer
Isolectin GS-IB4 (*Griffonia simplicifolia)* α-biotin Strep Conjugate	Thermofisher, 121414
Troponin T (1:40)	Invitrogen, MA5-12960
α-Smooth Muscle Actin Cy3 (1:100)	Sigma, C6198
Secondary antibodies (dilution)	**Manufacturer**
Streptavidin, Alexa Fluor^{Tm} 647 conjugate	Thermo Fisher, S21374
Goat anti mouse 568 (1:300)	Invitrogen, A-11004

was implemented when integrating datasets, following the standard workflow (21). The cells were clustered and projected using UMAP implementing the standard Seurat workflow and utilizing the corrected harmony reduction embedding values (20). Clusters were annotated based on the cluster marker genes, as described previously (15). Day 8 hESC-ECP scRNA-seq data were processed, as previously described (11).

At day 8, the cells were mixed 1:1 with trypan blue to identify dead cells, visualized, quantified (Bio-Rad, HertfordshiHuman orthologs for mouse genes were identified using the BioMart package (22) and used to replace mouse gene names in the dataset in order to run CellPhoneDB ligand–receptor analysis (16). Mouse genes with no identified human ortholog were removed from downstream analysis. Count values from the mouse cardiac MI data were then merged with count values from the hESC-ECP data, and data normalization performed using the standard Seurat NormalizeData method (20). Normalized count data were then used as input into the CellPhoneDB package, which was run using the statistical method with 100 iterations and a *P*-value threshold of 0.05.

Statistical analyses

At day 8, the cells were mixed 1:1 with trypan blue to identify dead cells, visualized, quantified (Bio-Rad, HertfordshiPower calculations were performed to determine the minimum sample size required to achieve statistical significance for left ventricular (LV) function at 14 d. For CAL procedures, with a power of 80% and a 5% chance of type I error, 12 mice/group are required. At an 80% survival rate, 15 mice/group are needed.

Data were analyzed in JMP 12 (SAS Institute, Inc., Cary, North Carolina, USA). Distribution was verified with the Shapiro–Wilk test, and non-parametric data were log-transformed, where necessary. Echocardiography outcomes were analyzed by ANOVA with Tukey's *post-hoc* testing, where appropriate. Student's *t*-test was conducted, where appropriate. Data were graphed in GraphPad Prism 9 (GraphPad Software Inc., USA) and are presented as the mean ± SEM and significance indicated.

Results

Human embryonic stem cell-derived endothelial cell product differentiation is efficient and reproducible

In total, three differentiations were produced. Cells (**Figure 2A**) comprised 69.6% ± 4.0 $CD31^+/CD144^+$ (EC) at day 6 and 83.5% ± 3.3 at day 8 (**Figures 2B,C**). Staining for pluripotent markers at day 8 revealed cells to be 0.08% ± 0.01 $TRA160^+/SSEA3^+$ (**Supplementary Figure 1**). Finally, 2.6 × 10^6 cells were harvested per T75 flask with 97% ± 0.6 viability.

Human embryonic stem cell-derived endothelial cell product injection reduces risk area, but not initial infarct area

At 1 day post-injection, the infarct risk area was significantly reduced in the CALC mice compared with CALM (**Figure 3A**), while there was no difference in the infarct area at 1 day post-ligation in CALM and CALC mice (**Figure 3B**), as determined by TTC staining (**Figure 3C**). The infarct area

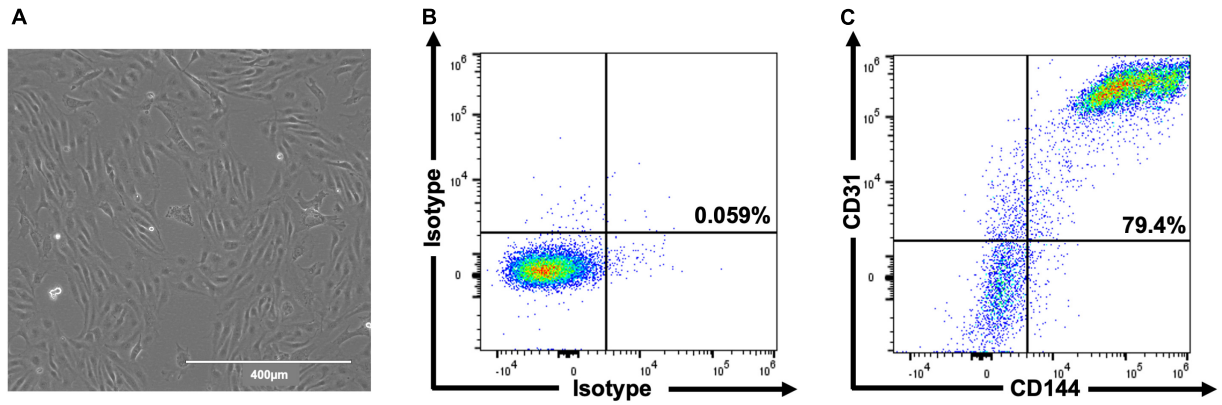

FIGURE 2
Representative images of hESC-ECP differentiation and phenotypic characterization. Day 8 morphology and confluency **(A)** and representative flow cytometric analysis **(B,C)** of isotype controls and hESC-ECP stained for CD31 (PECAM1) and CD144 (VE-cadherin).

10.3389/fcvm.2022.953211

of the CALD mouse that survived to 1 d post-injection was 88% of the risk area and 75% of the total left ventricle area.

Human embryonic stem cell-derived endothelial cell product injection preserves left ventricular function and structure

Cell injection prevented CAL-induced cardiac dilation at 7 and 14 days post-injection (**Figures 4C,D**), preserved ejection fraction at 7 days, and slowed progression of reduced ejection fraction in CALM mice at 14 days (**Figure 4A**). While there were no observed differences in the mitral valve E/A wave ratio (**Figure 4E**) or myocardial performance index (**Figure 4F**) amongst groups, global longitudinal strain analysis suggested that hESC-ECP injection slowed the progression toward heart failure (**Figure 4B**).

Human embryonic stem cell-derived endothelial cell product injection reduces infarct area and collagen deposition at 14 days

In order to study the effect of hESC-ECP injection on cardiac remodeling, we performed immunohistochemical assessment of the mature infarct area at 14 days by MT and PSR staining. Cell injection reduced collagen deposition (CALM: 35.6 ± 6.0%, CALC: 15.6 ± 5.8%) (**Figures 5A,E**), and infarct volume was significantly reduced in the CALC mice compared with CALM (CALM: 54.5 ± 5.0%, CALC: 21.3 ± 4.9%) (**Figures 5B,F**). There were no differences in isolectin B4 perfused vascular density (**Figures 5C,G**) or myocardial regeneration (**Figures 5D,H**) between the groups.

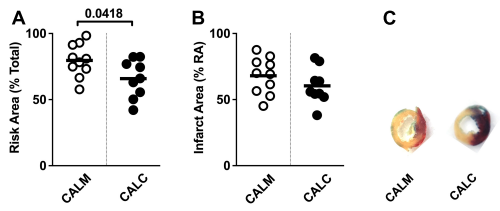

FIGURE 3
1-Day infarct area following hESC-ECP or media injection. Risk area (%) of LV area below the suture **(A)**, infarct area,% **(B)** within the risk area, and **(C)** representative sections 1 d post-infarct in CALM, n = 11, and CALC, n = 10 groups. Student's t-test; data are presented as individual points and as mean ± SEM.

Ligand–receptor interaction analysis reveals predicted interactions between the human embryonic stem cell-derived endothelial cell product and resident post-coronary artery ligation cardiac populations

Dimension reduction and clustering analysis of cardiomyocyte-free scRNA-seq data from C57BL/6J naive, 1 day, and 3 days post-infarcted hearts identified populations comparable to those originally identified by Forte et al. (15) (**Figure 6A**). Following merging with data from the day 8 hESC-ECP (11), ligand–receptor interaction (LRI) analysis predicted multiple interactions between component populations of the day 8 hESC-ECP (EC and mesenchymal) and resident cardiac immune (NK and macrophage) and stromal (myofibroblast and fibroblast) populations (**Figure 6B**). In keeping with our observation of modified infarct formation, both EC and mesenchymal populations of the hESC-ECP expressed fibronectin (*FN1*) and collagens (*COL3A1* and *COL4A1)* known to form complexes with integrins to modulate myofibroblast function (23) (**Figure 6C**). Both hESC-ECP component populations also expressed the *HLA-E* ligand, known to supress NK activity *via* the KLRD1/KLRC1 receptor (24).

Discussion

This study shows that hESC-ECP injection in the infarcted heart improves functional and structural outcomes in a mammalian paradigm of heart failure. LR complexes within immune and myo-/fibroblast niches suggest a potential mechanism for pathological reprogramming with delivery of live hESC-ECP independent of cellular integration. Potentially due to time-dependent LRIs between live hESC-ECs and -MESs, and resident endothelial cells, monocytes, macrophages, fibroblasts, and myofibroblasts, the acute tissue remodeling window through 3 days post-ligation is a powerful and dynamic environment in which to effect change in the infarcted heart.

Through ultrasound echocardiography and longitudinal strain analyses, we demonstrate that intracardiac hESC-ECP injection (CALC) of 1 × 10^6 cells within the peri-infarct region in the CAL model of myocardial infarction (MI) preserves the left ventricle ejection fraction (EF) and reduces ventricular dilation 14 days post-injection compared with media-injected (CALM) in Crl:CD1-*Foxn1*^{nu} mice. Greater end-diastolic volume (EDV) and end-systolic volume (ESV) in the CALM mice suggest that hESC-ECP injection preserves functional myocardium and abrogates CAL-induced ventricular dilation. Additionally, we demonstrate that at 1 day post-surgery, the infarct area is comparable in the CALC and CALM mice, suggesting that subsequent scar remodeling and myocardial

10.3389/fcvm.2022.953211

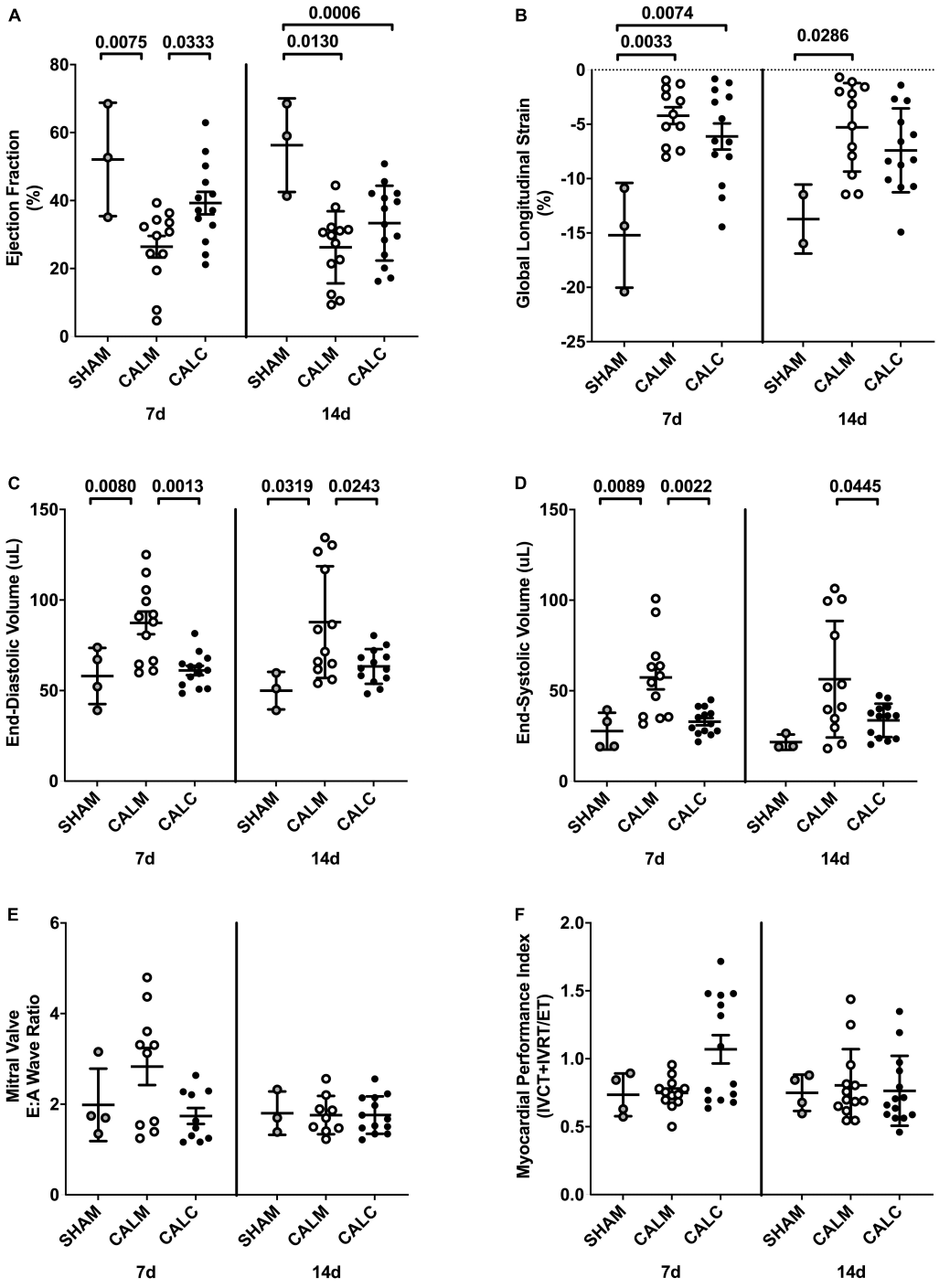

FIGURE 4
Echocardiography outcomes in hESC-ECP and media injected mice. Ejection fraction **(A)** was preserved in CALC mice compared to CALM at 7 d, but not at 14 d post-injection. Global longitudinal strain **(B)** was increased at 7 d in both CALC and CALM compared with SHAM, but only in CALM mice at 14 d. End-diastolic volume, EDV **(C)**, and end-systolic volume, ESV **(D)**, were preserved at 7 and 14 d in CALC compared with CALM mice. Mitral valve E/A wave ratio **(E)** and myocardial performance index **(F)** were not different amongst groups at either time point. ANOVA with Tukey's *post-hoc* test. Data are mean ± SEM.

function are independent of initial infarct size. Analyses suggest that hESC-ECP injection may influence acute myocardial survival, fibroblast maturation, and preserve contractile myocardium 14 days post-treatment, which integrates into the mature scar. These first studies in the setting of MI suggest that improved functional outcomes in parallel with clear,

10.3389/fcvm.2022.953211

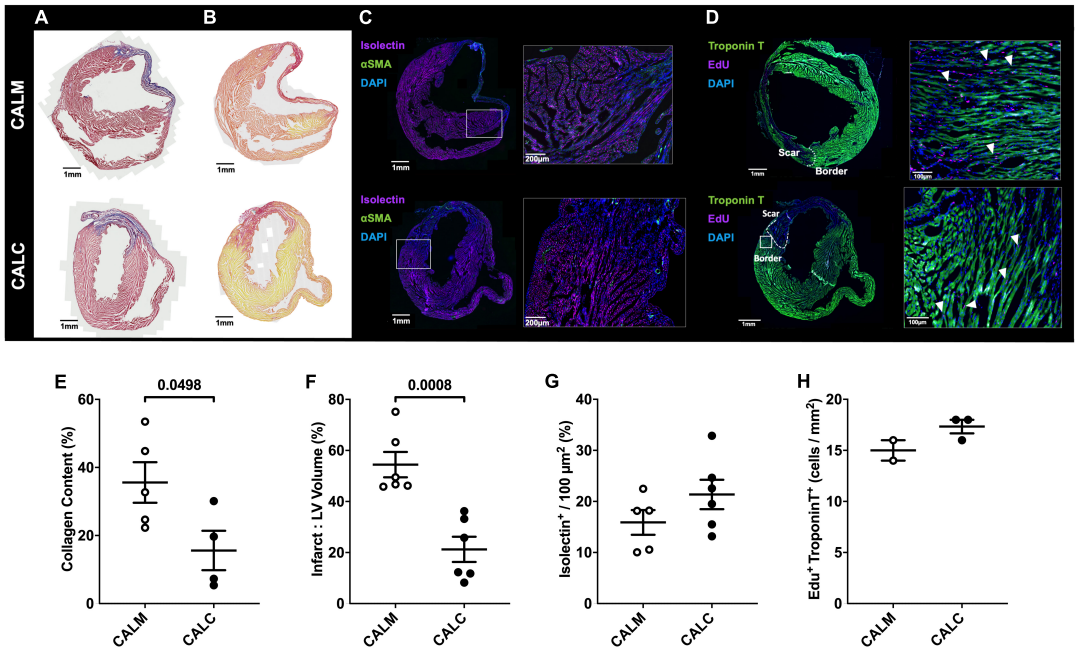

FIGURE 5
Immunohistochemical assessment of mature infarct area and myocardial characteristics. Collagen deposition **(A,E)** and infarct volume **(B,F)** were significantly reduced in CALC mice compared with CALM. There were no differences in isolectin B4 perfused vascular density **(C,G)** or myocardial regeneration **(D,H)** between the groups. Student's *t*-test; data are mean ± SEM. White arrows **(D)** indicate Edu + Troponin T + cells.

time-bound histological changes are indicative of divergent tissue remodeling pathways in hESC-ECP-injected mice.

Recent pre-clinical testing of other stem cell-based therapies suggests a complex mechanism of efficacy (5, 25). Rather than providing a consistent, well-described outcome in the preservation or recovery of cardiac tissue, these interventions demonstrate diverse effects on resident cardiac cell populations, inducing localized immune activation (15, 26), potentially *via* paracrine mechanisms (27). Vagnozzi and colleagues have recently reported that transplanted mouse-on-mouse cell products enhance inflammation and direct immune cell trafficking, modulating the chronic inflammatory profile post-MI due to cell death (6). However, based on our preliminary LRI, this conclusion may not be fully pertinent herein and not be generalizable to all stem cell-based therapies. The potential for direct interaction with resident cell populations suggests that a viable cell product may be necessary. LRI analyses suggest that the hESC-EC and -MES have the potential for cell–cell crosstalk with stromal and immune cell types, including cell signaling, that may influence immune cell recruitment and infiltration into the injured heart (CCL23, CCL4L2, KLRC1, KLRK1) and cardiac remodeling (IGF2R and collagen– and fibronectin–integrin complexes a1b1 and a5b1, respectively). Although historically transgenic immunocompromised mice have been used in cardiac cell therapy studies to avoid immune-induced xenograft failure and the effects of pharmacological immunosuppression, recent work suggests that transgenic mice are able to mount a robust immune response in CAL (28). Characterization of the modified LRI response in transgenic immunocompromised mice would help identify the biological factors influencing disease severity in CAL (15).

The extent of injury, quality of repair, and the breadth of myocardial remodeling are intricately linked to the intensity of the inflammatory response. Ischemic injury leads to the dynamic recruitment and mobilization of a range of innate and adaptive immune cells that contribute to the development of a mature scar, and modification of fibroblast and myofibroblast remodeling. As fibroblast proliferation and immune cell activation peak 2–4 days post-MI (15, 29), future investigations of the early post-treatment therapeutic response could identify druggable networks during the acute remodeling window. Neutrophils are initially recruited to clear necrotic tissue, in our studies peaking in the heart 24–48 h post-MI. Ly6C^{high} monocytes, precursors of the "classical" inflammatory macrophage, are recruited from splenic and bone marrow reservoirs and localize to the area of damage. Macrophages dominate during the early immune response, clearing apoptotic neutrophils and necrotic debris by 3–7 days post-infarct. Accumulating monocytes give rise to tissue macrophages with a reparative phenotype, initiating neo-angiogenesis and fibroblast collagen production, while attenuating inflammation. Within several weeks, monocyte recruitment subsides and a mature scar forms within the infarcted region (26, 30, 31). The dynamic post-MI inflammatory response is influenced by

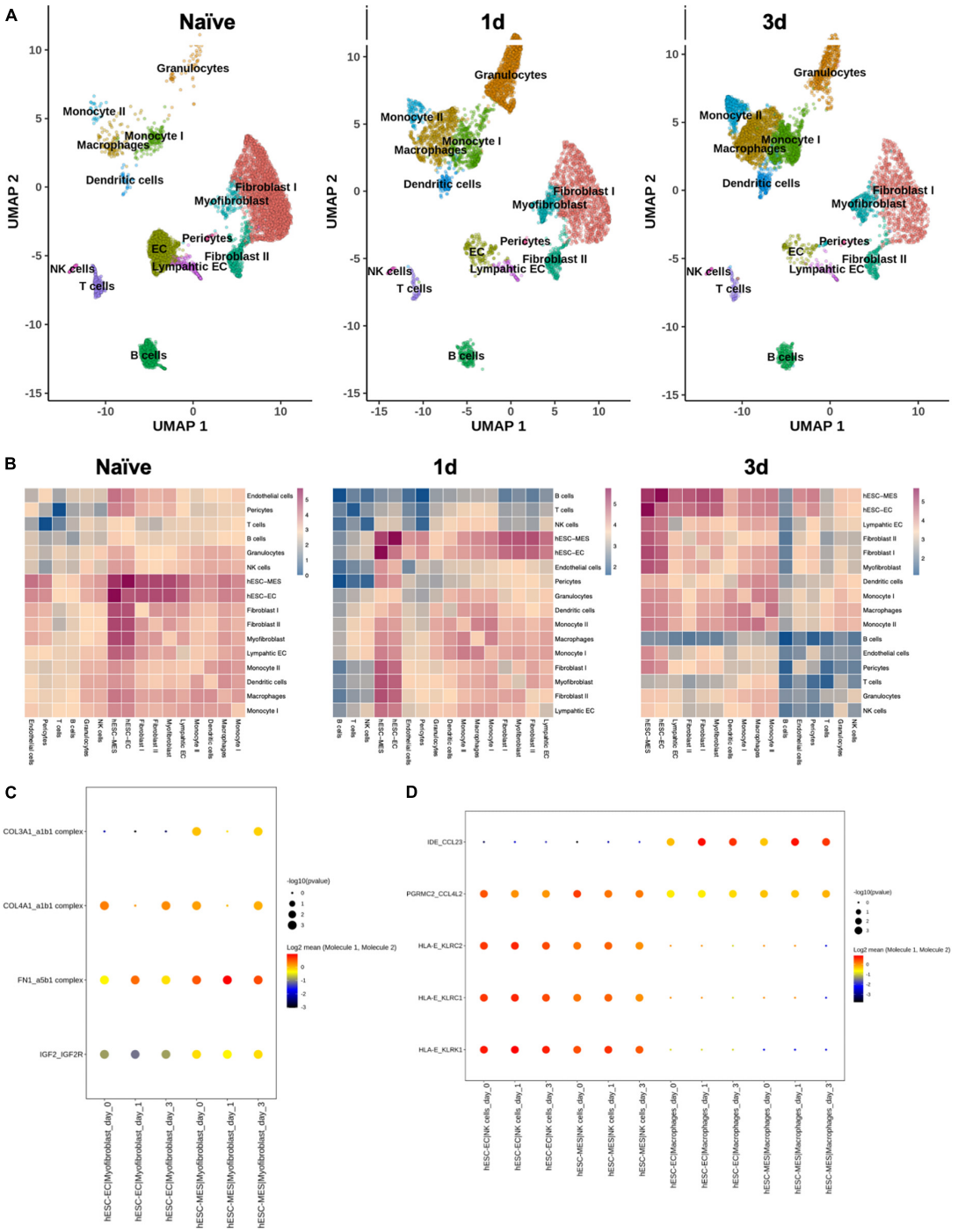

FIGURE 6
Ligand–receptor interactions between hESC-ECP constituents and resident cardiac populations. **(A)** UMAP projection of clusters identified from cardiomyocyte-free scRNA-seq data of C57BL/6J hearts taken either prior to CAL (naive), or 1 or 3 days post-CAL. **(B)** Ligand–receptor interaction (LRI) analysis between day eight hESC-ECP populations and resident cardiac populations at each timepoint. Heatmaps illustrate $\log_{10}$(number of predicted LRI) between each population. Dot plots of LRIs between hESC-ECP populations and **(C)** myofibroblasts and **(D)** NK and macrophages.

immune cell localization and expansion of immune cells within the associated pericardial adipose tissue, an organ rich in B cells (32–36). Adverse remodeling can be caused by excessive or deficient inflammatory cell recruitment into the heart post-MI (26, 30, 31, 37). Thus, targeted immunomodulation offers a powerful approach to improve pathological cardiac remodeling. hESC-ECP therapy could serve to reprogramme subsequent scar formation *via* inflammatory or immune

mechanisms, modifying fibroblast remodeling and preserving functional myocardium, subsequently improving clinically relevant physiological outcomes.

It is important to note the limitations of this study. We have focused on the effect in a relatively acute setting; thus, extended long-term studies need to be performed in the future to elucidate downstream effects in a more translational paradigm of heart failure. While we provide evidence of potential mechanisms of action, we have not formally assessed this and confirmed *via* independent techniques. Additionally, our ECP is a combination of both endothelial-like and mesenchymal-like cells (10, 11), and we do not know which component, or indeed if both populations, are required for the phenotype. Our utilization of dead cell materials, which has previously been suggested to induce immune-mediated remodeling, was unsuccessful and would require extensive development in the future. Furthermore, we were not able to demonstrate cellular integration. However, in a prior study, in the setting of peripheral limb ischemia, we demonstrated that our ECP is not likely to survive a prolonged period of time (beyond 24 h; 75% lost at 24 h) (10); thus, assessing cellular integration is unlikely to provide evidence of causality. Further studies will address these issues.

Data availability statement

The original contributions presented in this study are included in the article/**Supplementary material**, further inquiries can be directed to the corresponding author.

Ethics statement

The animal study was reviewed and approved by the University of Edinburgh Animal Welfare and Ethical Review Board (AWERB), under project (70/8933, approved 29/04/2016).

Author contributions

A-MS, IM, MB, JM, GG, and AHB: conceptualization. A-MS, IM, MM-P, AT, MB, JM, GG, and AHB: methodology. A-MS, IM, and MM-P: formal analysis. A-MS, MM-P, and AT: investigation. A-MS, GG, and AHB: resources. A-MS and IM: data curation and visualization. A-MS, MM-P, and CB: writing – original draft preparation. A-MS, JM, PH, GG, and AHB: supervision. A-MS and GG: project administration. MB and AHB: funding acquisition. All authors contributed to writing – review and editing, read, and agreed to the published version of the manuscript.

Funding

The British Heart Foundation supported this work (Program grant: RG/14/3/30706 to AHB, and project grant and FS/17/27/32698 to AHB). AHB was supported by the British Heart Foundation Chair of Translational Cardiovascular Sciences (CH/11/2/28733), European Research Council (EC 338991 VASCMIR). AHB, MB, and A-MS are supported by the BHF Centre for Vascular Regeneration (RM/17/3/33381), and AHB and MB are supported by the BHF Regenerative Medicine Centre (RM/13/2/30158). MB was supported by the British Heart Foundation (FS/16/4/31831).

Acknowledgments

We are grateful to the staff of the University of Edinburgh Biomedical and Veterinary Sciences for their excellent technical assistance. Cell culture was conducted in the MRC Centre for Regenerative Medicine facility, University of Edinburgh. Flow cytometry data were generated with support from the QMRI Flow Cytometry and cell sorting facility, University of Edinburgh. Histological stains were generated with support from the Shared University Research Facilities (SuRF), University of Edinburgh.

Conflict of interest

The authors declare that the research was conducted in the absence of any commercial or financial relationships that could be construed as a potential conflict of interest.

Publisher's note

Supplementary material

The Supplementary Material for this article can be found online at: https://www.frontiersin.org/articles/10.3389/fcvm.2022.953211/full#supplementary-material

SUPPLEMENTARY FIGURE 1
Day 8 representative flow cytometric analysis of **(A)** isotype controls and **(B)** hESC-ECP stained for pluripotent markers TRA160C and SSEA3C.

References

1. BHF (2020). Available online at: http://www.bhf.org.uk (2020). (accessed April 9, 2021).

2. WHO. *Cardiovascular Diseases (CVDs)*. Geneva: WHO (2015).

3. Roger VL, Go AS, Lloyd-Jones DM, Adams RJ, Berry JD, Brown TM, et al. Heart disease and stroke statistics–2011 update: a report from the American heart association. *Circulation.* (2011) 123:e18–209. doi: 10.1161/CIR.0b013e3182009701

4. Bargehr J, Ong LP, Colzani M, Davaapil H, Hofsteen P, Bhandari S, et al. Epicardial cells derived from human embryonic stem cells augment cardiomyocyte-driven heart regeneration. *Nat Biotechnol.* (2019) 37:895–906. doi: 10.1038/s41587-019-0197-9

5. Braunwald E. Cell-Based therapy in cardiac regeneration: an overview. *Circ Res.* (2018) 123:132.

6. Vagnozzi RJ, Maillet M, Sargent MA, Khalil H, Johansen AKZ, Schwanekamp JA, et al. An acute immune response underlies the benefit of cardiac stem cell therapy. *Nature.* (2020) 577:405–9. doi: 10.1038/s41586-019-1802-2

7. Li Z, Wilson KD, Smith B, Kraft DL, Jia F, Huang M, et al. Functional and transcriptional characterization of human embryonic stem cell-derived endothelial cells for treatment of myocardial infarction. *PLoS One* (2010) 4:e8443. doi: 10.1371/journal.pone.0008443

8. Madonna R, Van Laake LW, Davidson SM, Engel FB, Hausenloy DJ, Lecour S, et al. Position paper of the European society of cardiology working group cellular biology of the heart: cell-based therapies for myocardial repair and regeneration in ischemic heart disease and heart failure. *Eur Heart J.* (2016) 37:1789–98. doi: 10.1093/eurheartj/ehw113

9. Kane NM, Meloni M, Spencer HL, Craig MA, Strehl R, Milligan G, et al. Derivation of endothelial cells from human embryonic stem cells by directed differentiation: analysis of microRNA and angiogenesis in vitro and in vivo. *Arterioscler Thromb Vasc Biol.* (2010) 30:1389–97. doi: 10.1161/ATVBAHA.110.204800

10. MacAskill MG, Saif J, Condie A, Jansen MA, MacGillivray TJ, Tavares AS, et al. Robust revascularisation in multiple models of limb ischemia using a clinically translatable human stem cell-derived endothelial cell product. *Mol Ther.* (2018) 26:1669–84. doi: 10.1016/j.ymthe.2018.03.017

11. McCracken IR, Taylor RS, Kok FO, de la Cuesta F, Dobie R, Henderson BEP, et al. Transcriptional dynamics of pluripotent stem cell-derived endothelial cell differentiation revealed by single-cell RNA sequencing. *Eur Heart J.* (2020) 41:1024–36. doi: 10.1093/eurheartj/ehz351

12. Fadini GP, Spinetti G, Santopaolo M, Madeddu P. Impaired regeneration contributes to poor outcomes in diabetic peripheral artery disease. *Arterioscler Thromb Vasc Biol.* (2020) 40:34–44. doi: 10.1161/ATVBAHA.119.312863

13. Kilkenny C, Browne W, Cuthill IC, Emerson M, Altman DG. Animal research: reporting in vivo experiments: the ARRIVE guidelines. *Br J Pharmacol.* (2010) 160:1577–9.

14. Spiroski A-M, Sanders R, Meloni M, McCracken IR, Thomson A, Brittan M, et al. The influence of the LINC00961/SPAAR locus loss on murine development, myocardial dynamics, and cardiac response to myocardial infarction. *Int J Mol Sci.* (2021) 22:969. doi: 10.3390/ijms22020969

15. Forte E, Skelly DA, Chen M, Daigle S, Morelli KA, Hon O, et al. Dynamic interstitial cell response during myocardial infarction predicts resilience to rupture in genetically diverse mice. *Cell Rep.* (2020) 30:3149–63.e6. doi: 10.1016/j.celrep.2020.02.008

16. Efremova M, Vento-Tormo M, Teichmann SA, Vento-Tormo R. CellPhoneDB: inferring cell–cell communication from combined expression of multi-subunit ligand–receptor complexes. *Nat Protoc.* (2020) 15:1484–506. doi: 10.1038/s41596-020-0292-x

17. Wang Z, Cui M, Shah AM, Tan W, Liu N, Bassel-Duby R, et al. Cell-type-specific gene regulatory networks underlying murine neonatal heart regeneration at single-cell resolution. *Cell Rep.* (2020) 33:108472.

18. McCarthy DJ, Campbell KR, Lun AT, Wills QF. Scater: pre-processing, quality control, normalization and visualization of single-cell RNA-seq data in R. *Bioinformatics.* (2017) 33:1179–86. doi: 10.1093/bioinformatics/btw777

19. Haghverdi L, Lun AT, Morgan MD, Marioni JC. Batch effects in single-cell RNA-sequencing data are corrected by matching mutual nearest neighbors. *Nat Biotechnol.* (2018) 36:421–7. doi: 10.1038/nbt.4091

20. Stuart T, Butler A, Hoffman P, Hafemeister C, Papalexi E, Mauck WM III, et al. Comprehensive integration of single-cell data. *Cell.* (2019) 177:1888–902.

21. Korsunsky I, Millard N, Fan J, Slowikowski K, Zhang F, Wei K, et al. Fast, sensitive and accurate integration of single-cell data with harmony. *Nat Methods.* (2019) 16:1289–96. doi: 10.1038/s41592-019-0619-0

22. Durinck S, Spellman PT, Birney E, Huber W. Mapping identifiers for the integration of genomic datasets with the R/Bioconductor package biomaRt. *Nat Protoc.* (2009) 4:1184. doi: 10.1038/nprot.2009.97

23. Bagchi RA, Roche P, Aroutiounova N, Espira L, Abrenica B, Schweitzer R, et al. The transcription factor scleraxis is a critical regulator of cardiac fibroblast phenotype. *BMC Biol.* (2016) 14:21. doi: 10.1186/s12915-016-0243-8

24. Orr MT, Lanier LL. Natural killer cell education and tolerance. *Cell.* (2010) 142:847–56.

25. Baker AH, Brittan M. Lost in translation: progress and challenges in advanced therapies to treat CVDs. *Mol Ther.* (2021) 29:426–7. doi: 10.1016/j.ymthe.2021.01.014

26. Gray GA, Toor IS, Castellan RFP, Crisan M, Meloni M. Resident cells of the myocardium: more than spectators in cardiac injury, repair and regeneration. *Curr Opin Physiol.* (2018) 1:46–51. doi: 10.1016/j.cophys.2017.08.001

27. Gu M, Nguyen PK, Lee AS, Xu D, Hu S, Plews JR, et al. Microfluidic single-cell analysis shows that porcine induced pluripotent stem cell–derived endothelial cells improve myocardial function by paracrine activation. *Circ Res.* (2012) 111:882–93. doi: 10.1161/CIRCRESAHA.112.269001

28. van Zuylen V-L, den Haan MC, Roelofs H, Fibbe WE, Schalij MJ, Atsma DE. Myocardial infarction models in NOD/Scid mice for cell therapy research: permanent ischemia vs ischemia-reperfusion. *Springerplus.* (2015) 4:336. doi: 10.1186/s40064-015-1128-y

29. Fu X, Khalil H, Kanisicak O, Boyer JG, Vagnozzi RJ, Maliken BD, et al. Specialized fibroblast differentiated states underlie scar formation in the infarcted mouse heart. *J Clin Invest.* (2018) 128:2127–43.

30. Swirski FK, Nahrendorf M. Cardioimmunology: the immune system in cardiac homeostasis and disease. *Nat Rev Immunol.* (2018) 18:733–44.

31. Dittrich A, Lauridsen H. Myocardial infarction and the immune response - Scarring or regeneration? A comparative look at mammals and popular regenerating animal models. *J Immunol Regen Med.* (2019) 4:100016.

32. Wu L, Dalal R, Cao CD, Postoak JL, Yang G, Zhang Q, et al. IL-10–producing B cells are enriched in murine pericardial adipose tissues and ameliorate the outcome of acute myocardial infarction. *Proc Natl Acad Sci USA.* (2019) 116:21673–84. doi: 10.1073/pnas.1911464116

33. Jackson-Jones LH, Duncan SM, Magalhaes MS, Campbell SM, Maizels RM, McSorley HJ, et al. Fat-associated lymphoid clusters control local IgM secretion during pleural infection and lung inflammation. *Nat Commun.* (2016) 7:12651. doi: 10.1038/ncomms12651

34. Bénézech C, Luu N-T, Walker JA, Kruglov AA, Loo Y, Nakamura K, et al. Inflammation-induced formation of fat-associated lymphoid clusters. *Nat Immunol.* (2015) 16:819–28. doi: 10.1038/ni.3215

35. Horckmans M, Bianchini M, Santovito D, Megens RTA, Springael J-Y, Negri I, et al. Pericardial adipose tissue regulates granulopoiesis, fibrosis, and cardiac function after myocardial infarction. *Circulation.* (2018) 137:948–60. doi: 10.1161/CIRCULATIONAHA.117.028833

36. Mylonas KJ, Jackson-Jones LH, Andrews JPM, Magalhaes MS, Meloni M, Joshi NV, et al. The pericardium promotes cardiac repair and remodelling post-myocardial infarction. *bioRxiv.* (2019) [Preprint] 2019:771154. doi: 10.1101/771154

37. Toor IS, Rückerl D, Mair I, Thomson A, Rossi AG, Newby DE, et al. Enhanced monocyte recruitment and delayed alternative macrophage polarization accompanies impaired repair following myocardial infarction in C57BL/6 compared to BALB/c mice. *Clin Exp Immunol.* (2019) 198:83–93. doi: 10.1111/cei.13330

frontiers | Frontiers in Cardiovascular Medicine

TYPE Original Research
PUBLISHED 20 October 2022
DOI 10.3389/fcvm.2022.948281

OPEN ACCESS

EDITED BY
Ajit Magadum,
Temple University, United States

REVIEWED BY
Felix B. Engel,
University Hospital Erlangen, Germany
Miao Cui,
University of Texas Southwestern Medical Center, United States
Gabriele D'Uva,
University of Bologna, Italy

*CORRESPONDENCE
Catherine H. Wilson
chw39@cam.ac.uk

†These authors have contributed equally to this work

SPECIALTY SECTION
This article was submitted to Cardiovascular Biologics and Regenerative Medicine, a section of the journal Frontiers in Cardiovascular Medicine

RECEIVED 19 May 2022
ACCEPTED 27 September 2022
PUBLISHED 20 October 2022

CITATION
Boikova A, Bywater MJ, Quaife-Ryan GA, Straube J, Thompson L, Ascanelli C, Littlewood TD, Evan GI, Hudson JE and Wilson CH (2022) HRas and Myc synergistically induce cell cycle progression and apoptosis of murine cardiomyocytes.
Front. Cardiovasc. Med. 9:948281.
doi: 10.3389/fcvm.2022.948281

HRas and Myc synergistically induce cell cycle progression and apoptosis of murine cardiomyocytes

Aleksandra Boikova[1†], Megan J. Bywater[2,3†], Gregory A. Quaife-Ryan[3], Jasmin Straube[3], Lucy Thompson[1], Camilla Ascanelli[1], Trevor D. Littlewood[2], Gerard I. Evan[2], James E. Hudson[3] and Catherine H. Wilson[1*]

[1]Department of Pharmacology, University of Cambridge, Cambridge, United Kingdom, [2]Department of Biochemistry, University of Cambridge, Cambridge, United Kingdom, [3]QIMR Berghofer Medical Research Institute, Herston, QLD, Australia

Aim: Adult mammalian cardiomyocytes are incapable of significant proliferation, limiting regeneration after myocardial injury. Overexpression of the transcription factor Myc has been shown to drive proliferation in the adult mouse heart, but only when combined with Cyclin T1. As constitutive HRas activity has been shown to stabilise Cyclin T1 *in vivo*, we aimed to establish whether Myc and HRas could also act cooperatively to induce proliferation in adult mammalian cardiomyocytes *in vivo*.

Methods and results: Using a genetically modified mouse model, we confirmed that constitutive HRas activity ($HRas^{G12V}$) increased Cyclin T1 expression. $HRas^{G12V}$ and constitutive Myc expression together co-operate to drive cell-cycle progression of adult mammalian cardiomyocytes. However, stimulation of endogenous cardiac proliferation by the ectopic expression of $HRas^{G12V}$ and Myc also induced cardiomyocyte death, while Myc and Cyclin T1 expression did not.

Conclusion: Co-expression of Cyclin T1 and Myc may be a therapeutically tractable approach for cardiomyocyte neo-genesis post injury, while cell death induced by $HRas^{G12V}$ and Myc expression likely limits this option as a regenerative therapeutic target.

KEYWORDS

Myc (c-Myc), HRas gene, cardiomyocyte, proliferation, cell-cycle

Introduction

The adult heart is one of the least regenerative organs of the human body. Shortly after birth of a mammal, cardiomyocytes exit the cell cycle and are subsequently characterised by a reduced rate of turnover (<1% per year in humans) (1). Consequently, if the adult mammalian heart is damaged (e.g., myocardial infarction), the default response is to replace the lost cardiomyocytes with non-contractile fibrotic scar tissue and cardiomyocyte hypertrophy which frequently lead to heart failure. A number of strategies have been proposed to promote myocardial regeneration post damage, including the direct injection of stem cells or stem cell-derived cardiomyocytes, direct reprogramming of non-myocytes into cardiomyocytes and endogenous cardiomyocyte proliferation (2). Endogenous cardiomyocyte proliferation requires driving the resident quiescent cardiomyocytes into a productive mitogenic cell cycle. Genetic lineage tracing studies in the regenerative neonatal mouse and zebrafish hearts indicate that the majority of newly generated cardiomyocytes are derived from endogenous cardiomyocyte proliferation rather than differentiation from a mesenchymal progenitor (3–5). These studies suggest that forced cardiomyocyte proliferation is a viable strategy for myocardial regeneration and several potential factors capable of reactivating endogenous proliferation of cardiomyocytes in adult hearts have been identified, for example, inhibition of Hippo protein kinase signalling, enforced expression of cell cycle regulators, inactivation of thyroid hormone signalling, and hypoxia, all induce regeneration (6–10). We have recently shown that combined ectopic expression of Myc and Cyclin T1 can lead to extensive cardiomyocyte proliferation in the mouse heart (11), although exploitation of the therapeutic potential requires further exploration.

Myc is a pleiotropic transcription factor that, amongst other activities, regulates cell growth and proliferation in mammalian cells (12). Consequently, Myc expression in normal cells is tightly regulated. Following damage in a regenerative tissue, the release of mitogens stimulates a transient increase in the short-lived Myc protein followed by a transient proliferative response (13). In contrast, Myc transcriptional programmes decrease during postnatal cardiac maturation and fail to reactivate post-infarction (14). Moreover, even when Myc expression is driven ectopically in the adult mammalian heart, it is unable to activate transcription of many target genes and cardiomyocytes remain almost entirely resistant to proliferation (11, 15). We previously established that Myc-driven transcription, and consequently cell proliferation, are critically dependent on the level of Cyclin T1 in cardiomyocytes (11).

Cyclin T1 strongly associates with CDK9 to form the positive transcription elongation factor b (P-TEFb) (16) that phosphorylates paused RNA PolII and the elongation factors DSIF and NELF, leading to productive transcriptional elongation (16, 17). Both components of P-TEFb, Cyclin T1 and CDK9 are tightly regulated by various transcriptional and post-transcriptional mechanisms (18, 19). P-TEFb is also dynamically controlled by an association with an inactivation complex (7SK snRNA, Larp7, MEPCE, and HEXIM) (20, 21). Unlike other cyclin-dependent kinases, CDK9 protein stability is not cell cycle dependent (22), but is primarily determined by binding to Cyclin T1 (23, 24). The level of the Cyclin T1 protein is thus the key factor in controlling the amount of the P-TEFb complex in a cell (23, 24). During postnatal cardiac maturation in mice the level of P-TEFb and phosphorylated RNA PolII steadily decline (11). Transgenic overexpression of Cyclin T1 in the heart leads to increased levels of both CDK9 and phosphorylated RNA PolII and, when expressed throughout development, leads to cardiac hypertrophy (11, 25, 26).

The RAS proteins (K-RAS, N-RAS, and H-RAS in humans) are small GTPases that function as molecular switches, cycling between their "off" GDP-bound and "on" GTP-bound states in response to mitogenic signalling (27). Depending on the cellular context, Ras can activate several downstream pathways that regulate protein synthesis, cell growth, survival, and cell motility (28), in the heart, Ras activation leads to reversible cardiac hypertrophy (29, 30). Hypertrophy, be it transgenically induced by constitutively active RAS or secondary to pressure overload or other hypertrophic stimuli, is accompanied by an increase in total RNA content. This is a result of increased P-TEFb activity and phosphorylation of RNA Pol II that increases total RNA and protein synthesis (25, 31). Using a genetically modified mouse model that combines the elevated expression of $HRas^{G12V}$ and an ectopically switchable Myc allele ($MycER^{T2}$), we show that expression of constitutively active $HRas^{G12V}$ in the heart leads to increased P-TEFb levels that, when combined with constitutive Myc activity, drives signs of cardiomyocytes proliferation *in vivo*.

Materials and methods

Mice

All animals were kept under SPF conditions. Mice were maintained on regular diet in a pathogen-free facility on a 12 h light/dark cycle with continuous access to food and water. All mice were euthanised under the schedule 1 method of cervical dislocation. Mouse strain *Tg(Myh6-tTA)6Smbf/J* was obtained from the Jackson Laboratory, and mouse strain *Tg(tetO-HRAS)65Lc/Nci* was obtained from the NCI Mouse Repository. Mouse strain $R26^{CAG-c-MycER}$ was produced in house. 1 mg of (Z)-4-hydroxytamoxifen (4-OHT; Sigma, H7904) was i.p injected into adult mice in 10% ethanol and vegetable oil (5 mg/ml), and tissues were collected 4 h post injection. 1 mg of tamoxifen (Sigma, T5648) was i.p injected into adult mice in 10% ethanol and vegetable oil (10 mg/ml) twice over a 24-h period and tissues collected at 24 h post initial

i.p. injection. Animals requiring doxycycline treatment were supplied with drinking water containing doxycycline hyclate 100 mg/L (Sigma D9891) in water containing 3% sucrose to increase palatability, this was replenished two times per week in light-protected bottles. Ear biopsies were collected from 2 to 5 weeks old mice and genotyped by PCR with the following oligonucleotide primers: for *Rosa26CAG*; Universal forward: 5′-CTCTGCTGCCTCCTGGCTTCT-3′ Wild-type reverse: 5′-CGAGGCGGATCACAAGCAATA-3′ and CAG reverse: 5′-TCAATGGGCGGGGGTCGTT-3′. Primers for the TetO-HRas allele were; H003: 5′-TGAAAGTCGAGCTCGGTA-3′ and H004: 5′-CCCGGTGTCTTCTATGGA-3′. Primers for the Myh6-tTA allele were; oIMR8746: 5′-CGCTGTGGG GCATTTTACTTTAG-3′ and oIMR8747: 5′-CATGTCCAGAT CGAAATCGTC-3′.

Immunoblotting

Snap-frozen animal tissues were ground on liquid nitrogen and proteins extracted in buffer containing 1% SDS, 50 mM Tris pH 6.8, and 10% glycerol on ice for 10 min. Lysates were boiled for 10 min, followed by sonication for 15 min at room temperature. Total protein (50 μg) was electrophoresed on an SDS–PAGE gel and transferred onto immobilon-P (Millipore) membranes. These were then blocked in 5% non-fat milk and incubated with primary antibodies overnight at 4°C. Secondary antibodies were applied for 1 h followed by chemiluminescent visualisation (Thermo Scientific, 32106 or Millipore, WBKLS0500). Immunoblots were either developed on Fuji RX X-ray film and scanned on an Epson Perfection V500 Photo flatbed scanner or visualisation was performed on LiCOR Odyssey Fc. Protein quantifications were performed on the LiCOR Odyssey Fc.

Primary antibodies: GAPDH (D16H11) XP® (Cell Signaling Technology, 5174, used at 1:5,000), phospho-Rpb1 CTD (Ser2; E1Z3G; Cell Signaling Technology, 13499, used at 1:2,500), CDK9 (C12F7; Cell Signaling Technology, 2316, used at 1:1,000), Cyclin T1 (D1B6G; Cell Signaling Technology, 81464, used at 1:1,000), p-ERK is phospho-p44/42 MAPK (Thr202/Tyr204, Cell Signaling Technology, 9101, used at 1:500), anti-rabbit IgG HRP (Sigma, A0545, used at 1:10,000). Sample loading was normalised for equal protein content. Expression of GAPDH is included as a confirmation of efficiency of protein isolation and comparable loading between individual tissue samples.

Immunohistochemistry

Immunohistochemistry was performed on formalin-fixed paraffin-embedded 4 μm sections. Sections were de-paraffinized and rehydrated, followed by antigen retrieval by boiling in 10 mM citrate buffer (pH 6.0) for 10 min. Endogenous peroxidase activity was blocked with 0.3% hydrogen peroxide for 30 min. Sections were then treated with rabbit VECTASTAIN Elite ABC horseradish peroxidase kit (Vector Laboratories, PK-6101) following the manufacturer's protocols. Sections were blocked in normal goat serum for 20 min, followed by 1 h incubation in the primary antibody at room temperature. Sections were then washed three times in PBST and incubated for 1h in secondary antibody, sections were then washed again in PBST and then incubated in ABC complex for 30 min. Sections were developed in DAB (3,3'-diaminobenzidine) for 5 min, counterstained in haematoxylin, dehydrated, and mounted in DPX. Staining was imaged on a Zeiss Axio Imager using the Zeiss ZEN software using the AutoLive setting and interactive white balance.

Primary antibodies: p-ERK is phospho-p44/42 MAPK (Thr202/Tyr204, Cell Signalling Technology, 9101, used at 1:500), and anti-Cyclin T1 (AbCam, ab238940, use at 1:500).

Immunofluorescence

Sections were pre-processed followed by antigen retrieval in the same way as for immunohistochemistry. Sections were blocked in 2.5% goat serum, and 1% BSA in PBST for 20 mins at room temperature. Primary antibody, made up of blocking buffer, was added for 1 h at room temperature, followed by three 5 min PBST washes, and secondary antibodies were added for 1 h at room temperature. Nuclei were visualised using Hoechst (Sigma, 861405) and sections mounted in ProLong™ Gold Antifade Mountant (Thermo Fisher, P36930). Antibodies: anti-phospho-Histone H3 (Ser10; Merck Millipore, 06-570, use at 1:500), cardiac troponin T (13-11; Thermo Fisher, MA5-12969, use at 1:100) and (CT3, Santa Cruz Biotechnology, sc-20025, use at 1:50), anti-Aurora B antibody (Abcam, ab2254, use at 1:200), anti-Mklp1 (Abcam, ab174304, use at 1:400), anti-CD206 (R&D Systems, AF2535, use at 1:100), anti-PCM1 (Sigma-Aldrich, HPA023370, use at 1:100), anti-Ki67 (SolA15; Thermo Fisher, use at 1:100) and (Atlas Antibodies, HPA023374, use at 1:100), Alexa Fluor 555 goat anti-rabbit IgG (H+L; Life Technologies, A21428), Alexa Fluor 555 goat anti-mouse IgG (H+L; Life Technologies, A21422), Alexa Fluor 555 goat anti-rat IgG (H+L; Life Technologies, A21434), Alexa Fluor 488 goat anti-rabbit IgG (H+L; Life Technologies, A11008), Alexa Fluor 488 goat anti-rat IgG (H+L; Life Technologies, A11006), Alexa Fluor 350 goat anti-mouse (H+L; Life Technologies A11045), wheat germ agglutinin, Alexa Fluor™ 488 conjugate (Thermo Fisher, W11261). TUNEL staining we performed following the manufactures instructions using the ApopTag® Fluorescein *In Situ* Apoptosis Detection Kit (S7110 Sigma-Aldrich). Staining was imaged on a Zeiss Axio Imager using the Zeiss ZEN software using the AutoLive setting or Leica Stellaris 5 confocal microscope. Quantification was performed by counting the number of positive cardiomyocytes for at least five images per organ/mouse, the mean of five raw counts was calculated and

is represented by each data point per graph. Cardiomyocyte cell areas were quantified by encircling individual cardiomyocytes stained with cardiac troponin and wheat germ agglutinin.

Quantitative RT-PCR

Total RNA was isolated using TRIzol Reagent (Thermo Fisher, 15596-018) following manufacturer's instructions. cDNA was synthesised from 1 μg of RNA using the High-Capacity cDNA Reverse Transcription Kit with RNase Inhibitor (Thermo Fisher, 4374966) following manufacturer's instructions. qRT-PCR reactions were performed on an Applied Biosystems QuantStudio 5 Real-Time PCR System using Fast SYBR Green Master Mix (Thermo Fisher, 4385612), following manufacturer's instructions. Primers: Ccnd1; forward 5′- GCGTACCCTGACACCAATCTC-3′, reverse 5′-CTCCTCTTCGCACTTCTGCTC-3. Cdk4; forward 5′-ATGGCTGCCACTCGATATGAA-3′, reverse 5′-TCCTCCATTAGGAACTCTCACAC-3′. Cdk1; forward 5′- AGAAGGTACTTACGGTGTGGT-3′, reverse 5′-GAGAGATTTCCCGAATTGCAGT-3′. Ccnb1; forward 5′-AAGGTGCCTGTGTGTGAACC-3′, reverse 5′-GTCAGCCCCATCATCTGCG-3′. Cad; forward 5′- CTGCCCGGATTGATTGATGTC-3′, reverse 5′-GGTATTAGGCATAGCACAAACCA-3′. Pinx1; forward 5′-AGCAAGGAGCCACAGAACATA-3′, reverse 5′-GGTGAGCAATCCAGTTGTCTT-3′. Bzw2; forward 5′-AGCGACTGTCTCAGGAATGC-3′, reverse 5′-CTGTTTCCGGAAGGTCGTT-3′. Polr3d; forward 5′-AAAAGCGTGAACGGGACAGG-3′, reverse 5′-AATGGGACTGGATCACTTCCG-3′. St6galnac4; forward 5′-TGGTCTACGGGGATGGTCA-3′, reverse 5′-CTGCTCATGCAAACGGTACAT-3′. Actin; forward 5′-GACGATATCGCTGCGCTGGT-3′, reverse 5′-CCACGATGGAGGGGAATA-3′. Gapdh; forward 5′-AGGTCGGTGTGAACGGATTTG-3′, reverse 5′-TGTAGACCATGTAGTTGAGGTCA-3′. Fosl1; forward 5′-ATGTACCGAGACTACGGGGAA-3′, reverse 5′-CTGCTGCTGTCGATGCTTG-3′. Egr3; forward 5′-CCGGTGACCATGAGCAGTTT-3′, reverse 5′-TAATGGGCTACCGAGTCGCT-3′.

Bulk RNA sequencing

Total RNA was purified using PureLink RNA Mini Kit (Thermo Scientific). On-column DNA digestion was performed using PureLink DNase (Thermo Scientific). 1 μg of purified RNA was treated with Ribozero rRNA removal kit (Illumina). RNA quality and removal of rRNA were checked with the Agilent 2100 Bioanalyser (Agilent Technologies). Libraries for RNA-seq were then prepared with the NEBNext® Ultra™ II DNA Library Prep Kit for Illumina (NEB) following the manufacturer's instructions starting from the RNA fragmentation step.

Bulk RNA sequencing data analysis

Sequence reads were adapter trimmed using Cutadapt (32) (version 1.11) and aligned using BWA aln for short reads (version 2.5.2a) to the GRCm38 (mm10) assembly with the gene, transcript, and exon features of the Ensembl (release 70) gene model. Expression was estimated using RSEM (33) (version 1.2.30). Transcripts with zero read counts across all samples were removed prior to analysis. Normalisation of RSEM expected read counts was performed by dividing by million reads mapped to generate counts per million (CPM), followed by the trimmed mean of M-values (TMM) method from the edgeR package (34). Differential expression analysis was performed using edgeR.

RNA sequencing comparison to myocardial infarction reversion network

RNA-seq files from E-MTAB-7595, E-MTAB-7636, and GSE95755 were combined into a single count matrix. Before remapping, poor quality sequences (<30 phred score) and adapter sequences were trimmed with Trimmomatic (35). Reads were mapped with STAR (36) to the reference mouse genome sequence GCRm38.p4/mm10 using default settings. The combined count matrix was generated using HTSeq-count (37) on union mode. Differential expression analysis was performed with EdgeR(v3.20.8) (34) using the glmLRT function. Differential expression comparisons were considered significant if FDR $p < 0.05$. Gene ontological analysis was performed using DAVID and Heatmaps were assembled using GENE-E (Broad Institute).

Statistical analysis

Bioinformatic and statistical analyses were performed using R with Bioconductor packages and comEpiTools packages (38, 39). Gene lists from RNA and ChIP sequencing were analysed in Enrichr or GSEA/MSigDB[1] (40). Statistical analyses for IHC and q-RT-PCR were performed using GraphPad Prism v9.0d (GraphPad Software, Inc., San Diego, CA, USA) as indicated with $p \leq 0.05$ considered to be statistically significant. Venn diagrams were drawn in the Lucidchart.[2] Heatmaps were drawn in R and Morpheus.[3]

1 http://www.gsea-msigdb.org/gsea/index.jsp
2 www.lucidchart.com
3 https://software.broadinstitute.org/morpheus

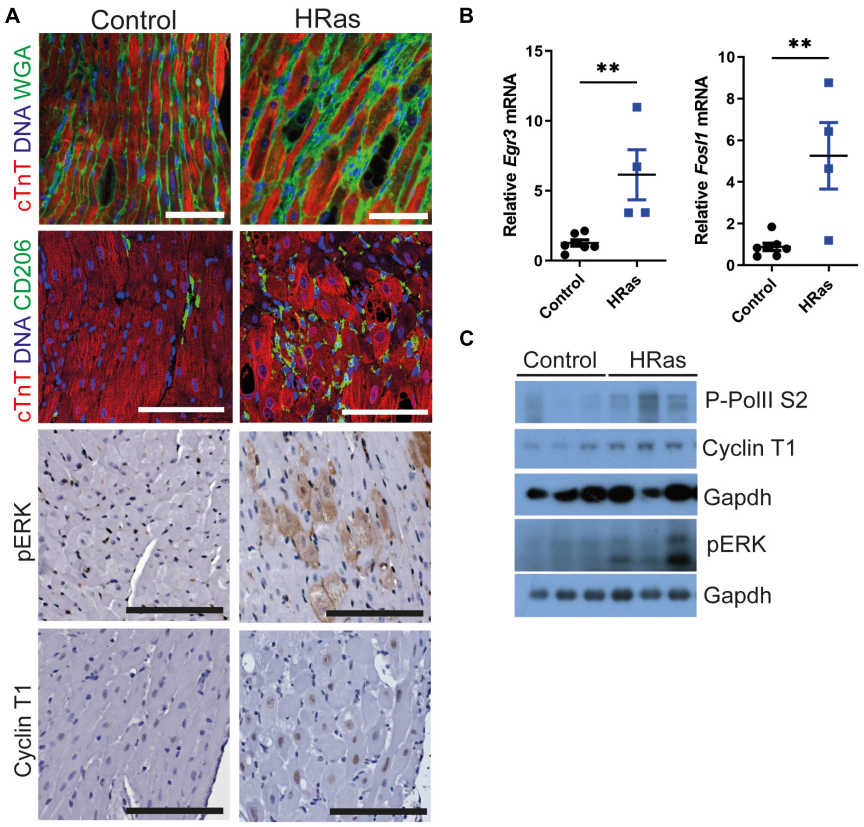

FIGURE 1
Ectopic cardiomyocyte HRas^{G12V} results in increased Cyclin T1 expression. **(A)** Top- Immunofluorescent staining of cardiac troponin (red) and wheat germ agglutinin or CD206 (green). middle- immunohistochemical analysis of pERK, bottom- immunohistochemical analysis of Cyclin T1 in hearts from wild type (Control) and *TetO-HRas; Myh6-tTA; R26*$^{+/+}$(*HRas*) mouse hearts 4 weeks post withdrawal of doxycycline. Bars are 100 μm. Representative images based on analysis of 5 images per mouse. **(B)** Quantitative RT-PCR analysis of control (*R26*$^{+/+}$*; TetO-HRas, R26*$^{+/+}$*; Myh6-tTA* or *R26*$^{+/+}$, *n* = 7) and *TetO-HRas; Myh6-tTA; R26*$^{+/+}$(*R26*$^{+/+}$*;HRas, n* = 4) mouse hearts 4 weeks post withdrawal of doxycycline. Expression is normalised to *Actin* and *Gapdh* and relative to the respective control. Replicate samples are derived from independent mice. Error bars show s.e.m. Two Way ANOVA with multiple comparisons test. $^{**}p < 0.01$. **(C)** Immunoblot analysis of the C-terminal domain of phosphorylated RNA Polymerase II [p-Rpb1(S2)], Cyclin T1 and pERK protein expression in hearts isolated from control (*R26*$^{+/+}$*; TetO-HRas, R26*$^{+/+}$*; Myh6-tTA* or *R26*$^{+/+}$) and *TetO-HRas; Myh6-tTA; R26*$^{+/+}$(*HRas*) mice 4 weeks post withdrawal of doxycycline. Expression of Gapdh is included as a loading control, for completeness, multiple Gapdh blots represent different gels (**top** – Cyclin T1 and P-RNA PolII S2, **bottom** – pERK). Replicate samples are derived from independent mice.

Results

Cardiac *HRas*^{G12V} expression leads to hypertrophy and amplified P-TEFb expression

We employed the cardiac-specific, doxycycline-controlled transgenic line *TetO-HRas* [*Tg(tetO-HRAS)65Lc/Nci]; Myh6tTA [Tg(Myh6-tTA)6Smbf/Jm*] (30) to overexpress HRas^{G12V} specifically in cardiomyocytes. Mice were generated and removed from doxycycline treatment at 4 weeks of age and the subsequent expression of constitutively active HRas^{G12V} led to an increase in hypertrophic cardiomyocytes (~10%, **Supplementary Figure 1A**) interspersed with CD206 positive macrophages and cardiomyocytes of normal volume (**Figure 1A**), as previously described (30). Hypertrophic cardiomyocytes displayed elevated pERK immunohistochemical staining (**Figure 1A**) and qRT-PCR analysis confirmed increased expression of the ERK-AP1 target genes Egr3 and Fos1L (**Figure 1B**), confirming enhanced HRas signalling. Despite the heterogeneity of the model, whole hearts expressing HRas^{G12V} displayed a moderate increase in Cyclin T1 and Phosphorylated RNA Pol II (**Figures 1A,C** and **Supplementary Figure 1B**).

HRas^{G12V} enables Myc-driven transcription in cardiomyocytes

To test the hypothesis that persistent HRas^{G12V} expression renders heart tissue Myc responsive, *TetO-HRas; Myh6tTA* mice were crossed to the *R26*$^{CMER/+}$ (*R26*$^{CAG-c-MycERT2}$) allele

to generate *TetO-HRas; Myh6-tTA; R26*$^{CMER/+}$ mice. In these mice, the MycER^{T2} fusion protein is constitutively expressed from a CAG-enhanced *Rosa26* promoter. MycER^{T2} is inert in the absence of a ligand but rapidly activated following administration of the ER^{T2} ligand 4OHT (4-hydroxytamoxifen), a primary metabolite of tamoxifen. In these mice, HRas^{G12V} and MycER^{T2} proteins can be independently activated by the withdrawal of doxycycline or administration of 4OHT (or tamoxifen), respectively (**Figure 2A**). Doxycycline was withdrawn from *TetO-HRas; Myh6-tTA; R26*$^{CMER/+}$ animals at weaning to induce expression of HRas^{G12V} and, once mice reached 8 weeks of age, MycER^{T2} was activated by injection of 4OHT for 4 h. We confirmed the elevated expression of Cyclin T1, CDK9, and phosphorylated RNA Pol II in the heart tissue of these animals compared to controls (**Figure 2B** and **Supplementary Figure 1C**).

We have previously determined that Myc-driven transcription is limited by the low level of endogenous P-TEFb within the adult heart. To establish if an HRas^{G12V}-driven increase in P-TEFb levels could enhance Myc-driven transcription, we quantified the expression of a panel of Myc target genes post MycER^{T2} activation. Cad, a Myc target gene previously shown to be transcribed following MycER^{T2} activation in all tissues, including the heart, showed increased expression in the heart tissue of both Myc activated (*R26*$^{CMER/}$) and HRas^{G12V}/Myc activated (*TetO-HRas; Myh6-tTA; R26*$^{CMER/+}$) tissues, confirming the functionality of the MycER^{T2} fusion in both conditions (**Figure 2C**). We then determined the expression of a panel of Myc target genes that we have previously observed as unchanged in the adult heart in response to MycER^{T2} activation alone. The co-expression of HRas^{G12V} sensitised the heart tissue to Myc-dependent expression of these targets over controls (**Figure 2C**). We also compared changes in global gene expression in heart of HRas^{G12V} (*TetO-HRas; Myh6-tTA; R26*$^{+/+}$) mice and Myc/HRas^{G12V} (*TetO-HRas; Myh6-tTA; R26* $^{CMER/+}$) mice 4 h after MycER^{T2} activation. We have previously observed marked induction of a Myc-driven transcriptional programme in the liver of MycER^{T2} expressing (*R26* $^{CMER/+}$) mice in the absence of co-expressed HRas^{G12V} (11) (**Figure 2D**). In contrast to the weak transcriptional response elicited by MycER^{T2} activation alone, in the presence of HRas^{G12V}, MycER^{T2} resulted in a marked transcriptional response (**Figure 2D**). MycER^{T2} and HRas^{G12V} expressing hearts displayed 1198 up-regulated DEGs and 693 down regulated DEGs (**Supplementary Table 1**) in comparison to HRas^{G12V} expression alone. Myc target gene identities overlapped with genes induced by MycER^{T2} in the adult liver, and in the adult heart in the presence of elevated Cyclin T1 expression (AAV9-driven cardiomyocyte-specific) (11) (**Figure 2E**). These genes are Myc targets, involved in direct Myc-regulated processes such as ribosomal biogenesis and RNA metabolic processes (**Figure 2E**, **Supplementary Figure 1D**, and **Supplementary Table 2**). In contrast, there was little overlap between downregulated genes observed following MycER^{T2} and HRas^{G12V} activation in the heart and genes downregulated by MycER^{T2} alone in the liver, suggesting a level of tissue specificity for Myc-dependent transcriptional repression. Consistent with this, genes downregulated in response to HRas^{G12V} and MycER^{T2} overlapped with those downregulated in the MycER^{T2} and Cyclin T1 expressing heart – these genes were characteristic of a homeostatic heart transcriptional programme, such as HCN4, MYOT (**Figure 2E** and **Supplementary Table 3**).

To determine if the transcriptional changes observed in response to combined activation of MycER^{T2} and HRas^{G12V} in the adult heart were similar to that observed in a regenerating neonatal heart, we analysed previous data to compare the transcriptional profiles of cardiomyocytes isolated from surgically infarcted hearts at different stages of development (14). Our unbiased comparison revealed that the P1 "neonatal regeneration gene expression signature" correlated most closely with the expression changes within the *TetO-HRas; Myh6-tTA; R26*$^{CMER/+}$ hearts (**Figure 3A**). Upregulated genes that overlapped with those also elevated in the "neonatal regeneration gene expression signature" enriched for GO terms including cell cycle control (**Figure 3B**). Interestingly, downregulated genes that overlapped with those also reduced in the "neonatal regeneration gene expression signature" contained genes involved in the negative regulation of mTOR signalling and we have previously observed a broad reprogramming of metabolism with a transition from neonatal to adult cardiac maturation (41). Furthermore, when regulated metabolic genes from our analysis are overlaid on the KEGG metabolic pathways *TetO-HRas; Myh6-tTA; R26*$^{CMER/+}$ hearts show broad reversion and reprogramming to neonatal metabolic pathways (**Supplementary Figure 2A**). Consistent with this reversion, gene set enrichment analysis (GSEA) indicated MycER^{T2} and HRas^{G12V} expressing hearts display enrichment of genes involved in glycolysis, characteristic of neonatal cardiomyocyte metabolism, and a reduction in genes involved with oxidative phosphorylation and fatty acid metabolism characteristic of adult cardiomyocyte metabolism (**Figure 3C**).

Combined HRas and Myc expression drives proliferation of cardiomyocytes *in vivo*

To determine if this Myc-dependent "regenerative transcriptional response" results in productive proliferation, MycER^{T2}/HRas^{G12V} expressing mice (*TetO-HRas; Myh6-tTA; R26*$^{CMER/+}$) or mice expressing either HRas^{G12V} or MycER^{T2} alone were administered tamoxifen via intraperitoneal injection at 8 weeks of age to activate MycER^{T2} and hearts collected after 24 h. Transcriptional analysis indicated that activation of MycER^{T2} in the presence of HRas^{G12V} induced robust

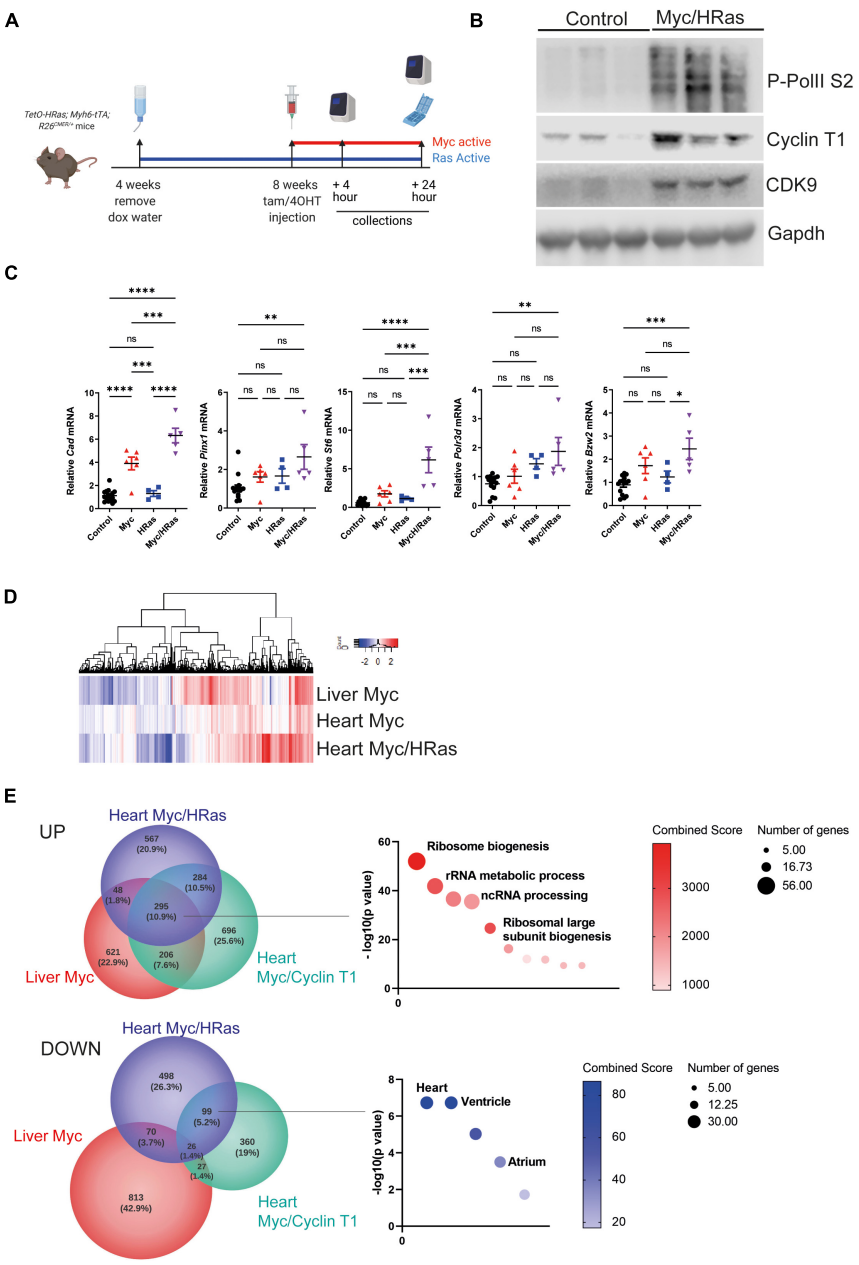

FIGURE 2
Cardiomyocyte HRas^{G12V} expression enables Myc-driven transcription. **(A)** Scheme of experimental work. **(B)** Immunoblot analysis of the C-terminal domain of phosphorylated RNA Polymerase II [p-Rpb1(S2)], Cyclin T1 and CDK9 protein expression in hearts isolated from control (*R26*$^{+/+}$; *TetO-HRas, R26*$^{+/+}$; *Myh6-tTA* or *R26*$^{+/+}$) and *TetO-HRas; Myh6-tTA; R26* $^{CMER/+}$(HRas/Myc) mice 4 weeks post withdrawal of doxycycline and at 24 h post administration of 4-OHT. Expression of Gapdh is included as a loading control. Replicate samples are derived from independent mice. **(C)** Quantitative RT-PCR analysis of *Cad, Bzw2, Pinx1, Polr3d, St6*, and *Cdc25a* in hearts from control (*R26*$^{+/+}$; *TetO-HRas, R26*$^{+/+}$; *Myh6-tTA* or *R26*$^{+/+}$, $n \geq 14$), *TetO-HRas; Myh6-tTA; R26*$^{+/+}$(*HRas, n = 4*), *R26*$^{CMER/+}$ (*Myc, n = 6*) and *TetO-HRas; Myh6-tTA; R26* $^{CMER/+}$ (*MycHRas, n = 5*) mice 4 weeks post withdrawal of doxycycline and 4 h post-administration of 4-OHT. Expression is normalised to *Actin* and *Gapdh* and relative to the respective control. Error bars show s.e.m. Two Way ANOVA with multiple comparisons test; control vs *R26*$^{CMER/+}$: *p**** = 0.001 (*Cad*), control vs *TetO-HRas; Myh6-tTA; R26* $^{CMER/+}$: *p*** = 0.01 (*Bzw2, Pinx1, Polr3d, Cdc25a*) *p**** = 0.001 (*St6*). Replicate samples are derived from independent mice. **(D)** Heat map showing the union of DEGs called in adult liver and adult heart. Shown are mRNA expression fold changes (Log2) upon MycER^{T2} activation relative to wild-type, as determined by RNA sequencing of *R26*$^{CMER/+}$ ($n \geq 3$) mice in comparison to wild-type (*R26*$^{+/+}$, $n \geq 3$) and *TetO-HRas; Myh6-tTA; R26* $^{CMER/+}$ mice (*Myc/HRas, n = 3*) in comparison to *TetO-HRas; Myh6-tTA; R26*$^{+/+}$ mice (*n = 3*) at 4 h post administration of 4-OHT. **(E)** Venn diagrams of overlap in the number of genes showing an increase (top) and decrease (bottom) in expression in response to supraphysiological Myc expression. The most significant GO Biological Process and ASCHS4 gene lists that overlap are shown. Comparisons included the liver of *R26*$^{CMER/+}$ (Myc liver, *n = 3*) compared to wild type. The adult mouse heart was isolated 4 weeks post systemic infection with an adeno associated virus encoding *Ccnt1* (*AAV9-Ccnt1*) compared to control and heart from *TetO-HRas; Myh6-tTA; R26* $^{CMER/+}$ (*n = 3*) 4 weeks after HRas^{G12D} expression and 4 h post Myc activation compared to control, as determined by RNA sequencing (FDR < 0.05 and abs(log2FC) > 0.5).

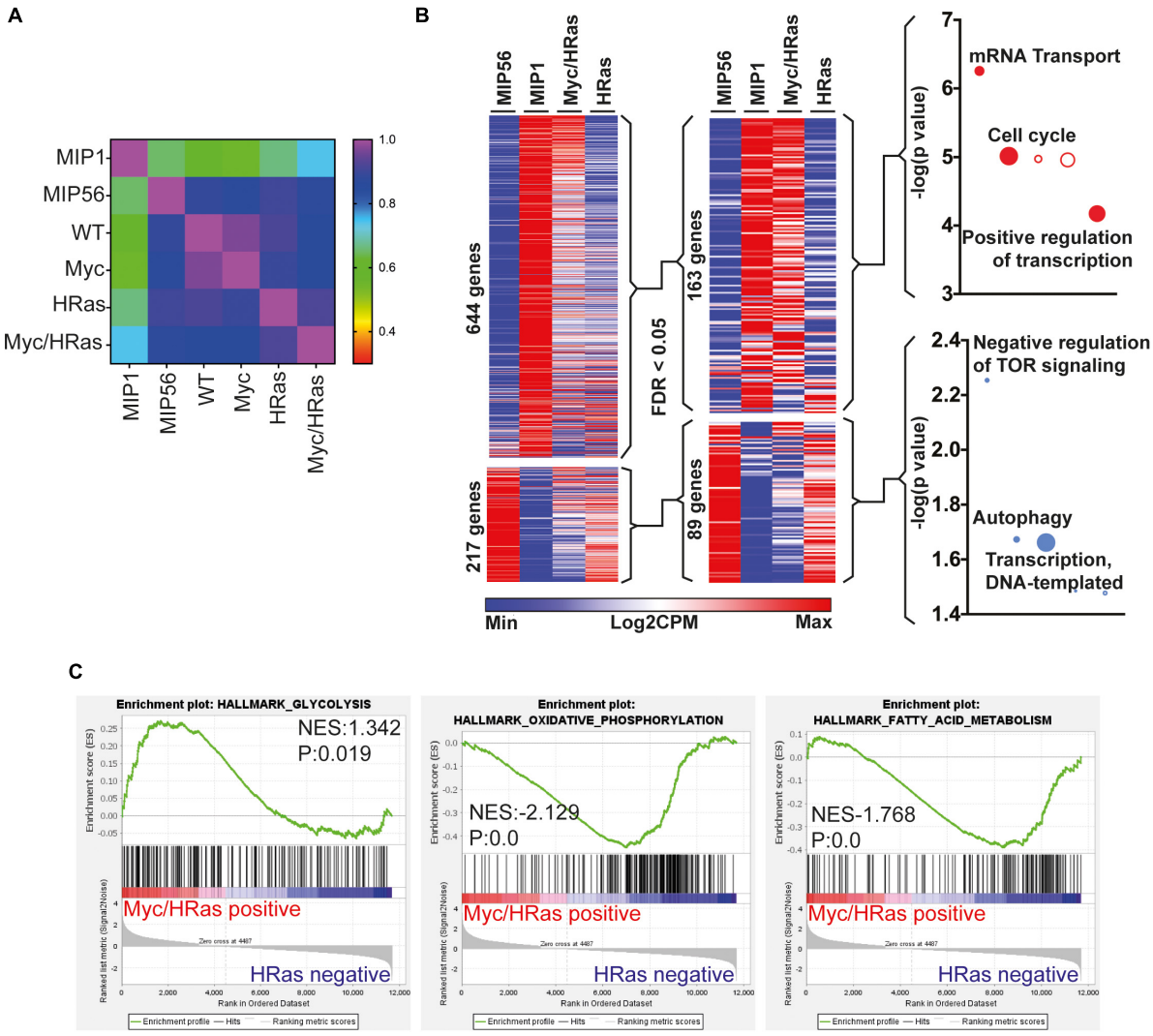

FIGURE 3
Cardiac MycER^{T2} and HRas^{G12V} expression result in signalling characteristic of neonatal cardiomyocytes. **(A)** Pearson correlative analysis of regenerative network genes (described in [14]) expressed in day 1 myocardial infarcted heart myocytes (MIP1), adult day 56 myocardial infarcted heart myocytes (MIP56), adult *R26*$^{+/+}$ (WT) hearts, adult *R26* $^{CMER/+}$ (Myc) hearts, adult *TetO-HRas; Myh6-tTA; R26*$^{+/+}$ (*HRas*) and adult *TetO-HRas; Myh6-tTA; R26* $^{CMER/+}$ (*Myc/HRas*) RNA-seq datasets. **(B)** Heat map depicts gene expression of the regeneration network genes (described in [14]) from RNA-seq of *TetO-HRas; Myh6-tTA; R26*$^{+/+}$ (*HRas*, $n = 3$) and *TetO-HRas; Myh6-tTA; R26* $^{CMER/+}$ P60 adult hearts (*Myc/HRas*, $n = 3$). MIP1.Myo and MIP56.Myo denotes neonatal (P1) or adult (P56) cardiomyocytes isolated from myocardial infarction-operated hearts ($n = 4$). Regeneration network genes were filtered for genes differentially expressed (DEGs) between *TetO-HRas; Myh6-tTA; R26*$^{+/+}$ (*HRas*) and *TetO-HRas; Myh6-tTA; R26* $^{CMER/+}$ (*Myc/HRas*) hearts (FDR < 0.05). **(C)** Gene set enrichment analysis of glycolysis, oxidative phosphorylation, and fatty acid metabolism gene lists in comparison to differential gene expression observed between *TetO-HRas; Myh6-tTA; R26* $^{CMER/+}$ mice (*Myc/HRas*, $n = 3$) and *TetO-HRas; Myh6-tTA; R26*$^{+/+}$ mice ($n = 3$) at 4 h post administration of 4-OHT.

expression of multiple cell cycle genes (*Cdk4*, *Ccnd1*, *Cdk1*, *Ccnb1*) that were not induced by HRas^{G12V} or Myc activation alone (except *Cdk4* which is a known Myc target, **Figure 4A**). Furthermore, markers of cytokinesis were upregulated in Myc and HRas^{G12V} expressing hearts (**Figure 4B**) and GSEA indicated that these hearts displayed significant enrichment for genes involved in cell cycle-related pathways such as E2F targets and G2/M checkpoints (**Supplementary Figure 2B**). These transcriptional events also underpinned significant markers of cell-cycle progression indicated by Ki67 (general cell cycle) and p-H3 (mitotic) positive cardiomyocytes specifically marked by PCM1 and cardiac troponin T, respectively (**Figures 4C,D**). In addition, Aurora B kinase displayed staining representative of cell cycle progression (prophase, metaphase, late anaphase/telophase, and mid body localisation) combined with features of disassembled sarcomeres that become marginalised to the cell periphery (4, 42) (**Figure 4E** and **Supplementary Figure 3**). Furthermore, Mklp1 expression was observed in cardiomyocytes at the cleavage furrow (**Figure 4F**).

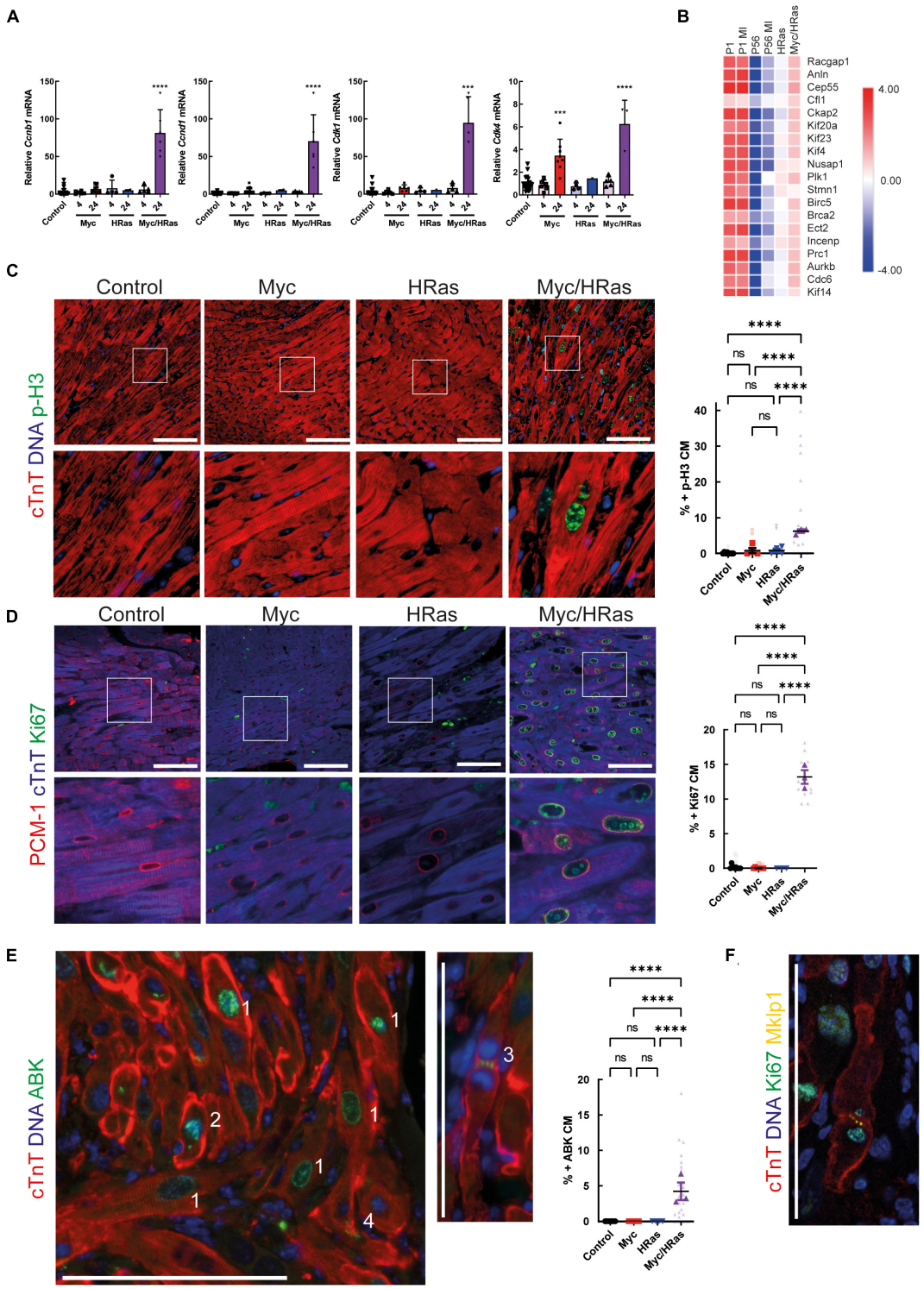

FIGURE 4
MycER^{T2} and HRas^{G12V} expression drive cardiomyocyte proliferation. **(A)** Quantitative RT-PCR analysis of *Cyclin D1, Cdk4, Cyclin B1*, and *Cdk1* in hearts of control (*R26*$^{+/+}$*; TetO-HRas, R26*$^{+/+}$*; Myh6-tTA* or *R26*$^{+/+}$, $n \geq 24$), *TetO-HRas; Myh6-tTA; R26*$^{+/+}$(*R26*$^{+/+}$*;HRas*, $n \geq 5$), *R26*$^{CMER/+}$ ($n \geq 14$) and *TetO-HRas; Myh6-tTA; R26* $^{CMER/+}$ (*R26* $^{CMER/+}$*;HRas*, $n = 8$) mice 4 weeks post withdrawal of doxycycline and 4 or 24 h post administration of 4-OHT. Expression is normalised to *Actin* and *Gapdh* and relative to the respective control. Error bars show s.e.m. One Way ANOVA with multiple comparisons test; control *vs* 24 h *R26*$^{CMER/+}$: $p = 0.001$*** (*Cdk4*), control *vs* 24 h *TetO-HRas; Myh6-tTA; R26* $^{CMER/+}$: p**** = 0.0001 (*Cyclin D1, Cdk4, Cyclin B1, Cdk1*). Replicate samples are derived from independent mice. **(B)** Heat map depicts gene expression (LogCPM) of cytokinesis genes in the regeneration network (described in [14]) from RNA-seq of adult *TetO-HRas; Myh6-tTA; R26*$^{+/+}$ (*HRas*, $n = 3$) and adult *TetO-HRas; Myh6-tTA; R26* $^{CMER/+}$ hearts (*Myc/HRas*, $n = 3$), neonatal (P1) or adult (P56) cardiomyocytes isolated from

(Continued)

FIGURE 4 (Continued)
sham and myocardial infarction-operated (MI) hearts (n = 4). **(C)** Left- immunofluorescent staining of heart from control, *TetO-HRas; Myh6-tTA; R26*$^{+/+}$ (*HRas*), *R26*$^{CMER/+}$ (Myc) and *TetO-HRas; Myh6-tTA; R26* $^{CMER/+}$ (Myc/*HRas*) mice 4 weeks post-withdrawal of doxycycline and 24 h post administration of tamoxifen. Cardiac troponin (red) and p-H3 positive mitotic nuclei (green). Representative images based on analysis of at least 3 independent mice. Right- quantification of percent p-H3 positive cardiomyocyte in hearts isolated from control (*R26*$^{+/+}$*; TetO-HRas, R26*$^{+/+}$*; Myh6-tTA* or *R26*$^{+/+}$, black, n = 8), *TetO-HRas; Myh6-tTA; R26*$^{+/+}$ (*HRas*, red, n = 3), *R26*$^{CMER/+}$ (Myc, blue, n = 4) and *TetO-HRas; Myh6-tTA; R26* $^{CMER/+}$ (*Myc/HRas,* purple, n = 3) mice 4 weeks post withdrawal of doxycycline and 24 h post administration of tamoxifen. Bold symbols = average per mouse heart, small faint symbols = each individual field quantified. Bars are 100 μm. Representative images based on analysis of 5 images per mouse; error bars show s.e.m. One Way ANOVA with multiple comparisons test: $p < 0.0001$****. **(D)** Left- Immunofluorescent staining of PCM-1 (red) and Ki67 (green) in the heart from control, *TetO-HRas; Myh6-tTA; R26*$^{+/+}$ (*HRas*), *R26*$^{CMER/+}$ (Myc) and *TetO-HRas; Myh6-tTA; R26* $^{CMER/+}$ (Myc/*HRas*) mice 4 weeks post withdrawal of doxycycline and 24 h post administration of tamoxifen. Right Myc/HRas image shows relocation of PCM1 and cardiac troponin signal in mitotic cardiomyocytes. Right- quantification of percent Ki67 positive cardiomyocytes in hearts isolated from control (*R26*$^{+/+}$*; TetO-HRas, R26*$^{+/+}$*; Myh6-tTA* or *R26*$^{+/+}$, black, n = 10), *TetO-HRas; Myh6-tTA; R26*$^{+/+}$ (*HRas*, red, n = 3), *R26*$^{CMER/+}$ (Myc, blue, n = 7) and *TetO-HRas; Myh6-tTA; R26* $^{CMER/+}$ (*Myc/HRas,* purple, n = 3) mice 4 weeks post withdrawal of doxycycline and 24 h post administration of tamoxifen. Bold symbols = average per mouse heart, small faint symbols = each individual field quantified. Bars are 100 μm. Representative images based on analysis of at least 3 independent mice. One Way ANOVA with multiple comparisons test: $p < 0.0001$****. **(E)** Left- Immunofluorescent staining of cardiac troponin (red) and Aurora B positive mitotic nuclei (green) in the heart of *TetO-HRas; Myh6-tTA; R26* $^{CMER/+}$ (Myc/*HRas*) mice 24 h post administration of tamoxifen. Numbers indicate differences in Aurora B localisation throughout the cell cycle. 1- Prophase and Prometaphase, 2- Metaphase, 3- Late anaphase/early telophase, 4 – centrally located mid-body. Right- quantification of percent ABK positive cardiomyocytes in hearts isolated from control (*R26*$^{+/+}$*; TetO-HRas, R26*$^{+/+}$*; Myh6-tTA* or *R26*$^{+/+}$, black, n = 8), *TetO-HRas; Myh6-tTA; R26*$^{+/+}$ (*HRas*, red, n = 4), *R26*$^{CMER/+}$ (Myc, blue, n = 7) and *TetO-HRas; Myh6-tTA; R26* $^{CMER/+}$ (*Myc/HRas,* purple, n = 3) mice 4 weeks post withdrawal of doxycycline and 24 h post administration of tamoxifen. Bold symbols = average per mouse heart, small faint symbols = each individual field quantified. Bars are 100 μm. Representative images based on analysis of at least 3 independent mice. Kruskal–Wallis with Dunn's multiple comparisons: $p < 0.01$**, $p < 0.001$***.
(F) Immunofluorescent staining of cardiac troponin (red), Ki67 (green) and Mklp1 (orange) in the heart of *TetO-HRas; Myh6-tTA; R26* $^{CMER/+}$ (Myc/*HRas*) mice 24 h post administration of tamoxifen. Bars = 100 μm.

Combined HRas^{G12V} and MycER^{T2} expression leads to apoptosis of cardiomyocytes

It has been previously noted that HRas^{G12V} hypertrophic hearts display increased levels of cell death, mononuclear cell infiltration, and damage that ultimately lead to heart failure (30). We observed an increase in the presence of mononuclear cell infiltration such as CD206 positive macrophages (**Figure 1A**) and the apoptosis marker cleaved caspase 3 (**Figure 5A**). We also observed increased cleaved caspase 3 when elevated HRas^{G12V} expression was combined with MycER^{T2} activation (**Figure 5A**) and an apoptotic gene expression signature was present (**Supplementary Figure 1D**). Therefore, longer-term analysis and cardiomyocyte dissociation and counting of these mice hearts were not possible. Although elevated levels of Myc expression are associated with apoptosis in some tissues (43) we did not observe apoptosis in hearts expressing activated MycER^{T2} in the absence of HRas^{G12V} (**Figure 5A**). Using a different system, we next determined if the cell death observed with HRas^{G12V} and Myc together was recapitulated by co-activation of MycER^{T2} and Cyclin T1. We infected, *R26*$^{CMER/+}$, and *R26*$^{LSL-CMER/+}$;*Myh6Cre* mice with cardiac-specific (cTnT promotor-dependent) overexpression of Cyclin T1 using *AAV9-cTnT-Ccnt1* or a control β-galactosidase virus (*AAV9-cTnT-LacZ*). In contrast, to control mice, MycER^{T2} activation in the presence of Cyclin T1 increased cardiomyocyte proliferation as previously described (11), increased heart weight to tibia size ratio, increased number of Ki67 and p-H3 positive cardiomyocyte nuclei (**Supplementary Figure 4**) (11). However, we found no evidence of apoptosis (cleaved caspase 3) in cardiomyocytes in hearts overexpressing Myc and Cyclin T1 (**Figure 5B**). To confirm negativity we also performed Terminal deoxynucleotidyl transferase dUTP nick end labelling (TUNEL) for cell death which also indicated that elevated Myc and Cyclin T1 activity does not induce cardiomyocyte cell death within 48 h (**Figure 5B**). While the method for overexpressing Cyclin T1 differed, we compared the upregulated gene expression profile of Myc/HRas expressing hearts and Myc/Cyclin T1 expressing hearts and found the GSEA hallmark signatures vastly overlapped. Myc/Ras expressing hearts showed additional gene set enrichment for apoptosis (including the pro-apoptotic proteins Bak and Bok), epithelial mesenchymal transition and inflammatory response (**Figure 5C** and **Supplementary Table 4**). The only GSEA pathway that was enriched in Myc/Cyclin T1 expressing hearts was Wnt/Beta Catenin. These data indicate that cell death is specific to HRas^{G12V} activation, not simply an inevitable consequence of enforced endogenous cardiomyocyte proliferation.

Discussion

Myc is a transcription factor that serves as a pivotal instructor of tissue regeneration following injury in a regenerative organ (13), however, in the heart both Myc transcription and Myc-driven transcription are attenuated. When Myc is acutely overexpressed in the heart it competently binds to DNA but only drives a limited transcriptional programme, and cell-cycle progression is not observed within 48 h (11). Protracted Myc expression in cardiomyocytes eventually leads to DNA synthesis, and myocyte hypertrophy but not to cardiomyocyte cytokinesis (15). We have previously shown that the ability of Myc to drive all the transcriptional

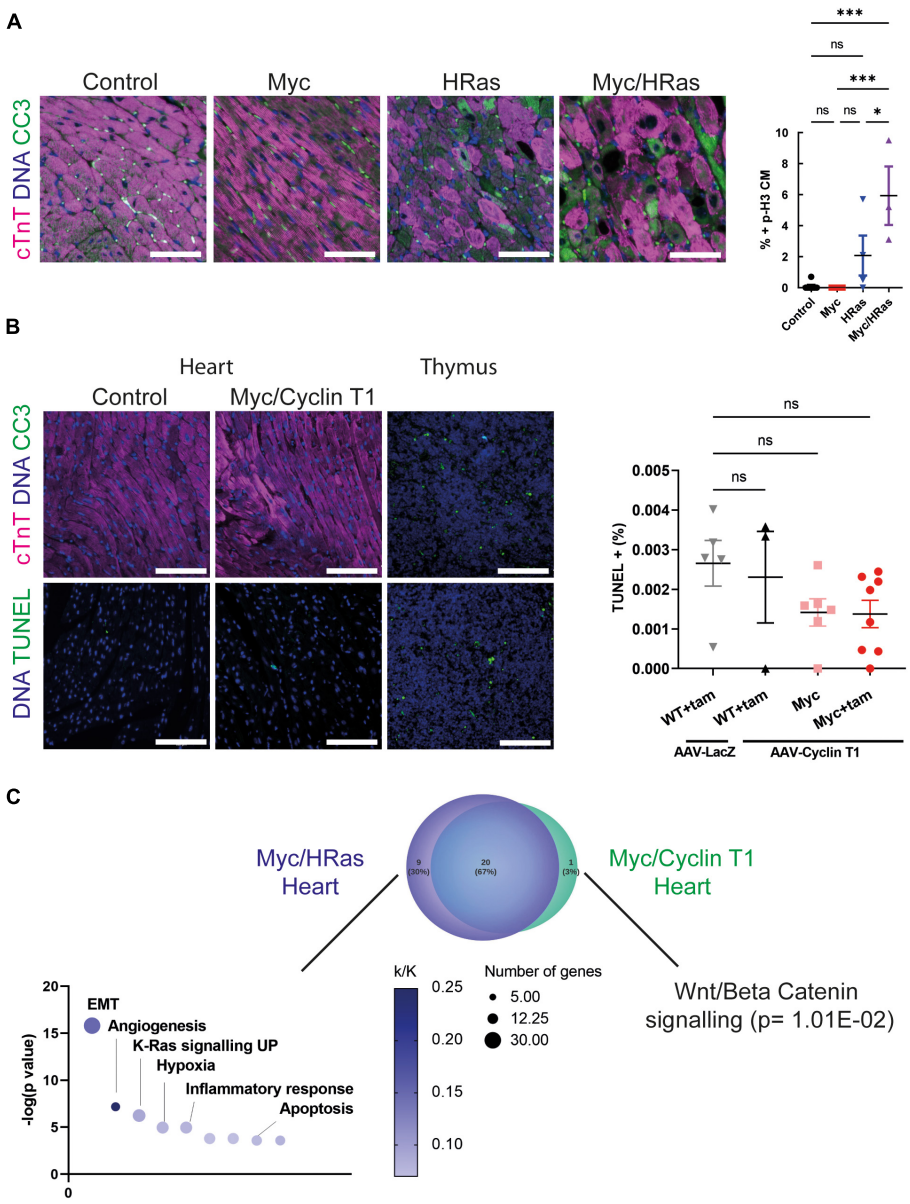

FIGURE 5
Cardiac HRas^{G12V} and MycER^{T2} expression results in cardiomyocyte apoptosis. **(A)** Left- immunofluorescent staining of cleaved caspase 3 (green) and cardiac troponin (pink) in heart from control, *TetO-HRas; Myh6-tTA; R26*$^{+/+}$ (*HRas*), *R26*$^{CMER/+}$ (Myc) and *TetO-HRas; Myh6-tTA; R26* $^{CMER/+}$ (Myc/*HRas*) mice 4 weeks post withdrawal of doxycycline and 24 h post administration of tamoxifen. Representative images based on analysis of at least 3 independent mice. Right- quantification of CC3 positive cardiomyocytes in hearts isolated from control (*R26*$^{+/+}$; *TetO-HRas, R26*$^{+/+}$; *Myh6-tTA* or *R26*$^{+/+}$, black, *n* = 8), *TetO-HRas; Myh6-tTA; R26*$^{+/+}$ (*HRas*, red, *n* = 4), *R26*$^{CMER/+}$ (Myc, blue, *n* = 4) and *TetO-HRas; Myh6-tTA; R26* $^{CMER/+}$ (*Myc/HRas,* purple, *n* = 3) mice 4 weeks post withdrawal of doxycycline and 24 h post administration of tamoxifen. Bars are 100 μm Representative images based on analysis of 5 images per mouse; error bars show s.e.m. One-Way ANOVA with multiple comparisons test; Myc/HRas *vs* control: $p = 0.0003$, Myc/HRas vs Myc: $P = 0.0006$, Myc/HRas vs HRas*; Myh6-tTA; R26*$^{+/+}$: $p = 0.0295$. **(B)** Left- immunofluorescent staining of heart from Control and *Myh6-Cre; R26*$^{LSL-CMER/+}$ (Myc/Cyclin T1) mice 4 weeks post systemic infection with an AAV-Cyclin T1 adeno-associated virus and 48 post administration of tamoxifen (tam) at adulthood. Top: Control is *R26*$^{+/+}$, cleaved caspase 3 (green) and cardiac troponin (pink), Bottom: Control is *Myh6-Cre; R26*$^{LSL-CMER/+}$ without tam treatment. TUNEL (green). Representative images based on analysis of 5 independent mice. Right- quantification of TUNEL positive cells in hearts isolated from *R26*$^{+/+}$ (WT) mice infected with AAV-LacZ and or AAV-Cyclin T1 and *Myh6-Cre; R26*$^{LSL-CMER/+}$ (Myc) mice 4 weeks post systemic infection with an adeno-associated virus and 48 post administration of tamoxifen (tam). Bars are 100 μm. Representative images based on analysis of 5 images per mouse; error bars show s.e.m. Thymus is shown as a positive control. One-Way ANOVA with multiple comparisons test. ns = not significant. **(C)** Venn diagram of the overlap of the GSEA hallmark signatures obtained from the upregulated gene expression profile of Myc/HRas expressing hearts or Myc/Cyclin T1 expressing hearts. Adult mouse hearts were either isolated 4 weeks post systemic infection with an adeno associated virus encoding *Ccnt1* (*AAV9-Ccnt1*) compared to control and heart from *TetO-HRas; Myh6-tTA; R26* $^{CMER/+}$ (*n* = 3) 4 weeks after HRas^{G12D} expression and 4 h post Myc activation compared to control, as determined by RNA sequencing (FDR < 0.05 and abs(log2FC) > 0.5). The significant non-overlapping GSEA hallmark signatures are shown below.

programmes necessary for cell division in cardiomyocytes depends on the level of P-TEFb (11). We and others have shown that the level of P-TEFb is dependent on the level of Cyclin T1 and elevated Cyclin T1 leads to a corresponding increase in CDK9 and phosphorylated RNA PolII (11, 25, 26). Since $HRas^{G12V}$ upregulates P-TEFb in cardiomyocytes (31) resulting in cardiac muscle hypertrophy, we hypothesised that Myc and Ras would co-operate to drive cardiomyocyte proliferation.

We employed a previously described mouse model of $HRas^{G12V}$ overexpression in which oncogenic *HRas*^{G12V} is under the control of a tetracycline response element (*TetO-HRas)* harbouring a cardiomyocyte-specific reverse tetracycline transactivator (*Myh6-tTA)*. Withdrawal of doxycycline at 4 weeks of age leads to cardiomyocyte-restricted $HRas^{G12V}$ overexpression and pathogenic myocardial hypertrophy. Cessation of $HRas^{G12V}$ activity after induction of hypertrophy leads to hypertrophy resolution (30). We confirmed that long-term overexpression of $HRas^{G12V}$ in cardiomyocytes led to increased HRas signalling and cardiomyocyte hypertrophy as previously reported (29, 30, 44–46). Four weeks after $HRas^{G12V}$ expression higher levels of CDK9, Cyclin T1, and phosphorylated RNA Pol II in $HRas^{G12V}$ were observed compared to control animals, confirming that long-term $HRas^{G12V}$ expression upregulates the transcriptional elongation machinery. The exact mechanism of increasing P-TEFb activity by Ras is not known, however, recently the downstream Ras effector AP-1 (heterodimeric transcription factors comprising members of the Fos and Jun families) has been shown to be critical for both Zebrafish and *Xenopus tropicalis* heart regeneration (47, 48). Fosl1 plays an essential role in cardiomyocyte proliferation by interacting with JunB and binding the Ccnt1 promoter, increasing the expression of Cyclin T1 (48). Here we show that $HRas^{G12V}$ overexpression in cardiomyocytes leads to increased Fosl1 and an increase in Cyclin T1 protein levels. We have previously demonstrated that Myc co-operates with elevated Cyclin T1 expression to drive cardiomyocyte proliferation *in vivo* (10), therefore, we hypothesised that Myc and HRas would also co-operate in cardiomyocyte proliferation. In the presence, but not the absence, of $HRas^{G12V}$, Myc activation competently elicited transcriptional programmes involved in cell growth, biogenesis, and metabolism that led to a cardiomyocyte proliferative response. Overlap of the genes altered in Myc and HRas activated hearts with those altered during regeneration of P1 neonatal cardiomyocytes indicated a strong correlation, suggesting that common regenerative transcriptional pathways are activated.

Quantification of cardiomyocyte division is notoriously challenging as cell-cycle re-entry does not necessarily lead to cell division (49–51), and the cell death observed in the HRas model prohibited long-term experimentation and cardiomyocyte number estimation by dissociation techniques. Ki67 is expressed during all active phases of the cell cycle while p-H3 expression begins in G2 and is present throughout mitosis. These markers relay no information regarding cytokinesis and hence they are technically markers of cell cycling and not necessarily proliferation. Here, we observe both Ki67 and p-H3 expression in cardiomyocytes (**Figure 4D**) demonstrating that combined Myc and HRas overexpression drive cardiomyocytes into the cell cycle. Aurora B kinase is expressed during G2, anaphase, metaphase, telophase, and cytokinesis, where it is detected within the mid-body and can be used as a marker of cardiomyocyte division. However, it is present in an asymmetrical location within cardiomyocytes undergoing bi-nucleation (49) and caution is needed when interpreting staining patterns (50). Here we observed Aurora B kinase localisation in cardiomyocytes in prophase, metaphase, anaphase/telophase and symmetrical mid-bodies. Mitotic kinesin-like protein 1 (Mklp1) is an additional marker of cardiomyocyte cytokinesis where it accumulates at the cleavage furrow (52, 53). Here we observed Mklp1 staining at the cleavage furrow of cardiomyocytes in Myc/HRas overexpressing hearts. While these data provide some evidence that Myc and HRas together drive cardiomyocytes' entry into the cell cycle with positivity for markers of cytokinesis, productive cell division cannot be formally confirmed without direct cardiomyocyte counting.

In healthy adult mammalian heart apoptosis is rare with only 0.01–0.001% TUNEL-positive cardiomyocytes observed. This rises to 2–12% apoptotic cardiomyocytes in MI ischaemia and reperfusion injury (54–56). Apoptotic death is also a common feature of cardiomyocytes driven into the cycle by overexpression of some cell cycle regulators such as E2F1, CDK1, and CCNB (8, 57). Paradoxically oncogenes, particularly Myc and Ras, promote both pro-proliferative and pro-apoptotic signals, and the cell fate outcome depends very much on the cell type and context (58). In cardiomyocytes, PI3K and ERK activation downstream of HRas has strong anti-apoptotic effects, promoting cardiomyocyte survival in pressure-overload hypertrophy and heart failure (59). However, hypertrophic cardiomyopathy resulting from HRas mutation associated with chronic constitutively activated Ras/Raf/MEK/ERK pathway and pathological hypertrophy leads to apoptosis (60), similar to the phenotype seen in *TetO-HRas; Myh6-tTA* mice used in this study. We show that MycER expression alone did not lead to cell death in agreement with similar models (15). However, prolonged/persistent ectopic $HRas^{G12V}$ signalling leads to apoptotic cell death, which was exacerbated by transient Myc signalling. Transcriptional profiling indicated Myc/HRas hearts expressed increased levels of the pro-apototic factors Bak, Bok and enhanced inflammatory response, which may be promoting apoptosis. These data indicate endogenous cardiac regeneration is unlikely to be effective with the combination of Myc and HRas. More importantly, the data suggest patients with elevation in Ras signalling in hypertrophic hearts may not benefit or may be harmed, from driving endogenous

cardiomyocyte regeneration via activation of cell cycle genes such as Myc. Here, we activated HRas for 4 weeks, further studies are required to establish whether a shorter period of HRas expression results in similar transcriptional changes and proliferation without hypertrophy and apoptosis.

More encouragingly, elevated Cyclin T1 expression, absent of HRas activation, co-operated with activated Myc to drive cardiomyocyte proliferation in the absence of apoptosis, suggesting that co-expression of Cyclin T1 and Myc may be a therapeutically tractable approach for heart regeneration after injury. Myc/Cyclin T1 hearts expressed an increased Wnt/Beta catenin signature, which has recently been shown to be cardioprotective in an adult mammalian setting (61), deciphering the key protective and destructive pathways will be key to translating these findings. As with all genes able to drive proliferation in cardiomyocytes the expression must be tightly regulated and localised. Promising modes of delivery are being developed including cell-specific viral expression vectors and transient modified mRNA technologies.

Study limitations

$HRas^{G12V}$ is restricted to the cardiomyocytes in the *TetO-HRas; Myh6-tTA;* $R26^{CMER/+}$ mice, but Myc is expressed across the whole animal, so care must be taken to draw conclusions from the bulk transcriptional data because the interaction between Myc activated non-myocytes and cardiomyocytes are possible. The different systems used to overexpress HRas (*TetO-HRas; Myh6-tTA;* $R26^{CMER/+}$ mice) and Cyclin T1 (*AAV9-cTnT-Ccnt1*) mean the apoptosis and proliferation efficiencies between these groups cannot be directly compared.

Data availability statement

All datasets generated and used in this study, have been deposited in ArrayExpress (www.ebi.ac.uk/arrayexpress) under accession codes: E-MTAB-7595, E-MTAB-8462, and E-MTAB-7636. Further information and requests for resources and reagents should be directed to, and will be fulfilled, by CW, chw39@cam.ac.uk.

Ethics statement

All experimental procedures received ethical approval and were conducted in accordance with the Home Office UK guidelines, under project licences 70/7586 and 80/2396 (GE) and PP2054013 (CW) that were evaluated and approved by the Animal Welfare and Ethical Review Body at the University of Cambridge.

Author contributions

MB and CW conceptualised the study. AB, MB, GQ-R, CA, and LT performed the experimental work. GQ-R and JS performed the sequencing analysis. AB, MB, and CW wrote the manuscript. GE and TL edited the manuscript. GE, JH, and CW obtained the funding. All authors contributed to the article and approved the submitted version.

Funding

This work was supported by the Cancer Research UK (Programme Grant CRUK-19013 to GE). MB was funded by an EMBO Long-term fellowship and an Australian National Health and Medical Research Council Early Career Fellowship. This work was also supported by funding from the Wellcome Trust Institutional Strategic Support Fund (204845/Z/16/Z to CW).

Acknowledgments

We thank the support staff in the Cambridge University Biomedical Services at the Gurdon Institute, CRUK Cambridge Institute and the Anne McLaren Building. We also like to thank the NGS library facility at the Wellcome – MRC Cambridge Stem Cell Institute and Steven Lane for laboratory support. Images were created with BioRender.com.

Conflict of interest

Authors MB and CW were named inventors on a patent (PCT/GB2020/050350) relating to data in this manuscript.

The remaining authors declare that the research was conducted in the absence of any commercial or financial relationships that could be construed as a potential conflict of interest.

Publisher's note

Supplementary material

The Supplementary Material for this article can be found online at: https://www.frontiersin.org/articles/10.3389/fcvm.2022.948281/full#supplementary-material

References

1. Bergmann O, Bhardwaj RD, Bernard S, Zdunek S, Barnabé- F, Walsh S, et al. Evidence for cardiomyocyte renewal in humans. *Science.* (2009) 324:98–103.

2. Sadek H, Olson EN. Toward the goal of human heart regeneration. *Cell Stem Cell.* (2020) 26:7–16.

3. Jopling C, Sleep E, Raya M, Martí M, Raya A, Belmonte JCI. Zebrafish heart regeneration occurs by cardiomyocyte dedifferentiation and proliferation. *Nature.* (2010) 464:606–9.

4. Porrello ER, Mahmoud AI, Simpson E, Hill JA, Richardson JA, Olson EN, et al. Transient regenerative potential of the neonatal mouse heart. *Science.* (2011) 331:1078–80.

5. Kikuchi K, Holdway JE, Werdich AA, Anderson RM, Fang Y, Egnaczyk GF, et al. Primary contribution to zebrafish heart regeneration by gata4+ cardiomyocytes. *Nature.* (2010) 464:601–5. doi: 10.1038/nature08804

6. Leach JP, Heallen T, Zhang M, Rahmani M, Morikawa Y, Hill MC, et al. Hippo pathway deficiency reverses systolic heart failure after infarction. *Nature.* (2017) 550:260–4.

7. Nakada Y, Canseco DC, Thet S, Abdisalaam S, Asaithamby A, Santos CX, et al. Hypoxia induces heart regeneration in adult mice. *Nature.* (2017) 541:222–7.

8. Mohamed T, Ang Y-S, Radzinsky E, Zhou P, Huang Y, Elfenbein A, et al. Regulation of cell cycle to stimulate adult cardiomyocyte proliferation and cardiac regeneration. *Cell.* (2018) 173:104–16.

9. Hirose K, Payumo AY, Cutie S, Hoang A, Zhang H, Guyot R, et al. Evidence for hormonal control of heart regenerative capacity during endothermy acquisition. *Science.* (2019) 364:184–8.

10. Monroe TO, Hill MC, Morikawa Y, Rodney GG, Martin JF, Monroe TO, et al. Article YAP partially reprograms chromatin accessibility to directly induce adult cardiogenesis In Vivo YAP partially reprograms chromatin accessibility to directly induce adult cardiogenesis In Vivo. *Dev Cell.* (2019) 48:765–79. doi: 10.1016/j.devcel.2019.01.017

11. Bywater MJ, Burkhart DL, Sabò A, Straube J, Pendino V, Hudson JE, et al. Reactivation of Myc transcription in the mouse heart unlocks its proliferative capacity. *Nat Commun.* (2020) 11:1827. doi: 10.1038/s41467-020-15552-x

12. Amati B, Littlewood TD, Evan GI, Land H. The c-Myc protein induces cell cycle progression and apoptosis through dimerization with Max. *EMBO J.* (1993) 12:5083–7. doi: 10.1002/j.1460-2075.1993.tb06202.x

13. Sodir NM, Evan GI. Nursing some sense out of Myc mitogenic stimuli. *J Biol.* (2009) 8:77.

14. Quaife-Ryan GA, Sim CB, Ziemann M, Kaspi A, Rafehi H, Ramialison M, et al. Multicellular transcriptional analysis of mammalian heart regeneration. *Circulation.* (2017) 136:1123–39. doi: 10.1161/CIRCULATIONAHA.117.028252

15. Xiao G, Mao S, Baumgarten G, Serrano J, Jordan MC, Roos KP, et al. Inducible activation of c-Myc in adult myocardium in vivo provokes cardiac myocyte hypertrophy and reactivation of DNA synthesis. *Circ Res.* (2001) 89:1122–9. doi: 10.1161/hh2401.100742

16. Jonkers I, Lis JT. Getting up to speed with transcription elongation by RNA polymerase II. *Nat Rev Mol Cell Biol.* (2015) 16:167–76. doi: 10.1038/nrm3953

17. Peterlin BM, Price DH. Controlling the elongation phase of transcription with P-TEFb. *Mol Cell.* (2006) 23:297–305. doi: 10.1016/j.molcel.2006.06.014

18. Marshall RM, Salerno D, Garriga J, Graña X, Marshall M, Salerno D, et al. Cyclin T1 expression is regulated by multiple signaling pathways and mechanisms during activation of human peripheral blood lymphocytes. *J Immunol.* (2005) 175:6402–11. doi: 10.4049/jimmunol.175.10.6402

19. Paparidis NF, Durvale MC, Canduri F. The emerging picture of CDK9/P-TEFb: More than 20 years of advances since PITALRE. *Mol Biosyst.* (2017) 13:246–76. doi: 10.1039/c6mb00387g

20. Kim YK, Mbonye U, Hokello J, Karn JT-. Cell receptor signaling enhances transcriptional elongation from latent HIV proviruses by activating P-TEFb through an ERK-dependent pathway. *J Mol Biol.* (2011) 410:896–916. doi: 10.1016/j.jmb.2011.03.054

21. Quaresma AJC, Bugai A, Barboric M. Cracking the control of RNA polymerase II elongation by 7SK snRNP and P-TEFb. *Nucleic Acids Res.* (2016) 44:7527–39. doi: 10.1093/nar/gkw585

22. Garriga J, Bhattacharya S, Calbo J, Marshall M, Truongcao M, Haines DS, et al. CDK9 is constitutively expressed throughout the cell cycle, and its steady-state expression is independent of SKP2. *Mol Cell Biol.* (2003) 23:5165–73. doi: 10.1128/MCB.23.15.5165-5173.2003

23. O'Keeffe B, Fong Y, Chen D, Zhou S, Zhou Q. Requirement for a kinase-specific chaperone pathway in the production of a Cdk9 / Cyclin T1 heterodimer responsible for P-TEFb-mediated tat stimulation of HIV-1 transcription. *J Biol Chem.* (2000) 275:279–87. doi: 10.1074/jbc.275.1.279

24. Chiu Y, Cao H, Jacque J, Stevenson M, Rana TM. Inhibition of human immunodeficiency virus type 1 replication by RNA interference directed against human transcription elongation factor P-TEFb (CDK9 / CyclinT1). *J Virol.* (2004) 78:2517–29. doi: 10.1128/jvi.78.5.2517-2529.2004

25. Sano M, Abdellatif M, Oh H, Xie M, Bagella L, Giordano A, et al. Activation and function of cyclin T-Cdk9 (positive transcription elongation factor-b) in cardiac muscle-cell hypertrophy. *Nat Med.* (2002) 8:1310–7. doi: 10.1038/nm778

26. Sano M, Wang SC, Scaglia F, Xie M, Sakai S, Tanaka T, et al. Activation of cardiac Cdk9 represses PGC-1 and confers a predisposition to heart failure. *EMBO J.* (2004) 23:3559–69. doi: 10.1038/sj.emboj.7600351

27. Karnoub AE, Weinberg RA. Ras oncogenes: Split personalities. *Nat Rev Mol Cell Biol.* (2008) 9:517–31.

28. Sugden PH. Ras, Akt, and mechanotransduction in the cardiac myocyte. *Circ Res.* (2003) 93:1179–92. doi: 10.1161/01.RES.0000106132.04301.F5

29. Hunter JJ, Tanaka N, Rockman HA, Ross J, Chien KR. Ventricular expression of a MLC-2v-ras fusion gene induces cardiac hypertrophy and selective diastolic dysfunction in transgenic mice*. *J Biol Chem.* (1995) 270:23173–8. doi: 10.1074/jbc.270.39.23173

30. Wei B-R, Martin PL, Spehalski SBHE, Kumar M, Hoenerhoff MJ, Rozenberg J, et al. Capacity for resolution of ras–MAPK-initiated early pathogenic myocardial hypertrophy modeled in mice. *Comp Med.* (2011) 61:109–18.

31. Abdellatif M, Packer SE, Michael LH, Zhang D, Charng MJ, Schneider MD. A ras-dependent pathway regulates RNA polymerase II Phosphorylation in cardiac myocytes: Implications for cardiac hypertrophy. *Mol Cell Biol.* (1998) 18:6729–36. doi: 10.1128/MCB.18.11.6729

32. Martin M. Cutadapt removes adapter sequences from high-throughput sequencing reads. *EMBnet J.* (2011) 17:10. doi: 10.14806/ej.17.1.200

33. Li B, Dewey CN. RSEM: Accurate transcript quantification from RNA-Seq data with or without a reference genome. *BMC Bioinformatics.* (2011) 12:323. doi: 10.1186/1471-2105-12-323

34. Robinson MD, McCarthy DJ, Smyth GK. edgeR: A bioconductor package for differential expression analysis of digital gene expression data. *Bioinformatics.* (2009) 26:139–40.

35. Bolger AM, Lohse M, Usadel B. Trimmomatic: A flexible trimmer for Illumina sequence data. *Bioinformatics.* (2014) 30:2114–20.

36. Dobin A, Davis CA, Schlesinger F, Drenkow J, Zaleski C, Jha S, et al. Ultrafast universal RNA-seq aligner. *Bioinformatics.* (2013) 29:15–21. doi: 10.1093/bioinformatics/bts635

37. Anders S, Pyl PT, Huber W. HTSeq-A Python framework to work with high-throughput sequencing data. *Bioinformatics.* (2015) 31:166–9. doi: 10.1093/bioinformatics/btu638

38. Gentleman R, Carey V, Bates D, Bolstad B, Dettling M, Dudoit S, et al. Bioconductor: Open software development for computational biology and bioinformatics. *Genome Biol.* (2004) 5:R80. doi: 10.1186/gb-2004-5-10-r80

39. Kishore K, de Pretis S, Lister R, Morelli MJ, Bianchi V, Amati B, et al. methylPipe and compEpiTools: A suite of R packages for the integrative analysis of epigenomics data. *BMC Bioinformatics.* (2015) 16:313. doi: 10.1186/s12859-015-0742-6

40. Chen EY, Tan CM, Kou Y, Duan Q, Wang Z, Meirelles GV, et al. Enrichr: Interactive and collaborative HTML5 gene list enrichment analysis tool. *BMC Bioinformatics.* (2013) 14:128. doi: 10.1186/1471-2105-14-128

41. Batho CAP, Mills RJ, Hudson JE. Metabolic regulation of human pluripotent stem cell-derived cardiomyocyte maturation. *Curr Cardiol Rep.* (2020) 22:73. doi: 10.1007/s11886-020-01303-3

42. Pianca N, Sacchi F, Umansky KB, Chirivì M, Iommarini L, Da Pra S, et al. Glucocorticoid receptor antagonization propels endogenous cardiomyocyte proliferation and cardiac regeneration. *Nat Cardiovasc Res.* (2022) 1:617–33. doi: 10.1038/s44161-022-00090-0

43. Murphy DJ, Junttila MR, Pouyet L, Karnezis A, Shchors K, Bui DA, et al. Distinct thresholds govern myc's biological output in vivo. *Cancer Cell.* (2008) 14:447–57. doi: 10.1016/j.ccr.2008.10.018

44. Zheng M, Dilly K, Dos Santos Cruz J, Li M, Gu Y, Ursitti JA, et al. Sarcoplasmic reticulum calcium defect in Ras-induced hypertrophic cardiomyopathy heart. *Am J Physiol Hear Circ Physiol.* (2004) 286:424–33. doi: 10.1152/ajpheart.00110.2003

45. Ruan H, Mitchell S, Vainoriene M, Lou Q, Xie LH, Ren S, et al. Giα1-Mediated cardiac electrophysiological remodeling and arrhythmia in hypertrophic cardiomyopathy. *Circulation.* (2007) 116:596–605. doi: 10.1161/CIRCULATIONAHA.106.682773

46. Mitchell S, Ota A, Foster W, Zhang B, Fang Z, Patel S, et al. Distinct gene expression profiles in adult mouse heart following targeted MAP kinase activation. *Physiol Genomics.* (2006) 25:50–9. doi: 10.1152/physiolgenomics.00224.2005

47. Beisaw A, Kuenne C, Guenther S, Dallmann J, Wu CC, Bentsen M, et al. AP-1 contributes to chromatin accessibility to promote sarcomere disassembly and cardiomyocyte protrusion during zebrafish heart regeneration. *Circ Res.* (2020) 126:1760–78. doi: 10.1161/CIRCRESAHA.119.316167

48. Wu H-Y, Zhou Y-M, Liao Z-Q, Zhong J-W, Liu Y-B, Zhao H, et al. Fosl1 is vital to heart regeneration upon apex resection in adult *Xenopus tropicalis*. *npj Regen Med.* (2021) 6:1–16. doi: 10.1038/s41536-021-00146-y

49. Heallen TR, Kadow ZA, Kim JH, Wang J, Martin JF. Stimulating cardiogenesis as a treatment for heart failure. *Circ Res.* (2019) 124:1647–57.

50. Engel FB, Schebesta M, Keating MT. Anillin localization defect in cardiomyocyte binucleation. *J Mol Cell Cardiol.* (2006) 41:601–12. doi: 10.1016/j.yjmcc.2006.06.012

51. Engel FB, Schebesta M, Duong MT, Lu G, Ren S, Madwed JB, et al. p38 MAP kinase inhibition enables proliferation of adult mammalian cardiomyocytes. *Genes Dev.* (2005) 19:1175–87. doi: 10.1101/gad.1306705

52. Capalbo L, Bassi ZI, Geymonat M, Todesca S, Copoiu L, Enright AJ, et al. The midbody interactome reveals unexpected roles for PP1 phosphatases in cytokinesis. *Nat Commun.* (2019) 10:1–17. doi: 10.1038/s41467-019-12507-9

53. Nishiyama C, Saito Y, Sakaguchi A, Kaneko M, Kiyonari H, Xu Y, et al. Prolonged myocardial regenerative capacity in neonatal opossum. *Circulation.* (2022) 146:125–39. doi: 10.1161/CIRCULATIONAHA.121.055269

54. Bennett MR. Apotosis in the cardiovascular system. *Heart.* (2002) 87:487.

55. Van Empel VPM, Bertrand ATA, Hofstra L, Crijns HJ, Doevendans PA, De Windt LJ. Myocyte apoptosis in heart failure. *Cardiovasc Res.* (2005) 67:21–9.

56. Chiong M, Wang ZV, Pedrozo Z, Cao DJ, Troncoso R, Ibacache M, et al. Cardiomyocyte death: Mechanisms and translational implications. *Cell Death Dis.* (2011) 2:1–11.

57. Agah R, Kirshenbaum LA, Abdellatif M, Truong LD, Chakraborty S, Michael LH, et al. Adenoviral delivery of E2F-1 directs cell cycle reentry and p53-independent apoptosis in postmitotic adult myocardium in vivo. *J Clin Invest.* (1997) 100:2722–8. doi: 10.1172/JCI119817

58. Cox AD, Der CJ. The dark side of Ras: Regulation of apoptosis. *Oncogene.* (2003) 22:8999–9006. doi: 10.1038/sj.onc.1207111

59. Gallo S, Vitacolonna A, Bonzano A, Comoglio P, Crepaldi TERK. A key player in the pathophysiology of cardiac hypertrophy. *Int J Mol Sci.* (2019) 20:1–21.

60. Sala V, Gallo S, Leo C, Gatti S, Gelb BD, Crepaldi T. Signaling to cardiac hypertrophy: Insights from human and mouse RASopathies. *Mol Med.* (2012) 18:938–47.

61. Quaife-Ryan GA, Mills RJ, Lavers G, Voges HK, Vivien CJ, Elliott DA, et al. β-Catenin drives distinct transcriptional networks in proliferative and nonproliferative cardiomyocytes. *Development.* (2020) 147:dev193417. doi: 10.1242/dev.193417

frontiers | Frontiers in Cardiovascular Medicine

TYPE Review
PUBLISHED 03 November 2022
DOI 10.3389/fcvm.2022.1000578

OPEN ACCESS

EDITED BY
Rajika Roy,
Temple University, United States

REVIEWED BY
Murugesan Velayutham,
West Virginia University, United States
Sudhahar Varadarajan,
Augusta University, United States
Motohiro Nishida,
National Institute for Physiological Sciences (NIPS), Japan

*CORRESPONDENCE
Guoan Zhao
guoanzhao@xxmu.edu.cn
Fei Lin
linfeixixi@aliyun.com

SPECIALTY SECTION
This article was submitted to Cardiovascular Biologics and Regenerative Medicine, a section of the journal Frontiers in Cardiovascular Medicine

RECEIVED 22 July 2022
ACCEPTED 18 October 2022
PUBLISHED 03 November 2022

CITATION
Miao R, Wang L, Chen Z, Ge S, Li L, Zhang K, Chen Y, Guo W, Duan X, Zhu M, Zhao G and Lin F (2022) Advances in the study of nicotinamide adenine dinucleotide phosphate oxidase in myocardial remodeling. *Front. Cardiovasc. Med.* 9:1000578. doi: 10.3389/fcvm.2022.1000578

Advances in the study of nicotinamide adenine dinucleotide phosphate oxidase in myocardial remodeling

Runran Miao[1], Libo Wang[1,2], Zhigang Chen[1,3,4], Shiqi Ge[1], Li Li[1], Kai Zhang[1], Yingen Chen[1], Wenjing Guo[1], Xulei Duan[1], Mingyang Zhu[1], Guoan Zhao[1,3,4]* and Fei Lin[1,3,4]*

[1]Department of Cardiology, The First Affiliated Hospital of Xinxiang Medical University, Heart Center of Xinxiang Medical University, Xinxiang, China, [2]College of Chemistry and Chemical Engineering, Henan Normal University, Xinxiang, China, [3]Cardiovascular Repair Engineering Technology Research Center, The First Affifiliated Hospital of Xinxiang Medical University, Xinxiang, China, [4]International Joint Laboratory of Cardiovascular Injury and Repair, The First Affifiliated Hospital of Xinxiang Medical University, Xinxiang, China

Myocardial remodeling is a key pathophysiological basis of heart failure, which seriously threatens human health and causes a severe economic burden worldwide. During chronic stress, the heart undergoes myocardial remodeling, mainly manifested by cardiomyocyte hypertrophy, apoptosis, interstitial fibrosis, chamber enlargement, and cardiac dysfunction. The NADPH oxidase family (NOXs) are multisubunit transmembrane enzyme complexes involved in the generation of redox signals. Studies have shown that NOXs are highly expressed in the heart and are involved in the pathological development process of myocardial remodeling, which influences the development of heart failure. This review summarizes the progress of research on the pathophysiological processes related to the regulation of myocardial remodeling by NOXs, suggesting that NOXs-dependent regulatory mechanisms of myocardial remodeling are promising new therapeutic targets for the treatment of heart failure.

KEYWORDS

heart failure, myocardial remodeling, NADPH oxidase, reactive oxygen species, oxidative stress

Introduction

Myocardial remodeling is a fundamental pathophysiological process in heart failure (HF) and is closely related to high morbidity and mortality of cardiovascular diseases (CVD) worldwide (1, 2). The main pathological features of myocardial remodeling are cardiomyocyte hypertrophy and apoptosis, excessive extracellular matrix protein (ECM) deposition, collagen deposition, and perivascular fibrosis, which lead to

myocardial stiffness, chamber dilation, cardiac insufficiency, and ultimately heart failure (1, 3). Furthermore, various cardiovascular diseases, such as myocardial infarction, cardiomyopathy, heart valve disease, myocarditis, and hypertension, can lead to myocardial remodeling, myocardial stiffness, and reduced compliance, followed by heart failure and death (4). Therefore, reversing myocardial remodeling and reducing morbidity and mortality of heart failure is the key to clinical treatment of cardiovascular diseases. Accumulating evidence suggests that ROS produced by nicotinamide adenine dinucleotide phosphate (NADPH) oxidases (NOXs) can regulate the level of oxidative stress and participate in the development of myocardial remodeling. This review explores the involvement of NADPH oxidase-related isoforms in the pathophysiological process of myocardial remodeling development through the regulation of complex molecular pathways and provides new ideas and approaches for the treatment of heart failure.

Nicotinamide adenine dinucleotide phosphate oxidase

NADPH oxidase, a multi-enzyme complex originally found in neutrophils, is involved in the non-specific host immune defense response against pathogenic microorganisms and is a key regulator of the redox homeostatic response. Seven mammalian isoforms of NOXs have been identified, including NOX1, NOX2, NOX3, NOX4, NOX5, double oxidase 1 (DUX1), and double oxidase 2 (DUOX2) (5, 6). All NOX isoforms contain NADPH-and flavin adenine dinucleotide (FAD)-binding domains. The different isoforms comprise homologs containing the NOX2 gp91Phox subunit but have different localization and regulatory roles (7). NOX1–4 consists of the NOX subunit catalytic subunit and p22phox as the only membrane-bound subunit. NOX5 is a structurally active enzyme body consisting of only the NOX subunit. DUOX 1 and DUOX2 consist of the DUOX-1/2 subunit, DUOXA1/2 subunit, and amino-terminal transmembrane structural domain with the peroxidase-like structural domain (8, 9). **Table 1** describes the composition, localization and related functions of NADPH oxidase.

The highest levels of NOX1, NOX2, NOX4, and NOX5 are found in the cardiovascular system (10), and the main isoforms expressed in the skeletal system are NOX1, NOX2, and NOX4. NOX3 is expressed only in fetal tissues and in the inner ear, especially in the cochlea, sensory epithelium, and spiral ganglia of the vestibule, which are essential for vestibular development and function (11, 12). DUOX1 and DUOX2 are mainly expressed in thyroid tissues (13). NOXs are composed of different regulatory subunits. NOX1 consists of p22Phox, NOXO1, NOXA1, and RAC1/2 regulatory subunits, NOX2 consists of Gp91Phox, p22Phox, p47Phox, p67Phox, p40Phox, and RAC1/2 regulatory subunits, and NOX3 consists of p22Phox and NOXO regulatory subunits. The p22Phox regulatory subunits regulate NOX4, and NOX5, DUOX 1, and DUOX2 are mainly regulated by the calcium-dependent mode of the N-terminal structural domain without p22Phox regulatory subunits (8, 14, 15).

NOXs are one of the main sources of reactive oxygen species (ROS) that are involved in the pathophysiological processes of CVD through redox reactions (11, 16). ROS in the heart is mainly produced through NOX1, NOX2, NOX4, and NOX5 catalysis (17). The main enzymatic sources of ROS are mitochondrial respiratory chain enzymes, xanthine oxidase (XO), uncoupled endothelial nitric oxide synthase (eNOS), and NOXs (18, 19). ROS, known as "second messengers," play a role in rapidly regulating the activity of signaling molecules and transcription factors. The main types of ROS include superoxide radical anion (O2·-), hydrogen peroxide (H_2O_2), and hydroxyl radicals (·OH). NOX1, 2, and 5 produce O2·-, while NOX4 mainly produces H_2O_2. NOX-induced oxidative stress that produces ROS can lead to eNOS dysregulation and endothelial dysfunction, reduce NO bioavailability, and induce myocardial damage (20). Under normal conditions, a small amount of ROS maintains the homeostasis of the cardiovascular system. However, excess ROS can cause redox imbalance, resulting in myocardial cell apoptosis and necrosis, fibroblast proliferation, activation of matrix metalloproteinases (MMPs), collagen deposition, and other pathophysiological processes, activating oxidative stress and causing pathological myocardial remodeling, leading to various diseases, such as myocardial infarction, hypertension, arrhythmia, heart failure, and vascular dysfunction (21–23). Excessive production of ROS also activates a variety of hypertrophic signaling kinases and transcription factors, disrupting the contractile function of excitation-contraction coupling core proteins, causing mitochondrial DNA(mtDNA) damage, lipid and protein peroxidation, abnormal ion channel function, leading to fibroblast proliferation, vascular endothelial dysfunction, interstitial fibrosis, atheromatous plaque formation, thromboembolism formation and inadequate cardiac energy supply, eventually progressing to heart failure (24–28). Recent studies have shown that ROS produced by mitochondria activate the oxidative stress process, causing apoptosis and interstitial fibrosis, resulting in functional and structural impairment, leading to deterioration of right ventricular (RV) function and pressure overload, which in turn leads to right heart failure (29). Studies have shown that NOX-related subtypes can mediate the development of cardiovascular diseases through the production of excess ROS. **Figure 1** shows the functional properties and basic activators of the four isoforms involved in myocardial remodeling.

NOX1

NOX1 was initially found in colon epithelial cells but can also be expressed in smooth muscle cells, fibroblasts, and

TABLE 1 Introduction to the composition, localization and related functions of NADPH oxidase.

	Essential regulatory subunits	Requirement for p22phox	Cell/tissue distribution	Cardiomyocyte expression	Regulating factors	Model building	References
NOX1	NOXO1 NOXA1 RAC	Yes	Smooth muscle cells Fibroblasts Endothelial cells	No	AngII NF-κB ET-1 IFN-γ VEGF PDGF ATF-1 GPER	ApoE$^{-/-}$, SHRs Tg^{SMCnox1} HFHS/STZ, NoxO1$^{-/-}$ Gper$^{-/-}$	(6, 8–12, 17, 20, 22, 26, 27, 29, 33, 36–39)
NOX2	Gp91Phox p47^{Phox} p67^{Phox} p40^{Phox} RAC	Yes	Cardiomyocytes, endothelial cells Vascular-smooth muscle cells Fibroblasts	Yes	AngII ET-1 TGF-β IFN-γ PDGF VEGF	Nox2$^{-/-}$, ApoE$^{-/-}$ LysM$^{Cre/WT}$ gp91phox$^{-/-}$ TLR5$^{-/-}$ TRPC3/C6 ectopic-expression	(6, 10–12, 17, 20, 31, 34, 41, 42, 44, 45, 47, 51, 52, 59, 104)
NOX3	NOXO	Yes	Fetal tissue inner ear	No			(11, 12)
NOX4	Calcium ions	Yes	Cardiomyocytes, endothelial cells Fibroblasts Vascular-smooth muscle cells	Yes	HIF-1 TGF-β TNF-α IFN-γ VEGF	NOX4$^{-/-}$, APOE$^{-/-}$ Tg-Nox4 HCAEC Cardio-Nox4$^{-/-}$ Endo-Nox4$^{-/-}$ ApoE$^{-/-}$/ p47phox$^{-/-}$ SHRs	(6, 7, 9, 22, 31, 35, 62, 63, 67–70, 75)
NOX5	Calcium ions	No	Endothelial cells Vascular-smooth muscle cells Extravascular fibroblasts	No	AngII TNF-α TGF-β PDGF IFN-γ	NOX5$^{±}$CRE$^{±}$ TeloHAEC cell line NOX5-siRNA	(6, 17, 20, 22, 31, 77–79, 81, 82, 84)

AngII, Angiotensin II; NF-Kb, nuclear factor kappa-B; ET-1,endothelin-1; IFN-γ, interferon-γ; VEGF, vascular endothelial growth factor; PDGF, platelet derived growth factor; ATF-1, activating transcription Factor 1; GPER, G-protein-coupled estrogen receptor; HIF-1, hypoxia-inducible factor-1; TNF, tumor necrosis factor; TGF-β, transforming growth factor-β; ApoE$^{-/-}$, ApoE knockout mice; SHRs, spontaneously hypertensive rats; Tg^{SMCnox1}, mice overexpressing Nox1 in SMCs; HFHS/STZ, high-fat and high-sugar diet/streptozotocin mouse model; NoxO1$^{-/-}$, Noxo1-knockout mice; Gper$^{-/-}$, G protein-coupled estrogen receptor gene deficient mice; Nox2$^{-/-}$, Nox2 knockout mice; LysM$^{Cre/WT}$, Model mice using the promoter of LysM gene to drive Cre recombinase; gp91phox$^{-/-}$, gp91phox knockout mice; TRPC3/C6, Canonical transient receptor potential; $^{-}$CRE, Cyclization Recombination Enzyme; Cardio-Nox4$^{-/-}$, Cardiomyocyte NOX4 knockout mice; Endo-Nox4$^{-/-}$, endothelial cell NOX4 knockout mice; Tg-Nox4 HCAEC, NOX4 overexpression in mouse coronary endothelial cells; TeloHAEC cell line, is a clonal cell line immortalized by stably expressing human telomerase catalytic subunit hTERT; NOX5-siRNA, NOX5-silenced.

endothelial cells. NOX1 is involved in the development of many diseases, such as atherosclerotic cardiovascular disease, lung disease, chronic kidney disease, cerebrovascular disease, and cancer (5, 30, 31). NOX1 is expressed on the X chromosome and determines the risk of sex-linked diseases (32). It is the main isoform regulating hypertensive diseases and aortic thickening. NOX1 has a self-regulatory function and is mainly regulated by the expression levels of various proteins such as AngII, NF-κB, endothelin-1 (ET-1), interferon-γ(IFN-γ), vascular endothelial growth factor (VEGF), platelet-derived growth factor (PDGF), activating transcription factor 1 (ATF-1), and G protein-coupled estrogen receptor (GPER), which play pro-proliferative and pro-inflammatory roles (6, 31, 33, 34).

Studies have shown that NOX1 promotes the progression of atherosclerotic disease, hypertensive disease, and myocardial remodeling through multiple signaling targets. Experimental studies showed that NOX1 expression was barely detectable in the left ventricle of adult rats and cultured cardiomyocytes of neonatal rats, but NOX2 and NOX4 could be detected, and the NOX2 expression level was higher than that of NOX4 (35). High NOX1 expression activates macrophage infiltration and promotes systemic inflammatory responses, thereby accelerating atherosclerosis development in female mice (36). Studies have found that NOX1 expression in ApoE$^{-/-}$ mouse models activates endothelial cell and macrophage proliferation and collagen deposition, significantly enlarging the intra-aortic plaque area and promoting atherosclerotic disease progression concurrently (33, 37). Studies have also reported that diabetic APOE$^{-/-}$ mice can increase the NOX1 level by mediating the overexpression of ET-1, increasing the production of ROS in peri-aortic adipose tissue, and promoting atherosclerosis progression (38). Vascular smooth muscle cell phenotype transition is a pathophysiological mechanism of atherosclerotic disease, and protein disulfide isomerase-A1 (PDIA1) is an upstream regulator of smooth muscle cell (SMC) phenotype transition, upregulating the expression levels of NOX1 and NOX4, causing cytoskeleton reconstruction and promoting atherosclerotic disease progression and exacerbating myocardial remodeling (39). AngII directly enhances the binding of NOX1 to angiotensin type 1 (AT1) receptors and stimulates vascular smooth muscle cell activation (5), which has pro-inflammatory and pro-atherosclerotic

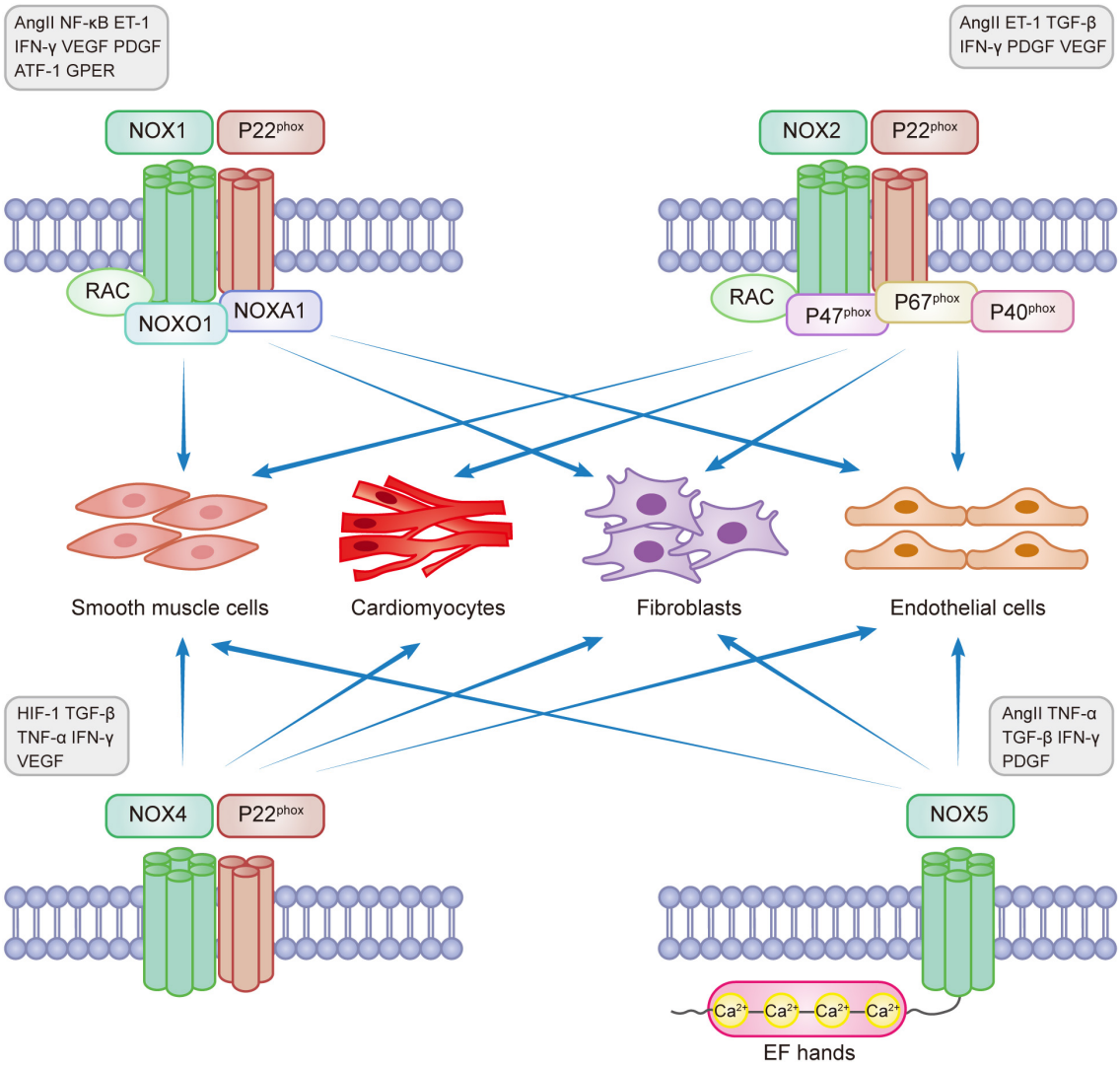

FIGURE 1
NADPH oxidase expression in myocardial remodeling.

effects. The epidermal growth factor receptor (EGFR), an important target of NOX1, upregulates ATF-1-mediated NOX1 expression levels and regulates cell proliferation and migration, promoting atherosclerosis progression (33). A study showed that NOX1 and NOX2 are highly expressed in aged spontaneously hypertensive rats (40). By constructing transgenic mice overexpressing NOX1 in vascular smooth muscle cells ($Tg^{SMCnox1}$), releasing excessive ROS from NOX1 could cause vascular endothelial cell dysfunction, leading to vessel wall hypertrophy and hypertension (41). In another study, NOX1-deficient mice (KO) had reduced expression of the surface adhesion molecules VCAM-1 and ICAM-1, reduced levels of myocardial inflammatory markers such as Mac-2, IL-1, and NLRP3, and downregulated myocardial metabolic remodeling in cardiac endothelial cells compared to male wild-type mice (WT) using a high-fat, high-sugar diet (HFHS)/streptozotocin (STZ) mouse model (42). GPER receptors promote ROS production by directly enhancing NOX1 binding to AT1, stimulating the proliferation of cardiomyocytes and vascular smooth muscle cells, affecting myocardial structural and morphological changes (43), and leading to myocardial remodeling.

NOX2

NOX2 (gp91Phox), present in phagocytes, is the first typical member of the NADPH oxidase family to be identified. NOX2 can be expressed in cardiomyocytes, endothelial cells, vascular smooth muscle cells, fibroblasts, and inflammatory cells and is

present in the heart, blood vessels, neural tissue, and kidney (14, 44, 45). NOX2 is a major enzyme involved in the membrane-bound release of ROS and the development of heart failure, dyskinesia, and myotonic diseases (46). Many factors could enhance the expression of NOX2, such as Hyperglycemia, hyperlipidemia, ischemia-reperfusion injury, Ang II, ET-1, transforming growth factor β (TGF-β), IFN-γ, PDGF, and VEGF (6, 7, 31, 34).

NOX2 is involved in the normal heart developmental process but aggravates the progression of diseases such as atherosclerosis, hypertension, arrhythmias, and heart failure. $NOX2^{-/-}$ embryonic hearts develop abnormal endocardial cushion development, which severely affects the endocardial-to-mesenchymal transition (EndMT) of atrial cushion explants, resulting in endocardial cell proliferation, apoptosis, and cardiac malformations (47). When cardiomyocytes are subjected to mechanical distortion by physiological stretch, they activate NOX2 in the sarcoplasmic and t-tubular membranes, induce ROS production through a microtubule-dependent network (X-ROS signaling), activate oxidative stress, sensitize ryanodine receptors (RyRs) around the sarcoplasmic reticulum (SR), induce massive cytoplasmic calcium ion (Ca^{2+}) release and increase the incidence of arrhythmias and cardiomyopathy (48). Studies have demonstrated that NOX2 expression in $ApoE^{-/-}$ mice reduces NO bioavailability, downregulates oxidative stress, decreases ROS release, and activates vascular smooth muscle cells, which can cause atherosclerosis (49). By constructing a post-infarction heart failure model in the left anterior descending branch of mice, AT1 receptor blockers acted on $NOX2^{+}$ myeloid cells, inducing inflammatory cell infiltration and activation of oxidative stress, causing vascular endothelial dysfunction and exacerbating heart failure (50). Transverse aortic constriction(TAC) induction model mice showed that the absence of NOX2 interfered with oxidative stress in the heart and produced a sustained protective effect against heart failure (45). By constructing $gp91phox^{-/-}$ mouse models, inhibition of NOX2 expression reduced the release of ROS and MMPs, decreased the activation of vascular endothelial cells owing to hypoxia and inflammatory response, and attenuated vascular remodeling (51). NOX2 and NOX4 in the hypothalamic paraventricular nucleus are key sources of aldosterone, leading to ROS release, causing sympathetic excitation, and contributing to the development of hypertensive disease (52). Activation of the renin-angiotensin system (RAS) promotes the high expression of NOX2 in cardiac endothelial cells, releasing excess superoxide, leading to NO inactivation, mediating inflammatory responses, and enhancing endothelial-mesenchymal transition (EMT), which leads to vasodilator dysfunction and increased cardiac interstitial fibrosis (53). Clinical studies have demonstrated a certain thrombotic risk in COVID-19 patients, correlating with oxidative stress caused by NOX2 activation (54, 55). Therefore, NOX2 is expected to be a novel pharmacological target for the treatment and prevention of COVID-19. This shows that NOX2 can be involved in the progression of cardiovascular diseases by participating in the pathogenesis of inflammatory response, apoptosis, and oxidative stress, providing novel ideas for clinical treatment.

NOX2 is involved in cellular hypertrophy and apoptosis during myocardial remodeling. Studies have shown that hyperglycemia can participate in NOX2-mediated oxidative stress in an AMPK-dependent manner, causing myocardial remodeling by causing apoptosis (56, 57). Ras-related C3 botulinum toxin substrate 1 (RAC1) is an important component of NADPH oxidase that promotes the transfer of cytoplasmic subunits to the membrane and induces NOXs activity. RAC1 is an important regulator that mediates NADPH oxidase activity to produce myocardial remodeling (58). RAC1 is involved in NOX2-induced hypertrophy of cardiomyocytes, causing myocardial remodeling (35). NOX2 expression mediates toll-like receptor 5 (TLR5) in adriamycin (Doxorubicin, DOX) toxicity, exacerbating cardiomyocyte death and interstitial fibrosis, leading to acute myocardial injury (59). Transient receptor potential canonical (TRPC) subfamily proteins are components of calcium channels that mediate calcium signaling and are key mediators involved in the development of myocardial remodeling. TRPC3 mediates pathological myocardial remodeling by forming a stable protein complex with NOX2 and p22phox, releasing ROS, amplifying redox signals, and inducing fibrotic responses in cardiomyocytes and fibroblasts through mechanical stimulation (60). Studies have shown that NOX2 is the main source of superoxide anion production by human atrial myocytes, causing apoptosis and interstitial fibrotic remodeling, which is an important basis for oxidative stress and electrophysiological remodeling in patients with atrial fibrillation (61). Therefore,NOX2 downregulation can act as an oxidative stress inhibitor and reduce ROS formation, providing long-term therapeutic value for the treatment of myocardial remodeling and the development of new drugs.

NOX4

NOX4 is the most widely expressed protein initially found in the kidney. NOX4 is present in the mitochondria, endoplasmic reticulum, cardiomyocytes, endothelial cells, vascular smooth muscle cells, fibroblasts, blood vessels, and various organs (31, 39). During various stress conditions, NOX4 is an important source of oxidative stress in myocardial mitochondria and is involved in the energy metabolic process of myocardial remodeling (62). TGF-β, TNF-α, and IFN-γ can activate high NOX4 expression (6, 31, 63, 64). NOX4 can be involved in the pathogenesis of various cardiovascular diseases and myocardial remodeling as a central component of endoplasmic reticulum

stress, participating in the oxidation of sarcoplasmic reticulum calcium ATPase (SERCA), increasing intracellular calcium ion transport, mediating myocardial electrophysiological activity, activating oxidative stress, and reducing autophagy (65).

NOX4 expression plays a partially protective role in the heart (66). NOX4 serves as a vasodilator through H_2O_2. $NOX4^{-/-}$ and $APOE^{-/-}$ mice can induce atherosclerotic disease progression by increasing endothelial cell inflammation and oxidative stress levels (67). NOX4 attenuates age-related mitochondrial oxidative stress and vascular inflammation and reduces the incidence of cardiovascular disease (62, 68). $NOX4^{-/-}$ mice (c-NOX4 KO) inhibited cysteine oxidation and nuclear withdrawal of HDAC4, and TAC-induced pathological myocardial hypertrophy was attenuated (69). During myocardial ischemia-reperfusion (I/R), cardiomyocyte NOX4 levels contributed to macrophage proliferation and polarization responses, and volume overload improved ventricular remodeling after myocardial infarction (MI) through NOX4 activation of Akt and an increase in downstream protein synthesis markers (S6 ribosomal protein and eIF4E-BP1), a therapeutic target (70).

High expression of NOX4, an endogenous anti-atherosclerotic enzyme, can cause damage to the heart. Lack of NOX4 in cardiac myocytes is beneficial, while the lack of NOX4 in blood vessels causes a decreased adaptive response, leading to post-ischemic and hypoxic myocardial injury. During hypoxia, NOX4 mediates the release of HIF-1α and vascular endothelial growth factor (VEGF), causing apoptosis and dysfunction of cardiomyocytes (7, 71). Excess ROS produced by NOX4 promotes cardiomyocyte apoptosis and mitochondrial dysfunction by mediating the upregulation of the pro-apoptotic proteins Bax and caspase-3 and the downregulation of the anti-apoptotic protein BCL2 and the survival protein p-AKTser473, resulting in myocardial structural damage and cardiac systolic and diastolic insufficiency (7, 72). Increased NOX4 expression in male Wistar rats treated with dexamethasone caused sympathetic excitation of the heart and blood vessels, upregulated oxidative stress levels, elevated blood pressure, and caused myocardial fibrosis. Simultaneously, the incidence of ventricular arrhythmias was significantly increased when induced by drugs or abrupt pacing (73). Clinically, the novel hypoglycemic GLP-1 agonist liraglutide exerts an anti-inflammatory effect by interfering with Sirtuin-1 (SIRT1)/NOX4/ROS signaling and NLRP3 inflammatory vesicle-dependent cellular scorching, downregulating NOX4 expression, reducing hypoxia-induced oxidative stress, and acting as a myocardial protector (74). JunD is a member of the activator protein 1 (AP-1) family of transcription factors and serves as a key target protein involved in anti-oxidative stress. $JunD^{-/-}$ mice upregulate oxidative stress levels by activating signaling pathways involved in JNK1 (c-Jun N-terminal kinases), increasing NOX2/4 expression, and inducing inflammatory response pathways involved in NF-κB signaling, causing left heart dysfunction (75). NOX1 and NOX4 mediate signaling pathways that promote smooth muscle cell proliferation, differentiation, and migration, causing vascular remodeling and exacerbating the progression of atherosclerosis and hypertension. Dual inhibitors of Nox1/4 increase blood pressure and perivascular macrophage infiltration, exacerbating perivascular inflammation and fibrosis levels in models of spontaneous hypertension (76). Thus, NOX4 exerts a dual regulatory effect on the myocardium and blood vessels to control the development of myocardial remodeling. The potential risk of cardiovascular disease should be considered when using NOX4 inhibitors.

NOX5

NOX5 is found only in humans and is not expressed in other mammals. It is mainly found in the vascular and renal systems and can be expressed in endothelial cells, vascular smooth muscle cells, and extravascular fibroblasts (77, 78). The NOX5 gene is located on chromosome 15 and includes six different splice isoforms: α, β, γ, δ, ε, and ζ, all of which are expressed in the vascular endothelial and smooth muscle cells. NOX5-α and NOX5-β are the most abundantly expressed and functional proteins for ROS production, and NOX5-ε may be a negative regulator of NOX5 (79). NOX5 does not require regulatory subunit activation and depends on an increased Ca^{2+} concentration for activation, causing a conformational change in the N-terminal structural domain containing the EF-hand loop (78).

Clinical studies have found that NOX5 is involved in the development of myocardial infarction, atherosclerosis, hypertension, and aortic aneurysm and aggravates myocardial remodeling. Hyperglycemia, TNF, TGF-β, IFN-γ, PDGF and Ang II promote increased intracellular calcium, and NOX5 binds directly to intracellular calcium and is activated for overexpression (6, 31, 79). Protein kinase C (PKC) also promotes NOX5 overexpression, regulates the endothelial cyclooxygenase-2 (COX-2)/prostaglandin-2 (PGE2) axis, causes ROS overproduction, and accelerates the progression of myocardial remodeling by activating the post-myocardial infarction (MI) inflammatory response (80, 81). NF-κB, a transcription factor involved in NOX5-induced adenocarcinoma, is involved in apoptosis through the upregulation of ROS-mediated activation of cyclooxygenase-2 (COX-2) (81). Recent studies have shown that NOX5, a gene newly associated with hypertension (82), ameliorates abnormal VSMC proliferation, inhibits oxidative stress, and attenuates hypertensive complications through the NOX5/ROS/c-Src signaling pathway (redox-sensitive protein) (83). In response to platelet-derived growth factor (PDGF) stimulation, NOX5 produces ROS to activate the JAK/STAT pathway to induce the proliferation of human aortic endothelial cells (84). NOX5

promotes the release of ROS from extracellular vesicles (EVS), induces phenotypic conversion of vascular smooth muscle cells, activates oxidative stress, promotes vascular smooth muscle cell proliferation, and induces myocardial remodeling (85). Therefore, NOX5 may be a new therapeutic target for the clinical treatment of heart failure.

Nicotinamide adenine dinucleotide phosphate and myocardial remodeling

NADPH is involved in oxidative stress-induced myocardial remodeling, mainly in endothelial dysfunction, ROS overproduction, and reduced antioxidant capacity (79, 86). ROS produced by NOXs can regulate the level of oxidative stress and participate in the development of myocardial remodeling, a response produced by the heart to pathological stimuli and consists of two main categories: physiological and pathological (87). Physiological myocardial remodeling is a compensatory and adaptive change of the heart to the body to maintain normal physiological functions of the heart. Pathological myocardial remodeling mainly occurs in structural, morphological, and energy metabolic remodeling, resulting in cardiac scarring, leading to myocardial stiffness, cavity dilation, and ventricular systolic dysfunction, resulting in arrhythmias and heart failure (1). The myocardial remodeling processes involve cardiomyocytes, fibroblasts, endothelial cells, vascular smooth muscle cells (VSMCs), and immune cells. Numerous studies have shown that modulation of NOX levels can improve the progression of myocardial remodeling. In contrast, NOXs produce ROS that act on mitochondrial enzymes, protein kinases, and transcription factors, causing cardiomyocyte hypertrophy, apoptosis, and necrosis, severely impairing cardiomyocyte energy metabolism and mitochondrial function, affecting myocardial excitation-contraction coupling, leading to myocardial hypertrophy and end-stage heart failure. Studies have confirmed that Ang II is important in regulating ROS generation by NOXs through AT1 receptors (86). Ang II inhibition also helps reduce the expression of NOXs and regulate myocardial remodeling.

Nicotinamide adenine dinucleotide phosphate oxidase affects myocardial structural remodeling

Myocardial structural remodeling includes cardiomyocyte hypertrophy, apoptosis, and interstitial fibrosis (14, 88). Cardiomyocyte hypertrophy is manifested by increased cardiomyocyte length, width, and mass, but the number of cardiomyocytes remains unchanged. Pathological myocardial hypertrophy is stimulated by cardiomyocyte apoptosis, fibroblasts, endothelial cells, smooth muscle cells and phagocytes activation and differentiation, extracellular matrix protein deposition, and interstitial and perivascular fibrosis (87), causing myocardial stiffness, abnormal cardiac function, and eventually heart failure (**Figure 2**).

Cardiomyocyte hypertrophy and apoptosis are the underlying features of myocardial structural remodeling. Studies have demonstrated that the main isoforms in cardiomyocytes are NOX2 and NOX4, with NOX2 mainly localized in the plasma membrane and NOX4 distributed in the nuclear membrane. Both are associated with the myocardial structural remodeling in chronic stress states. Intracellular NOX-mediated ROS, activated via the Ras-MEK1/2-ERK1/2 pathway, are involved in α1-adrenoceptor (α1-AR) mediated cardiomyocyte hypertrophy (22), which leads to myocardial structural and morphological remodeling. RAC1 is an important active regulator of NOXs. Ang II activates RAC1, upregulates the expression of NOXs, promotes cardiomyocyte hypertrophy, fibroblast proliferation, and myofibroblast differentiation, and induces myocardial remodeling (89). Studies have revealed that activation of NOX2 was induced after AngII, pressure overload and myocardial infarction, leading to cardiomyocyte hypertrophy, apoptosis, vascular smooth muscle cell proliferation and extracellular interstitial fibrosis, and aggravating myocardial structural remodeling (90–92). The AMPK/NOX2 pathway attenuates oxidative stress in diabetic hearts with ischemia/reperfusion injury and may reduce myocardial hypertrophic lesions by reducing cardiomyocyte death (93). NOX2, expressed in the heart, not only mediates oxidative stress, apoptosis, and inflammation through multiple target pathway proteins but is also subject to gene-level regulators, such as microRNAs (miRNAs) for its downstream products, to reduce its activity and slow the progression of cardiomyopathy and myocardial remodeling after MI (94). Cardiomyocyte hypertrophy caused by erythromycin (DOX) is associated with the activation of TRPC3/NOX2 signaling targets, which causes left ventricular hypertrophy, resulting in cardiac dysfunction (95). FYN is a tyrosine kinase of the Src family that negatively regulates NOX4 activity, attenuates oxidative stress and cardiomyocyte death, and slows myocardial remodeling through translational modification of the phosphorylated C-terminal Y566 of NOX4 (96). Another study indicated that high NOX4 expression activates the AKT/mTOR/NF-κB signaling pathway, mediates oxidative stress, releases excess ROS, causes cardiomyocyte hypertrophy and interstitial fibrosis, and leads to cardiac remodeling. Myocardial remodeling was significantly reduced after the treatment of mouse hearts with the NOX inhibitor GKT137831 (97).

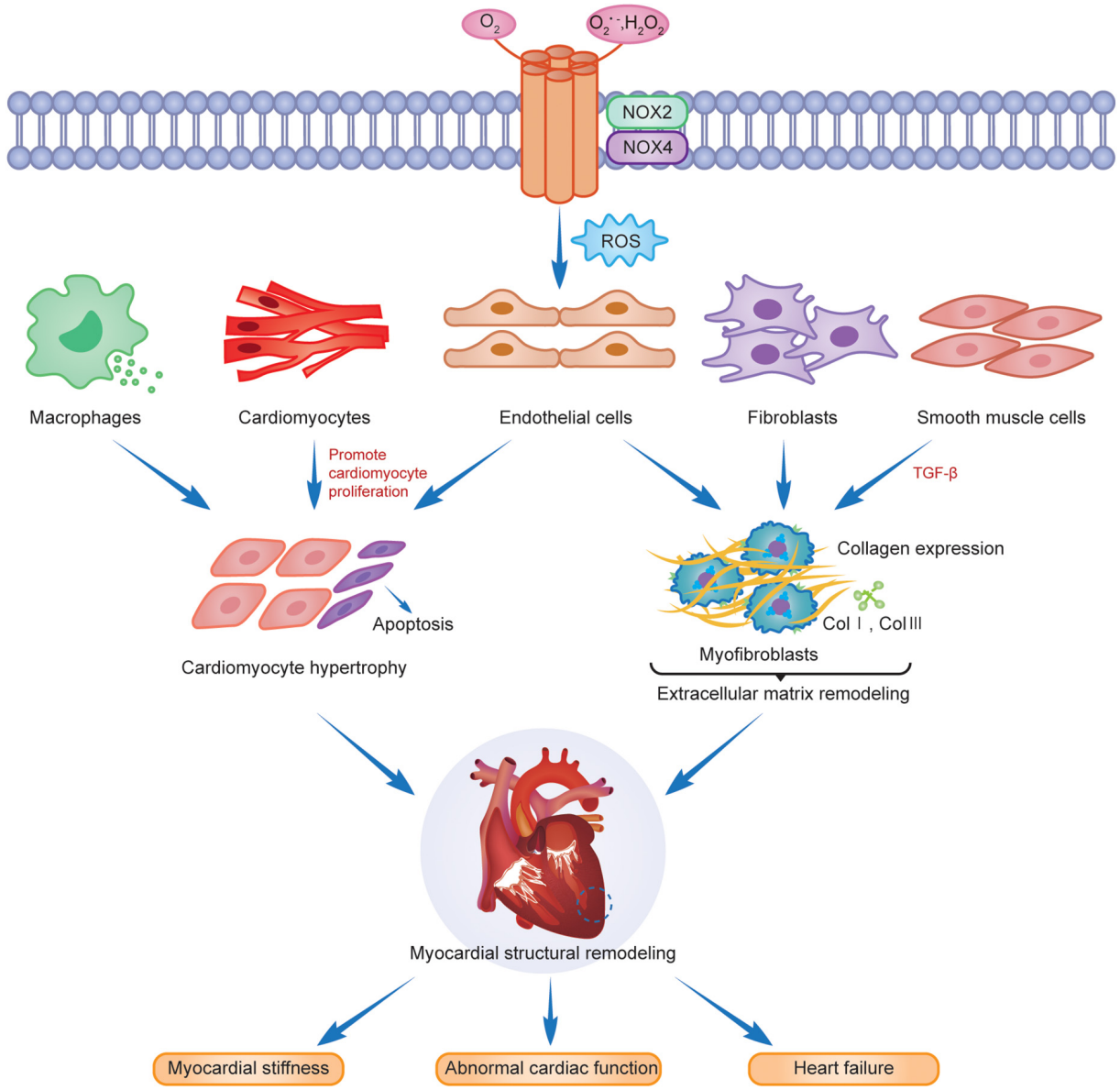

FIGURE 2
NOX2 and NOX4 are involved in myocardial remodeling.

Interstitial fibrosis is another characteristic change in the structural remodeling of the myocardium. Extracellular matrix protein deposition is an important component of interstitial fibrosis, and the main basic proteins included are type I and type III collagen while altering the myocardial meshwork. The proliferation and migration of cardiac fibroblasts are crucial in the interstitial fibrosis process of myocardial structural remodeling (1), and the two contribute to each other to aggravate myocardial remodeling progression. TGF-βis critical for the conversion of cardiac fibroblasts to a myofibroblast phenotype. Intervention in the TGF-β/Smad signaling pathway attenuates the activation and phenotypic conversion of fibroblasts due to Ang II induced NADPH oxidase activation and attenuates extracellular matrix remodeling due to cascade reactions (98). NOX4 induces TGF-β-induced actin upregulation and phenotypic transition in fibroblasts by stimulating Smads 2/3 phosphorylation and activation (99). ROS production after NOX4 expression upregulation can promote endothelial cell migration and vascular remodeling in an eNOS-dependent manner (100), which are jointly involved in promoting extracellular matrix remodeling. In the case of chronic hemodynamic overload, the NOX4 expression level in cardiomyocytes and endothelial cells increases, enhancing HIF-1 and VEGF signaling, activating

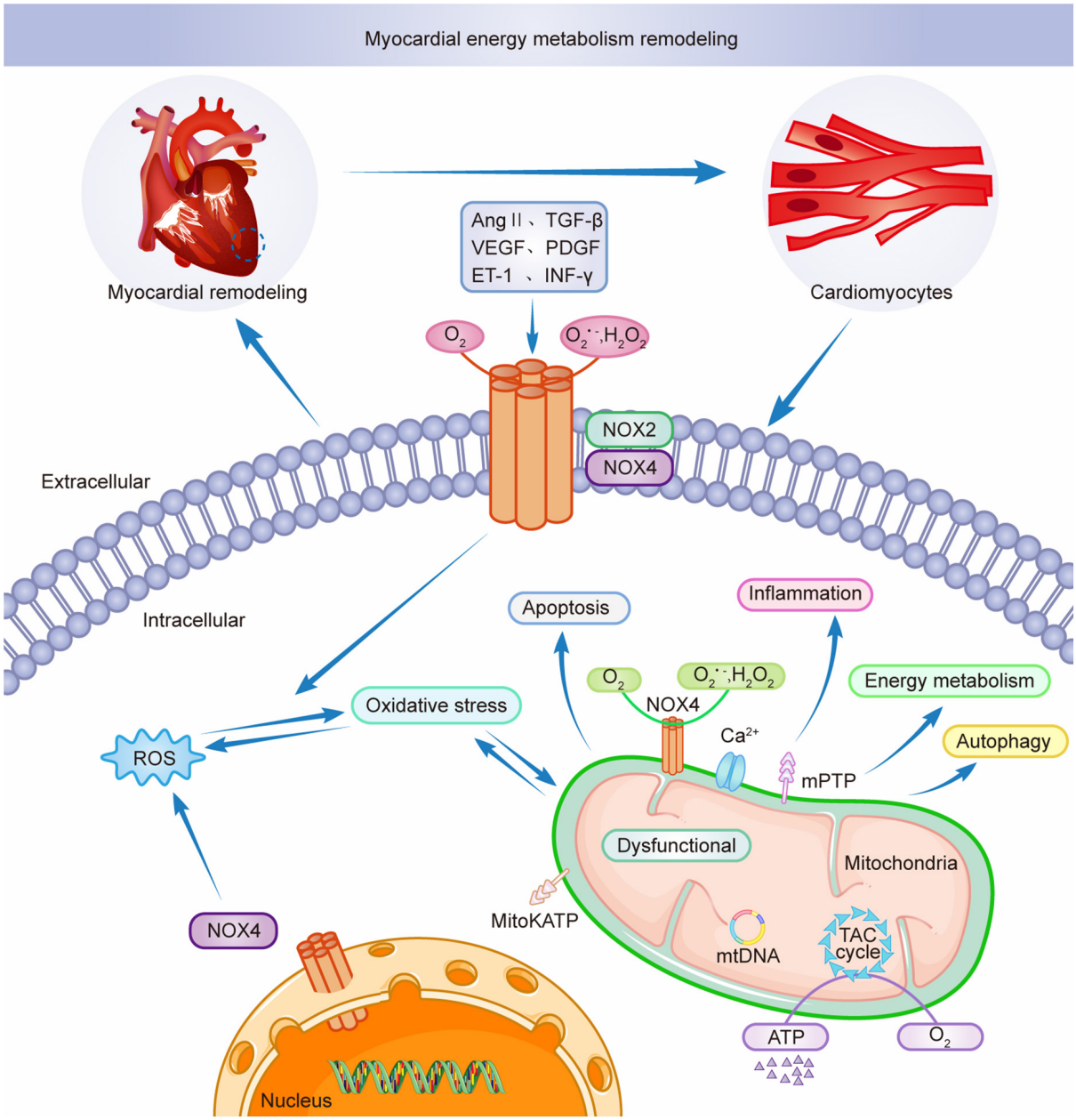

FIGURE 3
NOX2 and NOX4 participate in myocardial energy metabolism remodeling.

oxidative stress, causing myocardial fibrosis and vascular proliferation, increasing myocardial capillary density, and acting as a partial myocardial compensation but leading to the development of myocardial remodeling (66). However, NOX2 is deleterious in oxidative stress, and salusin-β is a bioactive peptide with 20 amino acids that can regulate the proliferative activity of vascular endothelial and smooth muscle cells. Salusin-β inhibits NOX-mediated ROS production, activates eNOS and NO production, causes dysregulation of the balance of contractile and vasodilator factors released from the vascular endothelium (101), improves endothelial dysfunction, cardiovascular remodeling, and cardiac dysfunction, and promotes early depolarization of rabbit cardiomyocytes by activating the calmodulin-dependent protein kinase II (CaMKII) pathway. Studies demonstrated its use as a downstream target of NOX2 to increase the incidence of arrhythmias in AngII-induced mouse models (102, 103), suggesting that NOX2 is involved in cardiac structural remodeling. Myocardial interstitial fibrosis due to pressure overload induced by Ang II injection, aldosterone, and aortic

ligation was significantly reduced in the NOX2$^{-/-}$ mouse model (104).

Nicotinamide adenine dinucleotide phosphate oxidase affects remodeling of myocardial energy metabolism

In cardiac energy metabolism, 95% of energy is provided by mitochondrial oxidative phosphorylation in the form of adenosine triphosphate (ATP), and the remaining 5% is provided by glycolysis. Mitochondria provide ATP mainly from the oxidation of fatty acids, approximately 40–60%, and the rest from the oxidation of ketone bodies, amino acids, and pyruvate (derived from glucose and lactate) (105, 106). Therefore, the remodeling of myocardial energy metabolism consists mainly of disorders of cardiac metabolic substrates and intracellular mitochondrial dysfunction (4, 107, 108).

NOX2 and NOX4 are involved in disrupting metabolic substrates for myocardial remodeling. The expression of NOX2 facilitates the polarization of M1 macrophages, promotes the coupling of inflammatory receptors to NOX2, activates the inflammatory cascade response, enhances the transport of glucose transporter proteins to the cytoplasmic membrane, and increases glucose uptake by glycolytic metabolic processes (109). Excitation-contraction coupling and metabolic disorders can cause increased mitochondrial respiratory chain superoxide synthesis, increased mitochondrial ROS release, and an imbalance between myocardial oxygen supply and demand, triggering oxidative stress and affecting various cellular survival rates during myocardial remodeling (110). NOX4 is mainly localized in the mitochondria and is involved in tricarboxylic acid cycle (TCA) and energy metabolism in the electron transport chain through redox reactions, thereby affecting nutrient metabolism (97).

Mitochondria are key to the remodeling of myocardial energy metabolism. Mitochondria are the center of intracellular processes of calcium homeostasis, energy metabolism, and oxidative stress. Intracellular Ca^{2+} and Na^{+} imbalance impede mitochondrial calcium overload, leading to the abnormal opening of the mitochondrial permeability transition pore (mPTP), resulting in abnormal mitochondrial energy metabolism, triggering oxidative stress, leading to excessive release of ROS from mitochondria, interfering with the excitation-contraction coupling process in the myocardium, and inducing cardiomyocyte death (111, 112). Studies have shown that NOX4 upregulation mediates mitochondrial dysfunction, cardiomyocyte hypertrophy, and apoptosis and is involved in myocardial structure and energy metabolism (97). AMPK is a physiological inhibitor of NOX and ROS production in endothelial cells. During pathological conditions, AMPK expression is reduced, and mitochondria produce excessive ROS, affecting myocardial energy supply and promoting inflammatory responses, exacerbating myocardial energy metabolic remodeling (113). Thus AMPK can be a therapeutic target for NOX-mediated remodeling of myocardial energy metabolism as a key mediator. AngII induces NADPH oxidase activation and ROS production, leading to mitochondrial microstructure and dysfunction by decreasing mitochondrial membrane potential and affecting mitochondrial morphology. Ang II stimulates NADPH oxidase through a protein kinase C (PKC)-mediated pathway-dependent stimulation, causing increased ROS release, activating mitochondrial Na^{+}-K^{+}-ATP channels, causing mitochondrial membrane potential abnormalities, disrupting the mitochondrial respiratory enzyme complex, resulting in mitochondrial dysfunction and remodeling of myocardial energy metabolism (114). NOX4 is mainly localized in the mitochondria of cardiomyocytes and endothelial cells. Mitochondrial DNA (mtDNA) is the main target of NADPH oxidase-mediated ROS action (25). NOX4 plays an adaptive role by promoting the oxidation of fatty acids and providing the energy required by cardiomyocytes (115). NOX4 and ROS produced by mitochondria are involved in NLRP3 inflammatory vesicles, dynamin-related protein 1 (Drp1) activation, and mitochondrial division induced by dilated cardiomyopathy (DCM) (116). NOX4 is crucial for myocardial energy metabolic remodeling. Therefore, mitochondrial dysfunction is critical in myocardial energy metabolic remodeling during pathological myocardial remodeling and simultaneously promotes myocardial pathological structural remodeling, leading to cardiac hypertrophy and functional decline (87). **Figure 3** shows the involvement of NOXs in the remodeling of myocardial energy metabolism through the release of ROS. The intervention of NADPH-activated oxidative stress provides new ideas for the treatment of myocardial remodeling and end-stage heart failure.

Nicotinamide adenine dinucleotide phosphate oxidase and therapeutic interventions

Drugs targeting NOX subtypes and related pathways are well researched and can be useful in the clinical management of cardiac and vascular disease. Numerous studies have shown that clinical agents acting on NOX family targets can slow the progression of myocardial remodeling and heart failure. RAC1 knockdown and NADPH oxidase inhibitors were shown to reduce myocardial apoptosis, inhibit the conversion of fibroblasts into myofibroblasts, provide antihypertrophic and antifibrotic effects, and improve the progression of myocardial remodeling (117). As an NOX inhibitor, celastrol directly binds to signal transduction and transcriptional activator proteins, reduces tyrosine phosphorylation and

nuclear translocation, and inhibits AngII involvement in NOX2-mediated myocardial remodeling, presumably leading to a protective effect on the myocardium through anti-oxidative stress (118, 119). Apocynin reduces DNA damage and telomere shortening in cardiomyocytes, inhibits the release of ROS from NOX, reduces oxidative stress levels, improves myocardial remodeling and reduces death in heart failure. Apocynin has been shown to reduce fibroblast activation, cardiomyocyte hypertrophy and apoptosis through anti-oxidative stress, preventing deterioration of cardiac function and pathological remodeling in Diabetic cardiomyopathy (DCM) mouse model (120, 121). Vitamin D deficiency is an important potential risk factor for cardiovascular disease. Vitamin D regulates NO synthesis by mediating the activity of eNOS. Studies have shown that vitamin D enhances oxidative capacity through the activity of antioxidant enzymes and can inhibit NOX production of ROS (122). The key to the development of NOX subtypes of cardiovascular disease and the exploration of NOX-mediated related targets provide potential therapeutic directions for the clinical treatment of cardiovascular disease caused by myocardial remodeling.

Conclusion

Myocardial remodeling is a common pathophysiological process in many cardiovascular diseases, accelerating disease progression and eventually leading to heart failure. There are few clinically effective drugs to reverse myocardial remodeling, and NADPH oxidases play a crucial role in the pathogenesis of cardiovascular diseases. NOX-mediated ROS production is associated with important cellular functions such as cell differentiation, proliferation, migration, apoptosis, and immune response. In addition, it is involved in different signaling pathways mediating the pathogenesis of cardiovascular diseases, such as inflammatory response, autophagy, apoptosis, and oxidative stress. Increased ROS release and oxidative stress-induced cellular damage lead to structural and functional alterations in the heart, leading to cardiac arrest, the major cause of death worldwide (123). Studies have confirmed that NADPH oxidase can induce ROS production and accelerate the morbidity and mortality associated with heart failure through different pathways and molecular mechanisms.

In this review, the basic pathophysiological process of myocardial remodeling was explored regarding the NADPH oxidase family mediating related signaling pathways through multiple signaling targets, upregulating oxidative stress levels, activating increased ROS expression levels, and severely affecting pathological changes such as cardiomyocyte hypertrophy, apoptosis, and interstitial fibrosis, and causing changes in myocardial structural and energy metabolic remodeling, leading to the deterioration of heart failure. However, its role in the signaling cascade and the associated molecular mechanisms involved in different pathological conditions are still unknown. Therefore, exploring the pathogenesis of myocardial remodeling and related therapeutic targets of oxidative stress is crucial. Although there are still some limitations to the clinical understanding of NOX in cardiovascular diseases, exploring relevant NOX inhibitory targets and developing new directions for clinical drugs provide potential applications for reversing myocardial remodeling and delaying the progression of heart failure in the clinical setting.

Author contributions

RM wrote the manuscript by reviewing and summarizing the relevant literature. LW and ZC revised the manuscript. SG, LL, and KZ prepared the figures. YC, WG, XD, and MZ involved in the work. GZ and FL supervised the progress of the entire manuscript to ensure completeness and accuracy and approved the submitted version. All authors contributed to the article and approved the submitted version.

Funding

This work was supported by the Key Specialized Research and Development Breakthrough in Henan Province (Nos. 212102310350 and 222102310442), the Research Projects of Higher Education Institutions in Henan Province (No. 22A360017), and the Medical Science and Technology Research Program Jointly Co-constructed Project in Henan Province (Nos. LHGL20200521 and LHGL20210513).

Acknowledgments

We thank Editage (www.editage.cn) for English language editing.

Conflict of interest

The authors declare that the research was conducted in the absence of any commercial or financial relationships that could be construed as a potential conflict of interest.

Publisher's note

References

1. Li L, Zhao Q, Kong W. Extracellular matrix remodeling and cardiac fibrosis. *Matrix Biol.* (2018) 68–9:490–506. doi: 10.1016/j.matbio.2018.01.013

2. Scofield SL, Amin P, Singh M, Singh K. Extracellular ubiquitin: role in myocyte apoptosis and myocardial remodeling. *Compr Physiol.* (2015) 6:527–60. doi: 10.1002/cphy.c150025

3. Gonzalez A, Schelbert EB, Diez J, Butler J. Myocardial interstitial fibrosis in heart failure: biological and translational perspectives. *J Am Coll Cardiol.* (2018) 71:1696–706. doi: 10.1016/j.jacc.2018.02.021

4. Gibb AA, Hill BG. Metabolic coordination of physiological and pathological cardiac remodeling. *Circ Res.* (2018) 123:107–28. doi: 10.1161/CIRCRESAHA.118.312017

5. Barton M, Meyer MR, Prossnitz ER. Nox1 downregulators: a new class of therapeutics. *Steroids.* (2019) 152:108494. doi: 10.1016/j.steroids.2019.108494

6. Lassegue B, San Martin A, Griendling KK. Biochemistry, physiology, and pathophysiology of NADPH oxidases in the cardiovascular system. *Circ Res.* (2012) 110:1364–90. doi: 10.1161/CIRCRESAHA.111.243972

7. Waghela BN, Vaidya FU, Agrawal Y, Santra MK, Mishra V, Pathak C. Molecular insights of NADPH oxidases and its pathological consequences. *Cell Biochem Funct.* (2021) 39:218–34. doi: 10.1002/cbf.3589

8. Lambeth JD. Nox enzymes and the biology of reactive oxygen. *Nat Rev Immunol.* (2004) 4:181–9. doi: 10.1038/nri1312

9. Bedard K, Krause KH. The NOX family of ROS-generating NADPH oxidases: physiology and pathophysiology. *Physiol Rev.* (2007) 87:245–313. doi: 10.1152/physrev.00044.2005

10. Konior A, Schramm A, Czesnikiewicz-Guzik M, Guzik TJ. NADPH oxidases in vascular pathology. *Antioxid Redox Signal.* (2014) 20:2794–814. doi: 10.1089/ars.2013.5607

11. Forstermann U, Xia N, Li H. Roles of vascular oxidative stress and nitric oxide in the pathogenesis of atherosclerosis. *Circ Res.* (2017) 120:713–35. doi: 10.1161/CIRCRESAHA.116.309326

12. Burtenshaw D, Kitching M, Redmond EM, Megson IL, Cahill PA. Reactive oxygen species (ROS), intimal thickening, and subclinical atherosclerotic disease. *Front Cardiovasc Med.* (2019) 6:89. doi: 10.3389/fcvm.2019.00089

13. De Deken X, Wang D, Many MC, Costagliola S, Libert F, Vassart G, et al. Cloning of two human thyroid CDNAS encoding new members of the NADPH oxidase family. *J Biol Chem.* (2000) 275:23227–33. doi: 10.1074/jbc.M000916200

14. Nabeebaccus A, Zhang M, Shah AM. NADPH oxidases and cardiac remodelling. *Heart Fail Rev.* (2011) 16:5–12. doi: 10.1007/s10741-010-9186-2

15. Hordijk PL. Regulation of NADPH oxidases: the role of RAC proteins. *Circ Res.* (2006) 98:453–62. doi: 10.1161/01.RES.0000204727.46710.5e

16. Cai H. Nad(P)H oxidase-dependent self-propagation of hydrogen peroxide and vascular disease. *Circ Res.* (2005) 96:818–22. doi: 10.1161/01.RES.0000163631.07205.fb

17. Maejima Y, Kuroda J, Matsushima S, Ago T, Sadoshima J. Regulation of myocardial growth and death by NADPH oxidase. *J Mol Cell Cardiol.* (2011) 50:408–16. doi: 10.1016/j.yjmcc.2010.12.018

18. Zhang Y, Murugesan P, Huang K, Cai H. NADPH oxidases and oxidase crosstalk in cardiovascular diseases: novel therapeutic targets. *Nat Rev Cardiol.* (2020) 17:170–94. doi: 10.1038/s41569-019-0260-8

19. Bubb KJ, Drummond GR, Figtree GA. New opportunities for targeting redox dysregulation in cardiovascular disease. *Cardiovasc Res.* (2020) 116:532–44. doi: 10.1093/cvr/cvz183

20. Meza CA, La Favor JD, Kim DH, Hickner RC. Endothelial dysfunction: is there a hyperglycemia-induced imbalance of NOX and NOS? *Int J Mol Sci.* (2019) 20:3775. doi: 10.3390/ijms20153775

21. Grieve DJ, Byrne JA, Siva A, Layland J, Johar S, Cave AC, et al. Involvement of the nicotinamide adenosine dinucleotide phosphate oxidase isoform Nox2 in cardiac contractile dysfunction occurring in response to pressure overload. *J Am Coll Cardiol.* (2006) 47:817–26. doi: 10.1016/j.jacc.2005.09.051

22. Xiao L, Pimentel DR, Wang J, Singh K, Colucci WS, Sawyer DB. Role of reactive oxygen species and Nad(P)H oxidase in alpha-adrenoceptor signaling in adult rat cardiac myocytes. *Am J Physiol Cell Physiol.* (2002) 282:C926–34. doi: 10.1152/ajpcell.00254.2001

23. Maytin M, Siwik DA, Ito M, Xiao L, Sawyer DB, Liao R, et al. Pressure overload-induced myocardial hypertrophy in mice does not require Gp91phox. *Circulation.* (2004) 109:1168–71. doi: 10.1161/01.CIR.0000117229.60628.2F

24. Panda P, Verma HK, Lakkakula S, Merchant N, Kadir F, Rahman S, et al. Biomarkers of oxidative stress tethered to cardiovascular diseases. *Oxid Med Cell Longev.* (2022) 2022:9154295. doi: 10.1155/2022/9154295

25. Tsutsui H, Kinugawa S, Matsushima S. Oxidative stress and heart failure. *Am J Physiol Heart Circ Physiol.* (2011) 301:H2181–90. doi: 10.1152/ajpheart.00554.2011

26. Nishihara T, Tokitsu T, Sueta D, Oike F, Takae M, Fujisue K, et al. Clinical significance of reactive oxidative metabolites in patients with heart failure with reduced left ventricular ejection fraction. *J Card Fail.* (2021) 27:57–66. doi: 10.1016/j.cardfail.2020.07.020

27. Krzeminska J, Wronka M, Mlynarska E, Franczyk B, Rysz J. Arterial hypertension-oxidative stress and inflammation. *Antioxidants.* (2022) 11:172. doi: 10.3390/antiox11010172

28. Shi X, Dorsey A, Qiu H. New progress in the molecular regulations and therapeutic applications in cardiac oxidative damage caused by pressure overload. *Antioxidants.* (2022) 11:877. doi: 10.3390/antiox11050877

29. Muller M, Bischof C, Kapries T, Wollnitza S, Liechty C, Geissen S, et al. Right heart failure in mice upon pressure overload is promoted by mitochondrial oxidative stress. *JACC Basic Transl Sci.* (2022) 7:658–77. doi: 10.1016/j.jacbts.2022.02.018

30. Gimenez M, Schickling BM, Lopes LR, Miller FJ Jr. Nox1 in cardiovascular diseases: regulation and pathophysiology. *Clin Sci.* (2016) 130:151–65. doi: 10.1042/CS20150404

31. Cave AC, Brewer AC, Narayanapanicker A, Ray R, Grieve DJ, Walker S, et al. NADPH oxidases in cardiovascular health and disease. *Antioxid Redox Signal.* (2006) 8:691–728. doi: 10.1089/ars.2006.8.691

32. AlSiraj Y, Chen X, Thatcher SE, Temel RE, Cai L, Blalock E, et al. XX sex chromosome complement promotes atherosclerosis in mice. *Nat Commun.* (2019) 10:2631. doi: 10.1038/s41467-019-10462-z

33. Sheehan AL, Carrell S, Johnson B, Stanic B, Banfi B, Miller FJ Jr. Role for NOX1 NADPH oxidase in atherosclerosis. *Atherosclerosis.* (2011) 216:321–6. doi: 10.1016/j.atherosclerosis.2011.02.028

34. Lassegue B, Clempus RE. Vascular Nad(P)H oxidases: specific features, expression, and regulation. *Am J Physiol Regul Integr Comp Physiol.* (2003) 285:R277–97. doi: 10.1152/ajpregu.00758.2002

35. Hingtgen SD, Tian X, Yang J, Dunlay SM, Peek AS, Wu Y, et al. Nox2-containing NADPH oxidase and AKT activation play a key role in angiotensin II-induced cardiomyocyte hypertrophy. *Physiol Genomics.* (2006) 26:180–91. doi: 10.1152/physiolgenomics.00029.2005

36. Buchmann GK, Schurmann C, Warwick T, Schulz MH, Spaeth M, Muller OJ, et al. Deletion of Noxo1 limits atherosclerosis development in female mice. *Redox Biol.* (2020) 37:101713. doi: 10.1016/j.redox.2020.101713

37. Jandeleit-Dahm K. Endothelin in diabetes-associated atherosclerosis: opportunity 'NOX'. *Cardiovasc Res.* (2021) 117:987–9. doi: 10.1093/cvr/cvab018

38. Ouerd S, Idris-Khodja N, Trindade M, Ferreira NS, Berillo O, Coelho SC, et al. Endothelium-restricted endothelin-1 overexpression in type 1 diabetes worsens atherosclerosis and immune cell infiltration via NOX1. *Cardiovasc Res.* (2021) 117:1144–53. doi: 10.1093/cvr/cvaa168

39. Fernandes DC, Wosniak J Jr, Goncalves RC, Tanaka LY, Fernandes CG, Zanatta DB, et al. PDIA1 acts as master organizer of Nox1/Nox4 balance and phenotype response in vascular smooth muscle. *Free Radic Biol Med.* (2021) 162:603–14. doi: 10.1016/j.freeradbiomed.2020.11.020

40. Wind S, Beuerlein K, Armitage ME, Taye A, Kumar AH, Janowitz D, et al. Oxidative stress and endothelial dysfunction in aortas of aged spontaneously hypertensive rats by NOX1/2 is reversed by NADPH oxidase inhibition. *Hypertension.* (2010) 56:490–7. doi: 10.1161/HYPERTENSIONAHA.109.149187

41. Dikalova A, Clempus R, Lassegue B, Cheng G, McCoy J, Dikalov S, et al. Nox1 overexpression potentiates angiotensin II-induced hypertension and vascular smooth muscle hypertrophy in transgenic mice. *Circulation.* (2005) 112:2668–76. doi: 10.1161/CIRCULATIONAHA.105.538934

42. Xu L, Balzarolo M, Robinson EL, Lorenz V, Verde GD, Joray L, et al. Nox1 mediates metabolic heart disease in mice and is upregulated in monocytes of humans with diastolic dysfunction. *Cardiovasc Res.* (2021) cvab349. doi: 10.1093/cvr/cvab349

43. Meyer MR, Fredette NC, Sharma G, Barton M, Prossnitz ER. GPER is required for the age-dependent upregulation of the myocardial endothelin system. *Life Sci.* (2016) 159:61–5. doi: 10.1016/j.lfs.2016.02.041

44. Laddha AP, Kulkarni YA. NADPH oxidase: a membrane-bound enzyme and its inhibitors in diabetic complications. *Eur J Pharmacol.* (2020) 881:173206. doi: 10.1016/j.ejphar.2020.173206

45. Parajuli N, Patel VB, Wang W, Basu R, Oudit GY. Loss of Nox2 (Gp91phox) prevents oxidative stress and progression to advanced heart failure. *Clin Sci.* (2014) 127:331–40. doi: 10.1042/CS20130787

46. Ferreira LF, Laitano O. Regulation of NADPH oxidases in skeletal muscle. *Free Radic Biol Med.* (2016) 98:18–28. doi: 10.1016/j.freeradbiomed.2016.05.011

47. Moazzen H, Wu Y, Engineer A, Lu X, Aulakh S, Feng Q. Nox2 is critical to endocardial to mesenchymal transition and heart development. *Oxid Med Cell Longev.* (2020) 2020:1679045. doi: 10.1155/2020/1679045

48. Prosser BL, Ward CW, Lederer WJ. X-ROS signaling: rapid mechano-chemo transduction in heart. *Science.* (2011) 333:1440–5. doi: 10.1126/science.1202768

49. Urner S, Ho F, Jha JC, Ziegler D, Jandeleit-Dahm K. NADPH oxidase inhibition: preclinical and clinical studies in diabetic complications. *Antioxid Redox Signal.* (2020) 33:415–34. doi: 10.1089/ars.2020.8047

50. Molitor M, Rudi WS, Garlapati V, Finger S, Schuler R, Kossmann S, et al. Nox2+ myeloid cells drive vascular inflammation and endothelial dysfunction in heart failure after myocardial infarction via angiotensin II receptor type 1. *Cardiovasc Res.* (2021) 117:162–77. doi: 10.1093/cvr/cvaa042

51. Tojo T, Ushio-Fukai M, Yamaoka-Tojo M, Ikeda S, Patrushev N, Alexander RW. Role of Gp91phox (Nox2)-containing Nad(P)H oxidase in angiogenesis in response to hindlimb ischemia. *Circulation.* (2005) 111:2347–55. doi: 10.1161/01.CIR.0000164261.62586.14

52. Xue B, Beltz TG, Johnson RF, Guo F, Hay M, Johnson AK. PVN adenovirus-sirna injections silencing either Nox2 or Nox4 attenuate aldosterone/Nacl-induced hypertension in mice. *Am J Physiol Heart Circ Physiol.* (2012) 302:H733–41. doi: 10.1152/ajpheart.00873.2011

53. Murdoch CE, Chaubey S, Zeng L, Yu B, Ivetic A, Walker SJ, et al. Endothelial NADPH oxidase-2 promotes interstitial cardiac fibrosis and diastolic dysfunction through proinflammatory effects and endothelial-mesenchymal transition. *J Am Coll Cardiol.* (2014) 63:2734–41. doi: 10.1016/j.jacc.2014.02.572

54. Sindona C, Schepici G, Contestabile V, Bramanti P, Mazzon E. Nox2 activation in Covid-19: possible implications for neurodegenerative diseases. *Medicina.* (2021) 57:604. doi: 10.3390/medicina57060604

55. Violi F, Oliva A, Cangemi R, Ceccarelli G, Pignatelli P, Carnevale R, et al. Nox2 activation in Covid-19. *Redox Biol.* (2020) 36:101655. doi: 10.1016/j.redox.2020.101655

56. Hafstad AD, Hansen SS, Lund J, Santos CXC, Boardman NT, Shah AM, et al. NADPH oxidase 2 mediates myocardial oxygen wasting in obesity. *Antioxidants.* (2020) 9:171. doi: 10.3390/antiox9020171

57. Wang C, Zhu L, Yuan W, Sun L, Xia Z, Zhang Z, et al. Diabetes aggravates myocardial ischaemia reperfusion injury via activating Nox2-related programmed cell death in an AMPK-dependent manner. *J Cell Mol Med.* (2020) 24:6670–9. doi: 10.1111/jcmm.15318

58. Satoh M, Ogita H, Takeshita K, Mukai Y, Kwiatkowski DJ, Liao JK. Requirement of RAC1 in the development of cardiac hypertrophy. *Proc Natl Acad Sci U.S.A.* (2006) 103:7432–7. doi: 10.1073/pnas.0510444103

59. Ma ZG, Kong CY, Wu HM, Song P, Zhang X, Yuan YP, et al. Toll-like receptor 5 deficiency diminishes doxorubicin-induced acute cardiotoxicity in mice. *Theranostics.* (2020) 10:11013–25. doi: 10.7150/thno.47516

60. Kitajima N, Numaga-Tomita T, Watanabe M, Kuroda T, Nishimura A, Miyano K, et al. TRPC3 positively regulates reactive oxygen species driving maladaptive cardiac remodeling. *Sci Rep.* (2016) 6:37001. doi: 10.1038/srep37001

61. Kim YM, Guzik TJ, Zhang YH, Zhang MH, Kattach H, Ratnatunga C, et al. A myocardial Nox2 containing Nad(P)H oxidase contributes to oxidative stress in human atrial fibrillation. *Circ Res.* (2005) 97:629–36. doi: 10.1161/01.RES.0000183735.09871.61

62. Ago T, Matsushima S, Kuroda J, Zablocki D, Kitazono T, Sadoshima J. The NADPH oxidase NOX4 and aging in the heart. *Aging.* (2010) 2:1012–6. doi: 10.18632/aging.100261

63. Sturrock A, Cahill B, Norman K, Huecksteadt TP, Hill K, Sanders K, et al. Transforming growth factor-beta1 induces Nox4 Nad(P)H oxidase and reactive oxygen species-dependent proliferation in human pulmonary artery smooth muscle cells. *Am J Physiol Lung Cell Mol Physiol.* (2006) 290:L661–73. doi: 10.1152/ajplung.00269.2005

64. Yoshida LS, Tsunawaki S. Expression of NADPH oxidases and enhanced HO-generating activity in human coronary artery endothelial cells upon induction with tumor necrosis factor-alpha. *Int Immunopharmacol.* (2008) 8:1377–85. doi: 10.1016/j.intimp.2008.05.004

65. Ochoa CD, Wu RF, Terada LS. Ros signaling and ER stress in cardiovascular disease. *Mol Aspects Med.* (2018) 63:18–29. doi: 10.1016/j.mam.2018.03.002

66. Zhang M, Mongue-Din H, Martin D, Catibog N, Smyrnias I, Zhang X, et al. Both cardiomyocyte and endothelial cell Nox4 mediate protection against hemodynamic overload-induced remodelling. *Cardiovasc Res.* (2018) 114:401–8. doi: 10.1093/cvr/cvx204

67. Schurmann C, Rezende F, Kruse C, Yasar Y, Lowe O, Fork C, et al. The NADPH oxidase Nox4 has anti-atherosclerotic functions. *Eur Heart J.* (2015) 36:3447–56. doi: 10.1093/eurheartj/ehv460

68. Vendrov AE, Vendrov KC, Smith A, Yuan J, Sumida A, Robidoux J, et al. Nox4 NADPH oxidase-dependent mitochondrial oxidative stress in aging-associated cardiovascular disease. *Antioxid Redox Signal.* (2015) 23:1389–409. doi: 10.1089/ars.2014.6221

69. Matsushima S, Kuroda J, Ago T, Zhai P, Park JY, Xie LH, et al. Increased oxidative stress in the nucleus caused by NOX4 mediates oxidation of HDAC4 and cardiac hypertrophy. *Circ Res.* (2013) 112:651–63. doi: 10.1161/CIRCRESAHA.112.279760

70. Mongue-Din H, Patel AS, Looi YH, Grieve DJ, Anilkumar N, Sirker A, et al. NADPH oxidase-4 driven cardiac macrophage polarization protects against myocardial infarction-induced remodeling. *JACC Basic Transl Sci.* (2017) 2:688–98. doi: 10.1016/j.jacbts.2017.06.006

71. Zhang M, Brewer AC, Schroder K, Santos CX, Grieve DJ, Wang M, et al. NADPH oxidase-4 mediates protection against chronic load-induced stress in mouse hearts by enhancing angiogenesis. *Proc Natl Acad Sci U.S.A.* (2010) 107:18121–6. doi: 10.1073/pnas.1009700107

72. Wen SY, Tamilselvi S, Shen CY, Day CH, Chun LC, Cheng LY, et al. Protective effect of HDL on NADPH oxidase-derived super oxide anion mediates hypoxia-induced cardiomyocyte apoptosis. *PLoS One.* (2017) 12:e0179492. doi: 10.1371/journal.pone.0179492

73. Macedo FN, Souza DS, Araujo J, Dantas CO, Miguel-Dos-Santos R, Silva-Filha E, et al. NOX-dependent reactive oxygen species production underlies arrhythmias susceptibility in dexamethasone-treated rats. *Free Radic Biol Med.* (2020) 152:1–7. doi: 10.1016/j.freeradbiomed.2020.03.005

74. Zhang L, Qi X, Zhang G, Zhang Y, Tian J. Saxagliptin protects against hypoxia-induced damage in H9c2 cells. *Chem Biol Interact.* (2020) 315:108864. doi: 10.1016/j.cbi.2019.108864

75. Hussain S, Khan AW, Akhmedov A, Suades R, Costantino S, Paneni F, et al. Hyperglycemia induces myocardial dysfunction via epigenetic regulation of jund. *Circ Res.* (2020) 127:1261–73. doi: 10.1161/CIRCRESAHA.120.317132

76. Nosalski R, Mikolajczyk T, Siedlinski M, Saju B, Koziol J, Maffia P, et al. Nox1/4 inhibition exacerbates age dependent perivascular inflammation and fibrosis in a model of spontaneous hypertension. *Pharmacol Res.* (2020) 161:105235. doi: 10.1016/j.phrs.2020.105235

77. Zhao GJ, Zhao CL, Ouyang S, Deng KQ, Zhu L, Montezano AC, et al. Ca(2+)-dependent Nox5 (NADPH oxidase 5) exaggerates cardiac hypertrophy through reactive oxygen species production. *Hypertension.* (2020) 76:827–38. doi: 10.1161/HYPERTENSIONAHA.120.15558

78. BelAiba RS, Djordjevic T, Petry A, Diemer K, Bonello S, Banfi B, et al. Nox5 variants are functionally active in endothelial cells. *Free Radic Biol Med.* (2007) 42:446–59. doi: 10.1016/j.freeradbiomed.2006.10.054

79. Jha JC, Watson AMD, Mathew G, de Vos LC, Jandeleit-Dahm K. The emerging role of NADPH oxidase NOX5 in vascular disease. *Clin Sci.* (2017) 131:981–90. doi: 10.1042/CS20160846

80. Pandey D, Patel A, Patel V, Chen F, Qian J, Wang Y, et al. Expression and functional significance of NADPH oxidase 5 (Nox5) and its splice variants in human blood vessels. *Am J Physiol Heart Circ Physiol.* (2012) 302:H1919–28. doi: 10.1152/ajpheart.00910.2011

81. Marques J, Cortes A, Pejenaute A, Ansorena E, Abizanda G, Prosper F, et al. Induction of cyclooxygenase-2 by overexpression of the human NADPH oxidase 5 (NOX5) gene in aortic endothelial cells. *Cells.* (2020) 9:637. doi: 10.3390/cells9030637

82. Touyz RM, Anagnostopoulou A, Camargo LL, Rios FJ, Montezano AC. Vascular biology of superoxide-generating NADPH oxidase 5-implications in hypertension and cardiovascular disease. *Antioxid Redox Signal.* (2019) 30:1027–40. doi: 10.1089/ars.2018.7583

83. Camargo LL, Montezano AC, Hussain M, Wang Y, Zou Z, Rios FJ, et al. Central role of C-Src in Nox5- mediated redox signalling in vascular smooth muscle cells in human hypertension. *Cardiovasc Res.* (2022) 118:1359–73. doi: 10.1093/cvr/cvab171

84. Jay DB, Papaharalambus CA, Seidel-Rogol B, Dikalova AE, Lassegue B, Griendling KK. Nox5 mediates Pdgf-induced proliferation in human aortic smooth muscle cells. *Free Radic Biol Med.* (2008) 45:329–35. doi: 10.1016/j.freeradbiomed.2008.04.024

85. Furmanik M, Chatrou M, van Gorp R, Akbulut A, Willems B, Schmidt H, et al. Reactive oxygen-forming NOX5 links vascular smooth muscle cell phenotypic switching and extracellular vesicle-mediated vascular calcification. *Circ Res.* (2020) 127:911–27. doi: 10.1161/CIRCRESAHA.119.316159

86. Yousefian M, Shakour N, Hosseinzadeh H, Hayes AW, Hadizadeh F, Karimi G. The natural phenolic compounds as modulators of NADPH oxidases in hypertension. *Phytomedicine.* (2019) 55:200–13. doi: 10.1016/j.phymed.2018.08.002

87. Nakamura M, Sadoshima J. Mechanisms of physiological and pathological cardiac hypertrophy. *Nat Rev Cardiol.* (2018) 15:387–407. doi: 10.1038/s41569-018-0007-y

88. Murdoch CE, Zhang M, Cave AC, Shah AM. NADPH oxidase-dependent redox signalling in cardiac hypertrophy, remodelling and failure. *Cardiovasc Res.* (2006) 71:208–15. doi: 10.1016/j.cardiores.2006.03.016

89. Lyu L, Chen J, Wang W, Yan T, Lin J, Gao H, et al. Scoparone alleviates ang II-induced pathological myocardial hypertrophy in mice by inhibiting oxidative stress. *J Cell Mol Med.* (2021) 25:3136–48. doi: 10.1111/jcmm.16304

90. Bendall JK, Cave AC, Heymes C, Gall N, Shah AM. Pivotal role of a Gp91(Phox)-containing NADPH oxidase in angiotensin II-induced cardiac hypertrophy in mice. *Circulation.* (2002) 105:293–6. doi: 10.1161/hc0302.103712

91. Greenberg HZE, Zhao G, Shah AM, Zhang M. Role of oxidative stress in calcific aortic valve disease and its therapeutic implications. *Cardiovasc Res.* (2022) 118:1433–51. doi: 10.1093/cvr/cvab142

92. Byrne JA, Grieve DJ, Bendall JK, Li JM, Gove C, Lambeth JD, et al. Contrasting roles of NADPH oxidase isoforms in pressure-overload versus angiotensin II-induced cardiac hypertrophy. *Circ Res.* (2003) 93:802–5. doi: 10.1161/01.RES.0000099504.30207.F5

93. Marino A, Hausenloy DJ, Andreadou I, Horman S, Bertrand L, Beauloye C. Amp-activated protein kinase: a remarkable contributor to preserve a healthy heart against ROS injury. *Free Radic Biol Med.* (2021) 166:238–54. doi: 10.1016/j.freeradbiomed.2021.02.047

94. Zhou H, Wang B, Yang YX, Jia QJ, Zhang A, Qi ZW, et al. Long noncoding RNAS in pathological cardiac remodeling: a review of the update literature. *Biomed Res Int.* (2019) 2019:7159592. doi: 10.1155/2019/7159592

95. Chen DS, Yan J, Yang PZ. Cardiomyocyte atrophy, an underestimated contributor in doxorubicin-induced cardiotoxicity. *Front Cardiovasc Med.* (2022) 9:812578. doi: 10.3389/fcvm.2022.812578

96. Matsushima S, Kuroda J, Zhai P, Liu T, Ikeda S, Nagarajan N, et al. Tyrosine kinase fyn negatively regulates NOX4 in cardiac remodeling. *J Clin Invest.* (2016) 126:3403–16. doi: 10.1172/JCI85624

97. Ago T, Kuroda J, Pain J, Fu C, Li H, Sadoshima J. Upregulation of Nox4 by hypertrophic stimuli promotes apoptosis and mitochondrial dysfunction in cardiac myocytes. *Circ Res.* (2010) 106:1253–64. doi: 10.1161/CIRCRESAHA.109.213116

98. Fu B, Su Y, Ma X, Mu C, Yu F. Scoparone attenuates angiotensin II-induced extracellular matrix remodeling in cardiac fibroblasts. *J Pharmacol Sci.* (2018) 137:110–5. doi: 10.1016/j.jphs.2018.05.006

99. Cucoranu I, Clempus R, Dikalova A, Phelan PJ, Ariyan S, Dikalov S, et al. Nad(P)H oxidase 4 mediates transforming growth factor-beta1-induced differentiation of cardiac fibroblasts into myofibroblasts. *Circ Res.* (2005) 97:900–7. doi: 10.1161/01.RES.0000187457.24338.3D

100. Craige SM, Chen K, Pei Y, Li C, Huang X, Chen C, et al. Nadph oxidase 4 promotes endothelial angiogenesis through endothelial nitric oxide synthase activation. *Circulation.* (2011) 124:731–40. doi: 10.1161/CIRCULATIONAHA.111.030775

101. Xu Y, Pan Y, Wang X, Chen A, Tang X, Liu X, et al. Knockdown of salusin-beta improves cardiovascular function in myocardial infarction-induced chronic heart failure rats. *Oxid Med Cell Longev.* (2021) 2021:8896226. doi: 10.1155/2021/8896226

102. Lu S, Liao Z, Lu X, Katschinski DM, Mercola M, Chen J, et al. Hyperglycemia acutely increases cytosolic reactive oxygen species via O-linked glcnacylation and camkii activation in mouse ventricular myocytes. *Circ Res.* (2020) 126:e80–96. doi: 10.1161/CIRCRESAHA.119.316288

103. Zhang M, Perino A, Ghigo A, Hirsch E, Shah AM. NADPH oxidases in heart failure: poachers or gamekeepers? *Antioxid Redox Signal.* (2013) 18:1024–41. doi: 10.1089/ars.2012.4550

104. Zhang M, Shah AM. ROS signalling between endothelial cells and cardiac cells. *Cardiovasc Res.* (2014) 102:249–57. doi: 10.1093/cvr/cvu050

105. Lopaschuk GD, Karwi QG, Tian R, Wende AR, Abel ED. Cardiac energy metabolism in heart failure. *Circ Res.* (2021) 128:1487–513. doi: 10.1161/CIRCRESAHA.121.318241

106. Wu C, Zhang Z, Zhang W, Liu X. Mitochondrial dysfunction and mitochondrial therapies in heart failure. *Pharmacol Res.* (2022) 175:106038. doi: 10.1016/j.phrs.2021.106038

107. Bertero E, Maack C. Metabolic remodelling in heart failure. *Nat Rev Cardiol.* (2018) 15:457–70. doi: 10.1038/s41569-018-0044-6

108. Yang J, Guo Q, Feng X, Liu Y, Zhou Y. Mitochondrial dysfunction in cardiovascular diseases: potential targets for treatment. *Front Cell Dev Biol.* (2022) 10:841523. doi: 10.3389/fcell.2022.841523

109. Griffiths HR, Gao D, Pararasa C. Redox regulation in metabolic programming and inflammation. *Redox Biol.* (2017) 12:50–7. doi: 10.1016/j.redox.2017.01.023

110. Vasquez-Trincado C, Garcia-Carvajal I, Pennanen C, Parra V, Hill JA, Rothermel BA, et al. Mitochondrial dynamics, mitophagy and cardiovascular disease. *J Physiol.* (2016) 594:509–25. doi: 10.1113/JP271301

111. Bertero E, Maack C. Calcium signaling and reactive oxygen species in mitochondria. *Circ Res.* (2018) 122:1460–78. doi: 10.1161/CIRCRESAHA.118.310082

112. Zhou B, Tian R. Mitochondrial dysfunction in pathophysiology of heart failure. *J Clin Invest.* (2018) 128:3716–26. doi: 10.1172/JCI120849

113. Wang S, Zhang M, Liang B, Xu J, Xie Z, Liu C, et al. Ampkalpha2 deletion causes aberrant expression and activation of Nad(P)H oxidase and consequent endothelial dysfunction in vivo: role of 26s proteasomes. *Circ Res.* (2010) 106:1117–28. doi: 10.1161/CIRCRESAHA.109.212530

114. Doughan AK, Harrison DG, Dikalov SI. Molecular mechanisms of angiotensin II-mediated mitochondrial dysfunction: linking mitochondrial oxidative damage and vascular endothelial dysfunction. *Circ Res.* (2008) 102:488–96. doi: 10.1161/CIRCRESAHA.107.162800

115. Nabeebaccus A, Hafstad A, Eykyn T, Yin X, Brewer A, Zhang M, et al. Cardiac-targeted NADPH oxidase 4 in the adaptive cardiac remodelling of the murine heart. *Lancet.* (2015) 385(Suppl. 1):S73. doi: 10.1016/S0140-673660388-9

116. Zeng C, Duan F, Hu J, Luo B, Huang B, Lou X, et al. Nlrp3 inflammasome-mediated pyroptosis contributes to the pathogenesis of non-ischemic dilated cardiomyopathy. *Redox Biol.* (2020) 34:101523. doi: 10.1016/j.redox.2020.101523

117. Li J, Zhu H, Shen E, Wan L, Arnold JM, Peng T. Deficiency of RAC1 blocks NADPH oxidase activation, inhibits endoplasmic reticulum stress, and reduces myocardial remodeling in a mouse model of type 1 diabetes. *Diabetes.* (2010) 59:2033–42. doi: 10.2337/db09-1800

118. Ye S, Luo W, Khan ZA, Wu G, Xuan L, Shan P, et al. Celastrol attenuates angiotensin II-induced cardiac remodeling by targeting Stat3. *Circ Res.* (2020) 126:1007–23. doi: 10.1161/CIRCRESAHA.119.315861

119. Jaquet V, Marcoux J, Forest E, Leidal KG, McCormick S, Westermaier Y, et al. NADPH oxidase (NOX) isoforms are inhibited by celastrol with a dual mode of action. *Br J Pharmacol.* (2011) 164:507–20. doi: 10.1111/j.1476-5381.2011.01439.x

120. Brandt M, Dorschmann H, Khraisat S, Knopp T, Ringen J, Kalinovic S, et al. Telomere shortening in hypertensive heart disease depends on oxidative DNA damage and predicts impaired recovery of cardiac function in heart failure. *Hypertension.* (2022) 79:2173–84. doi: 10.1161/HYPERTENSIONAHA.121.18935

121. Ding W, Feng H, Li WJ, Liao HH, Zhang N, Zhou ZY, et al. Apocynin attenuates diabetic cardiomyopathy by suppressing Ask1-P38/Jnk signaling. *Eur J Pharmacol.* (2021) 909:174402. doi: 10.1016/j.ejphar.2021.174402

122. Kim DH, Meza CA, Clarke H, Kim JS, Hickner RC. Vitamin D and endothelial function. *Nutrients.* (2020) 12:575. doi: 10.3390/nu12020575

123. Moris D, Spartalis M, Spartalis E, Karachaliou GS, Karaolanis GI, Tsourouflis G, et al. The role of reactive oxygen species in the pathophysiology of cardiovascular diseases and the clinical significance of myocardial redox. *Ann Transl Med.* (2017) 5:326. doi: 10.21037/atm.2017.06.27

frontiers | Frontiers in Cardiovascular Medicine

TYPE Review
PUBLISHED 12 January 2023
DOI 10.3389/fcvm.2022.981982

OPEN ACCESS

EDITED BY
Ajit Magadum,
Temple University, United States

REVIEWED BY
Alessandro Bertero,
University of Turin, Italy
Verena Schwach,
University of Twente, Netherlands
Jie Na,
Tsinghua University, China

*CORRESPONDENCE
Josef M. Penninger
✉ josef.penninger@ubc.ca

SPECIALTY SECTION
This article was submitted to Cardiovascular Biologics and Regenerative Medicine, a section of the journal Frontiers in Cardiovascular Medicine

RECEIVED 30 June 2022
ACCEPTED 29 December 2022
PUBLISHED 12 January 2023

CITATION
Wang J, An M, Haubner BJ and Penninger JM (2023) Cardiac regeneration: Options for repairing the injured heart. *Front. Cardiovasc. Med.* 9:981982. doi: 10.3389/fcvm.2022.981982

Cardiac regeneration: Options for repairing the injured heart

Jun Wang[1], Meilin An[1], Bernhard Johannes Haubner[2,3] and Josef M. Penninger[1,4]*

[1]Department of Medical Genetics, Life Sciences Institute, The University of British Columbia, Vancouver, BC, Canada, [2]Department of Internal Medicine III (Cardiology and Angiology), Innsbruck Medical University, Innsbruck, Austria, [3]Department of Cardiology, University Heart Center, University Hospital Zurich, Zurich, Switzerland, [4]Institute of Molecular Biotechnology of the Austrian Academy of Sciences, VBC – Vienna BioCenter, Vienna, Austria

Cardiac regeneration is one of the grand challenges in repairing injured human hearts. Numerous studies of signaling pathways and metabolism on cardiac development and disease pave the way for endogenous cardiomyocyte regeneration. New drug delivery approaches, high-throughput screening, as well as novel therapeutic compounds combined with gene editing will facilitate the development of potential cell-free therapeutics. In parallel, progress has been made in the field of cell-based therapies. Transplantation of human pluripotent stem cell (hPSC)-derived cardiomyocytes (hPSC-CMs) can partially rescue the myocardial defects caused by cardiomyocyte loss in large animals. In this review, we summarize current cell-based and cell-free regenerative therapies, discuss the importance of cardiomyocyte maturation in cardiac regenerative medicine, and envision new ways of regeneration for the injured heart.

KEYWORDS

cardiac regeneration, cell-free therapies, cell-based therapies, hPSC-CMs, transplantation

Introduction

Cardiovascular disease (CVD) remains a leading cause of morbidity and mortality globally. As cardiac regeneration is limited in adults, damaged cardiac regions form compensatory scars with very few functional cardiomyocytes, ultimately resulting in cardiac dysfunction and chronic heart failure. Current clinical therapies have been shown to enhance cardiac function, but none of them is designed to directly address the restoration of cardiomyocyte loss (1). Heart transplantation represents a standard treatment for patients with end-stage heart failure, however, the availability of organ donors is far from adequate to meet demand (2). It is therefore paramount to develop cardiac regenerative medicines.

Over the past two decades, fundamental advances have been made to uncover the cellular and molecular mechanisms of heart development (3, 4). The discovery of multiple signaling pathways and metabolic regulation of cardiac growth and homeostasis has shed light on potential endogenous mechanisms of cardiomyocyte regeneration. Novel drug delivery systems such as the adeno-associated virus 9 (AAV9) system or heart-targeted nanoparticles and the development of novel small molecules might allow for myocardial regeneration approaches in clinical settings (5–7). Moreover, human pluripotent stem cells (hPSCs)-derived cardiomyocytes (hPSC-CMs) have been extensively used for disease modeling and drug screening in CVD (8, 9). With the advancement of hPSC-CM research and cardiac organoid engineering, it has become possible to graft stem cell-derived-CMs into the injured heart, providing directions for

optimizing these approaches. In this review, we list some candidates for cell-free regenerative therapy, discuss the transplantation of adult stem cells and hPSC-CMs in cell-based therapy, and envision new regenerative approaches to repair damaged hearts.

Mechanisms underlying cardiac regeneration

Although the adult heart has been shown to lack regenerative capacity in mammals (10, 11), the heart can effectively regenerate within the first week after birth. Studies of apical resection (12, 13) and left anterior descending (LAD) coronary artery ligation (14–16) in neonatal rodents have shown that murine, as well as rat cardiomyocytes, have an intrinsic regenerative capacity within the first 7 days after birth. Similarly, the neonatal porcine heart is capable of regeneration after acute myocardial infarction (MI) during the first 2 days after birth (17). Furthermore, we recently reported the complete functional recovery after a massive MI in a human newborn (18). Compared to the neonatal mammalian heart, adult mammalian cardiomyocytes are highly differentiated and often contain more than one nucleus and well-aligned sarcomeres to maintain cardiac function (19); however, this in turn hinders myocardial regeneration in the adult heart once the heart is damaged (**Figure 1**). Therefore, inducing mature cardiomyocytes to re-enter the cell cycle from a quiescent state is one of the strategies to repair damaged hearts.

To date, extensive studies of neonatal heart regeneration and adult heart repair following injury in mammals have identified fundamental mechanisms underlying cardiac regeneration, providing directions for repair after myocardial injury. The transcription factor GATA4 (20), for example, is known to play an essential role in cardiomyocyte replication in neonatal mice. Myocardial Erbb2 (21) and BMP (22, 23) signaling were found to control cardiomyocyte proliferation. Inhibition of adrenergic receptor (AR) and thyroid hormone (TH) pathways promoted cardiomyocyte regeneration in mice after postnatal day 7 (24). Activation of Neuregulin1/ErbB4 signaling (25) or overexpression of a single transcription factor, namely Tbx20 (22), promoted the repair of damaged adult cardiomyocytes after myocardial infarction in mice and enhanced cardiomyocyte cell-cycle entry. Deletion of Salvador, a component in the Hippo pathway, improved heart function after myocardial infarction (26). Moreover, deletion of the hypoxia response element Meis1 increased the number of cardiomyocytes, especially mononucleated cardiomyocytes in adult mice (27).

In addition to directly inducing cardiomyocyte proliferation, several studies have demonstrated that other cardiac cell types, such as fibroblasts, can transdifferentiate into functional cardiomyocytes, which may be a potential and viable approach to heart regeneration *in vivo*. A classic combination of transcription factors Gata4, Mef2c, and Tbx5 (GMT) enabled direct reprogramming of postnatal cardiac or dermal fibroblasts into spontaneously contracting cardiomyocyte-like cells with cardiac-specific markers and contracted spontaneously (28). One study showed that blocking TGF-β and WNT signaling increased the efficiency of reprogramming in GMT-overexpressing cardiac fibroblasts. *In vivo*, mice treated with GMT, TGF-β inhibitor SB431542, and WNT inhibitor XAV939 for 2 weeks after myocardial infarction significantly improved reprogramming and cardiac function compared to mice treated with GMT only (29). In addition, the transcription factor Tead1 (Td) could efficiently replace Tbx5 in the GMT cocktail, enhancing reprogramming efficacy (30). Such reprogramming can also be achieved by chemical induction alone. A combination of nine compounds induced the transdifferentiation of fibroblasts into contracting cardiomyocyte-like cells (31). Importantly, fibroblasts can be directly reprogrammed to spontaneously contracting patches of differentiated cardiomyocytes without a pluripotent intermediate through transgenic expression of Oct4, Sox2, Klf4, and c-Myc (32). Recent studies have shown that in addition to fibroblasts, endocardial cells have the potential to generate cardiomyocytes (33). For example, the deletion of the stem cell leukemia (SCL) gene induces the expression of cardiac-specific proteins in endothelial cells (34).

Numerous studies have uncovered mechanisms that promote cardiac regeneration, and artificially increasing or decreasing these critical molecules *in vivo* may alleviate or even rescue the pathogenesis heart disease process. Thus, the discovery of druggable regenerative targets is vital to cell-free therapies.

Cell-free therapies

For cardiac repair, recombinant DNA, RNA-based, or recombinant protein therapeutics have been used in regenerative medicine. Here, we discuss some potential drug/molecule candidates for cell-free therapies based on preclinical reports of cardiac regeneration (**Table 1**).

In murine MI models, for example, injection of Neuregulin1 induced a sustained improvement in myocardial function and attenuated compensatory hypertrophy following MI (25). Adenoviral-based delivery of cyclin A2 increased myofilament density at the border zone of the MI and improved cardiac function (35). Moreover, cardiac-specific overexpression of FGF16 via AAV subtype 9 (AAV9) led to an upregulation of genes associated with cell proliferation in *Gata4*-ablated mouse hearts (20). Combined intramyocardial injection of CDK1/CCNB/CDK4/CCND significantly improved ejection fraction (EF), stroke volume, cardiac output, and markedly reduced the scar size (36). Down-regulation of Lrp6, a Wnt co-receptor, promoted adult post-MI cardiac repair by increasing cardiomyocyte proliferation (37). Delivery of IGF2BP3 through AAV9-Igf2bp3 into neonatal mouse hearts 3 days prior to LAD ligation significantly improved heart function as determined at 3-weeks post-injury (38). Some RNAs are potential targets for cardiac regeneration. For example, silencing miR-99/100 and Let-7 can induce cardiomyocyte dedifferentiation and improve heart function in adult LAD-treated mice (39). Knockdown of LncDACH1 using LncDACH1 shRNA (Adv-shLncDACH1) reactivated cardiomyocyte proliferation in adult mice and enhanced cardiac function in the injured heart (40). Delivery of Pkm2 modified RNA (modRNA) in mice hearts can increase cardiomyocyte cell proliferation and improve cardiac function after myocardial infarction (41). Moreover, one study showed chronic hypoxia-induced cardiac regeneration in adult mice. Long-term low oxygen treatment induced cardiomyocyte proliferation and angiogenesis *in vivo*, thereby reducing myocardial fibrosis and improving left ventricular systolic function in mice with myocardial infarction (42). In addition, induction of non-cardiomyocyte transdifferentiation into cardiomyocytes *in vivo* can also be achieved. Direct intramyocardial injection of GMT transdifferentiated non-cardiomyocytes into new cardiomyocyte-like cells, decreased infarct size, and attenuated cardiac dysfunction after myocardial infarction in mice hearts (43).

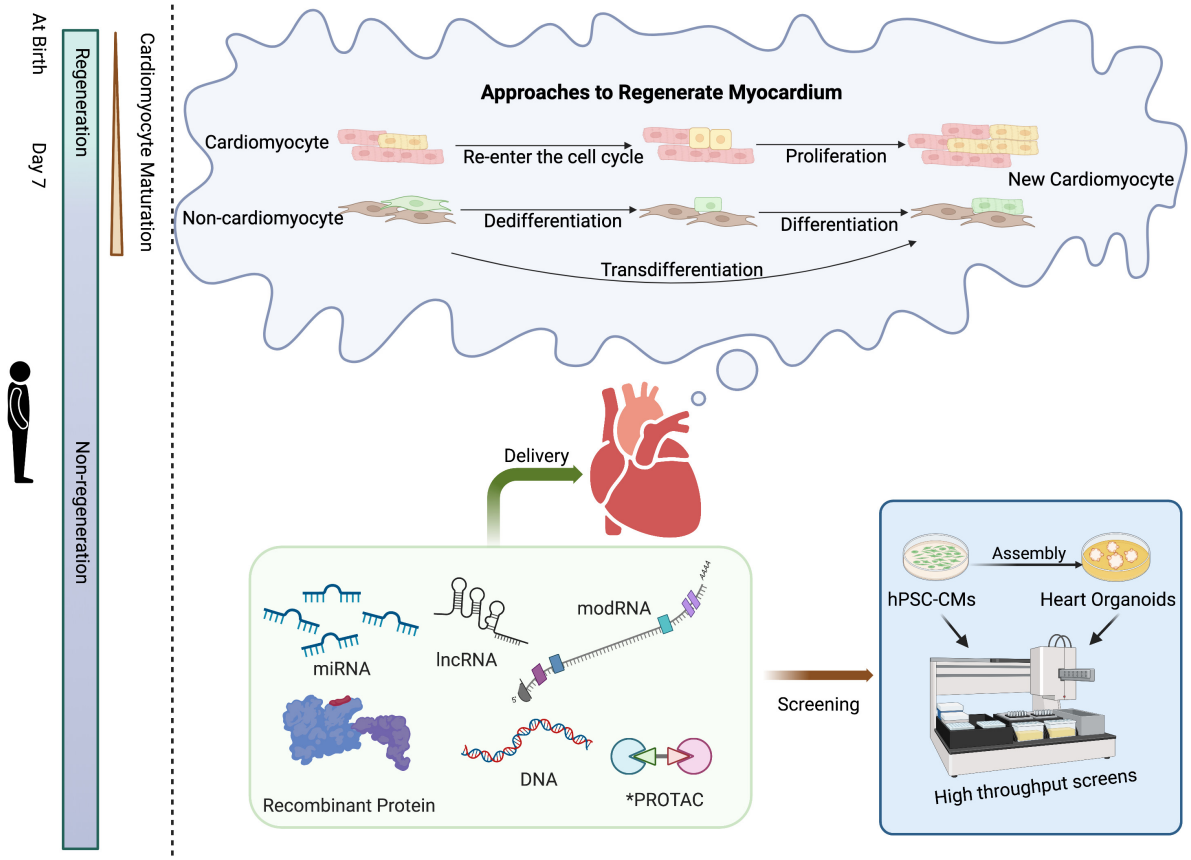

FIGURE 1
Schematic of approaches for cardiac regenerative medicine using cell-free therapies. Mammals have the intrinsic capability to structurally and functionally regenerate their hearts shortly after birth, a capacity that is subsequently lost. Approaches to cardiac regeneration involve the re-entry of cardiomyocytes into the cell cycle and/or transdifferentiation of other resident cell types into cardiomyocytes. Recombinant proteins, RNA-based drugs, PROTAC, or small molecules could serve as viable strategies for cardiac repair. High-throughput screening of drug candidates can be performed in hPSC-CMs or, at lower throughput, cardiac organoids prior to clinical application. Created with BioRender.com.

In swine MI models, cardiomyocyte hypertrophy and fibrosis following chronic MI were reduced when IGF-1/HGF was intramyocardially delivered into the injured area (44). Subcutaneous injection of a daily dose of growth hormone-releasing hormone agonist (GHRH-A) into pigs with a LAD ligation showed left ventricular structural and functional improvements, whereas cardiomyocyte proliferation was not significantly altered (45). In addition, the cardiomyogenic factor Follistatin Like 1 (FSTL1), produced by the epicardium, can stimulate recovery of contractile function within 2 weeks and limit fibrosis 4 weeks after MI injury, suggesting that FSTL1 has therapeutic efficacy in a large animal MI I/R swine model (46).

Although there many targets for cardiac regeneration have been identified and validated in animal models, the drugs currently available for clinical application are limited. The development of human cardiomyocytes from pluripotent stem cells will undoubtedly help test delivery systems and screen novel drugs for cardiac regeneration in a human "background" since hPSC-CMs from patients can also be used for preclinical tests for drug toxicity, thus enabling more precise and personalized treatments (47, 48). For example, one study designed an engineered bivalent neuregulin-1β that attenuates doxorubicin-induced double-strand DNA breaks in hPSC-CMs, with the vision to utilize such treatment to protect the heart from doxorubicin cardiotoxicity (49). hPSC-CMs from Arg663His-mutated patients can be treated with the L-type Ca2+ channel blocker verapamil to avoid the development of the hypertrophic cardiomyopathy phenotype *in vitro*. Therefore, verapamil might be a potential drug for patients with Arg663His-mutated hypertrophic cardiomyopathy (50). Compared with 2D hPSC-CMs, human cardiac organoids generated from human pluripotent stem cells through cell self-assembly (51) and 3D printing (52) are more similar in the structure and function of the human heart. Combined with gene editing, these 3D tissues can now be used to model various cardiovascular diseases such as myocardial infarction (51) and thus can ultimately be used as models for screening a collection of drug candidates (**Figure 1**).

Cell-based therapies for cardiac regeneration

Heart transplantation is currently the only restorative therapy for end-stage heart failure patients. Although the development of new drugs and surgical as well as improved storage techniques have led to an increase in successful heart transplantations, heart transplantation is still a high-risk medical procedure, and there remains an insufficient amount of donor hearts. In addition,

TABLE 1 Potential targets and candidates for cardiac regenerative cell-free therapies.

Candidates	Regulation	Application		Outcome	References
Tbx20	Up	Transgenic mice	Mice	Promotes cardiomyocyte proliferation	(22)
mir302-367	Up	Systemic delivery of miRNA	LAD mice	Induces cardiomyocyte proliferation and promotes cardiac regeneration post MI	(128)
miR-31a-5p	Up	miR-31a-5p antagomir	Neonatal rat	Promotes postnatal cardiomyocyte proliferation	(129)
NRG1	Up	Injection of NRG1 protein	LAD mice	Induces cardiomyocyte proliferation and promotes myocardial regeneration following MI	(25)
Jagged1	Up	–	–	Notch activation promotes immature cardiac myocyte proliferation and expansion at early time points in neonatal rats	(130)
GATA4	Up	–	–	GATA4 directly interacts with Cyclin D2 and Cdk4 promoters in cardiac myocytes from mice	(131)
CDK1, CDK4, Cyclin B1 and Cyclin D1	Up	Delivery of recombinant CDK1, CDK4, cyclin B1 and cyclin D1	LAD mice	Enhances cardiac function in mice after acute or sub-acute MI	(36)
Cyclin A2	Up	Adenoviral vector delivery	LAD rat	Induces cardiomyocyte mitotic activity and improves ventricular function after ischemic injury	(35)
IGF-1, HGF	Up	Administration of recombinant IGF-1/HGF	Intracoronary balloon occlusion in pigs	Improves cardiac function following MI	(44)
FGF16	Up	AAV9 delivery	Neonatal Gata4fl/fl mice with Cryoinjury	Rescues cryoinjury-induced cardiac hypertrophy and improved heart function after injury	(20)
Pkm2	Up	Delivery of Pkm2 modRNA	LAD mice	Increases cardiomyocyte cell division and improves cardiac function following MI	(41)
Agrin	Up	Recombinant Agrin	LAD mice	Stimulates cardiomyocyte proliferation in primary cardiac culture and is involved in cardiac regeneration in neonatal mice	(132)
PPARδ	Up	PPARδ agonist	LAD mice	Improves heart function in mice after myocardial infarction	(133)
hsa-miR-590, hsa-miR-199a	Up	AAV9-miRNA	Neonatal rat	Promotes cardiomyocyte proliferation in adult mice and improves cardiac function following MI	(134)
Hypoxia	Up	Hypoxia condition	LAD mice	Induces cell cycle re-entry of adult cardiomyocytes and improves functional recovery following MI in adult mice	(42)
ERBB2	Up	Transgenic mice	Erbb2-cKO mice	Transient induction of ERBB2 in adult mice is sufficient to reactivate CMs to proliferative and induce their regenerative potentials after ischaemic injury	(21)
FSTL1	Up	Patch with FSTL1 to the epicardium	LAD mice and pig	Stimulates cell cycle entry of CMs and improves cardiac function and survival in mouse and swine models of myocardial infarction	(46)
Yap1	Activated	–	–	Stimulates proliferation of postnatal cardiomyocytes in mice and in cultured rat cardiomyocytes	(135)
Gata4, Mef2c and Tbx5 (GMT)	Up	Injection of GMT-encoding retrovirus	LAD mice	Enhances cardiac reprogramming and cardiac function	(29, 43)
miR-99/100, Let-7a/c	Down	AAVs encoding for anti-miR-99/100 and anti-Let-7a/c	LAD mice	Adult cardiomyocyte dedifferentiation, enhances cardiomyocyte proliferation, and facilitates heart regeneration	(39)
LncDACH1	Down	Adv-LncDACH1, or Adv-shLncDACH1	LAD mice	Stimulates cardiac regenerative potential and enhanced cardiac function in the injured heart	(40)
LrP6	Down	AAV9-miRNAi-Lrp6 delivery	LAD mice	Reduces scar size in the infarcted hearts of mice and stimulates cardiomyocyte proliferation in the infarct border zone	(37)
Meis1	Down	Deletion of *meis1 in* mice	Adult mice	Induces cell cycle re-entry in mice	(27)

(Continued)

TABLE 1 (Continued)

Candidates	Regulation	Application		Outcome	References
FGF1, p38 MAP kinase	Down	FGF1/p38 inhibitor	LAD rat	Induces cardiomyocyte proliferation and rescue cardiac function following MI	(136)
Dag1	Down	–	TAC mice	The dystrophin– glycoprotein complex component dystroglycan 1 (Dag1) directly binds to the Hippo pathway effector Yap to inhibit cardiomyocyte proliferation in mice	(137)
α-catenins	Down	Gene depletion	αE- and αT-Catenin double KO mice	Leads to nuclear accumulation of Yap and induction of cardiomyocyte proliferation in mice	(138)
GSK-3β	Down	Gene depletion	GSK-3β conditional KO mice	Protects against post-MI remodeling and promotes cardiomyocyte proliferation in adult mice	(139)
GHRH-A	Down	Injection of a hormone-releasing hormone agonist (GHRH-A)	LAD pig	Reduces infarct size and improve cardiac function in pigs with subacute ischemic cardiomyopathy	(45)
Adrenergic receptor (AR), thyroid hormone (TH)	Down	AR and TH inhibitors	Neonatal mice	Extends postnatal cardiac regenerative capacity in part by promoting cardiomyocyte cell division	(24)

immunosuppression is required after heart transplantation, which is a risk factor for complications. In recent years, cell-based therapies have been proposed as a promising approach for treating advanced heart failure and repairing damaged myocardial tissue.

Adult stem cells transplantations

Early evidence suggested that adult stem cells such as bone marrow cells (BMCs), bone marrow-purified haematopoietic stem cells (HSCs), and bone marrow-purified mesenchymal stem cells (MSCs) can differentiate into cardiomyocytes. A 2001 study showed that 9 days after transplantation of c-kit+ BMCs in a LAD mouse model, newly formed myocytes occupied 68% of the infarcted region in the ventricle leading to an overall improvement in cardiac function (53). Then, one report claimed that the grafts of c-Kit+, stem cell antigen-1 positive (Sca-1+) BMCs migrated to ischemic areas where they differentiated into cardiomyocytes and endothelial cells (54). C-kit+ cells (55) and Sca-1+ cells (56, 57)were hence considered as adult cardiac stem/progenitor cells (CPCs). However, multiple follow-up studies showed negative results (58, 59). One study found that transplantation of HSCs into adult mouse hearts did not result in any detectable transdifferentiation into cardiomyocytes, nor was there a significant increase in cardiomyocytes in the HSCs-treated hearts (58). Likewise, multiple laboratories have demonstrated that the transplantation of c-kit+ cells into infarcted adult mouse hearts did not result in the differentiation of cardiomyocytes (60, 61). Additional studies further showed that Sca-1+ cells do not generate new cardiomyocytes (62–64), but are rather precursors of endothelial cells (62). Moreover, lineage-tracing techniques have confirmed that both c-kit+ and Sca1+ adult stem cells in transplanted mice cannot differentiate into cardiomyocytes *in vivo* (62–67). Thus, the concept of adult cardiac stem cells, as well as the idea that adult stem/progenitor cells can promote cardiac remuscularization, have been rejected.

Nonetheless, numerous clinical trials of bone marrow-derived adult stem cell transplantation have been conducted [reviewed in (68–70)]. As expected from foundational research, the overall clinical benefit was not significant. To date, there is growing evidence that the minute benefits of adult stem cell therapy could be attributed to the effects of secreted factors acting on neighboring cells through a paracrine mechanism (69, 70). Several key secreted growth factors have been identified, such as VEGF, HGF, IGF-1, and TGF-β, mediators that stimulate angiogenesis, inhibit apoptosis or modulate inflammatory pathways (71, 72). In addition, exosomes might be one of the reasons for the improvement of cardiac function after such adult stem cell transplantation. Treating the infarcted area with exosomes secreted by cardiac mesenchymal stem cells can enhance cardiac angiogenesis, promote cardiomyocyte proliferation, and maintain cardiac function in mouse hearts (73). In addition, one study found that both live and dead adult stem cells induced macrophage accumulation in the infarcted area of hearts, improving the heart function after I/R injury, which also occurred after the direct induction of innate immune response. Thus, the recovery of the infarcted area of the heart following adult stem cell therapy may attribute to an acute inflammatory wound-healing response through the accumulation of regional macrophages (74).

Pluripotent stem cell-based therapies for cardiac regeneration

Human embryonic stem cells (ESCs) have the ability to differentiate into multiple cell types and thus have great therapeutic potential in regenerative medicine. However, because human ESCs are extracted from blastocysts, both scientific research and clinical applications of human ESCs face ethical issues (75). In 2006, Takahashi and Yamanaka successfully induced pluripotent stem cells (iPSCs) from fibroblasts by the introduction of four factors, Oct3/4, Sox2, c-Myc and Klf4. The self-renewal and differentiation capacity of pluripotent stem cells is largely comparable to that of embryonic stem cells but avoids ethical issues (76). In recent years, many laboratories have reported the development of cardiomyocytes from ESCs (77, 78) and iPSCs (79–84). ESC-derived cardiomyocytes (ESC-CMs) and iPSC-derived cardiomyocytes (iPSC-CMs), here collectively referred to as hPSC-CMs, express molecular markers and exhibit subcellular structures and electrophysiology resembling primary, albeit immature cardiomyocytes.

TABLE 2 Preclinical and clinical studies of hPSC-CMs transplantations for treatment of cardiac disease.

Species	Disease model	Cell types	Delivery method	Heart function	Side effect	References
Mice	LAD	hiPSC-CMs	Intramyocardial injection	Enhance	No major side effects reported	(85, 87)
Rat	I/R	hESC-CMs	Intramyocardial injection			(90)
	LAD	hiPSC-CMs	Intramyocardial injection			(86)
	LAD	hiPSC-CMs and rat microvessels	Intramyocardial injection			(111)
Guinea-pig	Cryoinjury	Partly matured hESC-CMs	Intramyocardial injection		Arrhythmia but reduced	(99)
Pig	Ameroid ring placement	hiPSC-CMs	Cell sheet		Arrhythmia	(88)
	LAD	hESC-CMs	Direct image-guided transendocardial injection			(95)
	Cryoinjury	hiPSC-cardiac spheroids	Intramyocardial injection			(110)
Monkey	I/R	hESC-CMs	Intramyocardial injection			(93)
	LAD	hESC-CMs				(97)
	LAD	mPSC-CMs				(94)
Human	Patients	hiPSC-CMs	Injection	Not yet reported	Not yet reported	(120)
		hiPSC-CMs	Patches	Clinical symptoms improved	No adverse events	(114)

Several groups have transplanted hPSC-CM in experimental cardiovascular disease models *in vivo* (85–93), providing experimental feasibility studies for future clinical applications (**Table 2**). Studies have confirmed that hPSC-CMs can engraft, survive, and electrically couple with host myocardial tissue *in vivo* and improve contractile function after infarction. For example, in both acute myocardial infarction and chronic post-infarction heart disease in rats, transplanted hPSC-CMs can survive and form viable tissue containing striated cardiomyocytes. These hPSC-CM injections attenuated ventricular dilatation and preserved systolic function after acute myocardial infarction but are insufficient to alter adverse remodeling of chronic myocardial infarction rats (90, 91). In addition, transplanted hPSC-CMs could remuscularize cryoinjured guinea-pig hearts, thereby preserving cardiac function (92). Intramyocardial delivery of one billion hPSC-CMs into Macaques suffering an ischemia/reperfusion injury also resulted in the remuscularization of substantial areas of the infarcted monkey heart (93). The hPSC-CM engraftment is indeed promising as a cell-based therapy. However, there are key issues that remain to be solved.

Arrhythmias are considered the most critical side effect of engraftment, as they can be lethal, especially in pigs and primates. In ischemia/reperfusion-injured macaques, ventricular arrhythmias were observed despite remuscularization (93). Similar results were found in myocardial-infarcted cynomolgus monkeys. Ventricular tachycardias happened following the transplantation of monkey iPSC-derived cardiomyocytes (mPSC-CMs) (94). Studies in infarcted hearts of rats and pigs also showed the development of arrhythmias and tachyarrhythmias following injection of immature hPSC-CMs (95, 96). In infarcted hPSC-CM recipient pigs, frequent and fatal ventricular tachyarrhythmias were observed during the first few days of post-transplantation, and normal sinus rhythm was observed 28 days after transplantation (95). Such graft-related ventricular arrhythmias most likely originate from an ectopic pacemaker formed by the transplanted hPSC-CMs (97). To eliminate such arrhythmic events, several strategies have been considered. Pharmacologic treatment is one of the solutions to engraftment arrhythmia. One study showed that a combination of amiodarone and ivabradine could effectively suppress arrhythmia in infarcted hPSC-CM recipient pigs (98). In addition, the engraftment of more mature cardiomyocytes was beneficial in reducing arrhythmia events (99). This study showed that hPSC-CMs cultured on polydimethylsiloxane (PDMS) substrates exhibited increased expression of cardiac maturation markers and improved structural and functional properties of more mature cardiomyocytes *in vitro*. They then found that transplantation of this PDMS-treated hPSC-CMs in an infarcted guinea pig enhanced post-transplant structure and alignment, host-graft electromechanical integration, and importantly, reduced proarrhythmic behavior (99). To engraft matured hPSC-CMs, several studies have attempted to induce cardiomyocyte maturation *in vitro*. For example, using 3–6 months long-term cultures, hPSC-CMs exhibited an adult-like phenotype, including increased cell size or greater myofibril density and alignment (100, 101). In addition, electric pacing and mechanical stimulation were shown to promote hPSC-CMs maturation *in vitro* (102, 103). hPSCs-CMs treated with a maturation medium including a peroxisome proliferator-activated nuclear receptors alpha (PPARa) agonist, palmitate, dexamethasone, and Tri-iodo-l-thyronine (T3) (104) in the presence of low glucose resulted in hPSC-CMs with increased the expression of genes associated with fatty acid oxidation (FAO), mitochondrial respiration, and muscle function (105). In addition, insulin-like growth factor-1 (IGF-1) or low glucose in culture media was shown to promote cardiomyocyte maturation (106, 107). In contrast to monolayer cardiomyocyte cultures, hPSCs-CMs grown in 3D *in vitro* appear to be more mature and thereby better mimic bona fide cardiomyocytes (108). In particular, self-organizing cardiac organoids, as compared to 2D-grown hPSC-CMs, exhibit increased expression of cardiac ion

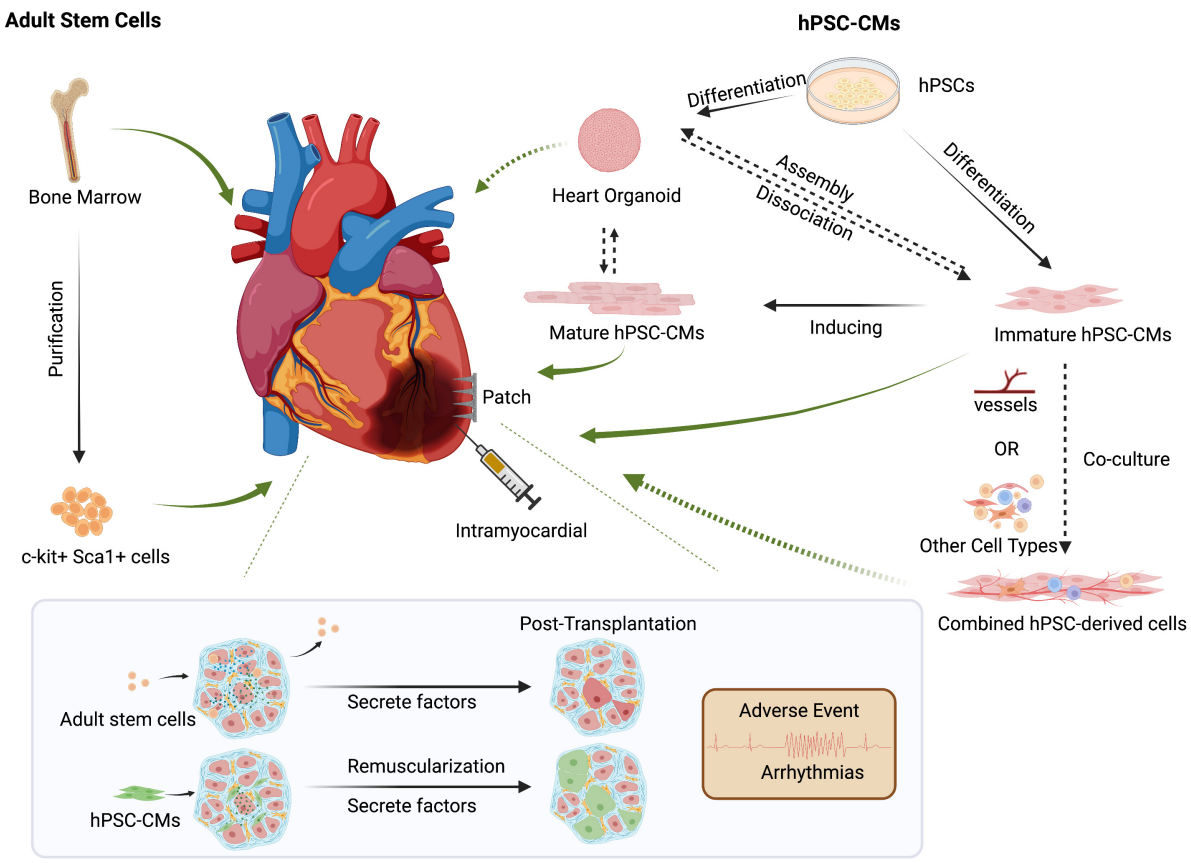

FIGURE 2
Cell-based approaches to cardiac regenerative medicine. Delivery methods such as intracardiac injection and cell patches can be used for cell-based therapies. Though controversial, transplanting bone marrow-derived adult stem cells could promote cardiac function via secreted factors. Human pluripotent stem cell-derived cardiomyocytes (hPSC-CMs) can repair damaged hearts through tissue replacement of lost cardiomyocytes and help promote cardiac function by secreting growth factors such as VEGF. However, preclinical models and clinical trials must carefully address post-transplant arrhythmias and other side effects. The increased maturity of hPSC-CMs might reduce unwanted and potentially lethal arrhythmic events. Co-delivery of multiple cell types, including endothelial cells or other cardiac cell types, might improve hPSC-CMs retention and thereby promote the repair of injured hearts. Created with BioRender.com.

channels (KCNH2), structural proteins (TNNI1, TTN, and MYH6), cardiac transcriptional factors (TBX5 and MEF2C), or sarcoplasmic reticulum proteins (RYR2 and ATP2A2), indicating improved maturity (108).

During the transplantation of exogenous hPSC-CMs, the nutrient-deprived and hypoxic environment in the infarcted area is a major challenge (109). Although studies demonstrated that hPSC-CMs could be engrafted in monkey hearts and survive up to 3 months (93, 94, 97), another report found that the engrafted hPSC-CMs were massively reduced in numbers after 8 weeks post-transplantation in pig hearts (110). Therefore, the addition of support cells may be beneficial for hPSC-CMs integration and survival. Indeed, co-transplantation of microvessels and hPSC-CMs into the ischemic area of the LAD-treated rats promoted the survival of hPSC-CMs *in vivo* and improved cardiac function compared with the transplantation of hPSC-CMs alone (111). Although the mechanisms involved in the functional integration and survival of hPSC-CMs in host tissues are not fully understood, studies have found vascularization occurs after hPSC-CMs transplantation and may be related to cytokines such as VEGF secreted by the grafted cells (109, 112). Therefore, the addition of VEGF (113) or other pro-angiogenic factors before transplantation may also contribute to the improvement of hPSC-CMs survival and subsequent enhanced cardiac function.

Besides cardiomyocyte maturation and vascularization, the mode of delivery might be critical. Intracardiac injection is the current delivery method, but grafts may be eluted with the circulatory system. To enhance hPSC-CMs survival, a multicomponent pro-survival cocktail was developed, and its co-injection with hPSC-CMs improved graft residency *in vivo* (90, 91). Bioengineering methods such as cell patches (114, 115) and cell sheets (116, 117) have also been devised to improve cell engraftment rates, however, integrating cells in biomaterials with host myocardium is a big challenge. For example, transplantation of hPSC-CMs sheets improved cardiac systolic function not attributable to graft integration into the host myocardium but most likely due to neovascularization (118). Recently microneedle patches were developed to be inserted into the myocardium, improving the connection between the graft and the host myocardium (119).

So far, there have been two clinical trials engrafting hPSC-CMs for heart disease. Two patients in China underwent an experimental treatment for heart disease based on hPSC-CMs, though the clinical outcomes have not yet been published (120). In Japan, one male patient who suffered from severe heart failure due to ischemic cardiomyopathy was treated with clinical-grade hPSC-CMs patches. The clinical symptoms apparently improved 6 months after surgery, without any major adverse events or changes in the cardiac wall

motion at the site of the transplant. However, more details need to be disclosed (114). Regardless, these first human clinical trials hold promises for the use of hPSC-CMs to repair cardiac damage (**Figure 2**).

Future directions and conclusion

The field of cardiac regeneration has made remarkable progress in recent years. Both cell-free and cell-based methods are vigorously researched and developed to promote and improve cardiac regeneration for clinical applications. Along the way, numerous molecular mechanisms and key factors involving cardiomyocyte's re-entry into the cell cycle or trans-differentiation of non-cardiomyocytes into cardiomyocytes were discovered and are now being translated to drug development. Although some molecules, such as recombinant proteins, small molecule inhibitors, or RNA-based therapies, are being developed, more effective drugs need to be discovered. Moreover, Proteolysis Targeting chimera (PROTAC) technologies might provide viable modes of drug delivery for targeted and time-resolved degradation of candidate drug targets (121, 122).

For cardiac repair using cell-based systems, hPSC-CMs have the potential to form functional tissue containing striated cardiomyocytes *in vivo*. To achieve clinical use, hPSC-CMs will be required to be mass-produced with strict quality standards. Therefore, allogeneic, off-the-shelf hPSCs-CMs must be developed. In addition to pharmacological immunosuppression, including new-generation drugs with fewer side effects, gene-edited hypoimmune hPSC-CM have been generated to overcome the rejection from the host (123). Another obstacle is the maturity of transplanted hPSC-CMs, in particular, addressing and reducing arrhythmic events triggered by the transplanted cardiomyocytes that have to be functionally integrated into the electrically coupled cardiac tissue. Compared to monolayer cultures, 3D hPSCs-CMs appeared to express more maturation markers and functionally mimic more mature cardiomyocytes, including the formation of tight junctions between cardiomyocytes. Thus, transplantation of hPSC-CM aggregates rather than loose single cardiomyocytes may contribute to graft survival, improve functionality and reduce arrhythmias. However, several studies suggest that the optimal timing of transplantation depends on the developmental stage of hPSC-CMs (124, 125). Moreover, the mode of delivery of such cell-based therapies will be critical. Balancing hPSC-CMs maturity, effective delivery, and transplantation timing must be the focus of future research.

Besides cardiomyocytes, the heart contains multiple other cell types, such as endothelial cells, fibroblasts, smooth muscle cells, or different types of immune cells, that might affect graft survival and improve the function of damaged hearts (126). As more hPSC-derived cell types can be faithfully generated, co-transplantation of multiple cell types might therefore greatly improve cell-based therapies for cardiac diseases. For instance, our group developed stem cell-derived self-organizing 3D blood vessel organoids (BVOs) that form bona fide and functionally perfused vascular trees containing arterioles, capillaries, and venules when transplanted into immunodeficient mice (127). Such BVOs and other approaches to generate human endothelial cells and blood vessels, such as 3D printing, could be utilized to enhance and maintain the engraftment of stem cell-derived cardiomyocytes.

Author contributions

JW wrote and revised the draft. JP designed and supervised and revised the study. MA designed the tables. BH revised the draft. All authors read and approved the submitted version.

Funding

JP was supported by a Canada 150 Chair in Functional Genomics, a Paul G. Allen Distinguished Investigator Award, and the T. von Zastrow Foundation.

Conflict of interest

JP was the founder of Angios Biotech which develops blood vessel organoids for drug screening and clinical use in humans.

The remaining authors declare that the research was conducted in the absence of any commercial or financial relationships that could be construed as a potential conflict of interest.

Publisher's note

References

1. Heidenreich P, Bozkurt B, Aguilar D, Allen L, Byun J, Colvin M, et al. 2022 Aha/Acc/Hfsa guideline for the management of heart failure: a report of the American college of cardiology/American heart association joint committee on clinical practice guidelines. *Circulation.* (2022) 2022:1063. doi: 10.1161/CIR.0000000000001063

2. Piperata A, Caraffa R, Bifulco O, Avesani M, Apostolo A, Gerosa G, et al. Marginal donors and organ shortness: concomitant surgical procedures during heart transplantation: a literature review. *J Cardiovasc Med.* (2022) 23:167–75. doi: 10.2459/jcm.0000000000001233

3. Cui Y, Zheng Y, Liu X, Yan L, Fan X, Yong J, et al. Single-cell transcriptome analysis maps the developmental track of the human heart. *Cell Rep.* (2019) 26:1934–50e5. doi: 10.1016/j.celrep.2019.01.079

4. Lescroart F, Zaffran S. Single cell approaches to understand the earliest steps in heart development. *Curr Cardiol Rep.* (2022) 2022:1682. doi: 10.1007/s11886-022-01681-w

5. Wang Q, Song Y, Chen J, Li Q, Gao J, Tan H, et al. Direct in vivo reprogramming with non-viral sequential targeting nanoparticles promotes cardiac regeneration. *Biomaterials.* (2021) 276:121028. doi: 10.1016/j.biomaterials.2021.121028

6. Fan C, Joshi J, Li F, Xu B, Khan M, Yang J, et al. Nanoparticle-mediated drug delivery for treatment of ischemic heart disease. *Front Bioengin Biotechnol.* (2020) 8:687. doi: 10.3389/fbioe.2020.00687

7. Naso M, Tomkowicz B, Perry W, Strohl W. Adeno-associated virus (Aav) as a vector for gene therapy. *BioDrugs.* (2017) 31:317–34. doi: 10.1007/s40259-017-0234-5

8. Matsa E, Burridge P, Wu J. Human stem cells for modeling heart disease and for drug discovery. *Sci Trans Med.* (2014) 6:s6–6. doi: 10.1126/scitranslmed.3008921

9. Smith A, Macadangdang J, Leung W, Laflamme M, Kim D. Human ipsc-derived cardiomyocytes and tissue engineering strategies for disease modeling and drug screening. *Biotechnol Adv.* (2017) 35:77–94. doi: 10.1016/j.biotechadv.2016.12.002

10. Jopling C, Sleep E, Raya M, Martí M, Raya A, Belmonte J. Zebrafish heart regeneration occurs by cardiomyocyte dedifferentiation and proliferation. *Nature.* (2010) 464:606–9. doi: 10.1038/nature08899

11. Laube F, Heister M, Scholz C, Borchardt T, Braun T. Re-programming of newt cardiomyocytes is induced by tissue regeneration. *J Cell Sci.* (2006) 119:4719–29. doi: 10.1242/jcs.03252

12. Porrello E, Mahmoud A, Simpson E, Hill J, Richardson J, Olson E, et al. Transient regenerative potential of the neonatal mouse heart. *Science.* (2011) 331:1078–80. doi: 10.1126/science.1200708

13. Mahmoud A, Porrello E, Kimura W, Olson E, Sadek H. Surgical models for cardiac regeneration in neonatal mice. *Nat Prot.* (2014) 9:305–11. doi: 10.1038/nprot.2014.021

14. Haubner B, Adamowicz-Brice M, Khadayate S, Tiefenthaler V, Metzler B, Aitman T, et al. Complete cardiac regeneration in a mouse model of myocardial infarction. *Aging.* (2012) 4:966–77. doi: 10.18632/aging.100526

15. Haubner B, Schuetz T, Penninger JMA. Reproducible protocol for neonatal ischemic injury and cardiac regeneration in neonatal mice. *Basic Res Cardiol.* (2016) 111:64. doi: 10.1007/s00395-016-0580-3

16. Wang Z, Cui M, Shah A, Tan W, Liu N, Bassel-Duby R, et al. Cell-type-specific gene regulatory networks underlying murine neonatal heart regeneration at single-cell resolution. *Cell Rep.* (2020) 33:108472. doi: 10.1016/j.celrep.2020.108472

17. Zhu W, Zhang E, Zhao M, Chong Z, Fan C, Tang Y, et al. Regenerative potential of neonatal porcine hearts. *Circulation.* (2018) 138:2809–16. doi: 10.1161/CIRCULATIONAHA.118.034886

18. Haubner B, Schneider J, Schweigmann U, Schuetz T, Dichtl W, Velik-Salchner C, et al. Functional recovery of a human neonatal heart after severe myocardial infarction. *Circ Res.* (2016) 118:216–21. doi: 10.1161/CIRCRESAHA.115.307017

19. Derks W, Bergmann O. Polyploidy in cardiomyocytes. *Circ Res.* (2020) 126:552–65. doi: 10.1161/CIRCRESAHA.119.315408

20. Yu W, Huang X, Tian X, Zhang H, He L, Wang Y, et al. Gata4 regulates fgf16 to promote heart repair after injury. *Development.* (2016) 143:936–49. doi: 10.1242/dev.130971

21. D'Uva G, Aharonov A, Lauriola M, Kain D, Yahalom-Ronen Y, Carvalho S, et al. Erbb2 triggers mammalian heart regeneration by promoting cardiomyocyte dedifferentiation and proliferation. *Nat Cell Biol.* (2015) 17:627–38. doi: 10.1038/ncb3149

22. Chakraborty S, Sengupta A, Yutzey K. Tbx20 promotes cardiomyocyte proliferation and persistence of fetal characteristics in adult mouse hearts. *J Mol Cell Cardiol.* (2013) 62:203–13. doi: 10.1016/j.yjmcc.2013.05.018

23. Wu C, Kruse F, Vasudevarao M, Junker J, Zebrowski D, Fischer K, et al. Spatially resolved genome-wide transcriptional profiling identifies bmp signaling as essential regulator of zebrafish cardiomyocyte regeneration. *Dev Cell.* (2016) 36:36–49. doi: 10.1016/j.devcel.2015.12.010

24. Payumo A, Chen X, Hirose K, Chen X, Hoang A, Khyeam S, et al. Adrenergic-thyroid hormone interactions drive postnatal thermogenesis and loss of mammalian heart regenerative capacity. *Circulation.* (2021) 144:1000–3. doi: 10.1161/CIRCULATIONAHA.121.054846

25. Bersell K, Arab S, Haring B, Kühn B. Neuregulin1/Erbb4 signaling induces cardiomyocyte proliferation and repair of heart injury. *Cell.* (2009) 138:257–70. doi: 10.1016/j.cell.2009.04.060

26. Leach J, Heallen T, Zhang M, Rahmani M, Morikawa Y, Hill M, et al. Hippo pathway deficiency reverses systolic heart failure after infarction. *Nature.* (2017) 550:260–4. doi: 10.1038/nature24045

27. Mahmoud A, Kocabas F, Muralidhar S, Kimura W, Koura A, Thet S, et al. Meis1 regulates postnatal cardiomyocyte cell cycle arrest. *Nature.* (2013) 497:249–53. doi: 10.1038/nature12054

28. Ieda M, Fu J, Delgado-Olguin P, Vedantham V, Hayashi Y, Bruneau B, et al. Direct reprogramming of fibroblasts into functional cardiomyocytes by defined factors. *Cell.* (2010) 142:375–86. doi: 10.1016/j.cell.2010.07.002

29. Mohamed T, Stone N, Berry E, Radzinsky E, Huang Y, Pratt K, et al. Chemical enhancement of in vitro and in vivo direct cardiac reprogramming. *Circulation.* (2017) 135:978–95. doi: 10.1161/CIRCULATIONAHA.116.024692

30. Singh V, Pinnamaneni J, Pugazenthi A, Sanagasetti D, Mathison M, Martin J, et al. Hippo pathway effector tead1 induces cardiac fibroblast to cardiomyocyte reprogramming. *J Am Heart Assoc.* (2021) 10:e022659. doi: 10.1161/JAHA.121.022659

31. Cao N, Huang Y, Zheng J, Spencer C, Zhang Y, Fu J, et al. Conversion of human fibroblasts into functional cardiomyocytes by small molecules. *Science.* (2016) 352:1216–20. doi: 10.1126/science.aaf1502

32. Efe J, Hilcove S, Kim J, Zhou H, Ouyang K, Wang G, et al. Conversion of mouse fibroblasts into cardiomyocytes using a direct reprogramming strategy. *Nat Cell Biol.* (2011) 13:215–22. doi: 10.1038/ncb2164

33. Zhang H, Lui K, Zhou B. Endocardial cell plasticity in cardiac development, diseases and regeneration. *Circ Res.* (2018) 122:774–89. doi: 10.1161/CIRCRESAHA.117.312136

34. Fioret Bryan A, Heimfeld Jeremy D, Paik David T, Hatzopoulos Antonis K. Endothelial cells contribute to generation of adult ventricular myocytes during cardiac homeostasis. *Cell Rep.* (2014) 8:229–41. doi: 10.1016/j.celrep.2014.06.004

35. Woo Y, Panlilio C, Cheng R, Liao G, Atluri P, Hsu V, et al. Therapeutic delivery of cyclin A2 induces myocardial regeneration and enhances cardiac function in ischemic heart failure. *Circulation.* (2006) 114:455. doi: 10.1161/CIRCULATIONAHA.105.000455

36. Mohamed T, Ang Y, Radzinsky E, Zhou P, Huang Y, Elfenbein A, et al. Regulation of cell cycle to stimulate adult cardiomyocyte proliferation and cardiac regeneration. *Cell.* (2018) 173:104–16e12. doi: 10.1016/j.cell.2018.02.014

37. Wu Y, Zhou L, Liu H, Duan R, Zhou H, Zhang F, et al. Lrp6 downregulation promotes cardiomyocyte proliferation and heart regeneration. *Cell Res.* (2020) 2020:411. doi: 10.1038/s41422-020-00411-7

38. Wang Z, Cui M, Shah A, Ye W, Tan W, Min Y, et al. Mechanistic basis of neonatal heart regeneration revealed by transcriptome and histone modification profiling. *Proc Natl Acad Sci USA.* (2019) 116:18455–65. doi: 10.1073/pnas.1905824116

39. Aguirre A, Montserrat N, Zacchigna S, Nivet E, Hishida T, Krause Marie N, et al. In vivo activation of a conserved microrna program induces mammalian heart regeneration. *Cell Stem Cell.* (2014) 15:589–604. doi: 10.1016/j.stem.2014.10.003

40. Cai B, Ma W, Wang X, Sukhareva N, Hua B, Zhang L, et al. Targeting lncdach1 promotes cardiac repair and regeneration after myocardium infarction. *Cell Death Different.* (2020) 27:2158–75. doi: 10.1038/s41418-020-0492-5

41. Magadum A, Singh N, Kurian A, Munir I, Mehmood T, Brown K, et al. Pkm2 regulates cardiomyocyte cell cycle and promotes cardiac regeneration. *Circulation.* (2020) 141:1249–65. doi: 10.1161/CIRCULATIONAHA.119.043067

42. Nakada Y, Canseco D, Thet S, Abdisalaam S, Asaithamby A, Santos C, et al. Hypoxia induces heart regeneration in adult mice. *Nature.* (2017) 541:222–7. doi: 10.1038/nature20173

43. Qian L, Huang Y, Spencer C, Foley A, Vedantham V, Liu L, et al. In vivo reprogramming of murine cardiac fibroblasts into induced cardiomyocytes. *Nature.* (2012) 485:593–8. doi: 10.1038/nature11044

44. Koudstaal S, Bastings M, Feyen D, Waring C, van Slochteren F, Dankers P, et al. Sustained delivery of insulin-like growth factor-1/hepatocyte growth factor stimulates endogenous cardiac repair in the chronic infarcted pig heart. *J Cardiovasc Trans Res.* (2014) 7:232–41. doi: 10.1007/s12265-013-9518-4

45. Bagno L, Kanashiro-Takeuchi R, Suncion V, Golpanian S, Karantalis V, Wolf A, et al. Growth hormone–releasing hormone agonists reduce myocardial infarct scar in swine with subacute ischemic cardiomyopathy. *J Am Heart Assoc.* (2015) 4:e001464. doi: 10.1161/JAHA.114.001464

46. Wei K, Serpooshan V, Hurtado C, Diez-Cuñado M, Zhao M, Maruyama S, et al. Epicardial Fstl1 reconstitution regenerates the adult mammalian heart. *Nature.* (2015) 525:479–85. doi: 10.1038/nature15372

47. Cao X, Jahng J, Lee C, Zha Y, Wheeler M, Sallam K, et al. Generation of three induced pluripotent stem cell lines from hypertrophic cardiomyopathy patients carrying myh7 mutations. *Stem Cell Res.* (2021) 55:102455. doi: 10.1016/j.scr.2021.102455

48. Thomas D, Cunningham N, Shenoy S, Wu J. Human Ipscs in cardiovascular research: current approaches in cardiac differentiation, maturation strategies, and scalable production. *Cardiovasc Res.* (2021) 118:20–36. doi: 10.1093/cvr/cvab115

49. Jay S, Murthy A, Hawkins J, Wortzel J, Steinhauser M, Alvarez L, et al. An engineered bivalent neuregulin protects against doxorubicin-induced cardiotoxicity with reduced proneoplastic potential. *Circulation.* (2013) 128:152–61. doi: 10.1161/CIRCULATIONAHA.113.002203

50. Lan F, Lee Andrew S, Liang P, Sanchez-Freire V, Nguyen Patricia K, Wang L, et al. Abnormal calcium handling properties underlie familial hypertrophic cardiomyopathy pathology in patient-specific induced pluripotent stem cells. *Cell Stem Cell.* (2013) 12:101–13. doi: 10.1016/j.stem.2012.10.010

51. Kim H, Kamm R, Vunjak-Novakovic G, Wu J. Progress in multicellular human cardiac organoids for clinical applications. *Cell Stem Cell.* (2022) 29:503–14. doi: 10.1016/j.stem.2022.03.012

52. Kupfer M, Lin W, Ravikumar V, Qiu K, Wang L, Gao L, et al. In situ expansion, differentiation, and electromechanical coupling of human cardiac muscle in a 3d bioprinted, chambered organoid. *Circ Res.* (2020) 127:207–24. doi: 10.1161/CIRCRESAHA.119.316155

53. Orlic D, Kajstura J, Chimenti S, Jakoniuk I, Anderson S, Li B, et al. Bone marrow cells regenerate infarcted myocardium. *Nature.* (2001) 410:701–5. doi: 10.1038/35070587

54. Jackson K, Majka S, Wang H, Pocius J, Hartley C, Majesky M, et al. Regeneration of ischemic cardiac muscle and vascular endothelium by adult stem cells. *J Clin Investigat.* (2001) 107:1395–402. doi: 10.1172/JCI12150

55. Beltrami A, Barlucchi L, Torella D, Baker M, Limana F, Chimenti S, et al. Adult cardiac stem cells are multipotent and support myocardial regeneration. *Cell.* (2003) 114:763–76. doi: 10.1016/S0092-867400687-1

56. Oh H, Bradfute S, Gallardo T, Nakamura T, Gaussin V, Mishina Y, et al. Cardiac progenitor cells from adult myocardium: homing, differentiation, and fusion after infarction. *Proc Natl Acad Sci USA.* (2003) 100:12313–8. doi: 10.1073/pnas.2132126100

57. Matsuura K, Nagai T, Nishigaki N, Oyama T, Nishi J, Wada H, et al. Adult cardiac sca-1-positive cells differentiate into beating cardiomyocytes *. *J Biol Chem.* (2004) 279:11384–91. doi: 10.1074/jbc.M310822200

58. Murry C, Soonpaa M, Reinecke H, Nakajima H, Nakajima H, Rubart M, et al. Haematopoietic stem cells do not transdifferentiate into cardiac myocytes in myocardial infarcts. *Nature.* (2004) 428:664–8. doi: 10.1038/nature02446

59. Balsam L, Wagers A, Christensen J, Kofidis T, Weissman I, Robbins R. Haematopoietic stem cells adopt mature haematopoietic fates in ischaemic myocardium. *Nature.* (2004) 428:668–73. doi: 10.1038/nature02460

60. van Berlo J, Kanisicak O, Maillet M, Vagnozzi R, Karch J, Lin S, et al. C-kit+ cells minimally contribute cardiomyocytes to the heart. *Nature.* (2014) 509:337–41. doi: 10.1038/nature13309

61. Sultana N, Zhang L, Yan J, Chen J, Cai W, Razzaque S, et al. Resident C-kit+ cells in the heart are not cardiac stem cells. *Nat Commun.* (2015) 6:8701. doi: 10.1038/ncomms9701

62. Vagnozzi R, Sargent M, Lin S, Palpant N, Murry C, Molkentin J. Genetic lineage tracing of sca-1$^+$ cells reveals endothelial but not myogenic contribution to the murine heart. *Circulation.* (2018) 138:2931–9. doi: 10.1161/CIRCULATIONAHA.118.035210

63. Zhang L, Sultana N, Yan J, Yang F, Chen F, Chepurko E, et al. Cardiac sca-1$^+$ cells are not intrinsic stem cells for myocardial development, renewal, and repair. *Circulation.* (2018) 138:2919–30. doi: 10.1161/CIRCULATIONAHA.118.035200

64. Neidig L, Weinberger F, Palpant N, Mignone J, Martinson A, Sorensen D, et al. Evidence for minimal cardiogenic potential of stem cell antigen 1–positive cells in the adult mouse heart. *Circulation.* (2018) 138:2960–2. doi: 10.1161/CIRCULATIONAHA.118.035273

65. Tang J, Li Y, Huang X, He L, Zhang L, Wang H, et al. Fate mapping of sca1$^+$ cardiac progenitor cells in the adult mouse heart. *Circulation.* (2018) 138:2967–9. doi: 10.1161/CIRCULATIONAHA.118.036210

66. Soonpaa M, Lafontant P, Reuter S, Scherschel J, Srour E, Zaruba M, et al. Absence of cardiomyocyte differentiation following transplantation of adult cardiac-resident sca-1$^+$ cells into infarcted mouse hearts. *Circulation.* (2018) 138:2963–6. doi: 10.1161/CIRCULATIONAHA.118.035391

67. He L, Han M, Zhang Z, Li Y, Huang X, Liu X, et al. Reassessment of C-kit$^+$ cells for cardiomyocyte contribution in adult heart. *Circulation.* (2019) 140:164–6. doi: 10.1161/CIRCULATIONAHA.119.039909

68. Hansson E, Lendahl U. Regenerative medicine for the treatment of heart disease. *J Int Med.* (2013) 273:235–45. doi: 10.1111/joim.12033

69. Gerbin K, Murry C. The winding road to regenerating the human heart. *Cardiovasc Pathol.* (2015) 24:133–40. doi: 10.1016/j.carpath.2015.02.004

70. Michler R. The current status of stem cell therapy in ischemic heart disease. *J Cardiac Surg.* (2018) 33:520–31. doi: 10.1111/jocs.13789

71. Mirotsou M, Jayawardena T, Schmeckpeper J, Gnecchi M, Dzau V. Paracrine mechanisms of stem cell reparative and regenerative actions in the heart. *J Mol Cell Cardiol.* (2011) 50:280–9. doi: 10.1016/j.yjmcc.2010.08.005

72. Sid-Otmane C, Perrault L, Ly H. Mesenchymal stem cell mediates cardiac repair through autocrine, paracrine and endocrine axes. *J Trans Med.* (2020) 18:336. doi: 10.1186/s12967-020-02504-8

73. Ju C, Shen Y, Ma G, Liu Y, Cai J, Kim I, et al. Transplantation of cardiac mesenchymal stem cell-derived exosomes promotes repair in ischemic myocardium. *J Cardiovasc Trans Res.* (2018) 11:420–8. doi: 10.1007/s12265-018-9822-0

74. Vagnozzi R, Maillet M, Sargent M, Khalil H, Johansen A, Schwanekamp J, et al. An acute immune response underlies the benefit of cardiac stem cell therapy. *Nature.* (2020) 577:405. doi: 10.1038/s41586-019-1802-2

75. Volarevic V, Markovic B, Gazdic M, Volarevic A, Jovicic N, Arsenijevic N, et al. Ethical and safety issues of stem cell-based therapy. *Int J Med Sci.* (2018) 15:36–45. doi: 10.7150/ijms.21666

76. Takahashi K, Yamanaka S. Induction of pluripotent stem cells from mouse embryonic and adult fibroblast cultures by defined factors. *Cell.* (2006) 126:663–76. doi: 10.1016/j.cell.2006.07.024

77. Kehat I, Kenyagin-Karsenti D, Snir M, Segev H, Amit M, Gepstein A, et al. Human embryonic stem cells can differentiate into myocytes with structural and functional properties of cardiomyocytes. *J Clin Invest.* (2001) 108:407–14. doi: 10.1172/JCI12131

78. Murry C, Keller G. Differentiation of embryonic stem cells to clinically relevant populations: lessons from embryonic development. *Cell.* (2008) 132:661–80. doi: 10.1016/j.cell.2008.02.008

79. Mendjan S, Mascetti Victoria L, Ortmann D, Ortiz M, Karjosukarso Dyah W, Ng Y, et al. Nanog and Cdx2 pattern distinct subtypes of human mesoderm during exit from pluripotency. *Cell Stem Cell.* (2014) 15:310–25. doi: 10.1016/j.stem.2014.06.006

80. Mauritz C, Schwanke K, Reppel M, Neef S, Katsirntaki K, Maier L, et al. Generation of functional murine cardiac myocytes from induced pluripotent stem cells. *Circulation.* (2008) 118:507–17. doi: 10.1161/CIRCULATIONAHA.108.778795

81. Karakikes I, Ameen M, Termglinchan V, Wu J. Human induced pluripotent stem cell–derived cardiomyocytes. *Circ Res.* (2015) 117:80–8. doi: 10.1161/CIRCRESAHA.117.305365

82. Sharma A, Marceau C, Hamaguchi R, Burridge P, Rajarajan K, Churko J, et al. Human induced pluripotent stem cell–derived cardiomyocytes as an in vitro model for coxsackievirus b3–induced myocarditis and antiviral drug screening platform. *Circ Res.* (2014) 115:556–66. doi: 10.1161/CIRCRESAHA.115.303810

83. Lian X, Zhang J, Azarin S, Zhu K, Hazeltine L, Bao X, et al. Directed cardiomyocyte differentiation from human pluripotent stem cells by modulating wnt/β-catenin signaling under fully defined conditions. *Nat Prot.* (2013) 8:162–75. doi: 10.1038/nprot.2012.150

84. Burridge P, Matsa E, Shukla P, Lin Z, Churko J, Ebert A, et al. Chemically defined generation of human cardiomyocytes. *Nat Methods.* (2014) 11:855–60. doi: 10.1038/nmeth.2999

85. Rojas S, Kensah G, Rotaermel A, Baraki H, Kutschka I, Zweigerdt R, et al. Transplantation of purified ipsc-derived cardiomyocytes in myocardial infarction. *PLoS One.* (2017) 12:e0173222. doi: 10.1371/journal.pone.0173222

86. Guan X, Xu W, Zhang H, Wang Q, Yu J, Zhang R, et al. Transplantation of human induced pluripotent stem cell-derived cardiomyocytes improves myocardial function and reverses ventricular remodeling in infarcted rat hearts. *Stem Cell Res Ther.* (2020) 11:73. doi: 10.1186/s13287-020-01602-0

87. Jiang X, Yang Z, Dong M. Cardiac repair in a murine model of myocardial infarction with human induced pluripotent stem cell-derived cardiomyocytes. *Stem Cell Res Ther.* (2020) 11:297. doi: 10.1186/s13287-020-01811-7

88. Ishida M, Miyagawa S, Saito A, Fukushima S, Harada A, Ito E, et al. Transplantation of human-induced pluripotent stem cell-derived cardiomyocytes is superior to somatic stem cell therapy for restoring cardiac function and oxygen consumption in a porcine model of myocardial infarction. *Transplantation.* (2019) 103:291–8. doi: 10.1097/tp.0000000000002384

89. Robey T, Saiget M, Reinecke H, Murry C. Systems approaches to preventing transplanted cell death in cardiac repair. *J Mol Cell Cardiol.* (2008) 45:567–81. doi: 10.1016/j.yjmcc.2008.03.009

90. Laflamme M, Chen K, Naumova A, Muskheli V, Fugate J, Dupras S, et al. Cardiomyocytes derived from human embryonic stem cells in pro-survival factors enhance function of infarcted rat hearts. *Nat Biotechnol.* (2007) 25:1015–24. doi: 10.1038/nbt1327

91. Fernandes S, Naumova A, Zhu W, Laflamme M, Gold J, Murry C. Human embryonic stem cell-derived cardiomyocytes engraft but do not alter cardiac remodeling after chronic infarction in rats. *J Mol Cell Cardiol.* (2010) 49:941–9. doi: 10.1016/j.yjmcc.2010.09.008

92. Shiba Y, Fernandes S, Zhu W, Filice D, Muskheli V, Kim J, et al. Human Es-cell-derived cardiomyocytes electrically couple and suppress arrhythmias in injured hearts. *Nature.* (2012) 489:322–5. doi: 10.1038/nature11317

93. Chong J, Yang X, Don C, Minami E, Liu Y, Weyers J, et al. Human embryonic-stem-cell-derived cardiomyocytes regenerate non-human primate hearts. *Nature.* (2014) 510:273–7. doi: 10.1038/nature13233

94. Shiba Y, Gomibuchi T, Seto T, Wada Y, Ichimura H, Tanaka Y, et al. Allogeneic transplantation of ips cell-derived cardiomyocytes regenerates primate hearts. *Nature.* (2016) 538:388–91.

95. Romagnuolo R, Masoudpour H, Porta-Sánchez A, Qiang B, Barry J, Laskary A, et al. Human embryonic stem cell-derived cardiomyocytes regenerate the infarcted pig heart but induce ventricular tachyarrhythmias. *Stem Cell Rep.* (2019) 12:967–81. doi: 10.1016/j.stemcr.2019.04.005

96. Kadota S, Pabon L, Reinecke H, Murry C. In vivo maturation of human induced pluripotent stem cell-derived cardiomyocytes in neonatal and adult rat hearts. *Stem Cell Rep.* (2017) 8:278–89. doi: 10.1016/j.stemcr.2016.10.009

97. Liu Y, Chen B, Yang X, Fugate J, Kalucki F, Futakuchi-Tsuchida A, et al. Human embryonic stem cell–derived cardiomyocytes restore function in infarcted hearts of non-human primates. *Nat Biotechnol.* (2018) 36:597–605. doi: 10.1038/nbt.4162

98. Nakamura K, Neidig L, Yang X, Weber G, El-Nachef D, Tsuchida H, et al. Pharmacologic therapy for engraftment arrhythmia induced by transplantation of human cardiomyocytes. *Stem Cell Rep.* (2021) 16:2473–87. doi: 10.1016/j.stemcr.2021.08.005

99. Dhahri W, Valdman T, Wilkinson D, Pereira E, Ceylan E, Andharia N, et al. In vitro matured human pluripotent stem cell-derived cardiomyocytes form grafts with enhanced structure and function in injured hearts. *Circulation.* (2022) 145:1412–26. doi: 10.1161/CIRCULATIONAHA.121.053563

100. Lundy S, Zhu W, Regnier M, Laflamme M. Structural and functional maturation of cardiomyocytes derived from human pluripotent stem cells. *Stem Cells Dev.* (2013) 22:1991–2002. doi: 10.1089/scd.2012.0490

101. Ebert A, Joshi A, Andorf S, Dai Y, Sampathkumar S, Chen H, et al. Proteasome-dependent regulation of distinct metabolic states during long-term culture of human ipsc-derived cardiomyocytes. *Circ Res.* (2019) 125:90–103. doi: 10.1161/CIRCRESAHA.118.313973

102. Ruan J, Tulloch N, Razumova M, Saiget M, Muskheli V, Pabon L, et al. Mechanical stress conditioning and electrical stimulation promote contractility and force maturation of induced pluripotent stem cell-derived human cardiac tissue. *Circulation.* (2016) 134:1557–67. doi: 10.1161/CIRCULATIONAHA.114.014998

103. Ronaldson-Bouchard K, Ma S, Yeager K, Chen T, Song L, Sirabella D, et al. Advanced maturation of human cardiac tissue grown from pluripotent stem cells. *Nature.* (2018) 556:239–43. doi: 10.1038/s41586-018-0016-3

104. Yang X, Rodriguez M, Pabon L, Fischer K, Reinecke H, Regnier M, et al. Tri-iodo-L-thyronine promotes the maturation of human cardiomyocytes-derived from induced pluripotent stem cells. *J Mol Cell Cardiol.* (2014) 72:296–304. doi: 10.1016/j.yjmcc.2014.04.005

105. Funakoshi S, Fernandes I, Mastikhina O, Wilkinson D, Tran T, Dhahri W, et al. Generation of mature compact ventricular cardiomyocytes from human pluripotent stem cells. *Nat Commun.* (2021) 12:3155. doi: 10.1038/s41467-021-23329-z

106. Huang C, Peres Moreno Maia-Joca R, Ong C, Wilson I, DiSilvestre D, Tomaselli G, et al. Enhancement of human ipsc-derived cardiomyocyte maturation by chemical conditioning in a 3d environment. *J Mol Cell Cardiol.* (2020) 138:1–11. doi: 10.1016/j.yjmcc.2019.10.001

107. Feyen D, McKeithan W, Bruyneel A, Spiering S, Hörmann L, Ulmer B, et al. Metabolic maturation media improve physiological function of human ipsc-derived cardiomyocytes. *Cell Rep.* (2020) 32:107925. doi: 10.1016/j.celrep.2020.107925

108. Hofbauer P, Jahnel S, Papai N, Giesshammer M, Deyett A, Schmidt C, et al. Cardioids reveal self-organizing principles of human cardiogenesis. *Cell.* (2021) 2021:34. doi: 10.1016/j.cell.2021.04.034

109. Zhao X, Chen H, Xiao D, Yang H, Itzhaki I, Qin X, et al. Comparison of non-human primate versus human induced pluripotent stem cell-derived cardiomyocytes for treatment of myocardial infarction. *Stem Cell Rep.* (2018) 10:422–35. doi: 10.1016/j.stemcr.2018.01.002

110. Kawaguchi S, Soma Y, Nakajima K, Kanazawa H, Tohyama S, Tabei R, et al. Intramyocardial transplantation of human ips cell–derived cardiac spheroids improves cardiac function in heart failure animals. *JACC Basic Trans Sci.* (2021) 6:239–54. doi: 10.1016/j.jacbts.2020.11.017

111. Sun X, Wu J, Qiang B, Romagnuolo R, Gagliardi M, Keller G, et al. Transplanted microvessels improve pluripotent stem cell–derived cardiomyocyte engraftment and cardiac function after infarction in rats. *Sci Trans Med.* (2020) 12:eaax2992. doi: 10.1126/scitranslmed.aax2992

112. Nagase K, Nagumo Y, Kim M, Kim H, Kyung H, Chung H, et al. Local release of vegf using fiber mats enables effective transplantation of layered cardiomyocyte sheets. *Macromol Biosci.* (2017) 17:1700073. doi: 10.1002/mabi.201700073

113. Ai X, Yan B, Witman N, Gong Y, Yang L, Tan Y, et al. Transient secretion of Vegf protein from transplanted hipsc-cms enhances engraftment and improves rat heart function post mi. *Mol Ther.* (2022) 2022:12. doi: 10.1016/j.ymthe.2022.08.012

114. Miyagawa S, Kainuma S, Kawamura T, Suzuki K, Ito Y, Iseoka H, et al. Transplantation of ipsc-derived cardiomyocyte patches for ischemic cardiomyopathy. *MedRxiv* [preprint]. (2022). doi: 10.1101/2021.12.27.21268295

115. Miyagawa S, Kawamura T, Ito E, Takeda M, Iseoka H, Yokoyama J, et al. Evaluation of the Efficacy and safety of a clinical grade human induced pluripotent stem cell-derived cardiomyocyte patch: a pre-clinical study. *bioRxiv* [preprint]. (2021). doi: 10.1101/2021.04.07.438744

116. Kawamura M, Miyagawa S, Fukushima S, Saito A, Miki K, Funakoshi S, et al. Enhanced therapeutic effects of human ips cell derived-cardiomyocyte by combined cell-sheets with omental flap technique in porcine ischemic cardiomyopathy model. *Sci Rep.* (2017) 7:8824. doi: 10.1038/s41598-017-08869-z

117. Kawamura M, Miyagawa S, Miki K, Saito A, Fukushima S, Higuchi T, et al. Feasibility, safety, and therapeutic efficacy of human induced pluripotent stem cell-derived cardiomyocyte sheets in a porcine ischemic cardiomyopathy model. *Circulation.* (2012) 126:S29–37. doi: 10.1161/CIRCULATIONAHA.111.084343

118. Masumoto H, Matsuo T, Yamamizu K, Uosaki H, Narazaki G, Katayama S, et al. Pluripotent stem cell-engineered cell sheets reassembled with defined cardiovascular populations ameliorate reduction in infarct heart function through cardiomyocyte-mediated neovascularization. *Stem Cells.* (2012) 30:1196–205. doi: 10.1002/stem.1089

119. Tang J, Wang J, Huang K, Ye Y, Su T, Qiao L, et al. Cardiac cell–integrated microneedle patch for treating myocardial infarction. *Sci Adv.* (2018) 4:eaat9365. doi: 10.1126/sciadv.aat9365

120. Mallapaty S. Revealed: two men in china were first to receive pioneering stem-cell treatment for heart disease. *Nature.* (2020) 581:249–51. doi: 10.1038/d41586-020-01285-w

121. Donovan K, Ferguson F, Bushman J, Eleuteri N, Bhunia D, Ryu S, et al. Mapping the degradable kinome provides a resource for expedited degrader development. *Cell.* (2020) 10:38. doi: 10.1016/j.cell.2020.10.038

122. Sun X, Wang J, Yao X, Zheng W, Mao Y, Lan T, et al. A chemical approach for global protein knockdown from mice to non-human primates. *Cell Dis.* (2019) 5:10. doi: 10.1038/s41421-018-0079-1

123. Deuse T, Tediashvili G, Hu X, Gravina A, Tamenang A, Wang D, et al. Hypoimmune induced pluripotent stem cell–derived cell therapeutics treat cardiovascular and pulmonary diseases in immunocompetent allogeneic mice. *Proc Natl Acad Sci USA.* (2021) 118:e2022091118. doi: 10.1073/pnas.2022091118

124. Peinkofer G, Maass M, Pfannkuche K, Sachinidis A, Baldus S, Hescheler J, et al. Persistence of intramyocardially transplanted murine induced pluripotent stem cell-derived cardiomyocytes from different developmental stages. *Stem Cell Res Ther.* (2021) 12:46. doi: 10.1186/s13287-020-02089-5

125. Funakoshi S, Miki K, Takaki T, Okubo C, Hatani T, Chonabayashi K, et al. Enhanced engraftment, proliferation and therapeutic potential in heart using optimized human ipsc-derived cardiomyocytes. *Sci Rep.* (2016) 6:19111. doi: 10.1038/srep19111

126. Varzideh F, Pahlavan S, Ansari H, Halvaei M, Kostin S, Feiz M, et al. Human cardiomyocytes undergo enhanced maturation in embryonic stem cell-derived organoid transplants. *Biomaterials.* (2019) 192:537–50. doi: 10.1016/j.biomaterials.2018.11.033

127. Wimmer R, Leopoldi A, Aichinger M, Wick N, Hantusch B, Novatchkova M, et al. Human blood vessel organoids as a model of diabetic vasculopathy. *Nature.* (2019) 565:505–10. doi: 10.1038/s41586-018-0858-8

128. Tian Y, Liu Y, Wang T, Zhou N, Kong J, Chen L, et al. A microrna-hippo pathway that promotes cardiomyocyte proliferation and cardiac regeneration in mice. *Sci Trans Med.* (2015) 7:ra38–38. doi: 10.1126/scitranslmed.3010841

129. Liu H, Shi J, Wang H, Xuan Q, Bei Y, Sun W, et al. Abstract 309: mir-31a-5p controls cardiomyocyte proliferation in postnatal hearts. *Circ Res.* (2015) 117:A309. doi: 10.1161/res.117.suppl_1.309

130. Collesi C, Zentilin L, Sinagra G, Giacca M. Notch1 signaling stimulates proliferation of immature cardiomyocytes. *J Cell Biol.* (2008) 183:117–28. doi: 10.1083/jcb.200806091

131. Rojas A, Kong S, Agarwal P, Gilliss B, Pu W, Black B. Gata4 is a direct transcriptional activator of *Cyclin D2* and *Cdk4* and is required for cardiomyocyte proliferation in anterior heart field-derived myocardium. *Mol Cell Biol.* (2008) 28:5420–31. doi: 10.1128/MCB.00717-08

132. Bassat E, Mutlak Y, Genzelinakh A, Shadrin I, Baruch Umansky K, Yifa O, et al. The extracellular matrix protein agrin promotes heart regeneration in mice. *Nature.* (2017) 547:179–84. doi: 10.1038/nature22978

133. Magadum A, Ding Y, He L, Kim T, Vasudevarao M, Long Q, et al. Live cell screening platform identifies pparδ as a regulator of cardiomyocyte proliferation and cardiac repair. *Cell Res.* (2017) 27:1002–19. doi: 10.1038/cr.2017.84

134. Eulalio A, Mano M, Ferro M, Zentilin L, Sinagra G, Zacchigna S, et al. Functional screening identifies mirnas inducing cardiac regeneration. *Nature.* (2012) 492:376–81. doi: 10.1038/nature11739

135. Gise A, Lin Z, Schlegelmilch K, Honor L, Pan G, Buck J, et al. Yap1, the nuclear target of hippo signaling, stimulates heart growth through cardiomyocyte proliferation but not hypertrophy. *Proc Natl Acad Sci USA.* (2012) 109:2394–9. doi: 10.1073/pnas.1116136109

136. Engel F, Hsieh P, Lee R, Keating M. Fgf1/P38 map kinase inhibitor therapy induces cardiomyocyte mitosis, reduces scarring, and rescues function after myocardial infarction. *Proc Natl Acad Sci USA.* (2006) 103:15546–51. doi: 10.1073/pnas.0607382103

137. Morikawa Y, Heallen T, Leach J, Xiao Y, Martin J. Dystrophin–glycoprotein complex sequesters yap to inhibit cardiomyocyte proliferation. *Nature.* (2017) 547:227–31. doi: 10.1038/nature22979

138. Li J, Gao E, Vite A, Yi R, Gomez L, Goossens S, et al. Alpha-catenins control cardiomyocyte proliferation by regulating yap activity. *Circ Res.* (2015) 116:70–9. doi: 10.1161/CIRCRESAHA.116.304472

139. Woulfe K, Gao E, Lal H, Harris D, Fan Q, Vagnozzi R, et al. Glycogen synthase kinase-3β regulates post–myocardial infarction remodeling and stress-induced cardiomyocyte proliferation in vivo. *Circ Res.* (2010) 106:1635–45. doi: 10.1161/CIRCRESAHA.109.211482

Frontiers in
Cardiovascular Medicine

Innovations and improvements in cardiovascular treatment and practice

Focuses on research that challenges the status quo of cardiovascular care, or facilitates the translation of advances into new therapies and diagnostic tools.

Discover the latest Research Topics

See more →

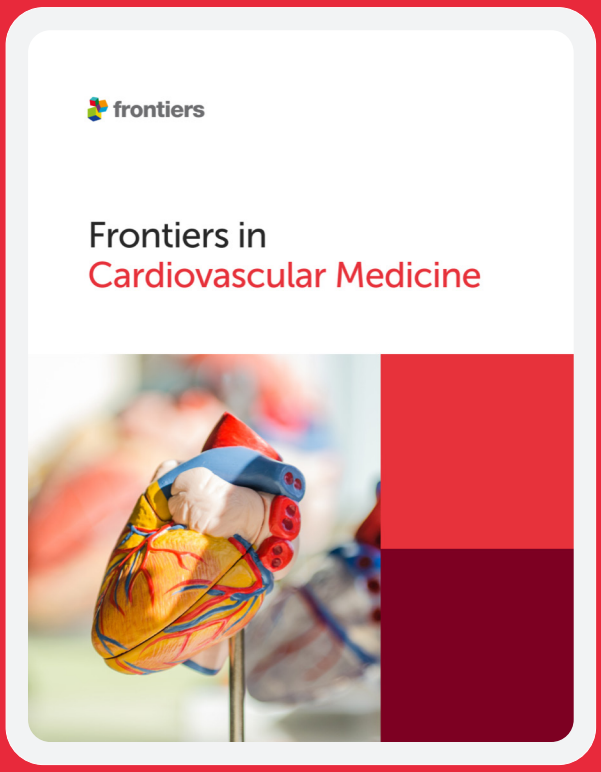

Frontiers

Avenue du Tribunal-Fédéral 34
1005 Lausanne, Switzerland
frontiersin.org

Contact us

+41 (0)21 510 17 00
frontiersin.org/about/contact